

# Assessing the Status and Trends of Spring Chinook Habitat in the Upper Grande Ronde River and Catherine Creek: Annual Report 2020

*publication date: April 12, 2021*

*Authors:* Seth White, Casey Justice, Lauren Burns, Ben Staton, and Matthew Kaylor



## Technical Report

Columbia River Inter-Tribal Fish Commission

700 NE Multnomah St, Ste 1200, Portland OR 97232 • (503)238-0667 • [www.critfc.org](http://www.critfc.org)

21-02

Funding for this work came from the Columbia Basin Fish Accords (2008-2021), a thirteen-year tribal/federal partnership between the Bonneville Power Administration, Bureau of Reclamation, Columbia River Inter-Tribal Fish Commission, The Confederated Tribes of the Umatilla Indian Reservation, The Confederated Tribes of the Warm Springs Reservation of Oregon, US Army Corps of Engineers, and The Confederated Tribes and Bands of the Yakama Nation.

# **Assessing the Status and Trends of Spring Chinook Habitat in the Upper Grande Ronde River and Catherine Creek**

BPA Project # 2009-004-00

Report covers work performed under BPA contract #(s) 73354 REL 22, 73354 REL 40

Report was completed under BPA contract #(s) 73354 REL 40

Report covers work performed from:

January – December 2020

Seth White<sup>1,2</sup>, Casey Justice<sup>1</sup>, Lauren Burns<sup>1</sup>, Ben Staton<sup>1</sup>, and Matthew Kaylor<sup>2</sup>

<sup>1</sup>Columbia River Inter-Tribal Fish Commission, Portland, OR 97232

<sup>2</sup>Department of Fisheries & Wildlife, Oregon State University, Corvallis, OR 97331

April 2021

This report was funded by the Bonneville Power Administration (BPA), U.S. Department of Energy, as part of BPA's program to protect, mitigate, and enhance fish and wildlife affected by the development and operation of hydroelectric facilities on the Columbia River and its tributaries. The views in this report are the author's and do not necessarily represent the views of BPA.

## Table of Contents

Executive Summary .....	3
Introduction.....	11
Study Area .....	14
Special Note on Progress in 2020 .....	16
References.....	17
Project Components.....	18
1.0 Habitat and Biotic Assessments.....	18
1.1 Refinement of a tributary habitat monitoring protocol .....	18
1.2 LiDAR data collection .....	27
1.3 Unmanned Aircraft Systems (UAS) for fish habitat assessments .....	33
1.4 Reanalysis of snorkel survey calibration methods.....	48
2.0 Riverscape Analyses .....	49
2.1 Spatial patterns and drivers of juvenile Chinook Salmon size and growth .....	49
2.2 Riverscape predictions of Chinook Salmon emergence timing.....	50
2.3 Long-term effects of cattle grazing on benthic macroinvertebrate assemblages .....	73
3.0 Fish-Habitat Modeling.....	82
3.1 Developing an index of Chinook Salmon parr capacity .....	82
3.2 Factors influencing Chinook Salmon pre-spawn survival.....	95
3.3 Update on the life cycle model .....	116
4.0 Adaptive Management.....	130
4.1 Progress on an adaptive management framework .....	130
Dissemination of Project Findings in 2020.....	133
Appendix A – CRITFC Tributary Habitat Assessment Protocol.....	135
Appendix B – Grande Ronde Basin Topobathymetric LiDAR Technical Data Report .....	179
Appendix C – Submitted paper on snorkel survey calibration methods.....	216
Appendix D – Published paper on spatial patterns on Chinook size and growth.....	262
Appendix E – Published Fisheries paper on the Grande Ronde basin as a case study ...	298



# Executive Summary

## Background and Objectives

The Columbia River Inter-Tribal Fish Commission is conducting a research, monitoring, and evaluation study designed to determine the effectiveness of aggregate restoration actions in improving freshwater habitat conditions and viability of ESA-listed spring Chinook Salmon (*Oncorhynchus tshawytscha*) populations. A critical uncertainty for fisheries managers in the Columbia Basin is whether freshwater habitat restoration actions will improve basin-wide habitat quantity/quality and thereby salmon productivity to a level sufficient to offset human-caused survival impairments elsewhere in the life cycle. Geographically, this project is focused on the upper Grande Ronde River and Catherine Creek basins (tributaries of the Snake River in the Columbia River basin), but with applications and testing of research, monitoring, and evaluation approaches also occurring in other Columbia River tributaries.

The objectives of this project are to: 1) Assess current status and trends in fish habitat characteristics considered to be key ecological concerns for viability of spring Chinook Salmon populations; 2) Evaluate effectiveness of aggregate stream restoration actions aimed at improving key ecological concerns; and 3) Develop a life cycle model to link biotic responses of spring Chinook Salmon populations to projected changes in stream habitat conditions.

We have categorized our work towards these objectives into the following project components:

- Component 1: Habitat and biotic assessments,
- Component 2: Riverscape analyses, and
- Component 3: Fish-habitat modeling.

These individual components are linked together conceptually in an overall cycle of research, monitoring, and evaluation, with analyses feeding into an adaptive management framework (Figure 1).



Figure 1. CRITFC's cycle of research, monitoring, and evaluation providing the basis for decision-making in an adaptive management framework.

### Special Note on Progress in 2020

The unprecedented circumstances of 2020—most notably the COVID-19 pandemic—made conducting research and monitoring especially challenging. However, by shifting our priority from intensive fieldwork to the collection of remote sensing data and continued focus on data analyses and development of models, we were able to make significant progress towards overall project objectives. In 2020 we pivoted towards light fieldwork (e.g., maintenance of temperature logger network, assistance to ODFW fish sampling crews) and collection of light detection and ranging (LiDAR) data over extensive regions of the Grande Ronde and Wallowa River basins in collaboration with regional partners. This new focus towards remote sensing allowed us to collect a rich data set that is being used to compare against past LiDAR data for assessment of decadal trends in riparian vegetation and for assessment of current status of fish-habitat conditions. Other notable progress in 2020 included completion of a new tributary habitat assessment protocol, analyses of datasets collected in the field in prior years (e.g., pre-spawn mortality, juvenile fish growth and phenology studies), and substantial progress on the life cycle model in collaboration with ODFW and NOAA.

## **Progress and Key Findings**

### Component 1: Habitat and Biotic Assessments

#### *Refinement of a Tributary Habitat Monitoring Protocol*

- A major project component is evaluating the effect that aggregate stream restoration actions have on improving the quantity and quality of habitat for ESA-listed spring Chinook Salmon. CRITFC and numerous other basin partners have been working to formalize new monitoring strategies that allow for the continuation of fish habitat status and trends assessment.
- During 2020, CRITFC made significant progress through the development of a new monitoring protocol and through continued engagement and creation of new partnerships.

#### *LiDAR Data Collection*

- In summer of 2020 we coordinated the collection of over 76,000 acres of topobathymetric (“green”) light detection and ranging (LiDAR) data in the Grande Ronde and Wallowa River watersheds, in collaboration with Grande Ronde Model Watershed and Bonneville Power Association.
- These data were collected for the purposes of (a) revisiting areas flown for terrestrial LiDAR in 2009-2011 for analysis of decadal changes to vegetation density/height and altered floodplain characteristics and (b) acquiring topobathymetric spatial data layers to calculate metrics of instream and near-stream fish habitat conditions.
- Subsequent data processing and QA/QC of LiDAR data revealed the data met quality targets in terms of point density and horizontal & vertical accuracy of classified points.
- Analyses in progress or planned include developing fish-habitat metrics, classification of large wood, and evaluation of inter-decadal change in riparian vegetation height and density using LiDAR data.

#### *Unmanned Aircraft Systems (UAS) for Fish Habitat Assessments*

- To test the feasibility of integrating remotely sensed methods into fish habitat monitoring we completed a comparative analysis of several channel unit and site level metrics using ground-based validation data and those derived from UAS imagery.
- Linear mixed effects models were used to examine the effects of geomorphic conditions (e.g., habitat unit types and morphology) and canopy densities on derived metrics across of the range of habitat conditions likely to be encountered by fish.
- At the scale of the entire river reach, some metrics showed promising correspondence between the two approaches; these metrics included total habitat area and volume.
- Riparian and geomorphic conditions affected the correspondence between ground- vs. UAS-derived estimates of water depth.

- Increasing canopy cover decreased our ability to quantify wood using UAS and significantly affected our ability to image the active wetted channel leading to larger error between the data collection methods. To a lesser degree than canopy density, reaches with constrained geomorphic conditions or slow water also resulted in significant increases in the error between the methods tested.
- The results of this study address a critical knowledge gap regarding the challenges and limitations that riparian canopy and in-stream conditions pose for fish habitat monitoring using UAS while also highlighting the need for additional investment and research into the potential of these rapidly evolving technologies.

#### *Reanalysis of snorkel survey calibration methods*

- We made refinements to a model relating juvenile salmon and steelhead counts in tributary rearing habitats observed via snorkeling to abundance estimates using a Bayesian hierarchical model. The model uses information about local abundance from mark-recapture surveys paired with snorkel surveys and physical habitat features. The model provides estimates of the effects of each habitat feature on the proportion of the local population counted by snorkel surveys, enabling correcting snorkel survey counts for partial detection for subsequent use in fish-habitat models and our life cycle model.
- We submitted a manuscript documenting this work and have received peer-review feedback and we have incorporated it into a new draft. We plan to resubmit revisions to the manuscript from this analysis to the journal *Fisheries Research*, also included as Appendix C of this report.
- The primary change from the previous version of the model is a revised likelihood function for mark-recapture data to allow evaluation of behavioral effects (e.g., active recapture avoidance) and incorporation if necessary. Although there were slight quantitative changes to the abundance estimates, very few qualitative inferences changed with the re-analysis.

#### Component 2: Riverscape Analyses

##### *Spatial patterns and drivers of juvenile Chinook Salmon size and growth*

- Chinook Salmon parr size, growth rates, and density were quantified at the network scale in the upper Grande Ronde River and Catherine Creek.
- In July, both basins exhibited clear size gradients with larger parr at downstream sites and decreasing size with distance upstream. In addition, parr were larger in Catherine Creek compared to upper Grande Ronde.
- Modeling of emergence timing indicated earlier fry emergence at downstream sites compared to upstream sites, and earlier emergence in Catherine Creek compared to upper Grande Ronde, which suggests that emergence timing was a main contributor to observed size patterns in July.

- Growth rates decreased with distance upstream in spring, but this pattern reversed in summer. As a result, fish downstream obtained the majority of growth in spring, whereas upstream fish obtained the majority of growth in summer.
- The manuscript has been accepted in the *Journal of Animal Ecology* and is attached as Appendix D in this report.

#### *Riverscape patterns of emergence phenology and fish size*

- We used year-round water temperature data and spawning surveys to estimate juvenile Chinook Salmon emergence timing throughout the spawning distributions of Catherine Creek, the upper Grande Ronde River, the Minam River, and the Middle Fork John Day River. We then related inter-annual variation in emergence timing to parr size and growth rates from 2011-2020.
- Key findings were that 1) emergence timing within each river was asynchronous and strongly spatially structured, 2) spatial patterns were not consistent among rivers, and 3) size was not greater in years with earlier emergence, as growth rates were higher in years with later emergence.
- These results are preliminary, but we plan to finalize analyses and submit the manuscript to a peer-reviewed journal in spring/summer 2021.

#### *Long-term effects of cattle grazing on benthic macroinvertebrate assemblages*

- CRITFC contributed to data collection and analysis of benthic macroinvertebrate assemblages in a study evaluating changes in geomorphology, fish habitat, and greenline and floodplain vegetation from 1996 to 2019 in the Middle Fork John Day River with various livestock management and stream restoration strategies. The study was initiated by collaborators from Confederated Tribes of the Warm Springs Reservation, University of Oregon, and Oregon State University and funded by the Oregon Watershed Enhancement Board.
- In this report, only results from the benthic macroinvertebrate portion are reported. Key findings include 1) overall taxonomic and EPT richness appeared to increase over time in all treatments except for active restoration, where EPT richness decreased; 2) invertebrate assemblage structure changed significantly over time, especially in actively restored sites where assemblages appeared to shift in a manner resembling higher elevation stream communities.
- These results are preliminary and warrant further analysis prior to making management recommendations. However, we recommend future monitoring should include continued benthic, drift, fish diet, and sampling for terrestrial invertebrates, which provide an important food source for salmonids and are more likely to be affected by near-stream livestock grazing.



### Component 3: Fish-Habitat Modeling

#### *Developing and index of Chinook rearing capacity*

- We analyzed the relationship between freshwater habitat conditions and abundance of Chinook Salmon summer parr measured across 125 sites over seven years (2011-2017; 304 unique observations) in the Grande Ronde River basin with the objective of developing an index of habitat capacity (i.e., weighted usable habitat).
- The model appeared to fit the data well (marginal  $R^2 = 0.82$ ), with variation in fish density explained by a combination of intrinsic habitat characteristics (mean annual flow, gradient, and base flow index) and dynamic habitat variables (water temperature, pool frequency, and large wood frequency) that can be affected by restoration actions.
- Using predicted fish density to weight the suitability of existing habitat, we intend to use this model to provide an index of summer parr rearing capacity in a life cycle model evaluating potential fish responses to restoration and climate change scenarios.

#### *Factors influencing Chinook pre-spawn survival and projected impacts of climate change*

- We used a 23-year time series (1993-2015) of Chinook Salmon carcass recovery data collected by ODFW in six populations and 87 survey reaches in the Grande Ronde River basin to evaluate the factors influencing pre-spawn survival rates.
- A logistic regression model was used to assess how reach-scale (0.1 – 10 km) estimates of pre-spawn survival were affected by riverine habitat conditions (pools, water temperature, streamflow) and biotic factors (spawner density, proportion hatchery origin, day of year). The best fitting model explained approximately 90% of the variation in pre-spawn survival, with fixed and random effects accounting for approximately 57% and 38% of the total variation, respectively.
- Pre-spawn survival was positively associated with day of year and mean summer flow and was negatively associated with the proportion of hatchery origin spawners and water temperature, while spawner density and pool frequency had little effect.
- Projected climate change impacts on pre-spawn survival varied considerably across populations with a mean predicted decrease from current (2006-2015) to the 2040s of only 0.02 in cooler wilderness streams such as the Minam River, and up to 0.19 in warmer streams such as the upper Grande Ronde (mean decrease across all populations = 0.13).
- These results contribute to our understanding of the environmental and biotic factors affecting pre-spawn survival of Pacific Northwest salmon populations and provide insights into potential future climate change impacts to a critical life stage for these threatened species.

### *Update on Life Cycle Model*

- We have made substantial progress towards completing an estimation life cycle model for Grande Ronde basin spring Chinook salmon, in close collaboration with NOAA and ODFW.
- The list of improvements we have made over previous efforts is long, but highlights include: (i) standardized, traceable, and reproducible sources of all information for all empirical data, (ii) addition of a process model for dynamics of hatchery-origin fish from release to return, (iii) addition of age-3 returns and sex composition, (iv) addition of auxiliary data sources, such as estimates of survival through the hydrosystem, to enable estimation of quantities that were previously assumed known without variability or uncertainty, such as ocean survival.
- The estimation phase is nearing completion; remaining steps include more detailed/accurate specification of mortality sources on the upstream migration, continued development of a revised habitat capacity index, and integration of the multiple populations into one model.
- We outline our plans for developing a set of scenarios to represent plausible future conditions and for assessing the relative likelihood of attaining desirable population status outcomes under different scenarios.

### Component 4: Adaptive Management

#### *Progress on an Adaptive Management Framework*

- We worked towards the goal of integrating adaptive management into the Grande Ronde basin restoration program via two major tasks: 1) publishing the results of a needs assessment workshop in *Fisheries* documenting progress and setbacks towards a comprehensive approach to habitat restoration (Appendix E) and 2) collaborating with the Grande Ronde Model Watershed (GRMW) and other partners to develop a 5- and 20-year adaptive management plan for the Grande Ronde basin.
- Steps planned for 2021 include continued development of the adaptive management framework, coordination with GRMW on our response to the Independent Scientific Review Panel (ISRP), development of management scenarios that will be run in the life cycle model, field tours of recent restoration projects, and presentation of findings at the State of the Science meeting hosted by GRMW.

### **Conclusions**

In 2020 we made significant advances towards understanding limiting factors and cumulative impacts of tributary habitat restoration on salmon populations in the Grande Ronde River subbasin, and by extension to the broader Columbia River basin. Our team finalized a tributary habitat

assessment protocol that can be applied in a rapid yet robust manner, taking advantage of emerging remote sensing technology. In collaboration with regional partners, we collected extensive LiDAR data over the project area that can be used to assess status and trends of riparian and fish-habitat conditions. We reevaluated statistical extrapolation of snorkel counts to fish abundance at the reach level, a critical variable in estimating tributary habitat capacity and assessing empirical fish-habitat relationships. Analyses of early life history data of juvenile Chinook Salmon and water temperature elucidated potential drivers of fish size, growth, and emergence phenology, which are important factors for juvenile fish survival, potentially leading to population bottlenecks. An analysis of Chinook Salmon pre-spawn mortality revealed that survival is expected to decrease across the Grande Ronde basin with future climate change, but less so in cold, wilderness streams that may provide a thermal refuge. We developed an improved model describing summertime distribution of juvenile Chinook Salmon in the Grande Ronde basin, linking habitat metrics that can be affected by restoration to an index of carrying capacity for subsequent use in our life cycle model. We made significant advances in our collaboration with NOAA and ODFW in the development of a revised LCM for Grande Ronde basin spring Chinook Salmon populations; these advances include standardization of input data, inclusion of hatchery-origin fish from release to return, addition of age-3 and sex composition, and incorporation of estimates of survival through the hydrosystem. Finally, we continued our engagement with Grande Ronde basin partners to articulate and formalize an adaptive management plan for the subbasin. This included publishing a manuscript focused on goals and overall vision of an adaptive management framework and assisting with the development of a 5- and 20-year adaptive management plan for the Grande Ronde basin. Overall, our team's activities in 2020—in collaboration with several tribal, federal, state, and local partners—represented important advances towards project objectives.

## Introduction

The Columbia River Inter-Tribal Fish Commission is conducting a research, monitoring, and evaluation study designed to determine the effectiveness of aggregate restoration actions in improving freshwater habitat conditions and viability of ESA-listed spring Chinook Salmon populations. A critical uncertainty for fisheries managers in the Columbia Basin is whether freshwater habitat restoration actions will improve basin-wide habitat quantity/quality and thereby salmon productivity to a level sufficient to offset human-caused survival impairments elsewhere in the life cycle. Geographically, this project is focused on the upper Grande Ronde River and Catherine Creek watersheds (tributaries of the Snake River in the Columbia River basin), but with applications and testing of approaches to research, monitoring, and evaluation occurring in other Columbia River tributaries.

Many studies in recent years have examined the current condition of fish habitat in Columbia River subbasins and how these habitat conditions influence salmon survival and productivity. Some of the most common impediments to the survival of salmon include high water temperatures, increased concentrations of fine sediment in spawning gravel, loss of riparian vegetation, channelization and diminished channel and floodplain complexity, loss of large wood in the channel, loss of large pools for adult fish holding and juvenile rearing, and depletion of summertime streamflow. We refer to these as *ecological concerns* (formerly known as *limiting factors*). More recent studies have additionally identified food webs (e.g., nutrient limitation, primary productivity, prey availability, or predation) as ecological concerns for salmonids (Naiman et al. 2012). Climate change presents an additional threat, as it can lead to changes in the quantity, timing, and type (i.e., snow vs rain) of precipitation as well as increased summer air and water temperatures (Mantua et al. 2010, Beechie et al. 2013).

Habitat restoration in the upper Grande Ronde River and Catherine Creek basins is being conducted by agencies including the U.S. Forest Service, Confederated Tribes of the Umatilla Indian Reservation (CTUIR), Oregon Department of Fish and Wildlife (ODFW), Union Soil and Water Conservation District (USWCD), Grande Ronde Model Watershed (GRMW), and U.S. Bureau of Reclamation (USBR). However, it remains unclear how these collective restoration actions affect salmon habitat quality and quantity in the freshwater tributary life stages, let alone how they impact salmon populations in the context of the complete life cycle. Fish-habitat relationships are inherently complex as they are influenced by interactions among intrinsic watershed factors (e.g., geology, valley form, flood regime) and anthropogenic factors (e.g., land use, climate change, restoration). These in turn affect ecological conditions and ultimately drive changes in fish abundance and productivity. This project incorporates several of these interacting factors in a holistic analytical framework.

The objectives of this project are to: 1) Assess current status and trends in fish habitat characteristics considered to be key ecological concerns for viability of spring Chinook Salmon

populations; 2) Evaluate effectiveness of aggregate stream restoration actions aimed at improving these ecological concerns; and 3) Develop a life cycle model to link biotic responses of spring Chinook Salmon populations to projected changes in stream habitat conditions that may result from restoration and climate change.

We have categorized our work towards these objectives into the following project components:

- Component 1: Habitat and biotic assessments,
- Component 2: Riverscape analyses,
- Component 3: Fish-habitat modeling, and
- Component 4: Adaptive management.

These individual components are linked together conceptually in an overall sequence of research, monitoring, and evaluation, with analyses feeding into an adaptive management framework (Figure 2).

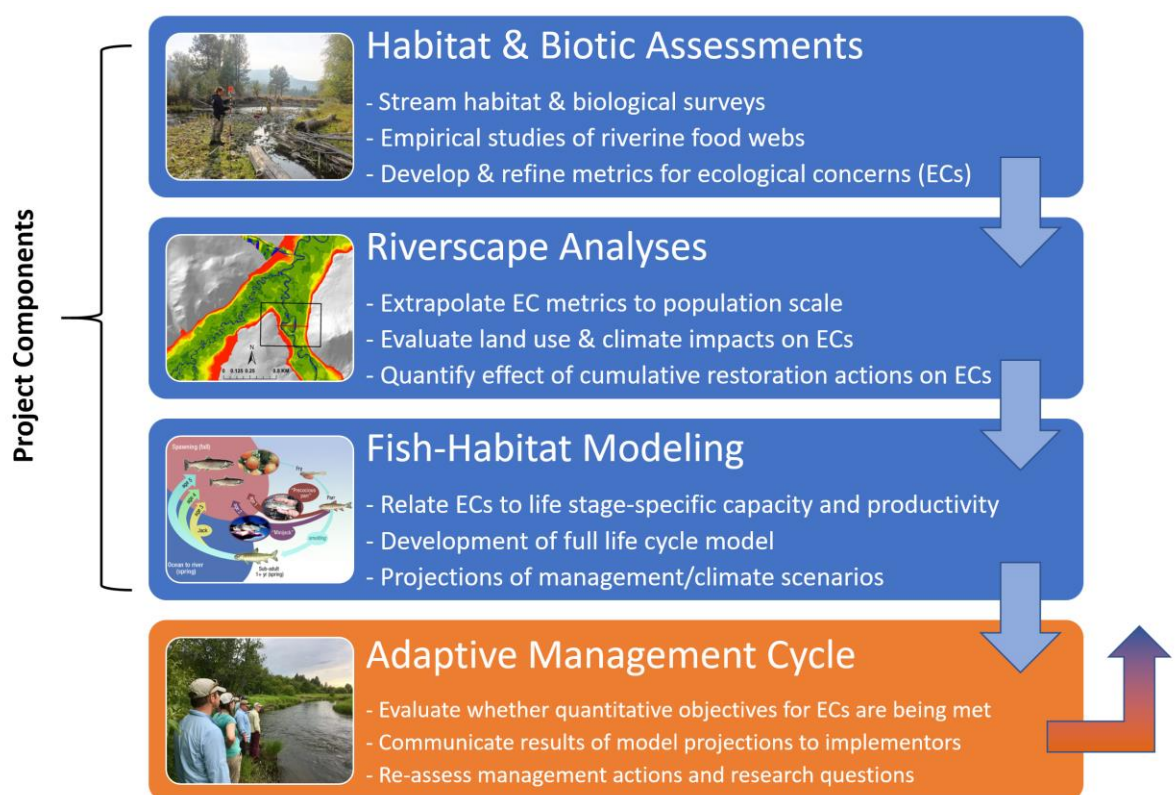


Figure 2. CRITFC's cycle of research, monitoring, and evaluation providing the basis for decision-making in an adaptive management framework.

*Component 1: Habitat and biotic assessments*—This component of our work involves collecting raw data from field surveys and remote sensing required to develop metrics for ecological concerns including habitat quality and quantity, site-specific estimates of fish capacity and productivity, and



condition of salmonid prey resources. Since 2010, CRITFC has monitored fish habitat conditions in the upper Grande Ronde River and Catherine Creek (impacted basins) and the Minam River (a wilderness reference system). We initiated our own habitat protocol in 2010, but in 2011 we were encouraged by Bonneville Power Administration (BPA) staff to adopt the Columbia Habitat Monitoring Program (CHaMP) stream habitat assessment survey. Data collected under these programs provided the basis for describing status and trends of key ecological concerns for Chinook Salmon in the study basins. In 2017, BPA commissioned a review of CHaMP which revealed several potential problems concerning both the collection of measurements and extrapolation of metrics. In response, our project initiated a revised habitat protocol in 2018 (finalized in 2020) that integrates ground-based habitat measurements with high-resolution aerial imagery from unmanned aircraft systems (UASs) to produce a pared-down list of metrics identified as having minimal observer bias and strong correspondence to known ecological concerns. Measurements of physical habitat can be paired with estimates of fish abundance derived from snorkel surveys and collection of macroinvertebrates. Additional work includes development and maintenance of an inter-agency stream temperature database in the upper Grande Ronde River, Catherine Creek, and Minam River watersheds.

*Component 2: Riverscape analyses*—This component of our work involves extrapolating metrics representing ecological concerns across stream networks and to the watershed/population scale using statistically rigorous approaches (e.g., GRTS-based averages or spatial stream-network [SSN] models). Additionally, we evaluate linkages among habitat conditions, land use, and climate conditions to understand watershed-scale processes affecting spatial and temporal trends in ecological conditions and investigate which management or policy scenarios will have the greatest impact. Quantifying the effects of cumulative restoration efforts in the subbasins is another aspect of this work, and includes developing a comprehensive restoration database for generating standardized metrics of restoration intensity. The above endeavors work towards assessing current patterns and trends of habitat quality and quantity that can be measured against historical or reference baselines.

Recovery of salmonid populations within the Columbia Basin may require an integrated approach involving management actions that consider food webs in addition to physical habitat availability (Naiman et al. 2012). To better understand the role of food webs in salmon recovery, we conducted a series of studies examining spatial patterns in nutrient concentrations and stream metabolism (Kaylor et al. 2019), carcass additions and the role of nutrient limitation and food availability on juvenile salmonid growth (Kaylor et al. 2020a; Kaylor et al. 2020b), and spatial patterns and drivers of juvenile Chinook Salmon size, growth, and emergence phenology. Collectively, efforts to assess salmonid size, growth, and phenology provide insight into the factors limiting juvenile salmonid productivity (e.g., water temperature and prey availability), actions that can be taken to increase productivity (e.g. carcass addition, floodplain restoration), and where in these basins

targeted restoration efforts may have the greatest impact on increasing juvenile salmonid productivity given the biophysical characteristics of these stream networks.

*Component 3: Fish-habitat modeling*—This component draws from the above data and analyses to relate ecological concerns to life stage-specific capacity or productivity, develop and apply a full spring Chinook Salmon life cycle model, and project the outcomes of alternative management and climate change scenarios. Life stage-specific models have thus far emphasized relationships between water temperature, instream habitat conditions, and abundance of rearing fish (parr); these models are then used to project anticipated changes to habitat capacity based on alternative management and climate change. The life cycle model is a tool to simulate fish population trends in relation to projected habitat conditions based on historical data and population dynamics, and to examine the relative benefits of habitat improvements on fish population recovery potential while accounting for out-of-basin impacts such as survival of out-migrating smolts at dams or mortality in the ocean phase. The fundamental basis of the model is that intrinsic watershed factors (such as geology, climate, or valley morphology) interact with human actions (such as forest harvest, cattle grazing, or stream restoration) to affect processes that drive known ecological concerns (e.g., water temperature, large wood and pool frequency, etc.), and therefore fish survival via both density-dependent and density-independent processes.

*Component 4: Adaptive management framework*—CRITFC plays an important role in development and application of the adaptive management framework for the Grande Ronde subbasin. Our project is involved in collection of data, development of models, and hypothesis testing regarding the types of cumulative management activities likely to be most effective for restoring fish populations. Local agencies (e.g., CTUIR, ODFW, USFS, SWCD, USBR) play a larger role in implementing restoration projects and conducting site-scale action effectiveness monitoring of individual restoration projects. CRITFC communicates results of model projections to local managers who re-assess the efficacy of management actions. CRITFC is currently working towards a clarified vision of adaptive management with Grande Ronde Model Watershed and its cooperating agencies (White et al. 2021).

## **Study Area**

This study is occurring in the Grande Ronde River and its tributaries, which originates in the Blue Mountains of NE Oregon and flows 334 km to its confluence with Snake River near the town of Rogersburg, Washington (Figure 3). Focal study watersheds include the upper Grande Ronde River upstream of the town of La Grande, Catherine Creek, and to a lesser extent, the Minam River, which drain areas of approximately 1,896, 1,051, and 618 km<sup>2</sup>, respectively.

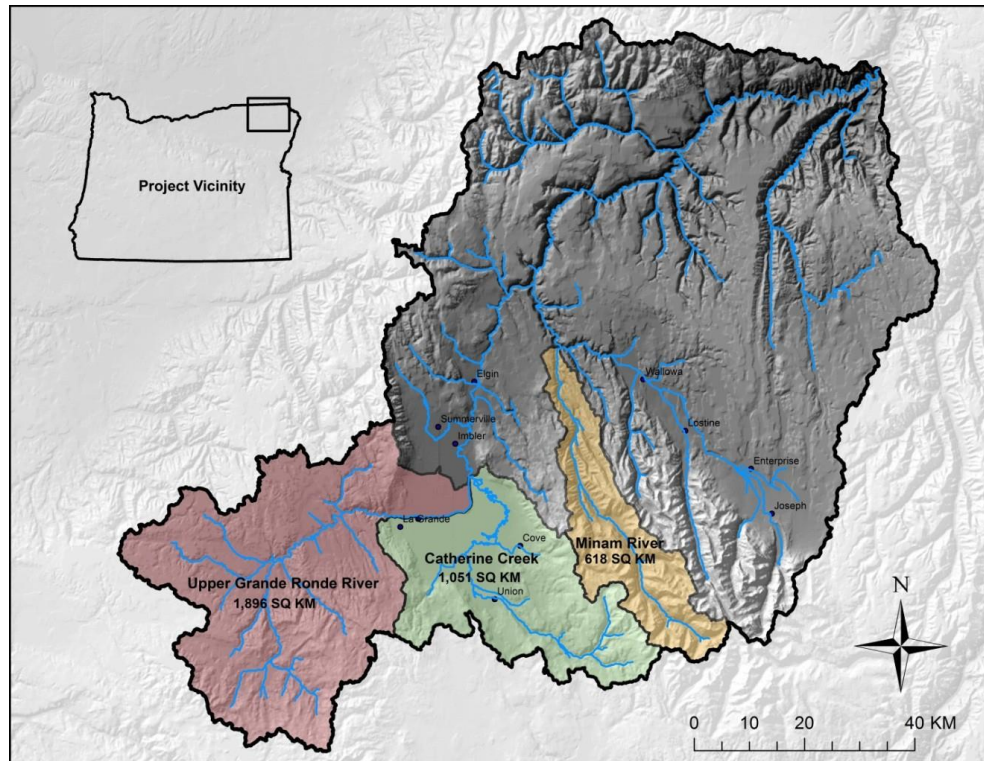


Figure 3. Study area in the Grande Ronde River basin, NE Oregon. Focal watersheds include the upper Grande Ronde River, Catherine Creek, and Minam River. The upper Grande Ronde and Catherine Creek are basins with significantly impacted habitat, currently undergoing restoration in various locations. The Minam River basin is the local reference area that has far less anthropogenic impact.

The topography of the upper portion of the subbasin (i.e., upstream of the Wallowa River confluence) is characterized by rugged mountains in the headwater areas and a broad, low gradient valley between the Blue and Wallowa Mountains. Peaks in the Wallowa Mountains reach a maximum elevation of 2,999 m and provide the source of many of the Grande Ronde's tributaries including Catherine Creek, the Minam River and the Wallowa River. The Blue Mountains reach elevations of 2,347 m and are the source of the Grande Ronde River, Wenaha River, and other tributaries. Due to the lower elevation of the Blue Mountains, snow melt generally occurs earlier in these tributaries, often resulting in very low flows during summer.

Surface geology of the Grande Ronde subbasin is dominated by rocks of the Columbia River Basalt group, with some older granitic intrusives and volcanics with associated sedimentary deposits present in the headwater areas of the upper Grande Ronde and Catherine Creek. The climate is characterized by cold, moist winters and warm, dry summers with mean daily air temperatures near La Grande averaging  $-0.42^{\circ}\text{C}$  in January and  $21^{\circ}\text{C}$  in July. Average annual precipitation ranges from 36 cm in the valleys to 152 cm in the mountains, with most of the precipitation in the mountains falling as winter snow.

The vegetation community at lower elevations is dominated by grasslands consisting of Idaho fescue/bluebunch wheatgrass (*Festuca idahoensis*-*Agropyron spicatum*) and bluebunch wheatgrass-Sandberg's bluegrass (*Agropyron spicatum*-*Poa sandbergii*) (Nowak 2004). As elevation increases, the grasslands transition to shrub/scrub plants, and eventually to coniferous forests in the mountains. Forest species consist of low elevation Ponderosa pine (*Pinus ponderosa*) and lodgepole pine (*Pinus contorta*) associations grading into Douglas-fir (*Pseudotsuga menziesii*), grand fir (*Abies grandis*), subalpine fir (*Abies lasiocarpa*), and mountain hemlock (*Tsuga mertensiana*) associations at higher elevations. Riparian vegetation is dominated by black cottonwood (*Populus trichocarpa*), willow (*Salix* spp.), black hawthorn (*Crataegus douglasii*), mountain alder (*Alnus incana*), and mountain maple (*Acer glabrum*).

Approximately 49% of the land in the Grande Ronde basin is publicly owned, of which about 97% is managed by the US Forest Service. The remaining public land is managed by the Bureau of Land Management and the States of Oregon and Washington. With the exceptions of the Eagle Cap and Wenaha-Tucannon Wilderness Areas, the National Forests are managed for multiple use including timber production, livestock grazing, and recreation. Private property comprises the remaining 51% of the land in the basin and is located primarily in lower elevation valleys and along rivers. A large proportion of the private property is used for agriculture including crop production, livestock grazing, and forestry. Only 0.1% of the land in the Grande Ronde Basin is currently owned by the tribes, although the tribes retain fishing and hunting access rights at all usual and accustomed locations as afforded under the treaties of 1855 and 1863.

Spring Chinook Salmon populations in these basins were listed as threatened under the Endangered Species Act in 1992. Population declines over the past century were due in part to overharvest, hydropower impacts, and degraded habitat conditions resulting from intensive anthropogenic disturbances including timber harvest, cattle grazing, levee and road construction, stream diversions for irrigation, and removal of beaver populations (*Castor canadensis*). Specifically, stream temperature, streamflow, fine sediment, habitat diversity, and quantity of key habitats such as large pools, have been identified as key ecological concerns for recovery of Chinook Salmon populations in these basins.

### **Special Note on Progress in 2020**

The unprecedented circumstances of 2020—most notably the COVID-19 pandemic—made conducting research and monitoring especially challenging. However, by shifting our priority from intensive fieldwork to the collection of remote sensing data and continued focus on data analyses and development of models, we were able to make significant progress towards overall project objectives. In 2020 we pivoted towards light fieldwork (e.g., maintenance of temperature logger network, assistance to ODFW fish sampling crews) and collection of light detection and ranging (LiDAR) data over extensive regions of the Grande Ronde and Wallowa River basins in collaboration with regional partners. This new focus towards remote sensing allowed us to collect

a rich data set that is being used to compare against past LiDAR data for assessment of decadal trends in riparian vegetation and for assessment of current status of fish-habitat conditions. Other notable progress in 2020 included completion of a new tributary habitat assessment protocol, analyses of datasets collected in the field in prior years (e.g., pre-spawn mortality, juvenile fish growth and phenology studies), and substantial progress on the life cycle model in collaboration with ODFW and NOAA.

## References

- Beechie, T., H. Imaki, J. Greene, A. Wade, H. Wu, G. Pess, P. Roni, J. Kimball, J. Stanford, P. Kiffney, and N. Mantua. 2013. Restoring salmon habitat for a changing climate. *River Research and Applications* 29:939–960.
- Naiman, R.J., J.R. Alldredge, D.A. Beauchamp, P.A. Bisson, J. Congleton, C.J. Henny, N. Huntly, R. Lamberson, C. Levings, E.N. Merrill, W.G. Pearcy, B.E. Rieman, G.T. Ruggerone, D. Scarnecchia, P.E. Smouse, and C.C. Wood. 2012. Developing a broader scientific foundation for river restoration: Columbia River food webs. *Proceedings of the National Academy of Sciences of the United States of America* 109(52): 21201–21207. doi:10.1073/pnas.1213408109. PMID:23197837.
- Kaylor, M.J., S.M. White, W.C. Saunders, and D.R. Warren (2019) Relating spatial patterns of stream metabolism to distributions of juvenile salmonids at the river network scale. *Ecosphere*, 10.6: e02781.
- Kaylor, M.J., S.M. White, E.R. Sedell, and D.R. Warren (2020a) Carcass additions increase juvenile salmonid growth, condition, and size in an interior Columbia River Basin tributary. *Canadian Journal of Fisheries and Aquatic Sciences*, 77(4):703-715.
- Kaylor, M.J., S.M. White, E.R. Sedell, A.M. Sanders, and D.R. Warren (2020b) Food webs respond to carcass additions along a temperature and fish assemblage gradient through direct and indirect pathways. *Ecosystems* 24: 168-184.
- Mantua, N., I. Tohver, and A. Hamlet. 2010. Climate change impacts on streamflow extremes and summertime stream temperature and their possible consequences for freshwater salmon habitat in Washington State. *Climatic Change* 102(1–2):187–223.
- White, S.M., S. Brandy, C. Justice, K.A. Morinaga, L. Naylor, J. Ruzycki, E.R. Sedell, J. Steele, A. Towne, J.G. Webster, and I. Wilson. 2021. Progress towards a comprehensive approach for habitat restoration in the Columbia Basin: Case study in the Grande Ronde River. *Fisheries*, fsh.10562. <https://doi.org/10.1002/fsh.10562>.



# Project Components

## 1.0 Habitat and Biotic Assessments

### *1.1 Refinement of a tributary habitat monitoring protocol*

**Note:** The protocol referenced in this section is available in Appendix A: “Tributary Habitat Assessment Protocol”.

#### **Introduction**

Since 2010 CRITFC has monitored fish habitat conditions in the upper Grande Ronde River, Catherine Creek, and Minam River. After initially drafting our own agency stream monitoring protocol, CRITFC supported the development and implementation of the Columbia Habitat Monitoring Program (CHaMP). Data collected from these programs provide the basis for describing status and trends of limiting habitat factors for Chinook Salmon in the study basins. In 2017, BPA commissioned a review of CHaMP which revealed several potential problems concerning both the collection of measurements and extrapolation of metrics to unsampled portions of the basin. In response to these concerns and feedback from the Independent Science Review Panel (ISRP), our project reassessed the components that would ensure the success and longevity of a new monitoring approach and allow for the continuation of status and trends analysis. We identified four major considerations when reconceptualizing a new monitoring strategy: 1) the methods used should be based on regionally accepted practices which are both repeatable and could reliably be used for comparison with a subset of previously derived metrics from other protocols, 2) it should incorporate measures of long-term impacts of land use and climate change, 3) it improves upon previous fish habitat survey methodologies by reducing the intensity of ground-based measurements and integrating unmanned aircraft systems (UAS), and 4) it promotes partnership and garners regional support as a means for funding and continued long-term monitoring.

Using these considerations as a guide, we developed the Tributary Habitat Assessment Protocol. This protocol includes a pared-down list of metrics identified as having minimal observer bias, clear linkage to common ecological concerns in Columbia basin tributaries (i.e., water temperature, channel and floodplain complexity, pool habitats, fine sediment, etc.; Table 1), and consistency (i.e., cross-walkability) with previously collected habitat monitoring data. This protocol was tested during the 2018 field season with the first phase of implementation planned to occur in 2021. The monitoring plans for this coming field season build upon preexisting partnerships and seek out new opportunities. The methods outlined in this protocol are based on widely accepted and previously implemented monitoring methods used throughout the Pacific Northwest (i.e., CHaMP, ODFW Aquatic Inventories Project (AqI)). Acknowledging previous criticisms, the monitoring approach outlined within the CRITFC Tributary Habitat Assessment

Protocol aims to cover more ground with less effort and cost, while obtaining high resolution aerial imagery using UAS that will provide a rich dataset with numerous current and future analytical opportunities. Our planned application of this monitoring protocol corresponds to biologically significant reaches (BSRs) in the project areas, with a specific focus on areas designated as high priority for habitat restoration (i.e., Tier 1 BSRs). However, the protocol is flexible enough to be tailored to the specific limiting factors or needs of a particular basin such as prioritization of stream segments with active or planned restoration.

## Habitat Survey Methods

While much is known about fish populations at microhabitat and basin scales, in this protocol we seek to address the gap in understanding at intermediate scales (e.g.,  $10^3 - 10^5$  m; Fausch et al. 2002). This protocol is designed to provide a more comprehensive and continuous riverscape perspective of the status and trends in fish habitat by ultimately merging datasets from multiple spatial scales. The major components of this protocol are split into ground and aerial-based methods. The ground-based methods are a fusion of two widely used and accepted protocols within the Columbia River Basin (CRB) including AqI (Moore et al 2019) and CHaMP (CHaMP 2016), while the aerial-based portion of the protocol utilizes drones. Drones have become ubiquitous in monitoring throughout a range of disciplines within the CRB. Drones are used in this protocol to collect imagery from multiple viewing angles (i.e., nadir and off-nadir), which together can be used to reconstruct continuous orthorectified mosaics (Figure 4) of the stream channel and immediate floodplain. To increase efficiency, improve reproducibility, and address the need for data collection at intermediate spatial scales, we reduced the frequency and total number of measurements collected within habitat units (i.e., channel units) by ground crews. We attempted to reduce the reliance on qualitative or visually estimated metrics to the degree possible with the intention of producing metrics that are robust enough to provide meaningful evaluations of habitat change over time.

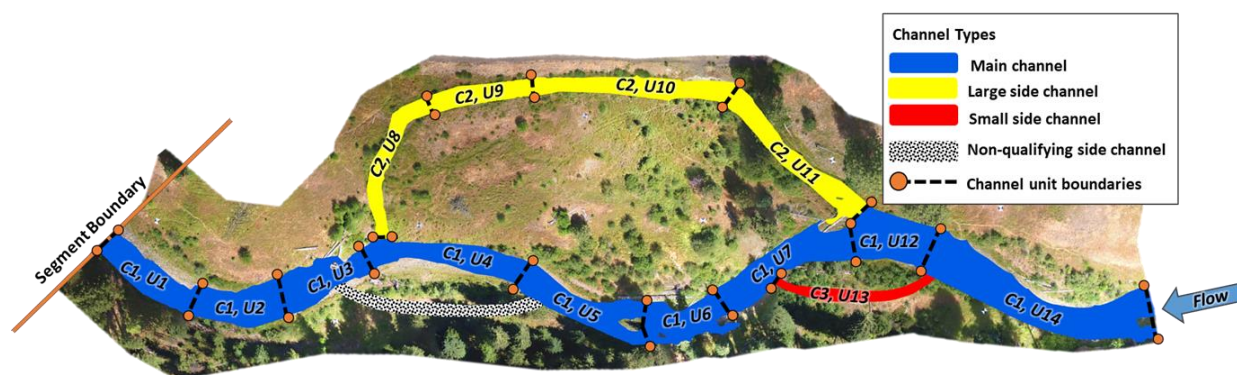


Figure 4. Example of an orthomosaic reconstructed from UAS imagery overlaid with segment and channel unit boundaries as outlined in the methods of the Tributary Habitat Assessment Protocol.

At a minimum, channel unit data will be summarized at the reach scale ( $\approx 20$  times bankfull width) for calculation of common habitat metrics (e.g., pool frequency, large wood frequency, side channel length; Table 1) and analysis of fish-habitat relationships. While the specific methods used to roll-up data to larger spatial scales are beyond the scope of this field protocol, we emphasize that aggregation methods should account for differences in natural channel morphology (i.e., slope, discharge, sediment supply, valley confinement; Montgomery and Buffington 1997; Beechie and Imaki 2014).

The approach outlined in this protocol is hierarchical, where the location of data collection will depend on the desired scale of inference. For example, if the goal is to quantify habitat conditions within a single stream segment or small watershed (1 – 50 km), then it is feasible to conduct a spatially continuous census of all available habitat during a single year. Organizations may also choose to collect census data covering different portions of a watershed over a number of years and then merge the data together. If the desired scale of inference is too extensive to census within a discreet time period (i.e., large watershed, Major Population Group (MPG), or Evolutionarily Significant Unit (ESU)), then a randomized sampling design is recommended in which a subsample of the total population is sampled to produce an estimate of average habitat conditions. One choice for this approach is the Generalized Random Tessellation Stratified (GRTS) design (Stevens and Olsen 2004), which provides a spatially balanced sample across a stream network and has been widely used for aquatic habitat monitoring in the Pacific Northwest (CHaMP 2016; Moore et al. 2019). Ideally, sample locations would be drawn from the Columbia River basin-wide master sample to facilitate integration of survey data across multiple monitoring programs (Larsen et al. 2008).

In addition to continuing the collection of physical stream habitat data, this protocol continues to document land use and climate impacts in the Grande Ronde through stream temperature monitoring. CRITFC made significant progress during 2020 to streamline temperature monitoring by compiling temperature records and metadata from basin partners. These data are now stored in a centralized data management system. We analyzed network coverage to reduce redundancies and set current and future priority monitoring locations. As part of an effort to prevent data loss and continue the efforts of previous monitoring programs, CRITFC also performed routine maintenance and data recovery of temperature loggers in the remote Minam River Wilderness area that were established initially for use during CHaMP. Beyond supporting the ongoing monitoring work outlined in this protocol, CRITFC's continued work investigating stream temperature as a limiting factor continues to support the needs of basin partners (i.e., Oregon Department of Environmental Quality (DEQ) Total Maximum Daily Load update; NorWeST water temperature model update) and larger riverscape studies and life cycle modelling.

## Partnering with local and regional entities

The success and continuation of any monitoring program is largely dependent on the strength of its partnerships. CRITFC's presence in the Grande Ronde basin over the last 10 years has fostered numerous partnerships that have resulted in organized planning, implementation, and cost-sharing related to monitoring and research efforts. Our ongoing partnership with PNAMP is of specific relevance to CRITFC and our monitoring efforts in the Grande Ronde which seek to increase the knowledge and application of using remote sensing in fish habitat and river health assessments. In late 2020, CRITFC and PNAMP staff worked together to recruit a diverse group of technical experts throughout the Pacific Northwest to serve as organizing committee members in a renewed PNAMP Remote Sensing Forum (RSF). The goals the forum are: 1) providing equitable opportunities for professional development or advancement of programmatic needs as they relate to remote sensing in the fields of fisheries and water resources in the Pacific Northwest, 2) increasing collaboration on the creation of regionally specific standardized methods for collecting and analyzing remotely sensed data, and 3) reducing barriers to entry/adoption of remote sensing practices by providing technical expertise and feedback in an online forum setting. In addition to this partnership with PNAMP, CRITFC continued to demonstrate the importance of building and maintaining strong partnerships in 2020 through: a) the adoption of our Tributary Habitat Assessment protocol by the Grande Ronde Model Watershed (GRMW) with partial funding from the US Forest Service, b) collaboration with GRMW and the Bonneville Power Administration for the acquisition of topobathymetric light detection and ranging data (LiDAR; see Appendix B of this report), and c) serving as project advisors and providing support to the Union Soil and Water Conservation District for upcoming Strategic Implementation Area monitoring.

Table 1. Metrics which can be generated from the Tributary Habitat Assessment Protocol.

Indicator type	Indicator	Metric	Description	Data source
<b>Habitat quality/diversity</b>	Floodplain/side channels	River complexity index	River complexity index (RCI) = $S \cdot (1+J)$ where S = stream sinuosity, J = # of side channel junctions (Brown 2002)	Field/LiDAR/UAS
	Floodplain/side channels	Side channel ratio	Length of side channels divided by length of main channel during base flow (Beechie et al. 2017)	Field/LiDAR/UAS
	Riparian condition	Riparian tree cover	Average percent tree canopy cover in the	UAS/LiDAR

Indicator type	Indicator	Metric	Description	Data source
			riparian zone (50 m stream buffer)	
	Riparian condition	Riparian tree height	Average tree height (m) in the riparian zone (50 m stream buffer)	UAS/LiDAR
	Riparian condition	Riparian vegetation departure	Average percentage departure in current vegetation from simulated historical vegetation reference conditions in the riparian zone (100 m buffer; LANDFIRE 2016)	Satellite/ Modeled
	River channel (cover)	Large wood area percentage	Percentage of stream surface area covered by large wood during base flow	UAS/LiDAR
	River channel (cover)	Large wood frequency bankfull	Number of large wood pieces within the bankfull channel per 100 m stream length (Moore et al. 2017)	Field
	River channel (cover)	Large wood frequency wetted	Number of large wood pieces within the wetted channel during base flow per 100 m stream length (Moore et al. 2017)	Field
	River channel (cover)	Overhanging vegetation	Percentage of stream surface area covered by vegetation during base flow	UAS/LiDAR
	River channel (cover)	Undercut bank percentage	Percentage of the total bank length that is undercut	Field/UAS
	River channel (pools)	Residual pool depth	Mean residual pool depth (max depth - thalweg exit depth in meters; Mossop and Bradford 2006)	Field/LiDAR

<b>Indicator type</b>	<b>Indicator</b>	<b>Metric</b>	<b>Description</b>	<b>Data source</b>
	River channel (pools)	Large pool frequency	Number of large pools (> 20 m <sup>2</sup> area and > 0.80 m max depth) per km stream length (McIntosh et al. 2000)	Field/UAS/LiDAR
	River channel (pools)	Medium pool frequency	Number of medium-sized pools (> 20 m <sup>2</sup> area and > 0.50 m max depth) per km stream length	Field/UAS/LiDAR
	River channel (substrate)	Median sediment particle size	Median sediment particle size on the streambed surface in riffles (Wolman 1954)	Field
	Water quality	Coldwater refuge density	Number of cold-water refuges per km stream length (Dugdale et al. 2015)	FLIR
	Water quality	Maximum weekly maximum temperature	Maximum 7-day running average of daily maximum temperature (EPA 2003)	Field/Modeled
	Water quality	Observed/Expected benthic macroinvertebrates	Ratio of observed to expected (O/E) benthic macroinvertebrate taxa as predicted by the River Invertebrate Prediction and Classification System (RIVPACS, Hawkins et al. 2000)	Field
<b>Habitat quantity</b>	Floodplain/side channels	Off-channel habitat bankfull	Surface area (m <sup>2</sup> ) of connected off-channel habitat during bankfull flow (Konrad et al. 2015)	LiDAR

Indicator type	Indicator	Metric	Description	Data source
	Floodplain/ side channels	Off-channel habitat base flow	Surface area (m <sup>2</sup> ) of connected off- channel habitat during base flow	LiDAR/UAS
	Floodplain/ side channels	Side channel length	Length (m) of side channels during low flow	Field/UAS
	Flow	Center of flow mass	Flow-weighted mean day of the water year (i.e., center of flow timing; USFS 2015)	Field/ Modeled
	Flow	Mean annual flow	Mean daily flow (m <sup>3</sup> ·s <sup>-1</sup> ) within a water year (Oct 1 - Sep 30; USFS 2015)	Field/ Modeled
	Flow	Mean summer flow	Mean daily flow (m <sup>3</sup> ·s <sup>-1</sup> ) during summer (Jun 1 - Sep 30; USFS 2015)	Field/ Modeled
	River channel (fast water)	Fast water area	Surface area (m <sup>2</sup> ) of fast water habitat (e.g., fast turbulent, fast non-turbulent, fast small side channels) during base flow	Field/UAS
	River channel (total length)	Length accessible anadromous fish habitat	Length (km) of accessible main channel habitat that is currently used by anadromous fish for spawning, rearing, or migration	Field/ Modeled
	River channel (pools)	Slow water area	Surface area (m <sup>2</sup> ) of slow water habitat (e.g., pools, off- channel units, slow small side channels) during base flow	Field/UAS



## References

- Beechie, T., and H. Imaki. 2014. Predicting natural channel patterns based on landscape and geomorphic controls in the Columbia River basin, USA: Predicting Channel Patterns in the Columbia Basin. *Water Resources Research* 50(1):39–57.
- Beechie, T. J., O. Stefankiv, B. Timpane-Padgham, J. E. Hall, G. R. Pess, M. Rowse, M. Liermann, K. Fresh, and M. J. Ford. 2017. Monitoring Salmon Habitat Status and Trends in Puget Sound: Development of Sample Designs, Monitoring Metrics, and Sampling Protocols for Large River, Floodplain, Delta, and Nearshore Environments. U.S. Department of Commerce, NOAA Technical Memorandum NMFSNWFSC-137. <https://doi.org/10.7289/V5/TM-NWFSC-137>
- Brown, A. G. 2002. Learning from the past: palaeohydrology and palaeoecology. *Freshwater Biology* 47(4):817–829.
- CHaMP (Columbia Habitat Monitoring Program). 2016. Scientific protocol for salmonid habitat surveys within the Columbia Habitat Monitoring Program.
- Dugdale, S. J., N. E. Bergeron, and A. St-Hilaire. 2015. Spatial distribution of thermal refuges analysed in relation to riverscape hydromorphology using airborne thermal infrared imagery. *Remote Sensing of Environment* 160:43–55.
- Fausch, K., Torgersen, C., Baxter, C., Li, H., 2009. Landscapes to Riverscapes: Bridging the Gap Between Research and Conservation of Stream Fishes. *BioScience* 52, 483–498.
- Hawkins, C. P., R. H. Norris, J. N. Hogue, and J. W. Feminella. 2000. Development and evaluation of predictive models for measuring the biological integrity of streams. *Ecological Applications* 10(5):1456–1477.
- Konrad, C. P. 2015. Geospatial assessment of ecological functions and flood-related risks on floodplains along major rivers in the Puget Sound Basin, Washington. Page 28. U.S. Geological Survey, Scientific Investigations Report 2015-5033.
- LANDFIRE. 2016. LANDFIRE Remap 2016 Vegetation Departure (VDep) CONUS dataset. Earth Resources Observation and Science Center (EROS), U.S. Geological Survey <https://www.landfire.gov/vdep.php>.
- McIntosh, B. A., J. R. Sedell, R. F. Thurow, S. E. Clarke, and G. L. Chandler. 2000. Historical Changes in Pool Habitats in the Columbia River Basin. *Ecological Applications* 10(5):1478.
- Moore, K., K. Jones, J. Dambacher, and C. Stein. 2019. Aquatic Inventories Project: methods for stream habitat surveys. Oregon Department of Fish and Wildlife, Version 29.1, Corvallis, OR.

- Montgomery, D. R., and J. M. Buffington. 1997. Channel-reach morphology in mountain drainage basins. *GSA Bulletin* 109(5):596–611.
- Mossop, B., and M. J. Bradford. 2006. Using thalweg profiling to assess and monitor juvenile salmon (*Oncorhynchus* spp.) habitat in small streams. *Canadian Journal of Fisheries and Aquatic Sciences* 63(7):1515–1525.
- Stevens, D. L., and A. R. Olsen. 2004. Spatially balanced sampling of natural resources. *American Statistical Association* 99(465):262–278.
- U.S. Environmental Protection Agency (EPA). 2003. EPA Region 10 Guidance for Pacific Northwest State and Tribal Temperature Water Quality Standards. EPA 910-B-03-002. Region 10 Office of Water, Seattle, WA.
- United States Forest Service (USFS). 2015. Western US stream flow metric dataset: modeled flow metrics for stream segments in the western United States under historical conditions and projected climate change scenarios. Page 7.
- Wolman, M. G. 1954. A method of sampling coarse river-bed material. *Transaction of the American Geophysical Union* 35:951–956.

## 1.2 LiDAR data collection

**Note:** A completed report of the work discussed in this section is available in Appendix B: "Grande Ronde Basin, Oregon, Topobathymetric Lidar Technical Data Report."

### Introduction

In summer 2020, CRITFC, Grande Ronde Model Watershed, and Bonneville Power Administration collaborated on the acquisition of topobathymetric light detection and ranging (LiDAR) to assess river conditions across 76,188 acres of the Grande Ronde River and Wallowa River watersheds, including not only mainstem riparian conditions and floodplains but also larger tributaries currently or historically occupied by Chinook Salmon and steelhead/rainbow trout (Figure 5).

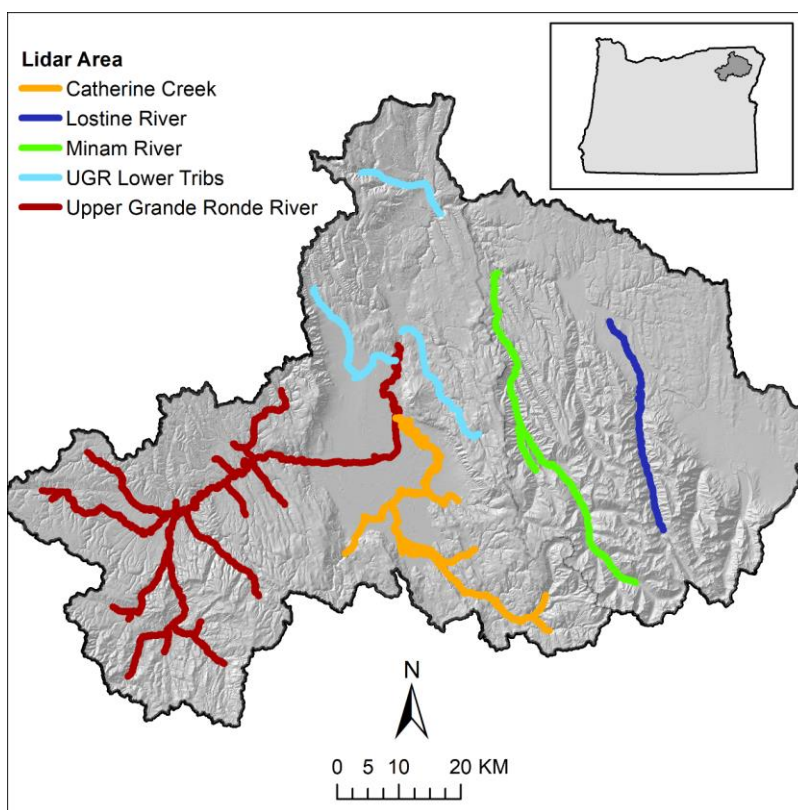


Figure 5. Major areas of interest (AOIs) for LiDAR acquisition in 2020.

Purposes of acquiring the LiDAR data included: 1) revisiting areas flown for terrestrial LiDAR in 2009-2011 for analysis of decadal changes to vegetation density/height and altered floodplain characteristics and 2) acquiring topobathymetric spatial data layers to calculate metrics of instream and near-stream fish habitat conditions. These sub-basins are central locations for life cycle monitoring and analysis for Chinook Salmon which is one of the key objectives of CRITFC's Monitoring Recovery Trends project.

This summary documents the data collection efforts in 2020 and preliminary results of QA/QC and data processing; detailed analyses of fish habitat metrics are in progress.

## Methods

Topobathymetric (“green”) LiDAR was collected by a private contractor, Quantum Spatial, Inc. (previously Watershed Sciences), the same company that collected LiDAR in 2009. The 2009 data collection project employed terrestrial (“red”) LiDAR that evaluated the height and density of riparian vegetation and width of the river channel, coupled with remotely sensed water temperature data (thermal infrared, or TIR), to create a water temperature model (i.e., Heat Source). This previous LiDAR dataset can be directly compared with the new data to assess riparian shrub and tree growth that has occurred over the last decade. This rare opportunity to evaluate vegetation change over a long time period and across a large spatial extent is expected to reveal insights into what kinds of restoration efforts were most effective in promoting riparian health.

In 2020, topobathymetric LiDAR was collected in multiple watersheds (Table 2) with buffer widths targeted for a minimum of 150 m on each stream bank, with additional buffer where the approximate 100-year floodplain (calculated independently by CRITFC) extended beyond 150 m. CRITFC provided QSI with a GIS shapefile with the precise area of interest (AOI) footprint. An additional buffer width was applied by QSI to ensure complete coverage of the AOI. Data collection occurred in low-flow, clear water conditions after leaf-out of terrestrial vegetation and roughly corresponding to timing of previous (2009) streamflow conditions, yet prior to significant growth of aquatic vegetation.

Table 2. River kilometers of major areas of interest for topobathymetric LiDAR acquisition in 2020.

LiDAR Area	Length (km)
Catherine Creek	141.5
Lostine River	43.4
Minam River	79.3
UGR Lower Tribs	86.7
Upper Grande Ronde River	300.0
Grand Total	650.9

Topobathymetric LiDAR was collected with appropriate sensors and in a manner that allowed for high-resolution data in typically clear, shallow streams often not exceeding 2 m in depth to achieve an average pulse density  $\geq 6$  pulses/m<sup>2</sup> (Table 3). Data products allow for discrimination of water, streambed and near-shore surfaces in shallow streams. Resulting data products were geo-spatially corrected, partly with the aid of ground survey points, to meet both project objectives (analysis of change from historical conditions and calculation of spatially explicit fish habitat conditions).

Table 3. LiDAR specifications and survey settings.

<b>Acquisition Dates</b>	8/17/2020 - 9/27/2020	8/17/2020 - 9/27/2020
<b>Aircraft Used</b>	Cessna Caravan	Cessna Caravan
<b>Sensor</b>	Riegl	Riegl
<b>Laser</b>	VQ-880-GII	VQ-880-GII-IR
<b>Maximum Returns</b>	15	15
<b>Resolution/Density</b>	Average 6 pulses/m <sup>2</sup>	Average 6 pulses/m <sup>2</sup>
<b>Nominal Pulse Spacing</b>	0.41 m	0.41 m
<b>Survey Altitude (AGL)</b>	400 m	400 m
<b>Survey speed</b>	145 knots	145 knots
<b>Field of View</b>	40°	42°
<b>Mirror Scan Rate</b>	80 lines per second	Uniform Point Spacing
<b>Target Pulse Rate</b>	200 kHz	150 kHz
<b>Pulse Length</b>	1.5 ns	3 ns
<b>Laser Pulse Footprint Diameter</b>	28 cm	8 cm
<b>Central Wavelength</b>	532 nm	1064 nm
<b>Pulse Mode</b>	Multiple Times Around (MTA)	Multiple Times Around (MTA)
<b>Beam Divergence</b>	0.7 mrad	0.2 mrad
<b>Swath Width</b>	1800 m	1800 m
<b>Swath Overlap</b>	55%	55 %
<b>Intensity</b>	16-bit	16-bit
<b>Accuracy</b>	RMSE <sub>z</sub> ≤ 15 cm	RMSE <sub>z</sub> ≤ 15 cm

QSI described LiDAR data processing steps undertaken to achieve quality deliverables, including but not limited to any corrections, calibrations, and accuracy assessments (e.g., RMSE of bathymetric surface accuracies). Final deliverables were to include the point cloud; several raster layers including topobathymetric bare earth DEM and highest hit DSM, water depth and surface rasters; and several vector layers including water edge breaklines, bathymetric coverage polygons, survey boundaries, etc.

Upon completion of data acquisition, QSI initiated a suite of automated and manual techniques to process the data into the requested deliverables. Processing tasks included GPS control computations, smoothed best estimate trajectory (SBET) calculations, kinematic corrections, calculation of laser point position, sensor and data calibration for optimal relative and absolute accuracy, and LiDAR point classification (Table 4Figure 6).

Table 4. ASPRS LAS classification standards applied to the Grande Ronde Basin dataset.

Classification Number	Classification Name	Classification Description
1	Default/Unclassified	Laser returns that are not included in the ground class, composed of vegetation and anthropogenic features
2	Ground	Laser returns that are determined to be ground using automated and manual cleaning algorithms
9	Water	NIR laser returns that are determined to be water using automated and manual cleaning algorithms
40	Bathymetric Bottom	Refracted Riegl sensor returns that fall within the water's edge breakline which characterize the submerged topography.
41	Water Surface	Green laser returns that are determined to be water surface points using automated and manual cleaning algorithms.
45	Water Column	Refracted Riegl sensor returns that are determined to be water using automated and manual cleaning algorithms.

Once bathymetric points were differentiated, they were spatially corrected for refraction through the water column based on the angle of incidence of the laser. The resulting point cloud data was classified using both manual and automated techniques. Processing methodologies were tailored for the landscape.

## Results

A detailed report of the 2020 LiDAR data collection effort can be found in Appendix B, with the key results summarized here. Average rates of pulse returns exceeded the target of  $\geq 6$  pulses/m<sup>2</sup> with first returns achieving a density of 31.28 points/m<sup>2</sup>, ground and bathymetric bottom classified returns achieving a density of 10.27 points/m<sup>2</sup>, and bathymetric bottom classified returns achieving a density of 7.00 points/m<sup>2</sup>.

The accuracy of the LiDAR data collection can be described in terms of absolute accuracy (the consistency of the data with external data sources) and relative accuracy (the consistency of the dataset with itself). Absolute accuracy was assessed using non-vegetated vertical accuracy (NVA) reporting designed to meet guidelines presented in the FGDC (2014) National Standard for Spatial Data Accuracy (Table 5). Horizontal accuracy was assessed at 0.03 m (RMSE). Bathymetric vertical accuracy and relative horizontal accuracy are additionally reported in Appendix B.

Table 5. Absolute vertical accuracy results.

	NVA, as compared to Classified LAS	NVA, as compared to Bare Earth DEM	Ground Control Points
<b>Sample</b>	116 points	116 points	2,435 points
<b>95% Confidence (1.96*RMSE)</b>	0.048 m	0.055 m	0.050 m
<b>Average</b>	0.001 m	0.003 m	0.000 m
<b>Median</b>	0.002 m	0.004 m	0.000 m
<b>RMSE</b>	0.025 m	0.028 m	0.025 m
<b>Standard Deviation (1<math>\sigma</math>)</b>	0.025 m	0.028 m	0.025 m

Final data products delivered by QSI to CRITFC are outlined in Table 6. These include points (classified returns; Figure 6), rasters (digital elevation models, water surface models, bathymetric depth model, GeoTiffs, etc.), and vector shapefiles (AOI, LiDAR tile index, water edge breaklines, etc.).

Table 6. LiDAR products delivered to CRITFC for the Grande Ronde basin.

<b>Points</b>	LAS v 1.4 <ul style="list-style-type: none"> <li>All Classified Returns</li> </ul>
<b>Rasters</b>	1.0 Meter ESRI Grids <ul style="list-style-type: none"> <li>Unclipped Topobathymetric Bare Earth Digital Elevation Model (DEM)</li> <li>Clipped Topobathymetric Bare Earth Digital Elevation Model (DEM)</li> <li>Highest Hit Digital Surface Model (DSM)</li> <li>Water Surface Model (WSM)</li> <li>Bathymetric Depth Model</li> </ul> 0.5 Meter GeoTiffs <ul style="list-style-type: none"> <li>Green Sensor Intensity Images</li> <li>NIR Sensor Intensity Images</li> </ul>
<b>Vectors</b>	Shapefiles (*.shp) <ul style="list-style-type: none"> <li>Area of Interest</li> <li>Lidar Tile Index</li> <li>Bathymetric Coverage Shape</li> <li>Water's Edge Breaklines</li> <li>Ground Survey Shapes</li> </ul>

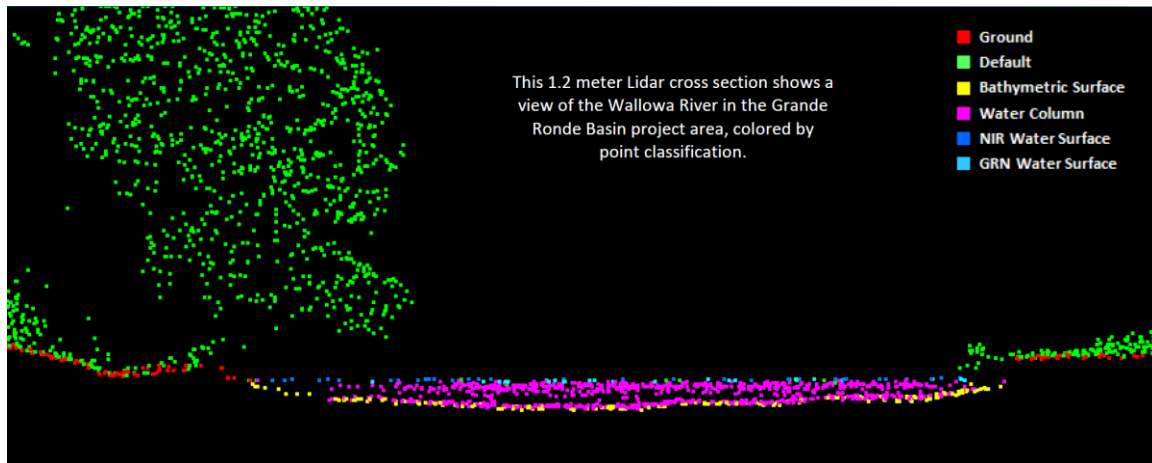


Figure 6. Example LiDAR cross section with classified points delineating ground, water surface, bathymetric surface, and vegetation.

While 2020 was focused on collection and initial processing of LiDAR data, we envision our next steps for using the LiDAR-derived products to include: (1) developing procedures and workflow for using LiDAR products to describe spatially-continuous fish habitat metrics, including linking LiDAR products to ground-measured habitat data; (2) developing refined methods for classifying LiDAR points as large wood apart from ground points; and (3) evaluating changes in riparian vegetation height and density from 2009 to 2020 using LiDAR collected in both time periods.

## References

- FGDC (Federal Geographic Data Committee). 2014. ASPRS Positional Accuracy Standards for Digital Geospatial Data, EDITION 1, Version 1.0. [https://www.asprs.org/a/society/committees/standards/Positional\\_Accuracy\\_Standards.pdf](https://www.asprs.org/a/society/committees/standards/Positional_Accuracy_Standards.pdf).
- QSI (Quantum Spatial, Inc.). 2021. Grande Ronde Basin, Oregon, Topobathymetric Lidar Technical Data Report. Prepared for the Columbia River Inter-Tribal Fish Commission. NV5 Geospatial, Corvallis, OR. 36 pgs.



### *1.3 Unmanned Aircraft Systems (UAS) for fish habitat assessments*

#### **Introduction**

Implementing regional habitat monitoring to assess the status and trends of tributary habitat for anadromous species has proven to be methodologically challenging. More specifically, the accuracy and resolution of data needed to answer broad questions of status and trends in salmon-bearing tributary habitats during any one life stage necessitates data collection at small spatial scales (e.g., meso-habitat; pool, riffle, etc.), where the intensity of sampling restricts large spatial coverage. Physical habitat surveys have historically been conducted by ground based crews, where depending on the spatial extent and project objectives, may range from less technical “stick and tape” based methods (e.g., the use of tape measures, depth rods; e.g., Aquatic Inventories Project) to those utilizing more technical high precision surveying equipment such as a total station or real time kinetic (RTK) GPS (e.g., Columbia Habitat Monitoring Program). In comparison to physical “stick and tape” measurements, technological improvements (e.g., total station, RTK) have increased survey accuracy and expanded the range of data applications (e.g., hydraulic models, DEM of difference); however, approaches remain labor intensive and expensive, which limits spatial and temporal replication. Thus, the development of new approaches and technologies to increase spatial and temporal replication, while maintaining a high degree of accuracy, are needed to better assess stream habitat conditions.

Aerial-based remote sensing approaches offer one possible solution for quantifying habitat at resolutions useful for exploring fish-habitat linkages (i.e., riverscape concept; Fausch et al., 2002) and over continuous spatial scales (Tamminga et al. 2015). Common aerial remote sensing applications range from light detection and ranging (LiDAR; terrestrial and topobathymetric), terrestrial laser scanning, and aerial imaging. Each of these applications have been well-studied and applied to riverine environments. Frequently, attempts to characterize river bathymetry are conducted using laser scanning (topobathymetric green LiDAR), spectral, and photogrammetric based approaches. However, these approaches require considerable financial investment and expertise for data processing. Structure-from-Motion (SfM) represents a more affordable option for characterizing habitat at spatial scales of less than 10 km (typically less than 2 km). Replacing traditional photogrammetry, SfM, takes advantage of known geometry and camera positions to reconstruct 2-dimensional pictures into a 3-dimensional reconstruction of the scene (Woodget et al. 2017). The application of unmanned aircraft systems (UAS or drones) has become increasingly common in the field of hydrology and fluvial geomorphology, facilitating easier acquisition of images over larger spatial extents. However, the combination of SfM photogrammetry and drones is a relatively new application (e.g., within the last decade) to the field of fluvial remote sensing, and further refinement of methodology and approaches are needed to improve and quantify accuracy and efficiency.

The most common application of drones in monitoring to date is the collection of true color imagery. Automated flight plans, increased safety features, and post-processing software allow restoration practitioners, videographers, and biologists to collect imagery, derive meaningful fish habitat data through image post-processing, and relay their findings on a level easily understood by the general public and policy makers. While drones can be additionally equipped with advanced sensors (e.g., multispectral, LiDAR, etc.) to allow for more quantitative approaches of assessing habitat, these approaches increase financial investment and require additional expertise, limiting use to those with considerable financial resources and expertise. Of specific interest to fish habitat surveys, drones are a relatively inexpensive technology that can reduce the time and effort spent collecting ground-based data, while yielding imagery that is rich enough to allow further data processing and discovery as new information in this field continues to grow. Furthermore, operating a drone and collecting imagery is a relatively unbiased method of collecting data that is not prone to the same subjectivity and transcription errors of ground-based measures.

There exists a wide range of applications for drones in fisheries related to topography, habitat assessments, and even population surveys (Tyler et al., 2017). However, to date studies examining the accuracy and precision of UAS derived data products have been limited and have focused on small spatial extents (i.e., single reaches) or ideal conditions (e.g., non-vegetated riparian areas) not representative of the variety of habitats utilized by fish (Dietrich 2017, Tamminga 2015). We collected stream habitat and topographic data using both ground- and drone-based approaches across 13 stream reaches representing gradients in physical habitat conditions and vegetative cover. This design allowed us to examine the agreement of these approaches when assessing common physical stream metrics relevant to fish habitat quality and quantity. This study addresses this current knowledge gap in the literature regarding the application of UAS for stream habitat surveys across a range of natural environmental conditions.

## **Methods**

### *Study Area*

This study was conducted within the upper portions of the Grande Ronde River and Catherine Creek watersheds in northeastern Oregon (Figure 7). These watersheds drain areas of 1896 and 1051 km<sup>2</sup>, respectively, before flowing northward to the confluence with the Snake River. Flows in the region are primarily driven by snowmelt from the Elkhorn and Wallowa Mountains, where a majority of annual precipitation is stored as snowpack during the winter months. The summer is characterized as hot and dry where base and low-flow conditions occur by late. Much of the upper Grande Ronde River is public land, characterized by broad, low-gradient meadows and steep constrained conifer-dominated reaches, while the lower elevations of both the Grande Ronde River and Catherine Creek are privately owned, low gradient, unconstrained valleys composed of mixed forest stands (Wells et al., 2015; White et al., 2017). Historic land use practices dating back to the early 19th century (e.g., splash damming, mining, road building) through today (e.g., agriculture

and cattle grazing) have had notable negative effects on the density and diversity of riparian vegetation, channel morphology, and basin-wide returns of spring Chinook Salmon (*Oncorhynchus tshawytscha*; Kelly and White, 2016; Wells et al., 2015; Phelps, 2011; Wissmar et al., 1994). Present day physical conditions throughout these watersheds are primarily low gradient riffle-run habitat with cobble-gravel streambeds and low turbidity, posing ideal conditions for light attenuation through the water column to the benthos.

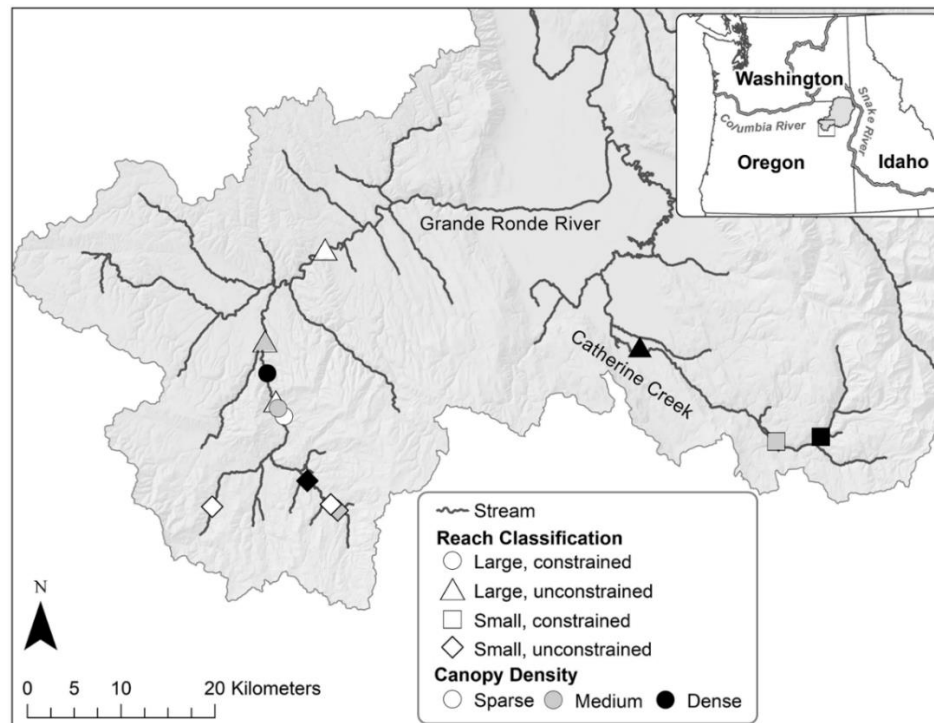


Figure 7. Map of sampled reaches for UAS mapping and topographic surveys of instream fish habitat in Catherine Creek and the upper Grande Ronde River. Aerial and ground-based habitat surveys were conducted at 13 sites representing a range of canopy densities (color) and geomorphic conditions (shapes).

### Site Selection

Thirteen study reaches were selected within the study area from locations associated with the Columbia Habitat Monitoring Program (CHaMP 2016), a protocol that used a spatially-balanced probabilistic survey design for evaluating spatial and temporal trends in fish habitat conditions in tributaries of the Columbia River basin. To evaluate how a UAS would perform in a variety of settings, we selected sites that represented a broad diversity of geomorphic and riparian conditions encountered by salmonids in the study area (Table 7). Sampling locations were chosen based on four criteria: 1) watershed size (i.e., small or large), 2) the combination of river confinement and gradient (i.e., constrained or unconstrained), 3) riparian canopy density (i.e., sparse, medium, or dense) and 4) primary occurrence on public land [e.g., US Forest Service land (USFS)]. Selection criteria (1) and (2) are based on the stream classification methodology developed by White et al.

(2011). Reach size was categorized as “small” or “large” based on a multivariate analysis of watershed characteristics (watershed area, elevation, stream order, and accumulated mean precipitation). Reaches were designated as “constrained” or “unconstrained” based on potential for lateral channel migration, with unconstrained reaches defined as those with  $\leq 10\%$  of the stream channel abutting bedrock or terrace features (Brierley and Fryirs, 2005) as determined from aerial photographs and 10-m digital elevation models. Density of the canopy layer (vegetation taller than 1.5 m), was evaluated using LiDAR collected in 2009 and classified by height strata by Wells et al. (2015). To account for the expected natural differences in canopy cover in unconstrained versus constrained reaches, thresholds for canopy density were classified using quartile values of vegetation density specific to stream channel constraint (Table 8). Access to public land was desirable during this initial study because of uncertainty regarding public perceptions of UASs, ease of land access (acquiring permits), and the benefits of increased safety and security measures of established USFS reporting and communication procedures.

Table 7. Sampling locations (n=13) and associated characteristics within the upper Grande Ronde and Catherine Creek Watersheds in northeastern Oregon.

Reach	Watershed Name	Size	River Confinement	Riparian Density	Canopy	Elevation (m)	Gradient (%)
CBW05583-138666	CC	Small	Constrained	Dense		1178	2.66
CBW05583-456106	CC	Small	Constrained	Medium		1044	1.11
CBW05583-099818	UGR	Small	Unconstrained	Medium		1359	0.58
CBW05583-280042	UGR	Small	Unconstrained	Sparse		1372	0.62
CBW05583-335162	UGR	Small	Unconstrained	Sparse		1334	0.86
CBW05583-468458	UGR	Small	Unconstrained	Dense		1306	2.49
CBW05583-321338	UGR	Large	Constrained	Sparse		1169	2.82
CBW05583-370490	UGR	Large	Constrained	Medium		1189	0.85
CBW05583-486202	UGR	Large	Constrained	Dense		1303	1.71
CBW05583-031546	UGR	Large	Unconstrained	Medium		1077	0.74
CBW05583-071770	UGR	Large	Unconstrained	Sparse		942	0.44
CBW05583-235322	UGR	Large	Unconstrained	Sparse		1154	0.92
CBW05583-430250	CC	Large	Unconstrained	Dense		847	0.69

Table 8. Thresholds of canopy density by stream channel constraint type.

	Canopy density values (%)		
Reach type	Sparse*	Medium <sup>†</sup>	Dense <sup>+</sup>
Constrained	15.8 – 30.4	35.9 – 42.8	44.9 – 53.1
Unconstrained	9.6 – 22.4	25.7 – 38.5	45.8 – 65.7
Quantile range:	* 5 <sup>th</sup> -25 <sup>th</sup>	<sup>†</sup> 35 <sup>th</sup> -65 <sup>th</sup>	+ 75 <sup>th</sup> -95 <sup>th</sup>

### *Ground surveys*

During the summer of 2018, field surveys were conducted to characterize the quantity and quality of available fish habitat at base and low-flow conditions. These surveys followed established, reach-based protocols used in the Pacific Northwest (e.g., CHaMP, 2016) to ensure consistency with other previously implemented regional approaches. In-stream physical habitat attributes were collected at the channel unit scale for each of the sampling locations using a two-tiered hierarchical classification scheme modified from Hawkins et al. (1993). Each channel unit was georeferenced and additional habitat attributes were collected based on classification type. Real time kinematic (RTK) GPS or total station were used to characterize the topography of the active channel and floodplain and to establish common ground control for use in aerial surveys.

### *Aerial surveys*

Imagery was captured for each site using a 15 mm Zenmuse X5 visible spectrum camera (equipped with a circular polarizing filter) mounted on a DJI Matrice 600 Pro (commercial-grade hexarotor UAS). Prior to each UAS flight mission, 1.5 x 1.5 m iron cross targets (Figure 8) were laid out over 10 ground control points (GCPs) established during the ground-based portion of the survey. Flight missions were planned with DJI Ground Station Pro at altitudes of 80-or-120 m resulting in average ground sampling distances (GSD) of 4.9 cm/pixel. Flights were limited between 10:00 and 14:00 to maximize solar noon lighting and reduce shadows from riparian vegetation. Resulting flight lines occurred at nadir (90 degrees) and oblique ( $\leq 26.5$  degrees) camera angles with an 80% forward and 70% side overlap and an average speed  $\leq 6$  m/s. To ensure high image quality and reduce potential image blur, imagery was collected while the UAS was hovering (i.e., stop-and-go shooting) and camera settings were generally left at defaults. A summary of the major flight parameters and field conditions at the time of survey are outlined in Table 9.

Table 9. Field conditions and flight parameters for aerial surveys.

Reach	Aerial Survey Date	Altitude (m AGL)	Area (HA)	Max depth (m)	Dominant substrate	Weather
CBW05583-031546	8/29/2018	120	5.13	1.08	Gravel	Sunny, clear
CBW05583-071770	9/24/2018	80	25.10	0.65	Cobble	Sunny, clear
CBW05583-099818	9/19/2018	80	0.92	0.75	Gravel	Sunny, clear
CBW05583-138666	9/7/2018	120	1.66	0.82	Cobble	Sunny, clear
CBW05583-235322	8/28/2018	120	2.76	0.70	Cobble	Sunny, clear
CBW05583-280042	9/21/2018	80	2.35	0.61	Gravel	Sunny, clear
CBW05583-321338	8/29/2018	120	2.39	1.94	Cobble	Sunny, hazy <sup>+</sup>
CBW05583-335162	9/11/2018	80	3.59	0.62	Gravel	Overcast
CBW05583-370490	8/25/2018	120	3.03	0.63	Cobble	Sunny, hazy <sup>+</sup>
CBW05583-430250	9/9/2018	80	2.18	1.51	Gravel	Sunny, clear
CBW05583-456106	9/6/2018	120	3.00	0.88	Cobble	Sunny, clear
CBW05583-468458	10/5/2018	80	1.84	0.78	Gravel	Overcast
CBW05583-486202	9/25/2018	120	2.76	0.67	Cobble	Sunny, clear

+ Smoke was present from regional wildfires at the time of the survey resulting in haze and reduced visibility.

### *Data post-processing*

The resulting photosets from each sampling location were processed in three stages as outlined in Figure 8: 1) image pre-processing in Agisoft Metashape, 2) post-processing in ArcMap and CloudCompare, and 3) data product corrections and error assessment in Python. Agisoft Metashape 1.4 was used to process imagery using a modified version of the USGS UAS Data Post-Processing structure-from-motion (SfM) workflow (Section 1 in USGS 2017). Images were imported with coordinates and checked for quality before adding GCP coordinate markers. After scale invariant feature transformation (SIFT) algorithms were run to identify common features and keypoints from overlapping images and coordinate markers were manually adjusted over each GCP center point in corresponding images. Imagery was then processed through SfM algorithms to perform bundle adjustments and image georeferencing. From the georectified images, a dense point cloud was built using quality and depth filtering parameters set to “high” and “moderate”, respectively. The resulting dense point cloud was then used as the basis to build a digital elevation model (DEM) and an orthomosaic. The resulting 10 cm resolution orthomosaic reconstructions of each sampling location were exported from Agisoft and used for feature classification in ArcMap 10.6.

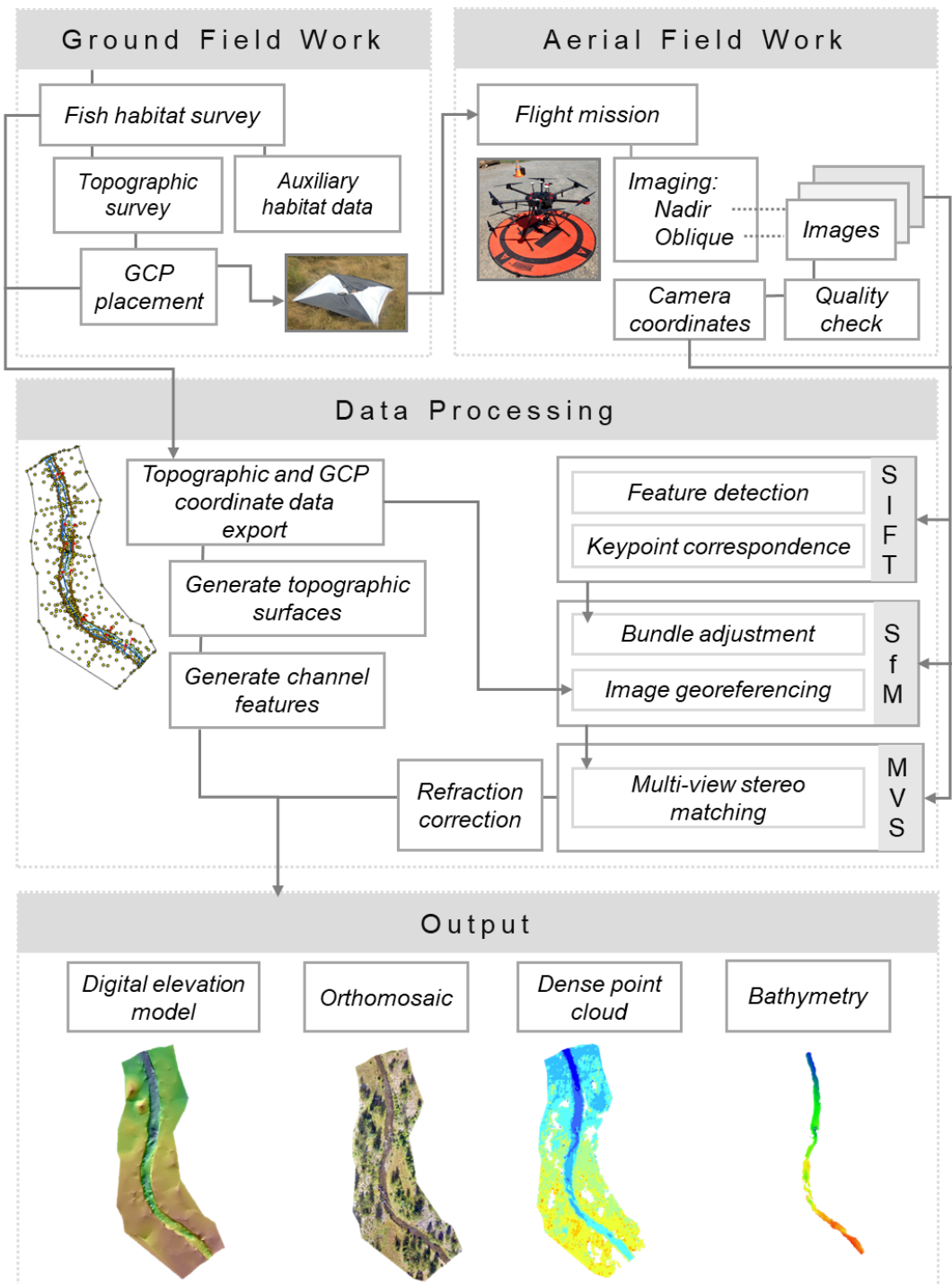


Figure 8. Workflow of ground and aerial mapping, data processing and outputs for riverine landscapes.

Because many of the metrics produced from CHaMP surveys relate to features within the wetted channel (e.g., wetted depths, volumes, and areas), a method to subsample and extract these features from the larger dense point cloud (DPC) was necessary. Using the Image Classification tool in ArcMap, a Maximum Likelihood Supervised Classification was performed to identify and extract

pixels corresponding to water in the active channel. Only pixels corresponding to water were retained, allowing us to exclude large wood, bare substrate, and vegetation features that would negatively influence the subsequent depth corrections. The wetted perimeter identified from the orthoimagery in ArcMap was then imported into CloudCompare (free and open source software; version 2.10.2). For each of the points falling within this wetted perimeter, depth corrections were performed following the multi-view stereo matching (MVS) refraction correction for SfM point clouds outlined by Dietrich (2017). Metrics were then computed using the corrected water depths and elevations.

Ground-based topographic data, collected following the CHaMP protocol (CHaMP, 2016a) at each of the 13 sampling locations, were processed using the CHaMP Topo Toolbar ArcMap add-in (<http://champtools.northarrowresearch.com/>). Metrics were generated by North Arrow Research, Inc. (Vancouver, British Columbia) for each of the sampling locations accounting for our modified survey design. Though the number of metrics generated is dependent on the site complexity (e.g., presence of multiple channels), the computed metrics from the CHaMP protocol typically result in > 100 metrics related to site level and channel unit level attributes.

### *Analytical approach*

Linear mixed effects models were used to account for the hierarchical structure of the data where multiple channel units were nested within each of our 13 sites. Introducing a site-level random effect enabled us to treat each channel unit as an observational unit while minimizing the effects of pseudoreplication. We structured the response variable as the difference between the two data collection methods (aerial minus ground) for a given channel unit – thus, if we view the ground-based measurement as the “true value”, then our response variable represents the error made by the aerial-based measurement. For each of six metrics of interest we constructed a set of global linear mixed effects models where canopy density (sparse, medium, dense), geomorphic classification (constrained or unconstrained), and channel unit type (fast water, slow water, or special case) were included as the explanatory variables in the global model. We automated the model selection process for all possible variable combinations using the ‘MuMIn’ package (Barton 2020) in R statistical software (R Core Team 2017). Akaike’s Information Criterion (AIC) was then used to compare model fits and determine the most parsimonious model and checked model assumptions and diagnostics using the ‘DHARMA’ package (Hartig 2020) in R.

## **Results and Discussion**

Quantifying the amount, quality, and changes to available in-stream habitat for fish is of critical importance throughout the Pacific Northwest where restoration actions are being used to improve viability of threatened and endangered species. UAS present new opportunities for monitoring and assessment of aquatic ecosystems through the collection of high-resolution data over continuous spatial extents in a variety of geomorphologic settings, without the need for interpolation from



reach-based samples (e.g., CHaMP 2016, PacFish InFish Biological Opinion (PIBO, Archer et al. 2016), Aquatic and Riparian Effectiveness Monitoring Program (AREMP, Reeves et al. 2004)). However, there is a need to thoroughly evaluate the utility of UAS approaches, including identifying sources of error stemming from natural variability in habitat conditions.

Obtaining stream habitat data representative of all habitat conditions utilized by fish has been difficult to achieve from ground-based habitat surveys or other remote sensing methods alone. We graphically assessed the quality of UAS derived data in comparison to those collected using ground-based methods and demonstrated the effects of geomorphology and canopy density on commonly computed habitat metrics (Figure 9). Among the limited metrics examined in this study, our findings support the challenges that numerous others have noted in attempting to obtain measures of river bathymetry from remotely sensed applications. We found metrics related to depth varied widely across the range of geomorphic and canopy densities examined. For pool residual depth, thalweg exit depth, and maximum depth, we found there to be a significant difference between the two survey methods evaluated (ground vs. aerial; Figure 9).

In addition to metrics related to channel unit geometries, the location and number of pieces of large wood are important measurements that influence stream morphology and biological productivity. Studies of large wood within streams are typically performed through surveys of wood distribution (ground-based or aerial counts), dating (residence time), and tracking (tagging) movement and accumulation (MacVicar et al., 2009). However, where large wood is abundant, measuring and geotagging each piece can be very time consuming. In this study, large wood pieces meeting our size criteria (15 cm in diameter and 3 m in length) were straightforward to identify from the UAS reconstructed orthoimagery using image classification schemes, and visually from orthophotos. However, despite the ease at which surficial pieces of wood meeting our criteria were identified, we observed a significant difference when comparing method types. Although the strength of the relationship between methods is relatively strong (Figure 9F) our failed ability to detect large wood pieces beyond those visible at the surface may partially be attributed to large wood structures spanning the channel that were both overlapping and partially sunken (e.g., into the bank, bedform, or underwater). Additionally, across all sites, we found water surface roughness/turbulence, shadows, overlapping sections, and riparian vegetation (grasses, trees) to impair our ability to identify all pieces counted on the ground. To a smaller degree, some of the variability in measurements between the two techniques may be attributable to crew observer error. Crews were trained to count pieces meeting our minimum criteria but were not required to measure each piece. This methodology may have resulted in over or undercounting pieces.

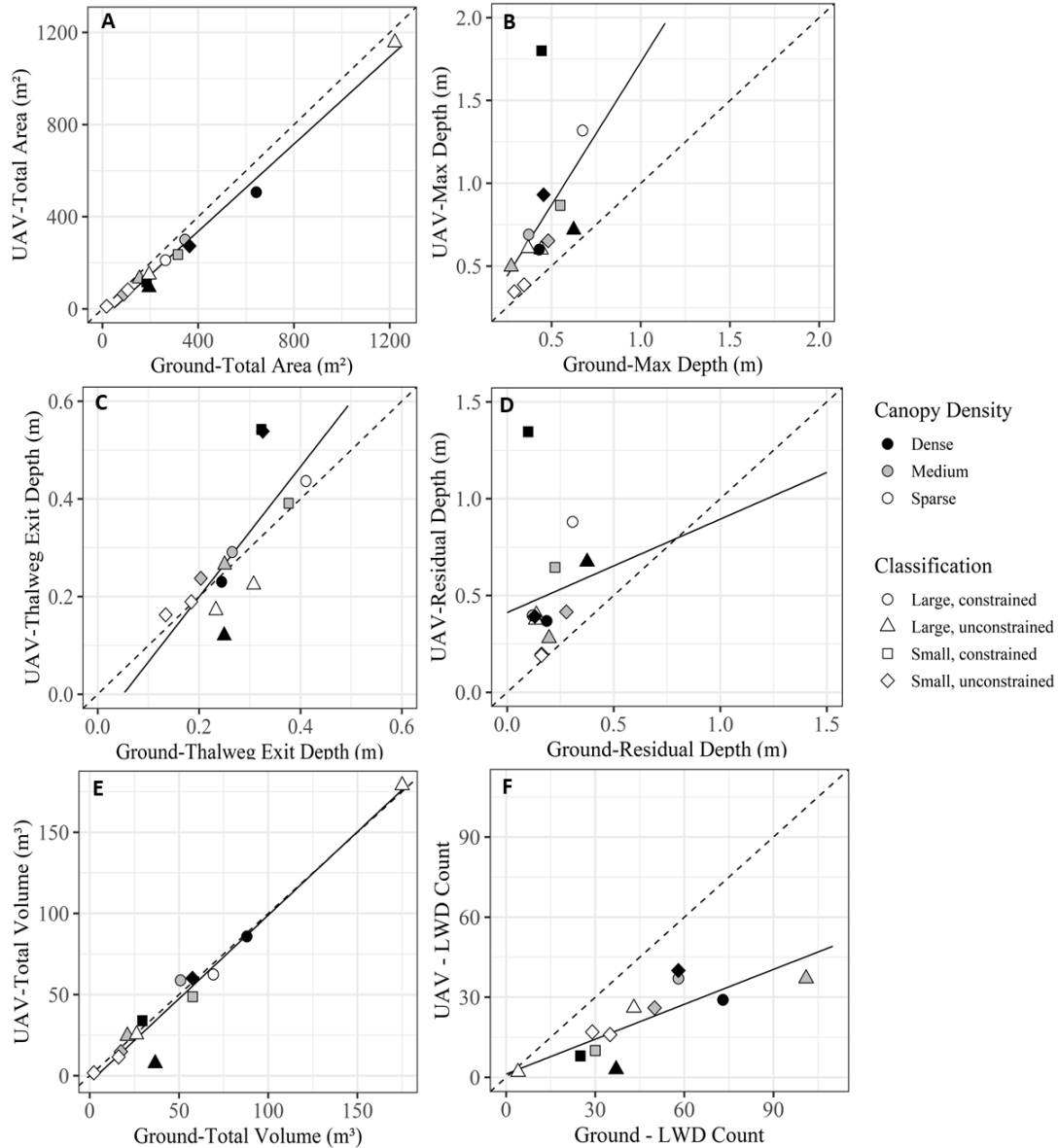


Figure 9. Relationships between ground-based and UAS-based metrics summarized by stream reach: A) mean total wetted area (m<sup>2</sup>), B) mean maximum depth (m), C) mean thalweg exit depth (m), D) mean residual depth (m), E) mean total wetted volume (m<sup>3</sup>), and F) sum of large wood counts. The solid line represents the regression line, while the dashed line is the 1:1 equality line.

We identified counts of large wood directly within or overhanging the active channel as the simplest quantifiable survey technique to obtain large wood distributions by unit type for a given stream reach. However, a hybridized approach using both ground-based count data coupled with UAS imagery could considerably enhance what we know about large wood movement, residence times, and volumes within streams. Though increasingly difficult to measure in complex channels (e.g., braided) or where obstructions are abundant, volumetric measures of large wood from imagery are possible. We found our average image resolution (4.9 cm/pixel) from UAS surveys at

80-or-120 meters to be sufficient to visually identifying and measuring large wood for validation. Furthermore, though we did not explicitly measure the length and diameter of each piece, Comiti et al. (2008b) found measurement errors from aerial imagery were greatly reduced (15%) when image resolution was at most twice that of the minimum large wood diameter. Continued work assessing the comparability between sampling locations with higher riparian canopy densities will be important in determining the feasibility of coupling UAS surveys with ground-based surveys of large wood.

### *Effects of canopy density and geomorphic conditions*

The best fitting models for explaining the error between the two measurement techniques (aerial vs. ground) for each of the six metrics evaluated are outlined in Table 10. Although unit type was included as an explanatory variable in the top models for four metrics the effect size was small in comparison to the effect of canopy density (Table 11). Canopy density was included as an explanatory variable in the top models for three of the metrics, where dense canopy had a large significant effect in many cases (e.g., total area, thalweg exit depth, large wood; Table 11). Channel morphology was included as explanatory variables in the top models for two metrics (max. depth and pool residual depth) where interestingly, both metrics included unit type and morphology as explanatory variables. In these models the effect of constrained morphologies and slow water unit types were highly significant ( $p < 0.0001$ ). Although diagnostic plots indicated that model assumptions were decently satisfied for many of the models, the assumptions of goodness of fit (Kirnoff-smithnoff) and for outliers failed with regard to the models for large wood, total volume, and total area.

Table 10. Model summary of the top ranked models for each of the six metrics evaluated based on Akaike's Information Criteria (AICc).

Response variable	Explanatory variables	df	logLik	AIC	Weight
Total Area	Canopy density + Unit type	7	-880.466	1775.6	0.483
Max. Depth	Morphology + Unit type	6	-25.456	63.5	0.665
Thalweg Exit Depth	Canopy density	5	37.658	-64.8	0.263
Pool Residual Depth	Morphology + Unit type	5	2.98	4.6	0.734
Total Volume	Unit type	5	-786.877	1584.1	0.266
Large Wood	Canopy density	5	-401.988	814.4	0.416

\*All models had  $\Delta AICc = 0$

Table 11. Summary of the top ranked models predicting each response variable.

Response variable	Fixed-effect covariates	Estimate	Std. Error	z-value	P-value
Total Area	Intercept	-103.49	11.85	-8.73	<0.001
	Canopy density - Medium	49.59	15.53	3.19	0.001
	Canopy density - Sparse	57.53	14.84	3.88	<0.001
	Unit type - Slow water	17.99	9.81	1.83	0.0668
	Unit type - Special case	80.45	34.76	2.31	0.0206
Max. Depth	Intercept	0.638	0.122	5.223	<0.001
	Morphology - Unconstrained	-0.393	0.154	-2.546	0.0109
	Unit type - Slow water	-0.175	0.0438	-3.999	<0.001
	Unit type - Special case	-0.176	0.136	-1.3	0.1935
Thalweg Exit Depth	Intercept	0.0943	0.0398	2.371	0.0178
	Canopy density - Medium	-0.0472	0.0483	-0.977	0.3285
	Canopy density - Sparse	-0.109	0.0463	-2.352	0.0187
Pool Residual Depth	Intercept	0.581	0.0994	5.846	<0.001
	Morphology - Unconstrained	-0.353	0.125	-2.828	0.00468
	Unit type - Slow water	-0.19	0.0432	-4.406	<0.001
Total Volume	Intercept	1.733	3.401	0.51	0.6103
	Unit type - Slow water	-11.372	5.255	-2.164	0.0305
	Unit type - Special case	-2.019	16.202	-0.122	0.9032
Large Wood	Intercept	-3.0235	0.541	-5.59	<0.001
	Canopy density - Medium	0.8416	0.715	1.18	0.239
	Canopy density - Sparse	1.819	0.677	2.69	0.00724

These findings highlight the importance of assessing UAS applications for stream habitat surveys over larger spatial scales and with replication that directly addresses challenges that restoration and monitoring practitioners should consider when evaluating the needs and data collection methods for a project or program. Although a variety of other remote sensing applications including structure-from-motion photogrammetry have demonstrated success in collecting remotely sensed topographic and bathymetric data with relatively good accuracy, the methods tested here and successfully demonstrated by Woodget et al. (2015, 2017) and Dietrich (2017) performed poorly when expanded to a more representative sample of riverine environments. As these fields continue to evolve, careful consideration should be given to sensor selection, post-processing algorithms, and data collection methodologies to determine the feasibility of obtaining the desired data products for a given study area.

## Conclusions

Imagery collected with UASs have the potential to provide continuous data at intermediate spatial scales. However, tree canopy and in-stream conditions can pose significant challenges to acquiring imagery and obtaining standard data products (e.g., dense point clouds, orthomosaics, and digital elevation models) from post-processing workflows. A primary component of this work was to assess the restrictions that riparian canopy density and geomorphic conditions would pose to a fish habitat survey methodology that incorporates the use of UAS for a component of the data collection process. As evidenced in this study, we found increasing canopy density to be the most prohibitive factor when deriving habitat metrics from imagery collected with a UAS. More specifically, in sampling locations where canopy was dense, channel overhanging vegetation, shadows cast by vegetation, and homogenous stands of species in some instances resulted in poor alignment of images, gaps in derived data products, and a reduction in the coverage and accuracy of derived elevation data.

By surveying fish habitat conditions both on the ground and from the air we were able to demonstrate the strengths and shortcoming of each method. The ground and aerial based methods used in this study present unique tradeoffs in the potential spatial coverage, time and cost investments, and data accuracy and precision. Ground based surveys using professional surveying equipment (e.g., total station or rtk GPS) produced high precision georectified data products of available instream fish habitat but require multi-day surveys with a minimum crew size of two persons. Aerial surveys, although also requiring some initial fieldwork with a two-person crew to establish GCPs, was typically completed in a fraction of the time (i.e., 30 minutes or less) required by ground methods. However, despite significant cost and time savings for the imagery acquisition portion of aerial surveys, the cost of specialized photogrammetric software for post-processing and the complex workflow to derive bathymetric data from imagery equate to overall similar time and cost investments of ground-based survey methods.

## References

- Archer, E.K., Henderson, R., Ojala, J.V., Gavin, A. and Burke, K.K., 2016. PacFish InFish Biological Opinion (PIBO) Monitoring Program: Effectiveness Monitoring Sampling Methods for Stream Channel Attributes.
- Barton, K. 2020. MuMIn: Multi-Model Inference. R package version 1.43.17. <https://CRAN.R-project.org/package=MuMIn>.
- Brierley, G.J., Brooks, A.P., Fryirs, K. and Taylor, M.P., 2005. Did humid-temperate rivers in the Old and New Worlds respond differently to clearance of riparian vegetation and removal of woody debris? *Progress in Physical Geography*, 29(1), pp.27-49.

- CHaMP (Columbia Habitat Monitoring Program). 2016. Scientific protocol for salmonid habitat surveys within the Columbia Habitat Monitoring Program. Prepared by CHaMP for the Bonneville Power Administration.
- Comiti F, Pecorari E, Mao L, Picco L, Rigon E, Lenzi MA. 2008b. New methods for determining wood storage and mobility in large gravel-bed rivers EPIC FORCE project Deliverable D20bis <https://research.ncl.ac.uk/epicforce/assets/D20bis.pdf>.
- Dietrich, J.T. 2017. Bathymetric Structure-from-Motion: extracting shallow stream bathymetry from multi-view stereo photogrammetry. *Earth Surf. Process. Landf.*, 42, 355–364.
- Flener, C.; Vaaja, M.; Jaakkola, A.; Krooks, A.; Kaartinen, H.; Kukko, A.; Kasvi, E.; Hyypä, H.; Hyypä, J.; Alho, P. 2013. Seamless Mapping of River Channels at High Resolution Using Mobile LiDAR and UAV-Photography. *Remote Sens.* 5, 6382–6407.
- Hartig, F. 2020. DHARMA: Residual Diagnostics for Hierarchical (Multi-Level / Mixed) Regression Models. R package version 0.3.2.0. <https://CRAN.R-project.org/package=DHARMA>.
- MacVicar, B.J., Piégay, H., Henderson, A., Comiti, F., Oberlin, C. and Pecorari, E., 2009. Quantifying the temporal dynamics of wood in large rivers: field trials of wood surveying, dating, tracking, and monitoring techniques. *Earth Surface Processes and Landforms*, 34(15), pp.2031-2046.
- Newson, M.D.; Newson, C.L. 2000. Geomorphology, ecology and river channel habitat: mesoscale approaches to basin-scale challenges. *Prog. Phys. Geogr.* 24, 195–217
- Reeves, G. H., D. B. Hohler, D. P. Larsen, D. E. Busch, K. Kratz, K. Reynolds, K. F. Stein, T. Atzet, P. Hays, and M. Tehan. 2004. Effectiveness monitoring for the aquatic and riparian component of the Northwest Forest Plan: conceptual framework and options. Page 71. U.S. Department of Agriculture, Forest Service, Pacific Northwest Research Station, General Technical Report PNW-GTR-577.
- Shintani, C.; Fonstad, M.A. 2017. Comparing remote-sensing techniques collecting bathymetric data from a gravel-bed river. *Int. J. Remote Sens.* 38, 2883–2902.
- Tamminga A, Hugenholtz C, Eaton B, Lapointe M. 2015. Hyperspatial remote sensing of channel reach morphology and hydraulic fish habitat using an unmanned aerial vehicle (UAV): a first assessment in the context of river research and management. *River Res Appl*, 31:379–391. <https://doi.org/10.1002/rra.2743>.
- Tamminga, A.D.; Eaton, B.C.; Hugenholtz, C.H. 2015. UAS-based remote sensing of fluvial change following an extreme flood event. *Earth Surf. Process. Landf.* 40, 1464–1476.

- Team, R. C. 2017. R: A language and environment for statistical computing. R Foundation for Statistical Computing, Vienna, Austria.
- Tyler, S., Jensen, O. P., Hogan, Z., Chandra, S., Galland, L. M., Simmons, J., & 2017 Taimen Research Team. (2018). Perspectives on the Application of Unmanned Aircraft for Freshwater Fisheries Census. *Fisheries*, 43(11), 510-516.
- USGS 2017. Unmanned Aircraft Systems Data Post-Processing. United States Geological Survey. UAS Federal Users Workshop 2017, <https://uas.usgs.gov/pdf/PhotoScanProcessingDSLRLMar2017.pdf>
- Wells, A.F., Crowe, E., Blaha, R., 2015. Riparian Vegetation Mapping in the Grande Ronde Watershed, Oregon: Monitoring and Validation of Spring Chinook Habitat Recovery and Population Viability. Prepared for Columbia River Inter-Tribal Fish Commission by ABR, Inc. (Alaska Biological Research, Environmental Research & Services, Anchorage, AK) and Elizabeth Crowe, Fort Collins, Colorado.
- Woodget, A.S.; Austrums, R.; Maddock, I.P.; Habit, E. 2017. Drones and digital photogrammetry: From classifications to continuums for monitoring river habitat and hydromorphology. *Wiley Interdiscip. Rev. Water*, 4, e1222
- Woodget, A. S., Dietrich, J. T., Wilson, Robin T. 2019. "Quantifying Below-Water Fluvial Geomorphic Change: The Implications of Refraction Correction, Water Surface Elevations, and Spatially Variable Error" *Remote Sens.* 11, no. 20: 2415. <https://doi.org/10.3390/rs11202415>

#### 1.4 Reanalysis of snorkel survey calibration methods

**Note:** we have received peer-reviews on a manuscript documenting a reanalysis of snorkel survey calibration methods; the complete and revised manuscript is included as Appendix C: “Accounting for uncertainty when estimating drivers of detection probability: an integrated approach illustrated with snorkel surveys for riverine fishes”. The abstract is provided below.

##### **Abstract**

Partial detectability is a common issue affecting the accuracy of surveys that quantify animal abundance and distribution. To estimate detection probability, counts are often calibrated to independent measures of abundance (e.g., via mark-recapture) but sampling variability in both data types is not typically accounted for. This practice may cause detection probability to be estimated inaccurately and lead to overly confident predictions for out-of-sample applications. Our objective was to develop, apply, and simulation-test an integrated approach for estimating detection probability that better-accommodates uncertainty. The method assumes mark-recapture and count surveys sample the same local abundance with error, allowing the construction of a joint likelihood function for both data sets. The model estimates coefficients that link detection probability to local covariates through a logit-linear model, allowing prediction of detection probability for locations without mark-recapture data. We illustrate the application of the model with an empirical data set of over 100 paired snorkel and mark-recapture surveys for riverine salmonids in northeastern Oregon. Selected covariates that best explained variability in detection probability for the empirical analysis included species, visibility, and channel unit type and depth, though much variability was attributed to random site effects. Estimated detection probability ranged from 0.02 to 0.92 among surveys and was higher for Chinook Salmon (*Oncorhynchus tshawytscha*) juveniles (mean: 0.38) than for steelhead/Rainbow Trout (*O. mykiss*; mean: 0.24). Simulation analyses revealed that accounting for rather than ignoring uncertainty in abundance data performed better in terms of selection of covariates, interval coverage, accuracy of estimated random variability terms, and reduced sensitivity to violated mark-recapture assumptions surrounding behavioral effects. This model represents an improvement over simpler calibration methods, particularly for snorkel surveys, by applying more a rigorous statistical treatment of sources of variability while explicitly describing the mechanistic link between local conditions and detection probability. The analytical methods we illustrate are general and could be broadly applied to quantify detection probability in other biological surveys with paired abundance and count data.



## 2.0 Riverscape Analyses

### 2.1 Spatial patterns and drivers of juvenile Chinook Salmon size and growth

**Note:** The accepted version of this manuscript can be found in Appendix D: “Temperature, emergence phenology, and consumption drive seasonal shifts in fish growth and production across riverscapes”. The abstract is provided below.

#### Abstract

1. Changes in biophysical conditions through time generate spatial and temporal variability in habitat quality across landscapes. For river ecosystems, researchers are increasingly able to characterize spatial and temporal patterns in habitat conditions, referred to as shifting habitat mosaics, yet rarely demonstrate how this translates into corresponding biological processes such as organism growth and production.
2. We assessed spatial patterns and processes determining seasonal changes in juvenile Chinook Salmon (*Oncorhynchus tshawytscha*) size, growth, and production over 30-40 km in two NE Oregon subbasins.
3. We quantified seasonal patterns of growth by combining estimated emergence dates and body size distributions in July and September. We then used analysis of bioenergetics, empirical fish diets, and spatial models incorporating temperature, habitat, and population density to evaluate mechanisms driving spatio-temporal patterns of growth. Lastly, we quantified seasonal contributions to individual fish growth and to total production as a function of position within the stream network.
4. Spatial heterogeneity in incubation temperatures corresponded to later emergence timing with distance upstream in both subbasins. During spring, estimated growth rates decreased with distance upstream, and coupled with emergence patterns, resulted in a pronounced longitudinal gradient in body size by July. During summer, spatial patterns of growth reversed, with greater diet ration sizes and growth efficiencies upstream than downstream. These opposing spatio-temporal patterns of emergence timing and seasonal growth rates produced spatial gradients in the proportion of fish growth achieved in spring versus summer, with up to 80% of an individual’s growth occurring prior to July at downstream sites but as low as 10% at upstream sites. Coupling longitudinal patterns of fish density and growth revealed that in one subbasin the majority of total production occurred in spring, while in the other, in which fish were concentrated in headwaters where they emerged late, the majority of production occurred in summer.
5. While recent work has emphasized inter-annual shifts in spatial patterns of fish production, this study demonstrates seasonally reversing gradients of fish growth and production across riverine landscapes, and reveals important contributions of warmer, downstream habitats to overall production that occurred during cooler times of the year.

## 2.2 Riverscape predictions of Chinook Salmon emergence timing and implications for juvenile size and growth

### Abstract

The success of organisms in any life stage is inherently linked to conditions experienced in prior life stages. For juvenile fish, temperature exposure during incubation largely controls embryonic development rates and the timing juveniles emerge from incubation substrates. The timing of emergence determines the biophysical conditions (temperature, flow, food supply) that recently emerged fish experience which in-turn can affect the duration of growth and subsequent survival during this critical life stage. While spatial variability in emergence timing has been evaluated across large spatial scales (i.e., among different streams and populations), it is unclear how emergence timing of a single population may vary within rivers. We evaluated spatial variability in spring Chinook Salmon (*Oncorhynchus tshawytscha*) emergence phenology throughout four NE Oregon rivers over 5-9 years and related inter-annual emergence timing estimates to juvenile salmon size and growth rates. Predicted emergence timing exhibited longitudinal variation in each river but these patterns did not follow a consistent trend among rivers: predicted emergence was progressively later with distance upstream in two rivers; progressively earlier with distance upstream in one river, and progressively later to a point and then earlier in the final river. Within years, the range in estimated median emergence timing among sites varied by 44 to 58 days in each river. Among years, the range in estimated emergence timing for a given location varied by 47 to 74 days in each river. Surprisingly, juvenile salmon in summer and fall were not larger in years exhibiting earlier emergence. Estimated growth rates from emergence to mid-summer and empirical growth rates from mid-summer to fall were positively correlated with later emergence. Spring and summer growth rates were negatively correlated with indices of juvenile density and mean water temperature, and positively associated with mean flow; however, the strength and significance of these relationships varied among rivers and growth interval (spring vs summer). Our results suggest considerable spatial and temporal variation in emergence timing in these rivers and that the shape of these patterns was related to longitudinal temperature trends in fall, winter, and spring. Further, results suggest that biophysical factors influencing growth rates (e.g., density, flow) were more important than emergence timing in determining juvenile size among years.

### Introduction

In riverine systems, abiotic (e.g., temperature, flow) and biotic (e.g., prey availability) conditions are spatially heterogeneous and interact with temporal processes at intra- and inter-annual scales to influence habitat conditions and biotic responses such as fish growth and production (Baldock et al. 2016; Brennan et al. 2019). For example, seasonal temperature changes can contribute to shifts in spatial patterns of fish growth, with greater growth rates in downstream sections during cooler seasons, reversing to higher growth rates in upstream sections in warmer months (Kaylor et al. *In press*; Armstrong et al. 2021). For poikilotherms, temperature is also a fundamental control

on embryo development rates and the timing of emergence from incubation habitats (Beacham and Murray 1990), thereby influencing growth duration and the biophysical conditions experienced by recently emerged fish. Longitudinal temperature profiles among rivers can be diverse (Fullerton et al. 2015), potentially structuring spatial patterns of emergence phenology. However, adult salmon may offset spawning to compensate for differential incubation durations, reducing spatial variation in emergence timing (Campbell et al. 2019). While studies have evaluated emergence timing among rivers (Austin et al. 2018; Adelfio et al. 2019; Campbell et al. 2019; Sparks et al. 2019), it is unclear how spatiotemporal patterns of spawn timing and temperature correspond to variation in emergence phenology within rivers.

Emergence timing has important implications for growth and survival (Egglishaw and Shackley 1977; Skoglund et al. 2012). Earlier emerging fish may achieve larger size than later emerging fish due to a longer growth duration and high spring growth rates (Kaylor et al. *In press*). For example, juvenile salmonids in Scotland streams were larger in years with earlier emergence, which was attributed to longer growth durations rather than inter-annual variation growth rates (Egglishaw and Shackley 1977). In addition to a longer growing duration, earlier emerging fish may also exhibit higher survival rates due to competitive advantages over later emerging, smaller fish (Einum and Fleming 2000). While there can be clear advantages to emerging early, there are also clear disadvantages. Emergence prior to high flows can reduce survival of newly emerged fry (Jensen and Johnsen 1999) and mismatches between emergence timing and optimal conditions for growth (i.e., temperature, prey availability, foraging ability) may reduce growth and survival.

Given the advantages and risks of variation in emergence timing, spawn timing is thought to be selected upon to promote emergence during long-term average optimal conditions for juvenile fitness. However, for populations spawning in warmer rivers and during warmer portions of the year, flexibility in spawn timing may be constrained, as high temperatures can increase embryo mortality (Geist et al. 2006). Thus, high temperatures may promote selection on spawn timing to limit mortality during early incubation (Beer and Anderson 2001). If spawning is constrained by temporal thermal barriers, spatial temperature patterns during the incubation period may correspond to pronounced emergence timing variation.

We evaluated spatial patterns of spring-run Chinook Salmon (*Oncorhynchus tshawytscha*) emergence timing over 5-9 years within four NE Oregon rivers. Emergence was predicted using empirical spawn timing data and annual temperature data from multiple locations in each river. Our goals were to 1) evaluate spatial patterns of predicted emergence in each river, 2) determine whether spatial patterns varied among years, and 3) relate inter-annual emergence estimates to juvenile salmon size and growth. Emergence modeling in two of these rivers for spawn year 2018 revealed later emergence with distance upstream (Kaylor et al. *In press*); we expected this trend to be consistent among basins but that the relationships would differ among years of contrasting environmental conditions, such as the 2014/2015 drought. We used historic juvenile Chinook Salmon sampling to relate inter-annual emergence timing predictions to fish size and growth rates.

We expected that fish would be larger in years with earlier emergence due to the prolonged duration of growth (Egglishaw and Chackley 1977). Quantifying spatial and temporal patterns of emergence timing has important implications for population dynamics and stability, especially in a changing climate in which emergence is expected to occur earlier (Adelfio et al. 2019; Sparks et al. 2019).

## **Methods**

### *Study area*

The study was conducted in four NE Oregon rivers (Figure 10). Three of the rivers – Catherine Creek (CC; 1,051 km<sup>2</sup>), the upper Grande Ronde River (UGR; 1,896 km<sup>2</sup>), and the Minam River (MIN; 618 km<sup>2</sup>) – are tributaries of the Grande Ronde River, which flows northward to its confluence with the Snake River. The Middle Fork John Day, although its origins are close in proximity to those of the Grande Ronde River, flows southwest into the John Day River before reaching the Columbia. The region is characterized by hot, dry summers and cool, wet winters with the majority of precipitation occurs as snow during winter months, resulting in snow-melt driven peak stream flows in spring. The drainages of MJFD (max elevation: 2478 m) and UGR (max elevation: 2414 m) originate from the lower elevation Blue Mountains, whereas CC (max elevation: 2640 m) and MIN (max elevation: 2791 m) drain higher elevations of the Wallowa Mountains. Consequently, snowmelt and associated peak flows typically occur earliest in MJFD, followed by UGR, CC, and MIN.

Numerous factors including habitat degradation, hydropower operations, altered predation, and overfishing have contributed to declines of returning spring Chinook Salmon in the Snake River basin (which includes the Grande Ronde basin), prompting the listing of this stock as threatened under the Endangered Species Act (NOAA 2008). As part of recovery efforts, there is a long history of hatchery supplementation in CC and UGR, with collection of local brood stock beginning in the late 1990s (Feldhaus et al. 2018). The Minam River is designated as a wilderness river and has undergone less habitat degradation (White et al. 2017) and no hatchery supplementation. Spring Chinook Salmon are not listed within the MJFD and no hatchery supplementation has occurred. Across all four rivers, adult Chinook Salmon enter natal tributaries in spring and spawn between early August and late September. Spawning typically occurs earlier in cooler, upstream sections and later in warmer downstream sections. Eggs incubate over the fall, winter, and spring with fry emerging from substrates in spring (Kaylor et al. In press; Lindsay et al. 1986).

### *Temperature and environmental covariates*

We collected year-round surface water temperature data over 5-9 years from 6-12 sites in each river (Figure 10) using Hobo Pro v2 and Tidbit data loggers (Onset Computer Corporation, Bourne, Massachusetts) recording at 15-minute intervals. Loggers were situated in a stout pvc

housing secured to a large boulder with epoxy, or in metal piping and secured to an adjacent tree with cable (Isaak et al. 2016). Data were downloaded every 1-5 years and the condition and location (e.g., detached, out of water) of loggers was noted upon retrieval. Loggers found out of the water or buried were excluded from analyses. Sufficient temperature data to estimate emergence timing was available for 9 years in CC, 9 years in UGR, 5 years in MIN, and 7 years in MFJD.

We expected inter-annual variability in environmental conditions over the incubation period to influence inter-annual emergence timing estimates. In addition, the study encompassed annual conditions ranging from an extreme drought from the winter of 2014 through the fall of 2015 to wetter, cooler years (e.g., 2019), which provides an opportunity to evaluate how climate change may influence emergence timing (Adelfio et al. 2019). We obtained historic winter air temperature and snow water equivalent (SWE, the amount of water stored in the snowpack) data from Oregon SNOTEL sites (<https://wcc.sc.egov.usda.gov/reportGenerator>) located near each river: CC (Taylor Green; elevation = 1749 m), UGR (Wolf Creek; 1716 m), MFJD (Tipton; 1570 m) and MIN (Aneroid Lake #2; 2256 m). To characterize annual conditions during the incubation period, we calculated mean annual temperature between October and March and SWE between January and March. We used linear regression models to evaluate the degree to which mean winter air temperature and mean SWE explained inter-annual variation in emergence timing estimates for each river.

### *Spawn timing*

Spawning date ranges were obtained from redd surveys conducted semi-continuously (some river sections were not accessible) throughout each river and in each year, as part of Oregon Department of Fish and Wildlife monitoring programs (Dowdy et al. 2019). Surveys were repeated every 7-10 days over a 3-6 week period, resulting in 3-5 surveys per river each year. During each survey, newly observed redds and their associated GPS location were recorded. Our goals were to 1) determine spatial patterns of spawn timing within each river (i.e., does spawning occur later downstream?), and 2) evaluate inter-annual variability in spawn timing. We fit linear models with the observation date of each redd as the dependent variable and river kilometer and year as fixed-effects. Two separate models were fitted: one for Grande Ronde basin tributaries (UGR, CC, and MIN) and the other for MFJD. Grande Ronde basin tributaries were included in the same model as they are close in proximity and within the same Evolutionary Significant Unit. Using data from multiple rivers allowed for estimation in years in which redd data in some rivers was data poor (consistent with Austin et al. 2021). In the Grande Ronde model, we included an interaction between each river and river kilometer to allow for different longitudinal patterns. In addition, there were slight differences in survey methods between Grande Ronde basin rivers and MFJD. In both models, spawn year was treated as a categorical fixed effect and we did not include an interaction with river kilometer (i.e., the intercept varied among years but slope did not). Although longitudinal patterns of spawn timing may vary among years, limited spatial data in low return

years prohibited rigorous evaluation of inter-annual variation in these relationships. Our approach produced similar results to an alternative approach of breaking each river into sections and evaluating cumulative distributions to determine median spawning dates (Austin et al. 2021).

### *Emergence timing*

Emergence timing was predicted using the relationship between water temperature and incubation development rates developed by Beacham and Murray (1990), but with modifications suggested by Sparks et al. (2019) to better account for variable temperature exposure:

$$E_i = 1/\exp [\log_e a - \log_e(T_i - b)]$$

where  $E_i$  is the daily contribution to development (0 to 1),  $T_i$  is the daily mean temperature (°C), and  $\log_e a$  (6.872) and  $b$  (-0.332) are coefficients derived from Beacham and Murray (1990). Beginning with the predicted spawn date, daily effective values are summed and emergence is predicted to occur on the first day that the sum exceeds 1. For each location and year, the mean spawn date was predicted as described above. To account for temporal variability in spawn timing at each location, we examined cumulative distributions of newly observed redds, which indicated that the majority of spawning at each site occurred over a 2-3 week window. We therefore established a distribution around mean spawn dates with a standard deviation of 4 days, resulting in 95% of spawn dates within each distribution occurring within a 16 day window, which is similar to the 14-day spawn window used by Beer and Anderson (2001). We ran 1000 simulations for each site and year combination in which each simulation drew from the spawn timing distribution.

### *Fish growth rates*

We used historic capture and tagging data from the Oregon Department of Fish and Wildlife to evaluate relationships between inter-annual variation in emergence timing and juvenile Chinook Salmon size and growth rates. Summer capture and tagging was conducted within specific sections of CC (between river kilometers 42-47), UGR (Rkm 318-326), and MIN (Rkm 35-43) in each year and at the same time of the year, providing consistent methodology. Data was not available for MFJD. During summer, juveniles were captured using snorkel-herding methodology in which snorkelers herded fish into a seine net (Tattam et al. 2017). Fish were anesthetized using MS-222 (tricaine methane sulfonate), and individuals 55 mm and larger were tagged with 12 mm passive integrated transponder (PIT) tags. If under-sized individuals were captured, a minimum of 15 were measured and the remainder were counted. In fall, fish were captured using screw traps located downstream of tagging locations. We calculated mean summer weight (including under-sized, untagged fish) and mean fall weight (including under-sized, untagged fish) for all years in which emergence timing estimates were available. We then estimated mass-standardized growth rates (MSGR; Ostrovsky 1995) from emergence to summer and from summer to fall:

$$\text{MSGR (\% d}^{-1}\text{)} = ((W_2^b - W_1^b)/(b * t)) * 100$$

where  $W_1$  and  $W_2$  represent fish weight during the first and second sampling event, respectively,  $t$  is the number of days, and  $b$  is the allometric mass exponent for Chinook Salmon (0.338; Perry et al. 2015). To estimate growth rates from emergence to summer, we assumed an initial mean weight of 0.5 g (Beacham and Murray 1990), and used the difference between mean weight in summer and initial weight to calculate MSGR (see Kaylor et al. In press). Emergence timing estimates were specific to the river kilometers in which fish were sampled. To account for variation in emergence timing, each river and year were randomly resampled (with replacement) from our emergence estimates and MSGR was recalculated with these different values of  $t$ . Growth rates from summer to fall were calculated using summer-tagged individuals that were recaptured at screw traps. We present the mean MSGR and 95% confidence intervals of all recaptured individuals between October 1 and November 31 of each year.

We evaluated relationships between annual predicted emergence timing and 1) summer mean size, 2) fall mean size, 3) emergence-to-summer MSGR, and 4) summer-to-fall MSGR for each river. We then used linear regression models to evaluate potential effects of density-dependence and environmental conditions on growth rates. We used the total number of previous year redds within tagging areas as a proxy for density-dependence, as the number of redds is strongly associated with the number of juveniles the following year. We calculated mean spring and summer temperature in each river and year using data loggers located within tagging areas. Spring was defined as April to June in CC, and April to July in UGR and MIN, because CC parr are consistently tagged in July whereas UGR and MIN parr are tagged in August. Summer was represented by July to October in CC and August to October in UGR and MIN. Lastly, we obtained continuous flow data from nearby gauging stations in each river (CC - station 13320000; UGR - station 13317850; MIN – station 13331500) to evaluate potential relationships between flow and growth rates. Similarly, we calculated mean flow in spring and summer for each river. Given the low sample size (5-9 years in each river), we were not able to include multiple covariates or interactions between covariates in linear models.

## Results

### *Temperature profiles*

Longitudinal patterns of incubation temperatures varied among rivers and seasons (Figure 11). For example, temperature increased with distance downstream in fall and spring in CC and UGR, but winter temperature was relatively homogenous. In contrast, spring and fall temperatures in MFJD were comparatively more homogenous, whereas winter temperature increased with distance upstream (upstream of river kilometer 100). A similar trend was apparent in MIN, in which winter temperatures were greatest at the farthest upstream location; in fall and spring, temperatures increased slightly with distance downstream.

Longitudinal temperature patterns were relatively consistent among years; however, there was considerable variation in seasonal mean temperatures (Figure 11b). In fall, spawn year 2019 (emergence year 2020) was consistently the coolest year, whereas 2014-2016 exhibited the warmest temperatures. In winter, spawn year 2014 was consistently the warmest year, in which mean temperature was 1.03, 0.51, and 0.98 °C greater than average temperature across all years in CC, UGR, and MFJD, respectively (no 2014 data for MIN). In spring, spawn years 2014 and 2015 exhibited the warmest temperatures, whereas 2018 and 2019 exhibited the coolest temperatures.

### *Spawn timing*

Estimated mean spawn timing was progressively earlier with distance upstream in each river (Figure 12). However, the slope of the relationship between river kilometer and median spawn date differed among rivers: -0.43 days km<sup>-1</sup> in UGR (95% CI = -0.46 - -0.40;  $p < 0.001$ ); -0.29 days km<sup>-1</sup> in CC (-0.33- -0.26;  $p < 0.001$ ); -0.22 days km<sup>-1</sup> in MIN (-0.24- -0.19;  $p < 0.001$ ); and -0.06 days km<sup>-1</sup> in MFJD (-0.08- -0.04;  $p < 0.001$ ). For Grande Ronde basin rivers (CC, UGR, and MIN), the inclusion of spawn year as a covariate improved model explanatory power ( $r^2 = 0.46$  vs 0.28) and was higher ranked than the model without spawn year ( $\Delta AICc = 1046$ ). Similarly, for MFJD, the model including spawn year explained more variation ( $r^2 = 0.18$  vs 0.02) and was ranked higher ( $\Delta AICc = 400$ ).

### *Emergence timing*

Predicted emergence timing exhibited clear spatial structuring in each river; however, patterns were not consistent among rivers (Figure 13). In CC and UGR, predicted emergence timing was progressively later with distance upstream, whereas the opposite pattern was observed in MFJD. Spatial patterns in MIN were mixed with later predicted emergence with distance upstream to a point and then earlier emergence at the farthest upstream locations. Models with an interaction between river kilometer and year were always ranked lower than models with year as an additive effect ( $\Delta AICc > 20$ ), indicating that spatial patterns of emergence timing were relatively consistent among years. Within years, the mean range of predicted emergence dates among sites was 58 days in CC (range 43-73), 44 days in UGR (range 36-56), 49 days in MIN (range 34-75), and 46 days in MFJD (range 36-58). Among years, the range in estimated emergence timing for a given location was 73 days in CC, 54 days in UGR, 47 days in MIN, and 74 days in MFJD. Predicted emergence was earliest in 2015 (spawn year 2014) and latest in 2018 (spawn year 2017).

Spatial patterns of winter temperature appear to be important in explaining earlier emergence timing at upstream locations in MFJD and MIN. For example, fall and spring temperatures were comparatively homogenous in MFJD, but winter temperatures were considerably warmer in upstream locations – a pattern consistent with the farthest upstream locations in MIN (Figure 11). In contrast, winter temperatures were relatively homogenous in CC and especially UGR (spawn



year 2014 excluded), whereas fall and spring temperatures increased considerably with distance downstream.

Among years, predicted emergence timing in each river was negatively correlated with mean air temperature from October through March but not with snow water equivalent (SWE) from January to March (Figure 14). For every 1°C increase in mean air temperature, median emergence timing was expected to be 22 days earlier in CC (95% CI: 7-37 days), 14 days earlier in UGR (95% CI: 1-28 days), 27 days earlier in MIN (95% CI: -14-68 days), and 21 days earlier in MFJD (95% CI: 0-41 days).

### *Fish size and growth*

Contrary to our expectations, earlier emergence did not result in larger parr in summer or fall (Figure 15a,b). In contrast, later emergence was positively correlated with mean parr size in fall in CC and UGR (Figure 15b), but this was not the case for summer size in which no relationship was evident (Figure 15a). Growth rates from emergence to mid-summer (hereafter spring) and from mid-summer to fall (hereafter summer) were positively correlated with later emergence (Figure 15c,d). Thus, although fish in years exhibiting early emergence had a longer estimated growing duration, their growth rates were slower, negating effects on inter-annual patterns in size.

Inter-annual variability in growth rates was explained by both abiotic and biotic factors; however, the strength of these relationships varied by river and growth interval (Figure 16). The number of redds from the previous year – a proxy for juvenile abundance in the growth year of interest – was negatively correlated with spring growth rates and weakly associated with summer growth rates in CC; in UGR and MIN, there was no statistically significant relationship. However, a single outlier in UGR (rearing year 2012) exhibited high leverage given the small sample size (8 years). With this year excluded, the relationships between the number of redds and juvenile growth rates during spring ( $r^2 = 0.52$ ;  $p = 0.04$ ) and summer ( $r^2 = 0.29$ ;  $p = 0.12$ ) were stronger. Mean spring temperature was negatively associated with spring growth rates in all three rivers; however, a statistically significant (at the  $\alpha = 0.05$  level) relationship was only evident in UGR. Mean summer temperature was negatively correlated with summer growth rates in CC, but not in UGR or MIN. Both mean spring discharge and mean summer discharge were positively related to spring growth rates in CC and UGR ( $p < 0.05$ ), but not in MIN.

## **Discussion**

Our results revealed strong spatial patterns in predicted emergence timing within these rivers and that these patterns were consistent among years in each river, despite considerable inter-annual variation in environmental conditions and estimated emergence dates. However, patterns were not consistent among rivers and were mediated by longitudinal temperature trends during fall, winter, and spring. For example, in CC and UGR, temperature increased with distance downstream in fall and spring, but was relatively homogenous in winter, leading to progressively later emergence

upstream. In contrast, fall and spring temperatures in MFJD were relatively homogenous, but winter temperatures were warmer upstream, resulting in earlier predicted emergence upstream attributed to greater winter contributions to embryo development. Thus, our results indicate that during the incubation period (fall-spring), longitudinal temperature trends varied among rivers, but also among seasons within rivers, leading to variable, and even opposing spatial patterns in predicted emergence timing. Across rivers of the Pacific Northwest, summer thermal profiles exhibit diverse longitudinal trends (Fullerton et al. 2015) that have important implications for fish physiology, growth, and distribution within watersheds. Consideration of spatiotemporal thermal profiles during the incubation period may reveal similar complexity, including shaping diverse patterns of emergence phenology.

### *Spatial patterns of emergence phenology*

The range of predicted emergence dates within each river and year was considerable. Fry emergence at the farthest upstream sites in CC and UGR was predicted to occur 6-8 weeks later than the farthest downstream sites, whereas emergence at the farthest upstream sites in MFJD was predicted to occur approximately 6 weeks earlier than downstream sites. Adult spawn timing is thought to be selected upon to promote emergence during optimal conditions for growth and survival (Crozier et al. 2008). If the timing of optimal conditions for emergence are uniform across space, spawn timing in adjacent tributaries with contrasting thermal regimes (e.g., ground water vs. surface water-dominated) may be offset to compensate for differential development rates, resulting in relatively synchronous emergence timing (Campbell et al. 2019). However, for populations spawning during warmer portions of the year (e.g., spring-run Chinook Salmon), high temperatures may present a temporal thermal barrier, in which spawn timing may be selected upon to reduce embryo mortality during early incubation (Beer and Anderson 2001). This is evidenced in rivers in our study by earlier spawning in upstream sections and progressively later spawning in warmer, downstream sections, especially in CC and UGR, in which there were greater increases in temperature with distance downstream during the spawning season. However, we estimated that mean spawn timing only varied by 3-14 days in each river. If spawning is constrained, variable thermal profiles during the incubation period are more likely to result in asynchronous, spatially-structured emergence phenology. Alternatively, the optimal window to emerge may vary within watersheds. For example, spring temperatures are greater in downstream sections of CC and UGR and optimal temperatures for spring growth may occur earlier downstream and progressively later upstream. Spatiotemporal patterns of temperature may also correspond with invertebrate production, such that prey availability also peaks earlier downstream.

Evaluating thermal contributions over the course of incubation revealed insights into potential mechanisms explaining spatial variation within rivers and temporal variation among rivers. For example, in MFJD, winter (defined here as Dec. – February) thermal contributions to development were minimal at downstream sites and greater at upstream sites, leading to earlier emergence upstream. This suggests that upstream sites are characterized by greater contributions of warmer

groundwater inputs and that groundwater influence decreases with distance downstream, which is consistent with decreasing baseflow index with distance downstream. In contrast, CC exhibited considerable thermal contributions to development in winter that were more consistent among sites, suggesting more stable and spatially homogenous groundwater inputs. UGR exhibited the lowest baseflow index of all rivers and winter contributions to development were minimal, resulting in the latest emergence timing of the four rivers. Thus consideration of hydrology and associated impacts on winter incubation temperature appears to be an important driver of spatial variation in emergence timing within basins and of temporal differences among basins.

Spatial structuring of emergence phenology has important implications for juvenile salmon ecology. For example, Kaylor et al. (*In press*) found that earlier emergence downstream, combined with greater spring growth rates, led to larger fish and progressively smaller mean size with distance upstream in early summer. Further, growth rates decreased with distance upstream in spring, but this pattern reversed direction in summer, resulting in downstream fish obtaining the majority of growth in spring whereas those in upstream sections obtained the majority of growth in summer. Temporal variation in emergence timing also influences the environmental conditions newly emerged fry are exposed to. In particular, emergence timing relative to snowmelt-driven spring peak flows has potential consequences for survival, dispersal, and habitat use. The coincidence of high flows and emergence can result in lower survival (Jensen and Johnsen 1999) and may also increase downstream dispersal (Saltveit et al. 1995). Flow is also directly related to floodplain inundation, and the accessibility of floodplains may only occur within a specific range of flows (Baldock et al. 2015). Floodplain habitats can provide velocity refuge and enhanced growth opportunities for juvenile salmon (Sommer et al. 2001; Jeffres et al. 2008). However, the timing of emergence relative to floodplain inundation may influence habitat use and the benefits floodplains provide to juvenile salmon. Evaluating how variation in emergence phenology influences these aspects of juvenile salmon ecology is an important avenue of future research.

#### *Inter-annual patterns of emergence timing*

While spatial patterns of emergence timing were consistent among years (i.e., the shape of emergence patterns), there was considerable inter-annual variation in emergence dates for a given location. Predicted emergence was earliest during the warm, drought conditions of 2014/2015, whereas cooler conditions in 2018/2019 resulted in the latest predicted emergence (e.g., 7-10 weeks later than in 2015). Adelfio et al. (2019) similarly predicted emergence to occur approximately 8 weeks earlier in warmer, rain-dominated winters compared to cooler, snow-dominated winters in precipitation-dominated Alaska rivers; however, in groundwater-dominated rivers, this difference was reduced to just 10 days. While winter temperature profiles in MIN and MFJD suggest groundwater influence in upstream sections, these sections exhibited warming trends consistent with downstream locations in all years, suggesting little ability for these groundwater sources to buffer warmer winters. Among the four rivers, mean incubation (October-March) air temperature accounted for 36-57% of the variation in inter-annual emergence estimates.

Winter air temperature in this region is anticipated to increase by approximately 3°C by the end of the century under regional climate change projections (Mote et al. 2019) and our results suggest that emergence timing could occur months earlier under these warming scenarios. It is unclear whether optimal timing to emerge will shift earlier at the same rate, or whether genetic selection in spawn timing will compensate for warmer incubation conditions and shorter incubation periods (Crozier et al. 2008).

#### *Implications of emergence timing on fish size and growth*

We expected parr to be larger in years with earlier emergence, owing to a longer duration of growth. However, we found no relationship between emergence timing and mean summer weight, and even observed positive relationships between later emergence and mean fall weight in two of the three rivers (MJFD not evaluated). This result contrasts with Egglshaw and Shackley (1977), who found that age-0 salmonids were larger in years with earlier emergence. Further, they found that seasonal growth rates were similar among years, and that greater size in years with earlier emergence was attributed to a longer growth duration. In contrast, we found that estimated growth rates from emergence to mid-summer (spring) and empirical growth rates from mid-summer to fall (summer) were not consistent among years, and instead were greater in years with later emergence.

There are a number of potential explanations for why earlier emergence did not lead to greater size. First, fish emerging later may have exhibited compensatory growth. However, compensatory growth typically occurs after a period of growth suppression (Ali et al. 2003), and our results suggest that later emergence was associated with higher initial (i.e., emergence-to-summer) growth rates. It is unclear whether prolonged incubation could lead to compensatory growth. Second, growth rates and size may have been more strongly controlled by density-dependence, rather than growth duration. The number of redds in the prior year (i.e., the redds contributing to the following year's abundance) was negatively correlated with spring and summer growth rates, but just one of the six relationships were statistically significant. However, sample size was low (5-9 years), and trends were consistent among rivers and between the two growth periods, suggesting density-dependence may contribute to observed growth rates. Lastly, the environmental conditions influencing emergence timing may have carry-over effects that influence growth after emergence. For example, warm winters with little snowpack accumulation may lead to faster development and earlier emergence, but also earlier onset of low-flow conditions, lower spring and summer discharge, and higher stream temperature, which may reduce growth rates. We found that spring and summer growth rates were negatively correlated with mean spring and summer water temperature and positively correlated with mean spring and summer flow. Reduced flow can decrease salmonid growth rates (Harvey et al. 2006), presumably by reducing drifting invertebrate prey and accessibility to adjacent habitats where foraging opportunities may be better. Given the non-linear relationship between water temperature and growth potential (Beauchamp 2009), warmer temperature in spring would be expected to increase growth rates, whereas warmer

temperature in summer may reduce growth rates. However, flow and temperature are inherently linked through climatic conditions, and we are therefore not able to evaluate whether increased temperature or reduced flow may have contributed to decreased growth in years exhibiting earlier emergence.

### *Caveats and limitations*

There are a number of caveats and limitations of our study. First, temperature data were from the water column rather than the substrates in which eggs are incubating. Studies have shown differences in temperature between surface water and incubation substrates (Adelfio et al. 2019), while others, including studies closer to our study sites (Groves et al. 2008), have found little difference. We acknowledge that our temperature data may differ from substrate temperature experienced during incubation, and thus may influence predictions of emergence dates. However, differences between surface water and substrate temperatures are unlikely to influence spatial patterns of emergence phenology predicted in this study. Second, emergence timing was modeled, and although we attempted to account for variability in spawn timing, we were not able to capture other sources of variability. For example, families within the same population can exhibit differential development rates (Beer and Steel 2018) and variation in dissolved oxygen can influence incubation duration (Geist et al. 2006). Additionally, we modeled median emergence timing, but fry emergence can occur over a period of weeks to months (Campbell et al. 2019) and at varying levels of development and yolk absorption (Beer and Anderson 2001). Thus the range in realized emergence is likely greater than we modeled. Lastly, when evaluating relationships between inter-annual conditions and growth rates, our sample size was low (5-9 years), limiting evaluation of interactions between covariates. It is likely that environmental covariates (i.e., flow and temperature) interacted with biotic conditions (i.e., density-dependence) to shape inter-annual patterns of growth rates, but we were not able to rigorously evaluate these interactions. This highlights the importance of and need for long-term data collection to understand drivers of population dynamics, especially under changing climatic conditions.

### **Conclusions**

There is increasing recognition that spatial and temporal variability in salmon population dynamics has a stabilizing effect on aggregate population productivity (i.e., portfolio effects; Schindler et al. 2015). Within these watersheds, spatial structuring of emergence timing may be a previously overlooked aspect of intra-population variability, contributing to population stabilization. This spatial variability may interact with temporal variation as environmental and biological (e.g., prey availability) conditions in some years may favor early emerging fry, whereas later emerging fry may exhibit greater growth and survival in other years. As salmon numbers decline, spawning may contract to core spawning areas (Isaak and Thurow 2006; Flitcroft et al. 2014), thereby reducing variability in emergence timing and the biophysical conditions newly emerged fry experience. Similarly, focusing habitat restoration efforts on narrow regions within spawning ranges may lead

to reduced variability. However, many questions remain about how spatiotemporal emergence patterns influence key aspects of juvenile salmon ecology including juvenile dispersal, floodplain use, and survival. Answering these questions has important implications for guiding management efforts and understanding how changing conditions may influence juvenile salmon ecology.

## References

- Adelfio, L. A., S. M. Wondzell, N. J. Mantua, and G. H. Reeves. 2019. Warm winters reduce landscape-scale variability in the duration of egg incubation for coho salmon (*Oncorhynchus kisutch*) on the copper river delta, Alaska. *Canadian Journal of Fisheries and Aquatic Sciences* 76(8):1362–1375.
- Armstrong, J. B., Fullerton, A. H., Jordan, C. E., Ebersole, J. L., Bellmore, J. R., Arismendi, I., Penaluna, B., & Reeves, G. H. (*In press*) The significance of warm habitat to the growth regime of coldwater fishes. *Nature Climate Change*.
- Austin, C. S., T. E. Essington, and T. P. Quinn. 2018. Spawning and emergence phenology of bull trout *Salvelinus confluentus* under differing thermal regimes. *Journal of Fish Biology* 94: 191-195
- Austin, C. S., T. E. Essington, and T. P. Quinn. 2021. In a warming river , natural-origin Chinook salmon spawn later but hatchery-origin conspecifics do not. *Canadian Journal of Fisheries and Aquatic Sciences* 77:68–77.
- Baldock, J. R., J. B. Armstrong, D. E. Schindler, and J. L. Carter. 2016. Juvenile coho salmon track a seasonally shifting thermal mosaic across a river floodplain. *Freshwater Biology* 61:1454–1465.
- Beacham, T. D., and C. B. Murray. 1990. Temperature, egg size, and development of embryos and alevins of five species of Pacific Salmon: A comparative analysis. *Transaction of the American Fisheries Society* 119(6):927–945.
- Beauchamp, D. A. 2009. Bioenergetic ontogeny: linking climate and mass-specific feeding to life-cycle growth and survival of salmon. *American Fisheries Society Symposium* 70(June):1–19.
- Beer, W. N., and J. J. Anderson. 2001. Effect of spawning day and temperature on salmon emergence: Interpretations of a growth model for Methow River chinook. *Canadian Journal of Fisheries and Aquatic Sciences* 58(5):943–949.
- Beer, W. N., and E. A. Steel. 2018. Impacts and Implications of Temperature Variability on Chinook Salmon Egg Development and Emergence Phenology. *Transactions of the American Fisheries Society* 147(1):3–15.

- Brennan, S. R., D. E. Schindler, T. J. Cline, T. E. Walsworth, G. Buck, and D. P. Fernandez. 2019. Shifting habitat mosaics and fish production across river basins. *Science*:783–786.
- Campbell, E. Y., J. B. Dunham, G. H. Reeves, and S. M. Wondzell. 2019. Phenology of hatching, emergence, and end-of-season body size in young-of-year coho salmon in thermally contrasting streams draining the Copper River Delta, Alaska. *Canadian Journal of Fisheries and Aquatic Sciences* 76(2):185–191.
- Crozier, L. G., A. P. Hendry, P. W. Lawson, T. P. Quinn, N. J. Mantua, J. Battin, R. G. Shaw, and R. B. Huey. 2008. Potential responses to climate change in organisms with complex life histories: evolution and plasticity in Pacific salmon. *Evolutionary Applications* 1(2):252–270.
- Dowdy, J. W., B. C. Power, G. A. McMichael, E. N. Branigan, K. J. Wauhkonen, C. R. Warnock, O. C. Davis, S. D. Favrot, E. R. Sedell, and J. R. Ruzycki. 2019. Investigations into the early life history of naturally produced spring Chinook Salmon and summer steelhead in the Grande Ronde River subbasin: Annual report 2018. La Grande, Oregon.
- Egglishaw, H. J., and P. E. Shackley. 1977. Growth, survival and production of juvenile salmon and trout in a Scottish stream, 1966-75. *Journal of Fish Biology* 11:647–672.
- Einum, S., and I. A. Fleming. 2000. Selection against late emergence and small offspring in Atlantic salmon (*Salmo salar*). *Evolution* 54(2):628–639.
- Isaak, D.J., Horan, D.L., and S.P. Wollrab. 2013. A simple protocol using underwater epoxy to install annual temperature monitoring sites in rivers and streams (No. RMRS-GTR-314). U.S. Department of Agriculture, Forest Service, Rocky Mountain Research Station, Ft. Collins, CO. <https://doi.org/10.2737/RMRS-GTR-314>
- Feldhaus, J. W., D. L. Eddy, P. J. Keniry, and J. R. Ruzycki. 2018. Lower Snake River compensation plan: Oregon spring Chinook Salmon evaluation studies 2016 annual progress report. Oregon Department of Fish and Wildlife, Salem, OR.
- Flitcroft, R., K. Burnett, J. Snyder, G. Reeves, and L. Ganio. 2014. Riverscape Patterns among Years of Juvenile Coho Salmon in Midcoastal Oregon: Implications for Conservation. *Transactions of the American Fisheries Society* 143(1):26–38.
- Fullerton, A. H., C. E. Torgersen, J. J. Lawler, R. N. Faux, E. A. Steel, T. J. Beechie, J. L. Ebersole, and S. G. Leibowitz. 2015. Rethinking the longitudinal stream temperature paradigm: region-wide comparison of thermal infrared imagery reveals unexpected complexity of river temperatures. *Hydrological Processes* 29:4719–4737.
- Geist, D. R., C. S. Abernethy, K. D. Hand, V. I. Cullinan, J. A. Chandler, and P. A. Groves. 2006. Survival, Development, and Growth of Fall Chinook Salmon Embryos, Alevins, and Fry

- Exposed to Variable Thermal and Dissolved Oxygen Regimes. *Transactions of the American Fisheries Society* 135(6):1462–1477.
- Groves, P. A., J. A. Chandler, and T. J. Richter. 2008. Comparison of Temperature Data Collected from Artificial Chinook Salmon Redds and Surface Water in the Snake River. *North American Journal of Fisheries Management* 28(3):766–780.
- Harvey, B. C., R. J. Nakamoto, J. L. White, B. C. Harvey, R. J. Nakamoto, and J. L. W. Reduced. 2006. Streamflow Lowers Dry-Season Growth of Rainbow Trout in a Small Stream Trout in a Small Stream. *Transactions of the American Fisheries Society* 135(4):998–1005.
- Isaak, D. J., and R. F. Thurow. 2006. Network-scale spatial and temporal variation in Chinook salmon (*Oncorhynchus tshawytscha*) redd distributions: Patterns inferred from spatially continuous replicate surveys. *Canadian Journal of Fisheries and Aquatic Sciences* 63(2):285–296.
- Jeffres, C. A., J. J. Opperman, and P. B. Moyle. 2008. Ephemeral floodplain habitats provide best growth conditions for juvenile Chinook salmon in a California river. *Environmental Biology of Fishes* 83:449–458.
- Jensen, A. J., and B. O. Johnsen. 1999. The functional relationship between peak spring floods and survival and growth of juvenile Atlantic Salmon (*Salmo salar*) and Brown Trout (*Salmo trutta*). *Functional Ecology* 13(6):778–785.
- Kaylor, M. J., Justice, C., Armstrong, J. B., Staton, B. A., Burns, L. A., Sedell, E., and S. M. White. *In press*. Temperature, emergence phenology, and consumption drive seasonal shifts in fish growth and production across riverscapes. *Accepted at Journal of Animal Ecology*.
- Lindsay, R. B., W. J. Knox, M. W. Flesher, B. J. Smith, E. A. Olsen, and L. S. Lutz. 1986. Study of wild Spring Chinook Salmon in the John Day River system. Portland, OR.
- Mote, P. W., J. Abatzoglou, K. D. Dello, K. Hegewisch, and D. E. Rupp. 2019. Fourth Oregon Climate Assessment Report - State of climate science: 2019.
- Perry, R. W., J. M. Plumb, and C. W. Huntington. 2015. Using a laboratory-based growth model to estimate mass-and temperature-dependent growth parameters across populations of juvenile Chinook Salmon. *Transactions of the American Fisheries Society* 144(2):331–336.
- Saltveit, S. J., T. Bremnes, and O. R. Lindå. 1995. Effect of sudden increase in discharge in a large river on newly emerged Atlantic salmon (*Salmo salar*) and brown trout (*Salmo trutta*) fry. *Ecology of Freshwater Fish* 4(4):168–174.
- Schindler, D. E., J. B. Armstrong, and T. E. Reed. 2015. The portfolio concept in ecology and evolution. *Frontiers in Ecology and the Environment* 13(5):257–263.



- Skoglund, H., S. Einum, T. Forseth, and B. T. Barlaup. 2012. The penalty for arriving late in emerging salmonid juveniles: Differences between species correspond to their interspecific competitive ability. *Functional Ecology* 26(1):104–111.
- Sommer, T. R., M. L. Nobriga, W. C. Harrell, W. Batham, and W. J. Kimmerer. 2001. Floodplain rearing of juvenile chinook salmon: evidence of enhanced growth and survival. *Canadian Journal of Fisheries and Aquatic Sciences* 58(2):325–333.
- Sparks, M. M., J. A. Falke, T. P. Quinn, M. D. Adkison, D. E. Schindler, K. Bartz, D. Young, and P. A. H. Westley. 2019. Influences of spawning timing, water temperature, and climatic warming on early life history phenology in western Alaska sockeye salmon. *Canadian Journal of Fisheries and Aquatic Sciences* 76:123–135.
- White, S. M., C. Justice, D. A. Kelsey, D. A. McCullough, and T. Smith. 2017. Legacies of stream channel modification revealed using General Land Office surveys, with implications for water temperature and aquatic life. *Elem Sci Anth* 5(0):3.

## Figures

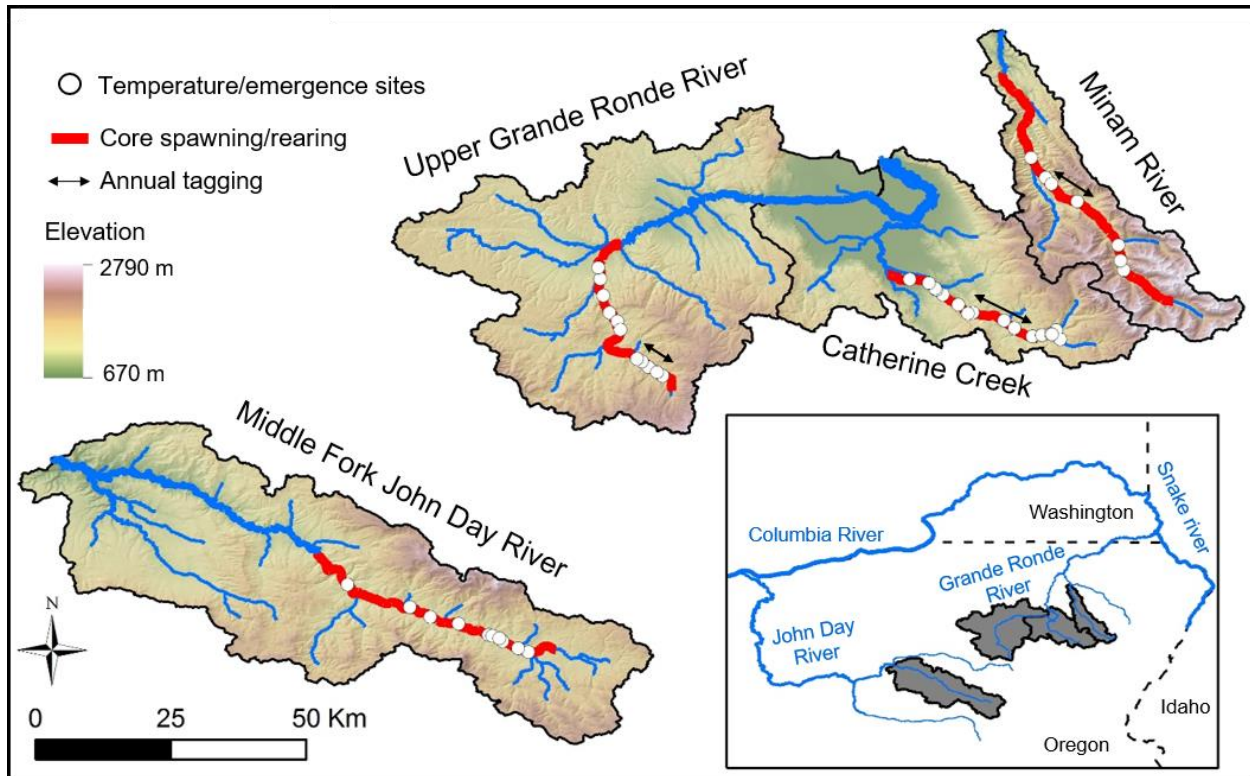


Figure 10: Map of study sites located within four NE Oregon river basins. Open points represent sites with annual temperature data in which emergence timing was predicted. Areas indicated in red represent core spawning and rearing extents of each river. Arrows indicate areas in which annual capture and tagging of juvenile Chinook Salmon occurred (not available for MFJD).

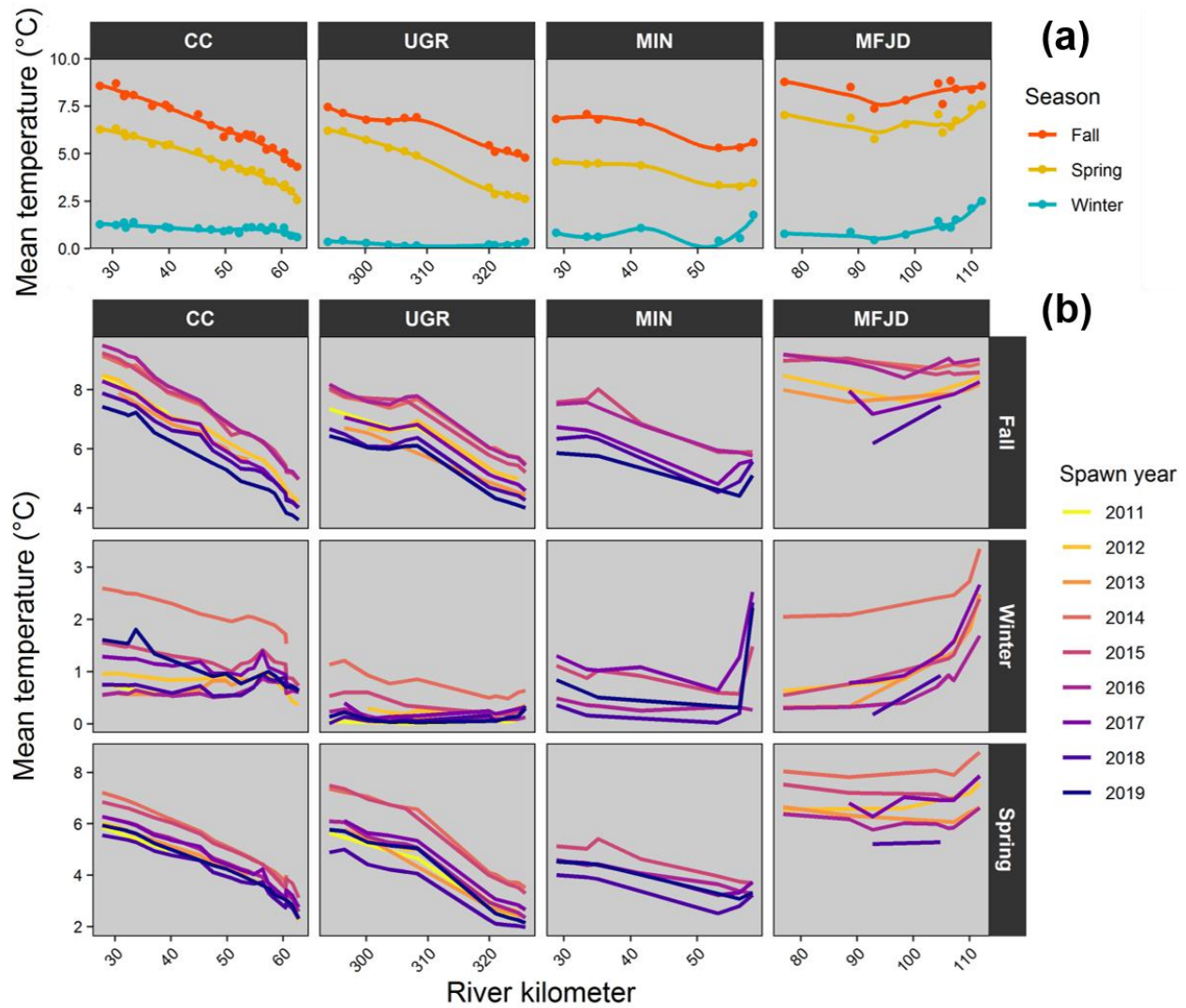


Figure 11: Seasonal temperature profiles within each river during seasons that incubating salmon experience prior to emergence: Fall = September-November; winter = December-February; Spring = March-May. (a) Mean seasonal temperature averaged across all years; (b) mean seasonal temperature in each year.

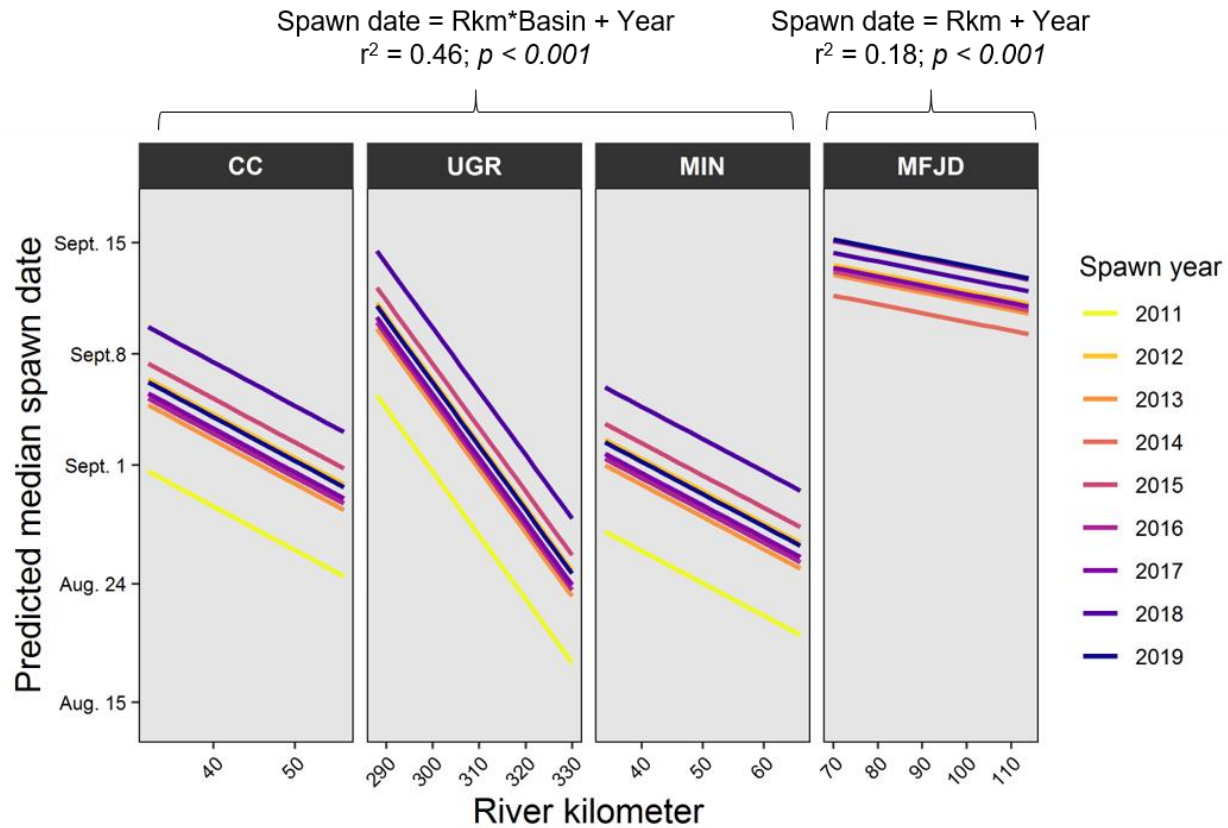


Figure 12: Modeled relationship between river kilometer and median spawn date in each river. Rivers within the Grande Ronde River basin (i.e., CC, UGR, and MIN) were included in a single model to allow for estimation in data poor years. MFJD, located in the John Day River basin, was analyzed separately due to geographic isolation and because Chinook Salmon are in a separate Evolutionary Significant Unit.

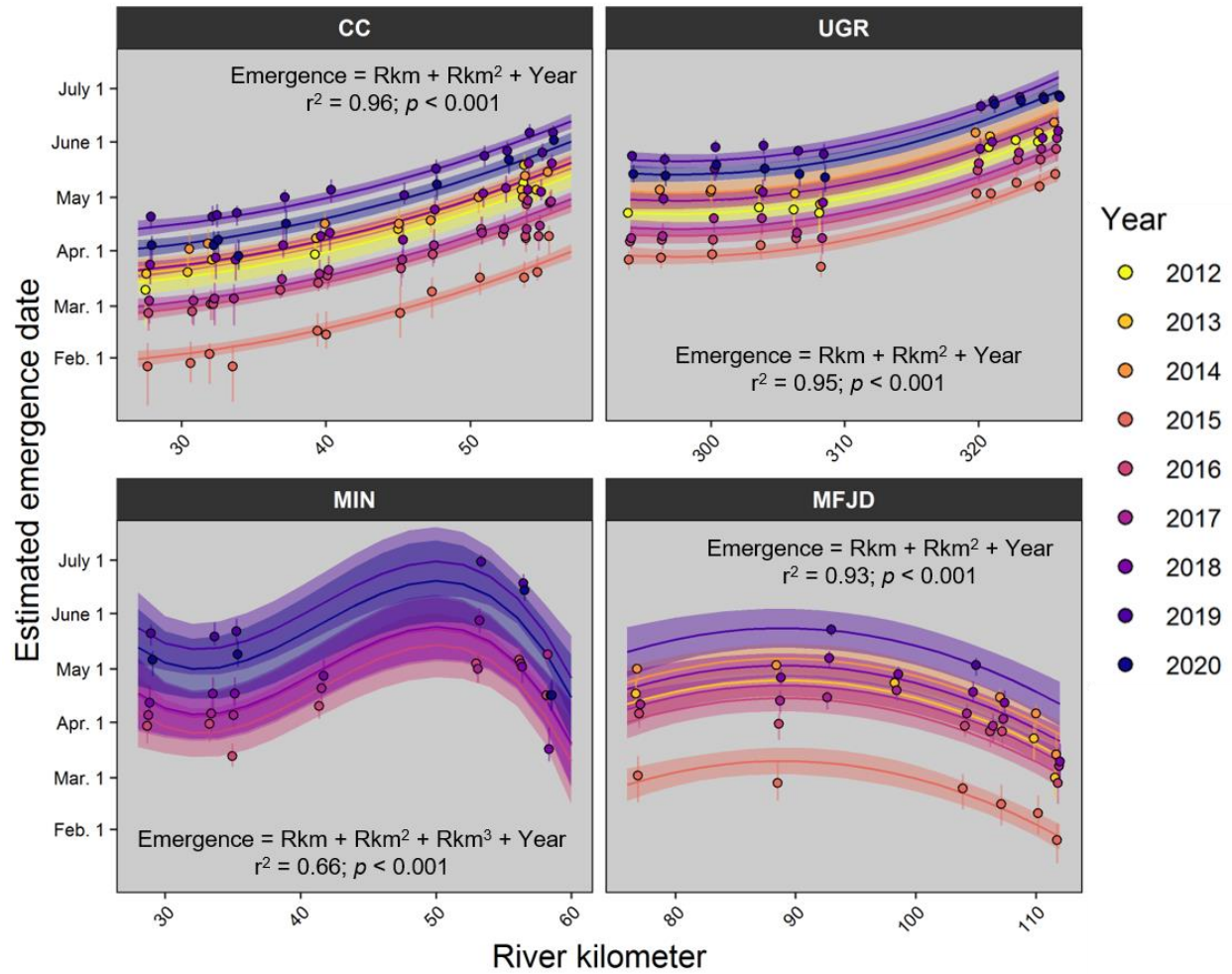


Figure 13: Spatial and temporal patterns of predicted emergence timing in each river. Points indicate sites in which emergence was predicted using annual empirical temperature data; vertical lines indicate the 25<sup>th</sup> and 75<sup>th</sup> percentile of simulated emergence estimates based on variability in spawn timing. Lines and shaded coloring indicate model fit and associated 95% confidence interval.

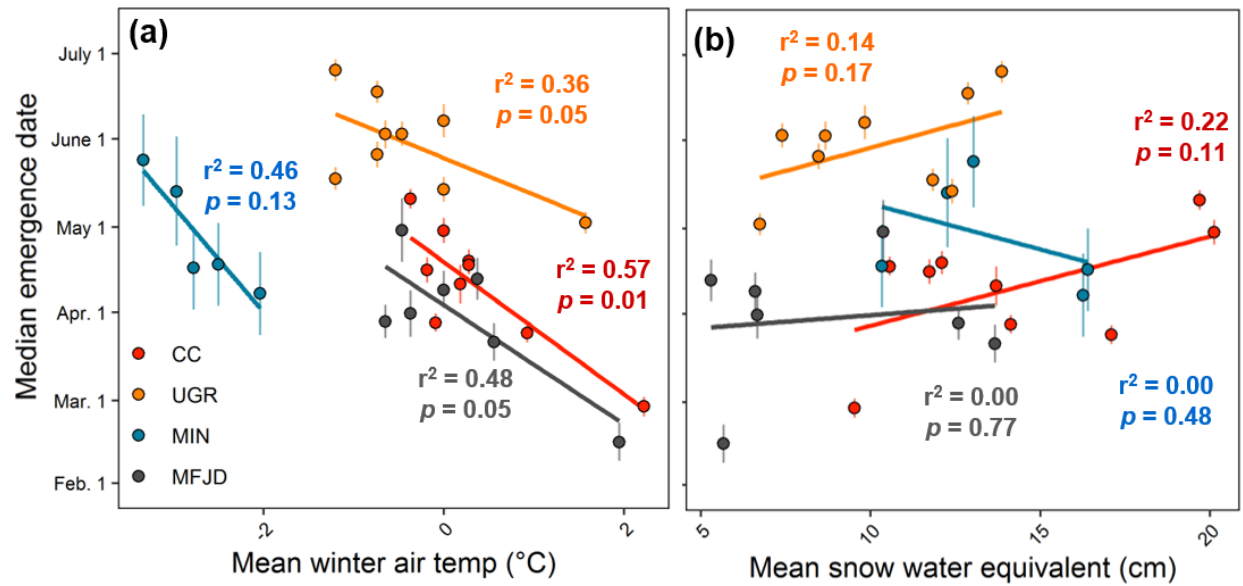


Figure 14: Relationship between mean winter air temperature (October-April) and median emergence timing (a) and between mean snow water equivalent (January-March) and median emergence timing (b). Air temperature and snowpack data were obtained from nearby monitoring stations. Each point represents a year.

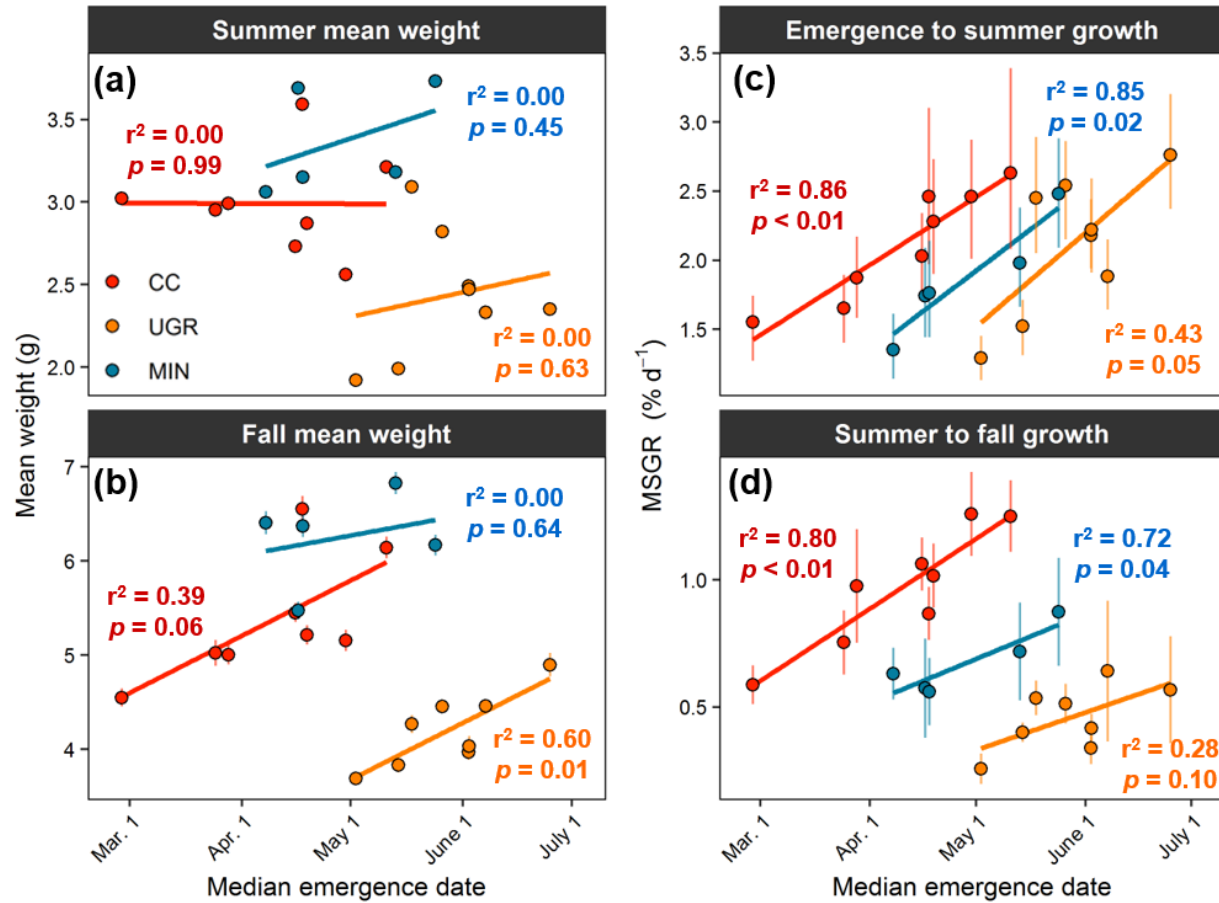


Figure 15: Relationships between estimated median emergence date and summer mean weight (a), fall mean weight (b), estimated mass-standardized growth rates from emergence to summer (c), and empirical growth rates from summer to fall (d). Each point represents a year and vertical error bars represent 95% confidence intervals. Among years, fish were sampled in a consistent location within each basin and at approximately the same dates.



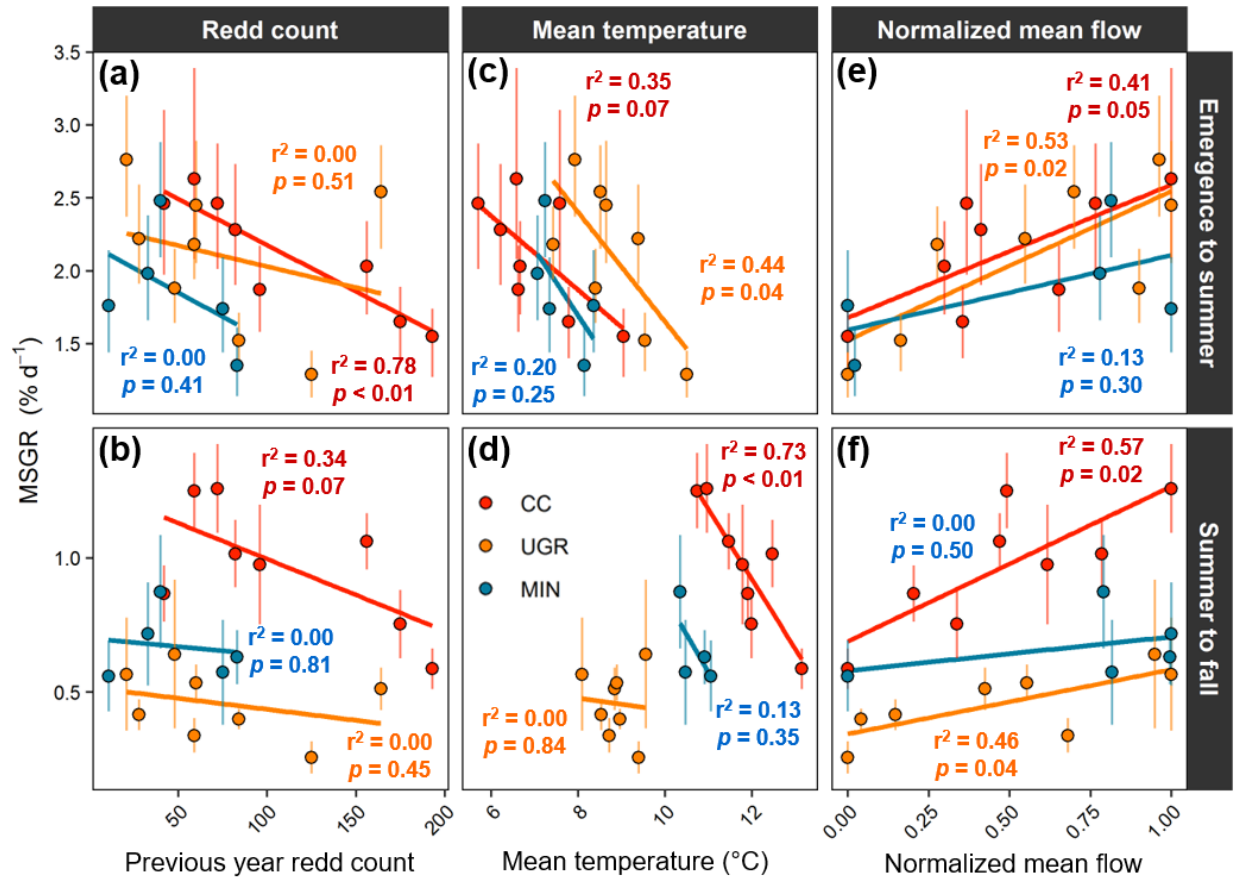


Figure 16: Estimated mass-standardized growth rates from emergence to mid-summer (a,c,e) and from mid-summer to fall (b,d,f) relative to the number of redds from the previous year (a,b), mean spring (c) and summer (d) water temperature, and mean spring (e) and summer (f) flow.



## *2.3 Long-term effects of cattle grazing on benthic macroinvertebrate assemblages*

### **Introduction**

In 2018, an Oregon Watershed Enhancement Board (OWEB)-funded project was initiated in the Middle Fork John Day River (MFJDR) to evaluate long-term effects of various cattle management and restoration treatments. Pre-treatment data was collected between 1996-1998, prior to the implementation and maintenance of treatments beginning in the late 1990s. The project originated from collaborators affiliated with the Confederated Tribes of the Warm Springs Reservation, University of Oregon, and Oregon State University to evaluate changes in (1) floodplain and greenline vegetation, and (2) instream geomorphology and habitat; CRITFC was able to additionally evaluate (3) benthic macroinvertebrate diversity and assemblage structure responses. This summary highlights results from the benthic macroinvertebrate portion of the study, whereas the results of the complete study are available as a project completion report (McDowell et al. 2021).

For all the objectives, change was compared over time (from 1996-1998 to 2018-2019) in the following five management categories:

1. Adaptive grazing: no passive or active restoration. Primary land use is domestic livestock grazing. Individual landowners manage animal numbers, timing, and type of grazing based on annual productivity and expert knowledge of the land
2. Partial passive restoration: reduced domestic livestock grazing in terms of stocking rate, season of use, or duration of grazing
3. Full passive restoration: complete removal of domestic livestock grazing
4. Full passive restoration in combination with active restoration projects
5. Full passive restoration in combination with recent earth-moving active restoration projects that have had limited recovery time. (This category is only used in the floodplain vegetation analysis)

Active restoration projects included constructing instream log structures, planting riparian shrubs, deepening pools, and opening side channels, although the specific elements varied somewhat among sites. Passive restoration projects involved removal of livestock or substantial reduction or changes in livestock grazing and browsing, although wild ungulate (elk and deer) browsing has continued.

### **Methods**

#### *Study area and sample design*

The study area covers approximately 57 km of the MFJDR, extending from Phipps Meadow to near Big Creek (Figure 17). We repeat-sampled several data sets describing vegetation, aquatic

invertebrates, and instream geomorphology and habitat that were first collected in 1996-1998, supplemented by an analysis of pre-restoration historical aerial imagery from 1989. The study area includes both unconstrained (wide floodplains) and constrained (narrow, canyon-like) reaches. Class 1 (large ranches) and Class 4 (retired ranches, now conservation areas) are found almost entirely within unconstrained, wide floodplains, and most of the constrained reaches are under USDA Forest Service management.

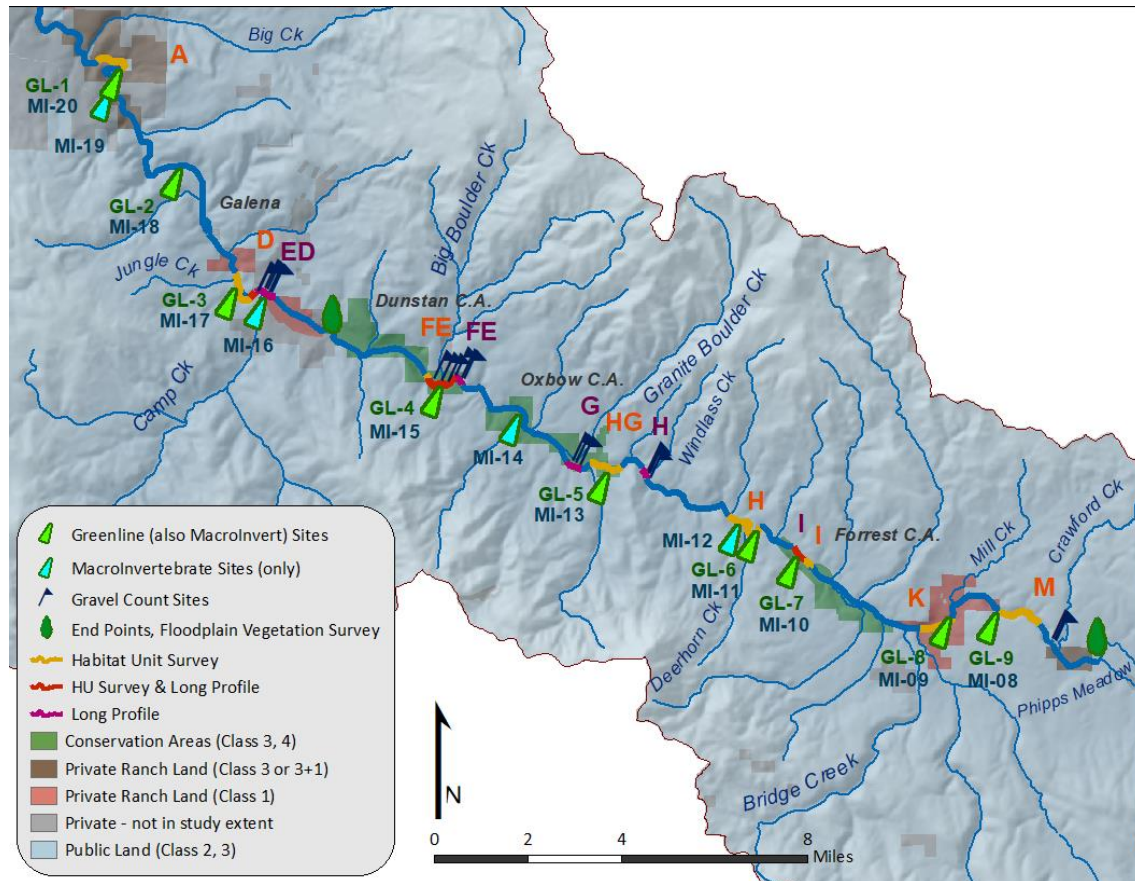


Figure 17. Map of study sites in the Middle Fork John Day River.

### *Field and laboratory sampling*

Benthic macroinvertebrate sampling and laboratory processing in 2018-2019 followed the original study design (Wright 2000). Invertebrate sampling, basic habitat measurements, and observations of fish distributions were conducted mid-summer to match the seasonal timing of temperature and flow conditions of the original study (Table 12; Figure 18). For each reach measuring 100 m in length by centerline, we first conducted a search for large and rare organisms at 6 equally-spaced transects using an Aqua Scope II. We then obtained 1 Surber sample (250  $\mu$ m mesh, 1 m<sup>2</sup> area) from random locations along each of the 6 transects, and combined contents into a single composite sample. Stream discharge, substrate characteristics, predominance of macrophytes, and fish species composition and abundance (via snorkeling) were additionally collected at each reach,

although we only report on the benthic macroinvertebrate data in this document. In 2019, we additionally collected invertebrate drift samples at most sites. Invertebrates from benthic and drift samples were stored in 95% ethanol and delivered to a contractor (Rhithron, Inc., Missoula, MT) for laboratory identification and enumeration at taxa resolution matching that of the original Wright (2000) study.

Table 12. Number of benthic macroinvertebrate samples available for direct comparison (univariate analysis) in the historical (1996-1998) vs. present (2018-2019) time periods by site and management treatment.

Site ID	<i>No. samples</i>		Treatment
	Historical	Present	
580 Pool (MI-10)	1	2	Pass+Act
Big Boulder (MI-15)	3	2	Pass+Act
Big Creek (MI-20)	1	2	Passive
Coyote Bluff (MI-13)	1	2	Pass+Act
Highway 7 (MI-08)	1	2	Part. Passive
Jungle Creek (MI-17)	2	2	Part. Passive
Mill Creek (MI-09)	1	2	Adapt. Man.
RM 22 (MI-18)	2	2	Passive
Scum Pool (MI-11)	3	2	Part. Passive

#### *Data analyses*

Original data from Wright (2000) were compared with the present-day data to evaluate long-term changes in two ways: first, through evaluation of invertebrate diversity as defined by median taxa richness and Ephemeroptera, Plecoptera, and Trichoptera (EPT) richness; and second by multivariate ordination of taxa presence-absence. We chose nonmetric multidimensional scaling (NMDS) as an analysis tool because it handles ecological data well including no assumption of linear relationships among variables. NMDS was performed on presence-absence data from the historical dataset using Sorensen's distance measure (32 samples, 63 taxa). We then employed the NMDS Scores procedure where the historical invertebrate assemblage was used as training data and new scores (18 samples, 52 taxa) were predicted with the original ordination held stable. NMDS and NMDS Scores were performed in PC-ORD v.7 software (McCune and Medford 2016).



Figure 18. Benthic macroinvertebrate sampling in the Middle Fork John Day River including (a) using a Surber sampler, (b) randomizing and marking sampling transect locations, and (c) measuring stream discharge.

## Results

### *Taxonomic diversity*

Benthic macroinvertebrate diversity as measured by taxa richness increased from the historical period to the present in most management treatments, except for Passive+Active where there was little detectable change (Figure 19a). There was only 1 site (Mill Creek) in the Adaptive Management treatment and hence only 1 sample from the historical period for this treatment, but the site was sampled twice in the present era (2018 and 2019) and yielded similar median values of taxa richness (41 taxa) as compared to historical (35 taxa). Benthic macroinvertebrate diversity as measured by EPT richness increased from the historical period to the present in most

management treatments, except for Passive+Active where there was a marked decrease (Figure 19b).

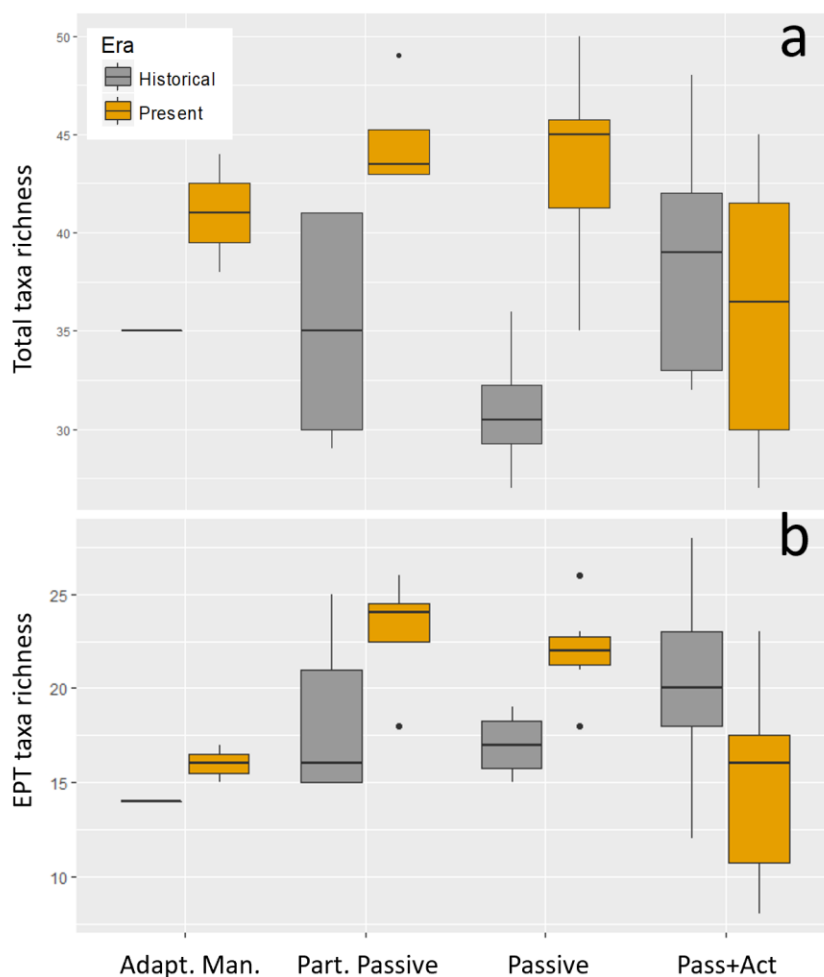


Figure 19. Median richness of (a) overall invertebrate taxa and (b) EPT taxa according to management treatment in the historical and present eras.

### *Assemblage structure*

The NMDS analysis revealed changes in assemblage structure over time, especially in the Passive+Active treatments (Figure 20). NMDS Axis 2 (y-axis) most notably discriminated between the historical and present assemblage structure with the exception of Mill Creek, which harbored an invertebrate assemblage similar to that of the historical period in 2018 (but the 2019 assemblage was consistent with other present samples). Historical samples tended to be represented by Veliidae (water striders), Hydraena (moss beetles), and Peltoperlidae (roach-like stoneflies); whereas samples in the present era tended to be represented by Petrophila (aquatic moths), Brychius (water beetles), and Tricorythidae (crawler mayflies). Additional differences were observed among management treatments in the present era, most notably between the



Passive+Active treatment and all others. Benthic invertebrate assemblages in actively restored sites shifted over time to resemble assemblages in higher elevation sites, as demonstrated by the positive correlation ( $r > 0.2$ ) between site elevation and NMDS axis 1, which discriminated actively restored assemblages from all others.

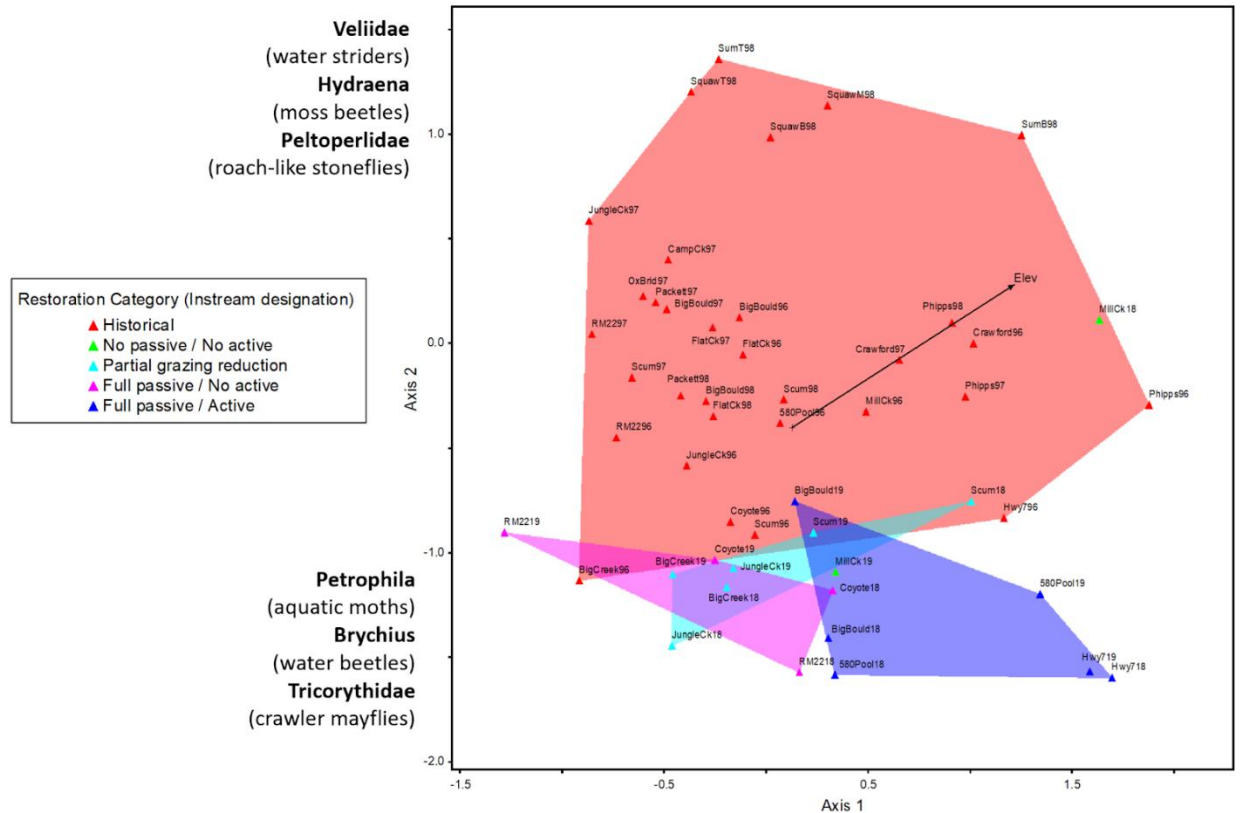


Figure 20. NMDS ordination of benthic macroinvertebrate taxa. Axes are composed of multivariate taxa presence-absence scores and points represent individual sampling events, grouped by historical period or present period according to management action. Biplot shows a positive correlation between site elevation and Axis 1.

## Discussion

Benthic macroinvertebrates are regarded as reliable indicators of changing instream and watershed conditions. Their abundance and composition integrate many environmental factors including various management practices occurring within watersheds (e.g., Irvine et al. 2015). In this study, it was notable that EPT taxa increased from the historical to the present period in most treatments, except for the Passive+Active management treatment where EPT taxa markedly decreased. The overall increase in invertebrate taxa may stem from several factors including succession of stream communities over time, unmeasured changes in land use or climate conditions, or a “lab effect” stemming from differences in laboratory identification or enumeration of taxa. However, evidence against the so-called lab effect consistently biasing our results came in the form of observing a decline in EPT taxa in the Passive+Active treatments. One possible reason for the observed decline

in EPT taxa in the Passive+Active treatment is that active restoration treatments could serve to reset the succession of invertebrate colonization and establishment. While active restoration has been shown to promote aquatic biodiversity in other studies (Miller et al. 2010), additional time may be required for these habitats to reach a mature successional stage. Active restoration furthermore promotes dynamic stream processes such as sorting of gravel and transport of large wood, both of which could increase ecological patchiness and biodiversity at larger scales, but may be associated with less diverse taxa at the site scale.

The general trend of increasing taxa richness over this long time period (1996-2019) corresponded with a concurrent study demonstrating a positive trend in benthic macroinvertebrate observed/expected (O/E) scores in the mainstem MFJDR from 2010-2019 (Saunders et al. 2020). However, the positive trend in O/E scores over time in that study was not statistically significant and was only observed in the mainstem river, with O/E scores in tributary streams (Camp and Lick Creeks) trending downward.

Along with the increasing trend in richness in most treatments, we noted a marked shift in the benthic invertebrate assemblage structure from the historical to the present period. Without further investigation we could not discern a clear pattern in the types of taxa that drove these shifts between the time periods. Likewise, the assemblages in the present-day Passive+Active treatment were markedly different from all other treatments as well as from the historical samples, but the causal drivers of this change cannot be determined without further investigation. One hypothesis suggested by results of both the taxa/EPT richness and assemblage structure analysis is that active restoration may have the effect of shifting site attributes towards upstream conditions, which may harbor lower taxa richness. This interpretation is supported by the association with the shift in actively restored assemblages to those resembling higher elevation assemblages. The effect of active restoration, therefore, would result in shifting benthic macroinvertebrate assemblages to resemble upstream assemblages along a longitudinal river profile as conceptualized in the river continuum concept (Vannote et al. 1980), in which narrower, upstream reaches are likely to have relatively greater input of organic material from stream-side vegetation.

Next steps outside the scope of this report include conducting a trait-based ordination of macroinvertebrate community to help understand which ecological characteristics of invertebrates responded to land use practices and other changes over time; analysis of invertebrate drift data (collected in 2019 only) to evaluate whether food quality and quantity for stream-dwelling fish (e.g., salmonids) differs among treatments; and analysis of fish assemblage data that was collected anecdotally alongside macroinvertebrates.

### *Management recommendations*

Until further analyses beyond the scope of this report are completed, we do not expect that findings from the macroinvertebrate portion of this study can provide specific management

recommendations for the Middle Fork John Day River. However, it is well understood from numerous other studies that benthic macroinvertebrates are sensitive to stream habitat quality, especially fine sediments, and that fine sediments are in turn increased with cattle grazing intensity. Our results did not point to a detrimental impact of cattle grazing management strategies on benthic macroinvertebrate communities over long time periods, but this interpretation is preliminary and warrants further investigation. We can, however, make recommendations for future invertebrate monitoring in the project area to help discern the effects of land management strategies on overall stream health.

Recommendations for future invertebrate monitoring include:

- Continue monitoring benthic macroinvertebrates on an annual or semi-annual basis at the reaches using the methods from the original Wright (2000) study, including expansion into the smaller tributary sites from the historical study that were not sampled in 2018-2019;
- Continue monitoring invertebrate drift samples at the historical sites although this was not an original component of Wright (2000);
- Include pan traps or other sampling for terrestrial invertebrates in monitoring the historical sites, as terrestrial invertebrates should represent a more immediate response to riparian conditions altered by cattle grazing;
- Include fish diet sampling in the monitoring at historical sites to evaluate food quantity and quality, which can be used in bioenergetics models or other analyses discerning the impact of energy intake on fish distribution, growth, and survival; and
- Finally, coordinate the invertebrate monitoring recommendations above (benthic, drift, terrestrial, and diet) with each other and with other fish and habitat studies in the watershed in a robust statistical design that can be evaluated over annual and decadal time scales.

## References

- Irvine, K.M., S.W. Miller, R.K. Al-Chokhachy, E.K. Archer, B.B. Roper, and J.L. Kershner. 2015. Empirical evaluation of the conceptual model underpinning a regional aquatic long-term monitoring program using causal modelling. *Ecological Indicators* 50: 8–23.
- McCune, B. and M.J. Mefford. 2016. PC-ORD. Multivariate Analysis of Ecological Data. Version 7. MjM Software Design, Gleneden Beach, Oregon, U.S.A.
- McDowell, P., M. Goslin, L. Ellsworth, and S.M. White. 2021. Long-term ecological effects of passive restoration in the Middle Fork John Day. Final Technical Report completed for Oregon Watershed Enhancement Board Project #218-6041.
- Miller, S.W., P. Budy, and J.C. Schmidt. 2010. Quantifying macroinvertebrate responses to in-stream habitat restoration: Applications of meta-analysis to river restoration. *Restoration Ecology* 18(1): 8–19.



- Saunders, W.C., J.V. Ojala, and R.V. Wagenen. 2020. Stream habitat condition for sites managed by the Oregon Watershed Enhancement Board (Amended for aquatic macroinvertebrates, February 2021). PacFish/InFish Biological Opinion (PIBO) Monitoring Program, USDA Forest Service, Logan, UT.
- Vannote, R. L., G. W. Minshall, K. W. Cummins, J. R. Sedell, and C. E. Cushing. 1980. The river continuum concept. *Canadian Journal of Fisheries and Aquatic Sciences* 37: 130–37.
- Wright, K.K. 2000. From continua to patches: Longitudinal patterns in the Middle Fork John Day River, Oregon. PhD Dissertation, Oregon State University, Corvallis, OR.

### 3.0 Fish-Habitat Modeling

#### *3.1 Developing an index of Chinook Salmon parr capacity in the Grande Ronde River basin*

##### **Introduction**

Despite considerable resources dedicated to restoration and monitoring of freshwater habitat conditions in the Columbia River basin, the collective benefits of past restoration actions as well as projected future impacts on salmon productivity and capacity remain unclear. Life cycle models are commonly used to evaluate the impact of alternative management and climate scenarios on salmon population viability, but these models require an accurate understanding of the environmental and biotic factors affecting productivity and capacity at different life stages. While recent life cycle modeling efforts have made considerable progress towards incorporating habitat restoration into model simulations (Pess and Jordan 2019, Crozier et al. 2021), freshwater dynamics are often represented by a single factor such as water temperature or habitat area and could be improved by evaluating a broader suite of habitat features that are commonly targeted by restoration practitioners (e.g., pool habitat, woody debris, off-channel habitat, and water temperature). Toward this aim, we used generalized linear mixed-effects modeling to analyze the relationship between freshwater habitat conditions and abundance of Chinook Salmon summer parr measured across 125 sites over seven years (2011-2017; 304 unique observations) in the Grande Ronde River basin in NE Oregon. The model was used to predict mean fish density (no. · 100m<sup>-1</sup>) throughout the current range of Chinook Salmon in the upper Grande Ronde and Wallowa River basins using spatially continuous ground-based habitat measurements from the Oregon Department of Fish and Wildlife's (ODFW) Aquatic Inventories Project (AqI; Moore et al. 2019) combined with modeled water temperature (NorWeST; Isaak et al. 2017) and other remotely-sensed data. Model predictions will be used as a weighting factor to compute total weighted usable habitat for rearing Chinook Salmon parr within each population of interest. This index of summer parr rearing capacity is intended be used in ongoing life cycle modeling efforts to evaluate population-level fish response to alternative management scenarios.

##### **Methods**

We used paired snorkel and habitat survey data collected at 125 sites in the upper Grande Ronde River, Catherine Creek and Minam River basins in NE Oregon between 2011 and 2017, totaling 304 unique site-year observations (Figure 21). Sites were randomly selected using a spatially balanced generalized random-tessellation stratified design (GRTS; Stevens and Olsen 2004) as part of the Columbia Habitat Monitoring Program (CHaMP 2016). Site length was approximately twenty times the bankfull channel width, ranging from 98 – 640 m (mean = 269 m). Each site was repeatedly surveyed every 1-3 years (i.e., repeated measures design) with the intent of assessing status and trends in fish habitat conditions.

Snorkel surveys were used to count Chinook Salmon parr during summer (July 1 – September 15) at each site using methods described in White et al. (2012). We expanded snorkel counts to total abundance using a Bayesian detection probability model based on local paired snorkel counts and mark-recapture abundance estimates (Staton et al. *in review*). Abundance estimates were converted to linear density ( $\text{no.} \cdot 100\text{m}^{-1}$ ) to account for differences in stream size across sites.

We selected a limited set of environmental covariates representing *a priori* hypotheses about the ecological processes influencing Chinook parr abundance (Table 13). Ground-based measurements from CHaMP were limited to four predictor variables (i.e., pools, wood, off-channel habitat, and water temperature) that were both biologically plausible and available as spatially continuous data from other data sources (i.e., Aquatic Inventories Program (AqI) and NorWeST). Metrics generated from remotely-sensed data (i.e., mean annual flow, gradient, and base flow index) were used to characterize differences in intrinsic channel characteristics that may have a strong influence on fish distribution but are minimally influenced by land use management. Mean annual flow and large wood frequency were log transformed (natural logarithm) prior to model fitting to correct for right skew in the covariate data and because we hypothesized an asymptotic relationship with fish density. A quadratic term for stream gradient was included based on observed patterns in the model residuals.

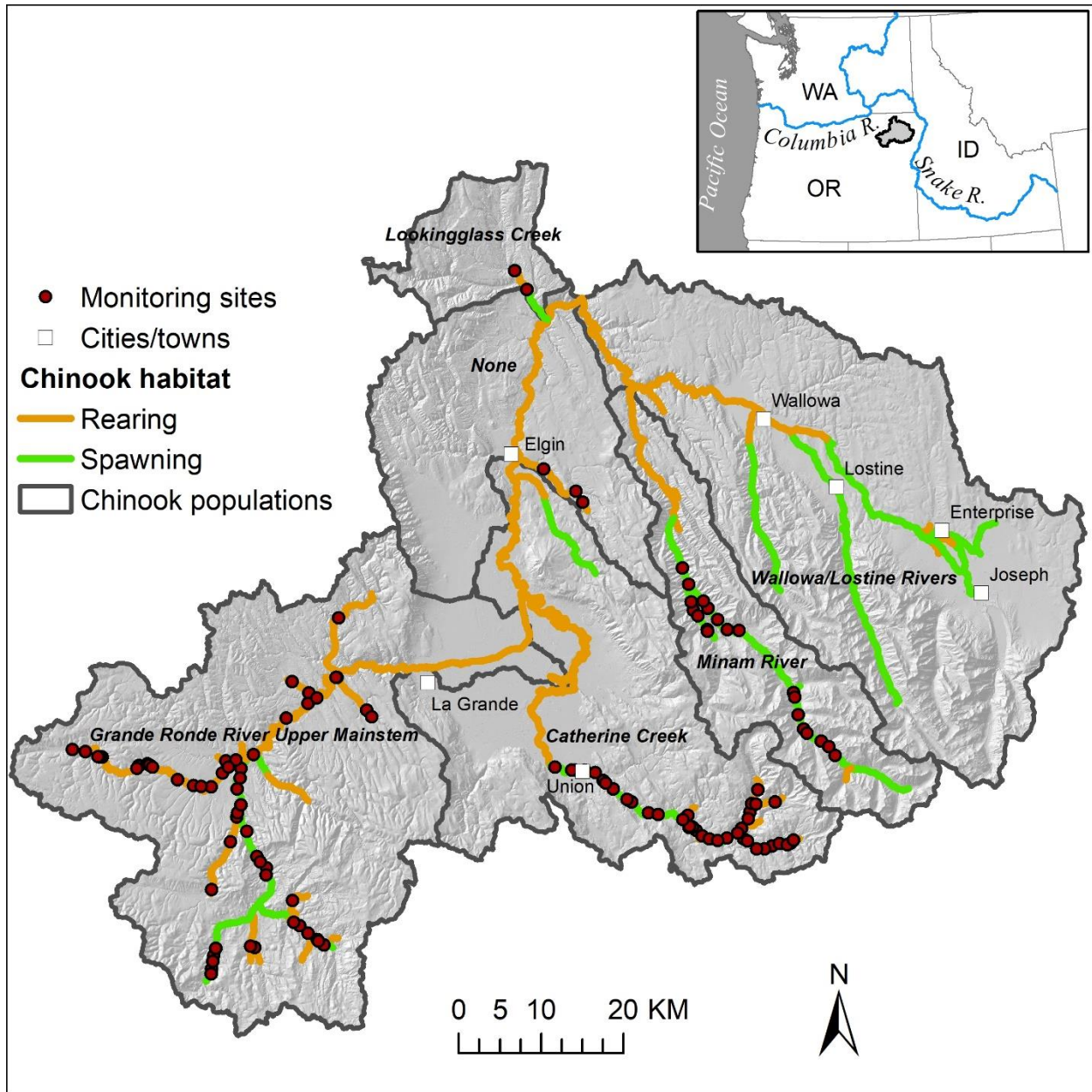


Figure 21. Map of study area showing 125 unique monitoring sites within the upper Grande Ronde and Minam River basins.

Table 13. Summary of fixed-effect covariates used in model fitting.

Covariate	Description	Data source
<i>BFI</i>	Base flow index. The ratio of baseflow to total flow, expressed as a percentage, within the watershed.	StreamCat database; Hill et al. (2016).
<i>Grad</i>	Stream gradient express as a percentage (%)	NetMap (2020)
<i>Grad2</i>	Stream gradient squared (for fitting quadratic curve)	NetMap (2020)
<i>LogLWFreq</i>	Log transformed number of large wood pieces ( $\geq 0.15$ m diameter and $\geq 3$ m length) per 100 meters within the bankfull channel	Model fitting data from CHaMP (2016). Prediction data from Aquatic Inventories Program (Moore et al. 2019).
<i>LogMAQ</i>	Log transformed mean annual flow in cubic meters per second (cms)	National Water Model Retrospective Analysis Dataset (NOAA 2019)
<i>MWMT</i>	Maximum weekly maximum water temperature ( $^{\circ}\text{C}$ ), or maximum seven-day running average of the daily maximum temperature. Missing values from CHaMP were filled in with modeled data from NorWeST model.	Model fitting data from CHaMP (2016). Prediction data from NorWeST model (Isaak et al. 2017).
<i>PIFreq</i>	Number of medium pools ( $> 0.5$ m max depth and $> 20$ m <sup>2</sup> surface area) per kilometer stream length	Model fitting data from CHaMP (2016). Prediction data from Aquatic Inventories Program.
<i>RCI</i>	River channel complexity index (RCI) = $S*(1+J)$ where $S$ = stream sinuosity, $J$ = # of side channel junctions	Model fitting data from CHaMP (2016). Prediction data from Aquatic Inventories Program. Metric definition from Brown (2002).

Spatially continuous covariate data from various publicly available data sources was used to make model predictions across the network where paired fish-habitat data was not available. The 1:24K scale National Hydrography Dataset Plus High Resolution stream layer (NHDPlus HR; USGS 2020) was used as the basis for summarizing habitat attributes and storing model predictions. We divided the NHDPlus HR layer into reaches with lengths approximately 20 times the modeled bankfull width, where bankfull width was calculated from regional hydraulic geometry curves (Clarke et al. 2008).

Channel unit scale data from the Aquatic Inventories Program (AqI) collected between 1991 and 2018 were used to characterize pool and wood frequencies throughout most of the Chinook bearing portions of our study area. We used ArcGIS (ESRI 2020) to join attributes from the AqI dataset to

the overlapping NHDPlus HR reaches. The most recent AqI survey from each location was selected to represent current habitat conditions. To ensure AqI and CHaMP wood and pool metrics were as comparable as possible, we recomputed these metrics from the raw data sources using consistent quantitative criteria (Table 13). In addition, a cross-walk analysis comparing selected CHaMP and AqI habitat metrics (i.e., pools and wood) found good general agreement between the two datasets (unpublished analysis, Seth White, CRITFC, *pers. comm.*).

We used maximum weekly maximum water temperature (*MWMT* °C) predictions (i.e., the maximum seven-day running average of daily max temperature) from the NorWeST model (Isaak et al. 2017) to characterize peak summer water temperatures. Prediction points, which were spaced approximately one kilometer apart, were joined to the nearest NHDPlus HR reach in ArcGIS. A comparison of NorWeST predictions with empirical measurements of *MWMT* from the Columbia Habitat Monitoring Program (CHaMP 2016) at 184 unique site/year observations in the Grande Ronde basin indicated the model was reasonably accurate with an  $R^2$  of 0.77 and median absolute error of 2 °C.

### *Statistical analysis*

The count of juvenile Chinook Salmon per 100 meters for each observation  $i$  ( $y_i$ ) was modeled using a negative binomial mixed-effects model, with random effects for site ( $j$ ) and year ( $k$ ). Model fitting was implemented with the ‘glmmTMB’ package using R statistical software (R Core Team 2020). Negative binomial regression was used to account for over-dispersion in the count data which precluded the use of standard Poisson regression. Initially we fit a “global model” using the full set of fixed-effect covariates and random effects. The linear predictor had the form:

$$\begin{aligned} \log(\mu_i) = & \beta_0 + \beta_1 BFI_i + \beta_2 Grad_i + \beta_3 Grad2_i \\ & + \beta_4 LogLWFreq_i + \beta_5 LogMAQ_i + \beta_6 MWMT_i \\ & + \beta_7 PlFreq_i + \beta_8 RCI_i + \varepsilon_{j[i]} + \gamma_{k[i]}. \end{aligned}$$

This equation produces the expected count for observation  $i$ , from which we assume  $y_i$  is a random deviate:

$$y_i \sim \mathcal{NB}(\mu_i, \alpha)$$

where:

- $\mu_i$  is the expected count for observation  $i$ , where ( $i = 1, 2, \dots, n_i = 304$ ), which occurred in site  $j[i]$  and year  $k[i]$ , of which there are  $n_j = 125$  and  $n_k = 7$ , respectively,
- $BFI_i$ ,  $Grad_i$ ,  $Grad2_i$ ,  $LogLWFreq_i$ ,  $LogMAQ_i$ ,  $MWMT_i$ ,  $PlFreq_i$ , and  $RCI_i$  are fixed-effect covariates for observation  $i$ , as described in Table 13,
- $\varepsilon_{j[i]}$  is a site random effect for observation  $i$ ; we assume that  $\varepsilon_j \sim \mathcal{N}(0, \sigma_\varepsilon^2)$ ,
- $\gamma_{k[i]}$  is a year random effect for observation  $i$ ; we assume that  $\gamma_k \sim \mathcal{N}(0, \sigma_\gamma^2)$ , and

- $\alpha$  is the dispersion parameter of the negative binomial distribution, common to all  $n_i$  observations, where  $Var(y_i) = \mu_i(1 + \alpha)$ .

We generated a set of candidate models consisting of all possible additive combinations of the fixed-effect covariates from the global model using the ‘dredge’ function from the MuMIn package (Barton 2020). Random effects for site and year were included in each of the candidate models to account for lack of independence among observations arising from the repeated measures survey design as well as year-specific variability not captured by the fixed-effects. Models were compared using Akaike’s Information Criterion corrected for small sample size (AICc) with AICc differences ( $\Delta AICc$ )  $< 2$  representing strong support as the best fitting model,  $\Delta AICc$  between 4 and 7 indicating considerably less support, and  $\Delta AICc > 10$  indicating essentially no support (Burnham and Anderson 2002).

We assessed the relative importance of predictor variables in part by calculating the summation of AICc weights (SW) over all models that contained each variable of interest (Burnham and Anderson 2002), with SW values closest to one indicating higher variable importance. Additionally, we used coefficient z-values—calculated as the parameter estimate divided by the standard error—to assess general variable importance, assuming that parameters with higher z-values (i.e., higher effect size relative to the parameter uncertainty) would have a greater influence on predicted fish density.

Goodness-of-fit of the global and best fitting models was assessed using residual diagnostic plots generated with the DHARMA package (Hartig 2020). The proportion of variance explained by each model (pseudo- $R^2$ ) was computed using methods described in Nakagawa and Schielzeth (2013) and implemented in package MuMIn. Specifically, the marginal pseudo-coefficient of determination ( $R_m^2$ ) represents the proportion of variance explained by the fixed effects in the model.

## Results and Discussion

Observed Chinook Salmon parr densities (fish  $\cdot$  100m<sup>-1</sup>) throughout the study area ranged widely from 0 to 2,560 (mean = 136), with the highest densities occurring in the Minam River wilderness area. Approximately 36% of the observation sites did not have any Chinook Salmon present, likely resulting from low seeding by spawning adults and suboptimal rearing conditions throughout much of the study area.

The best fitting model predicting fish density included mean annual flow, gradient, large wood frequency, maximum weekly maximum water temperature (*MWMT*), pool frequency, and base flow index as fixed-effect predictor variables (Table 14). The strongest competing model ( $\Delta AICc = 0.2$ ) included river complexity index (*RCI*) in addition to all covariates from the top model. No other models were considered strong competing models among the candidate set ( $\Delta AICc > 4$ ).

Residual diagnostic plots and goodness-of-fit tests for the global model and best fitting model indicated good correspondence with model assumptions (i.e., uniform distribution of residuals, homogeneity of variance in the y direction, no over- or under-dispersion). The fixed-effect covariates from the best fitting model explained approximately 82% of the variability in observed fish density (Table 14). Random effect standard deviations for *Site* and *Year* from the best fitting model were 0.45 and 0.48, respectively, suggesting moderately large variability associated with site and year after accounting for differences in fixed-effect covariates such as flow and temperature.

Variable importance, expressed as a summation of AICc weights (*SW*) from all candidate models, was relatively high ( $SW \geq 0.95$ ) for all predictor variables except *RCI* ( $SW = 0.48$ ). Similarly, covariate standardized effect size (*z*-values) from the global model indicated that mean annual flow had the strongest influence on predicted fish density (*z*-value = 6; Table 15), *RCI* had a relatively small influence (*z*-value = 1.4), while all other covariates had a moderate, albeit important, influence on fish density (*z*-value range = 2.2 – 3.4). All model coefficients from the global model except for the intercept and *RCI* were statistically significant ( $P < 0.05$ ). Because there were only two models with strong support based on AIC, and the second-best model contained an additional parameter (*RCI*) that was both non-significant and had minimal effect size, we chose to base model predictions on the more parsimonious top model (Table 15).

Modeled relationships between physical habitat variables and fish density were biologically plausible in their direction and magnitude, although there was considerable uncertainty in the predictions as evidenced by the relatively wide confidence intervals around the mean (Figure 22). Fish density was positively associated with mean annual flow, with mean predicted density across all sites and years increasing non-linearly from approximately 15 to 441 fish · 100m<sup>-1</sup> over the range of observed flows (Figure 22). Stream gradient had a slight positive influence on mean fish density up to a gradient value of about 1.5%, after which densities declined and approached near zero at gradients exceeding about 6%. Base flow index (*BFI*) was positively associated with fish density, with predicted mean density increasing by about 180 fish · 100m<sup>-1</sup> across the range of observed *BFI* values (55-69%). Water temperature had a pronounced negative influence on fish density, with predicted mean density declining from about 400 to 64 fish · 100m<sup>-1</sup> as maximum weekly temperatures increased from 12.5 to 29.5 °C. In contrast, pool frequency had a positive effect on fish density with mean densities increasing by about 365 fish · 100m<sup>-1</sup> as pool frequency increased from 0 to 47 pools · km<sup>-1</sup>. Finally, large wood positively influenced mean fish density, with the steepest increases in fish density occurring between wood frequencies of 0 and 10 pieces per 100 meters, with minimal additional gains in density beyond that.

Patterns in predicted mean fish density across the network based on out-of-sample habitat data from the most recent ODFW AqI surveys and recent 10-year average (2006-2015) flow and temperature predictions from regional flow and temperature models show substantially higher predicted fish density in the Minam and Wallowa/Lostine populations compared with other



portions of the basin (Figure 23). These findings are generally consistent with higher base flows, cooler water temperatures, and more intact physical habitat conditions in these parts of the basin. Projected densities in the upper Grande Ronde and Catherine Creek populations seem reasonable in the many portions of these watersheds, but fish densities appear to be overpredicted in the lower reaches near the Grande Ronde Valley where Chinook rearing is known to be very low or non-existent due in part to very high water temperatures and substantial water withdrawals during summer. In contrast, density predictions in the headwaters of the upper Grande Ronde River where water temperatures are cooler and pool densities are relatively high, appear to be lower than expected.

One reason for the apparent model inaccuracies in some portions of the study area could be that NorWeST model predictions of MWMT in the Grande Ronde basin are biased high (median error = 1.7 °C). Refitting the fish density model using Average August water temperature predictions from NorWeST, which were not found to be unbiased (median error = 0.1 °C), could possibly improve out-of-sample model accuracy. Additionally, the model doesn't account for location or density of spawners in the previous year, which could result in overpredictions of fish abundance in locations far from currently used spawning habitats. However, using current spawning density or redd distribution as a covariate in the model would be problematic for projecting the outcome of future restoration or climate scenarios because spawner abundance and distribution would also likely change in the future. Finally, incorporating spatial autocorrelation into the model using spatial statistical network modeling (SSN ; Ver Hoef et al 2006) could potentially improve model accuracy and may be explored in the future.

This model provides an index of summer parr rearing capacity which can be used in ongoing life cycle modeling efforts to evaluate potential fish response to restoration and climate scenarios. Next steps include converting the fish density predictions from this model to an estimate of weighted usable habitat, and then summing all weighted usable habitat within each population area that is assessed in the life cycle model—currently upper Grande Ronde River, Catherine Creek, Minam River, and Lostine River. Additionally, we plan to work closely with partners in the basin to develop realistic restoration scenarios reflecting planned near-term restoration actions as well as idealized future scenarios (e.g., complete restoration to reference conditions). This approach offers a direct tool for evaluating how spatially explicit alterations of commonly targeted habitat features (pools, wood, temperature) could translate into changes in juvenile fish abundance, and ultimately, population viability. This method of developing an index of parr carrying capacity will be compared with alternative approaches such as pool equivalent units (Pess and Jordan 2019) and estimates of carrying capacity from a quantile random forest model (See et al. 2021) to evaluate its utility for life cycle model projections.

## References

- Barton, K. 2020. MuMIn: Multi-Model Inference. R package version 1.43.17. <https://CRAN.R-project.org/package=MuMIn>.
- Brown, A. G. 2002. Learning from the past: palaeohydrology and palaeoecology. *Freshwater Biology* 47(4):817–829.
- Burnham, K. P., and D. R. Anderson. 2002. Model selection and multimodel inference, a practical information-theoretic approach. Second edition. Springer-Verlag New York, Inc., New York, NY.
- CHaMP (Columbia Habitat Monitoring Program). 2016. Scientific protocol for salmonid habitat surveys within the Columbia Habitat Monitoring Program.
- Clarke, S. E., K. M. Burnett, and D. J. Miller. 2008. Modeling Streams and Hydrogeomorphic Attributes in Oregon From Digital and Field Data1. *JAWRA Journal of the American Water Resources Association* 44(2):459–477.
- Crozier, L. G., B. J. Burke, B. E. Chasco, D. L. Widener, and R. W. Zabel. 2021. Climate change threatens Chinook salmon throughout their life cycle. *Communications Biology* 4(1):222.
- ESRI 2020. ArcGIS Desktop: Release 10.8. Redlands, CA: Environmental Systems Research Institute.
- Hartig, F. 2020. DHARMA: Residual Diagnostics for Hierarchical (Multi-Level / Mixed) Regression Models. R package version 0.3.2.0. <https://CRAN.R-project.org/package=DHARMA>.
- Hill, R. A., M. H. Weber, S. G. Leibowitz, A. R. Olsen, and D. J. Thornbrugh. 2016. The Stream-Catchment (StreamCat) Dataset: A Database of Watershed Metrics for the Conterminous United States. *JAWRA Journal of the American Water Resources Association* 52(1):120–128.
- Isaak, D. J., S. J. Wenger, E. E. Peterson, J. M. Ver Hoef, D. E. Nagel, C. H. Luce, S. W. Hostetler, J. B. Dunham, B. B. Roper, S. P. Wollrab, G. L. Chandler, D. L. Horan, and S. Parkes-Payne. 2017. The NorWeST Summer Stream Temperature Model and Scenarios for the Western U.S.: A Crowd-Sourced Database and New Geospatial Tools Foster a User Community and Predict Broad Climate Warming of Rivers and Streams: Stream climates in the Western U.S. *Water Resources Research* 53(11):9181–9205.
- Moore, K., K. Jones, J. Dambacher, C. Stein, and et al. 2019. Aquatic Inventories Project: methods for stream habitat and snorkel surveys. Page 89. Oregon Department of Fish and Wildlife, Version 29.1, Corvallis, OR.

- Nakagawa, S., and H. Schielzeth. 2013. A general and simple method for obtaining  $R^2$  from generalized linear mixed-effects models. *Methods in Ecology and Evolution* 4(2):133–142.
- NetMap. 2020. NetMap Tools, ArcMap 10.X Add-in Module, Version 3.2.0. Developed by Terrain Works. [http://www.netmaptools.org/Pages/NetMapHelp/technical\\_help.htm](http://www.netmaptools.org/Pages/NetMapHelp/technical_help.htm).
- NOAA (National Oceanic and Atmospheric Administration). 2019. NOAA National Water Model Reanalysis Model Data version 2.0. Accessed from <https://registry.opendata.aws/nwm-archive/>. Downloaded on October 2019.
- Pess, G., and C. E. Jordan. 2019. Characterizing watershed-scale effects of habitat restoration actions to inform life cycle models: case studies using data-rich vs. data-poor approaches. U.S. Department of Commerce, NOAA Technical Memorandum NMFS-NWFSC-151.
- R Core Team. 2020. R: A language and environment for statistical computing. R Foundation for Statistical Computing, Vienna, Austria. URL <https://www.R-project.org/>.
- See, K. E., M. W. Ackerman, R. A. Carmichael, S. L. Hoffmann, and C. Beasley. 2021. Estimating carrying capacity for juvenile salmon using quantile random forest models. *Ecosphere* 12(3).
- Staton, B.A., C. Justice, S. White, E.R. Sedell, L.A. Burns, M.J. Kaylor. *In review*. Accounting for uncertainty when estimating drivers of detection probability: a hierarchical approach illustrated with snorkel surveys for riverine fishes. Submitted to *Fisheries Research*.
- Stevens, D. L., and A. R. Olsen. 2004. Spatially balanced sampling of natural resources. *American Statistical Association* 99(465):262–278.
- USGS (U.S. Geological Survey). 2020. National Hydrography Dataset Plus High Resolution (NHDPlus HR), accessed June 16, 2020 at URL <https://www.usgs.gov/core-science-systems/ngp/national-hydrography/access-national-hydrography-products> White, S., Justice, C., & McCullough, D.. 2012. Protocol for Snorkel Surveys of Fish Densities. Columbia River Inter-Tribal Fish Commission : <https://www.monitoringmethods.org/Protocol/Details/499>
- Ver Hoef, J. M., E. Peterson, and D. Theobald. 2006. Spatial statistical models that use flow and stream distance. *Environmental and Ecological Statistics* 13(4):449–464.

Table 14. Model selection table showing candidate models with Akaike difference ( $\Delta AICc$ ) less than ten.

Fixed-effect coefficients									DF	LogLik	AICc	$\Delta AICc$	Weight	$R_m^2$
<i>Int</i>	<i>BFI</i>	<i>LogLWFreq</i>	<i>LogMAQ</i>	<i>MWMT</i>	<i>Grad</i>	<i>Grad2</i>	<i>PlFreq</i>	<i>RCI</i>						
-0.088	0.082	0.266	0.844	-0.106	0.643	-0.201	0.032	NA	11	-1269.5	2561.9	0.0	0.48	0.82
0.099	0.080	0.254	0.849	-0.112	0.662	-0.202	0.029	0.064	12	-1268.5	2562.1	0.2	0.43	0.81
-0.020	0.089	NA	0.766	-0.123	0.799	-0.230	0.035	0.080	11	-1272.8	2568.6	6.7	0.02	0.78
6.305	NA	0.281	1.087	-0.183	0.784	-0.209	0.027	0.076	11	-1273.0	2568.9	7.0	0.01	0.78
-0.138	0.092	NA	0.762	-0.120	0.797	-0.231	0.038	NA	10	-1274.2	2569.1	7.3	0.01	0.77
6.337	NA	0.292	1.096	-0.181	0.778	-0.208	0.030	NA	10	-1274.2	2569.2	7.4	0.01	0.77
-5.653	0.133	0.267	0.679	NA	0.755	-0.212	0.037	NA	10	-1274.4	2569.5	7.6	0.01	0.82
-5.713	0.133	0.258	0.678	NA	0.779	-0.215	0.035	0.053	11	-1273.7	2570.3	8.4	0.01	0.82
1.287	0.073	0.312	0.833	-0.134	0.566	-0.188	NA	0.105	11	-1273.8	2570.4	8.6	0.01	0.78

Table 15. Summary of fixed-effect model coefficients from the best fitting model.

Fixed effects	Estimate	Std. Error	z-value	P-value
<i>(Intercept)</i>	-0.088	2.134	-0.041	9.7E-01
<i>BFI</i>	0.082	0.026	3.214	1.3E-03
<i>GRAD</i>	0.643	0.292	2.199	2.8E-02
<i>GRAD2</i>	-0.201	0.058	-3.435	5.9E-04
<i>Log_MAQ</i>	0.844	0.141	5.969	2.4E-09
<i>LogLWFreq</i>	0.266	0.085	3.115	1.8E-03
<i>MWMT</i>	-0.106	0.035	-3.084	2.0E-03
<i>PlFreq</i>	0.032	0.008	3.833	1.3E-04

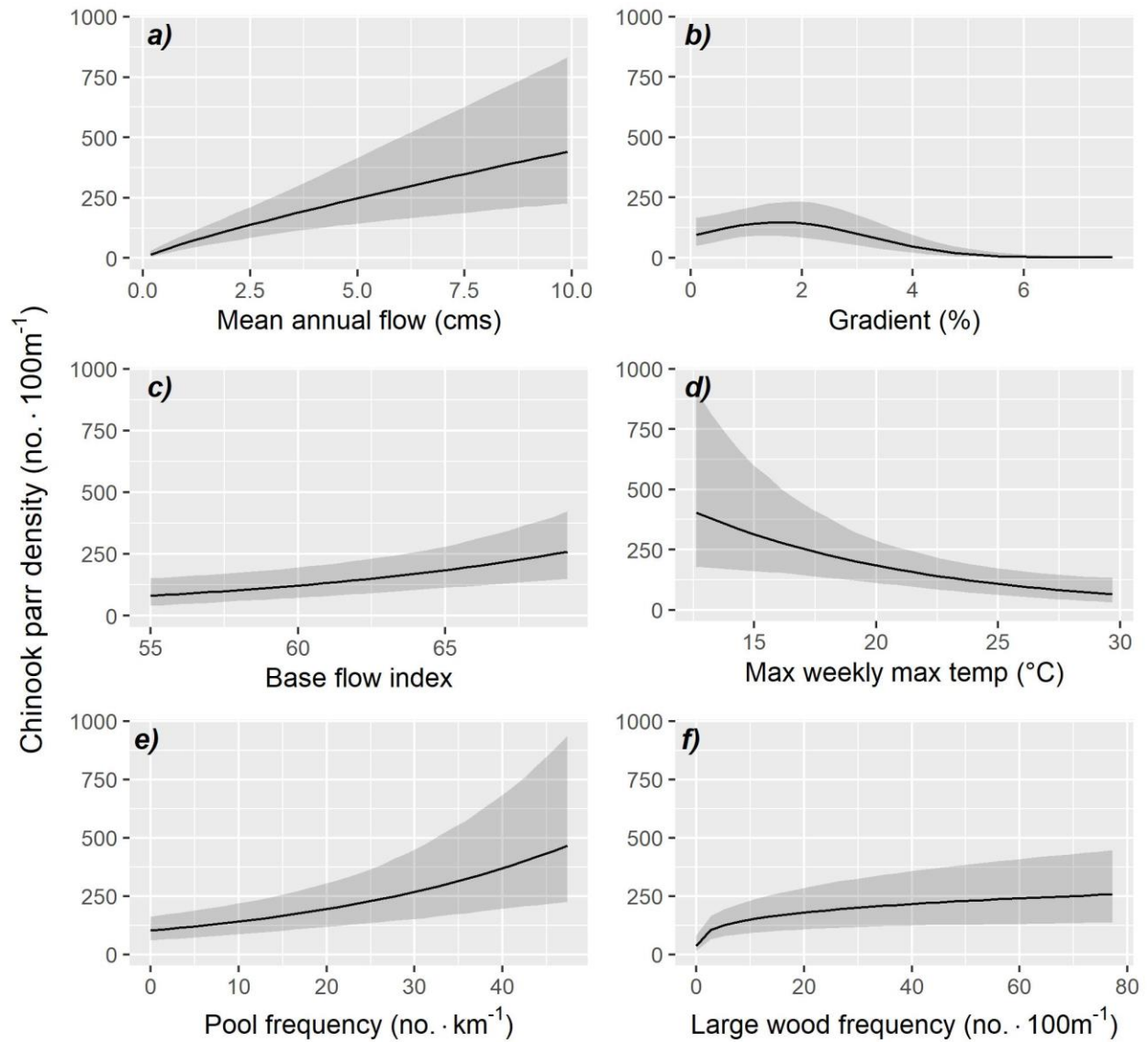


Figure 22. Marginal effects plot from the best-fitting model showing relationships between predicted Chinook parr density (no. · 100m<sup>-1</sup>) and fixed effect covariates. For each subplot (a-f), all other covariates were held at their mean value and random effects for site and year were turned off (i.e., predictions were not conditioned on the random effects). Shaded areas represent 95% confidence intervals around the mean generated via parametric bootstrap.

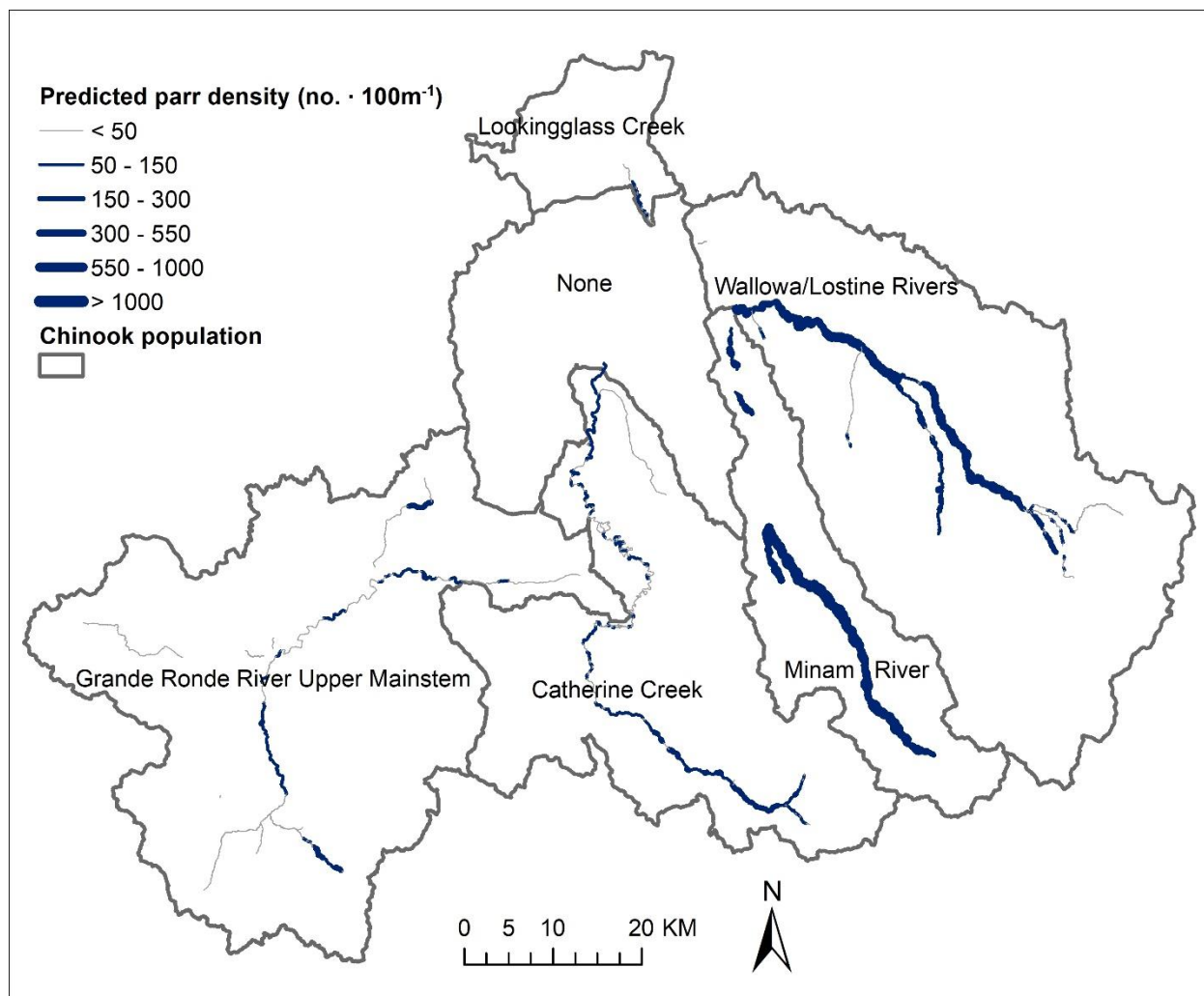


Figure 23. Map of predicted fish density (no. · 100m<sup>-1</sup>) for all stream reaches with available habitat data.

### *3.2 Factors influencing Chinook Salmon pre-spawn survival in eastern Oregon streams and projected impacts of future climate change*

#### **Abstract**

Low survival rates of adult salmon prior to spawning can adversely affect a population's long-term viability, a problem that is exacerbated by warming stream temperatures and reduced summer streamflow associated with climate change. In this study, we used a 23-year time series (1993-2015) of salmon carcass recovery data from spring-run Chinook Salmon (*Oncorhynchus tshawytscha*) collected in six populations and 87 survey reaches within the Grande Ronde River basin in Northeast Oregon to evaluate the environmental and biological factors influencing pre-spawn survival rates. A mixed-effects logistic regression model was used to assess how reach-scale (0.1 – 10 km) estimates of pre-spawn survival were affected by riverine habitat conditions (pools, water temperature, streamflow) and biotic factors (spawner density, proportion hatchery origin). Model results indicated a high degree of inter-annual and spatial variability in pre-spawn survival with reach-scale predictions ranging from 0.01 – 0.99 (mean = 0.88). Pre-spawn survival was positively associated with day of year and mean summer flow and was negatively associated with the proportion of hatchery origin spawners and water temperature, while spawner density and pool frequency had little effect. Predicted pre-spawn survival averaged across all populations and years declined from approximately 0.99 at 12 °C to 0.64 at 29 °C, although the temperature effect was more pronounced in some populations (e.g., upper Grande Ronde and Lostine). Projected climate change impacts on pre-spawn survival varied considerably across populations with a mean predicted decrease from current (2006-2015) to the 2040s of only 0.02 in cooler wilderness streams such as the Minam River, and up to 0.19 in warmer streams such as the upper Grande Ronde (mean decrease across all populations = 0.13). These results contribute to our understanding of the environmental and biotic factors affecting pre-spawn survival of Pacific Northwest salmon populations and provide insights into potential future climate change impacts to a critical life stage for these threatened species. These findings also highlight the pressing need for management actions that promote climate change resilience, particularly in temperature-impaired watersheds.

#### **Introduction**

Pacific salmon that have successfully migrated to their spawning grounds often die prior to spawning; a process commonly referred to as pre-spawn mortality. High pre-spawn mortality rates (i.e., low pre-spawn survival) observed in many salmon populations throughout the Pacific Northwest (up to 90% mortality; Bowerman et al. 2016) have raised awareness among natural resource managers of the potential threat that low pre-spawn survival can pose to population persistence and recovery potential (Keefer et al. 2010; Bowerman et al. 2016; Barnett et al. 2020). Low pre-spawn survival rates have been associated with elevated water temperature (Keefer et al. 2010; Roumasset 2012; Bowerman et al. 2018, 2021), low streamflow (Tillotson and Quinn 2017), pollutants (Feist et al. 2011; Scholz et al. 2011), infectious disease (CDFG 2004; Benda et al. 2015;

Barnett et al. 2020), high proportions of hatchery origin spawners (Bowerman et al. 2018, 2021), and high fish density (Quinn et al. 2007; Tillotson and Quinn 2017). Despite some understanding of the environmental and biotic factors influencing pre-spawn survival at the population scale, stream restoration practitioners could benefit from a clearer understanding of how these factors affect fish survival at finer spatial scales (i.e., reaches  $\approx 0.1 - 10$  km) so that restoration actions can prioritize those locations with the greatest potential benefit for spawning success. In addition, little is known about how physical habitat features at these scales such as pools—a common target of habitat restoration—influences salmon pre-spawn survival.

Human-caused climate change has already resulted in significant alterations to riverine habitats in North America including shifts in the magnitude and timing of seasonal flow patterns, increased frequency of extreme flow events such as flooding and drought, and long-term increases in mean annual stream temperatures (Lynch et al. 2016). Isaak et al. (2012) estimated that summer water temperatures in Pacific Northwest streams increased by approximately  $0.22$  °C/decade between 1980 and 2009, and August stream temperatures were projected to increase on average,  $+2.83$  °C by the 2080s (Isaak et al. 2017). Although the response of Pacific salmon to climate change is likely to be diverse (Crozier et al. 2008), a growing body of evidence suggests that recent climate change has already led to spatial and temporal shifts in salmon growth, phenology, and population dynamics (Lynch et al. 2016). Recent work by Bowerman et al. (2021) estimated that pre-spawn survival rates of spring Chinook salmon populations in the interior Columbia River Basin could decline by 0-17% by 2040. Given the increasing threat of climate change and associated warming of streams on fish populations across the Pacific Northwest and North America, it is important to evaluate the extent to which future climate-related changes to streamflow and water temperature may influence pre-spawn mortality especially in threatened salmon populations where climate change may pose a greater risk to population viability.

Although spatially continuous spawning ground surveys are commonly conducted throughout the Pacific Northwest to estimate salmon spawner abundance, distribution, and pre-spawn survival, corresponding data on environmental conditions is often lacking or is limited to a few selected points within the watershed (e.g., flow gauges). Researchers and managers often struggle to draw linkages between spawning survey data and environmental conditions because reach-specific data is difficult and expensive to acquire, or because the data was simply not collected historically. In this study, we draw from spatially extensive reach-scale ( $\sim 1$  km length) water temperature (NorWeST; Isaak et al. 2017) and streamflow model predictions (National Water Model; NOAA 2019) as well as ground-based fish habitat surveys (Moore et al. 2019) to evaluate relationships between environmental conditions and empirical reach-scale estimates of pre-spawn survival. We used a 23-year time series (1993-2015) of spawning ground surveys conducted across six distinct populations of spring-run Chinook Salmon (*Oncorhynchus tshawytscha*) and 87 survey reaches within the Grande Ronde River basin in Northeast Oregon to 1) evaluate the environmental and biological factors influencing salmon pre-spawn survival rates, and 2) predict how pre-spawn



survival rates would change in response to future climate change projections for the 2040s (2030-2059) and 2080s (2070-2099).

## **Methods**

### *Study Area*

The study area included 87 unique survey reaches distributed across 10 rivers and six distinct spring Chinook Salmon populations in the Grande Ronde River basin in northeast Oregon, USA (Figure 24). The Grande Ronde River is a major tributary of the Snake River, originating in the Blue Mountains of NE Oregon and flowing approximately 340 km north/northwest to its confluence with the Snake River in Southeast Washington. The Grande Ronde basin is typified by cold winters with ample snow in its headwaters, and hot, dry summers. Basin tributaries are primarily fed by snowmelt, with peak flows occurring during the spring, and base flows occurring during late summer, a period coinciding with Chinook Salmon spawning. Survey reaches spanned a wide range of stream sizes and habitat conditions with elevations ranging from 825 to 2,035 m (mean = 1,259 m) and mean summer flow (June 1 – September 30) ranging from approximately 0 to 21.4 cms (mean = 4.8).

Salmon populations evaluated in this study including the upper Grande Ronde River, Catherine Creek, Lookingglass Creek, Minam River, Lostine River, and Wallowa River are part of the Snake River Spring/Summer Chinook evolutionarily significant unit (ESU). Tributary and estuarine habitat degradation, combined with hydroelectric operations in the mainstem Snake and Columbia rivers, predation, and commercial and sport fishing contributed to the decline and subsequent listing of the ESU as threatened under the Endangered Species Act (ESA) in 1992 (NOAA 2008). While the Wallowa and Lostine rivers are technically considered part of the same population, they were treated separately in this analysis because spawner abundances and habitat conditions differed substantially between the two areas. In contrast with the other populations considered in this study, the Minam River is managed as a wilderness stream with no hatchery releases and has relatively undisturbed instream and riparian conditions. These focal populations were chosen because very low pre-spawn survival rates have been observed in some populations in recent years and managers need a better understanding of the factors affecting pre-spawn survival and how to prioritize restoration actions to address these factors.

### *Chinook Salmon spawning data*

We used Chinook Salmon spawning survey data collected by the Oregon Department of Fish and Wildlife (ODFW) to estimate pre-spawn survival rates within each survey reach from 1993-2015 (Figure 24). Surveys were intended to cover the entire spawning extent within each population with some gaps occurring in privately-owned areas with restricted access. Reaches ranged in length from 0.3 to 11.8 km (mean = 3.2 km) and were surveyed two to three times per year with the intention of covering the full range of spawn timing. For each female salmon carcass (age 3-

5) encountered during a survey, field crews recorded the “percent spawned” based on a visual estimate of the percentage of eggs remaining in the body cavity. Salmon carcasses were designated as successful spawners if fewer than 50% of the eggs were remaining in the carcass (Feldhaus et al. 2017). Male fish and carcasses that were severely degraded or missing their gonads were excluded from this analysis because percent spawned could not be reliably estimated. Counts of salmon carcasses within each survey reach ranged from 1 to 308 (mean = 11.2) with a total of 7,344 individual salmon carcasses observed across all reaches and years.

### *Covariate data*

We selected a limited set of environmental and biotic covariates representing *a priori* hypotheses about the ecological processes influencing pre-spawn survival (Table 16). Day of year (*DOY*) was included in our analysis to account for effects of within-season timing of carcass recoveries on pre-spawn mortality (Bowerman et al. 2021). We calculated *DOY* as the mean day of the year beginning on January 1 of all carcasses recovered within a given reach and year.

Mean summer (June 1 – September 30) streamflow was based on simulated data from the National Oceanic and Atmospheric Administration’s (NOAA) National Water Model Reanalysis Dataset (NOAA 2019). This model used precipitation and other meteorological data to predict hourly streamflow (cubic meters per second; cms) at each stream segment in the 1:100K National Hydrography Dataset (NHDPlusV2; average segment length  $\approx 1$  km) for a 26-year time period (January 1993 – December 2018). Model predictions were joined to the nearest overlapping spawning survey reach in ArcGIS (ESRI 2020) and mean daily flows within the summer period were then averaged by reach and year. This time period was chosen for consistency with available climate projections for streamflow (USFS 2020) and because it coincides with timing of adult salmon holding and spawning. A comparison of model predictions with observed mean summer streamflow at five gauging stations in the Grande Ronde basin from 1993-2018 confirmed that the model was very precise ( $R^2 = 0.97$ , median absolute error = 1.2 cms,  $n = 130$ ). Flow predictions were standardized by dividing mean summer flow by the upstream drainage area (expressed in 100s of square kilometers) to improve comparability across a broad range of stream sizes. Thus, summer streamflow per unit area ( $\text{cms} \cdot 100\text{km}^{-2}$ ) was more representative of interannual variation in streamflow than of position in the watershed per se.

We used maximum weekly maximum water temperature (*MWMT* °C) predictions (i.e., the maximum seven-day running average of daily max temperature) from the NorWeST model (Isaak et al. 2017) to characterize peak summer water temperatures within each survey reach and year. Prediction points, which are spaced approximately 1 km apart, were joined to each reach in ArcGIS and then averaged by reach and year. A comparison of NorWeST predictions with empirical measurements of *MWMT* from the Columbia Habitat Monitoring Program (CHaMP 2016) at 184 unique site/year observations in the Grande Ronde basin indicated the model was reasonably accurate with an  $R^2$  of 0.77 and median absolute error of 2 °C. The proportion of hatchery-origin

spawners (*PHOS*) was calculated as the fraction of total female carcasses recovered in each reach and year that were of hatchery origin. This covariate was included to account for potential differences in pre-spawn survival between hatchery and natural origin fish (Bowerman et al. 2018, 2021).

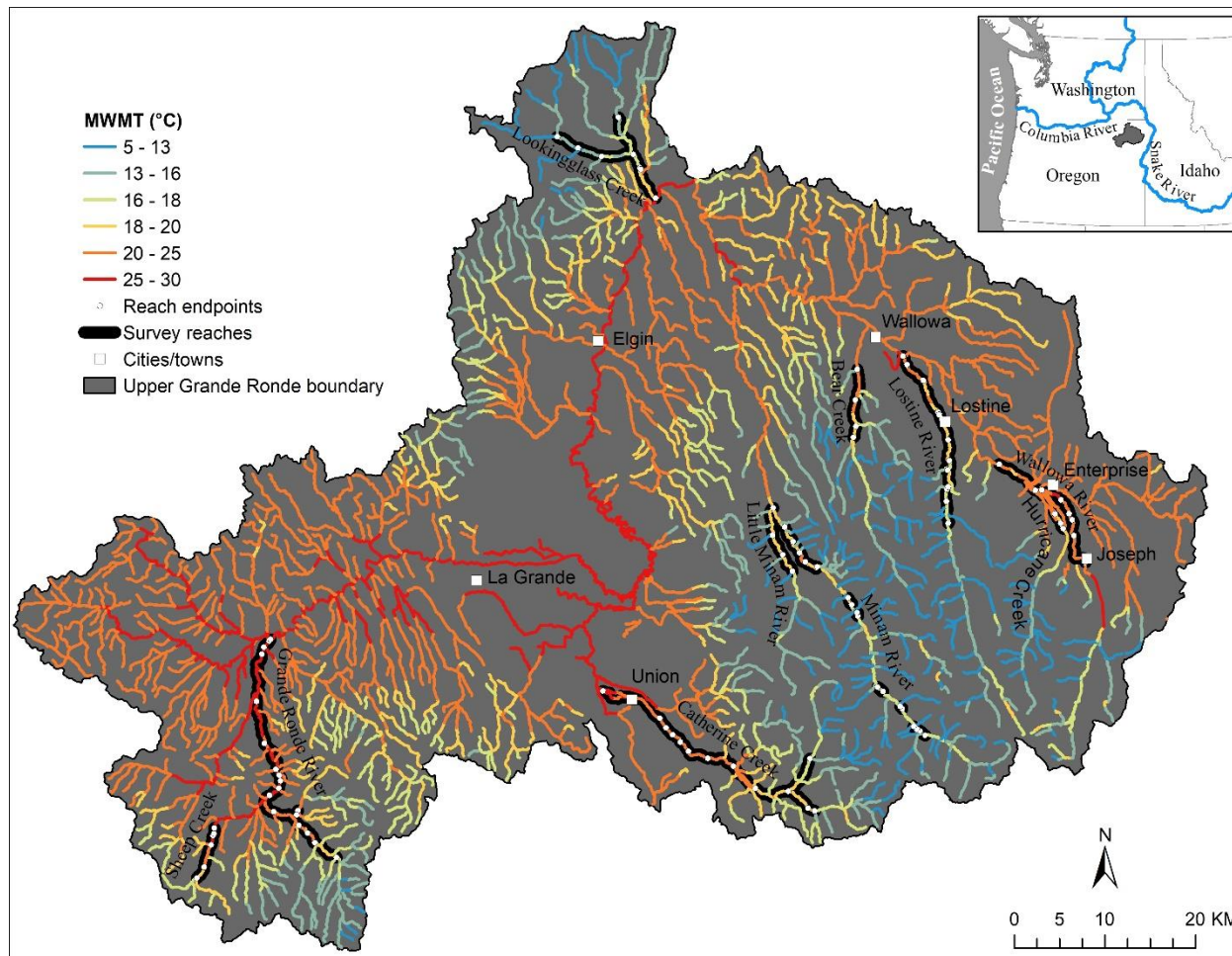


Figure 24. Upper Grande Ronde River study area in NE Oregon showing average maximum weekly maximum water temperature (MWMT °C) predictions from the NorWeST model from 2006-2015 and locations of spawning survey reaches used in the analysis.

Pool frequency data was obtained from ground-based stream habitat surveys conducted as part of ODFW's Aquatic Inventories Program (AqI; Moore et al. 2019) between 1991 and 2018. We hypothesized that reaches with more pools would be associated with higher pre-spawn survival because deep pools can provide cover from predators as well as energetically favorable refugia from high water velocities and temperatures. Because habitat survey data was not available for each year of interest (i.e., surveys were conducted approximately once every 10 years), we assigned the most recent pool frequency measurement to each reach. This assumes that pool habitat has not changed over the course of this study period. While this assumption is not true for some

selected reaches that have experienced intensive restoration or large-scale natural disturbances, analysis of broad-scale changes in pool habitat in the Grande Ronde has demonstrated that large pool frequency has remained relatively constant since the early 1990s when AqI surveys began (Seth White, CRITFC, pers. comm.). Because ground-based measurements of instream habitat were not available for all spawning survey reaches, we limited the dataset to include only those reaches that had corresponding physical habitat data (total reaches = 87).

Spawner density ( $\text{no.} \cdot \text{km}^{-1}$ ) was based on adult salmon abundance estimates provided by ODFW for each population and year. These estimates represent the number of potential spawners (age 3-5) in the population prior to pre-spawn mortality including both hatchery and natural origin fish. Spawner abundance was standardized across populations by dividing abundance estimates by the length of stream surveyed. Spawner density was represented at the population scale because abundance data was not available at the reach scale in most years. Thus, this covariate was intended to capture important inter-annual variability in pre-spawn survival associated with broad-scale density-dependent effects (i.e., high abundance years vs low abundance years).

#### *Climate change projections*

Future projections of mean summer streamflow were obtained from the Western U.S. Streamflow Metric Dataset (USFS 2020) corresponding to the 2040s (2030-2059) and 2080s (2070-2099) time periods. Streamflow predictions were generated from the Variable Infiltration Capacity (VIC) hydrologic model (Elsner et al. 2010) using projected meteorological data from an ensemble of 10 global climate models associated with the A1B gas emissions scenario (IPCC 2007). The A1B scenario lies between the middle and high end of the spectrum of projected anthropogenic greenhouse gas emissions. Streamflow predictions falling within the boundaries of each spawning survey reach were averaged to produce a single mean summer flow estimate per reach.

Projected water temperatures (*MWMT*) for the 2040s and 2080s were generated by the NorWeST model. Consistent with the Western Streamflow metrics, projections were based on simulated changes in air temperature and stream discharge from an average ensemble of 10 global climate models representing the A1B greenhouse gas emissions trajectory. For climate projection scenarios, all fixed-effect covariates besides flow and temperature were held fixed at their recent 10-year mean value (2006-2015). Additionally, random effects for year were excluded from predictions.

Table 16. Summary of covariates used in model fitting.

Covariate	Effect type	Description	Source
<i>DOY</i>	fixed	Mean day of year that carcasses were recovered within each reach and year	ODFW carcass recovery data (P. Gibson, La Grande Fish Research Office, pers. comm.)
<i>MSFPA</i>	fixed	Mean summer (Jun 1 - Sep 30) flow in cubic meters per second divided by the upstream drainage area in 100s of square kilometers within each reach and year ( $\text{cms} \cdot 100\text{km}^{-2}$ )	Historic data (National Water Model Retrospective Analysis Dataset; NWM 2019); Climate change projections (Western U.S. Stream Flow Metrics; USFS 2020)
<i>MWMT</i>	fixed	Maximum weekly maximum water temperature ( $^{\circ}\text{C}$ ) averaged within each reach and year	NorWeST model (Isaak et al. 2017)
<i>PHOS</i>	fixed	Proportion of total female carcass recoveries that were of hatchery origin within each reach and year	ODFW carcass recovery data
<i>PlFreq</i>	fixed	Pool frequency (i.e., number of pools with max depth $> 0.5$ meters and surface area $> 20$ square meters per kilometer within each reach; $\text{no.} \cdot \text{km}^{-1}$ )	ODFW Aquatic Inventories data (Moore et al. 2019)
<i>SpwnDen</i>	fixed	Spawner density (i.e., estimated number of natural and hatchery origin adult returns (age 3-6) divided by the length of habitat surveyed within each population and year ( $\text{no.} \cdot \text{km}^{-1}$ )	ODFW spawner abundance data (K. Bliesner, La Grande Fish Research Office, pers. comm.)
<i>Population</i>	random	Spring Chinook salmon population identifier	ODFW carcass recovery data
<i>Reach</i>	random	Spawning survey reach identifier	ODFW carcass recovery data
<i>Year</i>	random	Calendar year in which the spawning survey occurred.	ODFW carcass recovery data

## Statistical analysis

We used mixed-effects logistic regression implemented in the ‘glmmTMB’ package (Brooks et al. 2017) in R (R Core Team 2020) to model variability in Chinook Salmon pre-spawn survival probabilities ( $\pi_i$ ) for each survey  $i$ , where  $i$  is a specific carcass survey conducted in reach ( $j$ ) within population ( $k$ ) in year ( $l$ ). We initially fit a “global model” using the full set of fixed-effect covariates and random effects for each of the three survey identifiers such that the linear predictor had the form:

$$\begin{aligned} \text{logit}(\pi_i) = & \beta_0 + \beta_1 DOY_i + \beta_2 MSFPA_i + \beta_3 MWMT_i \\ & + \beta_4 PHOS_i + \beta_5 SpwnDen_i + \beta_6 PlFreq_i \\ & + \varepsilon_{j[i]} + \gamma_{k[i]} + \delta_{l[i]} \end{aligned}$$

This equation produces the expected pre-spawn survival probability for survey  $i$ , and we assume the count of examined carcasses that had successfully spawned ( $y_i$ ) is a binomial random variable with number of trials equal to the total number of carcasses examined in survey  $i$  ( $N_i$ ):

$$y_i \sim \mathcal{B}(N_i, \pi_i)$$

where:

- $\pi_i$  is the expected probability of spawning success (i.e., pre-spawn survival) for survey  $i$ , where ( $i = 1, 2, \dots, n_i = 654$ ), which occurred in reach  $j[i]$ , population  $k[i]$  and year  $l[i]$  of which there are  $n_j = 87$ ,  $n_k = 6$ , and  $n_l = 23$ , respectively.
- $DOY_i$ ,  $MSFPA_i$ ,  $MWMT_i$ ,  $PHOS_i$ ,  $SpwnDen_i$ ,  $PlFreq_i$ , are fixed-effect covariates for survey  $i$ , as described in Table 16.
- $\varepsilon_{j[i]}$  is the reach random effect for survey  $i$ ; we assume that  $\varepsilon_j \sim \mathcal{N}(0, \sigma_\varepsilon^2)$ .
- $\gamma_{k[i]}$  is the population random effect for survey  $i$ ; we assume that  $\gamma_k \sim \mathcal{N}(0, \sigma_\gamma^2)$ .
- $\delta_{l[i]}$  is a year random effect for survey  $i$ ; we assume that  $\delta_l \sim \mathcal{N}(0, \sigma_\delta^2)$ .

We then generated a set of candidate models consisting of all possible additive combinations of the fixed-effect covariates from the global model using the dredge function from the ‘MuMIn’ R package (Barton 2020). Random effects for population, site, and year were included in each of the candidate models to account for lack of independence among observations arising from the repeated measures survey design as well as population- and year-specific variability not captured by the fixed-effects. Models were compared using Akaike’s Information Criterion corrected for small sample size (AICc), and model averaging was used to compute AIC-weighted average coefficient values from all models in the candidate set (Burnham and Anderson 2002). Thus, model-averaged coefficients were heavily weighted by models with higher empirical support (i.e., lower AICc value and higher AICc weight) and were minimally influenced by models with low empirical support.

We assessed the relative importance of predictor variables in part by calculating the summation of AICc weights ( $SW$ ) over all models that contained each variable of interest (Burnham and Anderson 2002), with  $SW$  values closest to one indicating higher variable importance. Additionally, we compared z-values for each model parameter—calculated as the parameter estimate divided by the standard error—to assess general variable importance assuming that parameters with higher z-values (i.e., higher effect size relative to the parameter uncertainty) would have a greater influence on predicted pre-spawn survival probability.

Goodness-of-fit of the global model and top fitting models ( $\Delta AICc < 4$ ) was assessed using residual diagnostic plots generated with the DHARMA package (Hartig 2020). The proportion of variance explained by each model (pseudo- $R^2$ ) was computed using methods described in Nakagawa and Schielzeth (2013) and implemented in package MuMIn. Specifically, the marginal pseudo-coefficient of determination ( $R_m^2$ ) represents the proportion of variance explained by the fixed effects in the model and the conditional pseudo-coefficient of determination ( $R_c^2$ ) represents the proportion of variance explained by the entire model including both fixed and random effects.

## Results and Discussion

The best fitting models predicting Chinook Salmon pre-spawn survival rates among the set of candidate models we examined included day of year ( $DOY$ ), mean summer flow ( $MSFPA$ ), maximum weekly maximum water temperature ( $MWMT$ ), and proportion of hatchery origin spawners ( $PHOS$ ) as fixed-effect predictor variables, while spawner density ( $SpwnDen$ ) and pool frequency ( $PlFreq$ ) did not consistently appear in the top models (Table 17). Residual diagnostic plots and goodness-of-fit tests for the global model and top fitting models indicated that model assumptions were reasonably satisfied. The top fitting model explained approximately 90% of the variation in pre-spawn survival, with fixed and random effects accounting for approximately 57% and 38% of the total variation, respectively (Table 17).

Reach-scale pre-spawn survival predictions were highly variable both spatially (within and among populations) and temporally (across years) with survival predictions ranging from 0.01 to 0.99 (mean = 0.88; Table 18). Random effect standard deviations for *Reach*, *Population* and *Year* from the global model were 0.63, 0.62 and 0.44, respectively, indicating moderately high variability attributed to random effects. Pre-spawn survival rates declined over time in some populations (e.g., upper Grande Ronde and Lostine River) but were relatively stable in others (Table 18). For example, predicted survival probability in the upper Grande Ronde and Lostine populations declined by approximately 0.24 and 0.09, respectively, between the historic period (1993-2005) and the recent 10-year period (2006-2015). However, average survival rates in the other populations did not change appreciably over this time frame or could not be evaluated due to limited data during the early years (e.g., Lookingglass Creek sampling didn't begin until 2004). Recent 10-year mean pre-spawn survival rates (2006-2015) were lowest in the upper Grande

Ronde River population (mean = 0.65, range = 0.02 - 0.95), moderate in the Lostine River (mean = 0.74, range = 0.05 – 0.97), and highest in the Minam River (mean = 0.97, range = 0.91 - 1.00).

Pre-spawn survival rates did not follow a clear longitudinal trend as might be expected from spatial patterns in water temperature (Figure 25). For example, disproportionately low pre-spawn survival rates in some years were observed in reaches in close proximity to weirs located near the downstream extent of the spawning distribution, possibly indicating a weir effect on survival. In addition, pre-spawn survival was very low in some reaches of the upper Grande Ronde headwaters and upper Sheep Creek (a tributary of upper Grande Ronde). However, sample size was quite low in these reaches ( $n < 10$ ), and therefore their contribution to the overall population-scale pre-spawn survival rate would be minimal.

Variable importance, expressed as a summation of AICc weights ( $SW$ ) from all candidate models, ranged from 0.27 to 1, with the lowest  $SW$  values corresponding to pool frequency and spawner density ( $SW = 0.27$  and  $0.38$ , respectively) and high  $SW$  values ( $SW > 0.85$ ) for all other variables (Table 19). Model-averaged  $z$ -values for each predictor variable (an alternative measure of variable importance), indicated that day of year had the strongest influence on pre-spawn survival ( $z$ -value = 13.5; Table 19), whereas mean summer streamflow, water temperature and proportion of hatchery-origin spawners and had a weak to moderate effect ( $z$ -value = 2.2 - 4.9), and spawner density and pool frequency had a negligible effect ( $z$ -value  $< 0.9$ ). Model-averaged coefficients were statistically significant at the  $\alpha = 0.05$  level for all covariates except spawner density and pool frequency (Table 19).

Carcass recovery day was positively associated with pre-spawn survival, with mean predicted survival probability across all reaches, populations and years increasing from approximately 0.02 on day 187 (July 6) to 0.99 on day 272 (September 29) (Figure 26f). This result is consistent with observations from other salmon populations in the Columbia River basin (Bowerman et al. 2021) showing that salmon carcasses recovered early during the spawning period are more likely to be pre-spawn mortalities. This relationship reflects an inherent bias in the sampling methodology that is important to control for (Bowerman et al. 2016). Because we are only sampling dead fish rather than a representative sample of all fish (live and dead) within the population, it makes sense that carcasses recovered early in the spawning window will have had less time to complete the spawning process, and therefore will have a higher probability of dying prior to spawning.

Maximum weekly maximum water temperature had a negative effect on pre-spawn survival, with mean predicted survival rates across all populations remaining relatively high ( $> 0.95$ ) until temperatures exceeded approximately 19 °C, after which survival declined more steeply to a low of 0.64 at 29 °C (Figure 26b). The shape of the temperature-survival curve varied substantially across populations owing to differences in the population-specific intercept (i.e., *Population* random effect; Figure 27b). The temperature effect on pre-spawn survival was most pronounced in the upper Grande Ronde and Lostine River, and was relatively small in the Minam River,



Wallowa River, and Catherine Creek. For example, predicted mean pre-spawn survival rates in the upper Grande Ronde River declined steeply from approximately 0.94 at 17 °C to 0.49 at 29 °C, while survival rates in the Minam River population remained above 0.95 across the range of observed temperatures (15 - 21 °C).

The proportion of hatchery-origin spawners within each reach was an important biotic factor influencing pre-spawn survival, with higher hatchery fractions associated with lower predicted survival. Although the marginal effect of *PHOS* was relatively small when considered as an average across all populations (Figure 26), the influence of *PHOS* on survival was substantial for some populations such as the Lostine River and upper Grande Ronde (Figure 27). For example, mean predicted pre-spawn survival in the Lostine River declined from approximately 0.90 to 0.74 as *PHOS* increased from 0 to 1. In contrast, mean survival in Lookingglass Creek declined by only 0.04 (from 0.97 to 0.93) over the same *PHOS* range.

Mean summer flow per unit area was positively associated with pre-spawn survival, although the effect size was relatively small. Predicted pre-spawn survival averaged across all populations increased from about 0.91 to 0.97 as MSFPA increased from 0.1 to 8.6 cms · 100km<sup>-2</sup>, an increase of only 0.06 (6% survival) over the full range of observed flows. Similar to water temperature, the marginal effect of flow on pre-spawn survival differed considerably by population and was most pronounced in the Lostine and upper Grande Ronde rivers (Figure 27). For example, mean predicted survival probability in the Lostine River increased from about 0.75 to 0.89 as MSFPA increased from 0.1 to 8 cms · 100km<sup>-2</sup>, but only increased by about 0.02 (from 0.96 to 0.98) in the Minam River over a similar range of flows.

### *Climate projections*

Maximum weekly maximum water temperature was projected to increase by an average of 2.1 °C from the recent 10-year average (2006-2015) to the 2040s future time period (range across all populations = 0.6 – 2.5 °C), and by 2.8 °C by the 2080s (range = 1.3 - 3.2 °C). Similarly, mean summer flow was projected to decline by 68% on average (range = 50 – 75%) by the 2040s, and by 81% by the 2080s (range = 66 – 85%). Projected climate change impacts on pre-spawn survival varied considerably across populations with a mean predicted decrease from current (2006-2015) to the 2040s of only 0.02 (2% survival) in cooler wilderness streams such as the Minam River, and up to 0.19 (19% survival) in warmer streams such as the upper Grande Ronde (mean decrease across all populations = 0.13; Figure 28). Pre-spawn survival was projected to decline by an average of 0.15 by the 2080s (range of population means = 0.03 – 0.23).

### **Summary**

Chinook Salmon pre-spawn survival in the Grande Ronde basin varied considerably across populations and spatially within populations. After accounting for the effect of sampling date, pre-spawn survival was positively associated with mean summer flow and negatively associated with

the proportion of hatchery origin spawners and water temperature. On the other hand, spawner density and pool frequency appeared to have little effect on pre-spawn survival. Projected reductions in summer streamflow and elevated water temperatures associated with climate change had a variable effect on each population with predicted reductions in survival probability from current (2006-2015) to the 2040s ranging from 0.02 to 0.19 (mean decrease =0.13). These results provide spatially explicit predictions of pre-spawn survival that can be used to simulate potential fish response to alternative management or climate scenarios and to prioritize restoration actions. These findings also contribute to our understanding of the environmental and biotic factors affecting pre-spawn survival of Pacific Northwest salmon populations and provide insights into potential future climate change impacts to a critical life stage for these threatened species.

Table 17. Model selection table showing candidate models with Akaike difference ( $\Delta\text{AICc}$ ) less than ten.

Fixed-effect model coefficients							df	logLik	AICc	$\Delta\text{AICc}$	weight	$R_m^2$	$R_c^2$
<i>Intercept</i>	<i>DOY</i>	<i>MSFPA</i>	<i>MWMT</i>	<i>PHOS</i>	<i>SpwnDen</i>	<i>PlFreqAvg</i>							
-19.250	0.109	0.123	-0.241	-1.160	NA	NA	8	-611.4	1239.0	0.0	0.37	0.57	0.90
-19.322	0.109	0.160	-0.239	-1.057	-0.005	NA	9	-610.8	1239.8	0.8	0.25	0.57	0.90
-19.395	0.109	0.121	-0.235	-1.154	NA	0.009	9	-611.4	1241.0	2.0	0.14	0.58	0.90
-19.450	0.109	0.158	-0.233	-1.052	-0.005	0.008	10	-610.7	1241.8	2.8	0.09	0.57	0.90
-18.592	0.109	NA	-0.260	-1.108	NA	NA	7	-614.0	1242.1	3.1	0.08	0.54	0.89
-18.947	0.109	NA	-0.245	-1.105	NA	0.021	8	-613.8	1243.8	4.8	0.03	0.56	0.89
-18.607	0.109	NA	-0.260	-1.123	0.001	NA	8	-614.0	1244.2	5.1	0.03	0.54	0.89
-18.956	0.109	NA	-0.245	-1.117	0.000	0.021	9	-613.8	1245.9	6.8	0.01	0.56	0.89

Table 18. Summary of mean fixed-effect covariate values and predicted pre-spawn survival probabilities by population and time period. The range of values across all reaches and years are provided in parentheses.

Time period	Fixed-effect covariates						Pre-spawn survival	
	<i>PHOS</i>	<i>MWMT</i>	<i>MSFPA</i>	<i>SpwnDen</i>	<i>PIFreq</i>	<i>DOY</i>	Fit	Std. Err.
Catherine Creek (CATH)								
1993-2005	0.28 (0.00, 1.00)	21.0 (16.7, 24.5)	1.6 (0.5, 3.1)	3.3 (0.4, 7.9)	3.2 (0.6, 7.0)	250.5 (231.0, 258.5)	0.95 (0.55, 0.99)	0.02 (0.00, 0.17)
2006-2015	0.56 (0.00, 1.00)	21.0 (16.5, 25.7)	1.5 (0.5, 4.6)	10.7 (2.5, 24.4)	3.4 (0.3, 7.4)	247.5 (187.5, 265.0)	0.93 (0.01, 0.99)	0.02 (0.01, 0.08)
Total	0.43 (0.00, 1.00)	21.0 (16.5, 25.7)	1.5 (0.5, 4.6)	7.2 (0.4, 24.4)	3.3 (0.3, 7.4)	248.9 (187.5, 265.0)	0.94 (0.01, 0.99)	0.02 (0.00, 0.17)
Upper Grande Ronde River (GRUM)								
1993-2005	0.35 (0.00, 1.00)	23.1 (17.6, 27.5)	1.0 (0.5, 1.7)	2.8 (0.3, 7.1)	8.6 (2.6, 22.0)	250.6 (197.0, 265.0)	0.89 (0.04, 0.99)	0.04 (0.00, 0.10)
2006-2015	0.85 (0.00, 1.00)	23.2 (17.4, 28.7)	1.1 (0.5, 2.8)	15.6 (0.4, 26.2)	8.4 (0.0, 22.0)	240.0 (201.0, 266.0)	0.65 (0.02, 0.95)	0.06 (0.01, 0.16)
Total	0.65 (0.00, 1.00)	23.2 (17.4, 28.7)	1.1 (0.5, 2.8)	10.6 (0.3, 26.2)	8.4 (0.0, 22.0)	244.2 (197.0, 266.0)	0.74 (0.02, 0.99)	0.05 (0.00, 0.16)
Lookingglass Creek (LKGLS)								
2004-2005	0.95 (0.75, 1.00)	16.3 (13.1, 19.0)	0.9 (0.6, 1.2)	3.6 (1.8, 5.4)	1.1 (0.0, 2.0)	255.8 (252.1, 260.1)	0.96 (0.90, 0.99)	0.02 (0.01, 0.03)
2006-2015	0.85 (0.00, 1.00)	16.2 (11.8, 19.2)	0.9 (0.3, 1.6)	16.0 (3.3, 32.2)	1.3 (0.0, 3.7)	245.8 (191.5, 260.5)	0.87 (0.03, 1.00)	0.02 (0.00, 0.08)
Total	0.87 (0.00, 1.00)	16.2 (11.8, 19.2)	0.9 (0.3, 1.6)	14.2 (1.8, 32.2)	1.3 (0.0, 3.7)	247.2 (191.5, 260.5)	0.88 (0.03, 1.00)	0.02 (0.00, 0.08)
Lostine River (LOS)								
1993-2005	0.35 (0.00, 1.00)	18.8 (15.4, 22.0)	4.5 (1.3, 8.3)	8.9 (0.7, 16.2)	1.3 (0.0, 3.5)	246.2 (232.8, 268.3)	0.83 (0.33, 0.99)	0.05 (0.00, 0.14)
2006-2015	0.68 (0.00, 1.00)	19.0 (15.0, 21.8)	3.7 (0.0, 7.9)	38.0 (6.6, 93.2)	1.5 (0.0, 6.6)	243.5 (219.6, 261.0)	0.74 (0.05, 0.97)	0.04 (0.01, 0.16)
Total	0.54 (0.00, 1.00)	18.9 (15.0, 22.0)	4.1 (0.0, 8.3)	25.6 (0.7, 93.2)	1.4 (0.0, 6.6)	244.7 (219.6, 268.3)	0.78 (0.05, 0.99)	0.05 (0.00, 0.16)
Minam River (MIN)								
1993-2005	0.07 (0.00, 1.00)	18.6 (15.3, 21.1)	4.4 (1.2, 7.9)	16.6 (2.3, 28.7)	13.1 (9.7, 16.6)	245.1 (233.0, 257.0)	0.97 (0.88, 0.99)	0.02 (0.00, 0.07)
2006-2015	0.09 (0.00, 1.00)	18.5 (15.1, 20.9)	3.7 (0.8, 8.1)	31.2 (13.5, 48.9)	12.8 (9.7, 16.6)	243.8 (234.0, 262.0)	0.97 (0.91, 1.00)	0.02 (0.00, 0.05)
Total	0.08 (0.00, 1.00)	18.6 (15.1, 21.1)	4.1 (0.8, 8.1)	23.5 (2.3, 48.9)	13.0 (9.7, 16.6)	244.5 (233.0, 262.0)	0.97 (0.88, 1.00)	0.02 (0.00, 0.07)
Wallowa River (WAL)								
1993-2005	0.27 (0.00, 1.00)	22.1 (18.0, 25.4)	4.9 (1.7, 8.6)	2.9 (0.2, 4.2)	7.8 (1.2, 13.8)	251.6 (230.0, 272.0)	0.89 (0.45, 1.00)	0.04 (0.00, 0.14)
2006-2015	0.20 (0.00, 1.00)	21.9 (17.8, 25.2)	4.3 (1.1, 7.5)	7.1 (0.7, 14.3)	7.3 (1.2, 11.1)	251.2 (216.0, 265.0)	0.91 (0.29, 0.99)	0.03 (0.00, 0.16)
Total	0.23 (0.00, 1.00)	22.0 (17.8, 25.4)	4.5 (1.1, 8.6)	5.6 (0.2, 14.3)	7.4 (1.2, 13.8)	251.3 (216.0, 272.0)	0.90 (0.29, 1.00)	0.04 (0.00, 0.16)
Grand Total	0.40 (0.00, 1.00)	19.9 (11.8, 28.7)	3.0 (0.0, 8.6)	16.3 (0.2, 93.2)	6.4 (0.0, 22.0)	246.4 (187.5, 272.0)	0.88 (0.01, 1.00)	0.03 (0.00, 0.17)

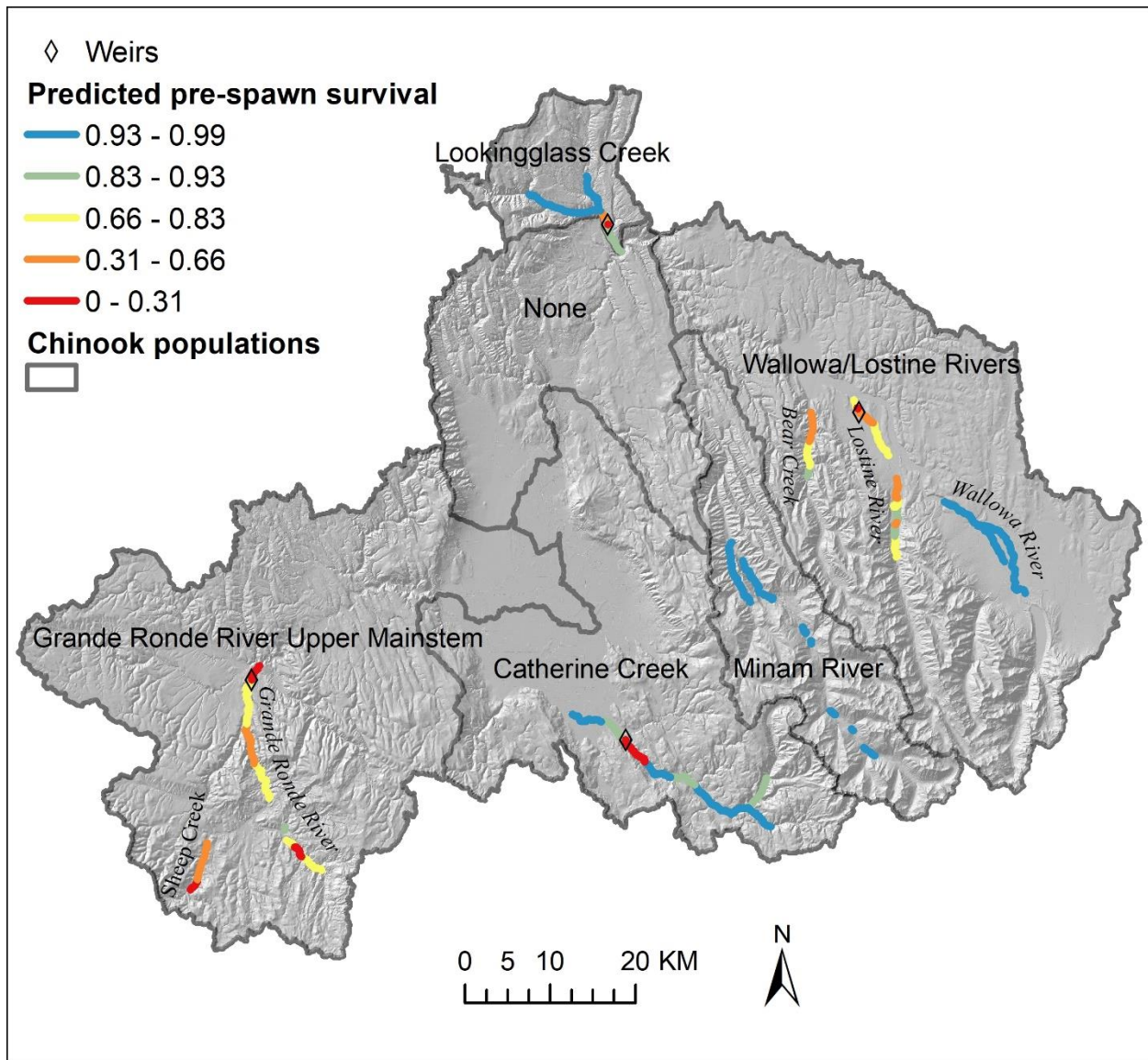


Figure 25. Map of mean pre-spawn survival predictions from 2006-2015 by survey reach.

Table 19. Summary of model-averaged fixed-effect coefficient estimates.

Fixed effect	Estimate	Std. Error	z-value	P-value	SW
(Intercept)	-19.224	2.152	8.917	< 2e-16	1.00
DOY	0.109	0.008	13.524	< 2e-16	1.00
MSFPA	0.137	0.062	2.221	0.026	0.85
MWMT	-0.241	0.049	4.902	9.00E-07	1.00
PHOS	-1.116	0.264	4.217	2.47E-05	1.00
SpwnDen	-0.004	0.004	0.930	0.352	0.38
PlFreq	0.011	0.033	0.324	0.746	0.27

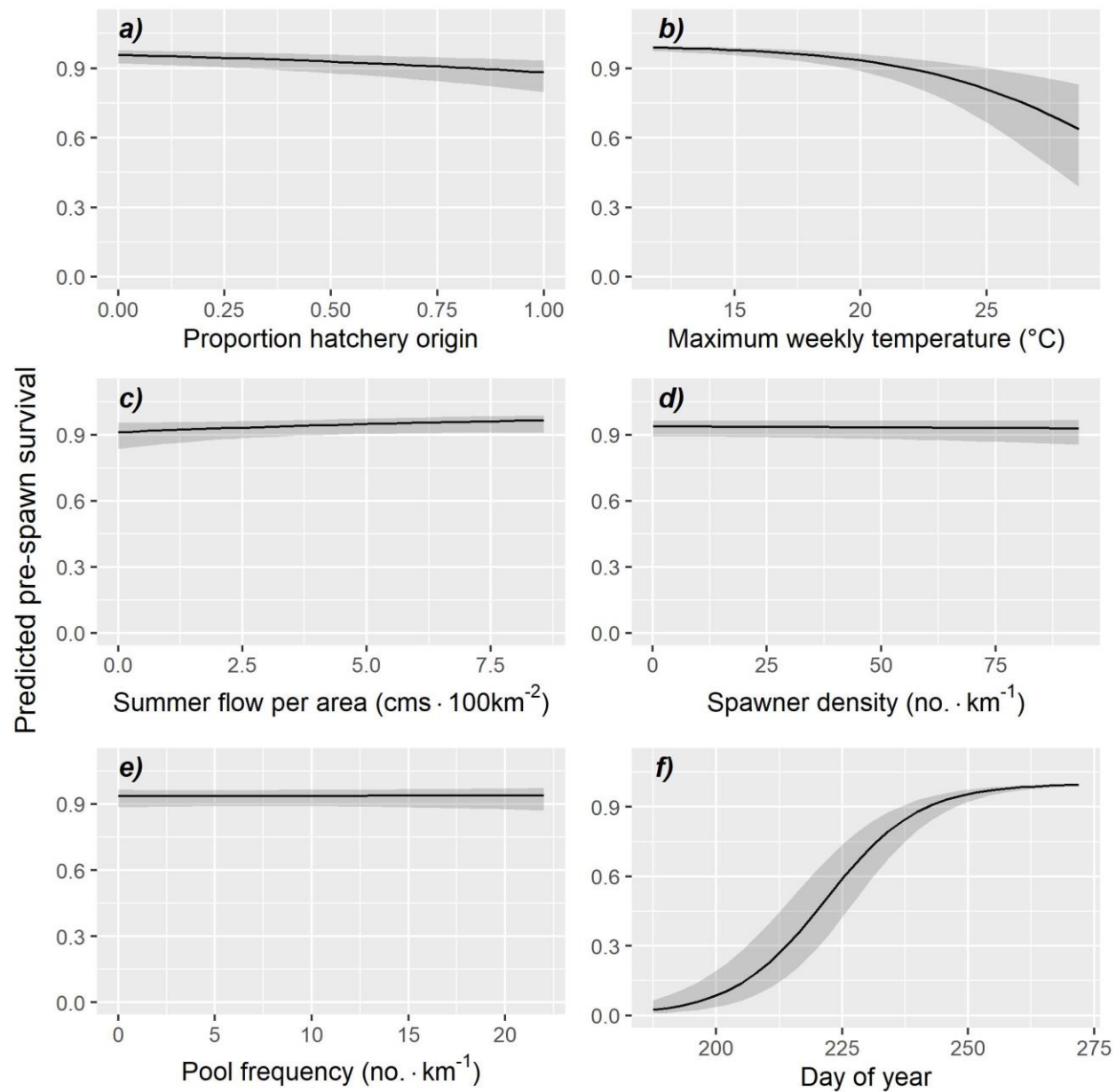


Figure 26. Marginal effects plot showing model-averaged predictions of mean pre-spawn survival as a function each fixed-effect covariate. Predictions for each subplot (a-f) were generated by holding all other fixed effects at their mean value and setting random effects to zero. Shaded areas represent 95% confidence intervals around the mean not accounting for random effect variances.

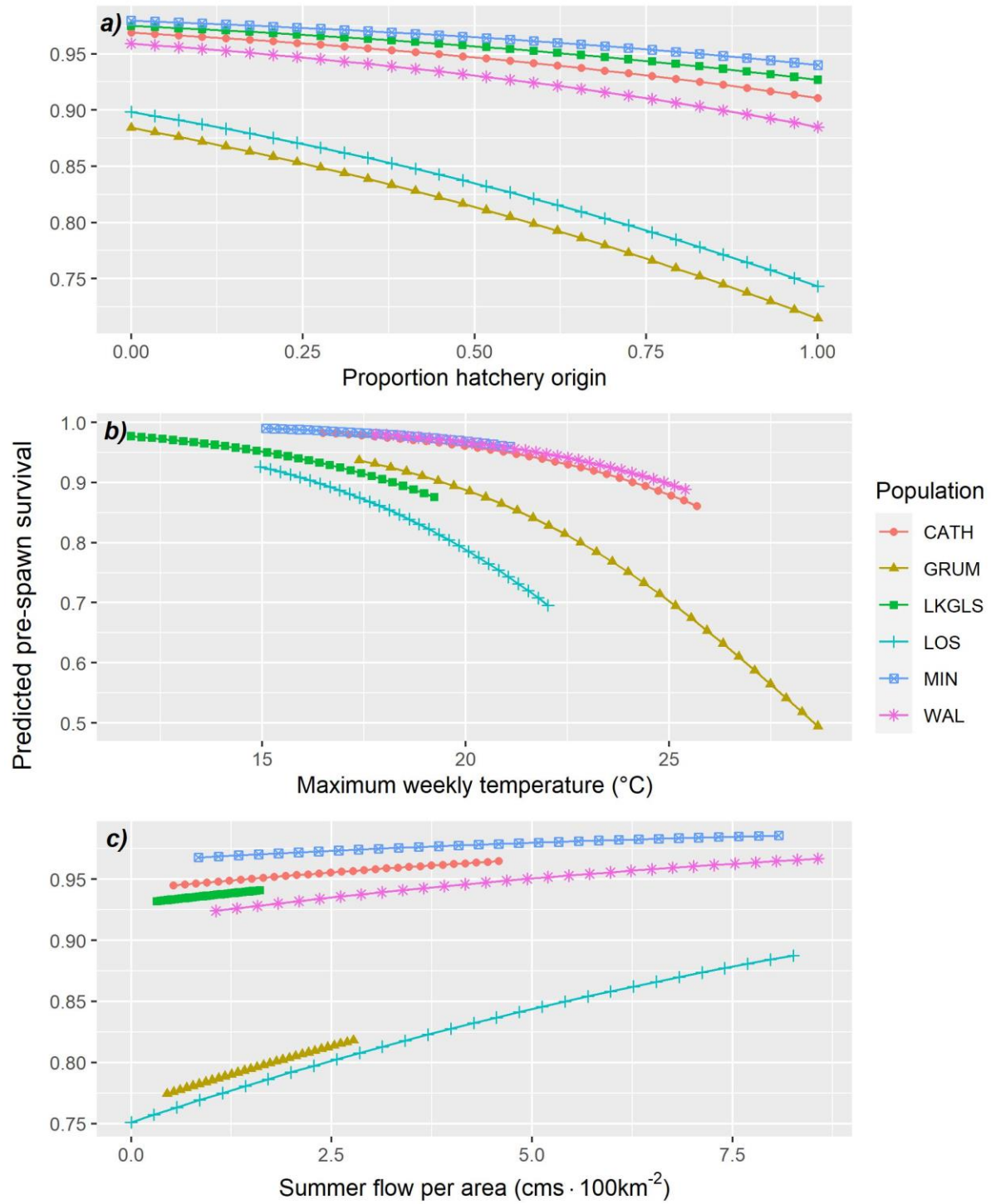


Figure 27. Model-averaged predictions of pre-spawn survival as a function of three fixed effect covariates grouped by population. For each subplot (a-c), all fixed-effect covariates except for the ones shown on the x-axis were fixed at their population-specific mean value and other random effects (i.e., reach and year) were set to zero.

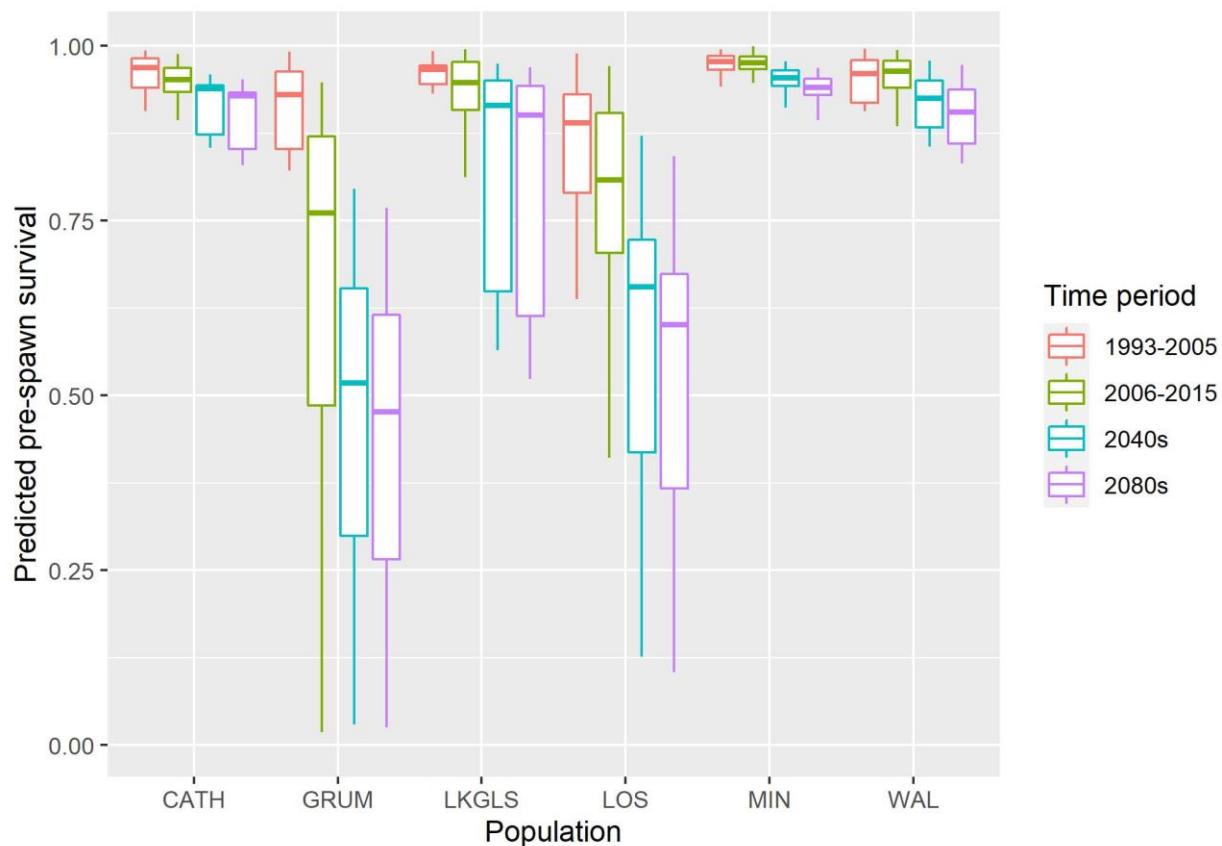


Figure 28. Distribution of reach-scale predicted pre-spawn survival rates by population and time period. Predictions for future years (2040s and 2080s) were not conditioned on the year random effect.

## References

- Barnett, H. K., T. P. Quinn, M. Bhuthimethee, and J. R. Winton. 2020. Increased prespawning mortality threatens an integrated natural- and hatchery-origin sockeye salmon population in the Lake Washington Basin. *Fisheries Research* 227:105527.
- Barton, K. 2020. MuMIn: Multi-Model Inference. R package version 1.43.17. <https://CRAN.R-project.org/package=MuMIn>.
- Benda, S. E., G. P. Naughton, C. C. Caudill, M. L. Kent, and C. B. Schreck. 2015. Cool, Pathogen-Free Refuge Lowers Pathogen-Associated Prespawn Mortality of Willamette River Chinook Salmon. *Transactions of the American Fisheries Society* 144(6):1159–1172.



- Bowerman, T. E., M. L. Keefer, and C. C. Caudill. 2021. Elevated stream temperature, origin, and individual size influence Chinook salmon prespawn mortality across the Columbia River Basin. *Fisheries Research* 237:105874.
- Bowerman, T., A. Roumasset, M. L. Keefer, C. S. Sharpe, and C. C. Caudill. 2018. Prespawn Mortality of Female Chinook Salmon Increases with Water Temperature and Percent Hatchery Origin. *Transactions of the American Fisheries Society* 147(1):31–42.
- Bowerman, T., M. L. Keefer, and C. C. Caudill. 2016. Pacific Salmon Prespawn Mortality: Patterns, Methods, and Study Design Considerations. *Fisheries* 41(12):738–749.
- Brooks, M. E., K. Kristensen, K. J. van Benthem, A. Magnusson, C. W. Berg, A. Nielsen, H. J. Skaug, M. Maechler and B. M. Bolker. 2017. glmmTMB Balances Speed and Flexibility Among Packages for Zero-inflated Generalized Linear Mixed Modeling. *The R Journal*, 9(2), 378-400.
- Burnham, K. P., and D. R. Anderson. 2002. Model selection and multimodel inference, a practical information-theoretic approach Second edition. Springer-Verlag New York, Inc., New York, NY.
- CDFG (California Department of Fish and Game). 2004. September 2002 Klamath River fish-kill: final analysis of contributing factors and impacts. CDFG, Sacramento, CA.
- Crozier, L. G., A. P. Hendry, P. W. Lawson, T. P. Quinn, N. J. Mantua, J. Battin, R. G. Shaw, and R. B. Huey. 2008. Potential responses to climate change in organisms with complex life histories: evolution and plasticity in Pacific salmon. *Evolutionary Applications* 1(2):252–270.
- Elsner, M. M., L. Cuo, N. Voisin, J. S. Deems, A. F. Hamlet, J. A. Vano, K. E. B. Mickelson, S.-Y. Lee, and D. P. Lettenmaier. 2010. Implications of 21st century climate change for the hydrology of Washington State. *Climatic Change* 102(1–2):225–260.
- ESRI 2020. ArcGIS Desktop: Release 10.8. Redlands, CA: Environmental Systems Research Institute.
- Feist, B. E., E. R. Buhle, P. Arnold, J. W. Davis, and N. L. Scholz. 2011. Landscape Ecotoxicology of Coho Salmon Spawner Mortality in Urban Streams. *PLoS ONE* 6(8):e23424.
- Feldhaus, J. W., T. L. Hoffnagle, D. L. Eddy, and K. N. Ressel. 2017. Lower Snake River compensation plan: Oregon spring Chinook Salmon evaluation studies 2014 annual progress report. Oregon Department of Fish and Wildlife, Salem, OR.
- Hartig, F. 2020. DHARMA: Residual Diagnostics for Hierarchical (Multi-Level / Mixed) Regression Models. R package version 0.3.2.0. <https://CRAN.R-project.org/package=DHARMA>.

- IPCC (Intergovernmental Panel on Climate Change). 2007. Climate change 2007: The physical science basis. Retrieved from <http://www.ipcc.ch/>
- Isaak, D. J., S. J. Wenger, E. E. Peterson, J. M. Ver Hoef, D. E. Nagel, C. H. Luce, S. W. Hostetler, J. B. Dunham, B. B. Roper, S. P. Wollrab, G. L. Chandler, D. L. Horan, and S. Parkes-Payne. 2017. The NorWeST Summer Stream Temperature Model and Scenarios for the Western U.S.: A Crowd-Sourced Database and New Geospatial Tools Foster a User Community and Predict Broad Climate Warming of Rivers and Streams: Stream climates in the Western U.S. *Water Resources Research* 53(11):9181–9205.
- Isaak, D. J., S. Wollrab, D. Horan, and G. Chandler. 2012. Climate change effects on stream and river temperatures across the northwest U.S. from 1980–2009 and implications for salmonid fishes. *Climatic Change* 113(2):499–524.
- Keefer, M. L., G. A. Taylor, D. F. Garletts, G. A. Gauthier, T. M. Pierce, and C. C. Caudill. 2010. Prespawn mortality in adult spring Chinook salmon outplanted above barrier dams: Chinook salmon prespawn mortality. *Ecology of Freshwater Fish* 19(3):361–372.
- Lynch, A. J., B. J. E. Myers, C. Chu, L. A. Eby, J. A. Falke, R. P. Kovach, T. J. Krabbenhoft, T. J. Kwak, J. Lyons, C. P. Paukert, and J. E. Whitney. 2016. Climate Change Effects on North American Inland Fish Populations and Assemblages. *Fisheries* 41(7):346–361.
- Moore, K., K. Jones, J. Dambacher, C. Stein, and et al. 2019. Aquatic Inventories Project: methods for stream habitat and snorkel surveys. Page 89. Oregon Department of Fish and Wildlife, Version 29.1, Corvallis, OR.
- Nakagawa, S., and H. Schielzeth. 2013. A general and simple method for obtaining  $R^2$  from generalized linear mixed-effects models. *Methods in Ecology and Evolution* 4(2):133–142.
- NOAA (National Oceanic and Atmospheric Administration). 2008. Supplemental comprehensive analysis of the Federal Columbia River Power System and mainstem effects of the Upper Snake and other tributary actions. NOAA Fisheries.
- NOAA (National Oceanic and Atmospheric Administration). 2019. NOAA National Water Model Reanalysis Model Data version 2.0. Accessed from <https://registry.opendata.aws/nwm-archive/>. Downloaded on October 2019.
- Quinn, T. P., D. M. Eggers, J. H. Clark, and H. B. Rich, Jr. 2007. Density, climate, and the processes of prespawning mortality and egg retention in Pacific salmon ( *Oncorhynchus* spp.). *Canadian Journal of Fisheries and Aquatic Sciences* 64(3):574–582.
- R Core Team. 2020. R: A language and environment for statistical computing. R Foundation for Statistical Computing, Vienna, Austria. URL <https://www.R-project.org/>.

- Roumasset, A. G. 2012. Pre-spawn mortality of upper Willamette River spring Chinook Salmon: associations with stream temperature, watershed attributes, and environmental conditions on the spawning grounds. Page 108. University of Idaho, Moscow Idaho.
- Scholz, N. L., M. S. Myers, S. G. McCarthy, J. S. Labenia, J. K. McIntyre, G. M. Ylitalo, L. D. Rhodes, C. A. Laetz, C. M. Stehr, B. L. French, B. McMillan, D. Wilson, L. Reed, K. D. Lynch, S. Damm, J. W. Davis, and T. K. Collier. 2011. Recurrent Die-Offs of Adult Coho Salmon Returning to Spawn in Puget Sound Lowland Urban Streams. PLoS ONE 6(12):e28013.
- Tillotson, M. D., and T. P. Quinn. 2017. Climate and conspecific density trigger pre-spawning mortality in sockeye salmon (*Oncorhynchus nerka*). Fisheries Research 188:138–148.
- USFS (United States Forest Service). 2020. Western U.S. Stream Flow Metrics – A dataset of modeled flow metrics for streams in major river basins of the Western US for historical and future climate change scenarios. Accessed from <https://data.fs.usda.gov/geodata/edw/datasets.php?xmlKeyword=hydro+flow+metrics+west>. Downloaded on December 2020.

### *3.3 Update on the life cycle model*

#### **Background**

Beginning in fall of 2019, CRITFC joined a team of modelers and biologists in a collaborative revision of existing life cycle models (LCMs) for Grande Ronde basin spring Chinook Salmon. The team is composed primarily of staff from CRITFC (B. Staton, C. Justice, and S. White), NOAA (M. Liermann and R. Sharma), and ODFW (P. Gibson and T. Sedell). The overarching objective of the LCM is to understand how likely management actions, such as restoration of juvenile rearing habitat, are to result in population recovery in the face of future conservation challenges, such as climate change. Projecting how Grande Ronde Chinook Salmon populations will respond to future conditions requires a firm understanding of historical population dynamics and responses to biological and environmental conditions. As such, we have organized the project into three primary phases:

- 1. Development of a statistical LCM** – wherein characteristics of the historical population dynamics are estimated from historical biological and physical habitat variables.
- 2. Development of plausible future scenarios** – wherein formalized expressions of potential future conditions representing alternative management actions or climate change are posited for evaluation.
- 3. Simulation of future population outcomes** – wherein the estimated population dynamics quantities from historical estimates are used to project possible outcomes under each of the potential future scenarios and a set of performance metrics is used to gauge the relative likelihood of population recovery under each scenario.

At the time of writing, we have made substantial progress on the topics of phase 1 and have initiated early planning discussions for phase 2. Given this level of completion, we have chosen to use this space primarily to elaborate on the model we are developing for phase 1 and to provide a high-level overview of our plans for phases 2 and 3.

#### **Phase 1: Development of a statistical LCM**

A statistical LCM is one that estimates characteristics of the salmon life cycle (e.g., productivity, survival, carrying capacity, transition probabilities) from available data. It is needed to provide baseline parameter estimates that represent the historical population dynamics, such that we can simulate the populations forward in time under phase 3.

In our 2019 annual report (White et al. 2020, Section 3.1 therein), we described a modeling effort developed by M. Liermann and R. Sharma for Grande Ronde basin spring Chinook Salmon and our plans to improve upon their work in a collaborative effort. We refer to this model as the “Liermann & Sharma model”, and unlike previous modeling efforts in the Grande Ronde basin, it is an integrated model: it fits simultaneously to all of the available data time series including

adult/juvenile abundance, juvenile survival, and adult composition (rather than performing piecemeal analyses and then stitching the output together as a complete life cycle). Further, it is a state-space model: it explicitly acknowledges that there are two sources of variability that create the data set; biological process noise creates the true underlying variability that we care about quantifying and measurement errors which result in differences between the observation and the true value. We use Bayesian inference to estimate model parameters – this approach works well for state-space models, and the output (i.e., samples from a joint posterior distribution) will be useful for propagating uncertainty estimated in phase 1 to the simulation analyses of phase 3.

In the three sections that follow under phase 1, we describe the (a) stages we model and the dynamics that link them in a narrative rather than mathematical presentation, (b) parameters that are estimated when modeling these stages and dynamics, and (c) the linkages we make to observations to enable parameter estimation from empirical data. We use footnotes to provide more details on which specific portions of the model differ from the Liermann & Sharma model. It is important to note that the final model will fit to the four populations (upper Grande Ronde River, Catherine Creek, Lostine River, and Minam River) simultaneously, but in its current form the model only handles one population at a time.

### *Stages and dynamics*

The model is structured by brood year, migratory strategy, origin, sex, and age – however brood year is the only structure that applies to all life stages. It tracks the latent (i.e., true, but only partially or imperfectly observed) abundance states at several discrete life stages according to this structure as defined by a set of process equations that have both deterministic and stochastic components. Reproduction and early life survival take the form of a Beverton-Holt (BH) recruitment relationship that produces total end-of-summer parr (deterministic BH prediction plus stochastic process noise) from spawning adults. These parr are then partitioned into one of two migratory strategies: those that rear overwinter in the headwaters and those that rear overwinter farther downstream in the basin (termed “spring migrants” and “fall migrants”, respectively). Density-dependent overwinter survival terms are applied to these parr to obtain the number of natural-origin smolts that migrate out of the basin in the spring. At this point, hatchery-origin fish are introduced based on historical records and migrate downstream with the natural-origin fish<sup>1</sup>.

---

<sup>1</sup> The Liermann & Sharma model did not track abundance or survival of hatchery origin juveniles, and only addressed them at the adult stage upon return. That model tracked the complete life cycle for only natural-origin fish, then “created” hatchery-origin fish via an expansion for the proportion of hatchery-origin returns that have been observed in the past. We thought it important to model the dynamics of hatchery-origin fish throughout the complete life cycle, as decision makers may wish to evaluate scenarios that manipulate hatchery inputs.

We assume out-of-basin movement survival is the same for both natural-origin migratory strategies, but different for hatchery-origin fish.

Upon reaching Lower Granite Dam, the first dam encountered during the seaward migration, the migratory strategy of natural origin fish is discarded, and smolt become structured only by the year they were spawned and their origin. Smolt move through the hydropower system on the Snake and mainstem Columbia rivers using internally estimated survival terms and eventually reach the estuary. At this point, we consider them to be age-0 ocean juveniles (total age-2) and apportion them to sex<sup>2</sup>. We assume there are three possible ages Chinook Salmon can mature and return as adults: ocean age-1 (total age-3)<sup>3</sup>, ocean age-2 (total age-4), or ocean age-3 (total age-5). The ocean age refers to how many winters the juveniles have spent at sea, and fish that do not mature at a given age suffer an age- and origin-specific mortality rate and only the survivors have the chance to return at the next age.

For the adult return, mature fish from the corresponding brood years and ages make the spawning migration upriver in a given calendar year (which becomes the brood year for a future cohort). We have included placeholder terms for mainstem upstream survival affected by sources such as sea lion predation, harvest, and passage failures, but these are currently uninformed by data – improving this aspect is a primary next-step in model development. Eventually, these adults reach their natal tributary at which point some are removed for broodstock (except from the Minam River population) or may suffer pre-spawn mortality. Those that remain, regardless of age/sex/origin, are counted as equally contributing spawners that produce the next generation<sup>4</sup>.

### *Estimated Parameters*

The model must estimate many parameters to control how these dynamics behave. Many quantities are modeled hierarchically, wherein the parameters of a hyperdistribution are freely estimated: a time-constant mean and inter-annual variance. Year-specific values are sampled from this hyperdistribution to enable more robust estimation in years with missing or poor-quality data.

---

<sup>2</sup> The Liermann & Sharma model did not track abundance separately by sex. However, sex composition data are available for returning adults, and we deemed this important since we included the possibility of returning at total age-3 – these are almost all males and there was a concern of biasing the index of reproductive output in years with a large age-3 male return if we did not account for sex.

<sup>3</sup> The Liermann & Sharma model tracked return abundances of only total age-4 and total age-5 adults.

<sup>4</sup> The Liermann & Sharma model assumed that an age-5 spawner was “worth” 1.2 age-4 spawners. Our current model treats all spawners equally in producing the next generation of parr, but we have plans to incorporate fecundity data such that the BH relationship is expressed in terms of parr produced per egg, and the total egg production is calculated as the sum product of spawners-at-age/sex and mean fecundity-at-age/sex.

Oftentimes, the parameter in question is a proportion (e.g., survival or some other transition probability such as a mature rate) and we use a logit-normal hyperdistribution to model such parameters. If a set of parameters follow this structure, we will refer to it as “hierarchical”. The productivity and capacity parameters of the BH relationship are exceptions to this hierarchical structure – we assume those parameters are time-invariant. We model the capacity parameter as a product of an index of habitat availability and an estimated scalar – this scalar will enable predicted changes in habitat availability to affect population dynamics in phase 3 analyses (more details on the habitat index below). Because of the state-space nature of the model, parr recruitment states are treated as latent random deviates from the expected BH relationship. Next, the model hierarchically estimates the proportion of parr that will be fall migrants each year, and the annual complement becomes spring migrants. The model assumes the density of parr in the summer affects their size moving into winter and subsequent overwinter survival: a logit-linear model with logit-normal random deviates serves this purpose (one intercept for each migratory strategy but one slope common to both migratory strategy types). Thus, there is a deterministic density-dependent prediction for overwinter survival, and this serves as the expectation from which logit-normal deviates are produced to serve as the year- and migratory strategy-specific value. Out-of-basin movement survival is hierarchically estimated separately for natural- and hatchery-origin fish; we assume that both fall migrants and spring migrants have the same survival out of the basin. To move fish from the top of Lower Granite Dam through the entire hydrosystem and to arrival in the estuary, we hierarchically estimate separate survival time series for natural- and hatchery-origin fish.

We hierarchically estimate separate sex apportionment time series for natural- and hatchery-origin fish and these take effect upon arrival to the estuary. Additionally, we hierarchically estimate separate maturation rates by age, sex, and origin (i.e., the fraction of fish of a given sex/origin surviving the previous year at sea that mature and make the spawning migration at that age (total age-5 maturation rate set to one). We also hierarchically estimate ocean survival<sup>5</sup>, but were required to impose certain assumptions for identifiability purposes. We hierarchically estimate the time series corresponding to the first and second years at sea for natural-origin fish. To simplify the model and enable estimation, we assume the third year ocean survival is identical as the second year, but lagged by a year such that fish making these transitions at different ages experience the same survival term in the same calendar year. To obtain hatchery-origin ocean survival, we estimate a single logit-scale scalar that serves to adjust the entire ocean survival time series up or down for each ocean age. Exploratory models that included more estimated parameters that control

---

<sup>5</sup> The Liermann & Sharma model assumed ocean survival was known and time-invariant. We were able to relax this assumption by fitting to auxiliary information on juvenile survival through the hydrosystem.

ocean survival dynamics failed to converge, showed signs of non-identifiability, or otherwise provided non-sensical estimates.

For the return migration, we hierarchically estimate pre-spawn survival (applied after broodstock removals and sampling at weirs). Additionally, there are two components that contain “nuisance” parameters, i.e., quantities we are not interested in from an inferential standpoint but are needed for valid treatment of the historical data. First, we found that hatchery-origin adults were present in the adult composition data before they would be expected to return based on the start date of the hatchery program. For this, we introduce a simple “straying model” to produce these fish in the process model when there is no other process to generate their presence; this involves estimating the number of hatchery strays that entered the system each year and their composition by age and sex (not year-specific). This stray model is only applied in years where it is necessary, i.e., only in the early years when hatchery fish were sampled unexpectedly. Second, we estimate a set of correction factors that enable fitting to adult composition data collected at both weirs and carcass surveys. In data exploration exercises, we found systematic differences between these two data sets, suggesting a sampling bias in one of them. Thus, we estimate a set of correction factors that essentially quantify the relative likelihood that an individual of each age/sex will be sampled during carcass surveys relative to weir sampling.

Table 20 Summary of the parameter types estimated by the statistical LCM. The "Shared?" column indicates whether that parameter type will be shared among populations once a multi-population model is developed.

Type of Parameter(s)	Hierarchical?	Structure	Shared?
BH productivity	No	None	No
BH capacity	No	None	No
BH variability	No	None	No
Proportion fall migrants	Yes	Brood year, natural-origin only	No
Overwinter survival coefficients	No	Migratory strategy	No
Overwinter survival realizations	Yes	Migratory strategy, brood year	No
Out-of-basin movement survival	Yes	Origin, brood year	No
Survival through hydrosystem	Yes	Origin, brood year	Yes
Sex apportionment	Yes	Origin, brood year	Yes
*First year ocean survival	Yes	Origin, brood year	Yes
*Second year ocean survival	Yes	Origin, brood year	Yes
*Third year ocean survival	No	Origin, brood year	Yes
Maturation rates	Yes	Origin, sex, brood year	Yes
Carcass survey correction factor	No	Sex, age	Yes
*Abundance of hatchery strays	No	Brood year	No
*Composition of hatchery strays	No	Age, sex	No

\*Please see the text in “Estimated Parameters” for details on how ocean survival and hatchery strays are treated.



## *Data Sources*

The model fits to many data sources to enable estimation of this large number of parameters. Each data source has an associated quantity that represents its observation uncertainty. For example, for survival observations, these values are really estimates derived from data (PIT tag detection histories). Rather than perform the necessary estimation of such survival terms from the raw tagging data internally within the state-space model, we fit to the externally derived estimate of survival and use the standard error of this estimate to structure its observation error variance. There are several such survival terms for natural origin-fish: (a) fish tagged in the summer, (b) fish tagged at the screw trap in the fall, (c) fish tagged at the screw trap in the spring. We additionally fit to the estimated juvenile abundance that passed the screw trap in the fall and the spring. For hatchery fish, we use the number of released smolt each spring directly to introduce these fish into the modeled population and do not fit to them; but we do fit to the externally estimated survival of these hatchery releases to Lower Granite Dam<sup>6</sup>. We also fit to externally derived estimates of survival from Lower Granite Dam through Bonneville Dam<sup>7</sup>: these are origin- and brood year-specific values that we extracted from the Comparative Survival Study 2020 draft report (Table A1 therein; “aggregate wild Chinook” used for natural-origin fish and “Catherine Creek AP” used for hatchery-origin fish; DeHart et al. 2020). No other data sources are currently used until the adults arrive in their natal tributaries, where estimates of total adult returns have been made (prior to broodstock removals and pre-spawn mortality). We fit to this abundance, and their composition (by age/sex/origin) sampled at the weir (where applicable)<sup>8</sup>. We use the proportion of these fish (by age/sex/origin) that were removed for broodstock to decrement this return abundance to obtain the number of adults that have a chance to spawn. We fit to the composition of adults sampled in carcass surveys as an additional data set to inform the composition of the adults that returned in a given year<sup>9</sup>. We fit to counts of carcasses that were found to have unsuccessfully spawned as information to estimate pre-spawn survival<sup>10</sup>.

---

<sup>6</sup> These data sets were not used by the Liermann & Sharma model.

<sup>7</sup> These data sets were not used by the Liermann & Sharma model, instead ocean survival was assumed known to allow estimation of hydropower survival without including explicit information on it.

<sup>8</sup> In the revised model, composition vectors have 12 elements: 3 ages by 2 sexes by 2 origins. The Liermann & Sharma model used vectors with two elements: one for each age-4 and age-5 samples. Expanding this vector provides the information to internally estimate the additional maturity, sex apportionment, and ocean survival parameters.

<sup>9</sup> The Liermann & Sharma model did not use carcass data to inform adult composition.

<sup>10</sup> The Liermann & Sharma model did not use carcass spawn status data to internally estimate pre-spawn survival, rather, an assumed known value was supplied.

We use log-normal likelihoods for abundance data (e.g., juveniles that passed the trap), logit-normal likelihoods for proportions (e.g., externally derived survival probabilities), multinomial likelihoods for adult composition vectors, and binomial likelihoods for counts of examined carcasses that unsuccessfully spawned. All observations are assumed independent when constructing the joint likelihood for all data types. Figure 29 - Figure 33 at the end of this chapter show examples of how the current version of the model fits to the data sources described here for the Catherine Creek population.

### *Next Steps in Phase 1*

Before considering phase 1 development complete, there are several aspects of the model we wish to improve upon.

- (1) **More detailed habitat availability index** – the Liermann & Sharma model used a quantity called “pool equivalent units” to represent the amount of available habitat for juvenile rearing capacity. It is essentially a weighted usable habitat metric, where the weights of different habitat types are calculated from juvenile densities obtained from snorkel surveys. We currently use this same index, but are simultaneously developing a revised habitat capacity index that uses similar concepts, but includes more covariates (such as large wood and stream temperature) with the intent that this will enable us to evaluate more detailed habitat scenarios in phases 2 and 3. More details can be found in the section on developing the index.
- (2) **More detailed treatment of upstream adult migration** – we currently assume that 70% of the adults that return to the mouth of the Columbia River survive to their natal tributaries and that this value is time constant and is applicable to all ages and origins. This is almost certainly an underestimate, and realities like mark-selective fishery harvests indicate that we have oversimplified it. We would like to quantify this mortality more realistically, and partition it to the various sources (e.g., harvest, predation, and dam passage failures), which will allow these quantities to be manipulated for future scenarios. Note that we do not plan to estimate these quantities internally within the state-space model, but rather pass the model values that are assumed to be known based on the best available information.
- (3) **Inclusion of fecundity information** – currently each adult that survives pre-spawn mortality is treated as an equal contributor to the next generation of parr. However, due to fluctuations in age/sex composition over time, the total reproductive output each year may not be accurately represented by this index, and we thus may be over-estimating the magnitude of process variance in recruitment to the parr stage. We have plans to weight the contribution of each spawner by the mean fecundity-at-age, which may help address this problem.
- (4) **Integration of single populations into one model** – we plan to incorporate the four populations into one model as was done in the Liermann & Sharma model, rather than fitting separate models for each population as our current version is structured. This will

accomplish three main things: (a) overall simpler workflow (all information is contained in one joint posterior), (b) we can model (and estimate) correlations in among-population dynamics, and (c) greater information content to estimate parameters that are shared among populations (e.g., ocean survival, maturity, etc.).

## **Phase 2: definition of plausible future scenarios**

In this phase, we will formalize expectations for the conditions faced by these populations in the future. This will include factors that are “background changes” (those resulting from, e.g., climate change and land use) as well as “actionable changes” (those resulting from, e.g., habitat restoration and hatchery practices). In this effort, we will coordinate closely with local decision makers to design a set of scenarios that describe what the future might look like. We will focus primarily on physical habitat features of the freshwater environment, as this is the area where local managers can have the most influence, however, we will also examine other scenarios following the interest of the group (e.g., alternatives for hatchery supplementation strategies, harvest management, or hydropower operations). To facilitate interpretation of the output generated in phase 3, we wish to avoid a “fully factorial” set of scenarios, where all possible combinations of changes are considered and instead prefer to limit the set to those that are most interesting and plausible to decision-makers.

The revised habitat capacity index (see the section on its development for more details) will play a central role in expressing the freshwater components of these scenarios. That approach assigns a weight to all stream reaches in the relevant area for a population and sums the weighted reach length to obtain the index value for each population. The weights are calculated based on how the combination of habitat attributes found within a reach (e.g., large wood, stream temperature) score on a habitat suitability scale (0 = worst possible habitat, 1 = best possible habitat). The habitat suitability scale is quantified by relationships between fish density (via snorkel surveys) and habitat characteristics and the fitted values are rescaled to the 0-1 scale. Performing this calculation with habitat attributes from recent history gives us a value that represents a current index of habitat capacity. We can express future habitat restoration and climate change scenarios by changing the habitat attributes found in each reach and recalculating the weights and the summed index. For example, one scenario may include a 20% increase in large wood in 50% of the high priority habitat over the next 10 years. These changes in habitat will result in changes in the capacity index, which will then be passed to the simulation model in phase 3 and will affect the capacity of the habitat to hold rearing parr and will also affect density-dependent overwinter survival.

A limitation of this approach is that we will only be able to defensibly quantify scenarios that impact the habitat attributes that are included in the habitat suitability model. For example, because that model does not include any variables describing the availability of off-channel habitat, we will not be able to use this approach to investigate restoration actions in that context. That being said, we will still have the ability to “pull the levers”, so to speak, relative to other components of the

life cycle. For example, if we have reason to believe (ideally from the literature) that climate change is expected to change ocean survival by some percentage, we can still evaluate scenarios that incorporate these expectations.

### **Phase 3: simulation of future population outcomes**

One advantageous feature of building the estimation LCM as a state-space model is that the set of process equations serve as an expression of how we believe the population dynamics operate, and it can thus serve as a biological operating model for simulating the populations forward in time. The estimation LCM from phase 1 will provide a joint posterior distribution for all unknown quantities – this captures the expectation, uncertainty, and covariability of the parameters needed to simulate the populations forward. For parameters that are estimated hierarchically, the year-specific parameters will be of little use (except to initialize the populations from their current states), but the mean and spread of the hyperdistributions will be very useful. There are some components that will require a process model to be created, for example, a control rule for how broodstock removals are conducted and how this impacts the hatchery-origin smolt inputs the populations will receive. Further, some aspects may be simplified. For example, time varying sex composition may have been important for explaining historical data, but perhaps it is not a key feature of the population dynamics that needs to be simulated. Within a scenario, we will conduct many replicates by sampling different values from the joint posterior to simulate different possible population trajectories based on the uncertainty in the estimates we made based on historical data.

Critical to this effort will be the definition of several performance metrics summarizing the status of the populations based on their simulated trajectories. In general, these metrics will be implemented as a “yes” or a “no” outcome for whether some population outcome occurred, which when summarized over the many replicates, will give an indication of how much confidence we should have that population outcome will occur under each scenario.

### **References**

- DeHart, M., McCann, J., Chockley, B., Cooper, E., Scheer, G., Haeseker, S., Lessard, B., Copeland, T., Ebel, J., Storch, A., Tinus, E., and Rawding, D. 2020. Comparative Survival Study of PIT-tagged Spring/Summer/Fall Chinook, Summer Steelhead, and Sockeye: Draft 2020 Annual Report. Annual report submitted to Bonneville Power Administration for Contract #19960200 for work performed between December 1, 2019 – November 30, 2020.
- White, S., Justice, C., Burns, L., Staton, B., Graves, D., and Kaylor, M. 2020. Assessing the Status and Trends of Spring Chinook Habitat in the Upper Grande Ronde River and Catherine Creek. Annual report submitted to Bonneville Power Administration for Project #2009-004-00 for work performed between January – December 2019.

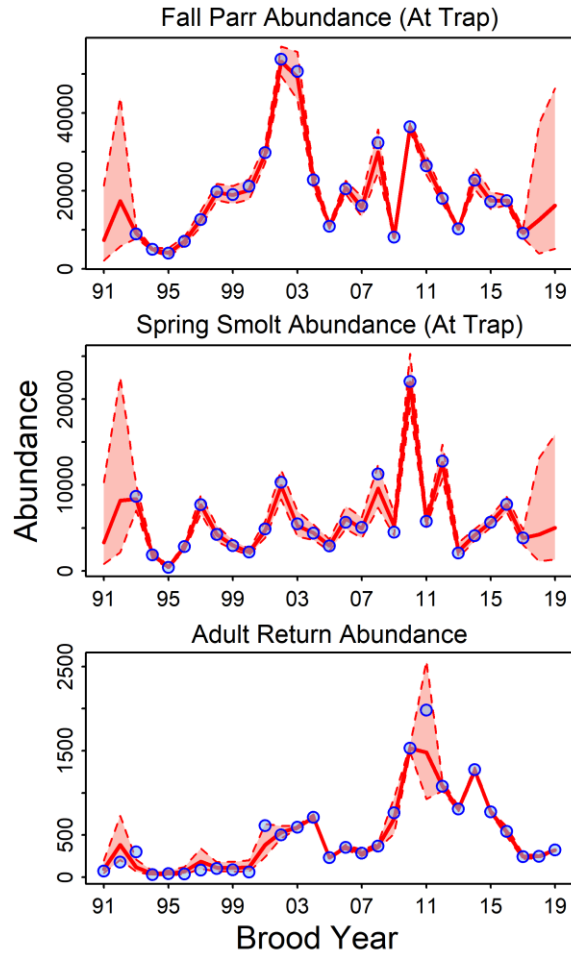


Figure 29 Posterior summaries (red) and observed values (blue) for abundance-related data sources. The thick red line is the posterior median and the red area is the 95% equal-tailed credible region. The displayed estimates/data are from the Catherine Creek population, but other populations look similar in terms of fit and amount of uncertainty.

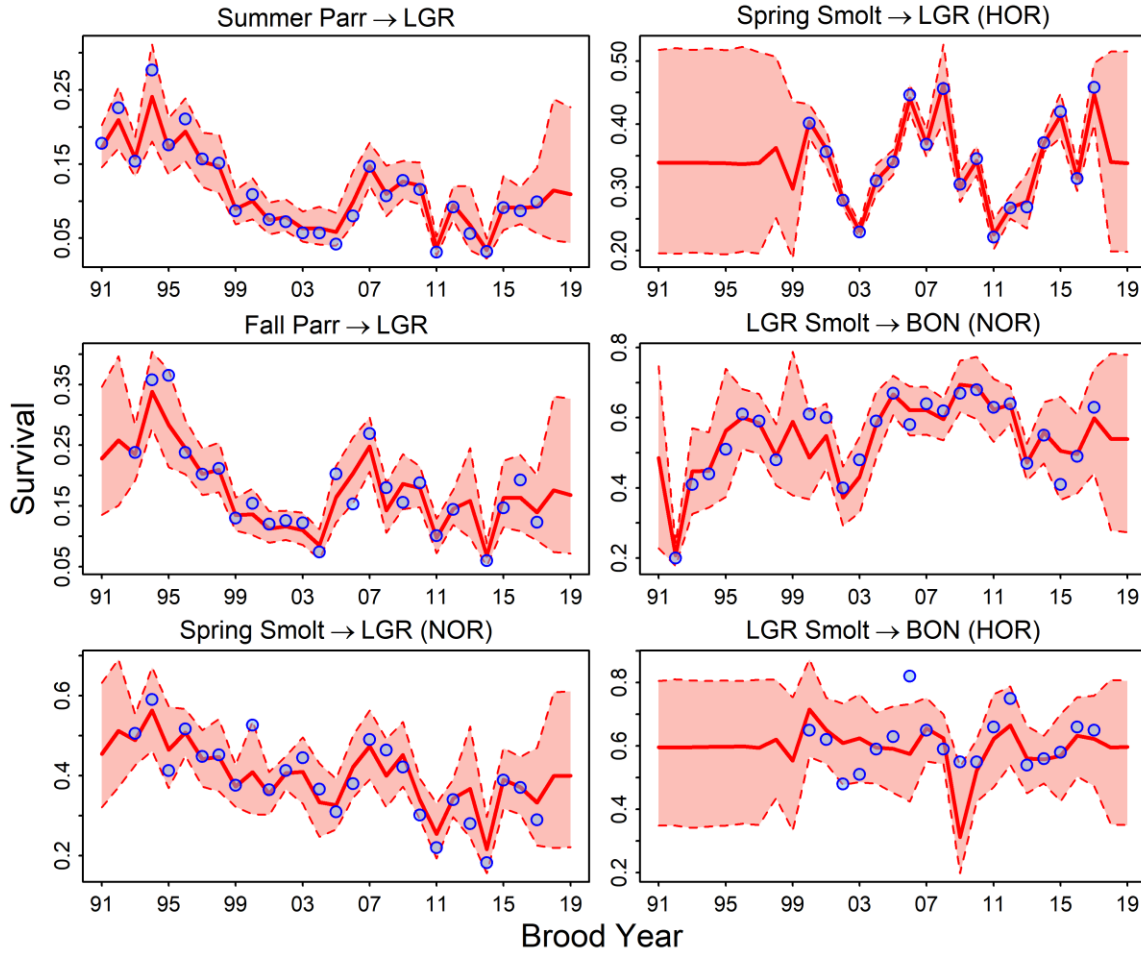


Figure 30 Posterior summaries (red) and observed values (blue) for juvenile survival-related data sources. The thick red line is the posterior median and the red area is the 95% equal-tailed credible region. The displayed estimates/data are from the Catherine Creek population, but other populations look similar in terms of fit and amount of posterior uncertainty.

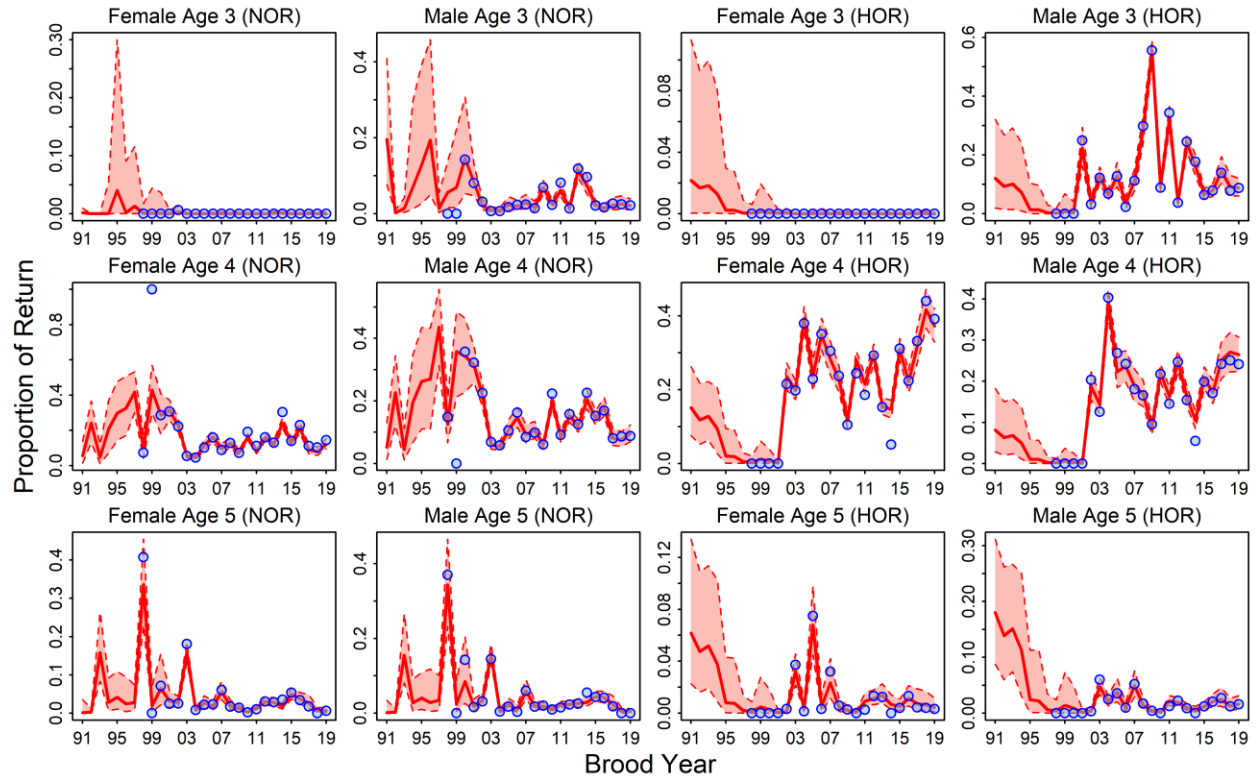


Figure 31 Posterior summaries (red) and observed values (blue) for adult composition data collected at the weir. The thick red line is the posterior median and the red area is the 95% equal-tailed credible region. Each panel represents the proportional contribution of each age/sex/origin type to the annual sample (the y-axis value summed across panels within one year is equal to 1). The displayed estimates/data are from the Catherine Creek population, but other populations look similar in terms of fit and amount of posterior uncertainty.

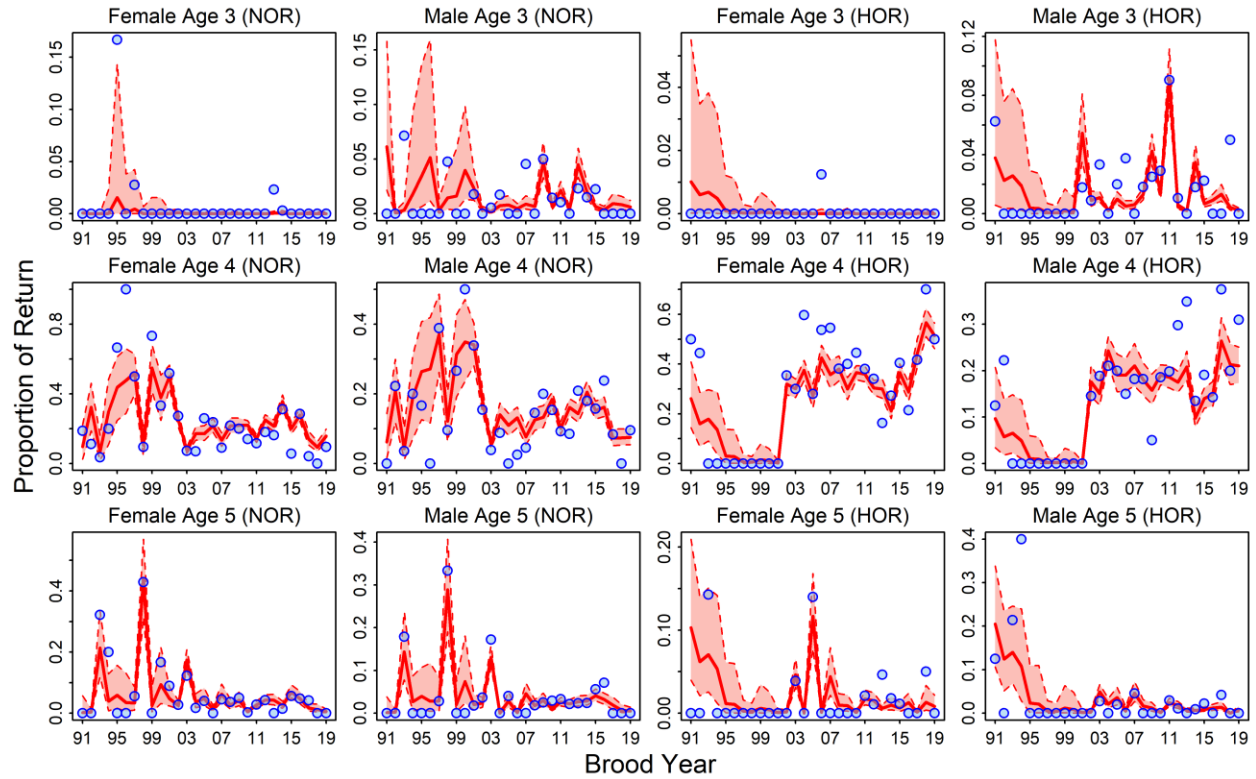


Figure 32 Posterior summaries (red) and observed values (blue) for adult composition data collected during carcass surveys. The thick red line is the posterior median and the red area is the 95% equal-tailed credible region. Each panel represents the proportional contribution of each age/sex/origin type to the annual sample (the y-axis value summed across all panels within one year is equal to 1). The displayed estimates/data are from the Catherine Creek population, but other populations look similar in terms of fit and amount of posterior uncertainty.



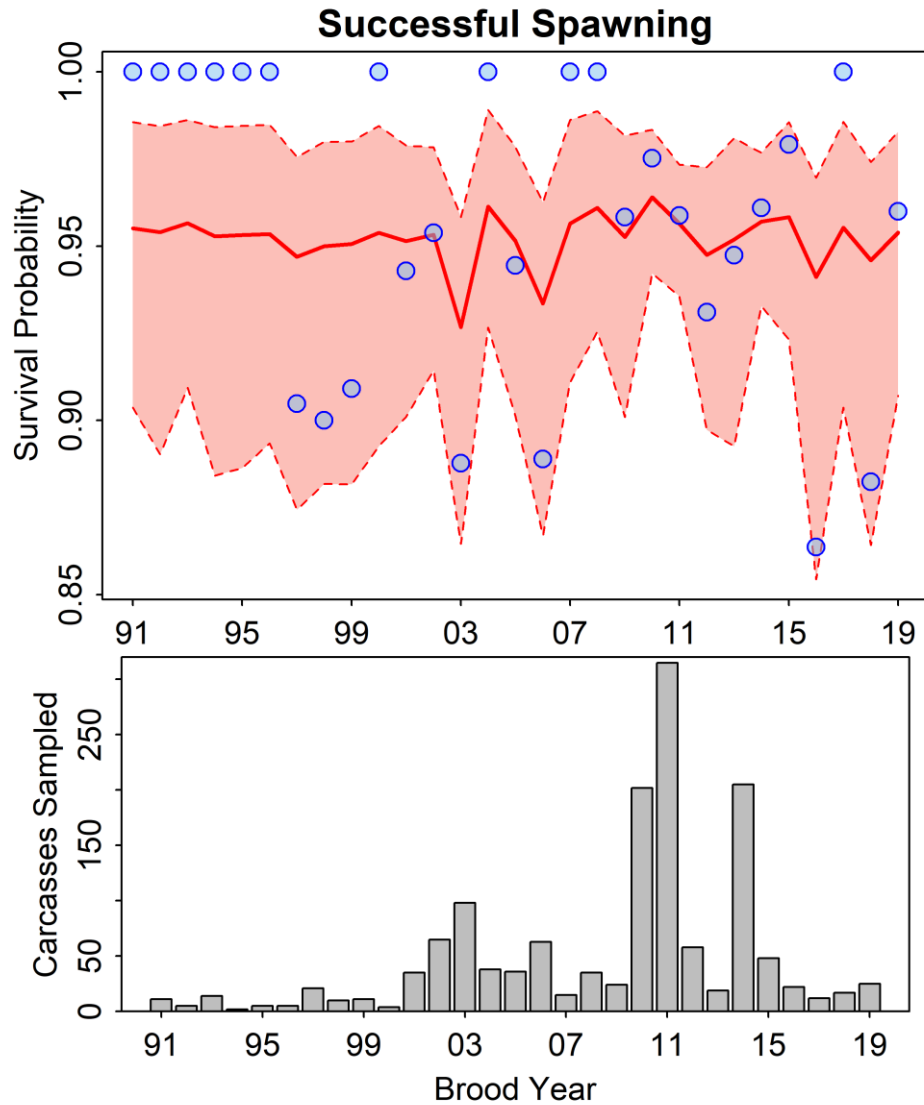


Figure 33 Top: posterior summaries (red) and observed values (blue) for the proportion of adults making it past broodstock removals that successfully spawn. The thick red line is the posterior median and the red area is the 95% equal-tailed credible region. Bottom: the number of carcasses examined for spawn status each year. In both panels, the displayed estimates/data are from the Catherine Creek population.

## 4.0 Adaptive Management

### 4.1 Progress on an adaptive management framework

**Note:** The published version of the manuscript discussed in this section is available in Appendix E – "Progress Towards a Comprehensive Approach for Habitat Restoration in the Columbia Basin: Case Study in the Grande Ronde River."

#### Summary

The Independent Science Review Panel (ISRP) previously recommended that our group engage with Grande Ronde Model Watershed (GRMW) in developing an adaptive management framework (ISRP 2018). In response to this recommendation, we worked with GRMW, Confederated Tribes of the Umatilla Indian Reservation (CTUIR), Oregon Department of Fish and Wildlife (ODFW), U.S. Forest Service (USFS), and several other partners on two related tasks: (a) a needs assessment workshop and manuscript documenting our progress and setbacks towards a comprehensive approach to habitat restoration in the Columbia River basin and (b) involvement in a multi-agency workgroup developing a 5- and 20-year adaptive management plan for the Grande Ronde basin.

#### **Progress Towards a Comprehensive Approach for Habitat Restoration in the Columbia Basin: Case Study in the Grande Ronde River**

Despite immense resources directed towards habitat restoration, recovering fish populations remains a daunting and perplexing issue. In 2015, recommendations for a comprehensive approach to habitat restoration in the Columbia River basin were published in *Fisheries* (Rieman et al. 2015), which included elements of landscape ecology and resilience, broad public support, governance for collaboration and integration, and capacity for learning and adaptation. Using the Grande Ronde River basin as a case study, we convened a working group consisting of local restoration practitioners, managers, and researchers involved in habitat restoration and research, monitoring, and evaluation to assess progress towards meeting these recommendations (White et al. 2021; Appendix E). We concluded that partnerships and collaborations in governance have been formed and research using a landscape perspective has been integrated into decision-making, but efforts would benefit from gaining broader public support, formalizing an adaptive management strategy (Figure 34), and defining objectives and indicators for biological and ecological diversity. Continued progress will require consistent policy and funding support from the broader region. We envision this self-assessment at the five-year milestone would be helpful to other groups facing similar challenges.

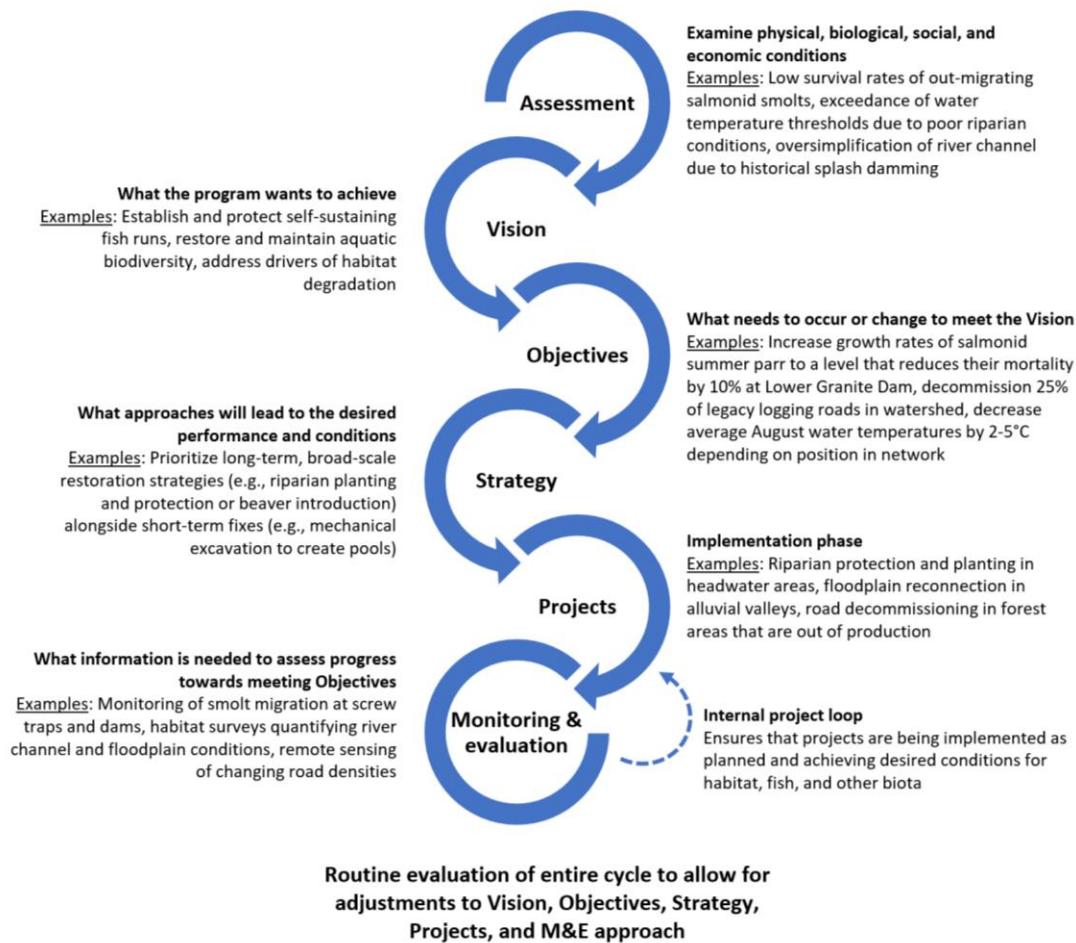


Figure 34. Adaptive management framework with examples from the Grande Ronde basin, from White et al. (2021) after ISRP (2018).

## Development of an Adaptive Management Framework

Building on lessons learned from our collaborative review of the Grande Ronde basin habitat restoration program (Appendix E), we are in the process of developing a formal adaptive management plan to guide future salmon habitat restoration actions. This process is being spearheaded by the Grande Ronde Model Watershed with active participation from numerous other partners including CTUIR, ODFW, and USFS. The primary goal of this project is to develop a comprehensive framework by which the progress of restoration actions towards meeting our objectives can be measured and used to inform future management actions. The adaptive management plan will consist of six key components including assessment, vision, objectives, strategy, projects, and monitoring and evaluation (Figure 34). Monitoring, evaluation, and assessment form the backbone of learning and revising the vision, goals, objectives, strategies, and projects intended to improve tributary habitat conditions in support of salmon recovery and river ecosystem health. While this plan is in the development phase, basin partners have recognized a

few critical aspects that will be needed to ensure its successful implementation. The first is that management objectives are quantified and not generalized (see “Objectives” in Figure 34 for examples). This is critical because it is the only way we will be able to measure progress and determine if we need to change course with our management actions. The second is that we need a consistent system for tracking restoration actions and reporting monitoring results across all organizations engaged in salmon restoration. It is not possible to track basin-wide progress towards salmon and ecosystem recovery if implementation and monitoring data are not reported in a consistent and tractable manner by all parties. Finally, a successful adaptive management plan will require steady financial and policy support for monitoring and research to ensure that sufficient quantitative data is available to evaluate progress and guide future management actions.

Next steps in development of the adaptive management plan include:

- Complete a draft of the adaptive management framework (May 2021);
- Coordinate with GRMW on response to ISRP regarding adaptive management (May 2021);
- Convene partners in Grande Ronde basin to develop habitat change scenarios (e.g., restoration, land management, climate change) to be run using the life cycle model being developed in collaboration between CRITFC, ODFW, and NOAA (June 2021);
- Field tours for qualitative evaluations of recent restoration projects in the Grande Ronde basin (summer 2021, depending on COVID status); and
- Present progress of adaptive management activities to basin partners at the GRMW State of the Science meeting (fall 2021).

## References

- ISRP (Independent Scientific Review Panel). 2018. Review of the Grande Ronde Model Watershed Synthesis, 1992-2016. ISRP 2018-11, Portland, Oregon.
- Rieman, Bruce E., Courtland L. Smith, Robert J. Naiman, Gregory T. Ruggerone, Chris C. Wood, Nancy Huntly, Erik N. Merrill, et al. 2015. A comprehensive approach for habitat restoration in the Columbia Basin. *Fisheries* 40 (3): 124–35. <https://doi.org/10.1080/03632415.2015.1007205>.
- White, Seth M., Sarah Brandy, Casey Justice, Kayla A. Morinaga, Leslie Naylor, James Ruzycki, Edwin R. Sedell, Jesse Steele, Alexandra Towne, James G. Webster, and Ian Wilson. 2021. Progress towards a comprehensive approach for habitat restoration in the Columbia Basin: Case study in the Grande Ronde River. *Fisheries*: fsh.10562. <https://doi.org/10.1002/fsh.10562>.

## Dissemination of Project Findings in 2020

### Publications

- Kaylor, M.J., Justice, C., Armstrong, J. B., Staton, B. A., Burns, L. A., Sedell, E., and S. M. White. 2021. Temperature, emergence phenology, and consumption drive seasonal shifts in fish growth and production across riverscapes. *Journal of Animal Ecology*, early online view: <https://doi.org/10.1111/1365-2656.13491>
- Kaylor, M.J., White, S.M., Sedell, E.R. et al. 2020. Carcass additions influence food webs through bottom-up and direct consumption pathways along a fish species assemblage gradient. *Ecosystems*. 24: 168-184. <https://doi.org/10.1007/s10021-020-00510-x>
- Kaylor, M.J., S.M. White, E.R. Sedell, and D.R. Warren. 2020. Carcass additions increase juvenile salmonid growth, condition, and size in an interior Columbia River Basin tributary. *Canadian Journal of Fisheries and Aquatic Sciences*, 77(4):703-715.
- McDowell, P., M. Goslin, L. Ellsworth, and S.M. White. 2021. Long-term ecological effects of passive restoration in the Middle Fork John Day. Final Technical Report completed for Oregon Watershed Enhancement Board Project #218-6041.
- White, S.M., S. Brandy, C. Justice, K.A. Morinaga, L. Naylor, J. Ruzycki, E.R. Sedell, J. Steele, A. Towne, J.G. Webster, and I. Wilson. 2021. Progress towards a comprehensive approach for habitat restoration in the Columbia Basin: Case study in the Grande Ronde River. *Fisheries*, fsh.10562. <https://doi.org/10.1002/fsh.10562>.

### Draft publications

- Staton, B.A., C. Justice, S. White, T. Sedell, L. Burns, and M. Kaylor. (In Revision). Accounting for uncertainty when estimating drivers of detection probability: an integrated approach illustrated with snorkel surveys for riverine fishes. Submitted to *Fisheries Research* Aug. 20, 2020, first round reviews received Jan. 25, 2020. (Revision draft is Appendix C, this document).

### Presentations

- Burns, L.A., S. White, C. Justice, B. Staton. 2020. Integrating unmanned aerial vehicles into large-scale habitat monitoring in the Columbia River Basin. Oregon Chapter of the American Fisheries Society, Bend, OR.
- Burns, L.A., S. White, C. Justice, B. Staton. 2020. Integrating unmanned aerial vehicles into large-scale habitat monitoring in the Columbia River Basin. Pacific Northwest Aquatic Monitoring

Partnership Emerging Technologies Information Session: Aerial Monitoring of Aquatic Systems.

Kaylor, M. J., Justice, C., Armstrong, J. B., Staton, B. A., Burns, L. A., Sedell, E., and S. M. White. 2020. Network-scale patterns of juvenile Chinook Salmon size, growth rates, and density in two NE Oregon tributaries. Oregon Chapter of the American Fisheries Society, Bend, OR.

Staton, B., C. Justice, S. White, T. Sedell, L. Burns, M. Kaylor. 2020. A hierarchical approach to joint estimation of juvenile salmon abundance and snorkel survey detection efficiency. Oregon Chapter of the American Fisheries Society, Bend, OR.

Staton, B. and H. Hershey. September 28, 2020. Workshop Instructed: Introductory Bayesian Inference with JAGS in Fisheries Science. Virtual Annual Meeting for the American Fisheries Society.

Staton, B. and H. Hershey. September 29, 2020. Workshop Instructed: Intermediate Bayesian Inference with JAGS in Fisheries Science. Virtual Annual Meeting for the American Fisheries Society.

White, S.M. 2020. Progress towards a comprehensive approach for habitat restoration in the Columbia Basin: Case study in the Grande Ronde River. Annual Meeting of the FCRPS BiOp Adaptive Management Plan workgroup, Seattle, WA.

White, S.M., Sullivan, S., Justice, C., Burns, L., Sedell, T., Staton, B. 2020. Food for thought (and salmon): Incorporating prey availability into habitat monitoring for Columbia River basin salmonids. Oregon Chapter of the American Fisheries Society, Bend, OR.

White, S.M. 2020. Guest lecture: Increasing tribal capacity to quantify salmonid prey in the Columbia basin. Fish Ecology course, University of Idaho, Moscow, ID.

### **Media reports**

White, S.M. 2020. What's all the buzz? Remote sensing to evaluate river health and fish habitat conditions (Public outreach article). *Ripples in the Grande Ronde*, Grande Ronde Model Watershed Education Outreach Program, Summer/Fall edition.

News article: "Grande Ronde River habitat review shows progress integrating science, management," Columbia Basin Bulletin, Bend, Oregon, 11 December 2020. <https://www.cbbulletin.com/grande-ronde-river-habitat-review-shows-progress-integrating-science-management-concern-efforts-may-not-overcome-rate-of-degradation/>

## **Appendix A – CRITFC Tributary Habitat Assessment Protocol**



# Tributary Habitat Assessment Protocol

Version 1.0



March 2021

Funded by:

Columbia Basin Fish Accords

BPA Project No. 2009-004-00

Prepared by Casey Justice, Lauren Burns and Seth White

Columbia River Inter-Tribal Fish Commission

Portland, OR



## Table of Contents

<b>ACKNOWLEDGMENTS .....</b>	<b>4</b>
<b>INTENTS AND MOTIVATIONS .....</b>	<b>4</b>
<b>SPATIO-TEMPORAL SCALE AND SURVEY DESIGN .....</b>	<b>4</b>
Stream segments .....	5
<b>SURVEY WORKFLOW .....</b>	<b>5</b>
<b>1.0 GROUND-BASED SURVEY METHODS .....</b>	<b>8</b>
1.1 Bankfull elevation.....	8
1.2 Channel types.....	9
1.3 Channel unit classification.....	9
1.3.1 Fast water units .....	10
1.3.2 Slow water units.....	12
1.3.3 Special case units .....	12
1.3.4 Steps.....	13
1.4 Channel unit dimensions.....	13
1.4.1 Unit length, width, and depth.....	13
1.4.2 Unit boundaries and edge-of-water points.....	15
1.5 Large wood .....	16
1.6 Undercut banks .....	17
1.7 Substrate size .....	18
1.8 Water temperature.....	20
<b>2.0 UAS SURVEY METHODS.....</b>	<b>24</b>
2.1 Regulations .....	26
2.2 Segment reconnaissance and pre-flight field work.....	26
2.3 Flight mission .....	27
2.4 Data products and metrics.....	29

**REFERENCES.....32**

**APPENDIX A: METRICS.....35**

**APPENDIX B: EQUIPMENT LIST .....38**

**APPENDIX C: FLIGHT MISSION CHECKLIST .....41**

**APPENDIX D: UAS FLIGHT LOG .....43**

## Acknowledgments

This protocol has been developed and refined based on lessons learned from many years of field data collected by dedicated field technicians and crew leaders whose hard work made this possible. Many of the methods described here were based directly on or were modified from the Columbia Habitat Monitoring Program (CHaMP 2016) and the Oregon Department of Fish and Wildlife (ODFW) Aquatic Inventories Project (AIP; Moore et al. 2019) and we thank all contributors to these programs for their excellent efforts. We also thank our funding source, Bonneville Power Administration (BPA) for supporting this program (BPA Project # 2009-004-00).

## Intents and motivations

This document describes field methods for collection of physical habitat data in wadable tributaries during low-flow with the overall goal of assessing habitat conditions and viability of Endangered Species Act (ESA)-listed salmonid populations. This protocol offers improved efficiency and repeatability over previously developed habitat assessment protocols by reducing the number of ground-based measurements, utilizing more objective survey methods, and leveraging new and emerging remotely sensed technologies and data products (e.g., LiDAR, unmanned aircraft systems (UAS; drone), and satellite imagery). In this protocol, ground-based measurements are coupled with UAS imagery to produce spatially referenced measurements of in-channel and floodplain-characteristics. These survey methods aim to strike a balance between intensive reach-scale monitoring programs such as CHaMP and PacFish InFish Biological Opinion (PIBO; Archer et al. 2016) and rapid-assessment watershed-scale surveys such as AIP. Taking stock of lessons learned from historic regional (ISEMP/CHaMP 2017; Roper et al. 2019) and tribal monitoring programs (Jones et al. 2015; White et al. 2019), we focused on methods that are both quantitative and repeatable (e.g., aerial imagery, simplified channel unit classification, measurement of large wood and channel dimensions, pebble counts), while excluding those that are more subjective (e.g., visual estimation of riparian cover and substrate size, complex channel unit classification, substrate embeddedness).

## Spatio-temporal scale and survey design

These methods are intended to describe fish habitat conditions in wadable streams during low-flow conditions. While some portions of this protocol could be applied to larger rivers or higher flow conditions (e.g., UAS-based methods, year-round temperature monitoring), alternative protocols should be utilized if detailed habitat assessments for large river or high flow conditions are required.

The protocol allows assessment of fish habitat conditions across a range of spatial scales from geomorphic channel unit (i.e., pool, fast turbulent, fast non-turbulent; length < 0.1 km), to reach (length  $\approx$  20 X bankfull width; 0.1 – 1 km), valley segment (1 – 5 km), or whole network/watershed scales. Ground-based data is collected at the channel unit scale (i.e., the finest grain of resolution), but can be aggregated to larger scales depending on the goals of the monitoring program. At a minimum, channel unit data will be summarized at the reach scale for calculation of common habitat metrics (e.g., pool frequency, large wood frequency, side channel area, etc.) and analysis of fish-habitat relationships. While the specific methods used to aggregate data to larger spatial scales are beyond the scope of this field protocol, we emphasize that aggregation methods should account for differences in natural channel morphology (i.e., slope, discharge, sediment supply, valley confinement; Montgomery and Buffington 1997; Beechie and Imaki 2014).

The location of data collection will depend on the desired scale of inference. For example, if the goal is to quantify habitat conditions within a single stream segment or small watershed (< 50 km total stream length), then it is feasible to conduct a spatially continuous census of all available habitat during a single season. Organizations may also choose to collect census data covering different portions of a watershed over a number of consecutive years and then merge the data together. If the desired scale of inference is too extensive to census (i.e., large watershed > 50 km stream length, Major Population Group (MPG), or Evolutionarily Significant Unit (ESU)), then a randomized sampling design is recommended where a subsample of the total extent is surveyed to produce an estimate of overall habitat conditions. A good choice for this approach is the Generalized Random Tessellation Stratified (GRTS) design (Stevens and Olsen 2004), which provides a spatially balanced sample across a stream network and has been widely used for aquatic habitat monitoring in the Pacific Northwest (CHaMP 2016; Moore et al. 2019). Ideally, GRTS sample locations would be drawn from the Columbia River basin-wide master sample to facilitate integration of survey data across multiple monitoring programs (Larsen et al. 2008). Spatial statistical network (SSN) models (Isaak et al. 2014) are another viable approach for extrapolating habitat conditions over large spatial extents.

The temporal frequency of data collection also depends on program goals and the habitat characteristics being measured. If a program aims to evaluate effectiveness of specific restoration actions at a relatively small number of sites and over a short time frame using a treatment versus control experimental design such as before-after-control-impact (BACI), it may make sense to collect data annually for multiple years both before and after treatment. If the goal is to evaluate status and trends in habitat conditions across a large spatial extent and over long time frames, then less frequent assessments (e.g., 5-10 years) are probably sufficient. Less frequent assessments are advisable for monitoring habitat characteristics that may take decades to change (e.g., riparian tree cover, natural large wood recruitment). However, depending on the spatial extent of the area of interest and the amount of habitat that can be measured in a season, multiple years of data collection may be required to complete a single assessment.

## Stream segments

Stream segments set the spatial boundaries for measurements of fish habitat and biota and help to organize the survey workflow into units of manageable size. Our goal was to select a segment size that was large enough that field crews would not be overburdened with frequent changes in segment boundaries, but small enough that corresponding UAS imagery and field data forms would not become unwieldy or overtaxing on computer processing capacity. We delineated stream segments using the National Hydrography Dataset High Resolution flowlines (NHDPlus HR, 1:24K scale; USGS 2016) as a starting point. Tributary junctions with a Strahler stream order  $\geq 4$  as determined from the NHDPlus value-added attributes were used as break points in the stream network, and all stream reaches falling between these break points were lumped together into a 'segment' and assigned a unique identification number. Segments were grouped by 12-digit hydrologic unit code (HUC) watershed boundaries consistent with the National Watershed Boundary Dataset (WBD; USGS et al. 2015) to facilitate data tracking and management. Topographic maps and spatial coordinates detailing segment boundaries will be provided to crews prior to each survey. While habitat surveys are organized by stream segment, metric calculations will span multiple spatial scales (channel unit – whole watershed) depending on the needs of monitoring program.

## Survey workflow

This protocol consists of two main components including a ground-based habitat survey and an unmanned aircraft system (UAS; drone) survey which work together to provide a comprehensive assessment of in-

channel and floodplain/riparian habitat characteristics. Ground-based measurements are intended to provide accurate yet efficient measurements of physical habitat features that can't be easily or reliably measured from UAS imagery or other remotely sensed data (e.g., LiDAR, satellite imagery) such as channel unit class, large wood counts, substrate size, water depth, water temperature, etc. UAS surveys provide precise and efficient measurements of stream surface area, riparian vegetation canopy cover and side channel habitats (i.e., length, area, node density) and will likely be used to produce numerous other relevant metrics as image processing tools are developed and refined. All data will be spatially referenced by surveying ground control points (aerial targets) and channel unit boundaries with a high-accuracy (sub meter) Global Navigation Satellite System (GNSS) or utilizing existing survey-grade ground control networks. Figure 1 provides a generalized workflow for the main components of the protocol—specific details about each component are provided in subsequent sections. A full list of habitat metrics generated from this protocol is provided in Appendix A.

The specific workflow of an organization or crew will depend upon the number of crew members, watershed size and complexity, and the availability of sampling equipment. Ground-based measurements require at least a two-person crew. One crew member will primarily be responsible for operating a high-accuracy GNSS receiver, while the second crew member collects habitat measurements. To prevent errors and improve data quality, it is essential that crew members keep a similar pace for ease of communication and to aid with measurements when needed. Crew members should maintain their role for the entirety of a stream segment to facilitate consistency in measurements. The UAS survey can be conducted with a one-person crew, but a second crew member is useful to help maintain line of site to the unmanned aerial vehicle (UAV) during flight and assist with set up and ground control layout.

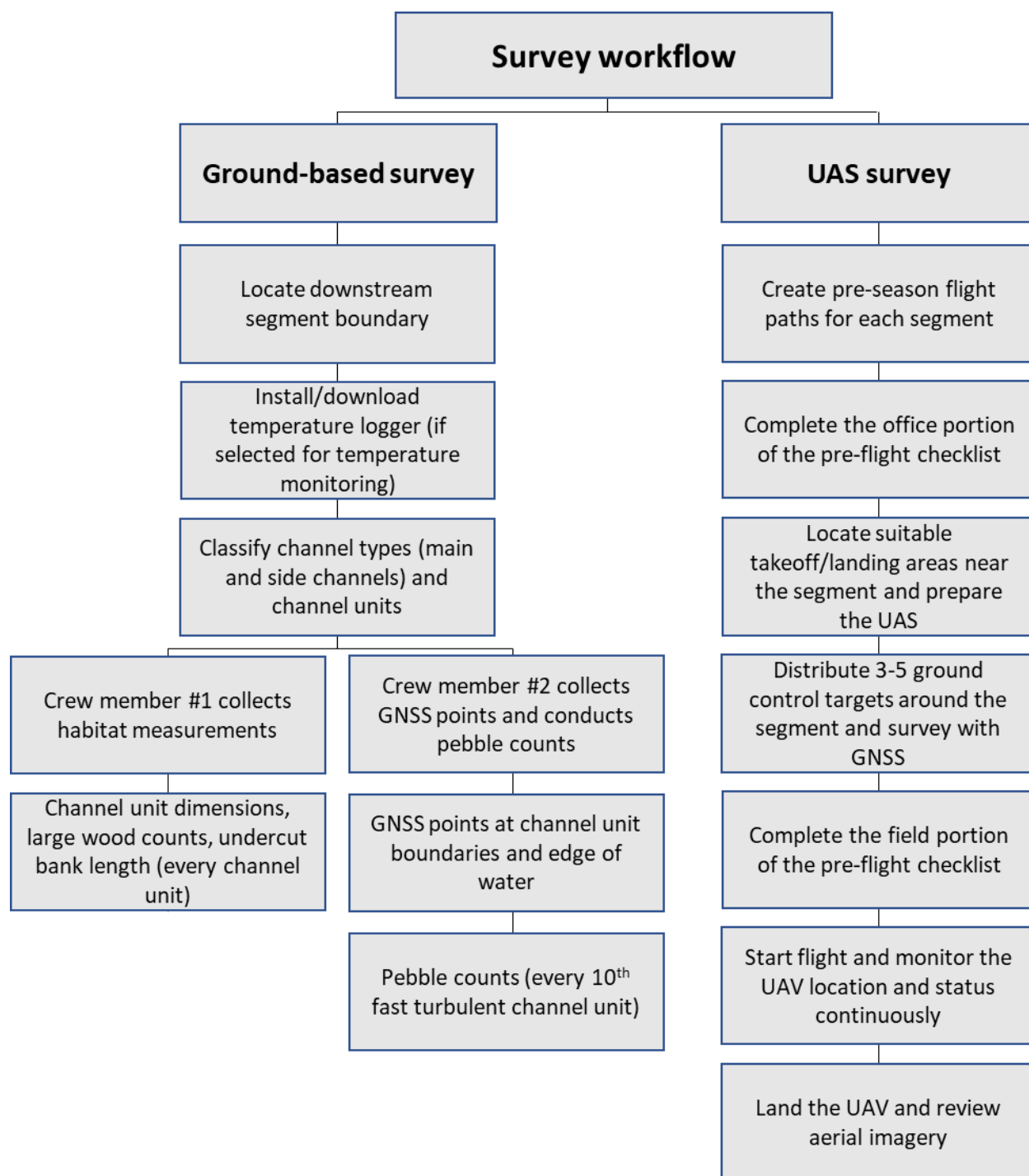


Figure 1. Generalized survey workflow.

## 1.0 Ground-based survey methods

### 1.1 Bankfull elevation

Some methods in this protocol depend on accurate identification of bankfull elevation including delineation of side channels and measurement of large wood and substrate size. Bankfull elevation is defined as the location along the stream banks where streamflow fills the channel to the top of the banks and water begins to overflow onto the floodplain (Leopold et al. 1964), an event that occurs approximately every 1.5 years. The portion of the stream channel that is at or below the bankfull elevation is termed the active channel.

Bankfull elevation is identified in the field using various physical indicators as defined by Harrelson et al. (1994; Table 1). Bankfull elevation is generally easier to distinguish in unconstrained channel types where streambanks are well defined and indicators such as abrupt changes in bank slope, tops of point bars, changes in substrate, and permanent vegetation are more prevalent. In deeply incised or constrained channels, especially those dominated by boulders and bedrock substrate, bankfull indicators may be more difficult to identify and the crew may have to depend on stain lines or move further up or downstream to find reliable indicators.

Regional hydraulic geometry curves (Castro and Jackson 2001, Bieger et al. 2015) provide modeled estimates of bankfull width and depth throughout a stream network as a function of watershed area and mean annual flow. These curves should be consulted prior to conducting field measurements to provide crews with an expected bankfull stage height and thereby help them to accurately identify bankfull elevation in the field.

*Table 1. Indicators used to determine bankfull elevation (Harrelson et al. 1994).*

Indicator	Description
Change in slope	The change from a vertical bank to a horizontal surface is the best identifier of bankfull, especially in low-gradient meandering streams. Many banks have multiple breaks, so examine banks at several locations for comparison. Slope breaks also mark the extent of stream terraces which are old floodplains above the active bankfull elevation. Terraces will generally have soil structure and perennial vegetation. Avoid confusing the elevation of the lower terrace with that of bankfull; they may be close in elevation.
Top of point bars	Point bars consist of bed material deposited on the inside of meander bends. The top elevation of point bars usually indicates the lowest possible bankfull stage. Multiple point bar elevations may be left from flows both above and below the bankfull elevation.
Change in vegetation	Look for the lower limit of perennial vegetation on the bank or a sharp break in the density or type of vegetation. Often willow and alders form root lines near the bankfull elevation. The lower limit of mosses or lichens on rocks or banks, or a break from mosses to other plants may also help identify the bankfull elevation.
Change in bank materials	Look for changes in bank particle size, usually from coarse particles to a finer particle matrix (which is often associated with a change in slope).

Indicator	Description
Undercuts banks	Look for bank sections where the perennial vegetation forms a dense root mat. Feel up beneath this root mat and estimate the upper extent of the undercut. This is usually slightly below bankfull stage. Undercut banks are best used as indicators in steep channels lacking floodplains.
Stain lines	Look for water lines on rocks that indicate where rocks are frequently inundated. Stain lines are often left by lower, more frequent flows, so stain lines should only be used to assist in identifying bankfull elevation along with another indicator or when no other indicators exist at a site.

## 1.2 Channel types

Channel types are used to differentiate the main channel from side channels. Unique channel type numbers within each segment are assigned to the main channel and all qualifying side channels in the sequential order in which they are encountered while working upstream (Figure 2).

The **main channel** is defined as the channel containing the largest amount of flow.

**Qualifying side channels** are defined as portions of the active channel (below bankfull elevation) that are separated from the main channel or other side channels by an island that has a surface elevation greater than or equal to the bankfull elevation for a length greater than or equal to the average bankfull width.

Note: If a channel is separated from another channel by a sediment deposit that is shorter than the average bankfull width or does not meet the height criteria (i.e., a sediment bar), then the channel is considered part of the adjacent channel.

All qualifying side channels are further classified as large or small based on a visual estimate of the percentage of streamflow in each channel. Qualifying side channels with  $\geq 25\%$  of the total flow (main channel plus side channel flow) are designated as **large side channels** and channel units within the side channel are uniquely classified (see 1.3 Channel unit classification; Figure 3). Qualifying side channels with  $< 25\%$  of the total flow are designated as **small side channels** and the entire side channel area is classified as either **slow water dominated** ("Small side channel - slow") or **fast water dominated** ("Small side channel - fast") based on the dominant habitat type. For small side channels with discontinuous flow, estimate the percentage of the channel length that is wet.

**Non-qualifying side channels** are distinguished from qualifying side channels by possessing one or more of the following characteristics:

- 1) The elevation of the streambed is above bankfull at any point.
- 2) The channel lacks a continuously defined streambed or developed streambanks.
- 3) The channel contains abundant terrestrial vegetation (i.e.,  $\geq 25\%$  of the streambed area is covered by terrestrial vegetation).

Non-qualifying side channels are not assigned channel numbers and channel units are not classified within them. However, if an off-channel unit occurs at the junction of a non-qualifying side channel and a larger channel, the off-channel unit is included in the survey and is considered part of the larger channel.

## 1.3 Channel unit classification

Channel geomorphic units are relatively homogeneous areas of the wetted channel with unique bedform shape, depth, velocity, and substrate characteristics from those of adjacent units. Measurements of



habitat and biota such as large wood, substrate size and fish abundance are collected individually by channel unit, thus making it the most basic level of data collection for these metrics. Channel units within each survey segment are classified using a two-tiered hierarchical classification system modified from Hawkins et al. (1993; Figure 3).

**With a few exceptions, channel geomorphic features must have a maximum surface dimension (length or width) that is at least as large as the average wetted channel width in that location to qualify as distinct channel units.** For example, a 3 m long by 2 m wide pool in a large side channel where the wetted width is 2 m would qualify, but a pool of the same size in the main channel where the wetted width is 8 m would not qualify. Additionally, channel-spanning features that are relatively short (e.g., plunge pools or short fast turbulent units) qualify as distinct channel units because they are at least as wide as the average wetted width. Features that do not meet this minimum size criteria are considered part of the adjoining channel unit.

Exceptions to this minimum size criterion include off-channel and special case units. Off-channel units must have a maximum length or width that is at least 50% of the average wetted width in the channel it is associated with to qualify. Dry channel units must be channel spanning (flow is completely subsurface) in at least one location to qualify. Other special case units do not have minimum size criteria.

### 1.3.1 Fast water units

**Fast turbulent (FT)** channel units are high points in the streambed profile that feature moderate to steep gradients ( $> 1\%$ ), coarse substrate (gravel to boulders) and supercritical flow (i.e., hydraulic jumps sufficient to entrain air bubbles and create localized patches of white water). The bedform of these units generally lacks lateral and longitudinal concavity. Fast turbulent units include several finer-scale channel unit types such as cascades, chutes, rapids, and riffles, but we do not distinguish among these to increase survey repeatability. Waterfalls, which typically have near-vertical gradients over very short distances, are classified as steps rather than fast turbulent units (see 1.3.4 Steps).

**Fast non-turbulent (FNT)** units, commonly called runs or glides, generally feature low gradients ( $< 1\%$ ), a uniform or planar bed profile and relatively smooth, non-turbulent flow. Fast non-turbulent units are distinguished from pools by their general lack of lateral and longitudinal concavity and often higher water velocity. These units are generally deeper than fast turbulent units and often contain substrate ranging from sand to cobbles. Fast non-turbulent units also include “sheets”, which are common in bedrock-dominated streams and occur where shallow water flows uniformly over smooth bedrock of variable gradient (often exceeding  $1\%$ ).

**Small side channels - fast (SSCF)** are small side channels ( $< 25\%$  of total flow) that are dominated by fast water habitat.

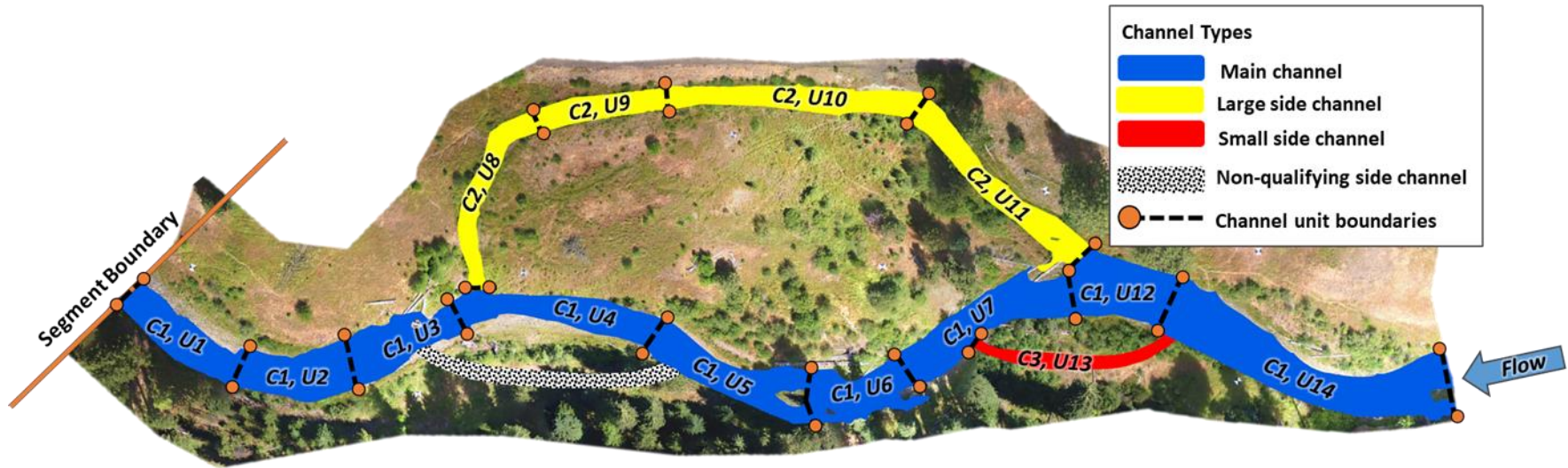


Figure 2. Example of a stream segment with correctly numbered channel types and units. Channel types have the prefix "C" followed by the sequential channel number (e.g., C1-C3) and channel units with the prefix "U" (e.g., U1-U14).

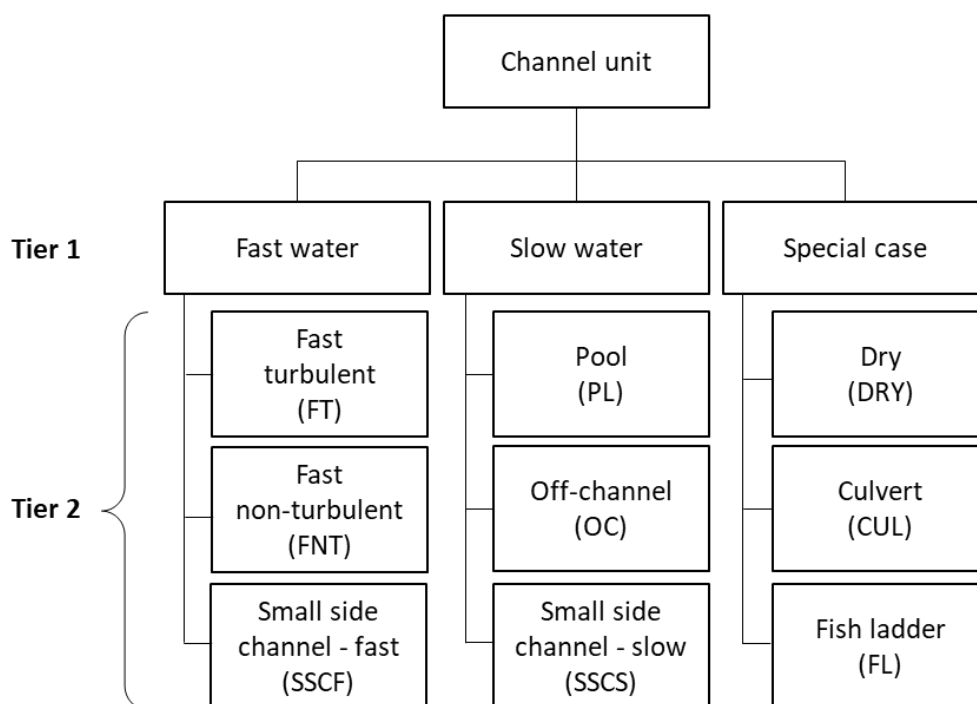


Figure 3. Hierarchical channel unit classification system

### 1.3.2 Slow water units

**Pools (PL)** are low points in the bed profile that feature very low gradients ( $< 1\%$ ), smooth non-turbulent flow, and a bed shape that possesses both lateral and longitudinal concavity. Substrate size in pools is variable (ranging from fines to boulders) but is typically smaller than faster water units. Pools consist of various types including scour, dammed, trench and plunge pools, though these are not distinguished separately to improve survey repeatability.

**Off-channel (OC)** units consist of low gradient (often  $0\%$ ) alcoves and backwaters along channel margins that are connected to the main channel or side channels but have little ( $< 1\%$ ) to no flow through them during low flow conditions. The bedform profile in off-channel units is generally similar to pools with substrate dominated by finer sediment (silt to gravel) and/or organic matter. Off-channel units are often formed during high flows by eddy scour around obstructions on the channel margins or flow through small side channels that are disconnected during low flow.

**Small side channels - slow (SSCS)** are small side channels ( $< 25\%$  of the total flow) dominated by slow water habitat. Small side channels lacking continuous flow will typically fall into this category.

### 1.3.3 Special case units

Special case units account for situations where typical channel geomorphic units do not apply due to low streamflow or man-made structures such as culverts and fish ladders.

**Dry (DRY)** units are channel-spanning sections of the main channel or large side channels that are dry at the time of the survey. Typical examples are riffles with subsurface flow or portions of side channels surrounding isolated pools. If small puddles exist within a mostly dry channel but they are shorter or narrower than the active channel width in that segment, they should be considered part of the surrounding dry channel unit.

**Culvert (CUL)** units are sections of stream that pass-through culverts. This classification does not apply to open-bottom culverts which have a defined streambed and can generally be classified as another unit type.

**Fish Ladders (FL)** are man-made structures often consisting of a series of step pools designed to facilitate fish passage. The entire fish ladder is considered a single channel unit.

### 1.3.4 Steps

Steps are abrupt, vertical, or near-vertical breaks in channel gradient formed by obstructions in the channel or drops over bedrock or other relatively immobile substrates. Steps usually occur over very short (almost negligible) distances, and therefore are not treated as separate channel units. However, the presence/absence of steps is documented due to their importance as potential fish migration barriers or in creating high quality fish habitat (e.g., beaver dams). Steps are classified according to the feature forming the step (i.e., dam, beaver dam, beaver dam analog, large wood, culvert, fish ladder, waterfall) and are assigned to the adjoining upstream channel unit.

Waterfalls sometimes consist of a series of vertical drops separated by lower-gradient channel unit types (usually fast-turbulent habitat). In these scenarios, vertical drops > 1.5 m are classified as steps while the lower-gradient portions are classified as either fast water or slow water channel units based on their physical characteristics as described above.

Short, channel-spanning sections of fast turbulent habitat commonly found separating pools in very low gradient (pool-riffle) and high gradient (step-pool) channel types are classified as fast turbulent channel units, not steps.

## 1.4 Channel unit dimensions

### 1.4.1 Unit length, width, and depth

Ground-based measurements of channel unit dimensions (length, width, and depth) provide the foundational information needed to quantify fish habitat and supplement UAS-based measurements where high canopy cover may be prohibitive.

Note: Future comparisons of ground- and UAS-based measurements of surface area across a range of canopy densities will be used to determine if there is a threshold below which ground-based measurements of channel unit dimensions will not be needed. In the meantime, channel unit dimensions will be measured on the ground at all channel units.

Channel units are visually divided into equally spaced transects located at approximately 25, 50, and 75% of the unit length. At each transect, the wetted width is recorded using a measuring tape or laser rangefinder and three depth measurements are taken perpendicular to flow at 25, 50, and 75% of the wetted width for a minimum of nine depth and three width measurements per channel unit (Figure 4). In slow water pool units, two additional depth measurements are collected at the pool tail crest and maximum depth (Figure 4; green squares in “U3”).

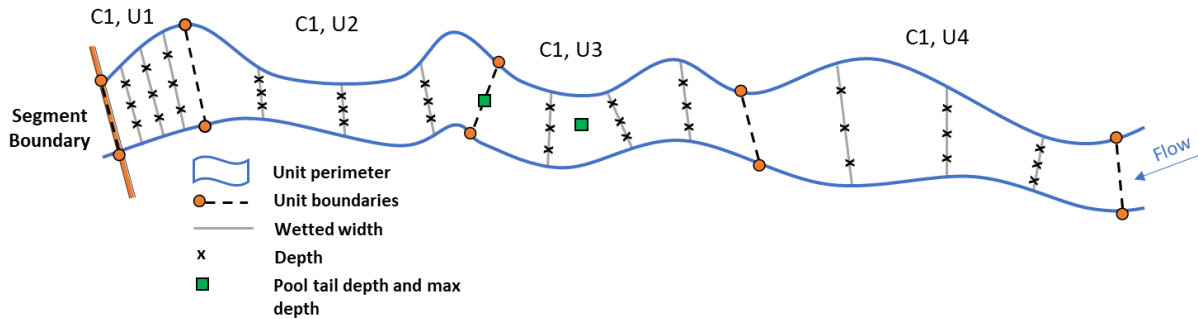


Figure 4. Aerial view of channel unit numbering and the location of wetted width and depth measurements taken within each unit.

Field procedures:

- 1) Starting from the downstream segment boundary and working upstream, assign channel numbers to the main channel and any qualifying side channels sequentially as they are encountered (C1, C2, C3, etc.; Figure 2). The main channel is always designated as channel 1 (C1).
- 2) Using the channel unit characteristics described above, classify and sequentially number each channel unit (U1, U2, U3, etc.) working upstream until the upstream boundary of the segment is reached. Reset the channel type and unit numbering sequences when starting a new stream segment.
  - a) If a side channel is encountered, continue numbering channel units sequentially in the channel with the most flow until the upstream start/inflow of the side channel is located, then move to the downstream end of the side channel.
    - i) For large side channels ( $\geq 25\%$  of the total flow), proceed with numbering channel units in the side channel, assigning them to a new channel number (Figure 2).
    - ii) For qualifying small side channels ( $< 25\%$  of the total flow), treat the side channel as a single channel unit and classify the dominant habitat type as fast or slow. If the small side channel has discontinuous flow, estimate the percentage of the small side channel length that is wet.
- 3) Record whether each channel unit is flow-connected. For a unit to be considered flow-connected, it must be connected by surface water (of any depth) to the downstream boundary of the stream segment.
- 4) If a stream segment has been selected for fish sampling, place flagging at channel unit boundaries labeled with the channel number, unit number, and unit type for fish survey crews to reference.
- 5) If a step is present at the downstream end of the channel unit, record the step type (dam, beaver dam, beaver dam analog, large wood, culvert, fish ladder, waterfall) and measure the step height from the water surface at the bottom of the step to the water surface at the top of the step.
  - a) For channel units classified as fish ladders, step type is recorded as “fish ladder” and step height is measured at a single step within the ladder that is representative of the average step height.
  - b) For channel units that have a dam at their downstream boundary that is bypassed by a fish ladder, step type is recorded as “dam” and step height is measured from the water surface at the base of the dam to the water surface at the top of the dam.

- 6) Measure the length of each channel unit along the unit's centerline to the nearest 0.1 m using a laser rangefinder or measuring tape. Capture channel curvature by taking multiple shorter measurements that follow the channel centerline and adding them together.
  - a) If a step is present at the downstream end of the channel unit, include the length of the step in the length measurement.
- 7) Measure the wetted width of each channel unit to the nearest 0.1 m at three equidistant transects located at approximately 25, 50, and 75% of the unit length and perpendicular to the direction of streamflow (Figure 4).
  - a) For channel units shorter than 2 m, measure width along a single transect located at the midpoint of the channel unit.
  - b) Record width of dry units as 0.
- 8) At each width transect, measure depth with a depth rod to the nearest 0.01 m at 25, 50, and 75% of the wetted width.
  - a) Record depth of dry units as 0.
- 9) Measure maximum depth at all slow water channel units. Be sure to probe the streambed thoroughly to find the deepest point in the channel unit.
- 10) Measure the pool tail depth (Figure 5) at all pool units (not including off-channel and slow small side channels). Pool tail depth is measured at the deepest point along the downstream pool boundary or pool tail crest.

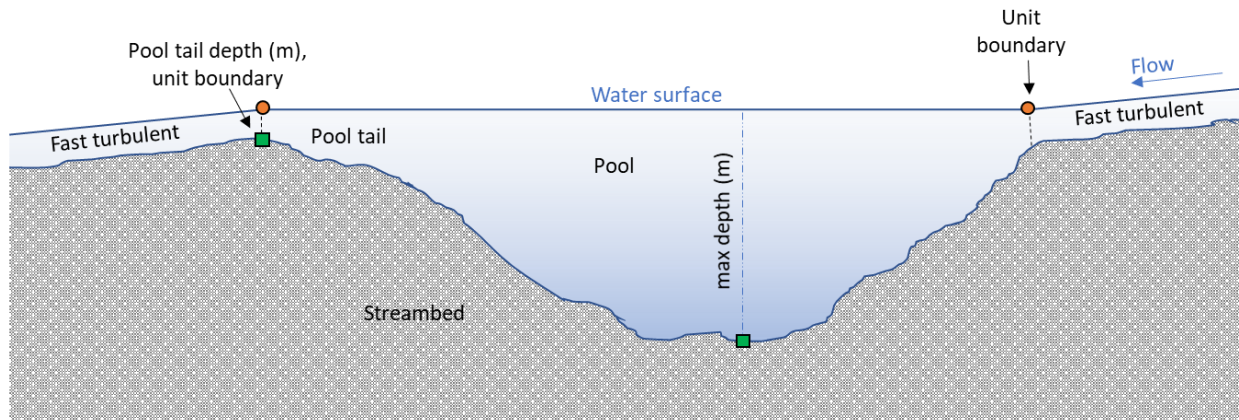


Figure 5. Cross-sectional view of the location of additional pool tail and maximum depth measurements taken within pool units.

#### 1.4.2 Unit boundaries and edge-of-water points

Boundaries of geomorphic channel units and the wetted stream channel are delineated using a high-accuracy (submeter) GNSS receiver to provide spatial reference for ground-based measurements and aid in processing of UAS-collected aerial imagery. Edge-of-water points represent the location where the water surface meets the stream bed or bank. The number and location of edge-of-water points is determined by the amount of channel overhanging canopy cover. At a minimum, every channel unit should have two edge-of-water points which mark the lower boundary of the channel unit (Figure 4).



Additional edge-of-water points are collected at major inflection points in channel morphology (e.g., around meander bends) where dense overhanging vegetation obstructs the view of the channel from the sky.

Field procedures:

- 1) Delineate the downstream boundaries of each channel unit by collecting at least two boundary points (one on each bank) with a high-resolution (submeter) GNSS receiver.
  - a) Unit boundary points should be collected at the edge-of-water and coded as “U” for unit combined with the sequential unit number (e.g., U1, U2, etc.; Figure 4).
  - b) If the unit geometry is complex, collect additional points within the wetted channel to accurately capture the perimeter of the unit. Unit boundary points collected within the wetted channel should be coded as “UW” for “unit wetted” combined with the sequential unit number (e.g., UW1, UW2, etc.).
- 2) If the adjoining upstream segment will not be surveyed during the same field season, collect a minimum of two additional boundary points at the upstream boundary of last channel unit in the segment.
- 3) Where dense riparian vegetation is present, collect edge-of-water points while working upstream through the unit capturing major inflection points in channel geometry. Code edge-of-water points as “LW” for “left wetted” and “RW” for “right wetted” corresponding to each bank (left or right) looking downstream.

## 1.5 Large wood

All large wood that meets the minimum size criteria and is within, partially within, or suspended over the active channel is counted using methods adapted from the ODFW Aquatic Inventories Project. The minimum size requirement for wood to be counted is 15 cm diameter and 3 m in length. Diameter is measured at 2 m from the base of the stem (i.e., where the root wad meets the stem) or, if no root wad exists, from the end of the stem with the largest diameter (Figure 6). Root wads < 3 m in length are an exception and are counted if the stem diameter is ≥ 15 cm. Large wood pieces must be dead or will be soon (i.e., newly fallen trees with detached roots are not to be counted).

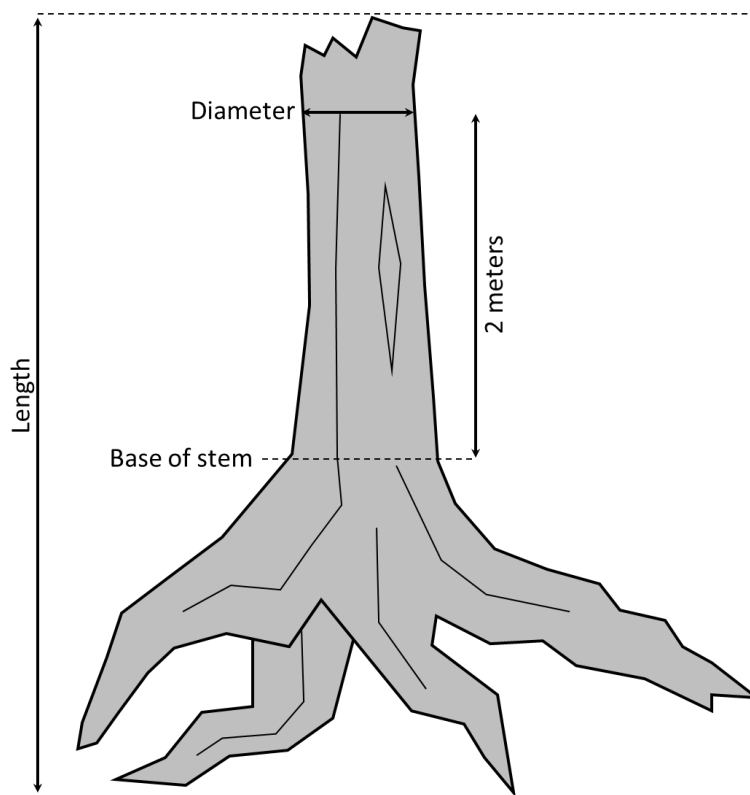


*Figure 6. Measurement locations for large wood.*

Field procedures:

- 1) Tally all large wood pieces within each channel unit that meet the minimum size criteria. The first 10 pieces encountered at the start of each day should be measured with a depth rod to calibrate visual estimates to the minimum size criteria. Any pieces that are close to the minimum size criteria (i.e., within about 0.5 m length and 10 cm diameter) should be measured to ensure accuracy. All remaining large wood pieces within the segment can be tallied without measuring.
  - a) If a piece of wood spans multiple channel units, assign that piece to the unit that contains the largest volume of the piece.
  - b) If the piece is not within the wetted perimeter of a channel unit, assign it to the nearest channel unit.
- 2) Record whether each piece of large wood is wet or dry. For a piece to be considered wet, any portion of the wood must be in contact with water.

## 1.6 Undercut banks

Undercut banks are important stream features that provide cover for fish. Undercuts can be identified where dense mats of roots or streambank material overhang the wetted channel.

Field procedures:

- 1) Record the length and associated channel unit of all undercuts that are  $\geq 1$  m long and  $\geq 20$  cm wide.
  - a) Undercut width is measured as the wetted horizontal distance from the outermost edge of the overhanging bank to the back “wall” of the undercut at its widest point (Figure 7).



- b) The undercut bank must be at least 20 cm wide at all points along its length.
- 2) If an undercut spans two channel units, split the length measurement at the channel unit boundary and record the length of undercut bank within each channel unit.

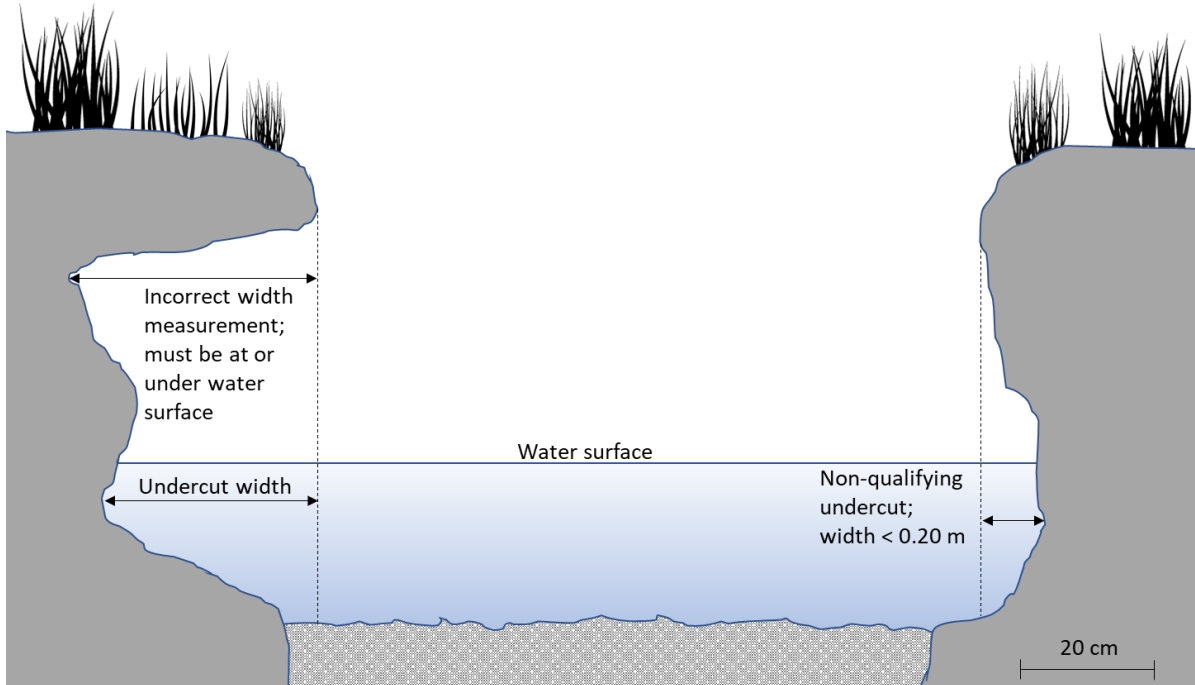


Figure 7. Channel cross-section showing where to measure undercut bank width.

## 1.7 Substrate size

Streambed particle size is measured using a Wolman pebble count procedure (Wolman 1954) at every 10<sup>th</sup> fast turbulent unit within each segment. Pebble counts are conducted along transects perpendicular to the stream channel and spanning the width of the bankfull channel (from toe of bank to toe of bank). The toe of bank refers to the line formed by the intersection of the general plane of the sloping side of the stream bank with the general plane of the channel bed. A minimum of 100 particles are measured within each stream segment using a square-hole template (gravelometer) with size classes corresponding to the Wentworth scale (Table 2).

### Field procedures:

- 1) Conduct a pebble count (100 particles) at the first fast turbulent unit in each segment and every 10<sup>th</sup> fast turbulent channel unit thereafter. Do not conduct pebble counts in small side channels (< 25% of the total flow).
- 2) Starting at the downstream unit boundary at the toe of either bank, select a particle by looking away and extending a finger straight down to the tip of a boot and picking up the first contacted particle.
  - a) Ensure that sampling occurs only within the active bankfull channel and do not measure stream bank particles.

- 3) Use a gravelometer to classify the intermediate axis (b-axis) of the particle (Figure 8). Record the size of the largest square hole that the particle does not fit through—this corresponds to the low end of the size category for that particle. For example, if a particle fits through the 180 mm square but does not fit through the 128 mm square, the size category is  $> 128 - 180$ .
- 4) After measuring the first particle, proceed to the next sample location by taking one pace. Scale your pace length relative to the size of the channel with the goal of measuring 100 pebbles within a single channel unit.
  - a) After you have begun your pebble count, avoid changing the pace or trajectory of sampling to avoid large boulders, deep water, or other obstacles. A consistent location on the boot should be used to minimize bias against smaller particles.
  - b) Do not measure the same particle twice and take extra caution, by tossing measured particles behind or downstream to prevent double counting.
  - c) For particles larger than 180 mm or particles that cannot be removed from the streambed, use the gradations along the edge of the gravelometer or a depth rod to measure the b-axis of the exposed portion of the particle (Figure 8). The edge of the gravelometer, which is 2 mm thick, can be used to identify particles less than 2 mm.
  - d) When bedrock is encountered at sample points, record the size as “bedrock” and measure additional particles as necessary to ensure a minimum of 100 particles (not including bedrock) are measured.
  - e) When the end of the first transect is reached, take a pace upstream using the same spacing to establish the next transect. Proceed with measuring particles along each transect in the same fashion described above until 100 particles have been measured.
- 5) If the upstream boundary of the unit is reached before completing the pebble count, continue to the next fast turbulent unit until 100 particles are measured. Record the channel unit number(s) that pebbles were measured in.
  - a) If the pebble count was extended into multiple channel units, conduct the next pebble count at the 10<sup>th</sup> fast turbulent unit after the last unit that was sampled.

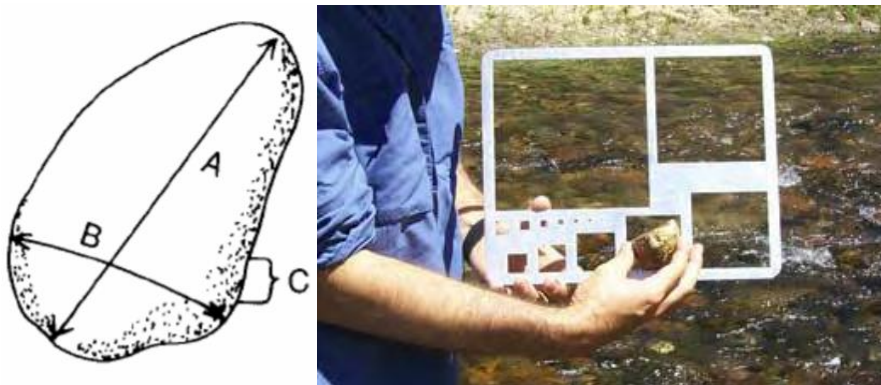


Figure 8. Left: particle axis from Harrelson et al. (1994). Right: Gravelometer used to measure the b-axis of each particle. Photo from CHaMP (2016).

*Table 2. Size gradation for sediment in the range of fines (sand, silt, clay) to boulders (Wentworth scale).*

Particle size description		Particle size (mm)	
		Minimum	Maximum
Bedrock		NA	NA
Boulder	mega	> 4096	NA
	very large	> 2896	4096
		> 2048	2896
	large	> 1448	2048
		> 1024	1448
	medium	> 724	1024
		> 512	724
	small	> 362	512
> 256		362	
Cobble	large	> 181	256
		> 128	181
	small	> 90.5	128
		> 64	90.5
Gravel	very coarse	> 45.3	64
		> 32	45.3
	coarse	> 22.6	32
		> 16	22.6
	medium	> 11.3	16
		> 8	11.3
	fine	> 5.66	8
		> 4	5.66
very fine	> 2.83	4	
	> 2	2.83	
Fines (Sand, Silt, Clay)		< 2	2

## 1.8 Water temperature

Year-round, hourly water temperature is measured using Onset HOB0 temperature data loggers ( $\pm 0.2$  °C accuracy) at pre-designated stream segments. Ideally, loggers should be installed no later than July 1 to ensure that peak summer temperatures are captured and downloaded again in the fall prior to high winter or spring flows.

Temperature monitoring locations will vary based on the monitoring program's resources and objectives. Generally, loggers should be placed in strategic locations to capture significant changes in water temperature such as near tributary junctions and across a range of stream sizes and elevations throughout the stream network of interest. Additionally, it is advisable to place loggers near the upstream and downstream extents of the study area (i.e., boundary conditions). Program leaders and/or crew supervisors will typically provide guidance to field technicians on the desired location of each logger.

There are two recommended options for logger installation: the epoxy method and the cable method. The epoxy method is the preferred option and should be used unless there is no suitable attachment surface for the epoxy (see Epoxy method below). In both cases, the logger is placed in a PVC housing unit to protect it from direct solar radiation and damage during high flows. Housing units are drilled with multiple holes (1/4 – 1/2 in diameter) to ensure adequate exchange of flowing water.

Optimal logger placement includes the following criteria for both epoxy and cable methods: 1) sufficient water depth to ensure loggers remain submerged year round, but outside of strong currents, 2) well-mixed streamflow, usually in fast-water channel units (i.e., avoid pools with stratified water temperatures), 3) non-depositional areas where the logger is unlikely to get buried by sediment, 4) not near groundwater seeps or other cold- or warm-water anomalies.

**Epoxy method:** Refer to Isaak et al. (2013) for complete details. Optimal placement locations for the epoxy method in addition to those described above include: 1) large rocks, boulders, or structures that will not move during high flows, 2) boulders large enough that they protrude above the low flow water surface and wide enough that they can effectively shield the logger from moving rocks or debris during high flows, 3) areas downstream of large rocks in pockets of relatively calm water with smaller substrate sizes, 4) a relatively flat downstream attachment surface that is deep enough to remain submerged in flowing water year-round. If a suitable attachment surface is not available, use the cable method.

Field procedures for epoxy method:

- 1) Clean the attachment surface of the boulder with a wire brush prior to installation.
- 2) Secure the temperature logger to the inside of the housing using a plastic zip tie.
- 3) Use a 2-part underwater epoxy (FX-764 Hydro-Ester® Splash Zone Epoxy manufactured by Fox Industries, Baltimore, MD, <http://www.foxind.com/>) to glue the PVC logger housing to the boulder.
  - a) Use approximately 1 golf ball sized portion of each part of the epoxy (white and grey) and mix together thoroughly with wet gloved hands for approximately 1 minute.
  - b) Apply the epoxy to the bottom of the housing in a thick layer (approximately 0.5 – 1 inch thick) and press the housing against the rock surface.
  - c) Gently smooth the epoxy with the gloved hand around the perimeter of the housing to maximize contact with the rock.
- 4) Brace the housing in place using a cobble and leave overnight to achieve a secure bond.

**Cable method:** Optimal placement locations for the cable method have the following attributes in addition to those described above: 1) a secure anchor point such as the base of a living tree or root (> 20 cm diameter) near the stream bank, 2) camouflaged or inconspicuous location when installed near high public use areas.

Field procedures for cable method:

- 1) Attach the logger housing to a tree or root using a stainless steel cable  $\geq 1/16$  in diameter and aluminum crimps. Note that galvanized cable will rust and break rapidly and is not recommended.
  - a) If a suitable tree or root is not present at the site, attach the cable to a metal stake or rebar driven securely into the streambed (nail stakes 2 – 2.5 ft long with holes for attaching cable are recommended).

- b) Use a long enough length of cable that the logger housing can be lifted out of the water during low flows to download the data without having to cut the cable.
- 2) Attach a 1-2 oz weight to the cable to ensure the logger and housing unit remain submerged.

Office procedures before leaving for the field:

- 1) Check the accuracy of all temperature loggers using an “ice bucket” method prior to installing in the field (Dunham et al. 2005). If the logger measurements are outside of the range of  $\pm 0.2$  °C, the logger should not be used.
- 2) Ensure the laptop computer battery is fully charged and the date and time are correct.
- 3) Open the HOBOWare software and check that it is set to standard international (SI) units (this ensures that temperature is recorded in degrees Celsius, not Fahrenheit).
- 4) Connect the HOBOS shuttle to the laptop using a USB cable and check the battery level on the HOBOS shuttle. Replace if necessary.
- 5) Sync the shuttle with the laptop. This ensures that any temperature loggers launched with the shuttle are programmed with the correct date and time. **Critical note: the shuttle must be re-synced with the laptop any time the shuttle batteries are replaced prior to launching or downloading any temperature loggers.**
- 6) If you’re planning to install temperature loggers at new locations (i.e., locations where a logger doesn’t already exist), it’s recommended to pre-launch several loggers in the office prior to departing for the field.
  - a) Attach the logger to the shuttle and squeeze the lever on the shuttle coupler to establish a connection with the logger. Once connected, launch the logger. Set the start date and time for 12:00 AM of the next day and set the logging interval to 1 hour. Setting the launch time for 12:00 AM ensures that air temperatures are not recorded prior to installation. Ensure that the launch was successful (see message at the bottom of the HOBOWare screen), then disconnect the logger.
  - b) Place pre-launched loggers in a labeled bag or otherwise mark them to ensure they are easily distinguished from unlaunched loggers.

Field procedures (installing new loggers):

- 1) Identify a suitable logger location and installation method using the guidance above.
- 2) Record the logger serial number.
- 3) If the logger was not pre-launched in the office, connect the shuttle to the laptop computer, attach the logger to the shuttle and squeeze the lever on the shuttle coupler to establish a connection with the logger. Once connected, launch the logger. Set the start date and time for the next hour (on the hour) of the current day and set the logging interval to 1 hour. Ensure that the launch was successful (see message at the bottom of the HOBOWare screen), then disconnect the logger.
- 4) Attach the logger to the inside of a PVC housing unit using plastic zip ties and install the logger.
- 5) Record spatial coordinates at the logger location (Preferred format UTM, NAD83).

- 6) Record the stream bank (facing downstream) that the logger is nearest to and the distance from the bank. If cable is attached to a tree on the bank, record the distance from bank as 0.
- 7) Record the attachment method (“Cabled to tree/roots”, “Cabled to stake”, or “Epoxy”).
- 8) Record the condition of the logger as “In flowing water”.
- 9) Record the action taken with the logger as “Installed new logger” and the date/time the action was taken.
- 10) Write a detailed description of the logger location. The description should include distance from nearby tributary junctions or other landmarks, and any other pertinent information for relocating the logger. For example: “Logger attached to grey, rectangular boulder 1 m in diameter near left bank, 5 m upstream from junction with Dry Creek, in a fast non-turbulent unit”.
- 11) Attach flagging to a nearby tree or other object to mark the location of the logger and take a photo of the logger location. Include enough of the surrounding environment to relocate the logger.

Field procedures (previously installed loggers):

- 1) Use existing spatial coordinates, photographs, and site notes to locate the previously installed logger. If the logger location is found but the logger is missing, search in the near vicinity for the missing logger using an underwater scope. If it cannot be found, install a new logger.
- 2) Remove the logger from the housing unit and confirm that the correct logger serial number was recorded when originally installed. Avoid removing the logger from the water when it will be recording one of its hourly temperature measurements (on the hour). Rubber gloves, large pliers, or an oil filter wrench may be helpful for unscrewing housings that are difficult to open (gloves are usually sufficient).
- 3) Attach the logger to the shuttle and squeeze the lever on the shuttle coupler to download the data. If working properly, the indicator light on the shuttle will blink orange during data transfer, and then blink green when the transfer is complete. If the light blinks red (indicating an error), clean the optical sensor on the logger and the shuttle connection surface and try again. If the data transfer fails after multiple tries, replace the logger and notify a project leader.
- 4) After downloading the logger, note whether the red light on the logger is blinking (indicating that it is launched and operational). If there is no blinking light, attempt to relaunch the logger. If there is still no blinking light, replace the logger and notify a project leader.
- 5) Record the condition of the logger (i.e., “Buried”, “Out of water”, “In flowing water”, “In non-flowing water”, or “Missing”). Loggers that are partially out of water are designated as out of water.
- 6) Record the action taken with the logger (i.e., “Installed new logger”, “Left in place”, “Moved”, “Removed”, “Replaced”, or “Didn’t replace”) and the date/time the action was taken. Move the sensor if it is in non-flowing water, out of water, or buried in sediment. Replace missing loggers with a new one unless otherwise instructed by a project leader.
- 7) Verify and update the logger location information as needed such as stream bank, distance from bank, attachment method, location description, and spatial coordinates. Only record new spatial coordinates if the logger was moved or if the original coordinates were erroneous. Take a new photo of the sensor only if the previous photo is no longer representative of the logger location or the photo is not stored in the temperature data entry application.

## 2.0 UAS survey methods

Unmanned aircraft systems (UAS) or drones have equipped biologists, restoration practitioners, and professional surveyors with the capabilities to investigate fish-habitat relationships at multiple spatial scales and in locations that are very challenging to survey with traditional ground-based methods (e.g., complex multi-threaded channels, deep water or broad floodplains). The UAS encompasses the entire package needed to operate the system including the unmanned aerial vehicle (UAV), ground control system, camera, GPS/GNSS, software, and the pilot in command. Of specific interest to fish habitat surveys, UASs are a relatively inexpensive technology that can reduce the time and effort spent collecting ground-based data, while yielding imagery allowing further processing and discovery as new insights in this field emerge. Furthermore, operating a drone and obtaining imagery is a relatively unbiased method of collecting data that is not prone to the same subjectivity and transcription errors of ground-based measures. UASs are used in this protocol to collect imagery from multiple viewing angles (i.e., nadir and off-nadir), which when coupled with ground-based data, can produce spatially accurate maps of complex channels, track changes in habitat over time, and compute accurate measures of habitat metrics. As UAS sensor technologies continue to improve and become more affordable, integrating their use in monitoring will allow for more efficient and accurate assessment of habitat conditions.

This section outlines an idealized workflow for the UAS-based portion of this protocol which can be broken down into four major steps: 1) adherence to regulations, 2) reconnaissance of river segments and pre-flight field work, 3) flight mission planning, and 4) development of data products. As with the ground-based portion of the survey, the specific workflow may further depend upon the number of crew members, tributary size and complexity, and available equipment. Our intent is to provide a high-level overview of standard considerations for integrating UASs into stream habitat surveys. However, careful consideration to align the project goals and objectives with the desired data products should be conducted as one of the first steps in this process as the resolution, accuracy, and completeness of resulting data products will be dependent on these factors. Figure 9Figure 1 provides a generalized workflow for the main components of the ground- and aerial-based field work—specific details about each component are provided in subsequent sections. A more detailed step-by-step checklist for pre-flight planning can be found in Appendix C along with an example flight log in Appendix D of this document.



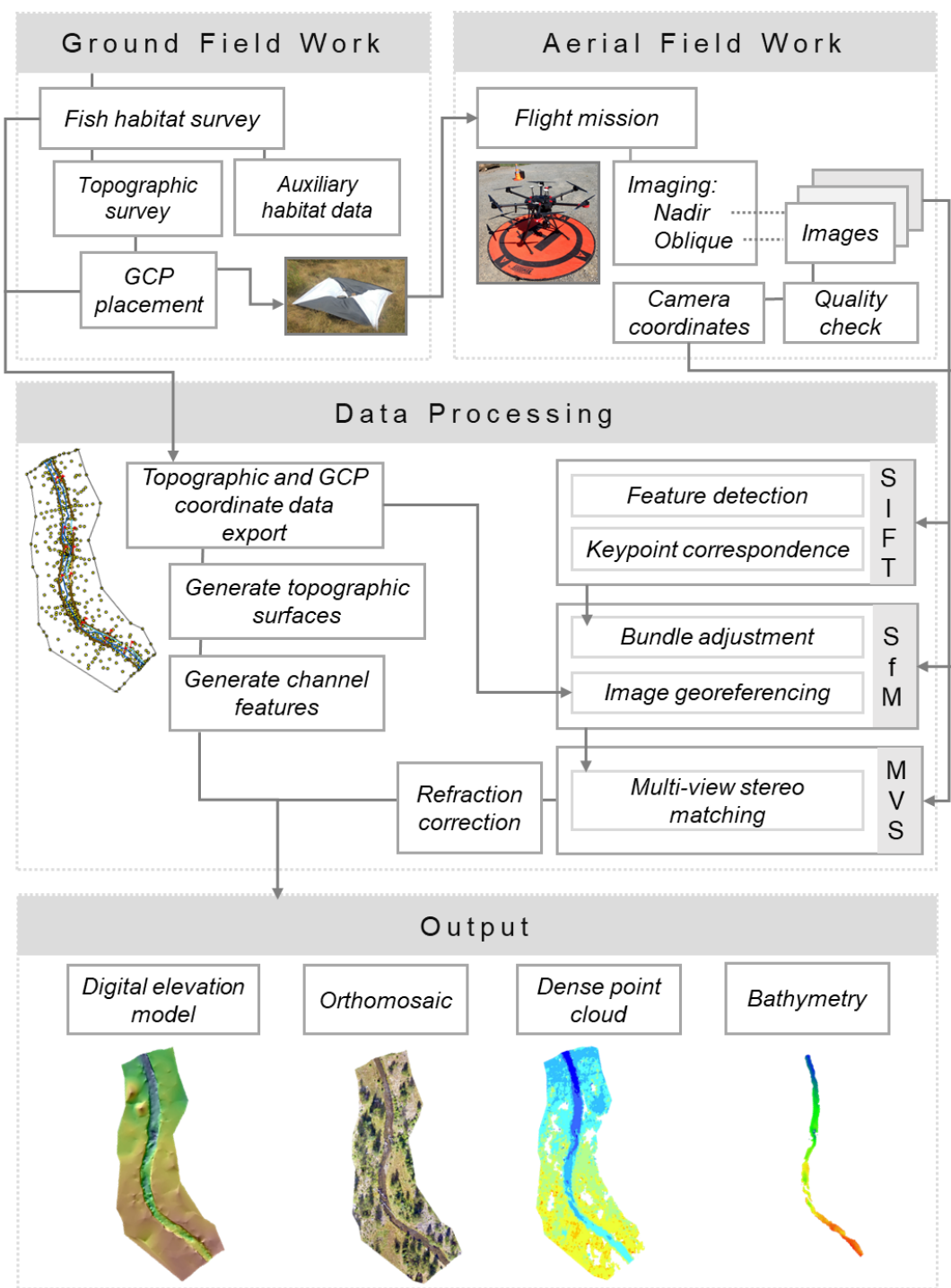


Figure 9. Workflow of ground and aerial mapping, data processing and outputs for tributary habitat assessments.



## 2.1 Regulations

Advancements in technology and availability of consumer grade UASs have resulted in an increased need to regulate their use by the Federal Aviation Administration (FAA) (Lusk 2017). To account for the rapidly growing number of UAS pilots and platforms, regulations are frequently evolving. As of the published date on this protocol, the FAA requires recurring remote pilot certification testing (every two years) and UAS registration (every three years). Commercial operators are required to hold a valid Part 107 (14 C.F.R. §107) remote pilot license issued by FAA and all UAVs must show proof of registration (FAA registration number) clearly displayed and visible on the hull of the UAV. The remote pilot must comply with all FAA regulations including proof of remote pilot certification and aircraft registration during all flight missions. It is the responsibility of each remote pilot to maintain their certification and UAV registration (FAA 2016a; FAA 2016b).

To ensure the safety and success of any flight mission, the pilot in command (PIC) and crew members should adhere to all outlined FAA flight rules. It is recommended that organizational standard operating procedures (SOPs) are generated, personal liability and aircraft insurance are obtained, and proper reporting (e.g., LAANC; FAA 2018) and record keeping are maintained for each mission. At a minimum, the PIC should complete a pre-flight checklist (one such suggested in Appendices C of this document) and keep a flight log (Appendix D). It is important to note that the PIC takes full responsibility for all aspects of a given flight including ensuring the safety of equipment, personnel, and surrounding area (people and landscape). The PIC must be physically and mentally prepared for flight and cognizant of any or external pressures (ego, outside stresses, etc.) Proper flight planning is a multistep process that should be completed by the crew supervisor or PIC prior to flight.

### Procedures:

- 1) Pass the FAA Part 107 remote pilot examine to obtain certification.
- 2) Register UAV(s) with the FAA and affix the aircraft registration number to the hull of the aircraft(s).
- 3) Identify temporary flight restrictions (TFR) and controlled or restricted airspace (i.e., wilderness areas, military flight lines, airports) within the geographic extent of the study area using aeronautical charts online (e.g., [Know Before You Fly](#); [SkyVector](#)).
- 4) Where necessary, request authorization to fly within restricted or controlled airspace (up to 90 days in advance) via a formal request to the proper parties (e.g., US Forest Service for wilderness areas) or using the Low Altitude Authorization and Notification Capability (LAANC) service. Approval may take up to 30 days depending on the airspace and location.
  - a) Permits or advance authorization may require proof of hull and liability insurance, mandatory flight reporting to local dispatch, and/or copies of standard operating procedures for conducting UAS work.
- 5) Conduct flight training for new pilots to provide hands-on flight experience and decrease the likelihood of an accident or emergency situation.
  - a) Accidents resulting in >\$500 damage to a UAV must be reported to the FAA.

## 2.2 Segment reconnaissance and pre-flight field work

Pre-season planning is conducted by the crew supervisor and/or PIC. Flight missions will be created for each stream segment of interest in a similar manner as the ground-based portion of this protocol. Depending on the flight planning software and additional resources available to each organization, a portion of the reconnaissance and mission planning can be completed before physically visiting the site.

For example, some flight planning software allows for automatic adjustments to flying altitude based on terrain. However, additional reconnaissance should be conducted once at each segment to identify local unforeseen hazards, alternative takeoff and landing locations for use during potential emergency procedures, and to verify the minimum safe flying altitude.

Additionally, establishing ground control within each stream segment should be conducted during this phase of pre-flight field work. Establishing ground control points (GCPs) have been shown to result in data that are 5-10 times more accurate than those collected with onboard GPS/GNSS of UASs alone (Turner et al. 2012) and are key in obtaining accurate data products from a flight mission. A minimum of three and up to five GCPs per kilometer should be distributed throughout the stream segment and be both visible in imagery from overhead and at locations that represent the topographic variability of the survey area. If no ideal locations exist within the segment to place ground control, permanent structures (e.g., houses, fence posts, etc.) or landforms (e.g., large boulders, rock outcroppings, etc.) can alternatively be used if pre-existing spatially referenced data are available (i.e., LiDAR, orthomosaics). At each GCP location, temporary survey markers (e.g., surveying nails and whiskers or capped rebar) should be hammered into the ground at each location representing the center point to place GCP targets. GPC work should occur in a relatively short timeframe (i.e., one week or less) prior to UAS flights to decrease the likelihood of tampering (e.g., humans or wildlife) or positional error due to ground settling.

#### Office and field procedures:

- 1) At the office, prepare pre-season flight paths for each stream segment.
  - a) Identify hazards (e.g., trees, cliffs, people, property, power lines) within each segment and adjust pre-flight paths and/or altitude to account for hazards.
  - b) Identify potential take-off and landing locations.
- 2) Ensure maps and flight plans are saved and cached to the iPad(s).
- 3) Within each stream segment, establish 3-5 ground control points (GCPs) per 1 km.
  - a) Using a high-accuracy GNSS or other surveying equipment (total station or real time kinematic GNSS), establish GCPs throughout the segment. Mark the center of each GCP with temporary surveying nails, whiskers, and flagging denoting the corresponding GCP number.
  - b) At each GCP, tamp down any tall grasses or woody vegetation that will prohibit the target from lying flat on the ground surface. Lay each ground control target over the surveying nail and ensure the target will remain secure using metal stakes or nearby rocks/wood pieces.
- 4) Meet with the crew to discuss the final flight plan, address additional concerns, and test radios.

## 2.3 Flight mission

Flight missions require a substantial amount of pre-planning and post-processing but the flight itself is typically completed in a very short amount of time (approximately 2-3 hours/stream segment). No flight should be conducted until the previous two steps (Regulations, Segment reconnaissance and pre-flight field work) have been completed. The use of a pre-flight checklist and flight log are suggested to maintain physical records of each flight; examples of each can be found in Appendices C and D respectively.

Collecting high-resolution imagery, coupled with ground control, is paramount to obtaining accurate data products. The accuracy and completeness of each product is dependent on flight altitude, the number, overlap and orientation of images collected, and the density of riparian vegetation. To reduce the effect of any one of these, it is recommended to collect imagery from multiple viewing angles (nadir and oblique;

90 and <30 degrees respectively), reduce the flight altitude below 80 m if possible to decrease the ground sampling distance and increase imagery resolution and accuracy, and collect more imagery which can generally be achieved by increasing image overlap to at least 70% for both sidelap and frontlap. Depending on the UAS platform and metrics of interest, additional factors such as stream orientation, time-of-day, lighting and weather conditions may need to be considered. In general, flights should primarily be conducted between 10:00 and 14:00 when the sun is highest in the sky, thus maximizing the amount of light reaching the stream and penetrating the water column. To reduce glare from the surface of the water and improve the image quality, a circular polarizing filter should be used with UAS sensors. The light conditions may be further affected by riparian vegetation, where stream orientation and solar angle can interact to cast shadows on the landscape and active channel. Tall, dense riparian vegetation are particularly challenging for image matching algorithms to reconstruct a scene. Where complex topography, dense vegetation, and highly sinuous channels are present, additional imagery should be collected from multiple viewing angles and different times of day (if time permits) to improve data products.

Field procedures:

- 1) Before leaving for the field, begin completing the pre-flight checklist.
  - a) The PIC should identify potential flight restrictions involving undesirable weather (e.g., high winds, precipitation, lightning, fog) or airspace restrictions prior to leaving Wi-Fi or cell service.
  - b) If no hazards are identified and if necessary, the PIC should proceed with notifying air traffic control (ATC), local dispatch, or minimally LAANC of the flight plan.
  - c) Equipment including software should be checked and maintained as they may limit the ability of the UAV to launch (e.g., software updates, battery levels, compass calibration).
- 2) At each segment, the PIC should conduct a final assessment to determine whether it is safe or suitable to fly.
- 3) Ensure take-off and landing location(s) are suitable in that they are relatively flat, free of large trees and branches within a 3 m radius of the landing zone, and situated away from roads or worksites where active traffic and operations may interfere. Partition off the launch/landing areas using a weighted pad to help flatten any surrounding tall grasses and lay out safety cones and signage noting drone operation in progress.
- 4) Populate or review the pre-planned flight path(s) for the segment and set or check camera parameters.
  - a) Update the minimum and maximum flight altitudes based on vegetation height and topography as measured with a laser rangefinder during pre-flight field work.
- 5) Unload the UAV, ensure equipment is fully charged, and visually inspect the equipment.
  - a) Inspect rotors and propellers, gimbal(s) and payload(s), and check for visible defects.
  - b) Ensure sufficient storage is available on the SD card within the camera and clean the lens to remove any dust, debris, or water particles prior to takeoff.
  - c) Install UAV batteries.
- 6) Prepare to launch the UAV.
  - a) Turn on the UAV and remote controller(s) and check connectivity.
  - a) Set camera parameters.

- b) Perform a final review of the flight path and mission details.
  - c) Set the “home” location and verify emergency protocols.
  - d) If present, check radio connection between PIC and visual observer(s).
  - e) Complete the pre-flight checklist and update the flight log.
  - f) If not yet complete and necessary, contact air traffic control (ATC) or local dispatch to receive authorization to launch the UAV.
  - g) After receiving authorization, emergency procedures have been reviewed, and potential hazards have been accounted for and identified, proceed with launching the UAV. Continue to monitor the location of the UAV both visually in the air and in the app to ensure it is adhering to the flight plan.
- 7) Continue to monitor the status of the UAV.
- a) Maintain line-of-sight with the UAV and utilize visual observers when necessary.
  - b) Monitor the flight path, connection between the UAV and controller(s), image exposure and clarity, and battery levels.
  - c) Be prepared to take control in the event of a system malfunction.
- 8) Verify that the landing area is clear and safely land the UAV.
- 9) Review photos ensuring the desired extent was captured including all ground control targets and determine whether a secondary flight is needed to collect additional imagery.
- 10) Power down the UAV.
- 11) Complete the Flight Log for the mission.
- 12) If not returning for additional flights, collect all ground control targets, nails and whiskers, and flagging.

## 2.4 Data products and metrics

Advancements in post-processing software have allowed UAS imagery to be used for purposes beyond qualitative comparisons including deriving spatial measurements and quantifying change. Structure-from-motion (SfM) photogrammetry infers the 3D structure of an object (e.g., a tree, stream reach, landscape) from multiple 2D perspectives (i.e., imagery collected in motion from varying camera positions and orientations). SfM algorithms are incorporated into many widely available post-processing software packages and allow for the generation of derivative data products from collected imagery. The data products generated from post-processing are numerous and at a minimum, 3D models and orthomosaics are needed to derive metrics which can be used to investigate fish-habitat relationships (Figure 9). These products allow for both quantitative analysis of available habitat areas and lengths in addition to providing the means to manually check the positional accuracy of features captured with a high-accuracy GNSS receiver during the ground-based portion of this survey. For example, orthomosaics are used to derive channel overhanging canopy cover and further as qualitative checks to ensure channel unit boundaries are aligned with the wetted channel and are representative of the defined channel unit classification. Similarly, 3D models are used to create canopy height models (CHM) for riparian tree height and density calculations. A list of UAS-derived metrics related to fish habitat quantity/quality are provided in Table 3, with the full list of metrics from both ground and UAS methods provided in Appendix A.

Table 3. Metrics derived from UAS imagery.

Indicator type	Indicator	Metric	Description	Data source
<b>Habitat quality/diversity</b>	Floodplain/side channels	River complexity index	River complexity index (RCI) = $S*(1+J)$ where S = stream sinuosity, J = # of side channel junctions (Brown 2002)	Field/LiDAR/UAS
	Floodplain/side channels	Side channel ratio	Length of side channels divided by length of main channel during base flow (Beechie et al. 2017)	Field/LiDAR/UAS
	Riparian condition	Riparian tree cover	Average percent tree canopy cover in the riparian zone (50 m stream buffer)	UAS/LiDAR
	Riparian condition	Riparian tree height	Average tree height (m) in the riparian zone (50 m stream buffer)	UAS/LiDAR
	River channel (cover)	Large wood area percentage	Percentage of stream surface area covered by large wood during base flow	UAS/LiDAR
	River channel (cover)	Overhanging vegetation	Percentage of stream surface area covered by vegetation during base flow	UAS/LiDAR
	River channel (cover)	Undercut bank percentage	Percentage of the total bank length that is undercut	Field/UAS
	River channel (pools)	Large pool frequency	Number of large pools (> 20 m <sup>2</sup> area and > 0.80 m max depth) per km stream length (McIntosh et al. 2000)	Field/UAS/LiDAR
	River channel (pools)	Medium pool frequency	Number of medium-sized pools (> 20 m <sup>2</sup> area and > 0.50 m max depth) per km stream length	Field/UAS/LiDAR
	Floodplain/side channels	Off-channel habitat base flow	Surface area (m <sup>2</sup> ) of connected off-channel habitat during base flow	LiDAR/UAS
<b>Habitat quantity</b>	Floodplain/side channels	Side channel length	Length (m) of side channels during low flow	Field/UAS
	River channel (fast water)	Fast water area	Surface area (m <sup>2</sup> ) of fast water habitat (e.g., fast turbulent, fast non-turbulent, fast small side channels) during base flow	Field/UAS

Indicator type	Indicator	Metric	Description	Data source
	River channel (pools)	Slow water area	Surface area (m <sup>2</sup> ) of slow water habitat (e.g., pools, off-channel units, slow small side channels) during base flow	Field/UAS

These targeted metrics represent a baseline starting point which can be easily produced by organizations with minimal training or experience required and at an overall low investment cost. However, depending on organizational capacity (e.g., expertise or staff time), funding, and limiting factors for data collection, additional metrics can be derived from standard true color imagery or using other sensors. Accurately georeferenced digital elevation models (DEMs) are another product commonly generated from UAS imagery, but the accuracy, resolution, and completeness can be negatively impacted by the type and density of riparian vegetation. Where vegetation is not a significant factor or where light detection and ranging (LiDAR) data are available, differencing of DEMs (DoD) collected at two or more snapshots in time can show topographic change. Furthermore, shallow-water bathymetry mapping and bathymetric change detection are possible using corrective procedures applied to dense point clouds from SfM or using green topobathymetric LiDAR. Spectral analyses that use classification techniques and those that factor in object shape (e.g., object based image analysis (OBIA) or mask R-CNN) from RGB, multispectral, or hyperspectral imagery is another rapidly advancing technology which can be useful for identifying features (e.g., large wood, water, boulders, vegetation) within imagery. However, to date most applications of these post-processing and analytical techniques have been proof of concept and not yet widely adopted or implemented in monitoring. Finally, forward-looking infrared (FLIR) technology may be particularly useful to provide spatially continuous maps of stream temperature and identify cold water refuges. As software, UAS platforms and sensors continue to progress, periodic reevaluation should be conducted to ensure the best available methods and practices are in place.

#### Procedures:

- 1) Remove the SD card from the UAS camera and backup the imagery to a network location and/or external hard drive in folders denoting which stream segment they correspond to.
  - a) After ensuring the imagery has been backed up, delete the files from the SD and place it back in the camera.
- 2) Export the coordinates of GCPs for each stream segment to text files (.txt).
- 3) Using a photogrammetric post-processing software (i.e., Agisoft Metashape, Pix4D, DroneDeploy):
  - a) Import the imagery in batches to prevent crashing the software or overburdening the PC.
  - b) Import the coordinates for GCPs and use them to improve the accuracy of the spatial coordinates collected from each image.
  - c) Ensure the image coordinates and GCP coordinates are in the same coordinate system and perform a coordinate transformation if necessary.
  - d) At a minimum, proceed with post-processing to produce, check, and export a DEM and orthomosaic.
- 4) Import these data products into a geographic information system (GIS; i.e., ArcMap, QGIS, etc.) along with the spatial data collected with the high-accuracy GNSS.
  - a) Use the orthomosaic to assess and fix any misaligned edge of water or unit boundary points.

- 5) Use these datasets to produce the desired metrics such as those provided in Table 3.

## References

- Archer, E. K., R. Henderson, J. V. Ojala, V. Jeffrey, A. Gavin, and K. K. Burke. 2016. PacFish InFish Biological Opinion (PIBO) Monitoring Program: effectiveness monitoring sampling methods for stream channel attributes. Page 162. Multi-federal agency monitoring program, Logan, UT.
- Beechie, T., and H. Imaki. 2014. Predicting natural channel patterns based on landscape and geomorphic controls in the Columbia River basin, USA: Predicting Channel Patterns in the Columbia Basin. *Water Resources Research* 50(1):39–57.
- Beechie, T. J., O. Stefankiv, B. Timpone-Padgham, J. E. Hall, G. R. Pess, M. Rowse, M. Liermann, K. Fresh, and M. J. Ford. 2017. Monitoring Salmon Habitat Status and Trends in Puget Sound: Development of Sample Designs, Monitoring Metrics, and Sampling Protocols for Large River, Floodplain, Delta, and Nearshore Environments. U.S. Department of Commerce, NOAA Technical Memorandum NMFSNWFSC-137. <https://doi.org/10.7289/V5/TM-NWFSC-137>
- Bieger, K., H. Rathjens, P. M. Allen, and J. G. Arnold (2015), Development and evaluation of bankfull hydraulic geometry relationships for the physiographic regions of the United States, *J. Am. Water Resour. Assoc.*, 51(3), 842–858, doi:10.1111/jawr.12282.
- Brown, A. G. 2002. Learning from the past: palaeohydrology and palaeoecology. *Freshwater Biology* 47(4):817–829.
- Castro, J.M. and P.L. Jackson, 2001. Bankfull Discharge Recurrence Intervals and Regional Hydraulic Geometry Relationships: Patterns in the Pacific Northwest, USA. *Journal of the American Water Resources Association* 37(5):1249-1262
- CHaMP (Columbia Habitat Monitoring Program). 2016. Scientific protocol for salmonid habitat surveys within the Columbia Habitat Monitoring Program.
- Dugdale, S. J., N. E. Bergeron, and A. St-Hilaire. 2015. Spatial distribution of thermal refuges analysed in relation to riverscape hydromorphology using airborne thermal infrared imagery. *Remote Sensing of Environment* 160:43–55.
- Dunham, J., G. Chandler, B. Rieman, and D. Martin. 2005. Measuring stream temperature with digital data loggers: a user's guide. Page 15. USDA Forest Service, Rocky Mountain Research Station, General Technical Report RMRS-GTR-150WWW, Fort Collins, CO.
- Federal Aviation Administration (FAA). 2016a. Operation and certification of small unmanned aircraft systems. *Federal Register* 81(124):42064–42214.
- Federal Aviation Administration (FAA). 2016b. Small unmanned aircraft systems. Advisory Circular AC 107-2, Washington, D.C.
- Federal Aviation Administration (FAA). 2018. Low Altitude Authorization Notification Capability—LAANC. Air Traffic Organization Policy Notice JO 7210.909. Washington, D.C.
- Harrelson, C. C., C. L. Rawlins, and J. P. Potyondy. 1994. Stream channel reference sites: an illustrated guide to field technique. Page 61. U.S. Department of Agriculture, Forest Service, Rocky Mountain Forest and Range Experiment Station, General Technical Report GTR-RM-245, Fort Collins, CO.



- Hawkins, C. P., J. L. Kershner, P. A. Bisson, M. D. Bryant, L. M. Decker, S. V. Gregory, D. A. McCullough, C. K. Overton, G. H. Reeves, R. J. Steedman, and M. K. Young. 1993. A hierarchical approach to classifying stream habitat features. *Fisheries* 18(6):3–12.
- Hawkins, C. P., R. H. Norris, J. N. Hogue, and J. W. Feminella. 2000. Development and evaluation of predictive models for measuring the biological integrity of streams. *Ecological Applications* 10(5):1456–1477.
- Isaak, D. J., D. L. Horan, and S. P. Wollrab. 2013. A simple protocol using underwater epoxy to install annual temperature monitoring sites in rivers and streams. Page 21. U.S. Department of Agriculture, Forest Service, Rocky Mountain Research Station, General Technical Report RMRS-GTR-314, Fort Collins, CO.
- Isaak, Daniel J., Erin E. Peterson, Jay M. Ver Hoef, Seth J. Wenger, Jeffrey A. Falke, Christian E. Torgersen, Colin Sowder, et al. 2014. Applications of Spatial Statistical Network Models to Stream Data. *Wiley Interdisciplinary Reviews: Water*. <https://doi.org/10.1002/wat2.1023>.
- ISEMP/CHaMP. 2017. Integrated Status and Effectiveness Monitoring Program (ISEMP) and Columbia Habitat Monitoring Program (CHaMP) Annual Combined Technical Report, January – December 2016, BPA Projects 2003-017-00 and 2011-006-00, 93 Electronic Pages.
- Jones, K. L., S. J. O’Daniel, T. J. Beechie, J. Zakrajsek, and J. G. Webster. 2015. Physical habitat monitoring strategy (PHAMS) for reach-scale restoration effectiveness monitoring. Page 58. U.S. Geological Survey, Department of the Interior, Open-File Report 2015–1069, Reston, VA.
- Konrad, C. P. 2015. Geospatial assessment of ecological functions and flood-related risks on floodplains along major rivers in the Puget Sound Basin, Washington. Page 28. U.S. Geological Survey, Scientific Investigations Report 2015-5033.
- LANDFIRE. 2016. LANDFIRE Remap 2016 Vegetation Departure (VDep) CONUS dataset. Earth Resources Observation and Science Center (EROS), U.S. Geological Survey <https://www.landfire.gov/vdep.php>.
- Larsen, D. P., A. R. Olsen, and D. L. Stevens. 2008. Using a Master Sample to Integrate Stream Monitoring Programs. *Journal of Agricultural, Biological, and Environmental Statistics* 13(3):243–254.
- Leopold, L. B., M. G. Wolman, and J. P. Miller. 1964. *Fluvial processes in geomorphology*. Dover Publications, Inc., New York.
- Lusk, R., and W. Monday. 2017. An Early Survey of Best Practices for the Use of Small Unmanned Aerial Systems by the Electrical Utility Industry. Retrieved from Oak Ridge National Laboratory: <https://info.ornl.gov/sites/publications/Files/Pub73072.pdf>
- McIntosh, B. A., J. R. Sedell, R. F. Thurow, S. E. Clarke, and G. L. Chandler. 2000. Historical Changes in Pool Habitats in the Columbia River Basin. *Ecological Applications* 10(5):1478.
- Montgomery, D. R., and J. M. Buffington. 1997. Channel-reach morphology in mountain drainage basins. *GSA Bulletin* 109(5):596–611.
- Moore, K., K. Jones, J. Dambacher, and C. Stein. 2019. Aquatic Inventories Project: methods for stream habitat surveys. Oregon Department of Fish and Wildlife, Version 29.1, Corvallis, OR.



- Mossop, B., and M. J. Bradford. 2006. Using thalweg profiling to assess and monitor juvenile salmon (*Oncorhynchus* spp.) habitat in small streams. *Canadian Journal of Fisheries and Aquatic Sciences* 63(7):1515–1525.
- NetMap. 2020. Version 3.2.0. TerrainWorks.  
[http://www.netmaptools.org/Pages/NetMapHelp/technical\\_help.htm](http://www.netmaptools.org/Pages/NetMapHelp/technical_help.htm)
- Roper, B. B., W. C. Saunders, and J. V. Ojala. 2019. Did changes in western federal land management policies improve salmonid habitat in streams on public lands within the Interior Columbia River Basin? *Environmental Monitoring and Assessment* 191(9):574.
- Stevens, D. L., and A. R. Olsen. 2004. Spatially balanced sampling of natural resources. *American Statistical Association* 99(465):262–278.
- Turner, D., A. Lucieer, and C. Watson. 2012. An automated technique for generating georectified mosaics from ultra-high resolution unmanned aerial vehicle (UAV) imagery, based on structure from motion (SfM) point clouds. *Remote Sensing* 4, 1392–1410.  
<https://doi.org/10.3390/rs4051392>
- U.S. Environmental Protection Agency (EPA). 2003. EPA Region 10 Guidance for Pacific Northwest State and Tribal Temperature Water Quality Standards. EPA 910-B-03-002. Region 10 Office of Water, Seattle, WA.
- U.S. Forest Service (USFS). 2015. Western US stream flow metric dataset: modeled flow metrics for stream segments in the western United States under historical conditions and projected climate change scenarios. Page 7.
- U.S. Geological Survey (USGS), U.S. Department of Agriculture – Natural Resource Conservation Service (NRCS), U.S. Environmental Protection Agency (EPA), et al. 2015. National Watershed Boundary Dataset (WBD). Downloaded as part of the NHDPlus HR dataset from <https://www.usgs.gov/core-science-systems/ngp/national-hydrography/access-national-hydrography-products> on 6/16/2020.
- U.S. Geological Survey (USGS). 2016. BETA - USGS National Hydrography Dataset Plus High Resolution (NHDPlus HR) Best Resolution for HU4-0101 (Subregion) Publication Date 20160512 HU-4 Subregion FileGDB 10.1. Downloaded from <https://www.usgs.gov/core-science-systems/ngp/national-hydrography/access-national-hydrography-products> on 6/16/2020.
- White, S., C. Justice, L. Burns, D. Graves, D. Kelsey, and M. Kaylor. 2019. Assessing the status and trends of spring Chinook habitat in the upper Grande Ronde River and Catherine Creek. Page 177. Columbia River Inter-Tribal Fish Commission, Annual Report BPA Project # 2009-004-00, Portland, Oregon.
- Wolman, M. G. 1954. A method of sampling coarse river-bed material. *Transaction of the American Geophysical Union* 35:951–956.

## Appendix A: Metrics

Indicator type	Indicator	Metric	Description	Data source
<b>Habitat quality/diversity</b>	Floodplain/side channels	River complexity index	River complexity index (RCI) = $S \cdot (1+J)$ where S = stream sinuosity, J = # of side channel junctions (Brown 2002)	Field/LiDAR/UAS
	Floodplain/side channels	Side channel ratio	Length of side channels divided by length of main channel during base flow (Beechie et al. 2017)	Field/LiDAR/UAS
	Riparian condition	Riparian tree cover	Average percent tree canopy cover in the riparian zone (50 m stream buffer)	UAS/LiDAR
	Riparian condition	Riparian tree height	Average tree height (m) in the riparian zone (50 m stream buffer)	UAS/LiDAR
	Riparian condition	Riparian vegetation departure	Average percentage departure in current vegetation from simulated historical vegetation reference conditions in the riparian zone (100 m buffer; LANDFIRE 2016)	Satellite/Modeled
	River channel (cover)	Large wood area percentage	Percentage of stream surface area covered by large wood during base flow	UAS/LiDAR
	River channel (cover)	Large wood frequency bankfull	Number of large wood pieces within the bankfull channel per 100 m stream length (Moore et al. 2017)	Field
	River channel (cover)	Large wood frequency wetted	Number of large wood pieces within the wetted channel during base flow per 100 m stream length (Moore et al. 2017)	Field
	River channel (cover)	Overhanging vegetation	Percentage of stream surface area covered by vegetation during base flow	UAS/LiDAR
	River channel (cover)	Undercut bank percentage	Percentage of the total bank length that is undercut	Field/UAS
	River channel (pools)	Residual pool depth	Mean residual pool depth (max depth - thalweg exit depth in meters; Mossop and Bradford 2006)	Field/LiDAR

Indicator type	Indicator	Metric	Description	Data source
	River channel (pools)	Large pool frequency	Number of large pools (> 20 m <sup>2</sup> area and > 0.80 m max depth) per km stream length (McIntosh et al. 2000)	Field/UAS/LiDAR
	River channel (pools)	Medium pool frequency	Number of medium-sized pools (> 20 m <sup>2</sup> area and > 0.50 m max depth) per km stream length	Field/UAS/LiDAR
	River channel (substrate)	Median sediment particle size	Median sediment particle size on the streambed surface in riffles (Wolman 1954)	Field
	Water quality	Coldwater refuge density	Number of cold-water refuges per km stream length (Dugdale et al. 2015)	FLIR
	Water quality	Maximum weekly maximum temperature	Maximum 7-day running average of daily maximum temperature (EPA 2003)	Field/Model ed
	Water quality	Observed/Expected benthic macroinvertebrates	Ratio of observed to expected (O/E) benthic macroinvertebrate taxa as predicted by the River Invertebrate Prediction and Classification System (RIVPACS, Hawkins et al. 2000)	Field
<b>Habitat quantity</b>	Floodplain/side channels	Off-channel habitat bankfull	Surface area (m <sup>2</sup> ) of connected off-channel habitat during bankfull flow (Konrad et al. 2015)	LiDAR
	Floodplain/side channels	Off-channel habitat base flow	Surface area (m <sup>2</sup> ) of connected off-channel habitat during base flow	LiDAR/UAS
	Floodplain/side channels	Side channel length	Length (m) of side channels during low flow	Field/UAS
	Flow	Center of flow mass	Flow-weighted mean day of the water year (i.e., center of flow timing; USFS 2015)	Field/Model ed
	Flow	Mean annual flow	Mean daily flow (m <sup>3</sup> ·s <sup>-1</sup> ) within a water year (Oct 1 - Sep 30; USFS 2015)	Field/Model ed
	Flow	Mean summer flow	Mean daily flow (m <sup>3</sup> ·s <sup>-1</sup> ) during summer (Jun 1 - Sep 30; USFS 2015)	Field/Modeled
	River channel (fast water)	Fast water area	Surface area (m <sup>2</sup> ) of fast water habitat (e.g., fast turbulent, fast non-turbulent, fast small side channels) during base flow	Field/UAS

Indicator type	Indicator	Metric	Description	Data source
	River channel (total length)	Length accessible anadromous fish habitat	Length (km) of accessible main channel habitat that is currently used by anadromous fish for spawning, rearing, or migration	Field/ Modeled
	River channel (pools)	Slow water area	Surface area (m <sup>2</sup> ) of slow water habitat (e.g., pools, off-channel units, slow small side channels) during base flow	Field/UAS

## Appendix B: Equipment list

Equipment	Quantity	Check	Notes
<b>HABITAT</b>			
Protocol	2	<input type="checkbox"/>	
iPads or tablets with loaded site data	2	<input type="checkbox"/>	
Topo maps and segment metadata	1	<input type="checkbox"/>	
Arrow 100 high-resolution GNSS receiver with spare battery	1	<input type="checkbox"/>	
2m fixed-height survey rod (for GNSS receiver)	1	<input type="checkbox"/>	
Measuring tape (50 m)	1	<input type="checkbox"/>	
Telescoping leveling rod (i.e., stadia rod; $\geq 3$ m)	1	<input type="checkbox"/>	
Gravelometer	1	<input type="checkbox"/>	
Flagging (2 colors)	4	<input type="checkbox"/>	
Permanent markers and pencils	4	<input type="checkbox"/>	
Waterproof laser rangefinder	1	<input type="checkbox"/>	
Compass	1	<input type="checkbox"/>	
Write-in-rain field notebooks	3	<input type="checkbox"/>	
Clipboard to store manuals and datasheets	2	<input type="checkbox"/>	
Backpack	2	<input type="checkbox"/>	
Candy cane stakes for bankfull cross-sections	4	<input type="checkbox"/>	
Small spring clamps to hold measuring tape	4	<input type="checkbox"/>	
<b>UAS (DRONE)</b>			
UAS with spare batteries	1	<input type="checkbox"/>	
Launch pad	1	<input type="checkbox"/>	
iPad or tablet with flight planning software and sun/shade hood	1	<input type="checkbox"/>	
Pre-flight checklist and log binder	1	<input type="checkbox"/>	
Controller	2	<input type="checkbox"/>	
Spare SD cards	3	<input type="checkbox"/>	
Circular polarizing (CP) camera filter	1	<input type="checkbox"/>	
"Drone pilot at work - Do not disturb" sign	1	<input type="checkbox"/>	
High visibility safety vests	4	<input type="checkbox"/>	
Safety cones	2	<input type="checkbox"/>	
Hex key / Allen wrench set	1	<input type="checkbox"/>	
Spare propellers	4	<input type="checkbox"/>	
Two-way radios with spare batteries	4	<input type="checkbox"/>	
<b>TEMPERATURE</b>			
HOBO Tidbit Temperature loggers	10	<input type="checkbox"/>	
HOBO Onset Shuttle and USB cable	2	<input type="checkbox"/>	
iPad with temperature data collection application			
Laptop computer	1	<input type="checkbox"/>	

Flagging	2	<input type="checkbox"/>	
Stainless steel wire (1/16" diameter or larger)	40 ft	<input type="checkbox"/>	
Cable crimps for 1/16" cable or larger	25	<input type="checkbox"/>	
Crimping tool	1	<input type="checkbox"/>	
Heavy duty pliers with cable cutter	10	<input type="checkbox"/>	
Thermometer	2	<input type="checkbox"/>	
1.5" PVC male adapter	3	<input type="checkbox"/>	
1.5" PVC female screw cap	3	<input type="checkbox"/>	
Two part epoxy (Fox Industries FX-764 Hydro-Ester® Splash Zone Epoxy)	1	<input type="checkbox"/>	
Wire brush	1	<input type="checkbox"/>	
Nitrile gloves	10 pairs	<input type="checkbox"/>	
Metal detector (optional)	1	<input type="checkbox"/>	
Sledge hammer 2 lb	1	<input type="checkbox"/>	
1/4" – 3/4" rebar or nail stakes (2-2.5 ft length)	20	<input type="checkbox"/>	
<b>SAFETY/OTHER</b>			
GPS/GNSS and spare batteries or other navigation device	2	<input type="checkbox"/>	
Road maps	1	<input type="checkbox"/>	
Topo maps	1	<input type="checkbox"/>	
Satellite phone or another remote emergency communication device	1	<input type="checkbox"/>	
First aid kit (2 regular, 1 Wilderness First Aid)	3	<input type="checkbox"/>	
AED (Automated External Defibrillator)	1	<input type="checkbox"/>	
Tool kit (wrench, pliers, screws drivers, etc.)	1	<input type="checkbox"/>	
Road safety kit (includes jumper cables, air compressor, flares, flashlight, etc.)	1	<input type="checkbox"/>	
Safety vests	4	<input type="checkbox"/>	
Water container (5 gal)	1	<input type="checkbox"/>	
Cooler	1	<input type="checkbox"/>	
Ice packs	2	<input type="checkbox"/>	
Large tarp	1	<input type="checkbox"/>	
Rope (100 ft)	1	<input type="checkbox"/>	
Scientific research permits	1	<input type="checkbox"/>	
Fire extinguisher	1	<input type="checkbox"/>	
Inverter	1	<input type="checkbox"/>	
<b>PERSONAL FIELD EQUIPMENT</b>			
Wading boots	1	<input type="checkbox"/>	
Neoprene wading socks	1	<input type="checkbox"/>	
Waders	1	<input type="checkbox"/>	
Rain gear	1	<input type="checkbox"/>	
Hat	1	<input type="checkbox"/>	
Sunscreen	1	<input type="checkbox"/>	
Polarized sunglasses	1	<input type="checkbox"/>	

Bug repellent	1	<input type="checkbox"/>	
Pocket knife or multi-tool	1	<input type="checkbox"/>	
Water bottle (1 qt)	2	<input type="checkbox"/>	
Backpack	1	<input type="checkbox"/>	
Cell phone	1	<input type="checkbox"/>	
Cell phone charger	1	<input type="checkbox"/>	
Toilet paper	2	<input type="checkbox"/>	
Food for lunch, snacks, and lunch bag	1	<input type="checkbox"/>	

## Appendix C: Flight mission checklist

### Regulations

- ☐ Print off VFR Sectional Chart of flight area at <https://skyvector.com/>
- ☐ Obtain the necessary permissions from partnering agencies and/or notify private landowners
- ☐ Check for NOTAMs and TFRs
- ☐ Check weather for location and time of flight
- ☐ File LAANC and/or DROTAM at [www.1800wxbrief.com](http://www.1800wxbrief.com) (if applicable) and complete flight log

### Segment reconnaissance and pre-flight field work

- ☐ Prepare pre-season flight paths for each stream segment
- ☐ Ensure maps and flight plans are saved and cached to the iPad(s)
- ☐ Identify additional unforeseen hazards (trees, cliffs, people, property, power lines) within each segment
- ☐ Establish 3-5 ground control points (GCPs) per 1 km
  - Using a high-accuracy GNSS receiver or other surveying equipment (total station or real time kinematic GNSS) establish randomly distributed GCPs throughout the segment flagging each with the corresponding number
- ☐ Adjust pre-established flight paths to account for hazards
- ☐ Stake out ground control targets
- ☐ Meet with the crew to layout flight plan, address additional concerns, and test radios

### Flight mission

- ☐ Establish primary takeoff and landing zones
  - These areas should be flat and free of obstacles such as trees or shrubs within a 3 m radius. The use of a launch pads or an alternative surface (e.g., plywood) should be used to help tamp down tall grasses when necessary
- ☐ If takeoff and landing locations are on or adjacent to a road, set out safety cones and signage to alert the public to an active work site
- ☐ Unload the UAV, ensure equipment is fully charged, and visually inspect the equipment
  - Inspect rotors and propellers, gimbal(s) and payload(s), and check for visible defects
  - Ensure sufficient storage is available on the SD card within the camera and clean the lens to remove any dust, debris, or water particles prior to takeoff
  - Install UAV batteries
- ☐ Prepare to launch the UAV
  - Turn on the UAV and remote controller(s) and check connectivity
  - Set camera parameters
  - Review flight path and mission details
  - Set the “home” location and verify emergency protocols
  - If present, check radio connection between PIC and visual observer(s).
  - Complete the pre-flight checklist and update the flight log



- If not yet complete and necessary, contact air traffic control (ATC) or local dispatch to receive authorization to launch the UAV
- After receiving authorization, emergency procedures have been reviewed, and potential hazards have been accounted for and identified proceed with launching the aircraft
- ☐ Continue to monitor the mission status and UAV
  - Maintain line-of-sight with the UAV and utilizes visual observers when necessary
  - Monitor the flight path, connection between the UAV and controller(s), and battery levels
  - Be prepared to take control in the event of a system malfunction
- ☐ Verify the landing area is clear and safe to land the UAV
- ☐ Land the aircraft and review imagery ensuring the desired extent was captured including all ground control targets and determine whether a secondary flight is needed to collect additional imagery
- ☐ Power down the UAV
- ☐ Complete the Flight Log for the mission

## Appendix D: UAS Flight Log

Pilot in Command (PIC): \_\_\_\_\_  
 Organization: \_\_\_\_\_ Proposed Flight Date: \_\_\_\_/\_\_\_\_/\_\_\_\_  
 Stream Segment ID: \_\_\_\_\_  
 Local Airport Code(s): \_\_\_\_\_ Proximity: \_\_\_\_\_ (miles) Airspace Class: \_\_\_\_\_  
 ATC/ Dispatch Contact Date: \_\_\_\_/\_\_\_\_/\_\_\_\_ Permission Granted: Y / N  
 ATC/ Dispatch Contact Info: \_\_\_\_\_  
 Airport Emergency Phone Number: \_\_\_\_\_ ATC/CTAF Freq: \_\_\_\_\_  
 LAANC or DROTAM Filed Date: \_\_\_\_/\_\_\_\_/\_\_\_\_  
 Flight Coordinates: \_\_\_\_\_ Radius: \_\_\_\_\_ ALT: \_\_\_\_\_  
 Flight Date /Time: \_\_\_\_\_  
 LAANC or DROTAM Number: \_\_\_\_\_ Phone Operator Initials: \_\_\_\_\_  
 METAR: \_\_\_\_\_

☐ Minimum 3 SM visibility, ceiling 500 (ft) MSL above flight max ALT

Temporary Flight Restriction (TFR): Y / N \_\_\_\_\_

NOTAM Check: Y / N

- ILLNESS
- MEDICATION
- STRESS
- ALCOHOL
- FATIGUE
- EMOTION

- PILOT
- AIRCRAFT
- ENVIRONMENT
- EXTERNAL PRESSURES (EGO, OUTSIDE STRESSES, ETC)
- PEOPLE
- PROPERTY NEARBY
- FORCED LANDING AREA
- PARTICIPANT WAIVER

Crew Brief (If present)

- EMERGENCY PROCEDURES
- MISSION BRIEF

Pre-flight Complete: \_\_\_\_/\_\_\_\_/\_\_\_\_

Flight Notes (Include Date, Start/Stop Time, Visual Observers, Any Training, Maneuvers, etc.):

---



---



---



---



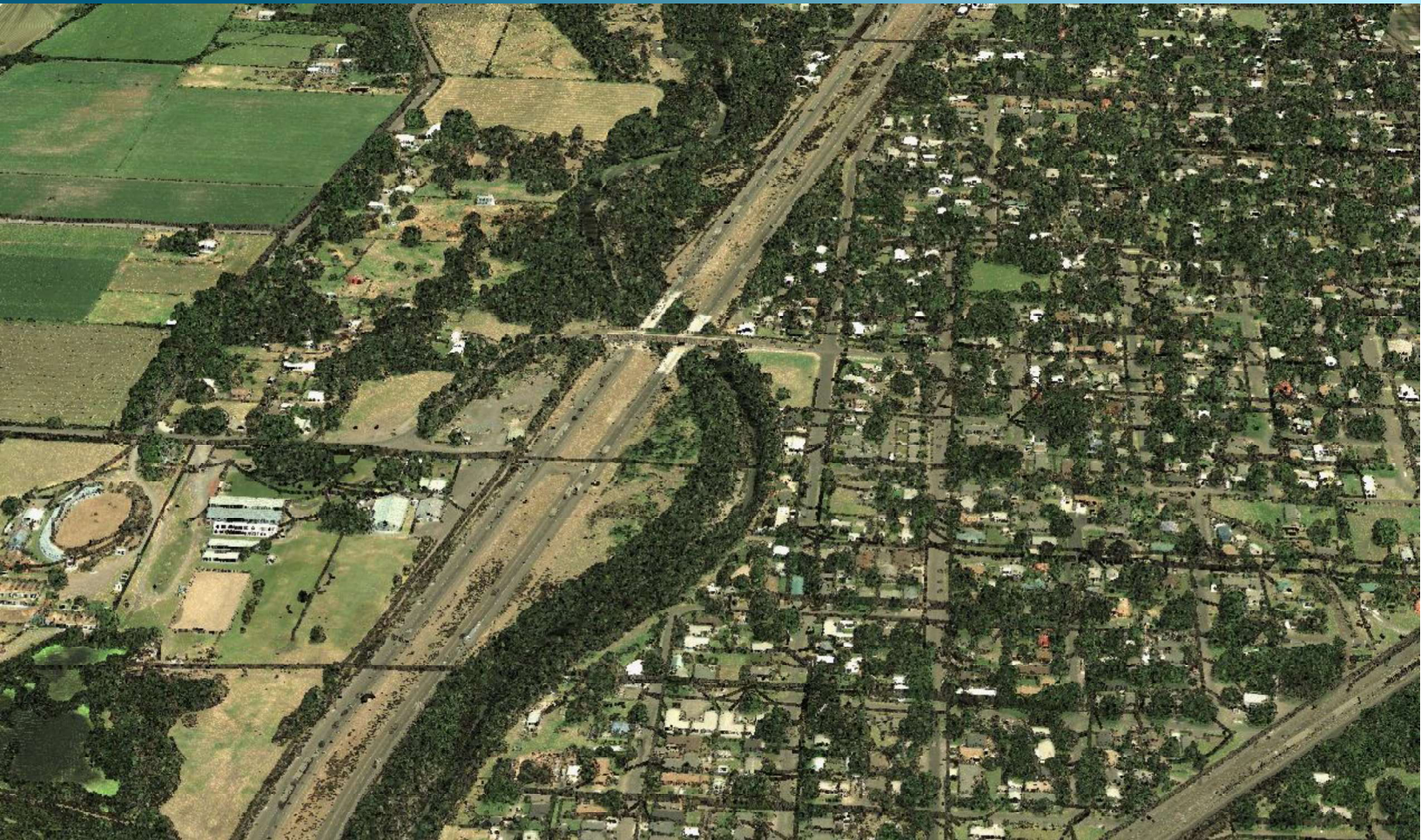
---



---

## **Appendix B – Grande Ronde Basin, Oregon, Topobathymetric LiDAR Technical Data Report**

February 12, 2021



# Grande Ronde Basin, Oregon

## Topobathymetric Lidar Technical Data Report

*Prepared For:*



**Seth M. White**

Columbia River Inter-Tribal Fish Commission  
Portland, OR 97232  
PH: 503-731-1300

*Prepared By:*



**NV5 Corvallis**

1100 NE Circle Blvd, Ste. 126  
Corvallis, OR 97330  
PH: 541-752-1204





# TABLE OF CONTENTS

INTRODUCTION ..... 1

    Deliverable Products ..... 2

ACQUISITION ..... 4

    Planning..... 4

    Airborne Lidar Survey ..... 8

    Ground Survey..... 10

        Base Stations..... 10

        Ground Survey Points (GSPs)..... 12

PROCESSING ..... 14

    Topobathymetric Lidar Data ..... 14

    Bathymetric Refraction ..... 17

    Water’s Edge Breaklines..... 17

    Lidar Derived Products ..... 17

        Topobathymetric DEMs ..... 17

RESULTS & DISCUSSION..... 18

    Lidar Point Density ..... 18

        First Return Point Density..... 18

        Bathymetric and Ground Classified Point Densities ..... 18

    Lidar Accuracy Assessments..... 23

        Lidar Non-Vegetated Vertical Accuracy..... 23

        Lidar Bathymetric Vertical Accuracies ..... 26

        Lidar Relative Vertical Accuracy ..... 28

        Lidar Horizontal Accuracy ..... 29

CERTIFICATIONS ..... 30

GLOSSARY ..... 31

APPENDIX A - ACCURACY CONTROLS ..... 32

**Cover Photo:** A view looking east over the Upper Grande Ronde River in La Grande, Oregon. The image was created from the Lidar point cloud and colored using imagery from the National Agriculture Imagery Program.



## INTRODUCTION

This photo taken by NV5 acquisition staff shows a view of the Minam River just south of Minam, Oregon in the Grande Ronde Basin site.



In August 2020, NV5 Geospatial (NV5) was contracted by Columbia River Inter-Tribal Fish Commission (CRITFC) to collect topobathymetric Light Detection and Ranging (Lidar) data in the summer of 2020 for the Grande Ronde Basin site in Oregon. The Grande Ronde Basin area of interest is located in northeastern Oregon and includes the Grande Ronde Lower Tributaries, Upper Grande Ronde, Lostine River, Catherine Creek, and Minam River. Traditional near-infrared (NIR) lidar was fully integrated with green wavelength return data (bathymetric) lidar in order to provide a seamless topobathymetric lidar dataset. Data were collected to aid CRITFC in assessing vegetation density and height, altered floodplain characteristics, and support analysis of instream and near-stream fish habitat conditions.

This report accompanies the delivered topobathymetric lidar data, and documents contract specifications, data acquisition procedures, processing methods, and analysis of the final dataset including lidar accuracy and density. Acquisition dates and acreage are shown in Table 1, a complete list of contracted deliverables provided to CRITFC is shown in Table 2, and the project extent is shown in Figure 1.

**Table 1: Acquisition dates, acreage, and data types collected on the Grande Ronde Basin site**

Project Site	Contracted Acres	Buffered Acres	Acquisition Dates	Data Type
Grande Ronde Basin, Oregon	76,189	93,681	08/17/2020 – 09/27/2020	Topobathymetric Lidar



# Deliverable Products

**Table 2: Products delivered to CRITFC for the Grande Ronde Basin site**

Grande Ronde Basin Lidar Products	
Projection: UTM Zone 11 North	
Horizontal Datum: NAD83 (2011)	
Vertical Datum: NAVD88 (GEOID18)	
Units: Meters	
Topobathymetric Lidar	
Points	LAS v 1.4 <ul style="list-style-type: none"> <li>All Classified Returns</li> </ul>
Rasters	1.0 Meter ESRI Grids <ul style="list-style-type: none"> <li>Uncropped Topobathymetric Bare Earth Digital Elevation Model (DEM)</li> <li>Cropped Topobathymetric Bare Earth Digital Elevation Model (DEM)</li> <li>Highest Hit Digital Surface Model (DSM)</li> <li>Water Surface Model (WSM)</li> <li>Bathymetric Depth Model</li> </ul> 0.5 Meter GeoTiffs <ul style="list-style-type: none"> <li>Green Sensor Intensity Images</li> <li>NIR Sensor Intensity Images</li> </ul>
Vectors	Shapefiles (*.shp) <ul style="list-style-type: none"> <li>Area of Interest</li> <li>Lidar Tile Index</li> <li>Bathymetric Coverage Shape</li> <li>Water's Edge Breaklines</li> <li>Ground Survey Shapes</li> </ul>

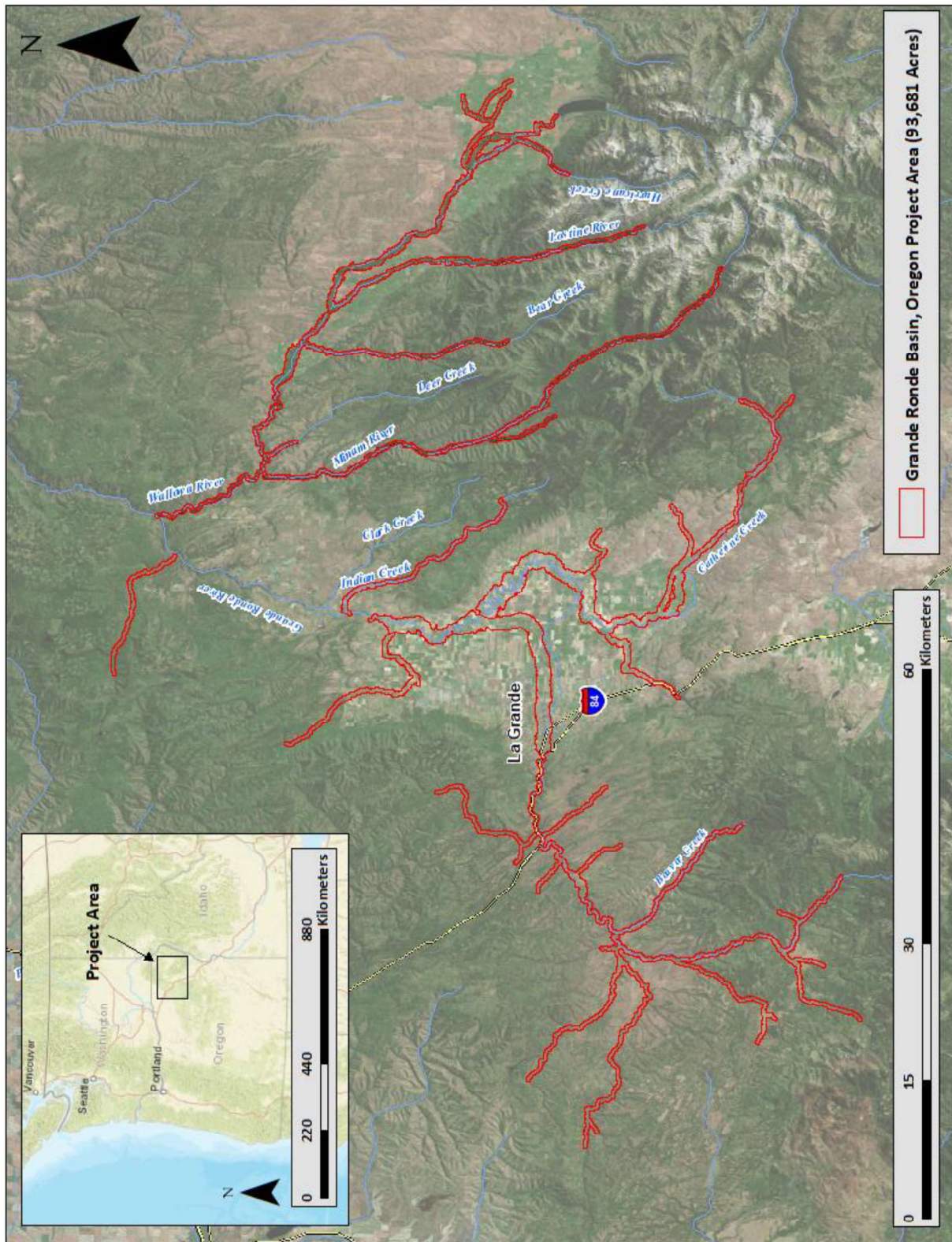


Figure 1: Location map of the Grande Ronde Basin site in Oregon

NV5's ground acquisition equipment set up in the Grande Ronde Basin Lidar study area.



## Planning

In preparation for data collection, NV5 reviewed the project area and developed a specialized flight plan to ensure complete coverage of the Grande Ronde Basin Lidar study area at the target combined point density of  $\geq 6$  points/m<sup>2</sup>. Acquisition parameters including orientation relative to terrain, flight altitude, pulse rate, scan angle, and ground speed were adapted to optimize flight paths and flight times while meeting all contract specifications.

Factors such as satellite constellation availability and weather windows must be considered during the planning stage. Any weather hazards or conditions affecting the flight were continuously monitored due to their potential impact on the daily success of airborne and ground operations. In addition, logistical considerations including private property access, potential air space restrictions, degree of perennial aquatic vegetation growth, channel flow rates (Figure 2 - Figure 5), and water clarity were reviewed.



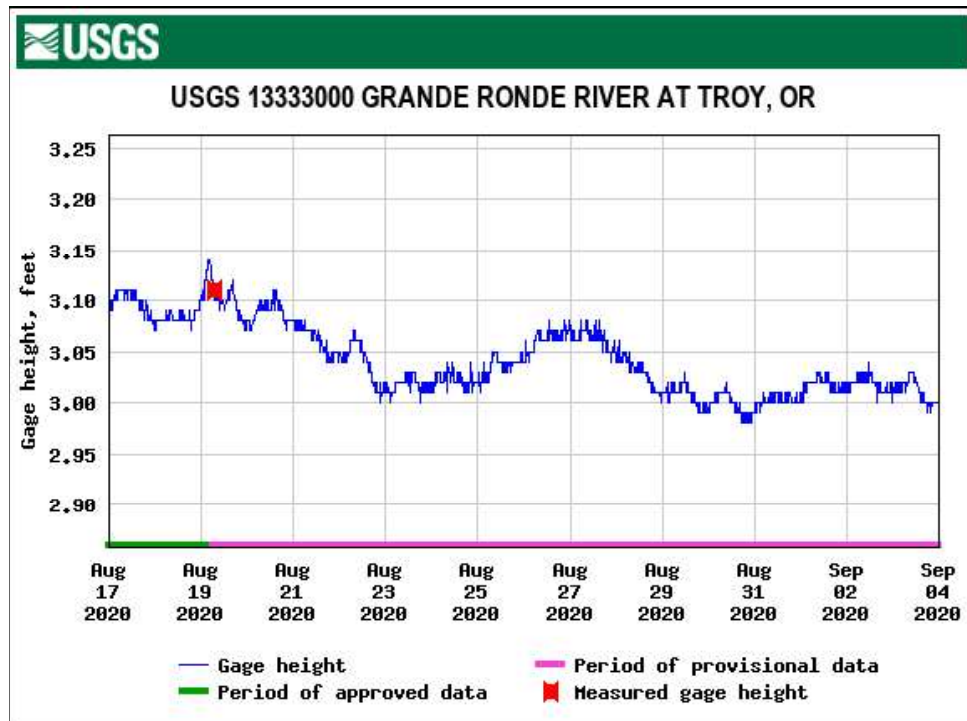


Figure 2: USGS Station 13333000 gage height along the Grande Ronde River at the time of Lidar acquisition.

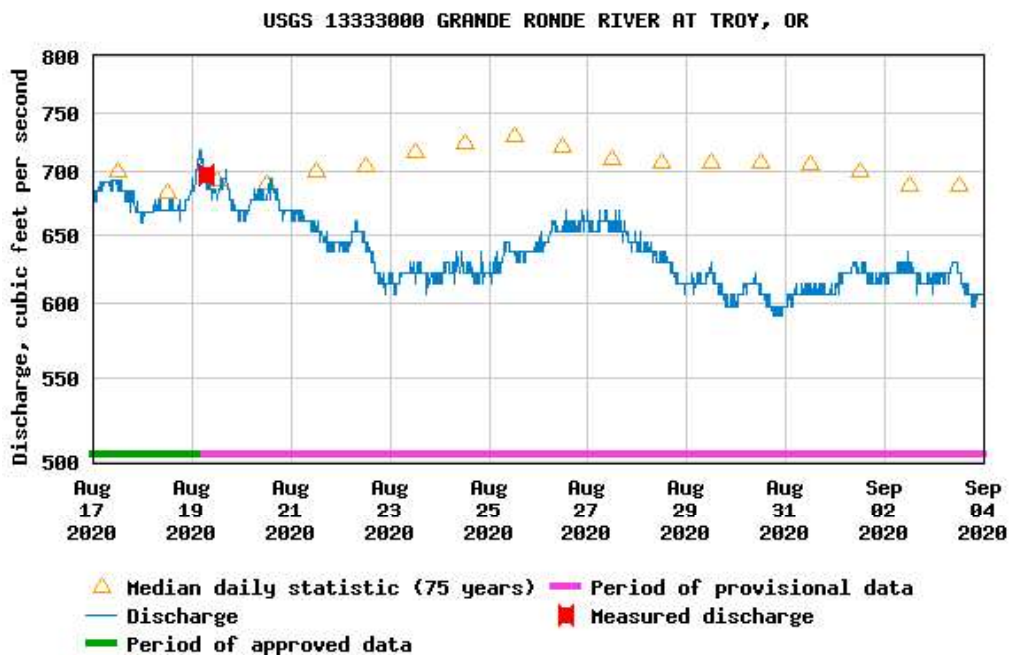


Figure 3: USGS Station 13333000 flow rates along the Grande Ronde River at the time of Lidar acquisition.

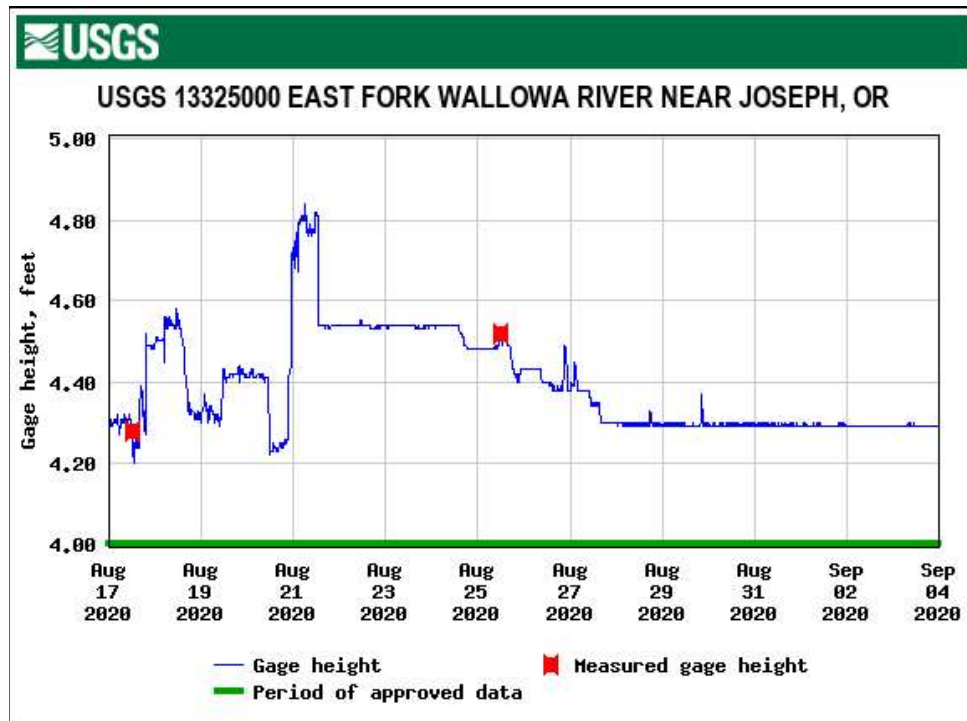


Figure 4: USGS Station 13325000 gage height along the East Fork Wallowa River at the time of Lidar acquisition.

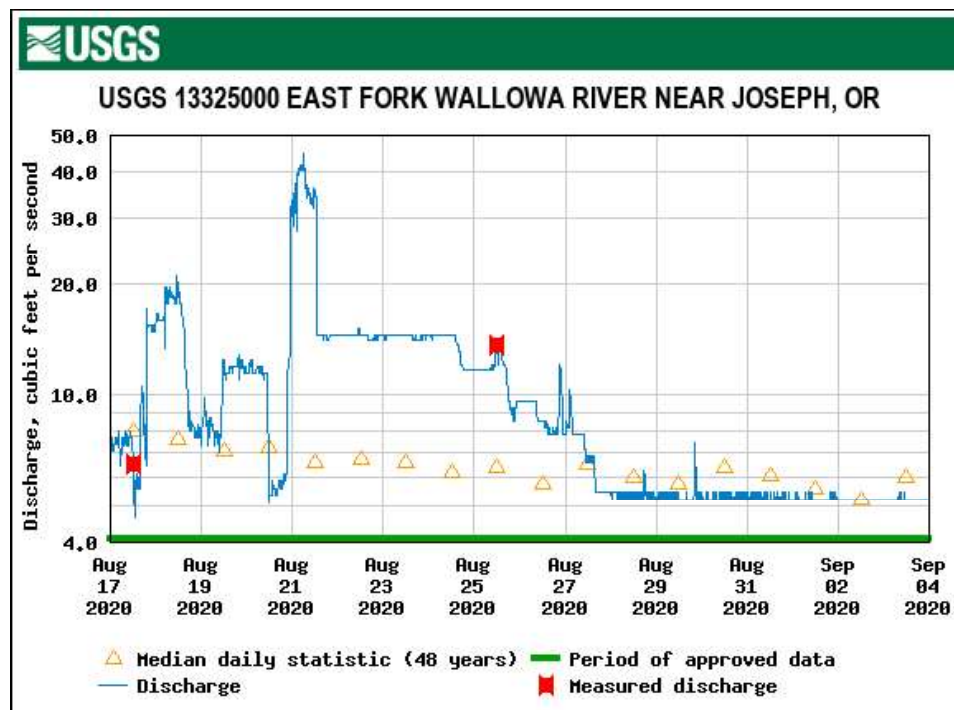
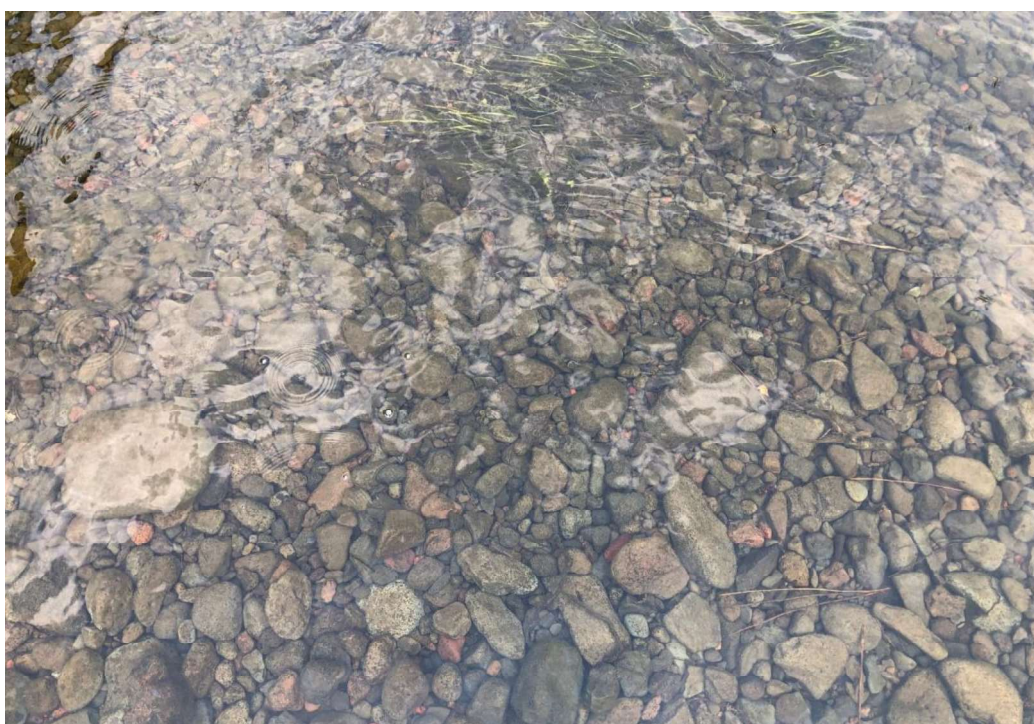


Figure 5: USGS Station 13325000 flow rates along the East Fork Wallowa River at the time of Lidar acquisition.





*These photos taken by NV5 acquisition staff display water clarity conditions near the confluence of Pelican Creek and Five Points Creek within the Grande Ronde Basin site.*



## Airborne Lidar Survey

The lidar survey was accomplished using a Riegl VQ-880-GII green laser system mounted in a Cessna Caravan. The Riegl VQ-880-GII boasts a higher repetition pulse rate (up to 550 kHz), higher scanning speed, small laser footprint, and wide field of view which allows for seamless collection of high resolution data of both topographic and bathymetric surfaces. The green wavelength ( $\lambda=532$  nm) laser is capable of collecting high resolution topography data, as well as penetrating the water surface with minimal spectral absorption by water. The Riegl VQ-880-GII contains an integrated NIR laser ( $\lambda=1064$  nm) that adds additional topography data and aids in water surface modeling. The recorded waveform enables range measurements for all discernible targets for a given pulse. The typical number of returns digitized from a single pulse range from 1 to 15 for the Grande Ronde Basin project area. It is not uncommon for some types of surfaces (e.g., dense vegetation or water) to return fewer pulses to the Lidar sensor than the laser originally emitted. The discrepancy between first return and overall delivered density will vary depending on terrain, land cover, and the prevalence of water bodies. All discernible laser returns were processed for the output dataset. Table 3 summarizes the settings used to yield an average pulse density of  $\geq 6$  pulses/m<sup>2</sup> over the Grande Ronde Basin project area.

**Table 3: Lidar specifications and survey settings**

Lidar Survey Settings & Specifications		
Acquisition Dates	8/17/2020 - 9/27/2020	8/17/2020 - 9/27/2020
Aircraft Used	Cessna Caravan	Cessna Caravan
Sensor	Riegl	Riegl
Laser	VQ-880-GII	VQ-880-GII-IR
Maximum Returns	15	15
Resolution/Density	Average 6 pulses/m <sup>2</sup>	Average 6 pulses/m <sup>2</sup>
Nominal Pulse Spacing	0.41 m	0.41 m
Survey Altitude (AGL)	400 m	400 m
Survey speed	145 knots	145 knots
Field of View	40°	42°
Mirror Scan Rate	80 lines per second	Uniform Point Spacing
Target Pulse Rate	200 kHz	150 kHz
Pulse Length	1.5 ns	3 ns
Laser Pulse Footprint Diameter	28 cm	8 cm
Central Wavelength	532 nm	1064 nm
Pulse Mode	Multiple Times Around (MTA)	Multiple Times Around (MTA)
Beam Divergence	0.7 mrad	0.2 mrad
Swath Width	1800 m	1800 m
Swath Overlap	55%	55 %
Intensity	16-bit	16-bit
Accuracy	RMSE <sub>z</sub> ≤ 15 cm	RMSE <sub>z</sub> ≤ 15 cm



All areas were surveyed with an opposing flight line side-lap of  $\geq 50\%$  ( $\geq 100\%$  overlap) in order to reduce laser shadowing and increase surface laser painting. To accurately solve for laser point position (geographic coordinates x, y and z), the positional coordinates of the airborne sensor and the attitude of the aircraft were recorded continuously throughout the Lidar data collection mission. Position of the aircraft was measured twice per second (2 Hz) by an onboard differential GPS unit, and aircraft attitude was measured 200 times per second (200 Hz) as pitch, roll and yaw (heading) from an onboard inertial measurement unit (IMU). To allow for post-processing correction and calibration, aircraft and sensor position and attitude data are indexed by GPS time.

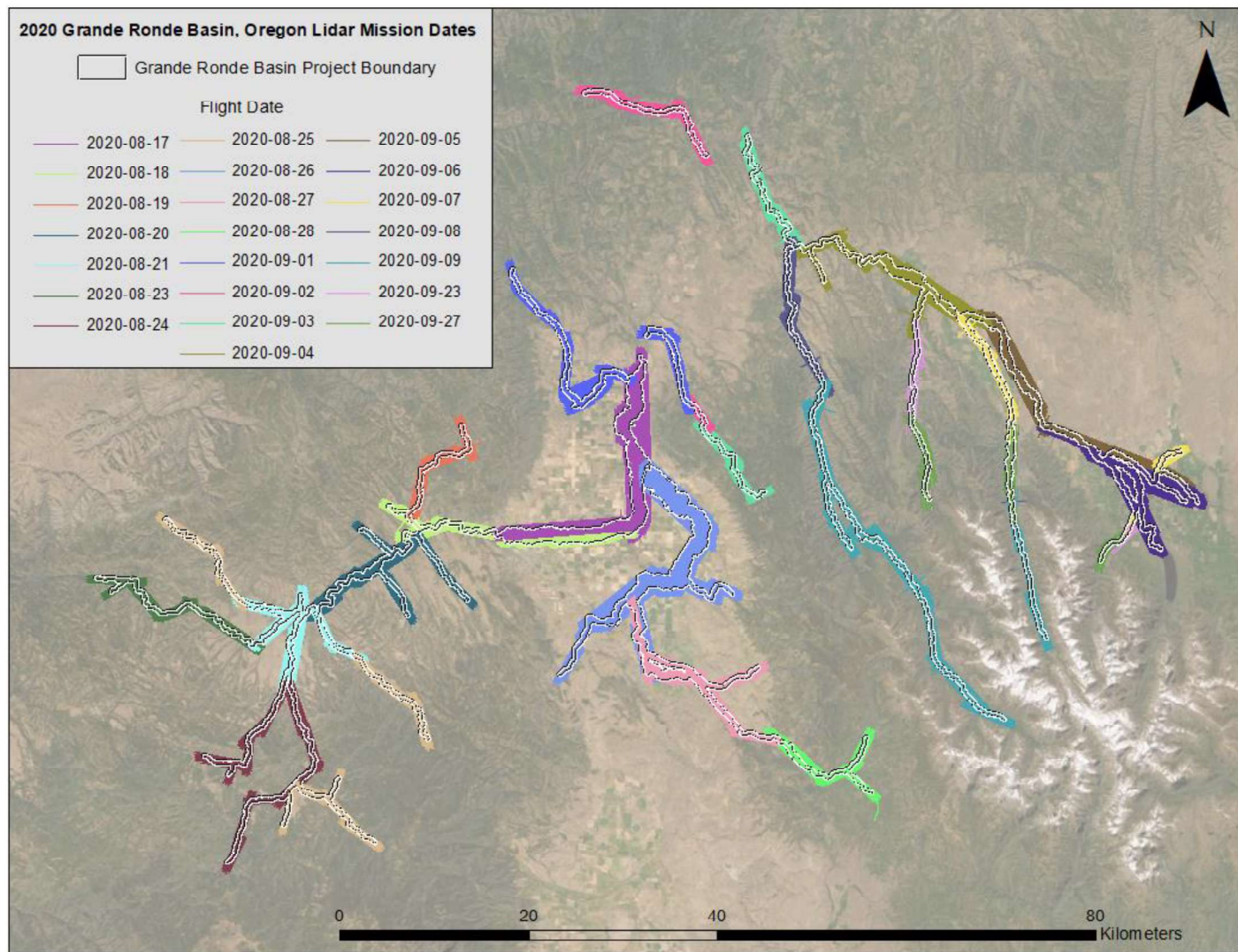


**Figure 6: 2020 Grande Ronde Basin, Oregon Lidar Mission Flight Dates**



## Ground Survey

Ground control surveys, including monumentation and ground survey points (GSPs), were conducted to support the airborne acquisition. Ground control data were used to geospatially correct the aircraft positional coordinate data and to perform quality assurance checks on final Lidar data.



NV5-Established Monument

## Base Stations

Base stations were used for collection of ground survey points using real time kinematic (RTK) , post processed kinematic (PPK), and fast static (FS) survey techniques.

Base station locations were selected with consideration for satellite visibility, field crew safety, and optimal location for GSP coverage. NV5 utilized three permanent active base stations from the Oregon Real-Time GNSS Network (ORGN) and established ten new monuments for the Grande Ronde Basin Lidar project (Table 4, Figure 7). New monuments are 6" survey nails set with washers. NV5's professional land surveyor, Evon Silvia (ORPLS#81104) oversaw and certified the ground survey.

**Table 4: Base station positions for the Grande Ronde Basin acquisition. Coordinates are on the NAD83 (2011) datum, epoch 2010.00**

Monument ID	Type	Latitude	Longitude	Ellipsoid (meters)
ELG2	ORGN	45° 33' 53.49145"	-117° 55' 42.27526"	816.489
ENTR	ORGN	45° 25' 52.50655"	-117° 17' 17.03741"	1127.055
P022	ORGN	45° 13' 54.41272"	-118° 00' 49.52589"	888.603
GRANDERONDE_01	Monument	45° 07' 28.48297"	-118° 24' 09.73070"	1716.444
GRANDERONDE_02	Monument	45° 36' 27.99906"	-117° 43' 47.78391"	772.675
GRANDERONDE_03	Monument	45° 20' 51.43296"	-118° 13' 18.25130"	891.243
GRANDERONDE_04	Monument	45° 15' 23.67625"	-118° 24' 33.09118"	1019.138
GRANDERONDE_05	Monument	45° 17' 00.13156"	-118° 32' 18.86449"	1282.184
GRANDERONDE_06	Monument	45° 08' 54.07071"	-118° 07' 42.31972"	1749.102
GRANDERONDE_07	Monument	45° 08' 37.58917"	-117° 42' 26.50403"	1103.04
GRANDERONDE_08	Monument	45° 43' 16.43177"	-117° 50' 30.51572"	909.444
GRANDERONDE_09	Monument	45° 16' 34.87642"	-117° 23' 25.45009"	1599.267
GRANDERONDE_10	Monument	45° 24' 39.86694"	-117° 25' 24.84674"	1120.229

NV5 utilized static Global Navigation Satellite System (GNSS) data collected at 1 Hz recording frequency for each base station. During post-processing, the static GNSS data was triangulated with nearby Continuously Operating Reference Stations (CORS) using the Online Positioning User Service (OPUS<sup>1</sup>) for precise positioning. Multiple independent sessions over the same monument were processed to confirm antenna height measurements and to refine position accuracy.

Monuments were established according to the national standard for geodetic control networks, as specified in the Federal Geographic Data Committee (FGDC) Geospatial Positioning Accuracy Standards for geodetic networks.<sup>2</sup> This standard provides guidelines for classification of monument quality at the 95% confidence interval as a basis for comparing the quality of one control network to another. The monument rating for this project is shown in Table 5.

**Table 5: Federal Geographic Data Committee monument rating for network accuracy**

Direction	Rating
1.96 * St Dev <sub>NE</sub> :	0.020 m
1.96 * St Dev <sub>Z</sub> :	0.050 m

For the Grande Ronde Basin Lidar project, the monument coordinates contributed no more than 5.6 cm of positional error to the geolocation of the final ground survey points and Lidar, with 95% confidence.

---

<sup>1</sup> OPUS is a free service provided by the National Geodetic Survey to process corrected monument positions.  
<http://www.ngs.noaa.gov/OPUS/>.

<sup>2</sup> Federal Geographic Data Committee, Geospatial Positioning Accuracy Standards (FGDC-STD-007.2-1998). Part 2: Standards for Geodetic Networks, Table 2.1, page 2-3. <http://www.fgdc.gov/standards/projects/FGDC-standards-projects/accuracy/part2/chapter2>

## Ground Survey Points (GSPs)

Ground survey points were collected using real time kinematic (RTK), post-processed kinematic (PPK), and fast-static (FS) survey techniques. For RTK surveys, a roving receiver receives corrections from a nearby base station or Real-Time Network (RTN) via radio or cellular network, enabling rapid collection of points with relative errors less than 1.5 cm horizontal and 2.0 cm vertical. PPK and FS surveys compute these corrections during post-processing to achieve comparable accuracy. RTK and PPK surveys record data while stationary for at least five seconds, calculating the position using at least three one-second epochs. FS surveys record observations for up to fifteen minutes on each GSP in order to support longer baselines. All GSP measurements were made during periods with a Position Dilution of Precision (PDOP) of  $\leq 3.0$  with at least six satellites in view of the stationary and roving receivers. See Table 6 for NV5 ground survey equipment information.

GSPs were collected in areas where good satellite visibility was achieved on paved roads and other hard surfaces such as gravel or packed dirt roads. GSP measurements were not taken on highly reflective surfaces such as center line stripes or lane markings on roads due to the increased noise seen in the laser returns over these surfaces. GSPs were collected within as many flightlines as possible; however, the distribution of GSPs depended on ground access constraints and monument locations and may not be equitably distributed throughout the study area (Figure 7).

**Table 6: NV5 ground survey equipment identification**

Receiver Model	Antenna	OPUS Antenna ID	Use
Trimble R7 GNSS	Zephyr GNSS Geodetic Model 2 RoHS	TRM57971.00	Static
Trimble R8 Model 2	Integrated Antenna	TRMR8_GNSS	Rover
Trimble R8 Model 3	Integrated Antenna	TRMR8_GNSS3	Rover

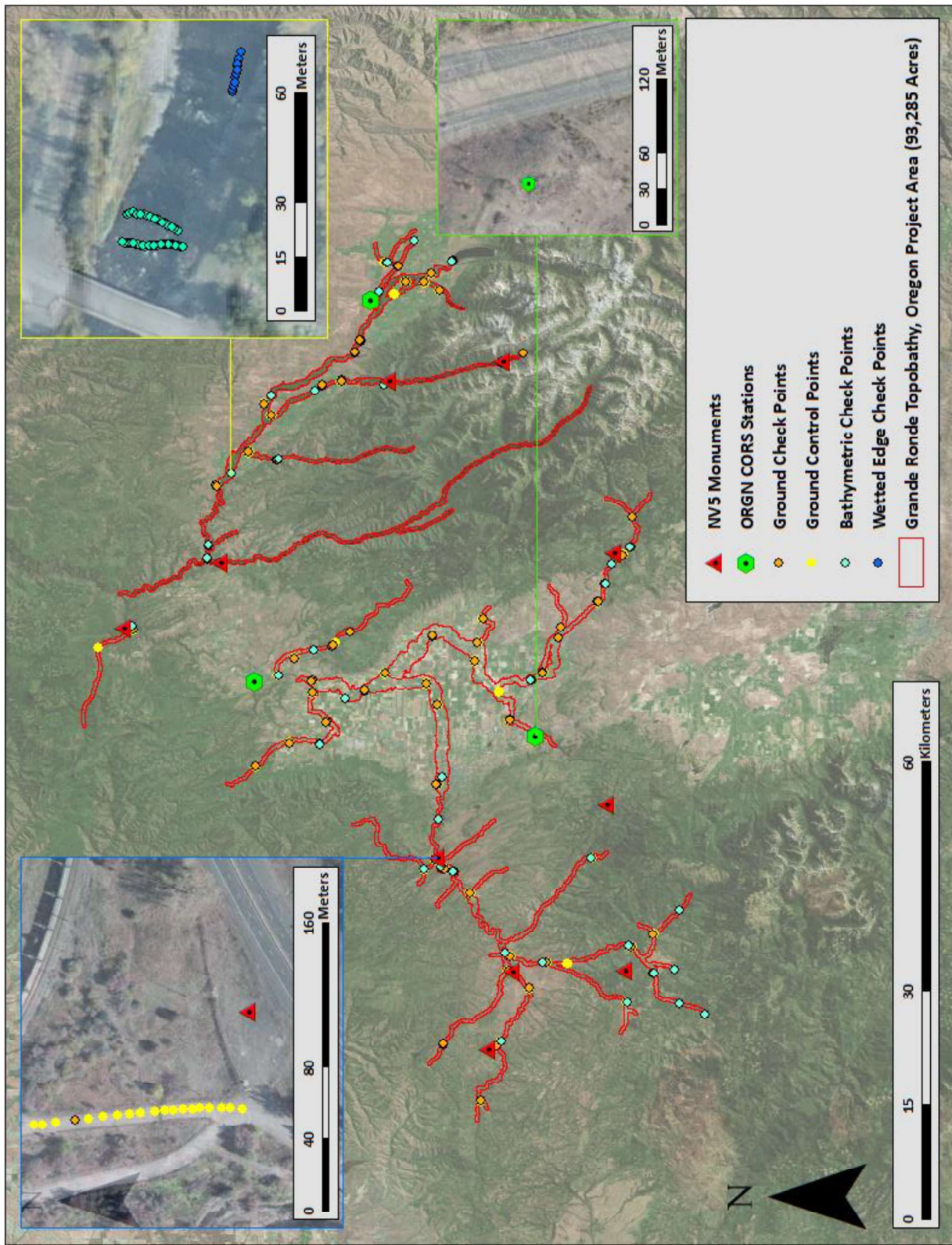
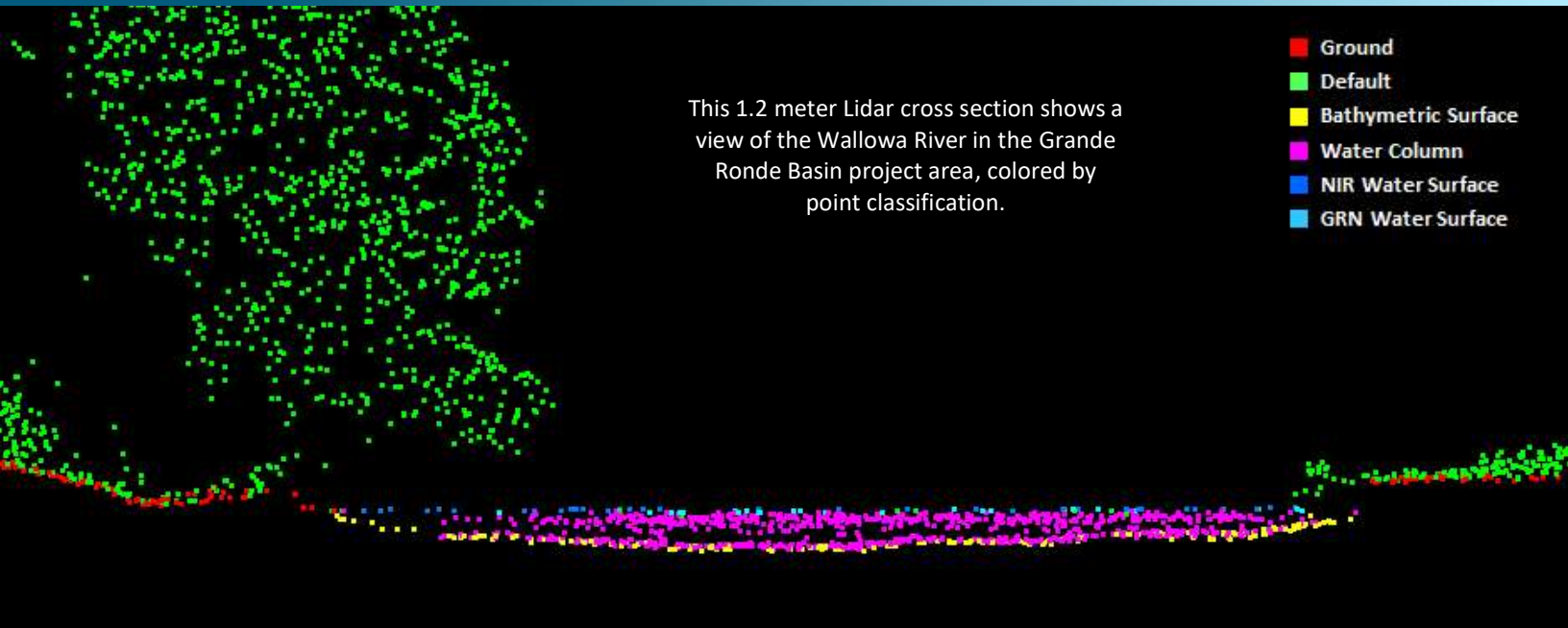


Figure 7: Ground survey location map



## PROCESSING



### Topobathymetric Lidar Data

Upon completion of data acquisition, NV5 processing staff initiated a suite of automated and manual techniques to process the data into the requested deliverables. Processing tasks included GPS control computations, smoothed best estimate trajectory (SBET) calculations, kinematic corrections, calculation of laser point position, sensor and data calibration for optimal relative and absolute accuracy, and Lidar point classification (Table 7).

Riegl's RiProcess software was used to facilitate bathymetric return processing. Once bathymetric points were differentiated, they were spatially corrected for refraction through the water column based on the angle of incidence of the laser. NV5 refracted water column points using NV5's proprietary LAS processing software, Las Monkey. The resulting point cloud data was classified using both manual and automated techniques. Processing methodologies were tailored for the landscape. Brief descriptions of these tasks are shown in Table 8.

**Table 7: ASPRS LAS classification standards applied to the Grande Ronde Basin dataset**

Classification Number	Classification Name	Classification Description
1	Default/Unclassified	Laser returns that are not included in the ground class, composed of vegetation and anthropogenic features
2	Ground	Laser returns that are determined to be ground using automated and manual cleaning algorithms
9	Water	NIR laser returns that are determined to be water using automated and manual cleaning algorithms
40	Bathymetric Bottom	Refracted Riegl sensor returns that fall within the water's edge breakline which characterize the submerged topography.
41	Water Surface	Green laser returns that are determined to be water surface points using automated and manual cleaning algorithms.
45	Water Column	Refracted Riegl sensor returns that are determined to be water using automated and manual cleaning algorithms.

**Table 8: Lidar processing workflow**

Lidar Processing Step	Software Used
Resolve kinematic corrections for aircraft position data using kinematic aircraft GPS and static ground GPS data. Develop a smoothed best estimate of trajectory (SBET) file that blends post-processed aircraft position with sensor head position and attitude recorded throughout the survey.	POSPac MMS v.8.5
Calculate laser point position by associating SBET position to each laser point return time, scan angle, intensity, etc. Create raw laser point cloud data for the entire survey in *.las (ASPRS v. 1.4) format. Convert data to orthometric elevations by applying a geoid correction.	RiProcess v1.8.5 LidarLauncher v1.1 (NV5 proprietary software) Las Monkey 2.6 (NV5 proprietary software)
Import raw laser points into manageable blocks to perform manual relative accuracy calibration and filter erroneous points. Classify ground points for individual flight lines.	TerraScan v.19
Using ground classified points per each flight line, test the relative accuracy. Perform automated line-to-line calibrations for system attitude parameters (pitch, roll, heading), mirror flex (scale) and GPS/IMU drift. Calculate calibrations on ground classified points from paired flight lines and apply results to all points in a flight line. Use every flight line for relative accuracy calibration.	TerraMatch v.19 Las Product Creator 3.0 (NV5 proprietary software)
Apply refraction correction to all subsurface returns.	Las Monkey 2.6 (NV5 proprietary software)
Classify resulting data to ground and other client designated ASPRS classifications (Table 7). Assess statistical absolute accuracy via direct comparisons of ground classified points to ground control survey data.	TerraScan v.19 TerraModeler v.19
Generate bare earth models as triangulated surfaces. Generate highest hit models as a surface expression of all classified points. Generate water surface models as triangulated water surface within bodies of water and ground surface elsewhere. Subtract bare earth models from water surface models to generate depth models. Export all surface models as ESRI GRIDs at a 1 meter pixel resolution.	TerraScan v.19 TerraModeler v.19 Las Product Creator 3.0 (NV5 proprietary software) ArcMap v. 10.3.1
Export intensity images as GeoTIFFs at a 0.5 meter pixel resolution.	ArcMap v. 10.3.1 Las Product Creator 3.0 (NV5 proprietary software)

## Bathymetric Refraction

Green lidar pulses that enter the water column must have their position corrected for refraction of the light beam as it passes through the water and its resulting decreased speed. NV5 has developed proprietary software (Las Monkey) to perform this processing based on Snell's law. The first step is to develop a water surface model (WSM) from the NIR Lidar water surface returns. The water surface model used for refraction is generated using the NIR channel. Points are filtered and edited to obtain the most accurate representation of the water surface and are used to create a water surface model TIN. A TIN model is preferable to a raster based water surface model to obtain the most accurate angle of incidence during refraction.

Once the WSM is generated, the Las Monkey refraction software then intersects the partially submerged green pulses with the WSM to determine the angle of incidence with the water surface and the submerged component of the pulse vector. This provides the information necessary to correct the position of underwater points by adjusting the submerged vector length and orientation. After refraction, the points are compared against bathymetric check points to assess accuracy.

## Water's Edge Breaklines

Water's edge breaklines were created to delineate the land/water interface within the Grande Ronde Basin project area. The breaklines were created automatically from post-refracted and post-edited point cloud data. All areas of water went through the refraction process and therefore bathymetric classing exists outside these breaklines .

## Lidar Derived Products

Because hydrographic laser scanners penetrate the water surface to map submerged topography, this affects how the data should be processed and presented in derived products from the lidar point cloud. The following discusses certain derived products that vary from the traditional (NIR) specification and delivery format.

## Topobathymetric DEMs

Bathymetric bottom returns can be limited by depth, water clarity, and bottom surface reflectivity. Water clarity and turbidity affects the depth penetration capability of the green wavelength laser with returning laser energy diminishing by scattering throughout the water column. Additionally, the bottom surface must be reflective enough to return remaining laser energy back to the sensor at a detectable level.

As a result, creating digital elevation models (DEMs) presents a challenge with respect to interpolation of areas with no returns. Traditional DEMs are "unclipped", meaning areas lacking ground returns are interpolated from neighboring ground returns (or breaklines in the case of hydro-flattening), with the assumption that the interpolation is close to reality. In bathymetric modeling, these assumptions are prone to error because a lack of bathymetric returns can indicate a change in elevation that the laser can no longer map due to increased depths. The resulting void areas may suggest greater depths, rather than similar elevations from neighboring bathymetric bottom returns. Therefore, NV5 created a water polygon with bathymetric coverage to delineate areas with successfully mapped bathymetry. This shapefile was used to control the extent of the delivered clipped topobathymetric model to avoid false triangulation (interpolation from TIN'ing) across areas in the water with no bathymetric returns.



This 1.2 meter lidar cross section shows a view of vegetation, bare ground, stream water surface, and stream bottom in the Grande Ronde Basin AOI, colored by point laser echo.

Only Echo  
First of Many  
Intermediate  
Last of Many

### Lidar Point Density

#### First Return Point Density

The acquisition parameters were designed to acquire an average first-return density of 6 points/m<sup>2</sup>. First return density describes the density of pulses emitted from the laser that return at least one echo to the system. Multiple returns from a single pulse were not considered in first return density analysis. Some types of surfaces (e.g., breaks in terrain, water and steep slopes) may have returned fewer pulses than originally emitted by the laser.

First returns typically reflect off the highest feature on the landscape within the footprint of the pulse. In forested or urban areas the highest feature could be a tree, building or power line, while in areas of unobstructed ground, the first return will be the only echo and represents the bare earth surface.

The average first-return density of the Grande Ronde Basin lidar project was 31.28 points/m<sup>2</sup> (Table 9). The statistical and spatial distributions of all first return densities per 100 m x 100 m cell are portrayed in Figure 8 and Figure 10.

#### Bathymetric and Ground Classified Point Densities

The density of ground classified lidar returns and bathymetric bottom returns were also analyzed for this project. Terrain character, land cover, and ground surface reflectivity all influenced the density of ground surface returns. In vegetated areas, fewer pulses may have penetrated the canopy, resulting in lower ground density. Similarly, the density of bathymetric bottom returns was influenced by turbidity, depth, and bottom surface reflectivity. In turbid areas, fewer pulses may have penetrated the water surface, resulting in lower bathymetric density.

The ground and bathymetric bottom classified density of lidar data for the Grande Ronde Basin project was 10.27 points/m<sup>2</sup> (Table 9). The statistical and spatial distributions ground classified and bathymetric bottom return densities per 100 m x 100 m cell are portrayed in Figure 9 and Figure 10.

Additionally, for the Grande Ronde Basin project, density values of only bathymetric bottom returns were calculated for areas containing at least one bathymetric bottom return. Areas lacking bathymetric returns (voids) were not considered in calculating an average density value. Within the successfully mapped area, a bathymetric bottom return density of 7.00 points/m<sup>2</sup> was achieved.

**Table 9: Average lidar point densities**

Density Type	Point Density
First Returns	31.28 points/m <sup>2</sup>
Ground and Bathymetric Bottom Classified Returns	10.27 points/m <sup>2</sup>
Bathymetric Bottom Classified Returns	7.00 points/m <sup>2</sup>

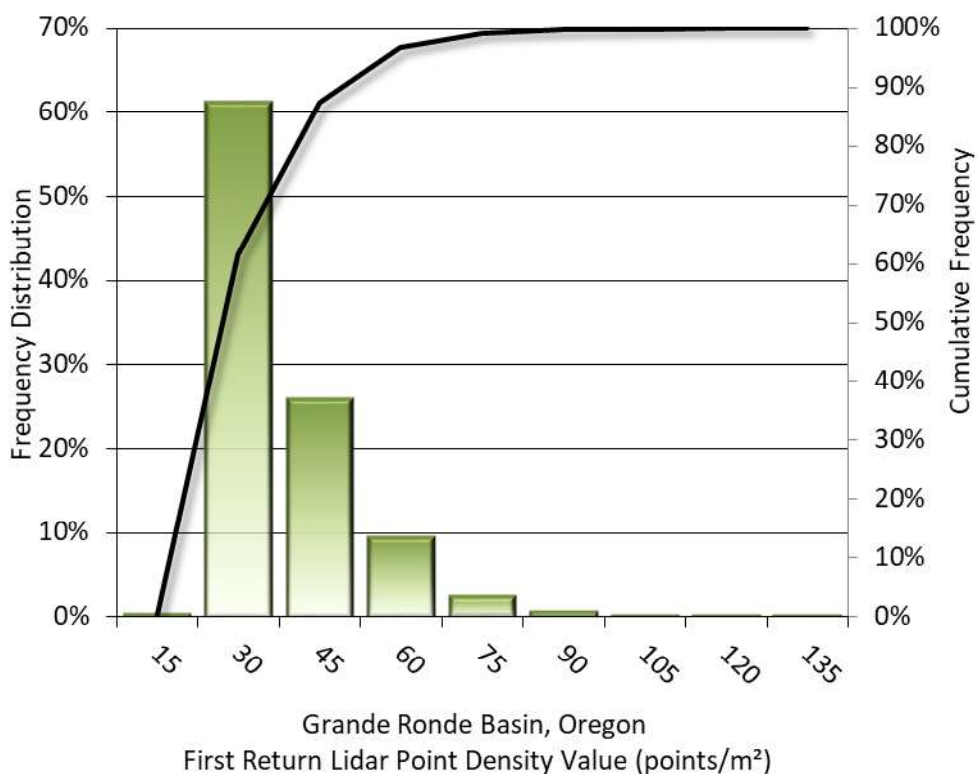


**Figure 8: Frequency distribution of first return densities per 100 x 100 m cell**

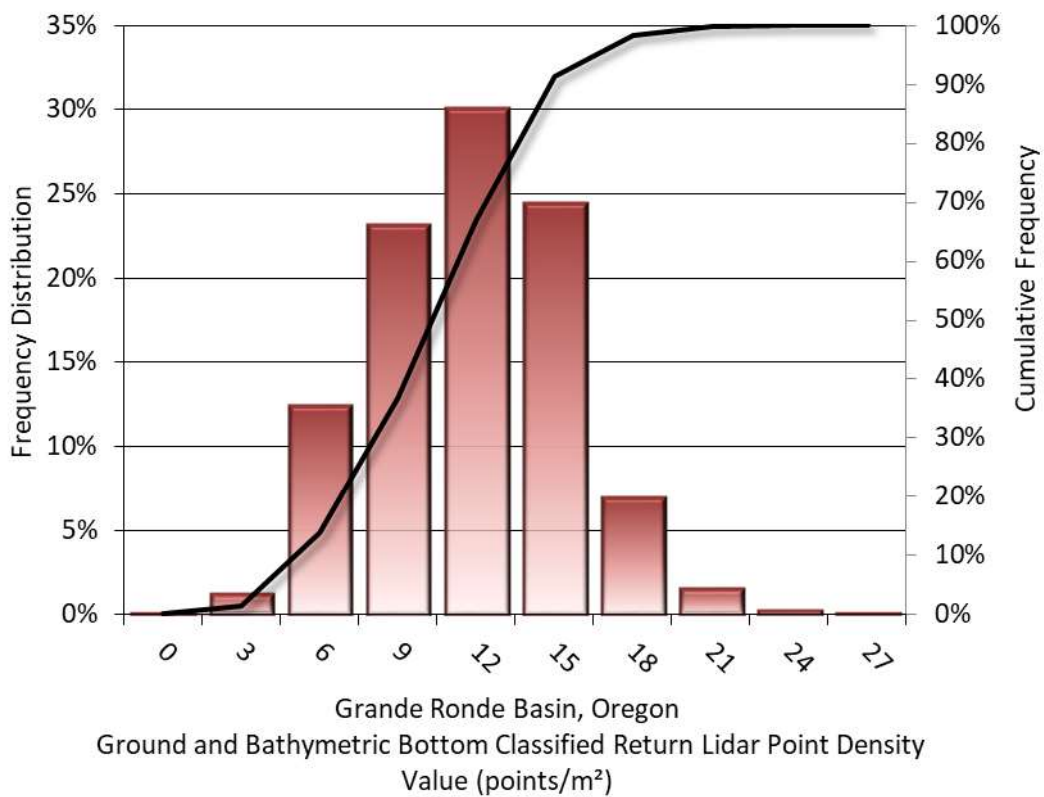


**Figure 9: Frequency distribution of ground and bathymetric bottom classified lidar return densities per 100 x 100 m cell**

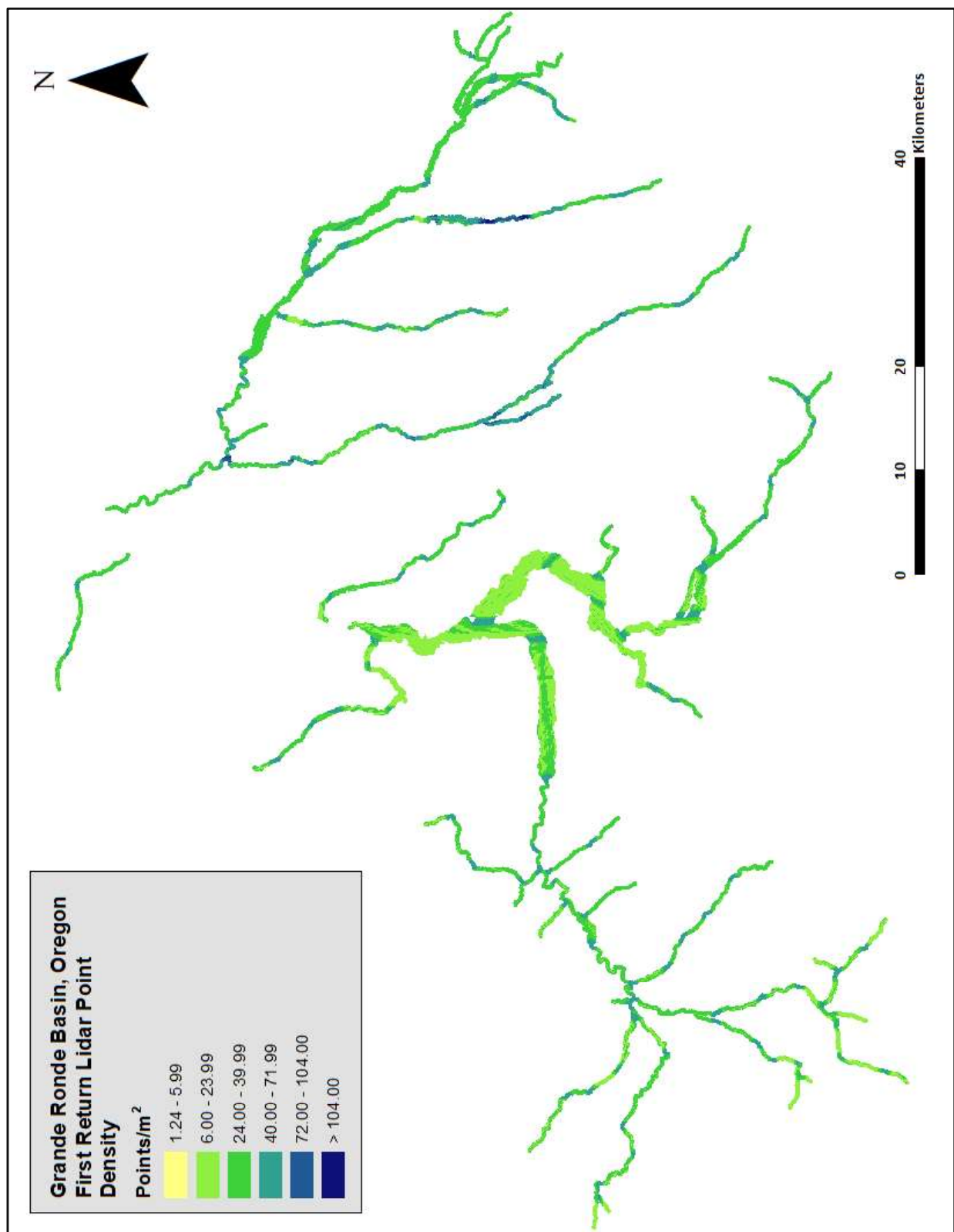


Figure 10: First return lidar density map for the Grande Ronde Basin site (100 m x 100 m cells)

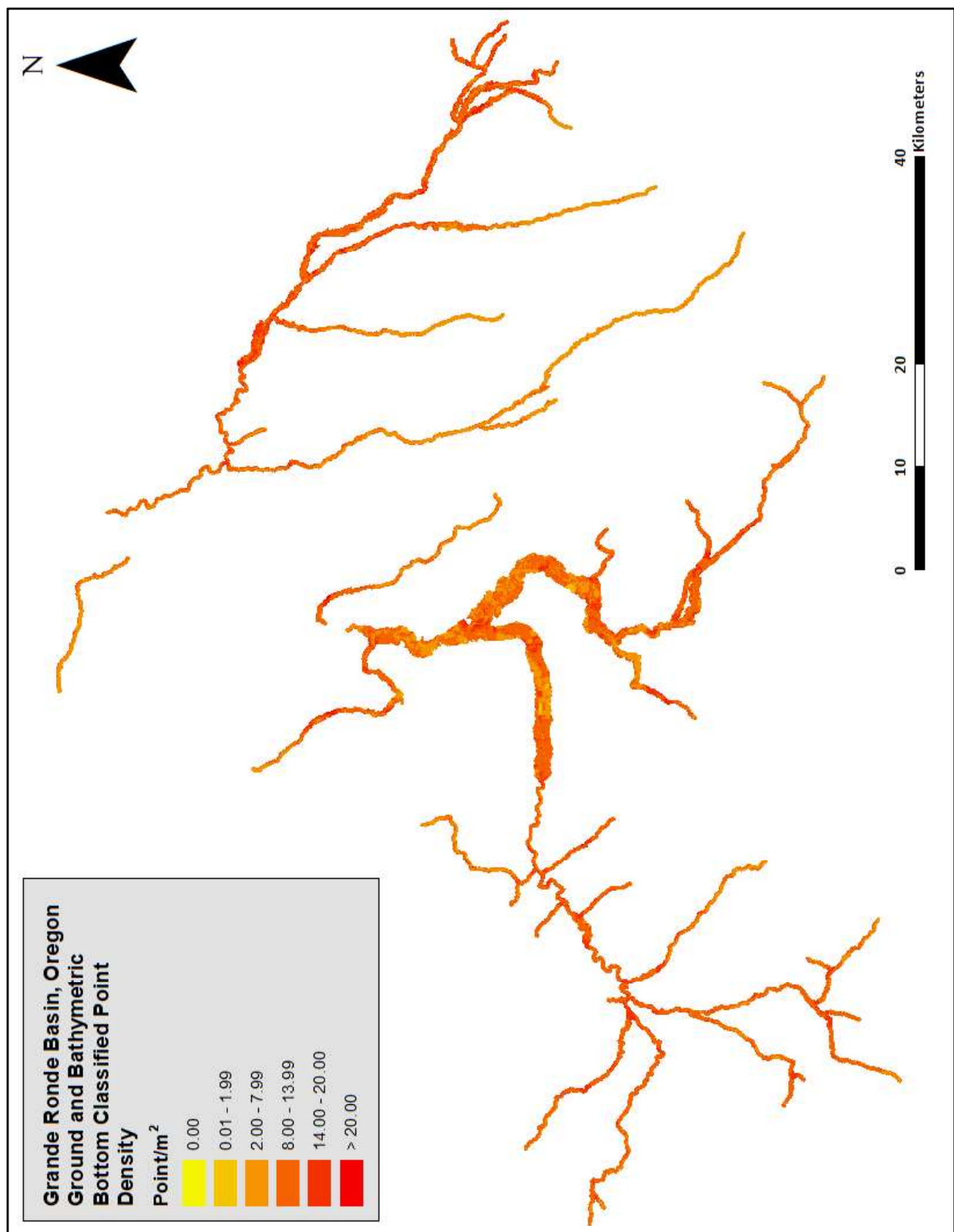


Figure 11: Ground and bathymetric bottom density map for the Grande Ronde Basin site (100 m x 100 m cells)

# Lidar Accuracy Assessments

The accuracy of the lidar data collection can be described in terms of absolute accuracy (the consistency of the data with external data sources) and relative accuracy (the consistency of the dataset with itself). See Appendix A for further information on sources of error and operational measures used to improve relative accuracy.

## Lidar Non-Vegetated Vertical Accuracy

Absolute accuracy was assessed using Non-vegetated Vertical Accuracy (NVA) reporting designed to meet guidelines presented in the FGDC National Standard for Spatial Data Accuracy<sup>3</sup>. NVA compares known ground check point data that were withheld from the calibration and post-processing of the lidar point cloud to the triangulated surface generated by the classified lidar point cloud as well as the derived gridded bare earth DEM. NVA is a measure of the accuracy of lidar point data in open areas where the Lidar system has a high probability of measuring the ground surface and is evaluated at the 95% confidence interval ( $1.96 * RMSE$ ), as shown in Table 10.

The mean and standard deviation ( $\sigma$ ) of divergence of the ground surface model from ground check point coordinates are also considered during accuracy assessment. These statistics assume the error for x, y and z is normally distributed, and therefore the skew and kurtosis of distributions are also considered when evaluating error statistics. For the Grande Ronde Basin survey, 116 ground check points were withheld from the calibration and post-processing of the lidar point cloud, with resulting non-vegetated vertical accuracy of 0.048 meters as compared to the classified LAS, and 0.055 meters against the bare earth DEM, with 95% confidence (Figure 12 and Figure 13).

NV5 also assessed absolute accuracy using 2,435 ground control points. Although these points were used in the calibration and post-processing of the lidar point cloud, they still provide a good indication of the overall accuracy of the lidar dataset, and therefore have been provided in Table 10 and Figure 14.

---

<sup>3</sup> Federal Geographic Data Committee, ASPRS POSITIONAL ACCURACY STANDARDS FOR DIGITAL GEOSPATIAL DATA EDITION 1, Version 1.0, NOVEMBER 2014.  
[https://www.asprs.org/a/society/committees/standards/Positional\\_Accuracy\\_Standards.pdf](https://www.asprs.org/a/society/committees/standards/Positional_Accuracy_Standards.pdf).



**Table 10: Absolute accuracy results**

Absolute Vertical Accuracy			
	NVA, as compared to Classified LAS	NVA, as compared to Bare Earth DEM	Ground Control Points
Sample	116 points	116 points	2,435 points
95% Confidence (1.96*RMSE)	0.048 m	0.055 m	0.050 m
Average	0.001 m	0.003 m	0.000 m
Median	0.002 m	0.004 m	0.000 m
RMSE	0.025 m	0.028 m	0.025 m
Standard Deviation (1σ)	0.025 m	0.028 m	0.025 m

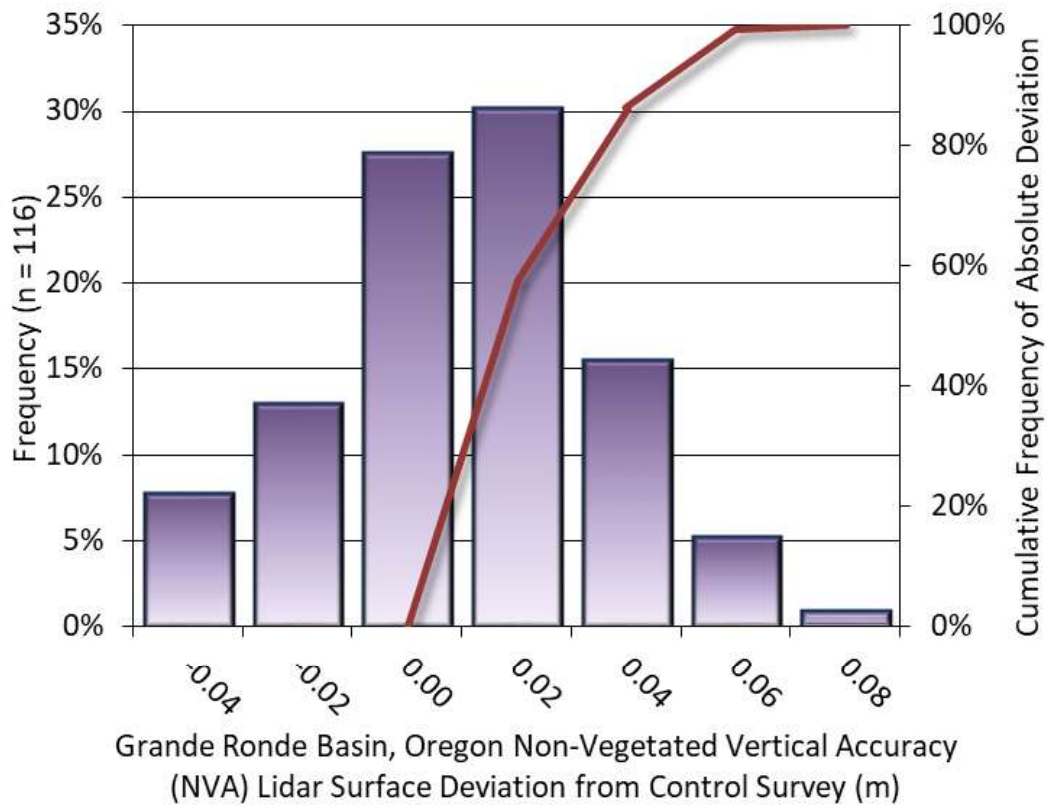


**Figure 12: Frequency histogram for classified LAS deviation from ground check point values**

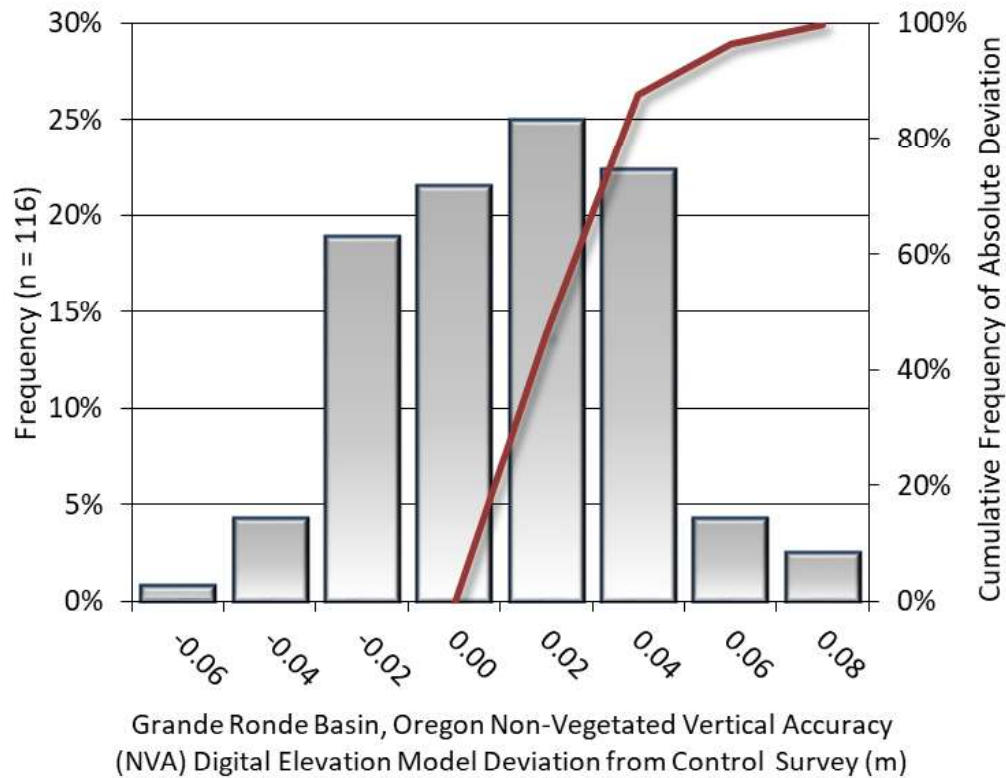


**Figure 13: Frequency histogram for lidar bare earth DEM deviation from ground check point values**

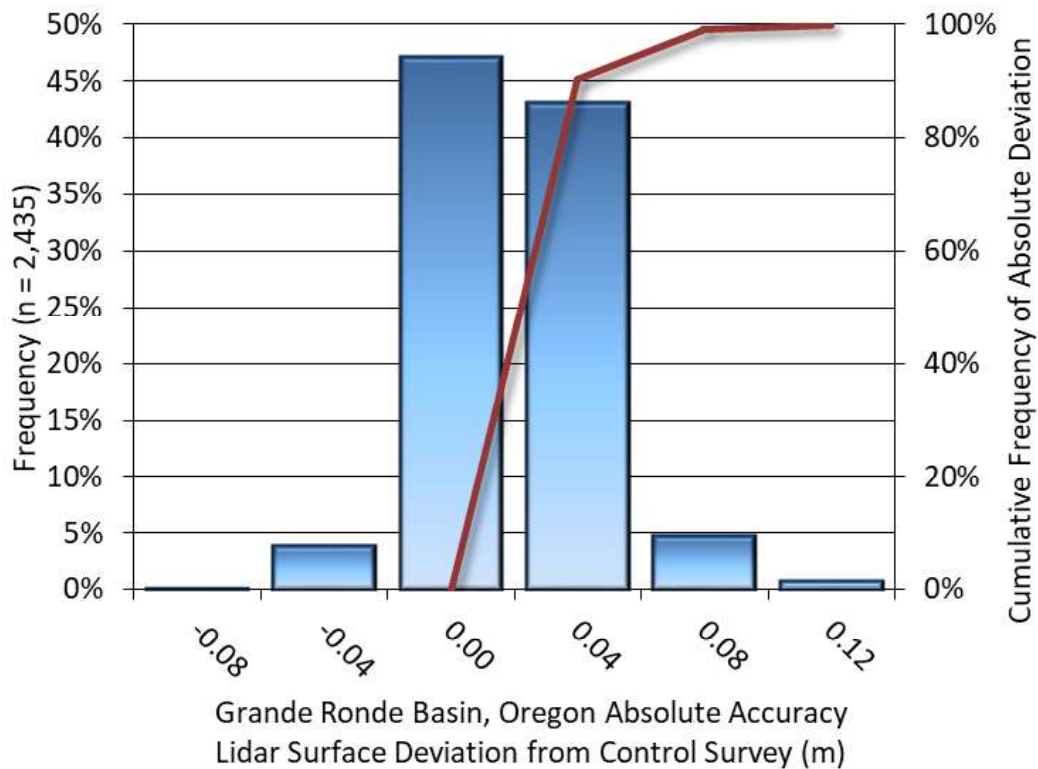


**Figure 14: Frequency histogram for lidar surface deviation ground control point values**



## Lidar Bathymetric Vertical Accuracies

Bathymetric (submerged or along the water's edge) check points were also collected in order to assess the submerged surface vertical accuracy. Assessment of 779 submerged bathymetric check points resulted in a vertical accuracy of 0.098 meters, while assessment of 200 wetted edge check points resulted in a vertical accuracy of 0.083 meters, evaluated at 95% confidence interval (Table 11, Figure 15, and Figure 16).

**Table 11: Bathymetric Vertical Accuracy for the Grande Ronde Basin Project**

Bathymetric Vertical Accuracy (VVA)		
	Submerged Bathymetric Check Points	Wetted Edge Bathymetric Check Points
Sample	779 points	200 points
95% Confidence (1.96*RMSE)	0.098 m	0.083 m
Average Dz	-0.026 m	-0.001 m
Median	-0.025 m	-0.001 m
RMSE	0.050 m	0.042 m
Standard Deviation (1σ)	0.043 m	0.042 m

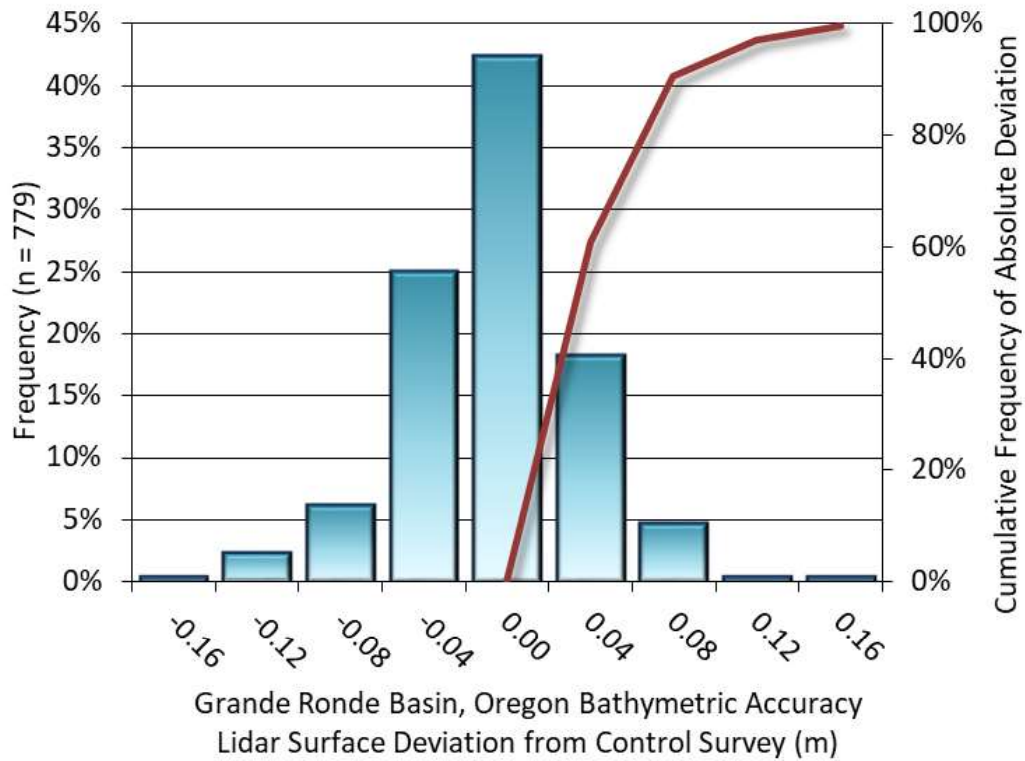


Figure 15: Frequency histogram for lidar surface deviation from submerged check point values

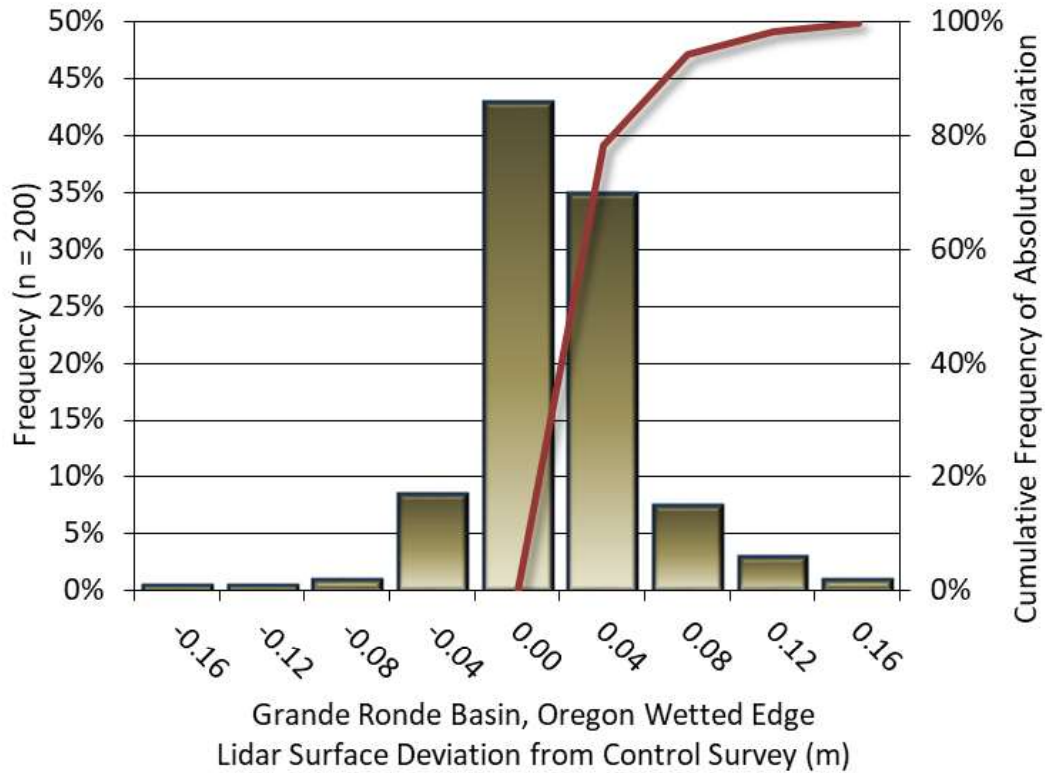


Figure 16: Frequency histogram for lidar surface deviation from wetted edge check point values

## Lidar Relative Vertical Accuracy

Relative vertical accuracy refers to the internal consistency of the data set as a whole: the ability to place an object in the same location given multiple flight lines, GPS conditions, and aircraft attitudes. When the Lidar system is well calibrated, the swath-to-swath vertical divergence is low (<0.10 meters). The relative vertical accuracy was computed by comparing the ground surface model of each individual flight line with its neighbors in overlapping regions. The average (mean) line to line relative vertical accuracy for the Grande Ronde Basin Lidar project was 0.033 meters (Table 12, Figure 17).

**Table 12: Relative accuracy results**

Relative Accuracy	
Sample	2663 flight line surfaces
Average	0.033 m
Median	0.031 m
RMSE	0.037 m
Standard Deviation ( $1\sigma$ )	0.013 m
1.96 $\sigma$	0.026 m

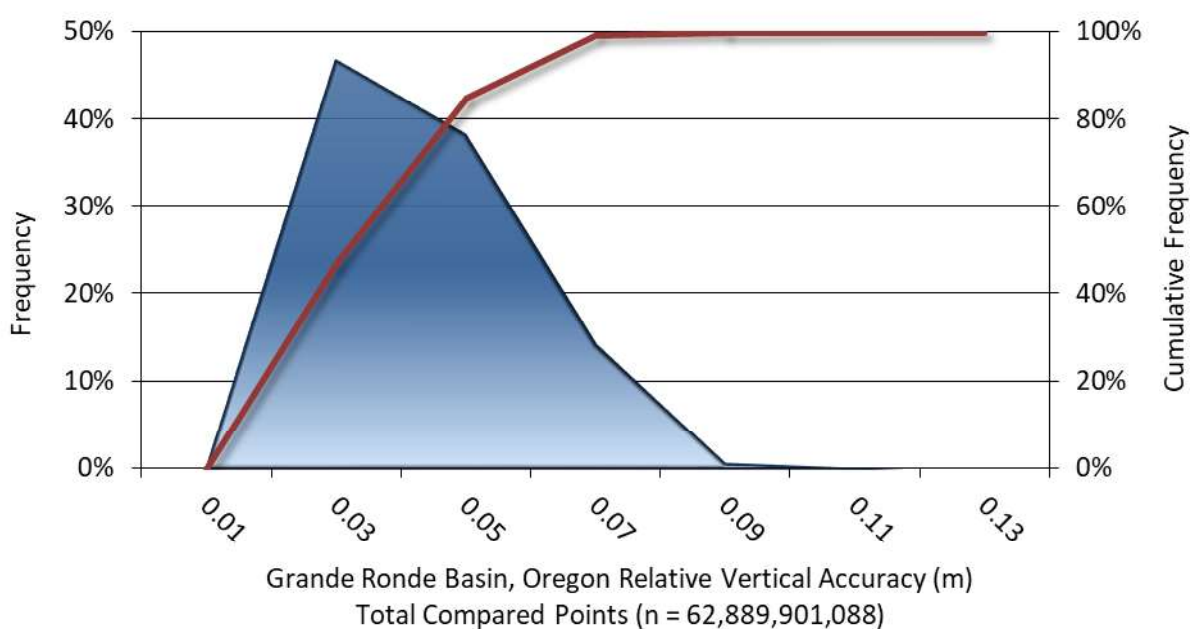


**Figure 17: Frequency plot for relative vertical accuracy between flight lines**

## Lidar Horizontal Accuracy

Lidar horizontal accuracy is a function of Global Navigation Satellite System (GNSS) derived positional error, flying altitude, and INS derived attitude error. The obtained  $RMSE_r$  value is multiplied by a conversion factor of 1.7308 to yield the horizontal component of the National Standards for Spatial Data Accuracy (NSSDA) reporting standard where a theoretical point will fall within the obtained radius 95 percent of the time. Based on a flying altitude of 400 meters, an IMU error of 0.002 decimal degrees, and a GNSS positional error of 0.015 meters, this project was compiled to meet 0.05 meters horizontal accuracy at the 95% confidence level.

**Table 13: Horizontal Accuracy**

Horizontal Accuracy	
$RMSE_r$	0.03 m
$ACC_r$	0.05 m

## CERTIFICATIONS

Quantum Spatial, Inc. provided Lidar services for the Grande Ronde Basin project as described in this report.

I, Shauna Gutierrez, have reviewed the attached report for completeness and hereby state that it is a complete and accurate report of this project.

Shauna Gutierrez  
Shauna Gutierrez (Feb 12, 2021 16:03 PST)

Feb 12, 2021

Shauna Gutierrez  
Project Manager  
Quantum Spatial, Inc.

I, Evon P. Silvia, PLS, being duly registered as a Professional Land Surveyor in and by the state of Oregon, hereby certify that the methodologies, static GNSS occupations used during airborne flights, and ground survey point collection were performed using commonly accepted Standard Practices. Field work conducted for this report was conducted between August 16, 2020 and September 27, 2020.

Accuracy statistics shown in the Accuracy Section of this Report have been reviewed by me and found to meet the "National Standard for Spatial Data Accuracy".

Evon P. Silvia

Feb 12, 2021

Evon P. Silvia, PLS  
NV5 Spatial, Inc.  
Corvallis, OR 97330

REGISTERED  
PROFESSIONAL  
LAND SURVEYOR

Evon P. Silvia

OREGON  
JUNE 10, 2014  
EVON P. SILVIA  
81104LS

EXPIRES: 06/30/2022

## GLOSSARY

**1-sigma ( $\sigma$ ) Absolute Deviation:** Value for which the data are within one standard deviation (approximately 68<sup>th</sup> percentile) of a normally distributed data set.

**1.96 \* RMSE Absolute Deviation:** Value for which the data are within two standard deviations (approximately 95<sup>th</sup> percentile) of a normally distributed data set, based on the FGDC standards for Non-vegetated Vertical Accuracy (FVA) reporting.

**Accuracy:** The statistical comparison between known (surveyed) points and laser points. Typically measured as the standard deviation ( $\sigma$ ) and root mean square error (RMSE).

**Absolute Accuracy:** The vertical accuracy of Lidar data is described as the mean and standard deviation ( $\sigma$ ) of divergence of Lidar point coordinates from ground survey point coordinates. To provide a sense of the model predictive power of the dataset, the root mean square error (RMSE) for vertical accuracy is also provided. These statistics assume the error distributions for x, y and z are normally distributed, and thus we also consider the skew and kurtosis of distributions when evaluating error statistics.

**Relative Accuracy:** Relative accuracy refers to the internal consistency of the data set; i.e., the ability to place a laser point in the same location over multiple flight lines, GPS conditions and aircraft attitudes. Affected by system attitude offsets, scale and GPS/IMU drift, internal consistency is measured as the divergence between points from different flight lines within an overlapping area. Divergence is most apparent when flight lines are opposing. When the Lidar system is well calibrated, the line-to-line divergence is low (<10 cm).

**Root Mean Square Error (RMSE):** A statistic used to approximate the difference between real-world points and the Lidar points. It is calculated by squaring all the values, then taking the average of the squares and taking the square root of the average.

**Data Density:** A common measure of Lidar resolution, measured as points per square meter.

**Digital Elevation Model (DEM):** File or database made from surveyed points, containing elevation points over a contiguous area. Digital terrain models (DTM) and digital surface models (DSM) are types of DEMs. DTMs consist solely of the bare earth surface (ground points), while DSMs include information about all surfaces, including vegetation and man-made structures.

**Intensity Values:** The peak power ratio of the laser return to the emitted laser, calculated as a function of surface reflectivity.

**Nadir:** A single point or locus of points on the surface of the earth directly below a sensor as it progresses along its flight line.

**Overlap:** The area shared between flight lines, typically measured in percent. 100% overlap is essential to ensure complete coverage and reduce laser shadows.

**Pulse Rate (PR):** The rate at which laser pulses are emitted from the sensor; typically measured in thousands of pulses per second (kHz).

**Pulse Returns:** For every laser pulse emitted, the number of wave forms (i.e., echoes) reflected back to the sensor. Portions of the wave form that return first are the highest element in multi-tiered surfaces such as vegetation. Portions of the wave form that return last are the lowest element in multi-tiered surfaces.

**Real-Time Kinematic (RTK) Survey:** A type of surveying conducted with a GPS base station deployed over a known monument with a radio connection to a GPS rover. Both the base station and rover receive differential GPS data and the baseline correction is solved between the two. This type of ground survey is accurate to 1.5 cm or less.

**Post-Processed Kinematic (PPK) Survey:** GPS surveying is conducted with a GPS rover collecting concurrently with a GPS base station set up over a known monument. Differential corrections and precisions for the GNSS baselines are computed and applied after the fact during processing. This type of ground survey is accurate to 1.5 cm or less.

**Scan Angle:** The angle from nadir to the edge of the scan, measured in degrees. Laser point accuracy typically decreases as scan angles increase.

**Native Lidar Density:** The number of pulses emitted by the Lidar system, commonly expressed as pulses per square meter.

## APPENDIX A - ACCURACY CONTROLS

### Relative Accuracy Calibration Methodology:

**Manual System Calibration:** Calibration procedures for each mission require solving geometric relationships that relate measured swath-to-swath deviations to misalignments of system attitude parameters. Corrected scale, pitch, roll and heading offsets were calculated and applied to resolve misalignments. The raw divergence between lines was computed after the manual calibration was completed and reported for each survey area.

**Automated Attitude Calibration:** All data was tested and calibrated using TerraMatch automated sampling routines. Ground points were classified for each individual flight line and used for line-to-line testing. System misalignment offsets (pitch, roll and heading) and scale were solved for each individual mission and applied to respective mission datasets. The data from each mission were then blended when imported together to form the entire area of interest.

**Automated Z Calibration:** Ground points per line were used to calculate the vertical divergence between lines caused by vertical GPS drift. Automated Z calibration was the final step employed for relative accuracy calibration.

### Lidar accuracy error sources and solutions:

Type of Error	Source	Post Processing Solution
<b>GPS (Static/Kinematic)</b>	Long Base Lines	None
	Poor Satellite Constellation	None
	Poor Antenna Visibility	Reduce Visibility Mask
<b>Relative Accuracy</b>	Poor System Calibration	Recalibrate IMU and sensor offsets/settings
	Inaccurate System	None
<b>Laser Noise</b>	Poor Laser Timing	None
	Poor Laser Reception	None
	Poor Laser Power	None
	Irregular Laser Shape	None

### Operational measures taken to improve relative accuracy:

**Low Flight Altitude:** Terrain following was employed to maintain a constant above ground level (AGL). Laser horizontal errors are a function of flight altitude above ground (about 1/3000<sup>th</sup> AGL flight altitude).

**Focus Laser Power at narrow beam footprint:** A laser return must be received by the system above a power threshold to accurately record a measurement. The strength of the laser return (i.e., intensity) is a function of laser emission power, laser footprint, flight altitude and the reflectivity of the target. While surface reflectivity cannot be controlled, laser power can be increased and low flight altitudes can be maintained.

**Reduced Scan Angle:** Edge-of-scan data can become inaccurate. The scan angle was reduced to a maximum of  $\pm 20^\circ$  from nadir, creating a narrow swath width and greatly reducing laser shadows from trees and buildings.

**Quality GPS:** Flights took place during optimal GPS conditions (e.g., 6 or more satellites and PDOP [Position Dilution of Precision] less than 3.0). Before each flight, the PDOP was determined for the survey day. During all flight times, a dual frequency DGPS base station recording at 1 second epochs was utilized and a maximum baseline length between the aircraft and the control points was less than 13 nm at all times.

**Ground Survey:** Ground survey point accuracy (<1.5 cm RMSE) occurs during optimal PDOP ranges and targets a minimal baseline distance of 4 miles between GPS rover and base. Robust statistics are, in part, a function of sample size (n) and distribution. Ground survey points are distributed to the extent possible throughout multiple flight lines and across the survey area.

**50% Side-Lap (100% Overlap):** Overlapping areas are optimized for relative accuracy testing. Laser shadowing is minimized to help increase target acquisition from multiple scan angles. Ideally, with a 50% side-lap, the nadir portion of one flight line coincides with the swath edge portion of overlapping flight lines. A minimum of 50% side-lap with terrain-followed acquisition prevents data gaps.

**Opposing Flight Lines:** All overlapping flight lines have opposing directions. Pitch, roll and heading errors are amplified by a factor of two relative to the adjacent flight line(s), making misalignments easier to detect and resolve.

## **Appendix C – Submitted Fisheries Research paper on snorkel survey calibration methods**



---

# Accounting for uncertainty when estimating drivers of detection probability: an integrated approach illustrated with snorkel surveys for riverine fishes

---

## **BENJAMIN A. STATON\***

Fisheries Science Department, Columbia River Inter-Tribal Fish Commission, NE Multnomah St., Ste. 1200, Portland, OR 97232

bstaton@critfc.org

## **CASEY JUSTICE**

Fisheries Science Department, Columbia River Inter-Tribal Fish Commission, NE Multnomah St., Ste. 1200, Portland, OR 97232

## **SETH WHITE**

Fisheries Science Department, Columbia River Inter-Tribal Fish Commission, NE Multnomah St., Ste. 1200, Portland, OR 97232

## **EDWIN R. SEDELL**

East Region Fish Research, Oregon Department of Fish and Wildlife, One University Blvd., La Grande, OR 97580

## **LAUREN A. BURNS**

Fisheries Science Department, Columbia River Inter-Tribal Fish Commission, NE Multnomah St., Ste. 1200, Portland, OR 97232

## **MATTHEW J. KAYLOR**

Department of Fisheries and Wildlife, Oregon State University, 2820 SW Campus Way, Corvallis, OR 97331

**Keywords:** abundance estimation, Bayesian analysis, detection probability, hierarchical models, snorkel surveys, variable selection

**Running Headline:** Abundance Uncertainty and Detection Probability

**Target Journal:** *Fisheries Research*

---

\*Corresponding Author

## Abstract

Partial detectability is a common issue affecting the accuracy of surveys that quantify animal abundance and distribution. To estimate detection probability, counts are often calibrated to independent measures of abundance (e.g., via mark-recapture) but sampling variability in both data types is not typically accounted for. This practice may cause detection probability to be estimated inaccurately and lead to overly confident predictions for out-of-sample applications. Our objective was to develop, apply, and simulation-test an integrated approach for estimating detection probability that better-accommodates uncertainty. The method assumes mark-recapture and count surveys sample the same local abundance with error, allowing the construction of a joint likelihood function for both data sets. The model estimates coefficients that link detection probability to local covariates through a logit-linear model, allowing prediction of detection probability for locations without mark-recapture data. We illustrate the application of the model with an empirical data set of over 100 paired snorkel and mark-recapture surveys for riverine salmonids in northeastern Oregon. Selected covariates that best explained variability in detection probability for the empirical analysis included species, visibility, and channel unit type and depth, though much variability was attributed to site-level random effects. Estimated detection probability ranged from 0.02 to 0.92 among surveys and was higher for Chinook Salmon (*Oncorhynchus tshawytscha*) juveniles (mean: 0.38) than for steelhead/Rainbow Trout (*O. mykiss*; mean: 0.24). Simulation analyses revealed that accounting for rather than ignoring uncertainty in abundance data performed better in terms of selection of covariates, interval coverage, accuracy of estimated random variability terms, and reduced sensitivity to violated mark-recapture assumptions surrounding behavioral effects. This model represents an improvement over simpler calibration methods, particularly for snorkel surveys, by applying more a rigorous statistical treatment of sources of variability while explicitly describing the mechanistic link between local conditions and detection probability. The analytical methods we illustrate are general and could be broadly applied to quantify detection probability in other biological surveys with paired abundance and count data.

# 1 Introduction

Spatial and temporal patterns in population abundance are key information sources for understanding the ecology of fish populations and forming the knowledge base for management and conservation. For example, quantifying abundance is critical for assessing the efficacy of preserves (Mosquera et al. 2000), measuring population response to restoration actions (Roni et al. 2008), and setting harvest quotas (Walters and Pearse 1996). Complete population censuses are often infeasible and therefore abundance is typically sampled using counts, which may be visual or capture-based in nature. Such counts are imperfect measures of population abundance primarily because they result from partial detectability, i.e., members of the population are counted with probability less than one. Partial detectability (also known as catchability for capture-based methods) introduces a directional bias that underestimates true abundance (Kéry and Schmidt 2008; Kellner and Swihart 2014). Further, the use of count data as an index of abundance (or other indices, such as catch-per-effort) typically requires the assumption that detection probability is constant across individuals, sampling locations, and time periods. Detection probability may not be constant and the same factors that influence its spatiotemporal variability may also affect local abundance (e.g., density of large wood for riverine fishes). For these reasons, estimation of detection probability is a cornerstone of population analyses based on count surveys.

Methods commonly used to quantify detection probability include those that assume some attenuation with increasing distance from the observer (distance sampling, Buckland et al. 2001), use spatially replicated counts (N-mixture models, Royle 2004), or use the frequency with which marked individuals are subsequently recaptured (mark-recapture methods, Seber 1986). Another method, sometimes referred to as “double sampling” (Williams et al. 2002, Section 12.6 therein) or “dual-gear validation” (e.g., Thurow et al. 2006), uses intensively monitored sites to estimate total abundance which, when paired with independent counts, provide an estimate of detection probability that may be applied to sites with count data but not abundance estimates. This practice of pairing independent abundance and count data has been widely used for quantifying detection probability or otherwise obtaining count correction factors for aquatic and terrestrial species. Examples include point counts paired with census counts in nesting bird survey plots (Bart and Earnst 2002), spotlight counts of crocodiles paired with mark-recapture (Hutton and Woolhouse 1989), spotlight counts of deer paired with abundance from thermal imagery (Collier et al. 2007), aerial counts of salmon paired with mark-recapture (Jones et al. 1998), and snorkel counts of fish paired with abundance estimates from mark-recapture (Jonasson et al. 2016), electrofishing (Thurow et al. 2006), or removal methods (Hankin and Reeves 1988; Hillman et al. 1992).

Given that detection probability estimated using the double sampling design is generally conducted on a small subset of sites and then applied to other locations, it is critical that relationships with covariates and their out-of-sample uncertainty be accurately characterized. To our knowledge, none of the examples of the double sampling design above accounted for sampling uncertainty in the abundance information when estimating detection probability, though granted, the amount of uncertainty varies intrinsically with the method used to obtain abundance. For example, Thurow et al. (2006) used beta-binomial regression to quantify covariate effects on detection probability wherein snorkel counts were considered successes and abundance estimates from catchability-adjusted electrofishing catch rates were treated as binomial trials – implicitly assuming perfect knowledge of abundance.

This practice of ignoring sampling variability in the data that inform abundance estimates likely inserts additional noise into detection probability relationships which could mask the true effects of covariates and hinder our ability to identify optimal predictive models. Further, unaccounted variability of independent abundance information is likely to inappropriately weight observations during model fitting and result in overstated confidence in estimated/predicted detection probability. These issues are problematic given the central role estimated detection probability and relationships with covariates serve in enabling comparisons of count data across space and time. Thus, it may be preferable to apply methods that estimate detection probability while explicitly acknowledging abundance is imperfectly known.

Snorkel surveys are commonly used to assess fish abundance and distribution as part of routine monitoring programs (e.g., Constable and Suring 2015; Fowler 2017) and directed ecological studies (Som et al. 2018; Flitcroft et al. 2013). They are frequently used in riverine habitats for salmonid fishes, both for juveniles (Thompson and Lee 2000; Flitcroft et al. 2013; Som et al. 2018) and adults (Pinter et al. 2018; Korman et al. 2002; Thurow et al. 2006) but have also been used for other fish taxa and in non-riverine environments (e.g., Lawson et al. 2011; Weaver et al. 2014; Ulibarri et al. 2017). Counts obtained from these surveys can inform fine-scale patterns of fish-habitat associations unavailable from larger-scale monitoring methods alone. Further, because fish are never handled during snorkel surveys, these methods are more rapid and less intrusive than other survey methods (e.g., multi-pass electrofishing), making them well-suited for monitoring the abundance and distribution of threatened species and at large spatial scales.

Given the difficult nature of counting small and mobile organisms in flowing water, snorkel surveys are subject to partial detectability and the double sampling approach has been used widely to estimate its magnitude (Hankin and Reeves 1988; Hillman et al. 1992; Thurow et al. 2006; Jonasson et al. 2016). N-mixture models have recently been used to address this issue (Som et al. 2018; Doll et al. 2020), however, this approach has not yet been widely applied for snorkel surveys and may not be ideal for all cases given the need for within-site replication (which could otherwise be distributed spatially) and strong assumptions (i.e., that abundance and detection probability are constant among repeated visits to the same site, Barker et al. 2017). Thus, it would be desirable to have a method for quantifying detection probability that (*a*) is suitable for commonly collected data sets (i.e., following a double sampling design), (*b*) accommodates uncertainty in independent abundance estimates, (*c*) allows direct modeling and selection of local covariates on detection probability, and (*d*) propagates uncertainty in estimated relationships to out-of-sample applications.

We present a widely applicable analytical method for quantifying detection probability from double sampling designs in snorkel and other biological surveys intended to meet these criteria. Our method jointly estimates abundance and covariate effects on detection probability within a single model rather than analyzing them sequentially. After describing the statistical structure and its assumptions, we illustrate an application of the method using empirical snorkel survey data collected in northeastern Oregon and use a simulation study to test its validity in the face of violated assumptions and varying data quality and quantity.

## 2 Methods

## 2.1 General data structure

The method we describe for quantifying detection probability requires paired abundance and count data from a variety of locations and associated variables that may influence the ease or difficulty of counting animals in each location. Our specific illustration assumes that abundance data take the form of a two-sample mark-recapture design but other designs could be accommodated by our approach. If possible, sampling locations should be selected at the smallest spatial scale of interest to provide the highest resolution for investigating the effects of local conditions on detection probability. For example, riverine sampling designs are often created hierarchically: channel units (i.e., individual pools, riffles, or runs) are nested within a site, sites are nested within a tributary, and tributaries are nested within a basin – in this case, channel units should be selected as the observational unit for conducting double sampling.

## 2.2 Modeling framework

### 2.2.1 Model of detection probability

Our goal was to develop a model to describe how detection probability (denoted by  $\psi_i$ ) for each observation ( $i$ ; a unique pair of abundance and count data) varies as a function of covariates. We define  $\psi_i$  as the probability that each member of the population (abundance denoted  $N_i$ ) is counted during the count survey. Thus, given known  $N_i$  and count ( $y_i$ ), a standard way to estimate the effects of covariates  $x_{1,i}, \dots, x_{n,i}$  on  $\psi_i$  is via logistic regression methodology:

$$\begin{aligned} \text{logit}(\psi_i) &= \alpha + \beta_1 x_{1,i} + \dots + \beta_n x_{n,i} + \epsilon_{j(i)}, \\ \epsilon_j &\sim N(0, \sigma^2) \end{aligned} \tag{1}$$

where  $\alpha$  is the intercept,  $\beta_1, \dots, \beta_n$  are coefficients quantifying covariate effects on the log odds of detection, and  $\epsilon_j$  is a random effect for level  $j$  of a blocking factor, and  $j(i)$  denotes the specific level that observation  $i$  belongs to. Logistic regression uses the assumption of binomial sampling:

$$y_i \sim B(\psi_i, N_i), \tag{2}$$

to build the likelihood function. However, this requires an abundance value  $N_i$ , and rarely is this quantity known with certainty. We therefore constructed an integrated model that uses this same logistic regression framework to model covariate effects on  $\psi_i$ , but simultaneously estimates  $N_i$  from mark-recapture data and thus acknowledges its uncertainty jointly with the uncertainty in count survey sampling. We chose to employ the Bayesian inferential framework because it is useful for (a) hierarchical and integrated models, (b) propagating uncertainty and parameter correlations to derived quantities, and (c) estimation of posterior model probabilities for model-averaging purposes.

### 2.2.2 Model for abundance

We designed the model to accommodate data collected by a two-sample mark-recapture design, in which the data for survey  $i$  are counts of the three observable capture histories; these include the number of individuals captured and marked in the first period and captured again in the second period ( $z_{i,11}$ ), the number of individuals captured and marked in the first period that were not captured in the second period ( $z_{i,10}$ ), and the number of individuals captured for the first time in the second period ( $z_{i,01}$ ). For one observation, we organize these counts into the vector  $\mathbf{z}_i$ :

$$\mathbf{z}_i = [ z_{i,11} \quad z_{i,10} \quad z_{i,01} ]. \tag{3}$$

We used the conditional likelihood expression (Huggins 1989, 1991) that removes the unobservable capture history ( $z_{i,00}$ ) from the calculation such that this three-element vector can be fitted assuming multinomial sampling conditional only on individuals captured in the study (more details in Williams et al. 2002, Section 14.1 therein). Consider the case where all individuals in the first period have capture probability  $p_{i,1}$  and all individuals in the second period have capture probability  $p_{i,2}$ . The probability that a member of  $N_i$  was captured at all (denoted  $p_i^*$ ) is then:

$$p_i^* = 1 - (1 - p_{i,1})(1 - p_{i,2}), \quad (4)$$

which can be used to create the vector ( $\pi_i$ ) of expected capture history probabilities:

$$\begin{aligned} \pi_{i,11} &= \frac{p_{i,1}p_{i,2}}{p_i^*} \\ \pi_{i,10} &= \frac{p_{i,1}(1 - p_{i,2})}{p_i^*} \\ \pi_{i,01} &= \frac{(1 - p_{i,1})p_{i,2}}{p_i^*}. \end{aligned} \quad (5)$$

This probability vector forms the expected proportions of observed capture histories, and is used in a multinomial likelihood by assuming:

$$\mathbf{z}_i \sim \mathbf{M}(\pi_i, r_i) \quad (6)$$

where  $r_i = z_{i,11} + z_{i,10} + z_{i,01}$ . Then, abundance can be derived as:

$$N_i = \frac{r_i}{p_i^*} \quad (7)$$

We embedded these calculations and their likelihood in the same model that includes the count survey data and logistic regression such that all unknowns could be simultaneously estimated.

Otis et al. (1978) introduced a family of mark-recapture models for closed population size estimation that vary in their assumptions about capture probabilities, and three of these models are relevant to the two-sample design we implemented. These models are commonly referred to as  $M_0$ ,  $M_t$ , and  $M_b$  (Table 1). Model  $M_0$  assumes that  $p_{i,1} = p_{i,2}$  whereas model  $M_t$  assumes that  $p_{i,1} \neq p_{i,2}$  and is equivalent to the well-known two-sample Lincoln-Peterson estimator. Model  $M_b$  assumes a behavioral response to capture and marking, such that capture probability in the second period depends on whether the individual was previously captured. Model  $M_b$  redefines  $p_{i,2}$  to be the probability a fish is captured for the first time in the second period (and assumes  $p_{i,1} = p_{i,2}$ ) and defines the recapture probability as  $c_{i,2}$ . For model  $M_b$ , the calculation to obtain  $\pi_i$  must be modified to accommodate these new definitions:

$$\begin{aligned} \pi_{i,11} &= \frac{p_{i,1}c_{i,2}}{p_i^*} \\ \pi_{i,10} &= \frac{p_{i,1}(1 - c_{i,2})}{p_i^*} \\ \pi_{i,01} &= \frac{(1 - p_{i,1})p_{i,2}}{p_i^*}, \end{aligned} \quad (8)$$

where the definition of  $p_i^*$  remains the same as in eq. 4. If behavioral effects are present, they can create large errors in abundance estimates when unaccounted for (e.g., Peterson et al. 2015). We thus designed our modeling approach to accommodate behavioral responses if evidence suggests they exist. We first assessed which model assumption ( $M_0$ ,  $M_t$ , or  $M_b$ ) was most supported by all observations with mark-recapture data only – we used the Watanabe-Akaike information criterion (WAIC) for this purpose (Watanabe 2013; Hooten and Hobbs 2015). Although discerning between  $M_t$  or  $M_b$  is problematic for one  $\mathbf{z}_i$  vector alone, by imposing the same assumption on all available  $\mathbf{z}_i$  vectors simultaneously and considering their likelihoods jointly, we were able to select the mark-recapture model that is most supported by the accumulation of multiple repeated mark-recapture studies (see the results of simulation block H presented in the Supplementary Material for a verification of this). We then fitted the integrated model that includes both count and mark-recapture data using the mark-recapture assumptions deemed most appropriate by WAIC.

### 2.2.3 Variable selection and model-averaging

Identifying which covariates are useful for explaining variability in detection probability ( $\psi_i$ ) in eq. 1 is a key step in building a model that allows robust predictions of detection probability in locations with count data only. Our model accounts for model uncertainty in this regard with additional parameters that enable estimation of the probability that each covariate should be included in an optimal predictive model. These “indicator variables” (Hooten and Hobbs 2015), denoted by  $\omega_1, \dots, \omega_n$ , were Bernoulli random variables that, when multiplied by each of the  $\beta$  coefficients, had the purpose of toggling on ( $\omega = 1$ ) or off ( $\omega = 0$ ) the effect of each covariate on the log odds of detection. This enabled evaluating multiple models during the fitting process (Kuo and Mallick 1998; Hooten and Hobbs 2015) while providing the posterior model probabilities needed for Bayesian multi-model inference. The posterior mean of each  $\omega$  term represents the probability that the corresponding covariate is a member of the optimal predictive model, with values greater than 0.5 indicating that the covariate should be included (Barbieri and Berger 2004). Model-averaged posteriors are calculated from  $\omega\beta$  rather than  $\beta$  and posterior model probabilities are calculated from the relative frequency with which the various  $\omega$  terms are jointly equal to 1 or 0.

### 2.2.4 Model assumptions

Our model makes simplifying assumptions to enable estimation, and for our description we divide these into three classes: those that apply to (a) random processes for mark-recapture sampling, (b) random processes for count sampling, and (c) the joint analysis of mark-recapture and snorkel data. All mark-recapture models we used assume (i) the population is closed between the first and second periods, (ii) capture/non-capture outcomes are the result of independent events across individuals, (iii) all individuals within a period have homogeneous (re)capture probabilities, (iv) there is no mark loss, and (v) marked and unmarked individuals are correctly identified as such. Mark-recapture models  $M_0$ ,  $M_t$ , and  $M_b$  all make different assumptions about how capture probability varies between periods and whether there is a behavioral effect of previous capture (described above, also Table 1). Assumptions of the binomial model as the count-generating process in equation 2 include (i) all members of  $N_i$  have homogeneous  $\psi_i$ , (ii) detection/non-detection outcomes are the result of independent events across individuals, and (iii) individuals are counted a maximum of one time and are correctly identified (e.g., to species). Integrating the two data types into a joint analysis introduces two additional assumptions. First, this requires the assumption that sampling variability is independent between mark-recapture and count surveys, e.g., negative errors

in abundance estimation are not associated with higher- or lower-than-expected outcomes from the count survey. Second, we must assume that the population abundance  $N_i$  is unchanged in the time elapsed between mark-recapture and count surveys. This assumption is less strict than complete closure as it does not assume no movement, but rather that any movement of individuals in or out of the study area between surveys results in net zero change on average across observations.

### 2.2.5 Computation

We fitted the model using Bayesian methods implemented with Markov chain Monte Carlo (MCMC) sampling using program JAGS (Plummer 2003) invoked through program R (R Core Team 2020) with the ‘jagsUI’ package (Kellner 2018). The R packages ‘postpack’ (Staton 2020b) and ‘posterior’ (Bürkner et al. 2020; Vehtari et al. 2021) were used for posterior summarization and MCMC sampling diagnostics, respectively. We selected prior distributions to be minimally informative while simultaneously discouraging implausible values from being sampled by the MCMC algorithm. We discuss MCMC sampling, diagnostics, and priors in greater detail in the Supplementary Material and provide JAGS model pseudocode therein as well. All code and data necessary to replicate the specific analyses described below are provided in Staton (2020a).

## 2.3 Empirical application

### 2.3.1 Study system

Data were collected in the Grande Ronde River basin which originates in the Blue Mountains of northeastern Oregon and flows northward to its confluence with the Snake River (Fig. 1). Local salmon populations have declined precipitously from their historical abundance (Nehlsen et al. 1991), prompting the listing of Snake River spring/summer-run Chinook Salmon (*Oncorhynchus tshawytscha*) and Snake River steelhead (*O. mykiss*) as threatened under the Endangered Species Act. Substantial resources have been invested in restoring freshwater habitat conditions in this region, and snorkel surveys have been used widely as a method for status and trends monitoring and evaluation of restoration effectiveness (e.g., White et al. 2019).

### 2.3.2 Field data collection

The study design and details of data collection are fully described in Jonasson et al. (2016) and we therefore provide only a brief overview here. Sampling occurred in the summers of 2012 and 2015 and spanned a range of habitat types and stream sizes in the upper Grande Ronde River, Catherine Creek, and their various tributaries (Fig. 1). Habitats were classified into channel units (i.e., pools, riffles, and runs) based on differences in bedform shape, gradient, and substrate size (CHaMP 2016). These channel unit delineations provided the spatial scale at which snorkel surveys were conducted following White et al. (2012), which is based on previously established protocols (Thurow 1994; O’Neal 2007). Essentially, a snorkeler entered each channel unit at the downstream end, identifying fish species and enumerating their abundance as they proceeded methodologically upstream. Two snorkelers were used in wider stream channels, in which case snorkelers communicated with each other during the survey to avoid duplicate counting. Data were temporarily recorded on an underwater slate and after the entire channel unit was surveyed, snorkelers permanently recorded the counts by species and the quality of visibility underwater as poor, average, or good based on a number of factors including water clarity, shade, and obstructions to line of sight. Target species were Chinook Salmon and steelhead/Rainbow Trout.



Prior to mark-recapture sampling, block nets were installed spanning the upstream and downstream ends of the channel unit to ensure population closure between capture events (Peterson et al. 2005). Fish were captured with backpack electrofishing in both events and marked using fin clips in the first event. We limited the data set to include only observations with valid data including non-zero marked and recaptured fish and paired snorkel and mark-recapture data that occurred within a two-day time frame (generally, snorkel surveys were conducted prior to mark-recapture sampling). This left 136 total observations (unique species by channel unit visit combinations) which included 100 unique channel units (45 and 59 channel units sampled in 2012 and 2015, respectively; four units were sampled in both years) across 44 unique sites; 38 of the observations were of Chinook Salmon and 98 were of *O. mykiss*.

We collected additional covariates intended to describe fish behavior and local habitat conditions that we hypothesized could influence snorkel detection probability. These covariates were measured using slight modifications to the CHaMP (2016) protocol and included: channel unit type classification (pool versus non-pool), average unit depth (m), density of large wood (greater than 15 cm in width and 3 m in length) in the wetted stream channel ( $\text{pieces} \cdot \text{m}^{-2}$ ), snorkeler-determined quality of visibility (poor, average, good), and species of observation.

### 2.3.3 Analysis

The model we applied to explain variability in snorkel survey detection probability had the form:

$$\begin{aligned} \text{logit}(\psi_i) = & \alpha + \omega_1\beta_1\text{Chinook}_i + \omega_2\beta_2\text{Pool}_i \\ & + \omega_3\beta_3\text{LWD2}_i + \omega_4\beta_4\text{LWD3}_i \\ & + \omega_5\beta_5\text{VIS1}_i + \omega_6\beta_6\text{VIS3}_i \\ & + \omega_7\beta_7\text{Depth}_i + \omega_8\beta_8\text{Depth}_i \times \text{Pool}_i + \varepsilon_{j(i)}. \end{aligned} \quad (9)$$

All variables were binary except  $\text{Depth}_i$ , which was continuous and z-transformed prior to analysis. We coded  $\text{Chinook}_i$  as 1 for Chinook Salmon and 0 for *O. mykiss*; likewise to discern pool and non-pool units in the case of  $\text{Pool}_i$ . We categorized large wood density because samples were not spread evenly along the observed continuum: we coded  $\text{LWD2}_i$  as 1 if large wood density was non-zero but less than the median density of all non-zero large wood density observations ( $0.026 \text{ pieces} \cdot \text{m}^{-2}$ ) and 0 otherwise; likewise for  $\text{LWD3}_i$  but for large wood densities greater than the median density. We coded  $\text{VIS1}_i$  as 1 for poor visibility and 0 otherwise; likewise for  $\text{VIS3}_i$  but for good visibility. Zero wood density ( $\text{LWD1}_i$ ) and average visibility ( $\text{VIS2}_i$ ) were the baseline categories and were quantified by the intercept ( $\alpha$ ). Coding the covariates this way and assigning  $\omega$  terms to each enabled us to evaluate models where, for example, high wood density has an effect relative to no wood but low wood density has no effect.

## 2.4 Simulation analysis

Stochastic simulation provides an opportunity to test the ability of the model to return robust estimates because they can be compared to true and known parameters. We designed the simulation analysis to address several questions:

- (1) Can the integrated model return unbiased estimates of true detection probability and abundance for both training data (locations with double sampling) and prediction data (locations with count and covariate data only)?

- (2) Are there benefits to accommodating the uncertainty in mark-recapture sampling, as measured by performance metrics such as accuracy, precision, and identification of ideal covariates?
- (3) Do the inferences in questions 1 and 2 depend on varying degrees of sample size, violated assumptions of the binomial count model and mark-recapture model, quality of mark-recapture data, and unmeasured covariate effects?
- (4) Does the variable selection approach we used perform well relative to a hypothetical case in which the covariates in the true model are known?

To investigate these questions, we developed a series of scenarios intended to isolate the effect of each factor on the reliability of the estimation model (scenarios and organization into blocks summarized in Table 2). Scenarios encompassed various combinations of data availability, data quality, violated assumptions, and effects of unmonitored covariates. We fitted two models to each simulated data set: the integrated model described in Section 2.2 and one identical in all ways except that the maximum likelihood estimate of abundance from mark-recapture data was used as known abundance with no uncertainty (referred to as the “external” approach). For each simulation scenario, we obtained 100 replicates of true states, data sets, and fitted estimates and calculated performance metrics reflecting accuracy, precision, variable selection, and credible interval coverage. Complete details of data simulation, model fitting, and calculation of performance metrics are provided in the Supplementary Material.

## 3 Results

### 3.1 Empirical application

Our analysis of mark-recapture data only strongly favored models  $M_t$  and  $M_b$  over the simplest model  $M_0$ , and favored model  $M_t$  over model  $M_b$  by over 20  $\Delta$ WAIC units. Thus, we used the assumptions of model  $M_t$  for fitting the integrated model. Averaged across all observations, capture probabilities were nearly equal between capture periods: posterior median of 0.41 (0.38 – 0.43; 95% CRL) for  $p_1$  and 0.42 (0.40 – 0.44) for  $p_2$ . We calculated the Pearson correlation coefficient between  $p_1$  and  $p_2$  across observations for each MCMC iteration and found them to be moderately correlated: 0.56 (0.44 – 0.67), indicating channel units that had higher-than-average capture probability in the first period were also likely to have higher-than-average capture probability in the second period as well. The integrated model fitted the mark-recapture data well, and estimated abundance generally agreed well with maximum likelihood estimates of abundance (Supplementary Material; Fig. 6). Across observations, Chinook Salmon abundance averaged 66 fish per channel unit (range of posterior medians: 2 – 624) and *O. mykiss* abundance averaged 53 fish per channel unit (range: 1 – 597).

We found strong evidence that snorkel survey detection probability varied by species, unit type, and depth, but that the depth effect was dependent on channel unit type (i.e., pool or non-pool; Fig. 2). Coefficients associated with these covariates all had parameter inclusion probabilities of 1, indicating their  $\omega$  terms took on the value of 1 for each MCMC iteration and suggesting we should have complete confidence that these covariates need accounting when predicting detection probability at new locations within the basin. The species effect was strongly positive, indicating that Chinook Salmon juveniles were seen with greater probability than *O. mykiss* (Fig. 2). Visibility was only important if the observer determined it was good (VIS3 effect). Poor visibility (VIS1) had a low probability of inclusion (0.15) and small effect size, indicating units with this attribute had

similar detection probabilities to those rated as average visibility. The covariates corresponding to non-zero density of large wood (LWD2 and LWD3) were assigned low parameter inclusion probabilities, indicating that channel units with these attributes had similar detection probability to units with no large wood at all. The single model with the highest posterior probability (0.44) included all covariates except both large wood density covariates and the poor visibility covariate (Supplementary Material, Table 3 therein).

Model-averaged detection probability response curves (Fig. 3) highlight the patterns suggested by the coefficient estimates. Most observations for both species occurred in channel units with no large wood present and average visibility; this limited our ability to investigate interactions among some habitat characteristics or species. The interaction between unit type and depth was strong, however, such that increasing depth had a positive effect on detection probability in non-pool units but a negative effect in pool units (Fig. 3). The estimated standard deviation of site-level random effects was large (1.12; 0.88 – 1.48) considering they are on the logit-scale. Posterior median detection probability for observations ranged from 0.11 to 0.84 (mean across observations: 0.38) for Chinook Salmon and 0.02 to 0.92 (mean: 0.24) for *O. mykiss*.

### 3.2 Simulation analysis

Due to the high dimensionality of the simulation results, only two blocks (B and D; Table 2) are displayed herein; complete block-specific results are presented in the Supplementary Material.

In cases where model assumptions were met and reasonable data quality was available (blocks A, B, and F), both the integrated and external (mark-recapture-derived abundance assumed to be the true value known without error) approaches returned nearly unbiased fits to the data and predictions for out-of-sample data. Average median percent error for abundance and detection probability across replicates was generally less than 5% (positive or negative) for both modeling approaches and rarely did the median percent error from any replicate exceed 10% positive relative bias. In terms of precision, the integrated model tended to produce fitted values and out-of-sample predictions closer to the true values, as evidenced by smaller median absolute percent error values, though the difference was modest (Fig. 4b). Performance of the variable selection approach was not perfect in all cases, but was at least as good or better when used in the integrated model rather than the external method. In particular, the external method incorrectly assigned high inclusion probabilities to truly unimportant covariates more frequently than the integrated model (Fig. 4c2). Credible interval coverage was generally better for detection probability than for abundance, and the integrated model had better coverage than the external abundance approach in most cases (Fig. 4d). Furthermore, the external abundance approach tended to over-estimate the standard deviation of site-level random effects – the integrated model suffered from this issue to a lesser degree (Fig. 4e).

As an example of model sensitivity to violated assumptions, we have included output summaries of simulation block D where it was possible to mistakenly count the same individual twice during count surveys. The primary effect of this violated assumption was to cause positive biases in the estimated and predicted detection probabilities (Fig. 5a3,a4). Estimation and prediction of abundance was not affected nearly to the same degree (Fig. 5a1,a2); this is because double-counting was possible in all count surveys, including those with and without mark-recapture sampling (training and prediction samples, respectively). So although we found the estimates of count survey detection probability to be positively biased relative to the true value in the presence of duplicate counts, largely unbiased predictions of abundance can still be obtained so long as the prevalence of

double-counts is the same in prediction samples as in the training samples.

## 4 Discussion

We have presented a modeling approach for integrating multiple information sources that are commonly collected when using a double sampling design to quantify detection probability. When applied to an empirical data set, the model uncovered several useful and intuitive patterns that demonstrated the effect of local conditions on detection probability. Through simulation trials, we demonstrated the method can return reasonably accurate and precise out-of-sample predictions. The simulation further revealed that there are benefits, albeit often modest in magnitude, to accounting for uncertainty in mark-recapture data, namely in terms of better selection of important covariates, better credible interval coverage, and greater accuracy in estimates of random variability. These findings suggest that investigators using the double sampling approach for quantifying the effects of covariates may see improved statistical performance by applying the integrated model we present (or similar) rather than treating abundance as a known quantity.

The magnitude and direction of estimated coefficients for the empirical data set were intuitive and for the most part aligned with our expectations. For example, in our experience with conducting snorkel surveys, *O. mykiss* are more evasive which makes them more difficult to see than Chinook Salmon, an observation supported to a limited extent by other studies (Hankin and Reeves 1988; Hillman et al. 1992). The depth by unit type interaction is also intuitive, as shallow, fast water, non-pool units have more turbulence and require more crawling (mask out of water) to progress through the survey; shallow pools do not suffer from this issue but deeper pools have their own characteristics that limit detection probability. We had expected to identify a negative effect of high large wood density, but we also had comparatively low replication at high large wood densities which likely affected our ability to identify an effect. Moreover, another study also found important effects of wood density, species, and visibility (Thurrow et al. 2006) and their estimates of detection probability for *O. mykiss* ranged between 0.15 and 0.2 (depending on size class), with individual observations ranging from 0 to 0.6 – our analysis estimated an average of 0.24 and a range of 0.02 to 0.92.

While covariates explained much of the variation in detection probability in the empirical data set, the estimated standard deviation of site-level random effects was large. This indicates that either some important covariates were not included or the count process was over-dispersed relative to the binomial process we assumed. Our simulation analyses illustrated that both cases can cause positive bias in the random variability term but that the accuracy of predictions was largely unaffected. Over-dispersion and failure to include all important covariates are common in ecological analyses, and our simulation analyses suggest that the integrated model showed better performance than the external approach in these situations. Although the random term was needed to accommodate otherwise unexplained variability in the empirical data, its magnitude indicates we should expect low precision in out-of-sample predictions.

We believe this integrated approach is general enough as to be applied to a wide variety of systems in which similar data (paired counts, independent abundance data, and explanatory covariates) have been collected. This is true so long as the count process can be reasonably approximated by a binomial process, as illustrated by our simulation analysis. In our simulation, the model generated snorkel count data using a binomial sampling process, yet the counts could

have instead been intended to represent counts from spotlight surveys, aerial surveys, camera traps, or other methods and the conclusions would be identical.

There are a variety of adaptations that could be made to the model for application to new use cases. First, the count component is essentially a binomial generalized linear model, meaning that its complexity can be tailored to available data. If suitable replication is conducted, then year- or observer-specific effects could be included as could higher order (e.g., quadratic) terms and more interaction terms. The indicator variable selection approach we embedded within the model to accommodate model uncertainty is general and can be altered to perform multi-model inference in more simplistic or complex cases (more examples of this approach in ecological settings can be found in Coggins et al. 2014; Dorazio et al. 2011; Gwinn et al. 2019a,b). Second, the mark-recapture likelihood could be altered to accommodate independent abundance data from more complex designs. In addition to our conditional multinomial likelihood approach, data augmentation (e.g., Royle and Dorazio 2010; Kéry and Schaub 2012, Ch. 6) is another method for expressing mark-recapture likelihoods that may show promise in this context. This would be particularly true if individual covariates (e.g., fish size) need to be accounted for, as data augmentation methods model sampling processes on an individual basis. Further, we believe non-mark-recapture designs for obtaining abundance estimates (e.g., depletion sampling, catchability-adjusted catch rate data, etc.) could be accommodated by our approach as well, so long as a sampling distribution can be assigned to the abundance estimate (or raw data) and an associated measure of statistical (i.e., observational) uncertainty is available. Finally, addressing particular research questions may necessitate assigning counts or captured individuals to multiple groups (e.g., size, age, or sex); it is plausible that the model could be extended to accommodate multinomial count outcomes.

A common goal of many ecological research, monitoring, and evaluation programs includes understanding and predicting animal abundance and distribution as influenced by habitat quality, climate change, species interactions, trophic relations, and other factors. However, the first step in any such program should include robust evaluation of the core response variable – animal abundance – which often includes assessment of detection probability. Our method that integrates the estimation of abundance and detection probability shows promise for rigorously quantifying the uncertainty in detection and abundance which should aid investigators using the double sampling/dual-gear validation design. The modeling approaches presented in this study point towards opportunities for future research that will help guide studies targeted at further quantifying the effects of covariates on survey detection probability.

## Acknowledgements

We thank the field personnel, who are too numerous to name individually, for collecting the data that informed our empirical analysis. We are grateful for C. Horn's contributions to the field study design. The analytical components of this research were supported by the Bonneville Power Administration as part of the Columbia Basin Fish Accords Agreement (Project #2009-004-00).

## Authors' Contributions

**B.A. Staton:** conceptualization, methodology, software, verification, formal analysis, writing – original draft, writing – review & editing; **C. Justice:** conceptualization, methodology, investigation, data curation, writing – review & editing; **S. White:** conceptualization, methodology, investigation, writing – review & editing, supervision, project administration; **E.R. Sedell:** conceptualization, methodology, investigation, writing – review & editing, supervision; **L.A. Burns:** conceptualization, methodology, writing – review & editing; **M.J. Kaylor:** conceptualization, methodology, writing – review & editing

## Data Availability

All data and code used to run analyses and generate figures found herein are documented on GitHub [DOI: 10.5281/zenodo.3928691; Staton (2020a)].

## References

- Barbieri, M. M. and Berger, J. O. 2004. Optimal predictive model selection. *The Annals of Statistics*, 32(3):870–897. doi: [10.1214/009053604000000238](https://doi.org/10.1214/009053604000000238).
- Barker, R. J., Schofield, M. R., Link, W. A., and Sauer, J. R. 2017. On the reliability of N-mixture models for count data. *Biometrics*, 74(1):369–377. doi: [10.1111/biom.12734](https://doi.org/10.1111/biom.12734).
- Bart, J. and Earnst, S. 2002. Double sampling to estimate density and population trends in birds. *The Auk*, 119(1):36–45. doi: [10.1093/auk/119.1.36](https://doi.org/10.1093/auk/119.1.36).
- Buckland, S. T., Anderson, D. R., Burnham, K. P., Laake, J. L., Borchers, D. L., and Thomas, L. 2001. *Introduction to distance sampling: estimating abundance of biological populations*. Oxford University Press, Oxford, UK.
- Bürkner, P.-C., Gabry, J., Kay, M., and Vehtari, A. 2020. *posterior: Tools for Working with Posterior Distributions*. R package version 0.1.3, URL: <https://mc-stan.org/posterior>.
- CHaMP 2016. *Scientific protocol for salmonid habitat surveys within the Columbia Habitat Monitoring Program*. Columbia Habitat Monitoring Program. URL: <https://www.champmonitoring.org/Program/RetrieveProgramDocumentFile/Tab/1126>.
- Coggins, L. G., Bacheler, N. M., and Gwinn, D. C. 2014. Occupancy models for monitoring marine fish: A Bayesian hierarchical approach to model imperfect detection with a novel gear combination. *PLoS ONE*, 9(9):e108302. doi: [10.1371/journal.pone.0108302](https://doi.org/10.1371/journal.pone.0108302).
- Collier, B. A., Ditchkoff, S. S., Raglin, J. B., and Smith, J. M. 2007. Detection probability and sources of variation in white-tailed deer spotlight surveys. *Journal of Wildlife Management*, 71(1):277–281. doi: [10.2193/2005-728](https://doi.org/10.2193/2005-728).
- Constable, Jr., J. and Suring, E. 2015. Juvenile salmonid monitoring in coastal Oregon and Lower Columbia streams, 2014. Monitoring Program Report OPSW-ODFW-2014-1, Oregon Department of Fish and Wildlife, Salem, OR. URL: <https://nrimp.dfw.state.or.us/CRL/reports/WORP/WORP2014AnnualReport.pdf>.
- Doll, J. C., Etchison, L., and Owensby, D. 2020. Population estimate of the state and federally threatened Spotfin Chub using underwater observations. *North American Journal of Fisheries Management*, 40(2):342–353. doi: [10.1002/nafm.10414](https://doi.org/10.1002/nafm.10414).
- Dorazio, R. M., Gotelli, N. J., and Ellison, A. M. 2011. Modern methods of estimating biodiversity loss from presence-absence surveys. In Grillo, O., editor, *Biodiversity Loss in a Changing Planet*, pages 277 – 302. InTech. URL: <https://www.intechopen.com/books/biodiversity-loss-in-a-changing-planet/modern-methods-of-estimating-biodiversity-from-presence-absence-surveys>.
- Flitcroft, R., Burnett, K., Snyder, J., Reeves, G., and Ganio, L. 2013. Riverscape patterns among years of juvenile coho salmon in midcoastal Oregon: Implications for conservation. *Transactions of the American Fisheries Society*, 143(1):26–38. DOI: [10.1080/00028487.2013.824923](https://doi.org/10.1080/00028487.2013.824923).
- Fowler, P. 2017. Southeast Alaska steelhead snorkel surveys of regional index streams, 2014 and 2015. Fishery Data Series 17-13, Alaska Department of Fish and Game, Anchorage, AK. URL: <http://www.adfg.alaska.gov/FedAidPDFs/FDS17-13.pdf>.
- Gwinn, D. C., Bacheler, N. M., and Shertzer, K. W. 2019a. Integrating underwater video into traditional fisheries indices using a hierarchical formulation of a state-space model. *Fisheries Research*, 219:105309. doi: [10.1016/j.fishres.2019.105309](https://doi.org/10.1016/j.fishres.2019.105309).
- Gwinn, D. C., Todd, C. R., Brown, P., Hunt, T. L., Butler, G., Kitchingman, A., Koehn, J. D., and Ingram, B. 2019b. Assessing a threatened fish species under budgetary constraints: Evaluating the use of

- existing monitoring data. *North American Journal of Fisheries Management*, 39(2):315–327. doi: [10.1002/nafm.10271](https://doi.org/10.1002/nafm.10271).
- Hankin, D. G. and Reeves, G. H. 1988. Estimating total fish abundance and total habitat area in small streams based on visual estimation methods. *Canadian Journal of Fisheries and Aquatic Sciences*, 45(5):834–844. doi: [10.1139/f88-101](https://doi.org/10.1139/f88-101).
- Hillman, T. W., Mullan, J. W., and Griffith, J. S. 1992. Accuracy of underwater counts of juvenile Chinook salmon, coho salmon, and steelhead. *North American Journal of Fisheries Management*, 12(3):598–603. doi: [10.1577/1548-8675\(1992\)012<0598:aoucoj>2.3.co;2](https://doi.org/10.1577/1548-8675(1992)012<0598:aoucoj>2.3.co;2).
- Hooten, M. B. and Hobbs, N. T. 2015. A guide to Bayesian model selection for ecologists. *Ecological Monographs*, 85(1):3–28. doi: [10.1890/14-0661.1](https://doi.org/10.1890/14-0661.1).
- Huggins, R. M. 1989. On the statistical analysis of capture experiments. *Biometrika*, 76(1):133–140. doi: [10.1093/biomet/76.1.133](https://doi.org/10.1093/biomet/76.1.133).
- Huggins, R. M. 1991. Some practical aspects of a conditional likelihood approach to capture experiments. *Biometrics*, 47(2):725–732. doi: [10.2307/2532158](https://doi.org/10.2307/2532158).
- Hutton, J. M. and Woolhouse, M. E. J. 1989. Mark-recapture to assess factors affecting the proportion of a Nile crocodile population seen during spotlight counts at Ngezi, Zimbabwe, and the use of spotlight counts to monitor crocodile abundance. *The Journal of Applied Ecology*, 26(2):381. doi: [10.2307/2404068](https://doi.org/10.2307/2404068).
- Jonasson, B. C., Sedell, E. R., Tattam, S. K., Garner, A. B., Horn, C., Bliesner, K. L., Dowdy, J. W., Favrot, S. D., Hay, J. M., McMichael, G. A., Power, B. C., Davis, O. C., and Ruzycki, J. R. 2016. Investigations into the life history of naturally produced spring Chinook salmon and summer steelhead in the Grande Ronde River subbasin. Annual Report BPA Project #1992-026-04, Oregon Department of Fish and Wildlife, La Grande, OR. URL: [https://nrimp.dfw.state.or.us/web%20stores/data%20libraries/files/ODFW/ODFW\\_40892\\_2\\_1992-026-04\\_2015\\_FinalReport\\_BPA\\_Version.pdf](https://nrimp.dfw.state.or.us/web%20stores/data%20libraries/files/ODFW/ODFW_40892_2_1992-026-04_2015_FinalReport_BPA_Version.pdf).
- Jones, E. L., Quinn, T. J., and Alen, B. W. V. 1998. Observer accuracy and precision in aerial and foot survey counts of pink salmon in a southeast Alaska stream. *North American Journal of Fisheries Management*, 18(4):832–846. doi: [10.1577/1548-8675\(1998\)018<0832:oaapia>2.0.co;2](https://doi.org/10.1577/1548-8675(1998)018<0832:oaapia>2.0.co;2).
- Kellner, K. 2018. *jagsUI: A Wrapper Around 'rjags' to Streamline 'JAGS' Analyses*. R package version 1.5.0.
- Kellner, K. F. and Swihart, R. K. 2014. Accounting for imperfect detection in ecology: A quantitative review. *PLoS ONE*, 9(10):e111436. doi: [10.1371/journal.pone.0111436](https://doi.org/10.1371/journal.pone.0111436).
- Kéry, M. and Schmidt, B. 2008. Imperfect detection and its consequences for monitoring for conservation. *Community Ecology*, 9(2):207–216. doi: [10.1556/comec.9.2008.2.10](https://doi.org/10.1556/comec.9.2008.2.10).
- Kéry, M. and Schuab, M. 2012. *Bayesian population analysis using WinBUGS: a hierarchical perspective*. Academic Press, Waltham, MA.
- Korman, J., Ahrens, R. N., Higgins, P. S., and Walters, C. J. 2002. Effects of observer efficiency, arrival timing, and survey life on estimates of escapement for steelhead trout (*Oncorhynchus mykiss*) derived from repeat mark-recapture experiments. *Canadian Journal of Fisheries and Aquatic Sciences*, 59(7):1116–1131. doi: [10.1139/f02-081](https://doi.org/10.1139/f02-081).
- Kuo, L. and Mallick, B. 1998. Variable selection for regression models. *Sankhyā: The Indian Journal of Statistics, Series B*, 60(1):65–81. URL: [https://www.jstor.org/stable/25053023?seq=1#metadata\\_info\\_tab\\_contents](https://www.jstor.org/stable/25053023?seq=1#metadata_info_tab_contents).
- Lawson, Z. J., Gaeta, J. W., and Carpenter, S. R. 2011. Coarse woody habitat, lakeshore residential development, and largemouth bass nesting behavior. *North American Journal of Fisheries Management*,



- 31(4):666–670. doi: [10.1080/02755947.2011.608990](https://doi.org/10.1080/02755947.2011.608990).
- Mosquera, I., Cote, I. M., Jennings, S., and Reynolds, J. D. 2000. Conservation benefits of marine reserves for fish populations. *Animal Conservation*, 3(4):321–332. doi: [10.1111/j.1469-1795.2000.tb00117.x](https://doi.org/10.1111/j.1469-1795.2000.tb00117.x).
- Nehlsen, W., Williams, J. E., and Lichatowich, J. A. 1991. Pacific salmon at the crossroads: Stocks at risk from California, Oregon, Idaho, and Washington. *Fisheries*, 16(2):4–21. doi: [10.1577/1548-8446\(1991\)016<0004:psatcs>2.0.co;2](https://doi.org/10.1577/1548-8446(1991)016<0004:psatcs>2.0.co;2).
- O’Neal, J. S. 2007. Snorkel surveys. In Johnson, D. H., Shrier, B. M., O’Neal, J. S., Knutzen, J. A., Augerot, X., O’Neil, T. A., and Pearsons, T. N., editors, *Salmonid Field Protocols Handbook: Techniques for Assessing Status and Trends in Salmon and Trout Populations*, pages 325–340. American Fisheries Society, Bethesda, MD.
- Otis, D. L., Burnham, K. P., White, G. C., and Anderson, D. R. 1978. Statistical inference from capture data on closed animal populations. *Wildlife Monographs*, (62):3–135.
- Peterson, J. T., Banish, N. P., and Thurow, R. F. 2005. Are block nets necessary?: Movement of stream-dwelling salmonids in response to three common survey methods. *North American Journal of Fisheries Management*, 25(2):732–743. doi: [10.1577/m04-051.1](https://doi.org/10.1577/m04-051.1).
- Peterson, J. T., Scheerer, P. D., and Clements, S. 2015. An evaluation of the efficiency of minnow traps for estimating the abundance of minnows in desert spring systems. *North American Journal of Fisheries Management*, 35(3):491–502. doi: [10.1080/02755947.2015.1017125](https://doi.org/10.1080/02755947.2015.1017125).
- Pinter, K., Lautsch, E., Unfer, G., and Hayes, D. S. 2018. Snorkeling-based fish stock assessment by anglers—a valuable method for managing recreational fisheries. *North American Journal of Fisheries Management*. doi: [10.1002/nafm.10246](https://doi.org/10.1002/nafm.10246).
- Plummer, M. 2003. JAGS: A program for analysis of Bayesian graphical models using Gibbs sampling. *3rd International Workshop on Distributed Statistical Computing (DSC 2003)*; Vienna, Austria, 124. URL: <https://www.r-project.org/conferences/DSC-2003/Drafts/Plummer.pdf>.
- R Core Team 2020. *R: A Language and Environment for Statistical Computing*. R Foundation for Statistical Computing, Vienna, Austria. Version 4.0.2.
- Roni, P., Hanson, K., and Beechie, T. 2008. Global review of the physical and biological effectiveness of stream habitat rehabilitation techniques. *North American Journal of Fisheries Management*, 28(3):856–890. doi: [10.1577/m06-169.1](https://doi.org/10.1577/m06-169.1).
- Royle, J. A. 2004. N-mixture models for estimating population size from spatially replicated counts. *Biometrics*, 60(1):108–115. doi: [10.1111/j.0006-341x.2004.00142.x](https://doi.org/10.1111/j.0006-341x.2004.00142.x).
- Royle, J. A. and Dorazio, R. M. 2010. Parameter-expanded data augmentation for Bayesian analysis of capture–recapture models. *Journal of Ornithology*, 152(S2):521–537. doi: [10.1007/s10336-010-0619-4](https://doi.org/10.1007/s10336-010-0619-4).
- Seber, G. A. F. 1986. A review of estimating animal abundance. *Biometrics*, 42(2):267. doi: [10.2307/2531049](https://doi.org/10.2307/2531049).
- Som, N. A., Perry, R. W., Jones, E. C., Juilio, K. D., Petros, P., Pinnix, W. D., and Rupert, D. L. 2018. N-mix for fish: Estimating riverine salmonid habitat selection via N-mixture models. *Canadian Journal of Fisheries and Aquatic Sciences*, 75(7):1048–1058. doi: [10.1139/cjfas-2017-0027](https://doi.org/10.1139/cjfas-2017-0027).
- Staton, B. 2020a. *bstaton1/snk-eff-ms-analysis*: Preliminary release. doi: [10.5281/zenodo.3928691](https://doi.org/10.5281/zenodo.3928691).
- Staton, B. 2020b. *postpack: Utilities for Processing Posterior Samples Stored in ‘mcmc.lists’*. R package version 0.5.2, URL: <https://bstaton1.github.io/postpack/>.
- Thompson, W. L. and Lee, D. C. 2000. Modeling relationships between landscape-level attributes and snorkel counts of Chinook salmon and steelhead parr in Idaho. *Canadian Journal of Fisheries and Aquatic*

- Sciences*, 57(9):1834–1842. doi: [10.1139/f00-135](https://doi.org/10.1139/f00-135).
- Thurrow, R. F. 1994. Underwater methods for study of salmonids in the intermountain West. General Technical Report INT-GTR-307, Department of Agriculture, U.S. Forest Service, Intermountain Research Station, Odgen, UT. doi: [10.2737/INT-GTR-307](https://doi.org/10.2737/INT-GTR-307).
- Thurrow, R. F., Peterson, J. T., and Guzevich, J. W. 2006. Utility and validation of day and night snorkel counts for estimating bull trout abundance in first- to third-order streams. *North American Journal of Fisheries Management*, 26(1):217–232. doi: [10.1577/m05-054.1](https://doi.org/10.1577/m05-054.1).
- Ulibarri, R. M., Bonar, S. A., Rees, C., Amberg, J., Ladell, B., and Jackson, C. 2017. Comparing efficiency of American Fisheries Society standard snorkeling techniques to environmental DNA sampling techniques. *North American Journal of Fisheries Management*, 37(3):644–651. doi: [10.1080/02755947.2017.1306005](https://doi.org/10.1080/02755947.2017.1306005).
- Vehtari, A., Gelman, A., Simpson, D., Carpenter, B., and Bürkner, P.-C. 2021. Rank-normalization, folding, and localization: An improved Rhat for assessing convergence of MCMC. *Bayesian Analysis*. doi: [10.1214/20-BA1221](https://doi.org/10.1214/20-BA1221).
- Walters, C. and Pearse, P. H. 1996. Stock information requirements for quota management systems in commercial fisheries. *Reviews in Fish Biology and Fisheries*, 6(1):21–42. doi: [10.1007/bf00058518](https://doi.org/10.1007/bf00058518).
- Watanabe, S. 2013. A widely applicable Bayesian information criterion. *Journal of Machine Learning Research*, 14:867–897.
- Weaver, D. M., Kwak, T. J., and Pollock, K. H. 2014. Sampling characteristics and calibration of snorkel counts to estimate stream fish populations. *North American Journal of Fisheries Management*, 34(6):1159–1166. doi: [10.1080/02755947.2014.951808](https://doi.org/10.1080/02755947.2014.951808).
- White, S., Justice, C., Burns, L., Graves, D., Kelsey, D., and Kaylor, M. 2019. Assessing the status and trends of spring Chinook habitat in the upper Grande Ronde River and Catherine Creek: Annual report 2018. Annual Report 19-04, Columbia River Inter-Tribal Fish Commission, Portland, OR. URL: <https://www.critfc.org/wp-content/uploads/2019/05/19-04.pdf>.
- White, S., Justice, C., and McCullough, D. 2012. *Protocol for snorkel surveys of fish densities*. Columbia River Inter-Tribal Fish Commission. URL: <https://www.monitoringmethods.org/Protocol/Details/499>.
- Williams, B. K., Nichols, J. D., and Conroy, M. J. 2002. *Analysis and Management of Animal Populations*. Academic Press, San Diego, CA.

**TABLE 1.** Three types of mark-recapture models for the two-sample case with closed populations. For models  $M_0$  and  $M_t$ ,  $p_{i,1}$  and  $p_{i,2}$  are capture probabilities for all individuals in each period. For model  $M_b$ ,  $p_{i,2}$  is the probability of first capture in the second period, and  $c_{i,2}$  is the probability of recapture. The  $\Delta\text{WAIC}$  column shows the difference in WAIC scores between each model and the lowest WAIC model for the Grande Ronde empirical analysis, which we used to inform which assumption should be made when fitting the integrated model.

Model	Assumptions	Description	$\Delta\text{WAIC}$
$M_0$	$p_{i,1} = p_{i,2}$	Time-constant capture probability	101
$M_t$	$p_{i,1} \neq p_{i,2}$	Period-specific capture probability	0
$M_b$	$p_{i,1} = p_{i,2} \neq c_{i,2}$	Behavioral response affects recapture probability	22

**TABLE 2.** Breakdown of the scenarios used for the simulation analysis. See the Supplementary Material for a description of how the scenarios were implemented.

Block	Description	Scenario	Training Samples	$\omega$ Known	Over-disp. Counts <sup>a</sup>	Double Count Prob.	$p_1, p_2^b$	$c_2^c$	Assumed Model <sup>d</sup>	Unobserved Covariates <sup>e</sup>
A	Model assumptions met, true model known, vary training sample size	1	25	Yes	None	0	beta(10, 10)	$p_2$	$M_t$	None
		2	50							
		3	100							
B	Model assumptions met, true model unknown, vary training sample size	4	25	No	None	0	beta(10, 10)	$p_2$	$M_t$	None
		5	50							
		6	100							
C	Homogenous $p_i$ assumption violated, vary the amount of over-dispersion	7	100	No	Little Some Lots	0	beta(10, 10)	$p_2$	$M_t$	None
		8								
		9								
D	Single count only assumption violated, vary the probability a fish is counted twice	10	100	No	None	0.05	beta(10, 10)	$p_2$	$M_t$	None
		11				0.1				
		12				0.2				
E	Model assumptions met, vary the quality of mark-recapture data	13	100	No	None	0	beta(20, 80)	$p_2$	$M_t$	None
		14					beta(50, 50)			
		15					beta(80, 20)			
F	Model assumptions met, vary the contribution of unobserved covariates	16	100	No	None	0	beta(10, 10)	$p_2$	$M_t$	Little
		17								Some
		18								Lots
G	Behavioral recapture response present, but not accounted for	19	100	No	None	0	beta(10, 10)	$p_2 \cdot 0.9$	$M_t$	None
		20						$p_2 \cdot 0.7$		
		21						$p_2 \cdot 0.5$		
H	Behavioral recapture response present, use WAIC to determine if it needs accounting	22	100	No	None	0	beta(10, 10)	$p_2 \cdot 0.9$	Use WAIC	None
		23				$p_2 \cdot 0.7$				
		24				$p_2 \cdot 0.5$				

<sup>a</sup> We used a beta-binomial count model to simulate over-dispersed counts of varying degrees by changing the sum of the two beta parameters; none =  $1 \times 10^{10}$ , little = 20, some = 10, lots = 5.

<sup>b</sup> Capture probabilities for each period were sampled from the listed beta distribution for each observation.

<sup>c</sup> Recapture probability for the second period is a function of the capture probability in that period.

<sup>d</sup> For block H, WAIC was used to select the best mark-recapture assumptions to make prior to fitting the model with count data.

<sup>e</sup> We used observation-level logit-normal deviates to simulate the effects of unobserved covariates. We varied their standard deviation: none = 0, little = 0.1, some = 0.3, lots = 0.5.

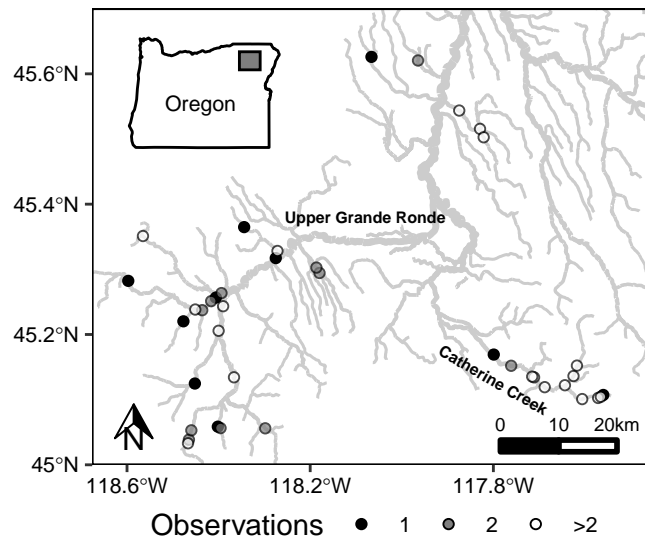


**FIGURE 1.** Map of the portion of the Grande Ronde River basin that served as the study area for the empirical application of the integrated model. Point colors denote the number of observations made at each site, i.e., the number of replicates for the site-level random effect.

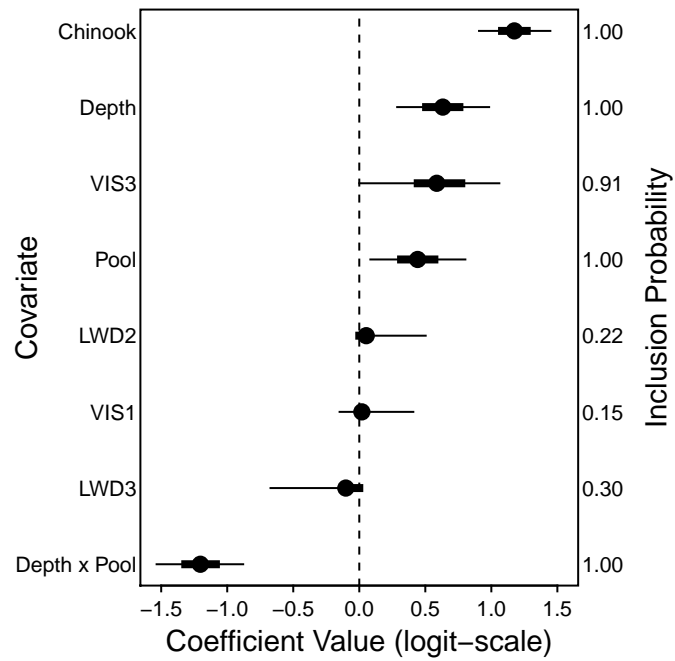


**FIGURE 2.** Model-averaged coefficient estimates ( $\omega\beta$ ) from the empirical application of the integrated model. Positive coefficient values indicate that covariate increases snorkel detection probability; points represent posterior means, thick bars represent central 50% credible limits and thin bars represent 95% credible limits. Along the right axis are posterior probabilities that each covariate should be included in an optimal predictive model (posterior mean of each  $\omega$  term).

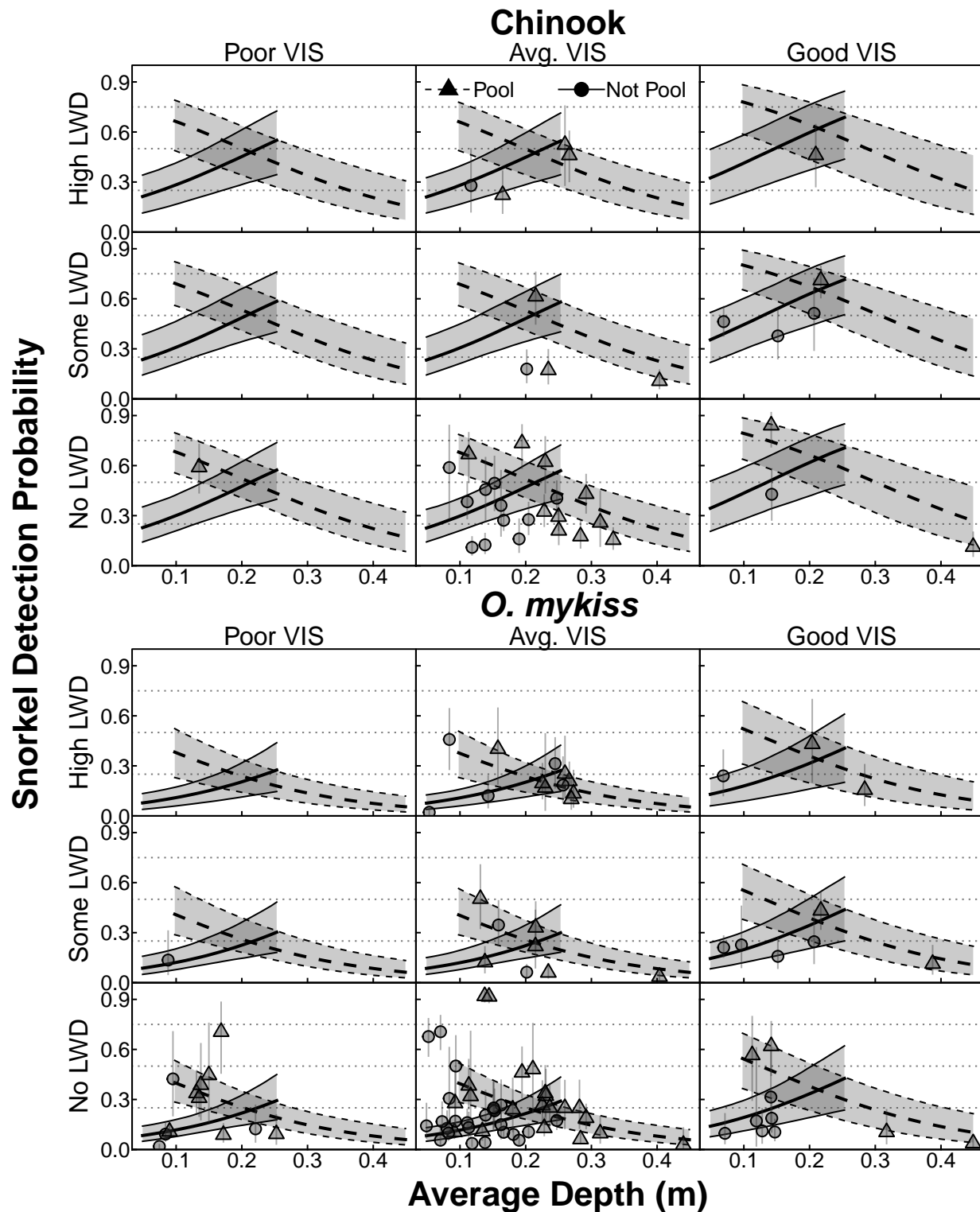


**FIGURE 3.** Response of snorkel survey detection probability to various covariates for two salmonid species in the empirical analysis. Each panel shows a unique combination of large wood density (LWD; rows) and snorkeler-determined visibility (VIS; columns) grouped by species (axes extent equal for all panels). Curves and points display the model-averaged posterior median fixed-effect relationship and observation-specific detection probability, respectively, for non-pool and pool units. Grey bands and error bars denote 95% equal-tailed credible intervals.

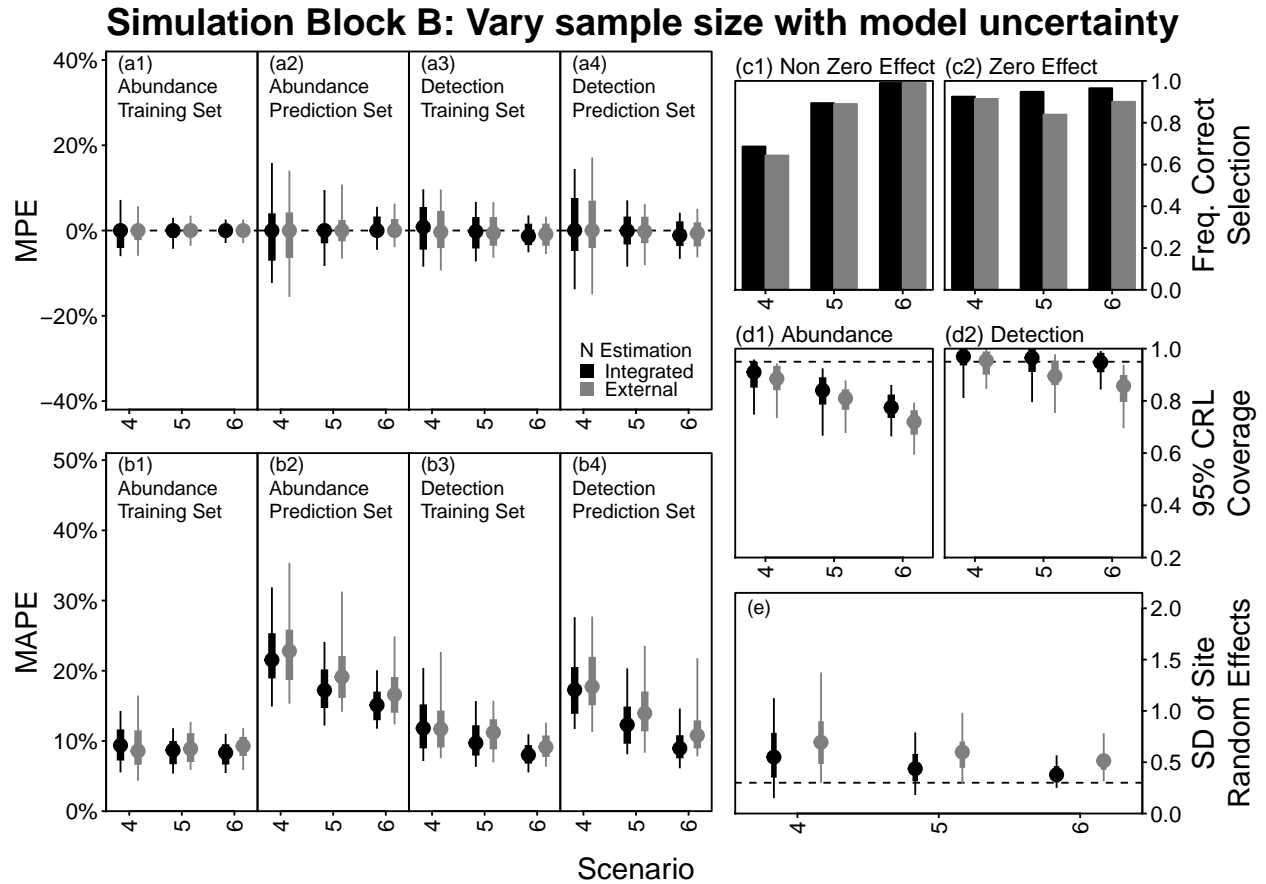


**FIGURE 4.** Summary of output from block B of the simulation trials, in which all model assumptions were met and the sample size was varied. Points represent medians across 100 replicate data sets, thick error bars represent the central 50% of outcomes, and thin error bars represent the central 95% of outcomes. (a) Distribution of median percent errors (MPE) across replicate data sets for abundance (a1 and a2) and detection probability (a3 and a4) – dashed line at 0 shows no error. (b) Same layout as (a), except for median absolute percent errors (MAPE). (c1) Proportion of the simulations in which truly non-zero effects were assigned probability of inclusion greater than 0.5. (c2) Proportion of the simulations in which truly zero-valued effects were assigned probability of inclusion less than 0.5. (d) Distribution of coverage statistics for abundance (d1) and detection (d2) – i.e., the fraction of 95% credible intervals that contained the true value (reference dashed line at 0.95 shows optimal coverage). (e) Distribution of estimated standard deviation of site-level random effects – dashed line shows the true value used to simulate the data. Matching figures for all simulation blocks are shown in the Supplementary Material.



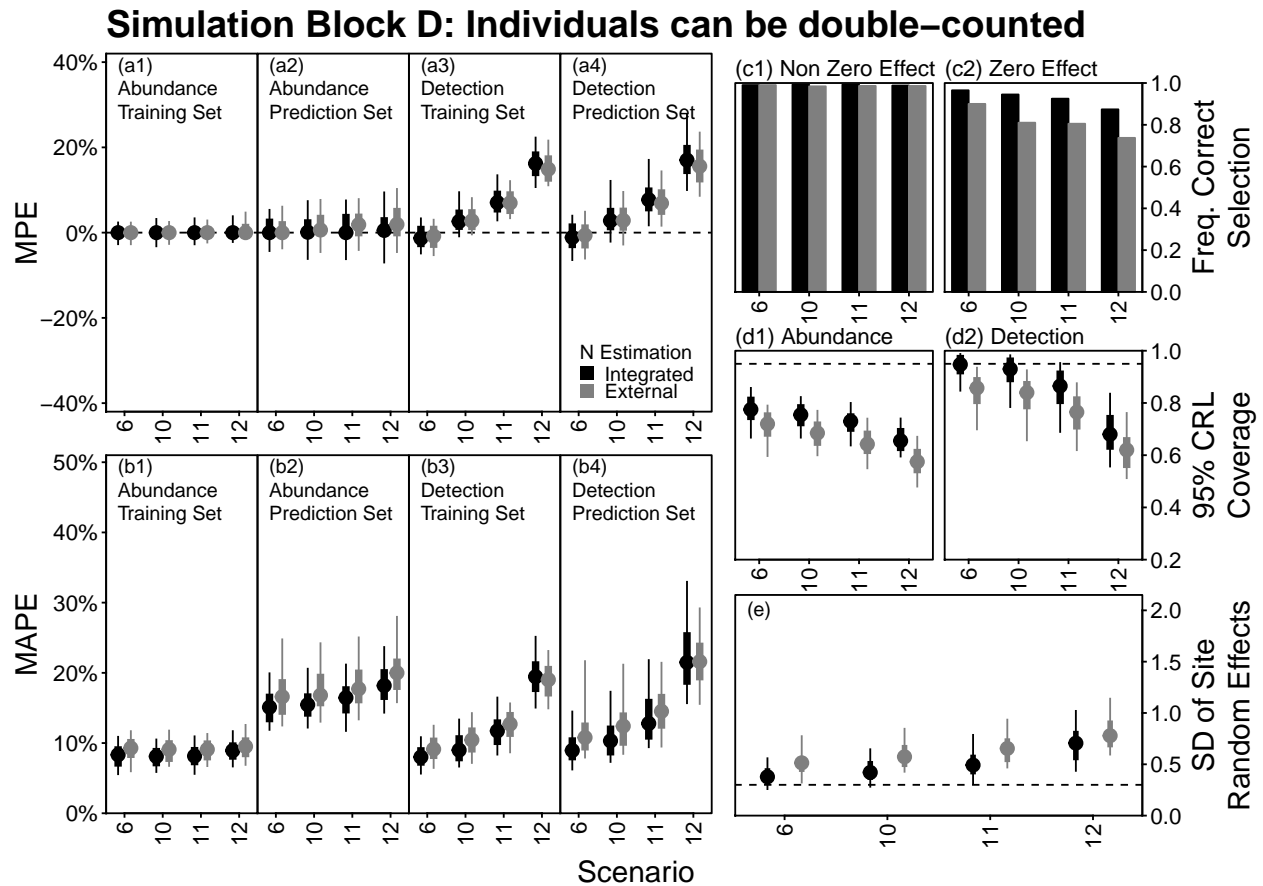


**FIGURE 5.** Summary of output from block D of the simulation trials in which it was possible to double-count individuals but the models did not account for it. Scenarios 6, 10, 11, and 12 had probabilities of double counting individuals of 0, 0.05, 0.1, and 0.2, respectively, and are identical in all other ways. Layout of this figure is identical to Figure 4, consult that figure caption for a description of the various panels.

---

# Supplementary Material

---

*Staton et al.: Accounting for uncertainty when estimating drivers of detection probability: an integrated approach illustrated with snorkel surveys for riverine fishes*

## 1 Additional methods

### 1.1 Posterior estimation

We conducted Markov chain Monte Carlo (MCMC) sampling with 29,000 iterations per each of three chains, each with a burn-in period of 5,000 iterations and thinned by 8 leaving a total of 9,000 retained samples for posterior inference. We assessed convergence of MCMC algorithms visually using trace plots and quantitatively using the rank-normalized  $\hat{R}$  statistic described in Vehtari et al. (2021). To further assess adequate sampling behavior, we used the estimated effective number of MCMC samples available for estimating the posterior median and 2.5th and 97.5th quantiles, which provided an indication of how many of the 9,000 retained samples contributed independent information for estimating these quantiles. These calculations were performed using the R package ‘posterior’ (Bürkner et al. 2020); all other posterior summarization tasks were performed using the R package ‘postpack’ (Staton 2020). For the simulation analysis, we discarded simulation replicates in which any of the estimated parameters had  $\hat{R}$  values greater than 1.1; this occurred very rarely: out of 100 replicates per scenario, at most seven replicates were discarded for this reason and most scenarios had between zero and two replicates discarded. For the empirical analysis, we evaluated model fit to the data visually by comparing the observed data against the corresponding posterior predictive values to verify the data were generally within the range of variability expected by the model assumptions.

### 1.2 Prior distributions

We selected all prior distributions to be minimally informative while simultaneously discouraging implausible values from being sampled by the MCMC algorithm. For logit-scale parameters ( $\alpha$  and  $\beta_1, \dots, \beta_n$ ), we assigned a prior  $t$ -distribution with standard deviation and degrees of freedom parameters of 1.566 and 7.763, respectively, as suggested by Dorazio et al. (2011) because it is uniform from 0 to 1 on the inverse logit-scale. We assigned the standard deviation of site-level random effects ( $\sigma$ ) a uniform prior bounded by [0,5]. For mark-recapture capture probabilities, we used independent beta(1,1) priors. Finally, for Bernoulli indicator variables ( $\omega_1, \dots, \omega_n$ ), we assigned prior probabilities of 0.5. The exception was for those  $\omega$  parameters corresponding to interaction terms, in which case we used prior probability equal to  $\omega_u \omega_v 0.5$  where  $u$  and  $v$  correspond to the main effects altered by the interaction term in question (i.e., the interaction would only be considered if both main effects were also considered). We show the implementation of these prior distributions in the JAGS model pseudocode below.

### 1.3 JAGS pseudocode for integrated model

```
model {  
  
  # --- COUNT SURVEY MODEL ---#  
  
  # PRIORS: COEFFICIENTS  
  a ~ dt(0, 1/1.566^2, 7.763)  
  b1 ~ dt(0, 1/1.566^2, 7.763)  
  b2 ~ dt(0, 1/1.566^2, 7.763)  
  b3 ~ dt(0, 1/1.566^2, 7.763)  
  
  # PRIORS: INDICATOR VARIABLES  
  w1 ~ dbern(0.5)  
  w2 ~ dbern(0.5)  
  w3 ~ dbern(0.5 * w1 * w2)  
  
  # PRIORS: RANDOM EFFECTS  
  sig ~ dunif(0, 5)  
  for (j in 1:nsites) {epi[j] ~ dnorm(0, 1/sig^2)}  
  
  # LINEAR PREDICTOR + LIKELIHOOD  
  for (i in 1:nobs) {  
    logit(psi[i]) <-  
      a + b1 * w1 * x1[i] + b2 * w2 * x2[i] + b3 * w3 * x1[i] * x2[i] + epi[site[i]]  
  
    y[i] ~ dbin(psi[i], N[i])  
  }  
  
  # --- MARK-RECAPTURE MODEL --- #  
  for (i in 1:nobs) {  
    # PRIORS: CAPTURE PROBABILITY: M_t  
    p1[i] ~ dbeta(1,1)  
    p2[i] ~ dbeta(1,1)  
  
    # PROBABILITY OF BEING CAPTURED AT ALL  
    p_star[i] <- 1 - (1 - p1[i]) * (1 - p2[i])  
  
    # MARGINAL PROBABILITY OF EACH CAPTURE HISTORY TYPE  
    pi[i,1] <- (p1[i] * p2[i])/p_star[i] # 11  
    pi[i,2] <- (p1[i] * (1 - p2[i]))/p_star[i] # 10  
    pi[i,3] <- ((1 - p1[i]) * p2[i])/p_star[i] # 01  
  
    # LIKELIHOOD  
    Z[i,1:3] ~ dmulti(pi[i,1:3], r[i])  
  
    # DERIVE ABUNDANCE  
    N[i] <- max(round(r[i]/p_star[i]), minN[i])  
  }  
}
```

## Pseudocode inputs

- `nobs`: number of observations (pairs of mark-recapture and count data); one or more observations per site
- `nsites`: number of sites included in analysis – could be any blocking factor
- `site[i]`: site identifier for observation  $i$
- `y[i]`: (snorkel) count for observation  $i$
- `Z[i, 1:3]`: a row vector containing the capture histories for observation  $i$
- `r[i]`: the number of unique individuals captured in mark-recapture; equal to  $\text{sum}(Z[i, 1:3])$
- `minN[i]`: minimum possible abundance for observation  $i$ , equal to  $\max(r[i], y[i])$
- `x1[i]`, `x2[i]`: covariates; if continuous should be  $z$ -transformed

## Pseudocode outputs

- `N[i]`: estimated abundance for observation  $i$
- `a`: logit-scale intercept
- `b1`: logit-scale coefficient for the effect of `x1`
- `b2`: logit-scale coefficient for the effect of `x2`
- `b3`: logit-scale coefficient for the effect of `x1*x2`
- `w1`: indicator variable for including a non-zero effect of `x1`
- `w2`: indicator variable for including a non-zero effect of `x2`
- `w3`: indicator variable for including a non-zero effect of `x1*x2`
- `sig`: standard deviation of site-specific random effects
- `epi[j]`: site-specific random effect for site  $j$
- `psi[i]`: detection probability for observation  $i$

## 1.4 Simulation analysis

We organized the simulation into a set of eight blocks that addressed one topic at a time. By “topic”, we are referring to the effect that specific situations have on the estimation and predictive performance of our integrated modeling approach, for example, whether and to what extent it is sensitive to sample size or violated assumptions. Within each block, we used three levels (levels referred to as “scenarios”), where the topic in question was varied with increasing “intensity.” The blocks, and the specific scenarios that they are made of, are summarized in Table 2 of the main text. The text below describes the specific features of our simulation approach and how the various scenarios were implemented.

### 1.4.1 State-generating model

We assumed abundance was distributed randomly across sampling units with mean and variance approximately equal to the distribution of fish abundances in the Grande Ronde River snorkel data set and followed the overall sampling structure of that data set (i.e., channel units nested within sites). We simulated five units at a given site and each unit had six associated covariate values recorded: three continuous (all on the  $z$ -scale) and three categorical (all binary). These covariates were not correlated with each other nor were they correlated with abundance. These characteristics of our code can be edited to reflect some new hypothetical case.

### 1.4.2 Data-generating model

We selected a portion of the units at random to be members of the training data set in which both mark-recapture and count data would be collected and the remaining portion had only count sampling conducted (prediction data set). We used 200 units in the prediction set and varied the size of the training set among 25, 50, and 100 observations depending on the scenario. We assumed covariates were measured without error at all units.

#### Mark-recapture data simulation

Most scenarios (those constituting blocks A – F) had mark-recapture data collection simulated following the assumptions of model  $M_t$ , except that we repeated sampling within a unit until both marks released and recaptured were non-zero. We sampled unit-specific capture probabilities  $p_{i,1}$  and  $p_{i,2}$  from a beta distribution with shape parameters  $a$  and  $b$ . Altering the  $a$  and  $b$  parameters changes the central tendency and variability in the beta random variable, which we used to control the quality of mark-recapture information: lower capture probabilities (expected value is  $a/(a+b)$ ) lead to more variable data, less informative mark-recapture estimates, and can result in large biases in two-sample closed population estimators. We controlled among-unit variability in capture probability by the scale of  $a$  and  $b$  while holding their ratio constant – higher values result in less variability. For most scenarios, we set  $a = b = 10$ , which we obtained by simulating data while tuning  $a$  and  $b$  until the estimated capture probabilities followed a similar beta distribution as found for the empirical data set. To generate high quality mark-recapture data, we used  $a = 80$  and  $b = 20$ , and reversed these to generate low quality mark-recapture data.

We also wished to evaluate how robust our model is in the face of behavior effects in mark-recapture sampling. Thus, for the scenarios in blocks G and H we simulated mark-recapture data under model  $M_b$ , where only  $p_{i,1}$  was beta-distributed with parameters  $a$  and  $b$ ,  $p_{i,2} = p_{i,1}$ , and  $c_{i,2} = C \cdot p_{i,2}$ . The quantity  $C$  took on the value of 0.9, 0.7, or 0.5 depending on the scenario, and served to simulate varying degrees of active avoidance behavior of previously captured individuals. For example,  $C = 0.5$  implies an initial capture probability that is 200% greater than the probability of recapture. In block G, the estimation models assumed that model  $M_t$  was correct and did not consider model  $M_b$ , whereas block H first fitted models  $M_0$ ,  $M_t$ , and  $M_b$  to mark-recapture data only and used WAIC to inform the estimation models which assumption to use, just as we did for the Grande Ronde empirical analysis. The contrast between these two blocks enabled us to assess whether our modeling framework can detect and account for behavioral effects on capture probabilities, and how consequential it might be if falsely ignored.

#### Count data simulation

We simulated count data collection using a beta-binomial random process, which allowed us to vary the extent to which the binomial sampling assumption made by the estimation models was met. Common to all scenarios was a true logit-linear detection probability model, which had non-zero effects for two continuous covariates, two categorical covariates, one interaction, and site effects – the remaining covariates had zero-valued effects (we were interested in how well the model could discern important from unimportant covariates). This model provided an expected overall detection probability at a given unit, around which three beta random variables were drawn to apply to individuals randomly assigned to one of three “groups” within each unit. These groups were intended to represent clusters of individuals, or individuals occupying microhabitats within

a unit that may have variability in detection probability beyond that explained by the unit-level covariates. We altered the scale of the beta distribution parameters to introduce more/less within-unit heterogeneity in detection probability. This has the effect of creating over-dispersion in the counting process and violates the assumption of strict binomial sampling (simulation block C; a similar approach was used by Martin et al. 2011). If  $a'$  and  $b'$  are the parameters of the beta distribution governing the mean and heterogeneity in detection probability in a given unit, then the expectation for any given group within the unit is  $a'/(a' + b')$  and the beta-binomial process approaches the binomial process as  $a' + b' = B' \rightarrow \infty$ ; we altered this sum ( $B'$ ) to introduce more/less over-dispersion and obtained the components as  $a' = \psi B'$  and  $b' = (1 - \psi)B'$ , where  $\psi$  is the overall expected detection probability for that unit as predicted by the true logit-linear model and unit-specific covariates. We used  $B'$  values of  $1 \times 10^{10}$  to represent no over-dispersion, and 20, 10, and 5 to represent “little”, “some”, and “lots” levels of over-dispersion, respectively.

In another block of scenarios (block D), we violated binomial sampling in an alternative way by allowing individuals to be double counted: individuals in a unit had some probability (one of 0, 0.05, 0.1, or 0.02) of being double counted conditional on being counted once. For an additional block of scenarios (block F), we added extra unit-level random effects (logit-normal scale) to the true detection probability in each unit that were not included in the estimation model to simulate the effects of unmonitored covariates. These effects were mean zero and had standard deviation values of 0, 0.1, 0.3, and 0.5 to represent no, “little”, “some”, and “lots” levels of variability caused by covariates not included in the analysis, respectively.

#### 1.4.3 Estimation models

We fitted two estimation models to each simulated data set. One model exactly mimicked the integrated approach described in Section 2.2 of the main text and the other differed only by using the maximum likelihood estimate of abundance from mark-recapture data as known without error. We refer to the latter approach as the “external” abundance estimation approach and the former as the “integrated” approach. In one block of scenarios (block A), the estimation models were constrained to include only the truly non-zero effect covariates and in all other scenarios (those in blocks B – H) the indicator variable selection and model-averaging framework described in Section 2.2.3 of the main text was used.

#### 1.4.4 Performance metrics

For all observations from each data set, we obtained the model fitted values (for training data) or predicted values (prediction data) for detection probability ( $\hat{p}_i$ ) and abundance ( $\hat{N}_i = y_i/\hat{p}_i$ ) and calculated the error from the true quantity (error = estimate - true value). We used posterior medians from each of the two models separately as the point estimates in these calculations. We summarized errors within each simulated data set using the median proportional error (MPE; error/true value) as a measure of accuracy (MPE should be near zero if method is accurate) and the median absolute proportional error (MAPE; |error|/true value) as a measure of precision (smaller MAPE reflects greater precision). Across models and scenarios and grouped by whether the data were in the training or prediction sets, we compared the resulting distributions of MPE and MAPE for detection probability and abundance. We compared the standard deviation of site-level random effects to the true value to investigate which cases tended to estimate more or less variability unaccounted for by fixed effects. To summarize performance with respect to variable selection, we calculated how frequently the approach placed high weight (posterior probability of  $\omega > 0.5$ ) on covariates with truly

non-zero effects and placed low weight (posterior probability of  $\omega < 0.5$ ) on covariates with truly zero effects. Finally, we calculated the fraction of true values that fell within the obtained credible intervals (prediction set only) at the 95% level as a measure of coverage – if model accounting for uncertainty is ideal, then true values should fall within the 95% credible intervals for 95% of the predictions within a data set.

## 2 Additional results

### 2.1 Empirical model fit/convergence

Fit of the integrated model to the empirical data was good (Fig. 6), and we did not detect any evidence of a lack of fit – certainly nothing that would indicate egregious inconsistencies between the model assumptions and the data. Of the three capture histories (i.e., elements of the multinomial vector  $\mathbf{z}_i$ ) the model fitted to capture history ‘10’ most closely. In general, integrated model estimates of abundance were similar to abundance estimates obtained by applying a Huggins conditional maximum likelihood estimator external to the integrated model (Fig. 7) – discrepancies in these two estimates are due to the need of the integrated model to explain sampling variability in both the mark-recapture and snorkel data. Convergence of MCMC sampling was also quite good – all estimated parameters had  $\hat{R}$  statistics less than 1.01 and the majority of parameters had effective sample sizes (for each the 50th, 2.5th, and 97.5th percentiles) well above 1,000 and all greater than 400 (the minimum number adequate suggested by Vehtari et al. 2021).

### 2.2 Detailed simulation output

The figures showing the patterns described in the following text are displayed at the end of this supplement. A broad-level overview of simulation results is provided in the main text – this text highlights the specific finding of each block of scenarios.

#### 2.2.1 Block A: Effect of sample size without model uncertainty

When the models were forced to consider only covariates that truly had a non-zero effect on detection probability, the primary effect of increasing sample size from 25 channel units to 50 or 100 channel units was to improve the precision of predictions (Fig. 8). This is seen by reduced ranges of MPE outcomes and lower overall values of MAPE in both predicted detection probability and abundance. Contrary to what might be expected, increasing sample sizes also had the effect of reducing credible interval coverage for the prediction set, primarily for abundance.

#### 2.2.2 Block B: Effect of sample size with model uncertainty

Increasing sample size resulted in a larger improvement in model performance when the true model was unknown (block B; Fig. 9) than when the true model was known (block A). In particular, the scale of the errors (MAPE) made when predicting abundance at sites without mark-recapture data was more responsive to increasing sample size in block B than in block A. For both estimation methods, the ability to assign high weight to covariates with truly non-zero effects was a function of the sample size, but the ability to identify which covariates had a truly zero effect was largely unaffected.

#### 2.2.3 Block C: Effect of unaccounted over-dispersed binomial counts

Challenging the models with over-dispersed counts of varying degrees had little effect on the accuracy of either estimation method, but had a much more substantial effect on the precision (Fig.

10). For example, the average MAPE of abundance predictions for scenario 9 (highly over-dispersed counts) was nearly double that of scenario 6 (equivalent in all ways to scenario 9 except that counts were not at all over-dispersed). The ability of the integrated model to correctly place low weight on unimportant covariates was sensitive to the amount of over-dispersion, however not as much so as for the external abundance method – a similar result was found for credible interval coverage. Both methods tended to overestimate the amount of variability that should be attributed to the site-level random effect in the face of over-dispersion, and the size of the errors increased with the amount of over-dispersion. Additionally, there was a slight tendency for the integrated model to have smaller errors for this parameter.

#### 2.2.4 *Block D: Effect of double-counted individuals*

When the possibility of double-counting individuals in the count survey was introduced, the primary effect was to result in positive biases in the estimated and predicted detection probabilities (Fig. 11). This makes intuitive sense: mark-recapture data remained the same, yet the observer reported counting more individuals, leading the model to believe that a larger fraction of the population was counted than truly was. Estimation and prediction of abundance was not affected nearly to the same degree (Fig. 11); this is because double-counting was possible in all count surveys, including those with and without mark-recapture sampling (training and prediction samples, respectively). So although we found the estimates of count survey detection probability to be positively biased relative to the true value in the presence of duplicate counts, largely unbiased predictions of abundance can still be obtained so long as the prevalence of double-counts is the same in prediction samples as in the training samples.

#### 2.2.5 *Block E: Effect of mark-recapture data quality*

Low quality mark-recapture data were simulated by having a low probability of capture in mark-recapture sampling (scenario 13; expected probability of capture of 0.2) which produced low sample sizes, which are known to create biases for two-sample closed population abundance estimators. However, the errors made by the integrated model for this most extreme poor data quality case were much larger than for the external approach (Fig. 12). Presumably this is due to the incredibly poor information to estimate  $p_{i,1}$  and  $p_{i,2}$ , which caused the beta(1,1) prior we used to become informative such that the truly low values of 0.2 had posterior expectations closer to the prior expectation of 0.5. Recognizing this, we recommend future work be applied to identifying less informative priors for estimation of these parameters in the case of incredibly low sample sizes. Very high mark-recapture data quality (scenario 15) resulted in nearly perfect estimates for both approaches.

#### 2.2.6 *Block F: Effect of unobserved covariate effects*

Introducing additional effects of covariates that the models were completely ignorant of had little effect on the performance of either estimation approach in terms of accuracy or ability to correctly identify important covariates (among those collected; Fig. 13). The primary effect was with increasing degrees of unaccounted covariates, the precision of both methods became lower. Similar to block C (over-dispersed binomial counts), both methods tended to over-estimate the amount of random variability that should be attributed to site-level effects, but the integrated model to a slightly lesser degree.



### 2.2.7 Block G: Effect of ignored behavioral avoidance to recapture

Ignoring the presence of a recapture avoidance behavioral response affected the performance of both methods, but to a much lesser degree for the integrated model than for the external approach (Fig. 14). The specific consequence was positively biased estimates of abundance and negatively biased estimates of detection probability. Presumably, the integrated model performed better in this regard because of its need to have satisfactory fits to both the count data and mark-recapture data.

### 2.2.8 Block H: Effect of accounted behavioral avoidance to recapture

By conducting an additional step to select the appropriate mark-recapture model with WAIC prior to fitting the detection probability model, we found that the biases displayed in block G were vastly reduced or eliminated in the case of the integrated model (Fig. 15). The WAIC approach was able to select the correct mark-recapture assumptions in only 10% of the simulated data sets under scenario 22 ( $p_{i,2} = p_{i,1}$  and  $c_{i,2} = 0.9 \cdot p_{i,2}$ ). In this scenario, model  $M_0$  was primarily selected, which makes intuitive sense given the similarity between the true model  $M_b$  and  $M_0$ . However, in scenarios 23 and 24 where  $c_{i,2} = 0.7 \cdot p_{i,2}$  and  $c_{i,2} = 0.5 \cdot p_{i,2}$ , respectively, model  $M_b$  was overwhelmingly selected (correctly) as the best (99% and 100% of replicates, respectively). When the integrated model correctly used the assumptions of model  $M_b$ , the biases apparent in the block G scenarios all but disappeared. This is in stark contrast to the external approach, which continued to show positive bias in predicted abundance and negative bias in detection probability – the cause of this difference is presently unclear.

## References

- Bürkner, P.-C., Gabry, J., Kay, M., and Vehtari, A. 2020. *posterior: Tools for Working with Posterior Distributions*. R package version 0.1.3, URL: <https://mc-stan.org/posterior>.
- Dorazio, R. M., Gotelli, N. J., and Ellison, A. M. 2011. Modern methods of estimating biodiversity loss from presence-absence surveys. In Grillo, O., editor, *Biodiversity Loss in a Changing Planet*, pages 277 – 302. InTech. URL: <https://www.intechopen.com/books/biodiversity-loss-in-a-changing-planet/modern-methods-of-estimating-biodiversity-from-presence-absence-surveys>.
- Martin, J., Royle, J. A., Mackenzie, D. I., Edwards, H. H., Kéry, M., and Gardner, B. 2011. Accounting for non-independent detection when estimating abundance of organisms with a Bayesian approach. *Methods in Ecology and Evolution*, 2(6):595–601. doi: 10.1111/j.2041-210x.2011.00113.x.
- Staton, B. 2020. *postpack: Utilities for Processing Posterior Samples Stored in ‘mcmc.lists’*. R package version 0.5.2, URL: <https://bstaton1.github.io/postpack/>.
- Vehtari, A., Gelman, A., Simpson, D., Carpenter, B., and Bürkner, P.-C. 2021. Rank-normalization, folding, and localization: An improved Rhat for assessing convergence of MCMC. *Bayesian Analysis*. doi: 10.1214/20-BA1221.

**TABLE 3.** Posterior model probabilities obtained from different combinations of  $\omega$  terms for the Grande Ronde basin empirical analysis. Models are shown as rows; the symbols ■ and × are used to show which covariates were included or excluded from the model, respectively. Only models with posterior probabilities greater than 0.01 are shown.

Covariate								Pr(Model)
Chinook	Pool	LWD2	LWD3	VIS1	VIS3	Depth	Depth × Pool	
■	■	×	×	×	■	■	■	0.436
■	■	×	■	×	■	■	■	0.189
■	■	■	×	×	■	■	■	0.105
■	■	×	×	■	■	■	■	0.081
■	■	■	■	×	■	■	■	0.037
■	■	×	■	■	■	■	■	0.034
■	■	■	×	×	×	■	■	0.031
■	■	×	×	×	×	■	■	0.021
■	■	■	×	■	■	■	■	0.020
■	■	×	■	×	×	■	■	0.017
■	■	■	■	×	×	■	■	0.010

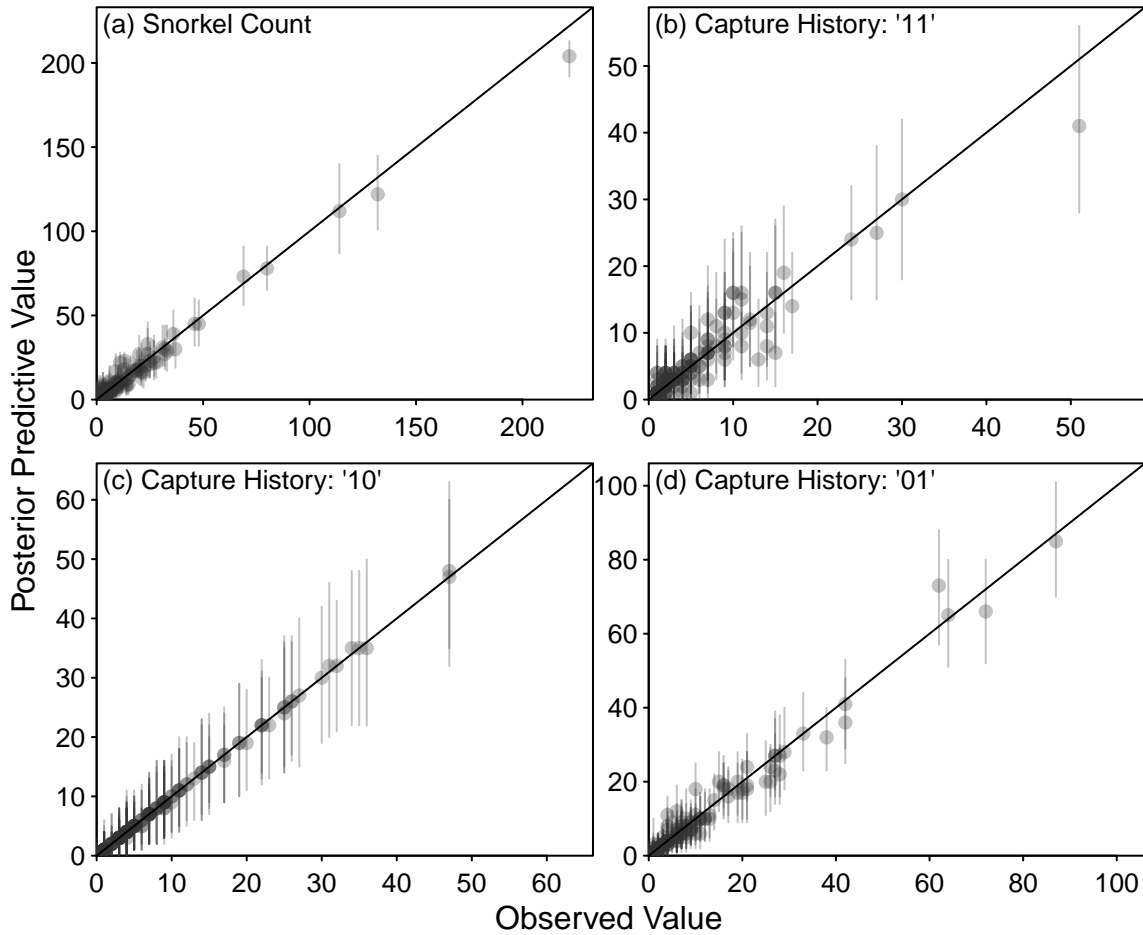


**FIGURE 6.** Posterior median predictive values versus observed values in each observation for (a) the snorkel count data and (b) the number of fish with mark-recapture history '11', (c) the number of fish with history '10', and (d) the number of fish with history '01'. The y-axis is similar to a fitted value, but includes all sources of uncertainty in the model; error bars represent 95% equal-tailed credible intervals.

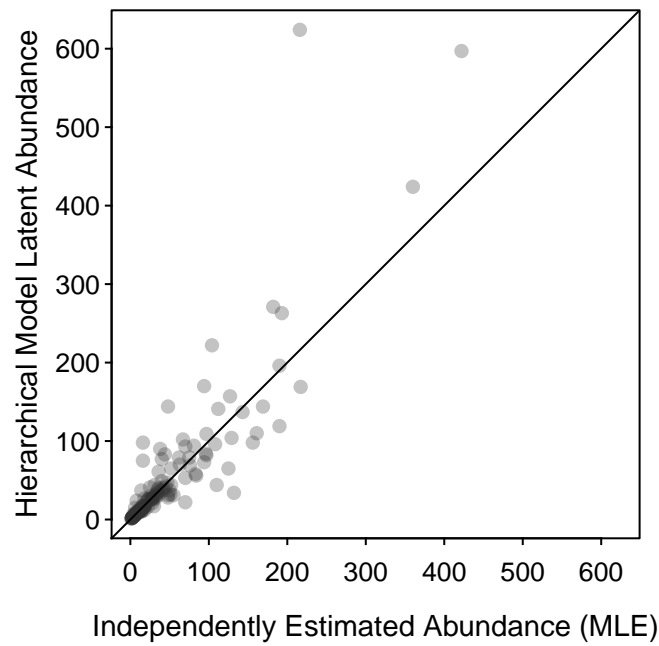


**FIGURE 7.** Comparison of posterior median abundance estimates from the integrated snorkel detection probability model (y-axis) and independent conditional maximum likelihood estimators (x-axis) fitted to empirical data from the Grande Ronde basin.

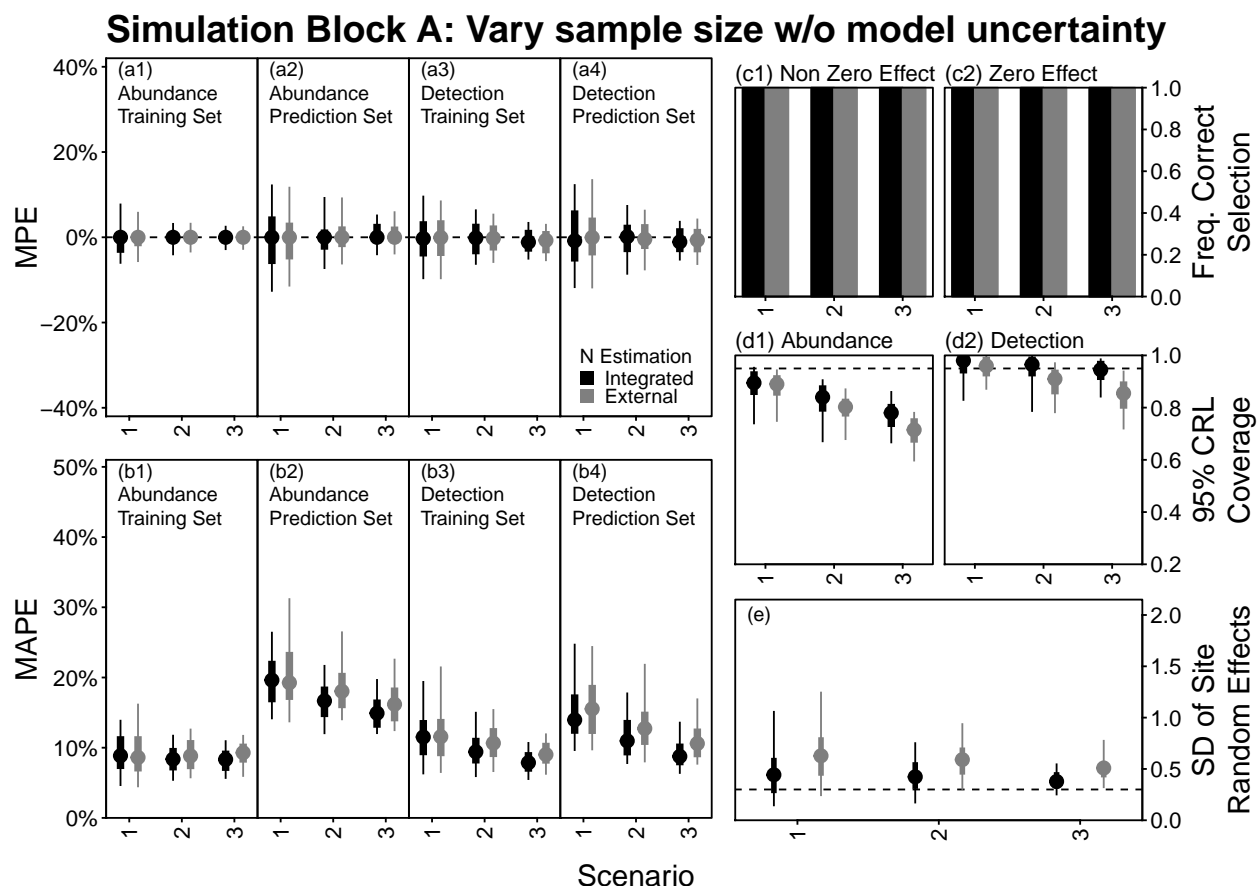


**FIGURE 8.** Summary of output from block A of the simulation trials, in which all model assumptions were met and the sample size was varied (scenario 1 = 25 training data sample size; scenario 2 = 50; scenario 3 = 100), but it was assumed the analyst knew exactly which covariates should be included (i.e.,  $\omega$  fixed rather than estimated). Points represent medians across 100 replicate data sets, thick error bars represent the central 50% of outcomes, and thin error bars represent the central 95% of outcomes. (a) Distribution of median percent errors (MPE) across replicate data sets for abundance (a1 and a2) and detection probability (a3 and a4) – dashed line at 0 shows no error. (b) Same layout as (a), except for median absolute percent errors (MAPE). (c1) Proportion of the simulations in which truly non-zero effects were assigned probability of inclusion greater than 0.5. (c2) Proportion of the simulations in which truly zero-valued effects were assigned probability of inclusion less than 0.5. (d) Distribution of coverage statistics for abundance (d1) and detection (d2) – i.e., the fraction of 95% credible intervals that contained the true value (reference dashed line at 0.95 shows optimal coverage). (e) Distribution of estimated standard deviation of site-level random effects – dashed line shows the true value used to simulate the data.

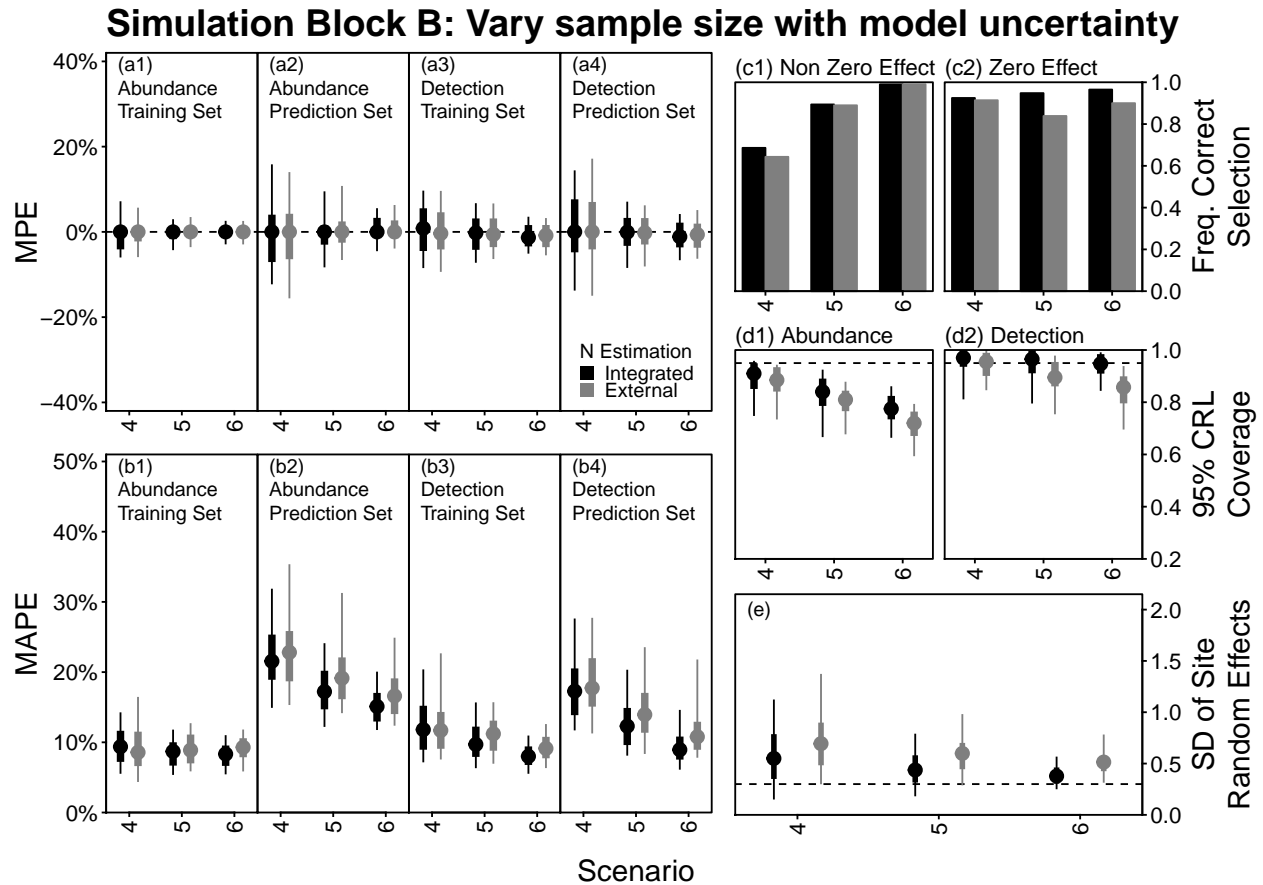


**FIGURE 9.** Summary of output from block B of the simulation trials, in which all model assumptions were met and the sample size was varied (scenario 4 = 25 training data sample size; scenario 5 = 50; scenario 6 = 100), but it was assumed that analyst did not know exactly which covariates should be included (i.e.,  $\omega$  estimated). See the caption in Fig. 8 for a description of the various panels.

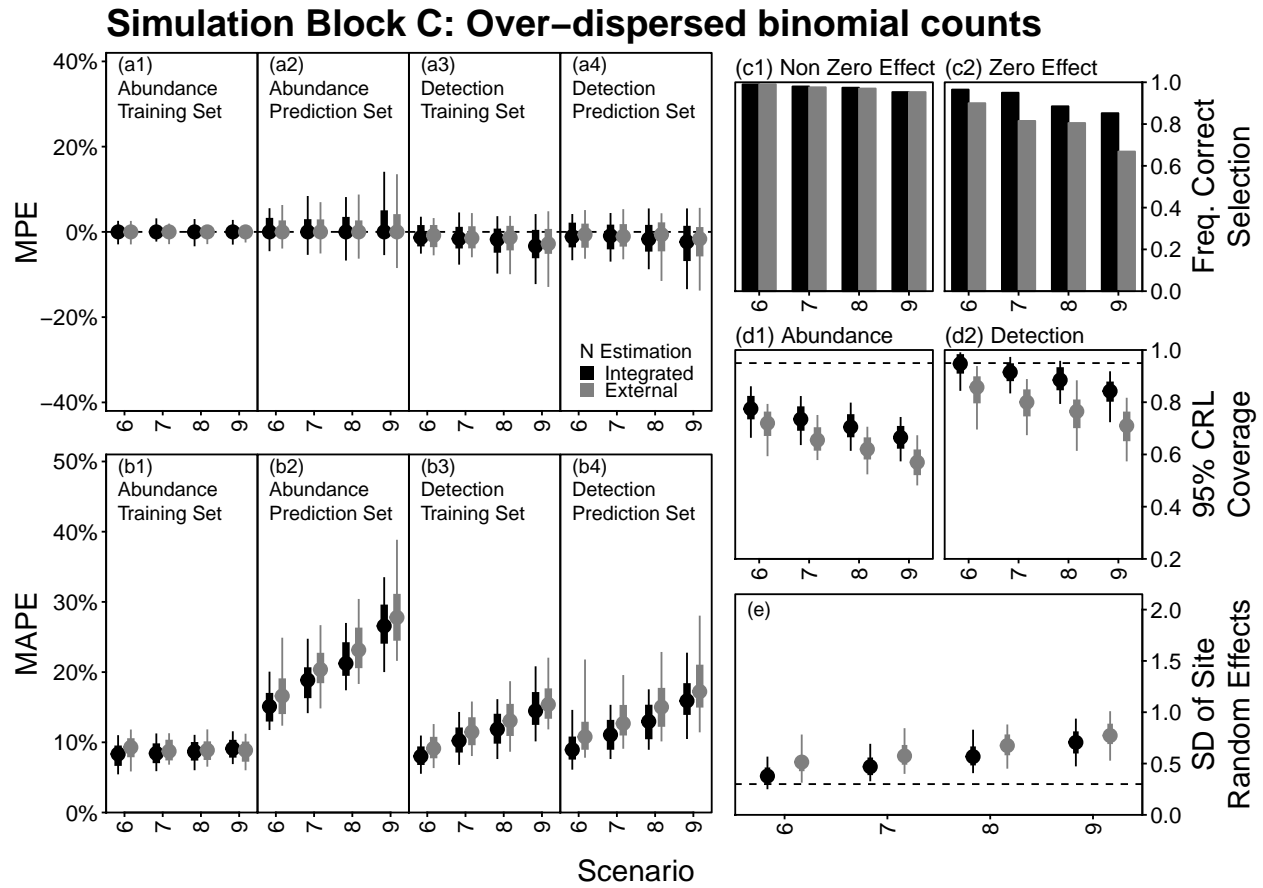


**FIGURE 10.** Summary of output from block C of the simulation trials, in which count surveys were over-dispersed to varying degrees (scenario 6 = no over-dispersion; scenario 7 = little; scenario 8 = some; scenario 9 = lots), but otherwise identical to scenario 6. See the caption in Fig. 8 for a description of the various panels.



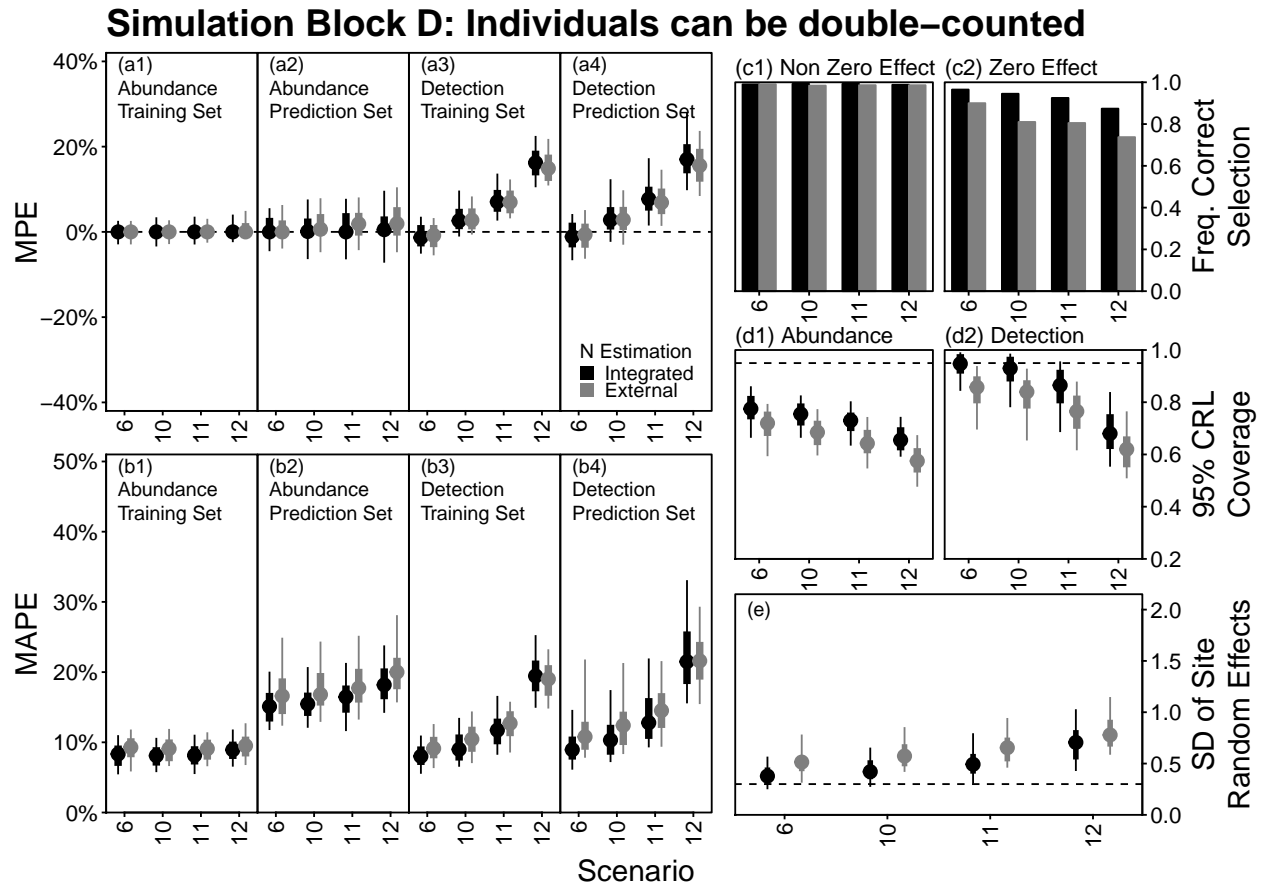


**FIGURE 11.** Summary of output from block D of the simulation trials, in which it was possible to double count individuals during the count surveys with varying probabilities (scenario 6 = 0; scenario 10 = 0.05; scenario 11 = 0.1; scenario 12 = 0.2), but otherwise identical to scenario 6. See the caption in Fig. 8 for a description of the various panels.

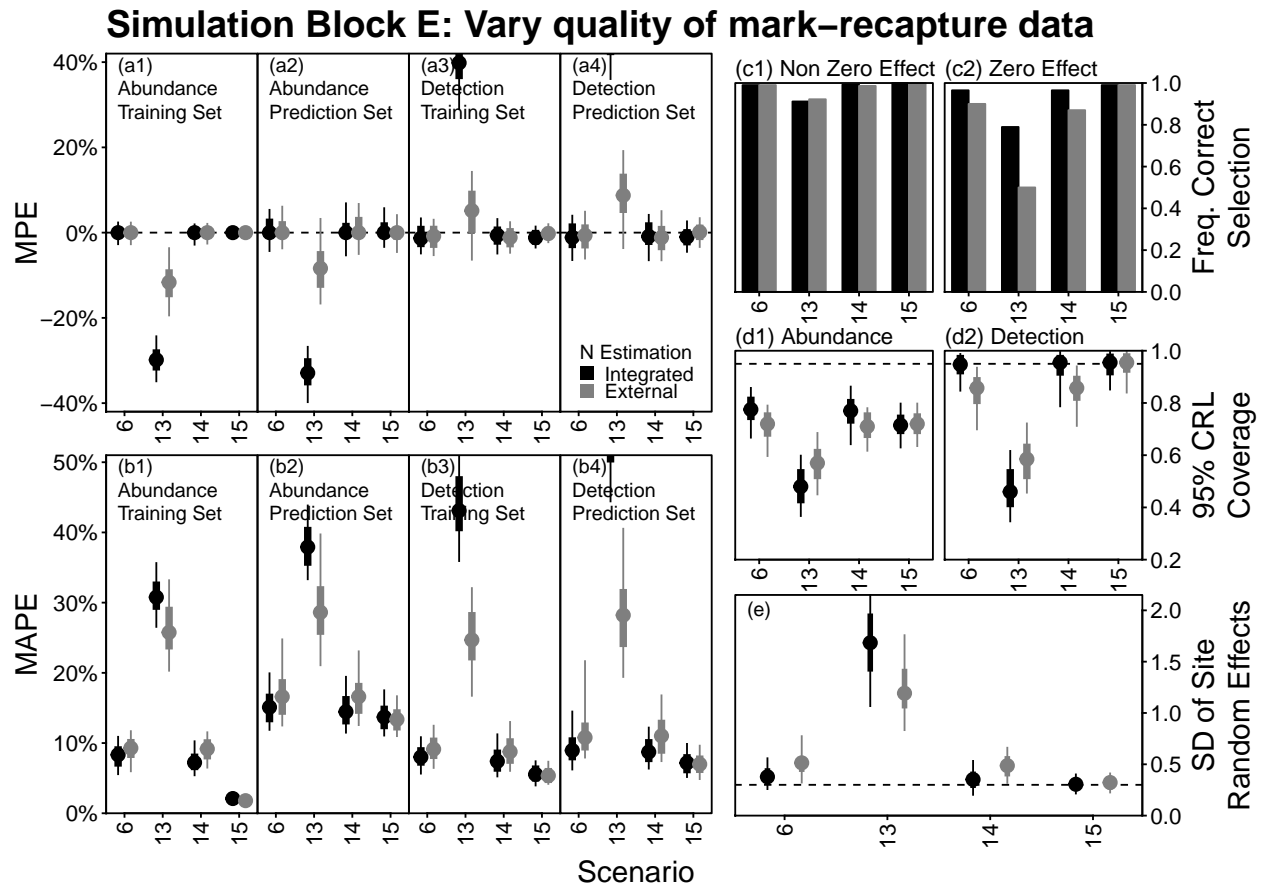


**FIGURE 12.** Summary of output from block E of the simulation trials, in which the probability of capture were simulated with low among-unit variability but of varying magnitudes (scenario 6 = expected capture probability of 0.5 but with high among-unit variability; scenario 13 = expected capture probability of 0.2; scenario 14 = 0.5; scenario 15 = 0.8), but otherwise identical to scenario 6. See the caption in Fig. 8 for a description of the various panels.

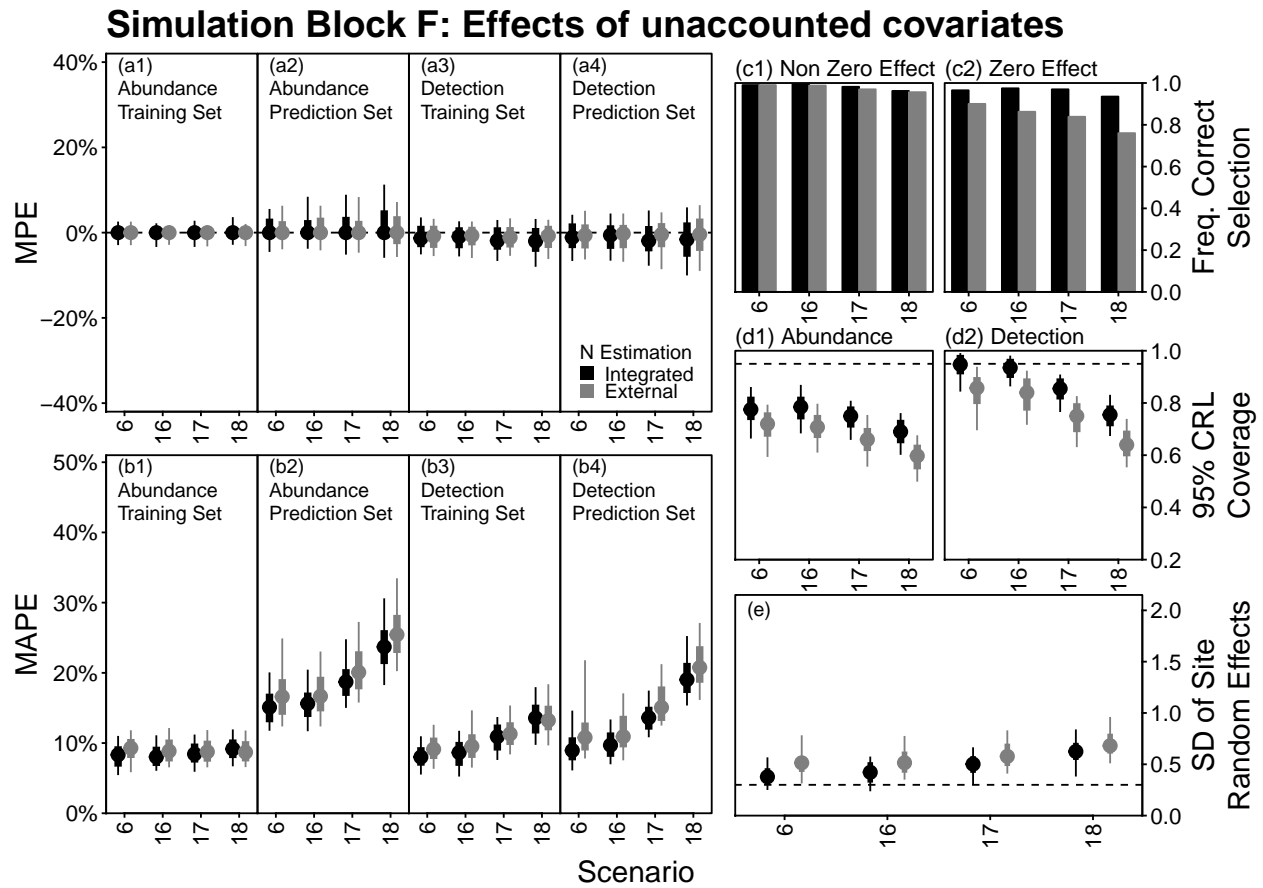


**FIGURE 13.** Summary of output from block F of the simulation trials, in which additional variability was added to the detection probability model to simulate the effects of important but unmonitored covariates (scenario 6 = no extra variability; scenario 16 = logit-scale SD of unit-level random effects set at 0.1; scenario 17 = SD set at 0.3; scenario 18 = SD set at 0.5), but otherwise identical to scenario 6. See the caption in Fig. 8 for a description of the various panels.

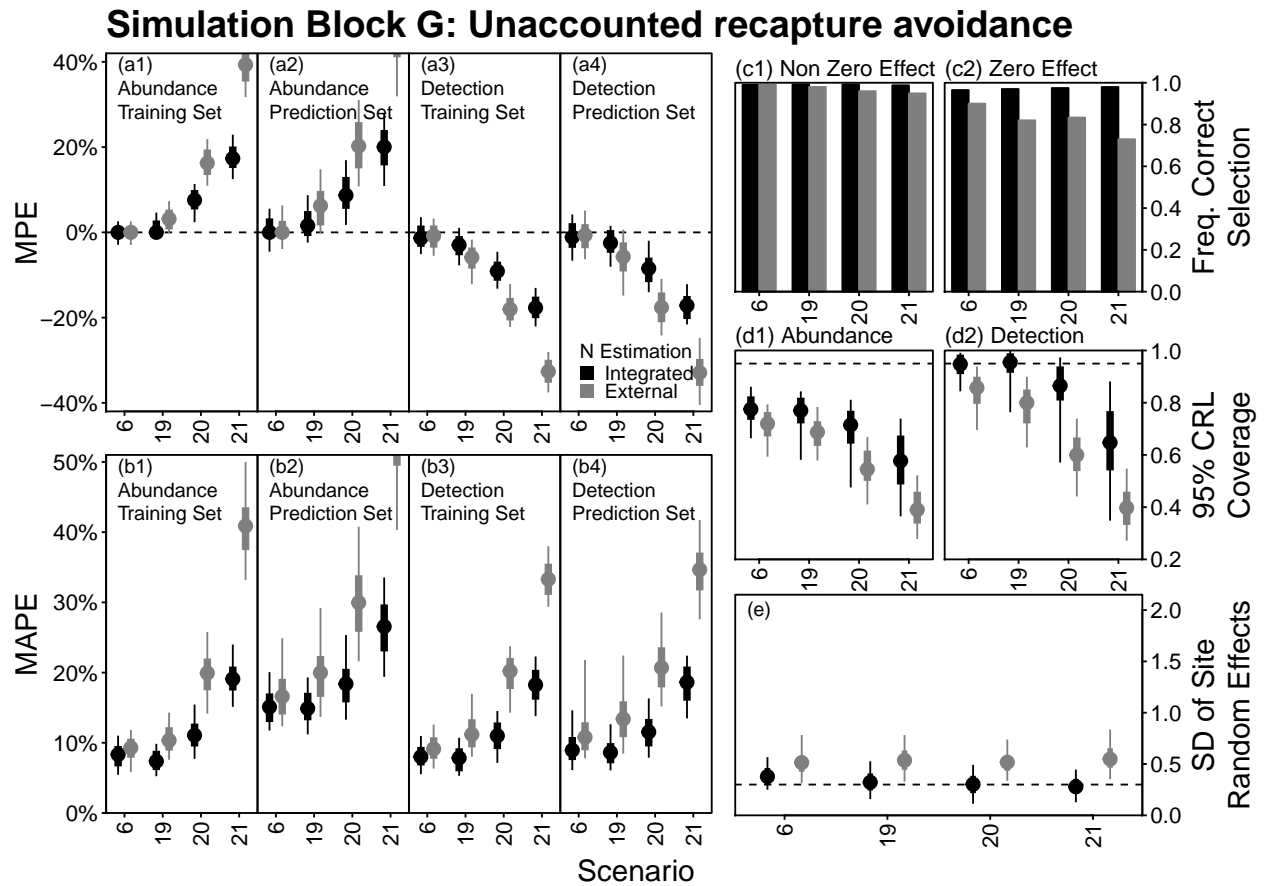


**FIGURE 14.** Summary of output from block G of the simulation trials, in which mark-recapture data were collected with varying degrees of trap shy behavioral responses but the estimation models assumed it was absent (scenario 6 = no behavioral response; scenario 19 = recapture probability set at 0.9 times initial capture probability; scenario 20 = recapture probability 0.7 times initial capture probability; scenario 21 = recapture probability 0.5 times initial capture probability), but otherwise identical to scenario 6. See the caption in Fig. 8 for a description of the various panels.

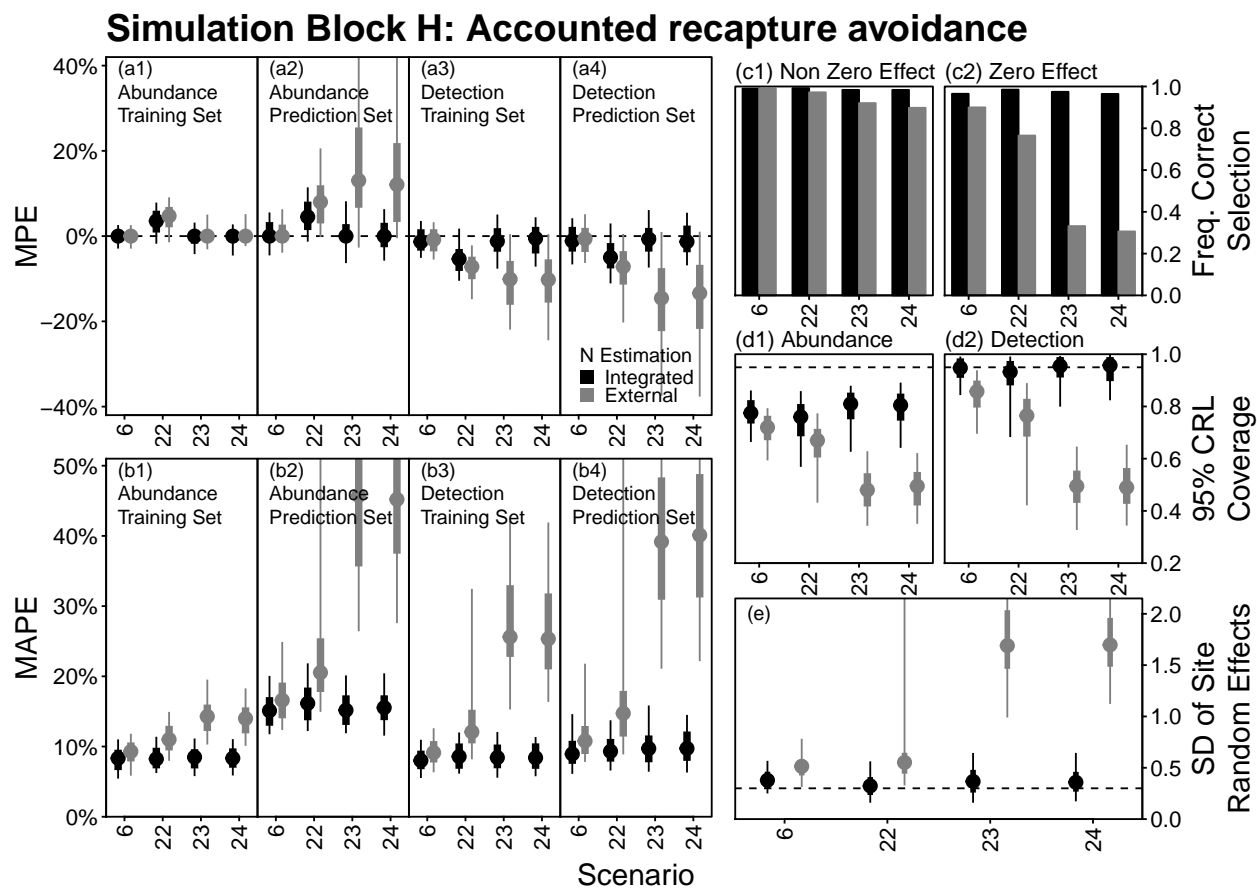


**FIGURE 15.** Summary of output from block H of the simulation trials, in which mark-recapture data were collected with varying degrees of trap shy behavioral responses and the assumption made by the estimation models was first selected using WAIC (scenario 6 = no behavioral response; scenario 22 = recapture probability set at 0.9 times initial capture probability; scenario 23 = recapture probability 0.7 times initial capture probability; scenario 24 = recapture probability 0.5 times initial capture probability), but otherwise identical to scenario 6. See the caption in Fig. 8 for a description of the various panels.

**Appendix D – Published Journal of Animal Ecology paper on spatial patterns and drivers of juvenile Chinook Salmon size and growth**

## **Temperature, emergence phenology, and consumption drive seasonal shifts in fish growth and production across riverscapes**

Matthew J. Kaylor<sup>1</sup>, Casey Justice<sup>2</sup>, Jonathan B. Armstrong<sup>1</sup>, Benjamin A. Staton<sup>2</sup>, Lauren A. Burns<sup>2</sup>, Edwin Sedell<sup>3</sup>, Seth M. White<sup>2</sup>

<sup>1</sup> Oregon State University, Department of Fisheries and Wildlife, Corvallis, Oregon

<sup>2</sup> Columbia River Inter-Tribal Fish Commission, Portland, Oregon

<sup>3</sup> Oregon Department of Fisheries and Wildlife, East Region Fish Research, La Grande, Oregon

### **Abstract**

Changes in biophysical conditions through time generate spatial and temporal variability in habitat quality across landscapes. For river ecosystems, researchers are increasingly able to characterize spatial and temporal patterns in habitat conditions, referred to as shifting habitat mosaics, yet rarely demonstrate how this translates into corresponding biological processes such as organism growth and production. We assessed spatial patterns and processes determining seasonal changes in juvenile Chinook Salmon (*Oncorhynchus tshawytscha*) size, growth, and production over 30-40 km in two NE Oregon subbasins. We quantified seasonal patterns of growth by combining estimated emergence dates and body size distributions in July and September. We then used analysis of bioenergetics, empirical fish diets, and spatial models incorporating temperature, habitat, and population density to evaluate mechanisms driving spatio-temporal patterns of growth. Lastly, we quantified seasonal contributions to individual fish growth and to total production as a function of position within the stream network. Spatial heterogeneity in incubation temperatures corresponded to later emergence timing with distance upstream in both subbasins. During spring, estimated growth rates decreased with distance upstream, and coupled with emergence patterns, resulted in a pronounced longitudinal gradient in body size by July. During summer, spatial patterns of growth reversed, with greater diet ration sizes and growth efficiencies upstream than downstream. These opposing spatio-temporal patterns of emergence timing and seasonal growth rates produced spatial gradients in the proportion of fish growth achieved in spring versus summer, with up to 80% of an individual's growth occurring prior to July at downstream sites but as low as 10% at upstream sites. Coupling longitudinal patterns of fish density and growth revealed that in one subbasin the majority of total production occurred in spring, while in the other, in which fish were concentrated in headwaters where they emerged late, the majority of production occurred in summer. While recent work has emphasized inter-annual shifts in

spatial patterns of fish production, this study demonstrates seasonally reversing gradients of fish growth and production across riverine landscapes, and reveals important contributions of warmer, downstream habitats to overall production that occurred during cooler times of the year.

## **Introduction**

Spatial heterogeneity in physical conditions across landscapes interacts with temporal variation ranging from climate forcing (Dobrowski, 2011) to diel temperature fluctuations (Huey, 1991; Sears et al., 2011) to influence dynamics of habitat quality. The result is a shifting habitat mosaic (SHM), in which optimal conditions are not static, but instead are continually redistributed across landscapes (Stanford et al., 2005). Studies evaluating how species interact with and respond to SHMs have revealed a variety of important ecological phenomena. For example, thermoregulating poikilotherms (e.g., most reptile and fish species) exploit diel shifts in thermal microhabitats to prolong their exposure to optimal temperatures (Cowles & Bogert, 1944), and mobile consumers exploit intra-annual shifts in optimal foraging conditions by tracking the distribution of resources through time (Aikens et al., 2017; Deacy et al., 2016). The heterogeneity generated by SHMs can confer stability at larger scales through portfolio effects, as seen in the habitat composition of river floodplains (Whited et al., 2007) or the reliability of fisheries stocks integrating asynchronous population productivity (Brennan et al., 2019; Schindler et al., 2010).

Understanding SHM's and how animals respond to them requires characterizing physical and biological aspects of the landscape across both space and time. This can be particularly challenging for freshwater ecosystems, where remote sensing is limited and organisms are often difficult to observe or sample. However, recent work across a large network of connected lakes and rivers showed how intra- and inter-annual shifts in climatic drivers generate corresponding shifts in the distribution of fish production (Brennan et al., 2019). At a finer spatial scale (within a single tributary stream), fish moved among floodplain habitats at weekly timescales to track optimal temperatures for growth as water levels receded (Baldock et al., 2016). Despite calls to generate continuous data throughout rivers (i.e., intermediate spatial scales; 10s-100s of kilometers) to understand reciprocal relationships between pattern and process (i.e., Fausch et al., 2002), studies have not related spatio-temporal patterns of habitat quality to impacts on organism growth and production at this scale.

The mechanisms underlying temporal shifts in productivity at large spatial scales may often be too complex to resolve or to apply to other systems (Rogers et al., 2013; Schindler & Hilborn, 2015), yet the spatial and temporal dynamics of water temperature in rivers ecosystems are relatively predictable and their effects on fish physiology are well understood. In particular, temperature usually increases with distance downstream (but not



always; Fullerton et al., 2015) and predictably changes throughout seasons in temperate regions. Most freshwater biota are poikilotherms, and temperature exerts strong control on growth potential as it exponentially increases metabolic costs and has a dome-shaped effect on digestive capacity (which sets maximum consumption rates). From these relationships, spatial heterogeneity in temperature can be translated into spatial heterogeneity in growth potential (Brandt et al., 1992; Sloat et al., 2005), yielding optimal temperatures for growth that shift seasonally throughout a watershed (Armstrong et al., *In press*).

Growth represents surplus in the energy budget, i.e., the difference between gains from consumption and losses from metabolic energy expenditures. While growth potential can be modeled using heterogeneity in temperature alone, realized growth depends on the interaction between temperature and consumption rates, which should increase with prey quantity or quality and decrease with consumer density (i.e., competition; Einum et al., 2008, Crozier et al., 2010). Spatially explicit bioenergetics models have been applied to predict summer growth across river systems as a function of temperature and consumption rates (Falke et al., 2019), but consumer density is rarely quantified at these scales and consumption rates can be highly variable at daily and seasonal time scales (Hansen & Beauchamp, 2015). Previous studies have estimated riverscape heterogeneity in growth rates based on single snapshots of body size (Anderson et al., 2008; Pess et al., 2011), but these do not reveal how growth accrues through time; juvenile fish body size may be more correlated with the duration of the growth interval – determined by emergence timing – rather than growth rates (Egglishaw & Chackley, 1977). Studies that do quantify temporal variation in growth typically trade off spatial contrast to allow tracking growth over longer periods, relying on a handful of sites to represent the range of conditions experienced by consumers across space.

Increased understanding of riverscape patterns of growth and the processes underlying these patterns could provide much needed information for designing conservation strategies. For example, Pacific salmon (*Oncorhynchus* spp.) are threatened or endangered throughout much of their southern range, and body size is linked to survival at multiple freshwater and marine life stages (Ebersole et al., 2006; Holtby et al., 1990; Zabel & Achord, 2004). Knowledge of riverscape patterns and processes of growth and size could help practitioners strategically allocate limited resources within a watershed to restore habitat and recover populations. Information on the riverscape phenology of growth is needed because freshwater climate adaptation is increasingly focused on summer conditions, evaluating streams based on growth conditions during a narrow, albeit important, time window (Isaak et al., 2015; Ruesch et al., 2012). As the coolest summer habitat is often prioritized in conservation planning, there is a need to evaluate whether and to what extent warmer portions of the riverscape (in summer) contribute to growth and production at other times of the year.

In this study, we characterize spatial and temporal patterns of juvenile Chinook Salmon (*Oncorhynchus tshawytscha*) growth across a riverscape and link these patterns to a suite of direct (e.g., temperature, consumption, growth duration) and indirect factors (e.g., density, spawn timing, winter incubation temperature) we expected to explain variation in growth at these scales (Figure D1). Specifically, we (1) quantified seasonal patterns of growth at sites spanning 30-40 kilometers in each of two NE Oregon subbasins by combining estimated emergence dates and body size distributions at two points in time: July and September. We then (2) explored the mechanisms underlying spatio-temporal patterns in growth through analysis of bioenergetics, evaluation of fish diets, and spatial models incorporating temperature, habitat, and population density. Lastly, we (3) evaluated seasonal contributions to individual fish growth and to total production as a function of position within the stream network.

## **Methods**

### *Study area and species*

The study was conducted in two subbasins (watersheds with distinct populations of Chinook Salmon) of the Grande Ronde River in NE Oregon: the upper Grande Ronde River (UGR; drainage area = 1,896 km<sup>2</sup>) and Catherine Creek (CC; drainage area = 1,051 km<sup>2</sup>). The region is characterized by cold winters in which most precipitation falls as snow, and hot, dry summers with little precipitation. Snowmelt drives peak flows occurring in spring that transition to base flow conditions from July through October – a period coinciding with maximum stream temperatures (Justice et al., 2017). Historically, these subbasins supported abundant returns of Spring Chinook Salmon; however, returns have declined precipitously owing to a range of human impacts, prompting the listing of Snake River Spring Chinook Salmon in 1992 as threatened under the Endangered Species Act. Spring Chinook Salmon spawn between early August and mid-September, with spawning occurring later in warmer river sections. Juveniles emerge from the substrate in the spring or early summer and the majority spend approximately one year rearing in freshwater before migrating to the ocean the following spring.

### *Sampling design and site selection*

Our target sample size to quantify juvenile Chinook Salmon (i.e., parr) density, size, and growth was 60 sites (30 per subbasin). We established a set of candidate sites based on areas associated with previously surveyed habitat monitoring and fish sampling within the geographic extent of Chinook Salmon parr rearing (N = 91). We then assigned sites to five temperature strata based on modeled August water temperatures (Isaak et al., 2017; temperature range 11.7 – 18.4 °C) and we randomly selected approximately 12 sites (range = 7 – 16 as some strata did not contain enough sites) within each stratum. Initial sampling

revealed that some sites did not have sufficient parr abundance to capture and obtain a reasonable sample size to estimate mean size and growth rates (minimum criteria was 25 fish) and we therefore sampled nearby sites from the initial set of candidate sites when this occurred. Logistical constraints, including low abundance at many sites, reduced our sample size for size and growth rates to 53 sites: 27 sites in CC and 26 sites in UGR (Figure D2). We were able to estimate density at 59 of the original 60 sites: 30 in CC and 29 in UGR (Figure D2). We estimated fry emergence timing at a subset of the sites (four in each subbasin) representing the range of environmental conditions experienced by incubating and rearing Chinook Salmon.

#### *Emergence timing estimation*

To predict emergence timing, we used the Effective Value Model (Sparks et al., 2019) which accounts for variable temperature experienced during incubation:

$$E_i = 1/\exp [\log_e a - \log_e (T_i - b)]$$

where  $E_i$  is the daily contribution to development (0 to 1),  $T_i$  is the daily mean temperature, and  $\log_e a$  (6.872) and  $b$  (-0.332) are coefficients derived from Beacham and Murray (1990). Emergence was predicted to occur on the date in which the sum of first exceeded 1 (Sparks et al., 2019). Spawning date ranges were obtained from weekly redd (i.e., nests excavated by spawning salmon) surveys conducted continuously throughout each subbasin in 2018, as part of an Oregon Department of Fish and Wildlife monitoring program (Dowdy et al., 2019). For each site in which emergence timing was modeled, we used the dates of nearby observed redds to obtain a range of spawning dates corresponding to three spawning periods: early, middle (peak), and late spawning (Lisi et al., 2013). This approach allowed us to estimate emergence windows that accounted for variability in spawn timing.

#### *Field surveys*

We sampled each site to obtain mean parr size in July (7/9-7/18 in UGR; 7/22-8/1 in CC) and then again in September (9/6-9/12 in UGR; 9/13-9/24 in CC), approximately eight weeks later. We captured parr using snorkel-herding methods in which snorkelers herded fish into a seine net (Tattam et al., 2017). Captured parr were anesthetized, measured (fork length, nearest mm), and weighed (wet mass, nearest 0.1 g). We used changes in mean weight between July and September at each site to estimate summer growth rates. However, comparisons of growth rates among sites required standardization for fish size, as growth potential is linked to body size. We therefore used mass-standardized growth rates (MSGR; Ostrovsky, 1995), in which growth is scaled to the specific growth rate of a 1 g fish:

$$\text{MSGR (\% d}^{-1}\text{)} = ((W_2^b - W_1^b)/(b * t)) * 100$$

where  $W_1$  and  $W_2$  are the mean fish weight during the first and second sampling event, respectively,  $t$  is the number of days, and  $b$  is the allometric mass exponent for Chinook Salmon (0.338; Perry et al., 2015). We used a bootstrap method to estimate the standard error of MSGR wherein individual fish weights from each site were randomly resampled (with replacement) to obtain different plausible values of  $W_1$  and  $W_2$  and MSGR was calculated for each. Additionally, we estimated spring MSGR at each of the sites where emergence timing was predicted using the estimated dates of emergence, size at emergence ( $W_1 = 0.5$  g; Beacham & Murray, 1990), and size in July ( $W_2$ ). We calculated MSGR over the estimated range of emergence dates to obtain a reasonable estimate that accounted for variability in emergence timing.

To validate that using changes in mean parr weight between sampling events was an appropriate method to characterize site-specific growth rates, we compared growth rates estimated using the above method to individual growth rates assessed using parr tagged with 12 mm passive integrated transponder (PIT) tags at 21 sites (2711 parr tagged). We found strong evidence for a positive relationship between the two methods ( $r^2 = 0.74$ ,  $p < 0.001$ ) and the slope did not differ from 1 (slope = 0.88; 95% CI = 0.65-1.11; Figure D-A1); we therefore proceeded using changes in mean weight to approximate MSGR.

We estimated Chinook Salmon parr densities (fish  $100\text{ m}^{-1}$ ) and habitat attributes at each site by conducting snorkel and habitat surveys. Each site had a length of approximately 15x the average bankfull channel width. Sites were delineated into habitat units (e.g., pools, riffles, runs) and snorkelers progressed worked upstream counting all salmonids. For each unit, we measured length (parallel to flowing water), width (at three transects perpendicular to flow), and depth (at 5 equidistant locations along each transect), and enumerated large wood (greater than 3.0 m in length and 0.15 m in diameter) within the bankfull channel. Snorkel counts for each unit were translated to abundance using predictions of detection probability which incorporated habitat attributes fitted to paired mark-recapture and snorkel count data collected from these two subbasins in previous years (Staton et al. *in review*).

Variation in consumption rates were expected to be an important driver of patterns in growth (Figure D1). Given sampling constraints in spring (high flows, parr not large enough to sample with non-lethal methods), we were only able to empirically sample diets in summer. Diets were collected at eight sites in each subbasin at three time periods: early August, late August, and early September. For each sampling event, 12 diet samples were obtained using non-lethal gastric lavage (Meehan & Miller, 1978) for a total of 36 samples per site and 576 total diet samples. Samples were preserved in 90% ethanol until they were processed at a professional laboratory (Rhithron Associates, Inc., Missoula, Montana). All invertebrates were identified, measured (length, nearest mm), and converted to dry mass using established length–mass relationships. The energy density of each invertebrate taxon

was calculated from dry mass based on equations in Cummins and Wuycheck (1971). We express the energy content of prey in the gut as a function of fish size (joules g fish<sup>-1</sup>).

### *Seasonal contributions to growth and production*

Throughout each subbasin, we estimated the proportion of total growth (emergence to September) that occurred in spring (defined as emergence to July) and summer (July to September). For each sampled and prediction site (see below for predicting response variables in non-sampled locations), spring and summer proportional growth were calculated as follows:

$$\text{Spring proportion} = (W_{\text{July}} - W_{\text{Emergence}}) / (W_{\text{Sept}} - W_{\text{Emergence}})$$

$$\text{Summer proportion} = (W_{\text{Sept}} - W_{\text{July}}) / (W_{\text{Sept}} - W_{\text{Emergence}})$$

where  $W_{\text{Emerg}}$  is the weight at emergence (0.5 g; Beacham & Murray, 1990),  $W_{\text{July}}$  is the mean weight in July, and  $W_{\text{Sept}}$  is the mean weight in September. Spring and summer parr production (kg 100 m<sup>-1</sup>) were estimated in a similar manner but took into account density and differences in weights rather than proportions:

$$\text{Spring production} = (W_{\text{July}} - W_{\text{Emergence}}) * \text{Density}$$

$$\text{Summer production} = (W_{\text{Sept}} - W_{\text{July}}) * \text{Density}$$

Estimates of uncertainty were obtained by bootstrapping, similar to how uncertainty in MSGR was obtained.

### *Bioenergetics modeling*

We used a bioenergetics model to estimate how close prey consumption rates were to the maximum rates set by digestive capacity ( $C_{\text{max}}$ ), which is a function of fish size and water temperature. From observed growth rate (i.e., change in fish mass), daily water temperature, and predator/prey energy densities, one can estimate the proportion of  $C_{\text{max}}$  that fish achieved (i.e.,  $pC_{\text{max}}$ ) by running bioenergetics simulations to iteratively solve for the  $pC_{\text{max}}$  that generates the observed final fish mass (Hanson et al., 1997). All simulations were conducted using Fish Bioenergetics 4.0 (Deslauriers et al., 2017) in R (R Core Team, 2017) and metabolic coefficients for Chinook Salmon were updated to better represent juveniles as opposed to adult salmon (Plumb & Moffitt, 2015; Trudel et al., 2005). Inputs included site-specific temperature (hourly time step), initial weight, final weight; and general values of predator energy density (assumed to be 4,200 J g<sup>-1</sup>; Trudel et al., 2005; Rosenthal, 2019), prey energy density (assumed to be 4,000 J g<sup>-1</sup>), and diet proportion (assumed that all prey were invertebrates). To estimate summer  $pC_{\text{max}}$  and associated uncertainty, we ran 100 simulations per site with each simulation drawing from

the bootstrapped distributions of initial (July) and final (September) weight. Empirical temperature data were collected at 26 of the 53 sites in summer 2019, and temperatures at sites without sensors were interpolated from nearby sensors and warming trends between the nearest upstream and downstream sensor. We modeled spring  $pC_{max}$  at the sites in which emergence timing was estimated using assumed weight at emergence (0.5 g), observed weight in July, and observed temperature over this interval.

### *SSN modeling*

We used spatial stream-network (SSN) models to predict key response variables (density, July weight, September weight, summer MSGR, and summer  $pC_{max}$ ) continuously throughout the Chinook Salmon rearing extent of CC and UGR and to evaluate relationships between covariates and response variables. We established prediction sites with segment lengths consistent with those of sampled locations (~ 15x bankfull width). We then merged this layer with network-scale continuous habitat data from the Aquatic Inventories Project (Moore et al., 2017). For each sampled site and prediction segment, we calculated percent pool area and large wood abundance (# pieces 100 m<sup>-1</sup>). Temperature was derived from the NorWeST model representing the mean August temperature (hereafter temperature) from 2006-2015 (Isaak et al., 2017). We calculated the number of redds within two km upstream of each site using redd surveys conducted in 2018 (consistent with Justice et al., 2017). Spatial data were formatted and processed in ArcGIS (STARs package v 2.0.7; Peterson & Ver Hoef, 2014) and spatial processing to produce an SSN object followed procedures outlined in Ver Hoef et al. (2014).

We restricted models to a maximum of five potential fixed-effect coefficients (covariates and interaction terms) in addition to the intercept, and selected variables based on plausible biological connections (Figure D1) and availability of data at all sampled and unsampled sites. For the density model, initial covariates included subbasin (UGR or CC), percent pool area, large wood density, redd count, temperature, and squared temperature as a quadratic term to account for a potential non-linear relationship between temperature and density. Initial covariates predicting July weight, September weight, growth (MSGR), and  $pC_{max}$  included density (observations and predictions from the density SSN model), subbasin (UGR or CC), temperature and interactions between these terms.

For each response variable we fitted a global model with tail-up and tail-down covariance structure (see Peterson & Ver Hoef, 2010) and assessed model residuals for normality. Among all response variables, only density showed concerning residual patterns, which was corrected using a square-root transformation. Next, we formulated a set of models with the same fixed-effect covariates as the global model but all combinations of covariance structures to determine the best covariance structure given the data, as assessed using AICc (Burnham & Anderson, 2004). We then formulated a set of candidate models with plausible

combinations of fixed-effect covariates and the best covariance structure selected in the previous step. The model with the lowest AICc score was selected to predict the response variable at unsampled locations. For the top-ranked model predicting each response variable, we present the model structure, the leave-one-out cross validation (LOOCV) coefficient of determination, the variance composition, and coefficient estimates with associated *p*-values (top three models presented in Table S1). In addition to evaluating the best candidate models explaining each response variable, we also fitted spatial models with only river kilometer and the interaction between river kilometer and subbasin to evaluate longitudinal patterns of each response variable.

## Results

### *Emergence timing*

Spatial patterns of estimated emergence timing were apparent in both subbasins, with later emergence upstream (Figure D3), even after accounting for earlier spawning in upstream sections. In CC, emergence at the most downstream site was predicted to occur between late March and early May, but between early May and early June at the most upstream site located 22 km upstream. In UGR, emergence at the most downstream site was estimated to occur between early and late May, but between late May and late June at the most upstream site located 30 km upstream. Earlier emergence in CC compared to UGR appeared to be partially driven by greater degree day accumulation in winter and early spring (Figure D3B).

### *Size and growth*

Consistent with spatial and temporal patterns of emergence, parr weight in July decreased with distance upstream in both subbasins (Figure D4A,B). Mean weight was estimated to decrease by 0.19 g in CC (95% CI: 0.16 - 0.21 g;  $p < 0.001$ ) and by 0.06 g in UGR (95% CI: 0.04-0.08 g;  $p < 0.001$ ) for every kilometer upstream (spatial model with river kilometer and subbasin as fixed-effects;  $n = 53$  sites). Parr were substantially larger in CC (mean weight range 2.31-7.38 g) compared to UGR (mean weight range 0.65-3.02 g). The top-ranked model included subbasin, temperature, density, and the interaction between subbasin and temperature. All fixed-effect covariates were significant ( $\alpha < 0.05$ ) and the model explained 95% of the variation in observed weights (Table D1; top three models shown in Table D-A1). Size gradients persisted through September with an estimated decrease of 0.12 g and 0.07 g for every kilometer upstream in CC (95% CI: 0.09-0.16 g;  $p < 0.001$ ) and UGR (95% CI: 0.04-0.09 g;  $p < 0.001$ ), respectively ( $n = 53$  sites). The top-ranked model had the same model structure as for mean July weight, explained 89% of the variation in observed weights, and all covariates had a detectable effect (Table D1; Table D-A1).

MSGR exhibited opposing spatial patterns in spring and summer; in spring, MSGR decreased with distance upstream, but in summer MSGR increased with distance upstream (Figure D4C,D). This resulted in large differences between spring and summer growth rates in downstream sections, and comparatively smaller differences in upstream sections. During summer, MSGR was estimated to increase by 0.069 % d<sup>-1</sup> in CC (95% CI: 0.048-0.090 % d<sup>-1</sup>;  $p < 0.001$ ), and by 0.024 % d<sup>-1</sup> in UGR (0.007-0.041 % d<sup>-1</sup>;  $p = 0.007$ ) for every additional kilometer upstream ( $n = 53$  sites). The top-ranked model explained 58% of the variation in observed summer MSGR and included subbasin, temperature, and the interaction between subbasin and temperature (Table D1). Contrary to our expectations, Chinook Salmon parr density was not included in the top-ranked model, and while it was included in the second and third ranked model, it was not significant and had a small effect relative to other covariates (Table D-A1).

### *Bioenergetics and diet*

Bioenergetic estimates of  $pC_{max}$  and empirical diet data were generally consistent with spring and summer growth rates. In spring,  $pC_{max}$  was greater (range = 0.63-1.0) compared to summer (range = 0.40-0.55) for all locations (Figure D5A,B). In summer,  $pC_{max}$  increased with distance upstream; by 0.0038 (95% CI: 0.0013-0.0063;  $p = 0.004$ ) in CC and by 0.0027 (95% CI: 0.0004-0.0049;  $p = 0.024$ ) in UGR for every kilometer upstream ( $n = 53$  sites). The top-ranked model included temperature and density and this model explained 51% of the observed variation (Table D1). Empirical summer prey rations (joules g fish<sup>-1</sup>) also generally increased with distance upstream in both subbasins (Figure D5C,D). In CC, for every increase in kilometer upstream, consumption was estimated to increase by 4.10 J g fish<sup>-1</sup> in early August (linear regression;  $n = 8$  sites; 95% CI: 2.61-5.59;  $r^2 = 0.80$ ;  $p = 0.002$ ) and by 3.93 J g fish<sup>-1</sup> in late August ( $n = 8$  sites; 95% CI: 2.15-5.71;  $r^2 = 0.72$ ,  $p = 0.005$ ), but this relationship was no longer present in September ( $n = 8$  sites; 95% CI: -1.10-2.21;  $r^2 = 0.07$ ,  $p = 0.535$ ). Similarly, in UGR for every increase in kilometer upstream, consumption was estimated to increase by 2.10 J g fish<sup>-1</sup> in early August ( $n = 8$  sites; 95% CI: 0.90-3.30;  $r^2 = 0.61$ ;  $p = 0.014$ ), by 1.82 J g fish<sup>-1</sup> in late August ( $n = 8$  sites; 95% CI: 0.30-3.34;  $r^2 = 0.39$ ;  $p = 0.056$ ), and by 0.92 J g fish<sup>-1</sup> in September ( $n = 8$  sites; 95% CI: 0.01-1.825;  $r^2 = 0.29$ ;  $p = 0.094$ ).

### *Parr distribution*

Parr were distributed differently in CC and UGR during summer (Figure D6), and modeling results suggest differences in density were attributed to spatial differences in physical habitat quality and proximity to spawning locations (Table D1). In UGR, the highest densities were in the upper portion of the watershed, with 55% of total abundance concentrated in the uppermost 10 km. In CC, the highest densities were in middle sections, whereas the farthest upstream sections exhibited low densities. The top-ranked model



explained 67% of the variation in observed densities and included wood density, prior year redd count, and percent pool habitat as fixed effects, all of which were statistically significant (Table D1).

#### *Seasonal contributions to growth and production*

In both subbasins, the proportion of individual growth that occurred in spring decreased with distance upstream (Figure D7A,B). This was especially apparent in CC where early emergence, high spring growth rates, and low summer growth rates in downstream sections resulted in over 80% of total growth occurring prior to July sampling while in the farthest upstream sections nearly 75% of total growth occurred in summer. In UGR proportional spring and summer growth in the downstream sections were evenly split, but in upstream sections, up to 90% of total growth occurred in summer. Because high densities were observed in the middle and downstream portions of CC, the majority of total CC production (65%) occurred in spring (Figure D7C,D). In contrast, high densities in the headwaters of UGR resulted in the majority of UGR production (60%) occurring in summer (Figure D7E,F). Thus, the spatial distribution of parr, coupled with spatio-temporal patterns of emergence and growth dictated seasonal contributions to total parr production.

#### **Discussion**

By sampling across seasons and at many sites along the longitudinal profile of two rivers, we were able to characterize a shifting mosaic of fish growth and elucidate its underlying mechanisms. Our results suggest that longitudinal gradients in incubation temperatures caused juvenile Chinook Salmon to emerge earlier downstream, where they fed at rates approximating their digestive capacity. Thus, in spring, warmer downstream reaches had a longer duration and higher rate of growth, while cooler upstream reaches exhibited slower incubation, later emergence, and lower growth rates. In summer we found the opposite longitudinal pattern of growth, arising from a different set of processes. Growth rates increased upstream where cooler temperatures reduced metabolic costs and prey rations were higher, despite high fish densities in some upstream locations (e.g., UGR). Fish growth shifted seasonally within the longitudinal profiles of these streams which provides empirical support of modelling efforts predicting seasonal growth reversals as temperatures changed (Armstrong et al., *In press*). As a result of seasonal growth patterns and emergence phenology, juveniles in downstream sections accrued the majority of growth in spring whereas those in cooler upstream sections accrued the majority of growth in summer. This illustrates how seasonal bias in research and conservation can translate into spatial bias in how we interpret the potential for landscapes to support fish. Field sampling is biased towards summer low flow periods (Brady et al., *In press*) and climate adaptation frameworks for coldwater fishes focus on summer conditions (Isaak et al., 2015). Through this lens, warmer downstream habitat ranks poorly. However, by considering multiple

seasons, we found that the major landscape contrast was not in the magnitude of habitat quality (as measured by growth) but rather its phenology. Devaluing downstream habitat may not only result in lost production potential, but may also make production more temporally synchronous, which likely reduces population stability (Moore et al., 2010).

#### *Processes regulating seasonal growth patterns*

Emergence timing was an important driver of spatial patterns in Chinook Salmon parr size and growth within and among the two subbasins. Despite increasing summer growth rates with distance upstream, size gradients apparent in July persisted into September, demonstrating the carry-over effects of winter and spring temperatures on incubation, emergence timing, and spring growth. Earlier emerging fish not only had a longer spring growth interval, but also a higher spring growth rate, compounding the effect of emergence timing on parr size by July. Spatial gradients in emergence timing may reflect evolutionarily selection on spawn timing to promote emergence during optimal conditions for growth and survival (Einum & Fleming, 2000) or, alternatively, selection to spawn during time periods when cooler temperatures reduce mortality in the embryonic life stage (Beer & Anderson, 2001; Dahlke et al., 2020). Given the similarities in summer temperature and spawn timing in CC and UGR, but considerably different emergence timing between the two subbasins, we believe it is more likely that temperature is a primary control on spawn timing with emergence timing reflecting temperature exposure during incubation. In UGR, winter temperature remained near 0, resulting in minimal degree day accumulation, while warmer winter temperatures and earlier spring warming in CC resulted in faster development and earlier predicted emergence. While these alternative hypotheses require further research to tease out mechanisms regulating spatiotemporal patterns of emergence, it is clear that emergence was key in structuring the growth and size achieved by juvenile Chinook Salmon.

Following emergence, temperature interacted with consumption rates to shape spatio-temporal patterns in growth. In spring, juvenile Chinook Salmon fed at rates near their digestive capacity (i.e.,  $C_{max}$ ), so observed growth rates were likely limited by thermal constraints on physiological performance (Wurtsbaugh & Neverman, 1988). Estimated  $pC_{max}$  integrates over the growth interval (i.e., it is an average) and foraging opportunities tend to vary substantially over time, so  $pC_{max}$  values need not equal 1 to imply physiological constraints on growth (Armstrong et al., 2010). In summer,  $pC_{max}$  was comparatively lower, ranging between 0.4 and 0.6, suggesting growth was limited by prey availability. Under food limitation, the primary effect of temperature on fish energy budgets is increased metabolic costs (Fry, 1947), and in summer metabolic costs were lower upstream where diet rations were also higher, which is consistent with higher growth rates upstream. Utilizing bioenergetics and consumption data provided insight into how longitudinal patterns of growth can reverse as temperature and prey availability seasonally

shift within the riverscape. Bioenergetics results also suggest that fish rearing in downstream habitats experience alternating constraints of sub-optimally cool temperatures in spring (i.e., growth was constrained by thermally mediated digestive capacity, demonstrated by  $pC_{max}$  near 1) and sub-optimally warm temperatures in summer. This illuminates the complexity of how thermal regimes affect growth and the strong trade-offs that seasonality may impose on the evolution of thermal performance.

Contrary to our expectations, the density of parr explained little variation in July size and summer growth rates across these subbasins. This contrasts with a number of studies finding a negative effect of density on size and growth (Ebersole et al., 2009; Walters et al., 2013; Zabel & Achord, 2004); however, the spatial and temporal scale considered in these studies yielded different density-dependent effects. At large spatial scales (e.g., whole subbasins) and multiple years, the total population abundance of Chinook Salmon smolts has been negatively correlated with mean smolt size (Walters et al., 2013; Zabel & Achord, 2004). At finer spatial scales (habitat units within a site) density was an important predictor of Coho Salmon (*O. kisutch*) size but not at larger spatial scales representing sites within and among streams (Ebersole et al., 2009). Sites in our study covered 30-40 kilometers of mainstem habitat in each subbasin and biophysical factors scaling with watershed position (e.g., temperature, prey availability, size gradients) may have been more important in driving spatial patterns of growth at this scale. In addition, the number of spawning adults in 2018 was among the lowest recorded in these subbasins and low parr densities in 2019 may have weakened density-dependent effects on growth in this year.

#### *Seasonal patterns of productivity*

At the population scale, the effects of longitudinal gradients in seasonal growth are dependent on the distribution of parr. Because parr were distributed comparatively lower in the watershed in CC, where emergence was earlier and spring growth rates were high, approximately 65% of total Chinook Salmon production occurred prior to July. The opposite occurred in UGR, where parr concentrated in the headwaters emerged late, and consequently most of the total production (60%) occurred in summer. The distinction between spring and summer is arbitrary, reflecting when we sampled; nonetheless, results clearly show that areas of CC experienced high production prior to July (the onset of low-flow conditions) and comparatively low production from July-September, while areas of UGR clearly exhibited greater production from July-September. An important caveat is that we estimated density in August and sources of mortality and emigration prior to this time are unaccounted for. Therefore, estimates of spring production represent the production of fish that survived and do not account for production lost to mortality and emigration out of the study area.

Determining the processes and habitat relationships underlying fish distributions in these subbasins is important because management efforts may be able to improve habitat quality in targeted areas, thereby altering fish distribution. Pool habitat and large wood were important predictors of parr density. Pools are more abundant in the upper portions of UGR and are less frequent in the mid and lower portions, while in CC, pools are scarce in the upper portions and more frequent in the mid and lower portions, which aligns with spatial patterns in parr distribution. Both subbasins have experienced drastic habitat simplification resulting in loss of pools and pool-forming large wood, contributing to these patterns (White et al., 2017). The dispersal of fry shortly after emergence is often limited (Einum & Nislow, 2005) and not surprisingly, the number of redds within two kilometers of a site was also an important predictor of parr density (consistent with Justice et al., 2017). Therefore, observed parr distributions likely reflect rearing habitat quality as well as biophysical controls on adult spawning locations (Beechie et al., 2008). Given spatial structuring of emergence timing and size, and the relationship between size and survival in these subbasins (Kaylor et al., 2020) and others (Ebersole et al., 2006; Zabel & Achord, 2004), restoration that improves spawning and rearing habitat quality in lower portions of each subbasin may shift the distribution towards larger fish, potentially increasing survival. However, survival can also decrease at high temperatures (McCormick et al., 1972), potentially negating the positive effect of size on survival in warm sections. Further research linking spatial patterns in parr survival as they relate to size gradients, thermal regimes, and habitat would improve restoration prioritization efforts.

#### *Context of shifting seasonal growth*

Longitudinal size gradients have been observed in other systems, although the spatial pattern and mechanisms may differ. For resident fishes which tend to be more mobile, size patterns are thought to be structured by habitat selection mediated by species' thermal tolerances, stream thermal profiles, and prey availability (Hughes, 1998). For juvenile salmonids, which may exhibit limited dispersal (Einum & Nislow, 2005), biophysical factors influencing growth duration and rate likely exert strong controls on spatial size gradients. In a study examining a stream recently colonized by Coho Salmon, size increased with distance upstream (the opposite of what we observed), and the authors suggested that low densities in these upstream sections may have allowed for higher growth rates (Pess et al., 2011) or that larger fish migrated farther upstream than smaller fish (Anderson et al., 2013). In an Alaska river, modeled Chinook Salmon growth rates in summer exhibited the same downstream-increasing pattern that we observed in spring (Falke et al., 2019), likely because temperatures remained below the physiological optimum. Food abundance interacts with temperature to mediate growth, such that prey availability may dampen (Campbell et al., 2020), or greatly amplify (Armstrong et al., 2010) the spatial relationship between temperature and growth. Thus, to understand spatial

patterns of size and growth, it is crucial to also evaluate spatial gradients in the processes generating these patterns.

### *Caveats*

There are a number of limitations and caveats that our study design could not address. First, an assumption underlying our findings is that juvenile movement was restricted. In summer, we believe this assumption is valid, as only 46 of the 2,971 parr that were PIT-tagged were detected in a site other than the site they were tagged, and 78% of these fish were detected within 2 km from where they were tagged. Movement of fry shortly after emergence is a potential source of error. However, several studies have found that juvenile salmonid movement following emergence was limited to just a few hundred meters (Einum & Nislow, 2005, Einum et al., 2011), and a recent study that challenged the idea that movement is restricted still found that the majority of fish dispersed less than 2 km (Eisenhauer et al., 2020). Given the spatial scales evaluated in this study (30-40 km in each subbasin), the consistent gradients of juvenile size in July in both basins, and how well gradients in size aligned with patterns of estimated emergence, we believe that large-scale movement and mixing of juveniles did not occur. However, there is clearly a need to better evaluate early life history dispersal to understand how movement may interact with shifting habitat mosaics to influence population dynamics. Second, we were able to evaluate patterns of growth and mechanisms driving growth at large scales (i.e., entire rivers) but this came at the expense of overlooking mechanisms driving growth at smaller spatial scales. Finer-scale variation in temperature (e.g., tributary inputs, ground water sources, thermal refuge), prey availability (e.g., variation among habitat types), and density (discussed previously) may be important sources of variation in growth that we were not able to capture. Last, size-selective mortality and movement may have contributed to observed size and growth patterns. For example, larger individuals may have exhibited higher survival rates than smaller individuals (Zabel & Achord, 2004) and may have been more likely to disperse farther (Anderson et al., 2011). Addressing these caveats would provide further understanding of juvenile salmon early life history and mechanisms driving landscape patterns of growth.

### **Conclusions**

The size achieved by juvenile salmon has important implications for survival through multiple life stages. Our results indicate that downstream portions of the network provided significant growth opportunities, mainly in spring, leading to larger parr size compared to sites farther upstream. Summer growth rates at these downstream locations were lower compared to upstream sites and we attribute the large size these individuals achieved to earlier emergence and high spring growth rates. Thus, these habitats may be important to overall production in these subbasins, but the phenology of growth opportunities differs.

In addition to effects of emergence timing on size, variability in emergence timing may be an important aspect of population stability (Schindler et al., 2010). For example, in some years earlier emergence may be more favorable as it provides increased growth opportunities (Egglshaw & Chackley, 1977; Einum et al., 2008), while in other years, earlier emergence may result in reduced survival due to harsh environmental conditions (e.g. high spring flows). In this regard, focusing habitat restoration efforts on spreading the distribution of fish throughout potential rearing habitat may be an effective strategy for achieving long-term stability in population productivity.

### **Acknowledgements**

We thank M. Cottingham, K. Schmidt, J. Dowdy, B. Power, S. Power, and the ODFW early life history crew for their assistance with field work. D. Graves assisted with geospatial analyses. G. Pess provided feedback on interpreting results. Numerous landowners allowed access to the stream through their property. This research was supported by the Bonneville Power Administration as part of the Columbia Basin Fish Accords Agreement (Project # 2009-004-00).

### **Author contributions**

MK, CJ, and SW conceived the idea and initial study design; MK, CJ, SW, BS, LB, and ES conducted field sampling or assisted sampling efforts; MK analyzed the data with assistance from CJ, JA, SW, and BS; All authors contributed towards interpreting results; MK, CJ, JA, SW, BS, and LB wrote the manuscript.

### **Data availability statement**

All data will be made publicly available and permanently archived using GitHub (github.com) after the manuscript is published.

### **Literature cited**

- Aikens, E. O., Kauffman, M. J., Merkle, J. A., Dwinnell, S. P. H., Fralick, G. L., & Monteith, K. L. (2017). The greenscape shapes surfing of resource waves in a large migratory herbivore. *Ecology Letters*, 20, 741–750. doi: 10.1111/ele.12772
- Anderson, J. H., Kiffney, P. M., Pess, G. R., & Quinn, T. P. (2008). Summer distribution and growth of juvenile Coho Salmon during colonization of newly accessible habitat. *Transactions of the American Fisheries Society*, 137(3), 772–781. doi: 10.1577/T07-013.1
- Anderson, J. H., Pess, G. R., Kiffney, P. M., Bennett, T. R., Faulds, P. L., Atlas, W. I., & Quinn, T. P. (2013). Dispersal and tributary immigration by juvenile coho salmon

contribute to spatial expansion during colonisation. *Ecology of Freshwater Fish*, 22, 30–42. doi: 10.1111/j.1600-0633.2012.00589.x

Armstrong, J. B., Fullerton, A. H., Jordan, C. E., Ebersole, J. L., Bellmore, J. R., Arismendi, I., Penaluna, B., & Reeves, G. H. (*In press*) The significance of warm habitat to the growth regime of coldwater fishes. *Nature Climate Change*. Accepted.

Armstrong, J. B., Schindler, D. E., Omori, K. L., Ruff, C. P., & Quinn, T. P. (2010). Thermal heterogeneity mediates the effects of pulsed subsidies across a landscape. *Ecology*, 91(5), 1445–1454.

Baldock, J. R., Armstrong, J. B., Schindler, D. E., & Carter, J. L. (2016). Juvenile coho salmon track a seasonally shifting thermal mosaic across a river floodplain. *Freshwater Biology*, 61, 1454–1465. doi: 10.1111/fwb.12784

Beacham, T. D., & Murray, C. B. (1990). Temperature, egg size, and development of embryos and alevins of five species of Pacific Salmon: A comparative analysis. *Transaction of the American Fisheries Society*, 119(6), 927–945. doi: 10.1577/1548-8659(1990)119

Beechie, T. J., Moir, H., & Pess, G. (2008). Hierarchical physical controls on salmonid spawning location and timing. *American Fisheries Society Symposium*, 65(January), 83–101.

Beer, W. N., & Anderson, J. J. (2001) Effect of spawning day and temperature on salmon emergence: interpretations of a growth model for Methow River chinook. *Canadian Journal of Fisheries and Aquatic Sciences*, 58, 943-949.

Brady, M. E., Chione, A. M., Armstrong, J. B. (*In press*). Missing pieces in the full annual cycle of fish ecology: a systematic review of the phenology of freshwater fish research. *Biology*. Preprint available. doi: <https://doi.org/10.1101/2020.11.24.395665>.

Brandt, S. B., Mason, D. M., & Patrick, E. V. (1992). Spatially-explicit models of fish growth rate. *Fisheries*, 17(2), 23–33.

Brennan, S. R., Schindler, D. E., Cline, T. J., Walsworth, T. E., Buck, G., & Fernandez, D. P. (2019). Shifting habitat mosaics and fish production across river basins. *Science*, 783–786.

Burnham, K. P., & Anderson, D. R. (2004). Multimodel inference: understanding AIC and BIC in model selection. *Sociological Methods & Research*, 33(2), 261–304. doi: 10.1177/0049124104268644

- Campbell, E. Y., Dunham, J. B., & Reeves, G. H. (2020). Linkages between temperature, macroinvertebrates, and young-of-year Coho Salmon growth in surface-water and groundwater streams. *Freshwater Science*, 39(July). doi: 10.1086/710042.
- Cowles, R. B., & Bogert, C. M. (1944). Preliminary study of the thermal requirements of desert reptiles. *Bulletin of the American Museum of Natural History*, 83, 261–296.
- Crozier, L. G., Zabel, R. W., Hockersmith, E. E., & Achord, S. (2010). Interacting effects of density and temperature on body size in multiple populations of Chinook salmon. *Journal of Animal Ecology*, 79, 342–349. doi: 10.1111/j.1365-2656.2009.01641.x
- Cummins, K. W., & Wuycheck, J. C. (1971). Caloric equivalents for investigations in ecological energetics. *International Association of Theoretical and Applied Limnology*, 18, 1–158.
- Dahlke, F. T., Wohlrab, S., & Butzin, M. (2020). Thermal bottlenecks in the life cycle define climate vulnerability of fish. *Science*, 2(July), 65–70.
- Deacy, W., Leacock, W., Armstrong, J. B., & Stanford, J. A. (2016). Kodiak brown bears surf the salmon red wave: direct evidence from GPS collared individuals. *Ecology*, 97(5), 1091–1098.
- Deslauriers, D., Chipps, S. R., Breck, J. E., Rice, J. A., & Madenjian, C. P. (2017). Fish Bioenergetics 4.0: An R-based modeling application. *Fisheries*, 42(11), 586–596. doi: 10.1080/03632415.2017.1377558
- Dobrowski, S. Z. (2011). A climatic basis for microrefugia: the influence of terrain on climate. *Global Change Biology*, 17, 1022–1035. doi: 10.1111/j.1365-2486.2010.02263.x
- Ebersole, J. L., Colvin, M. E., Wigington, P. J. J., Leibowitz, S. G., Baker, J. P., Church, M. R., ... Cairns, M. A. (2009). Hierarchical modeling of late-summer weight and summer abundance of juvenile Coho Salmon across a stream network. *Transaction of the American Fisheries Society*, (Mason 1976), 1138–1156. doi: 10.1577/T07-245.1
- Ebersole, J. L., Wigington, P. J., Baker, J. P., Cairns, M. A., Church, M. R., Hansen, B. P., ... Leibowitz, S. G. (2006). Juvenile Coho Salmon growth and survival across stream network seasonal habitats. *Transactions of the American Fisheries Society*, 135, 1681–1697. doi: 10.1577/T05-144.1
- Egglishaw, H. J., & Chackley, P. E. (1977). Growth, survival and production of juvenile salmon and trout in a Scottish stream, 1966-75. *Journal of Fish Biology*, 11, 647–672.



- Einum, S., & Fleming, I. A. (2000). Selection against late emergence and small offspring in Atlantic salmon (*Salmo salar*). *Evolution*, 54(2), 628–639. doi: 10.1111/j.0014-3820.2000.tb00064.x
- Einum, S., & Nislow, K. H. (2005). Local-scale density-dependent survival of mobile organisms in continuous habitats: An experimental test using Atlantic salmon. *Oecologia*, 143(2), 203–210. doi: 10.1007/s00442-004-1793-y
- Einum, S., Nislow, K. H., McKelvey, S., & Armstrong, J. D. (2008). Nest distribution shaping within-stream variation in Atlantic salmon juvenile abundance and competition over small spatial scales. *Journal of Animal Ecology*, 77(1), 167–172. doi: 10.1111/j.1365-2656.2007.01326.x
- Einum, S., Robertsen, G., Nislow, K. H., McKelvey, S., & Armstrong, J. D. (2011) The spatial scale of density-dependent growth and implications for dispersal from nests in juvenile Atlantic salmon. *Oecologia*, 165, 959-969.
- Falke, J. A., Huntsman, B. M., & Schoen, E. R. (2019). Climatic Variation Drives Growth Potential of Juvenile Chinook Salmon along a Subarctic Boreal Riverscape. *American Fisheries Society Symposium*, 90, 1–26.
- Fausch, K. D., Torgersen, C. E., Baxter, C. V., & Li, H. W. (2002). Landscapes to riverscapes: bridging the gap between research and conservation of stream fishes. *BioScience*, 52(6), 483–498. doi: 10.1641/0006-3568(2002)052[0483:LTRBTG]2.0.CO;2
- Fry, F. E. J. (1947). Effects of the environment on animal activity. In *Publication of the Ontario Fisheries Research Laboratory No. 68* (pp. 1–62). The University of Toronto Press.
- Fullerton, A. H., Torgersen, C. E., Lawler, J. J., Faux, R. N., Steel, E. A., Beechie, T. J., ... Leibowitz, S. G. (2015). Rethinking the longitudinal stream temperature paradigm: region-wide comparison of thermal infrared imagery reveals unexpected complexity of river temperatures. *Hydrological Processes*, 29, 4719–4737. doi: 10.1002/hyp.10506
- Hansen, A. G., & Beauchamp, D. A. (2015). Latitudinal and photic effects on diel foraging and predation risk in freshwater pelagic ecosystems. *Journal of Animal Ecology*, 84, 532–544. doi: 10.1111/1365-2656.12295
- Hanson, P. C., Johnson, T. B., Schindler, D. E., & Kitchell, J. F. (1997). *Fish bioenergetics 3.0*. Madison, WI: University of Wisconsin Sea Grant Institute.

- Holtby, L. B., Andersen, B. C., & Kadowaki, R. K. (1990). Importance of smolt size and early ocean growth to interannual variability in marine survival of Coho Salmon (*Oncorhynchus kisutch*). *Canadian Journal of Fisheries and Aquatic Sciences*, 47(11), 2181–2194.
- Huey, R. B. (1991). Physiological consequences of habitat selection. *The American Naturalist*, 137, S91–S115.
- Hughes, N. F. (1998). A model of habitat selection by drift-feeding stream salmonids at different scales. *Ecology*, 79(1), 281–294.
- Isaak, D. J., Wenger, S. J., Peterson, E. E., Hoef, J. M. Ver, Nagel, D. E., Luce, C. H., ... Parkes-payne, S. (2017). The NorWeST summer stream temperature model and scenarios for the western U.S.: A crowd-sourced database and new geospatial tools foster a user community and predict broad climate warming of rivers and streams. *Water Resources Research*, 53, 1–25. doi: 10.1002/2017WR020969
- Isaak, D. J., Young, M. K., Nagel, D. E., Horan, D. L., & Groce, M. C. (2015). The cold-water climate shield: delineating refugia for preserving salmonid fishes through the 21st century. *Global Change Biology*, 21, 2540–2553. doi: 10.1111/gcb.12879
- Justice, C., White, S. M., McCullough, D. A., Graves, D. S., & Blanchard, M. R. (2017). Can stream and riparian restoration offset climate change impacts to salmon populations? *Journal of Environmental Management*, 188, 212–227. doi: 10.1016/j.jenvman.2016.12.005
- Kaylor, M. J., White, S. M., Sedell, E. R., & Warren, D. R. (2020). Carcass additions increase juvenile salmonid growth, condition, and size in an interior Columbia River Basin tributary. *Canadian Journal of Fisheries and Aquatic Sciences*, 77, 703–715.
- McCormick, J. H., Hokanson, E. F., & Jones, B. R. (1972). Effects of temperature on growth and survival of young brook trout, *Salvelinus fontinalis*. *Journal of the Fisheries Research Board of Canada*, 29, 1107–1112.
- Meehan, W. R., & Miller, R. A. (1978). Stomach flushing: Effectiveness and influence on survival and condition of juvenile salmonids. *Journal of the Fisheries Research of the Board of Canada*, 35, 1359–1363.
- Moore, J. W., McClure, M., Rogers, L. A., & Schindler, D. E. (2010) Synchronization and portfolio performance of threatened salmon. *Conservation letters*, 3, 340–348.
- Moore, K., Jones, K., Dambacher, J., & Stein, C. (2017). Aquatic Inventories Project: Methods for stream habitat and snorkel surveys. Corvallis, OR.

- Ostrovsky, I. (1995). The parabolic pattern of animal growth: determination of equation parameters and their temperature dependencies. *Freshwater Biology*, 33, 357–371. doi: 10.1111/j.1365-2427.1995.tb00398.x
- Perry, R. W., Plumb, J. M., & W. Huntington, C. (2015). Using a laboratory-based growth model to estimate mass-and temperature-dependent growth parameters across populations of juvenile Chinook Salmon. *Transactions of the American Fisheries Society*, 144(2), 331–336. doi: 10.1080/00028487.2014.996667
- Pess, G. R., Kiffney, P. M., Liermann, M. C., Bennett, T. R., Anderson, J. H., & Quinn, T. P. (2011). The influences of body size, habitat quality, and competition on the movement and survival of juvenile Coho Salmon during the early stages of stream recolonization. *Transactions of the American Fisheries Society*, 140(4), 883–897. doi: 10.1080/00028487.2011.587752
- Peterson, E. E., & Ver Hoef, J. M. (2010). A mixed-model moving-average approach to geostatistical modeling in stream networks. 91(3), 644–651.
- Peterson, E. E., & Ver Hoef, J. M. (2014). STARS: An ArcGIS toolset used to calculate the statistical models to stream network data. *Journal of Statistical Software*, 56(2), 1:17.
- Petty, J. T., Thorne, D., & Mazik, P. M. (2014). The temperature – productivity squeeze: constraints on brook trout growth along an Appalachian river continuum. *Hydrobiologia*, 727, 151–166. doi: 10.1007/s10750-013-1794-0
- Plumb, J. M., & Moffitt, C. M. (2015). Re-Estimating Temperature-Dependent Consumption Parameters in Bioenergetics Models for Juvenile Chinook Salmon. *Transactions of the American Fisheries Society*, 144(2), 323–330. doi: 10.1080/00028487.2014.986336
- Rogers, L. A., Schindler, D. E., Lisi, P. J., Holtgrieve, G. W., Leavitt, P. R., Bunting, L., ... Walsh, P. B. (2013). Centennial-scale fluctuations and regional complexity characterize Pacific salmon population dynamics over the past five centuries. *PNAS*, 110(5), 1750–1755. doi: 10.1073/pnas.1212858110
- Rosenthal, E. (2019). Growth rate variation among juvenile Chinook Salmon (*Oncorhynchus tshawytscha*) cohorts and rearing conditions. California State University, Fresno.
- Ruesch, A. S., Torgersen, C. E., Lawler, J. J., Olden, J. D., Peterson, E. E., Volk, C. J., & Lawrence, D. J. (2012). Projected climate-induced habitat loss for salmonids in the

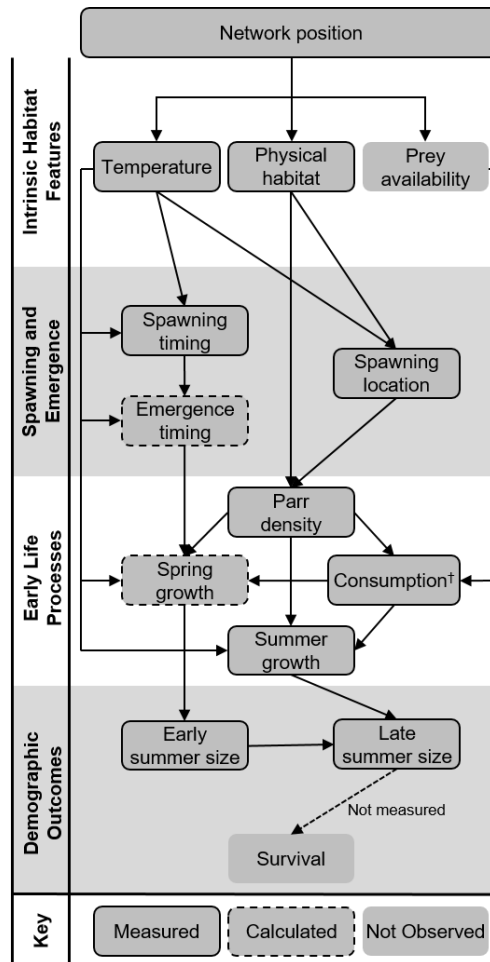
- John Day River network, Oregon, U.S.A. *Conservation Biology*, 26(5), 873–882. doi: 10.1111/j.1523-1739.2012.01897.x
- Schindler, D. E., Armstrong, J. B., & Reed, T. E. (2015). The portfolio concept in ecology and evolution. *Frontiers in Ecology and the Environment*, 13(5), 257–263. doi: 10.1890/140275
- Schindler, D. E., & Hilborn, R. (2015). Prediction, precaution, and policy under global change. *Science*, 347(6225), 953–954.
- Schindler, D. E., Hilborn, R., Chasco, B., Boatright, C. P., Quinn, T. P., Rogers, L. a, & Webster, M. S. (2010). Population diversity and the portfolio effect in an exploited species. *Nature*, 465(7298), 609–612. doi: 10.1038/nature09060
- Sears, M. W., Raskin, E., & Angilletta, M. J. J. (2011). The world is not flat: Defining relevant thermal landscapes in the context of climate change. *Integrative and Comparative Biology*, 51(5), 666–675. doi: 10.1093/icb/icr111
- Sloat, M. R., Shepard, B. P., White, R. G., & Carson, S. (2005). Influence of stream temperature on the spatial distribution of westslope cutthroat trout growth potential within the Madison River basin, Montana. *North American Journal of Fisheries Management*, 25, 225–237. doi: 10.1577/M03-165.1
- Sparks, M. M., Falke, J. A., Quinn, T. P., Adkison, M. D., Schindler, D. E., Bartz, K., ... Westley, P. A. H. (2019). Influences of spawning timing, water temperature, and climatic warming on early life history phenology in western Alaska sockeye salmon. *Canadian Journal of Fisheries and Aquatic Sciences*, 76, 123–135.
- Stanford, J. A., Lorang, M. S., & Hauer, F. R. (2005). The shifting habitat mosaic of river ecosystems. *Verhandlungen International Verein Limnologie*, 29, 123–136. doi: 10.1080/03680770.2005.11901979
- Tattam, I. A., Li, H. W., Giannico, G. R., & Ruzycki, J. R. (2017). Seasonal changes in spatial patterns of *Oncorhynchus mykiss* growth require year-round monitoring. *Ecology of Freshwater Fish*, 26, 434–443. doi: 10.1111/eff.12287
- Team, R. C. (2017). *R: A language and environment for statistical computing*. Vienna, Austria: R Foundation for Statistical Computing. Retrieved from <http://www.r-project.org/>
- Trudel, M., Tucker, S., Morris, J. F. T., Higgs, D. A., & Welch, D. W. (2005). Indicators of energetic status in juvenile coho salmon and Chinook salmon. *North American Journal of Fisheries Management*, 25(1), 374–390. doi: 10.1577/m04-018.1

- Ver Hoef, J. M., Peterson, E. E., Clifford, D., & Shah, R. (2014). SSN: An R package for spatial statistical modeling on stream networks. *Journal of Statistical Software*, 56(3), 1–45.
- Walters, A. W., Copeland, T., & Venditti, D. A. (2013). The density dilemma: limitations on juvenile production in threatened salmon populations. *Ecology of Freshwater Fish*, 22, 508–519.
- White, S. M., Justice, C., Kelsey, D. A., McCullough, D. A., & Smith, T. (2017). Legacies of stream channel modification revealed using General Land Office surveys, with implications for water temperature and aquatic life. *Elem Sci Anth*, 5(0), 3. doi: 10.1525/elementa.192
- Whited, D. C., Lorang, M. S., Harner, M. J., Hauer, F. R., Kimball, J. S., & Stanford, J. A. (2007). Climate, hydrologic disturbance, and succession: Drivers of floodplain pattern. *Ecology*, 88(4), 940–953.
- Wurtsbaugh, W. A., & Neverman, D. (1988). Post-feeding thermotaxis and daily vertical migration in larval fish. *Nature*, 333, 846–848.
- Zabel, R. W., & Achord, S. (2004). Relating size of juveniles to survival within and among populations of Chinook salmon. *Ecology*, 85(3), 795–806.

Table D1: Summary of top ranked models predicting each response variable: Parr density (sqrt (fish 100 m<sup>-1</sup>)); July mean weight; September mean weight; summer mass-standardized growth rates (MSGR); and summer *pCmax*. Basin is an indicator variable for CC (0) and UGR (1). LOOCV R<sup>2</sup> indicates the leave-one-out cross validation relationship between observed values and model-predicted values for the response variable, *b* represents the fixed-effect coefficient value of each predictor, standardized *b* represents the *b* coefficient divided by the standard error which provides a unitless effect size, and variance composition indicates the proportion of the explained variation by fixed-effects, spatial autocovariance, and the independent nugget component (residual variation at finer spatial scales than evaluated in models).

Response variable	<i>N</i> sites	LOOCV R <sup>2</sup>	Fixed-effects	Fixed-effect <i>p</i> -value	<i>b</i>	Standardized <i>b</i>	Variance composition		
							Fixed-effects	Spatial	Nugget
Density	59	0.67	Intercept	0.030	4.230	2.231	0.51	0.37	0.12
			Redd count	0.007	0.592	2.806			
			Wood count	0.035	0.080	2.164			
			Percent pool	<0.001	0.188	4.838			
July size	53	0.93	Intercept	<0.001	-14.112	-5.202	0.69	0.29	0.02
			Temp	<0.001	1.167	9.886			
			Basin	<0.001	15.810	4.142			
			Density	<0.001	-0.081†	-3.500			
			Temp*basin	<0.001	-1.122	-5.498			
August size	53	0.89	Intercept	0.021	-8.927	-2.390	0.58	0.41	0.01
			Aug. temp	<0.001	1.020	6.780			
			Basin	0.036	11.384	2.156			
			Density	<0.001	-0.131†	-4.695			
			Temp*basin	0.003	-0.858	-3.097			
Summer MSGR	53	0.58	Intercept	<0.001	6.371	3.580	0.14	0.71	0.16
			Temp	0.008	-0.292	-2.760			
			Basin	0.110	-5.194	-1.628			
			Temp*basin	0.104	0.338	1.656			
Summer <i>pCmax</i>	53	0.51	Intercept	<0.001	0.810	10.433	0.30	0.20	0.50
			Temp	<0.001	-0.022	-4.567			
			Density	0.095	-0.004†	-1.783			

† represents 100 Chinook/100 m



† Consumption included empirical diet data and bioenergetics modeling of consumption rates relative to theoretical assimilative capacity (i.e.,  $pC_{max}$ ).

Figure D1: Conceptual diagram of the biophysical factors shaping Chinook salmon parr growth, size, and survival. Direction of arrows indicates the hypothesized influence of one factor on another; border type denotes whether a factor was measured, calculated (estimated), or not measured by this study.

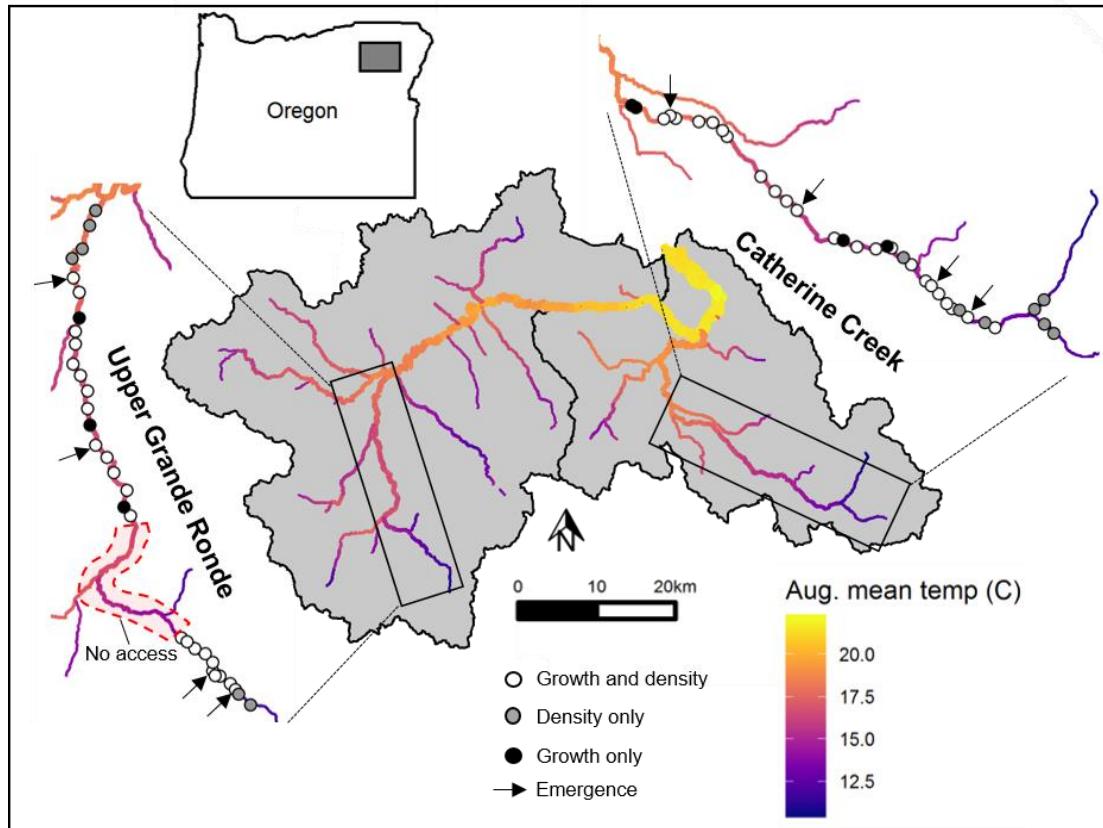


Figure D2: Map of study sites within the core rearing extent of Chinook Salmon in Catherine Creek and upper Grande Ronde. Size, summer growth rates, and summer bioenergetics estimates of consumption ( $pC_{max}$ ) were estimated at 53 sites and density was estimated at 59 sites, with 46 sites of these sites overlapping. Arrows indicate sites where emergence timing, spring growth rates, and spring bioenergetics  $pC_{max}$  were estimated. Mean August temperature was derived from the NorWeST stream temperature model for the years 2006-2015 (Isaak et al. 2017).



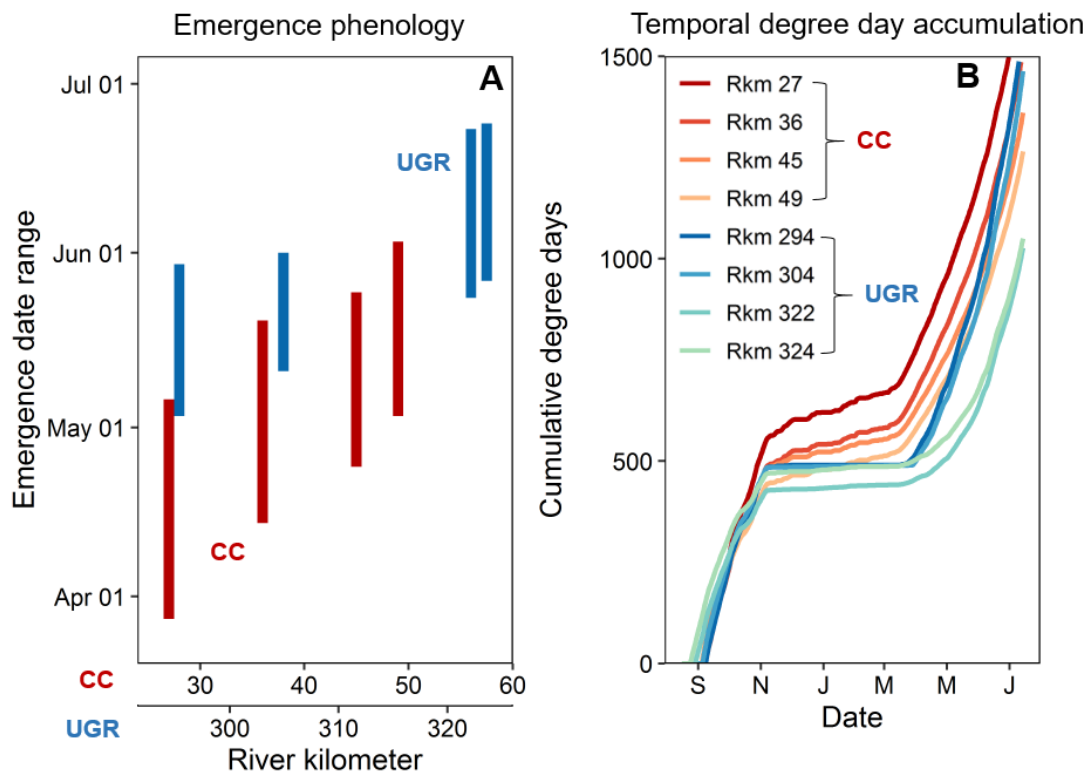


Figure D3: Estimated Chinook Salmon fry emergence timing (A) at four locations in Catherine Creek (red bars) and upper Grande Ronde (blue bars) and cumulative degree day accumulation from spawning to early July for each site (B). Emergence timing date ranges correspond to ranges in observed spawning dates near each site. Panel (B) represents cumulative degree days from the midpoint of the observed spawning range for each site.

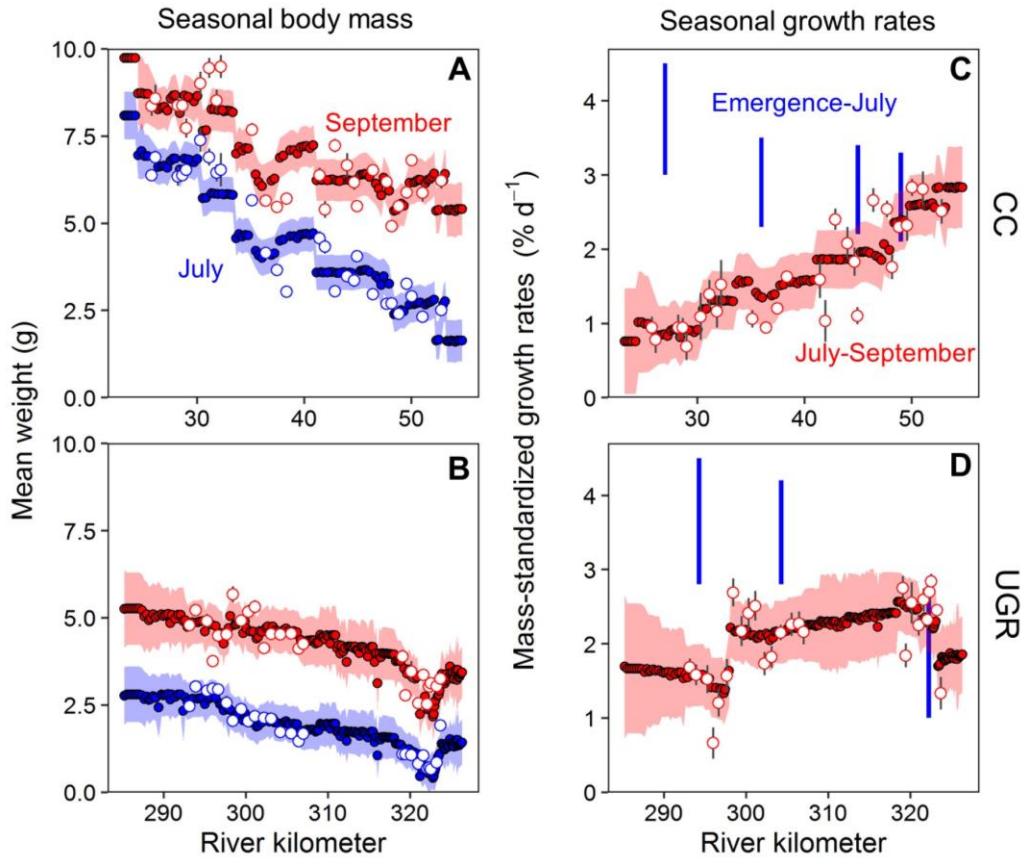


Figure D4: Mean juvenile Chinook Salmon weight (A,B) in July (blue) and September (red) and mass-standardized growth rates (C,D) from emergence to July (blue vertical lines) and from July to September (red points) in Catherine Creek (A,C) and upper Grande Ronde (B,D). Estimated growth rates from emergence to July are only available for the limited number of sites in which emergence was estimated (see Fig. 3). Open points indicate sampled sites and vertical grey lines of these points indicate sampled standard error. Filled points indicate sites where mean weight and MSGR were modeled and colored shading indicates prediction standard error. Blue vertical lines in C and D, represent estimated spring MSGR based on estimated emergence timing, emergence weight (0.5 g), and weight in July.

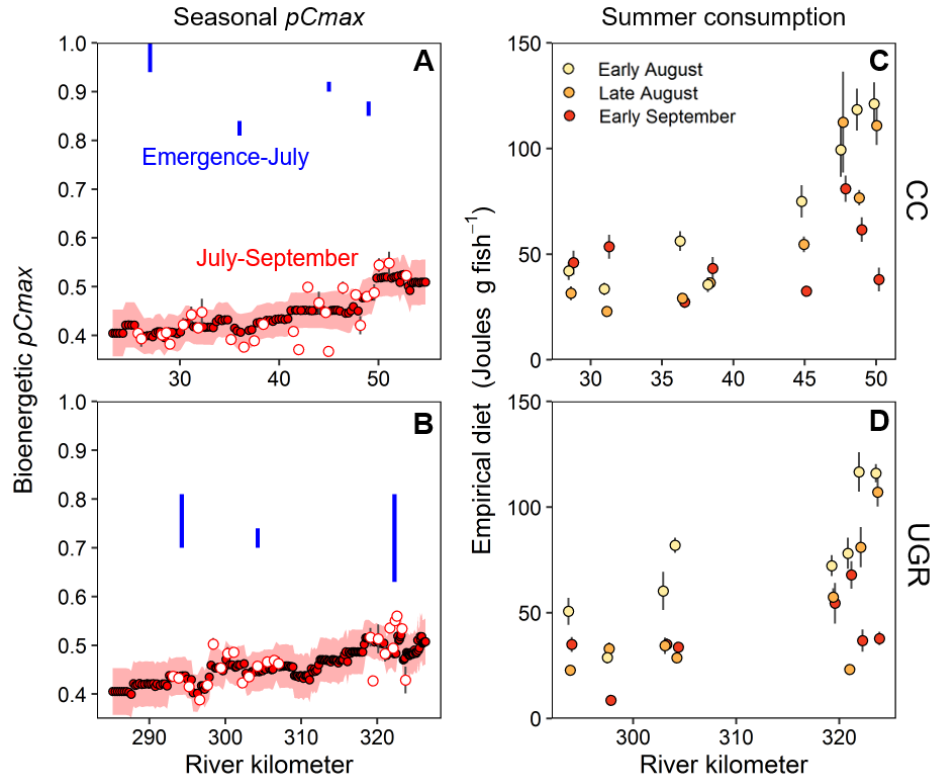


Figure D5: Estimated bioenergetics  $pC_{max}$  (A,B) in spring (blue vertical lines) and summer (red points and shading) and empirical energy content of diets at three sampling periods in summer (C,D) in Catherine Creek (A,C) and upper Grande Ronde (B,D). For A and B, open points indicate sampled sites and vertical grey lines of these points indicate estimated standard error; filled points indicate sites where  $pC_{max}$  was predicted and red shading indicates prediction standard error. Vertical lines in C and D indicate 95% confidence intervals of the mean.

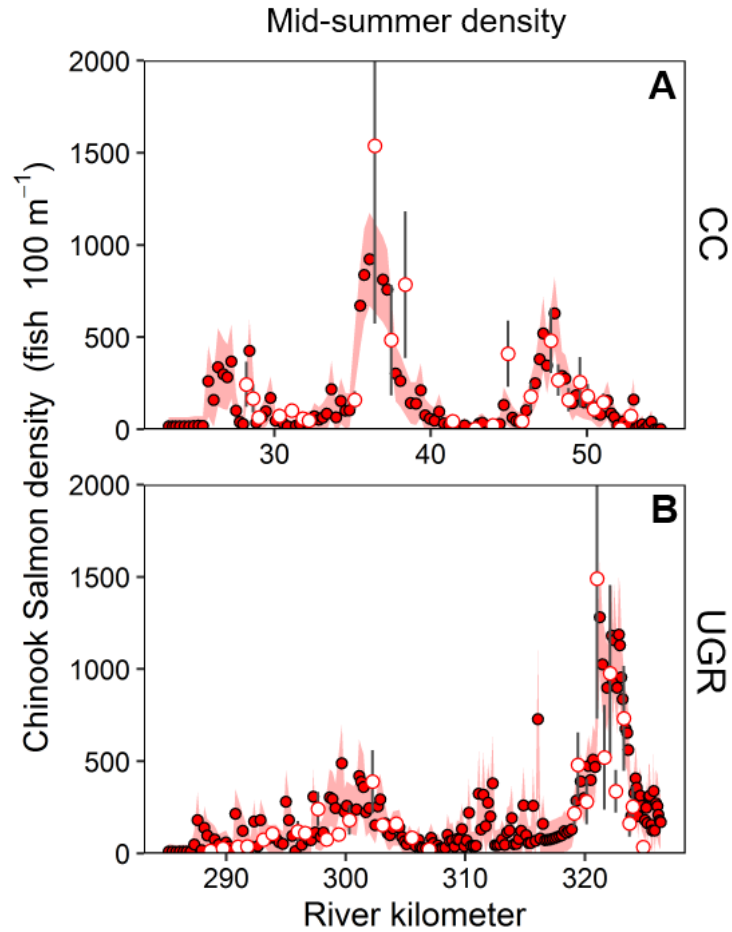


Figure D6: Estimated Chinook Salmon density at sites where snorkel surveys were conducted (open points) and sites where density was modeled (closed points) using continuously available habitat metrics and spatial autocorrelation in Catherine Creek (A) and upper Grande Ronde (B). Vertical grey lines represent standard error of density estimates at sampled sites whereas red shading indicates prediction standard error at unsampled locations.

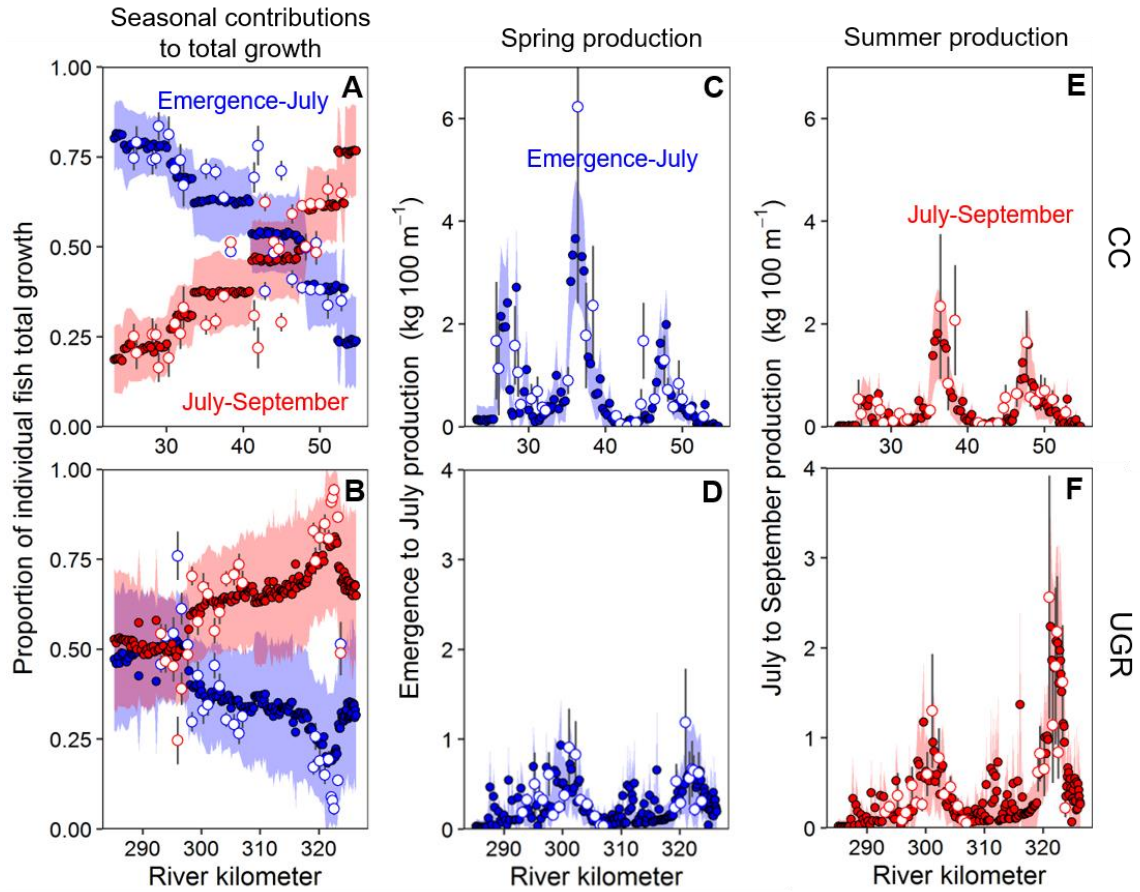


Figure D7: The proportion of individual fish growth accrued (A,B) in spring (blue) and summer (red), total spring production (C,D), and total summer production (E,F) in Catherine Creek (A,C,E) and upper Grande Ronde (B,D,F). Open circles indicate sampled sites and filled circles indicate unsampled sites where response variables were modeled. Vertical grey lines indicate estimated standard error and colored shading indicates prediction standard error. Production estimates represent growth rates multiplied by mid-summer density. Therefore, they represent the production of fish observed in mid-summer and do not account for production lost through mortality.

# Appendix D – supplemental tables and figures

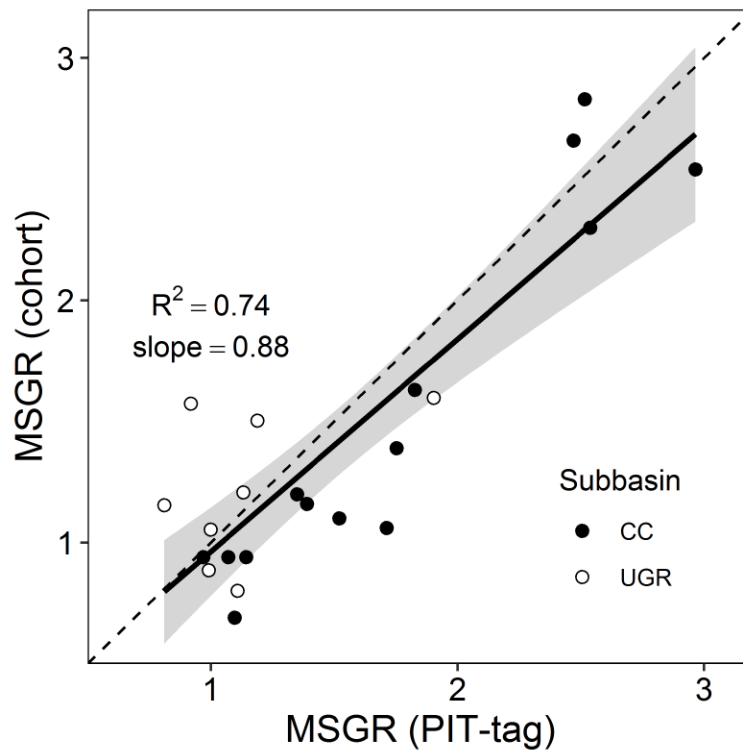


Figure D-A1: Fitted relationship between two methods of measuring mass-standardized growth rates (MSGR): from individuals that were individually tagged and recaptured (x-axis) versus using changes in mean cohort size (y-axis). Each point represents a site in either Catherine Creek (filled points) or upper Grande Ronde (open points). The solid line represents the fitted relationship to all points and grey shading represents the 95% CI of the relationship. Parr in CC were PIT-tagged in July while parr in UGR were PIT-tagged at the end of August. When parr were PIT-tagged and subsequently recaptured, a larger number of parr were sampled and length and weight were recorded, which were used to estimate cohort growth rates. All sites were revisited in mid-September, and as a result, the growth interval for CC was approximately 8 weeks while the growth interval for UGR was 3-4 weeks. These differences in when parr were tagged and the duration of time between sampling events likely explains why MSGR in UGR is lower and exhibits a narrower range compared to CC. Nonetheless, each point represents a valid comparison of cohort growth rates and PIT-tagged growth rates. This serves as a validation that using changes in cohort size is an adequate representation of empirical individual growth in our study.

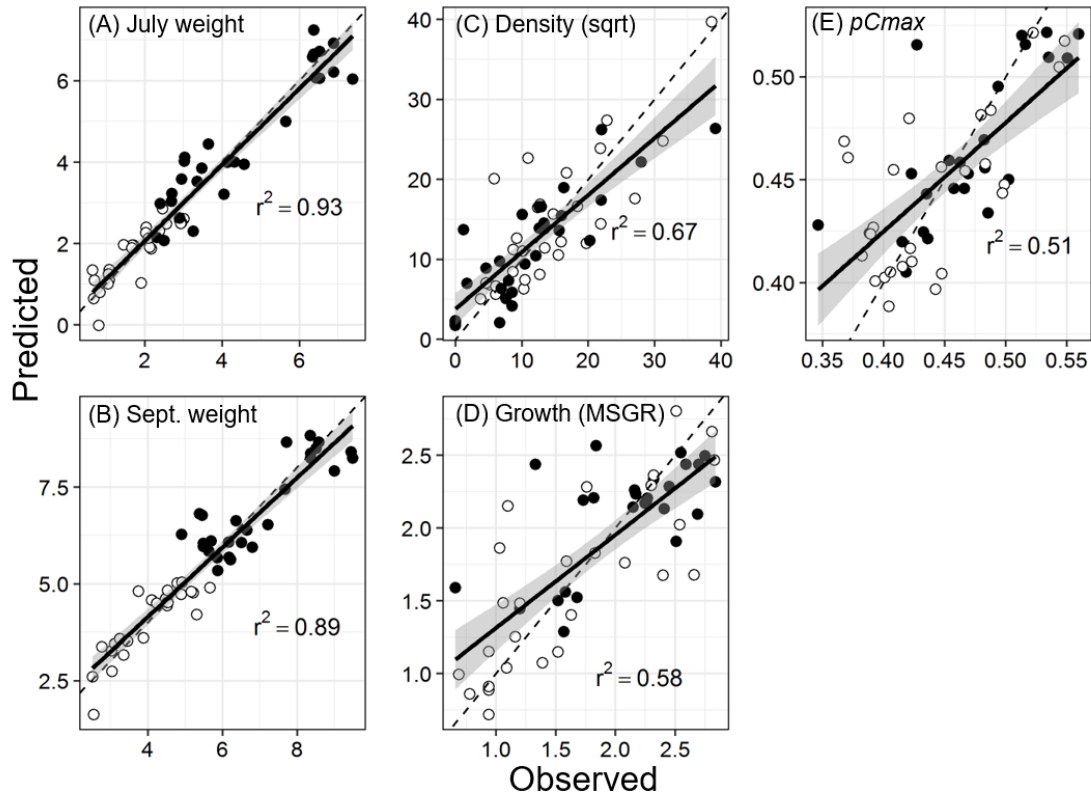


Figure D-A2: Comparison of leave-one-out cross validation (LOOCV) predictions for July mean weight (A), September mean weight (B), density (square-root transformed; C), mass-standardized growth rate (MSGGR; D), and bioenergetics  $pCmax$  (E) using the top-ranked model for each response variable. Filled points represent Catherine Creek and open points represent upper Grande Ronde. The dashed line indicates a 1:1 relationship and the solid line represents the regression relationship. Grey shading represents the 95% confidence interval for the relationship.

Table D-A1: Summary of the top three models predicting each response variable as ranked by AICc: Parr density (sqrt (fish 100 m<sup>-1</sup>)); July mean weight; September mean weight; summer mass-standardized growth rates (MSGR); and summer *pCmax*. Basin is an indicator variable for CC (0) and UGR (1). LOOCV R<sup>2</sup> indicates the leave-one-out cross validation relationship between observed values and model-predicted values for the response variable, *b* represents the fixed-effect coefficient value of each predictor, standardized *b* represents the *b* coefficient divided by the standard error which provides a unitless effect size, and variance composition indicates the proportion of the explained variation by fixed-effects, spatial autocovariance, and the independent nugget component (residual variation at finer spatial scales than evaluated in models).

Response variable	<i>n</i> sites	$\Delta AICc$	LOOCV R <sup>2</sup>	Fixed-effects	Fixed-effect <i>p</i> -value	<i>b</i>	Standardized <i>b</i>	Variance composition		
								Fixed-effects	Spatial	nugget
Density (sqrt)	59	0.0	0.67	Intercept	0.030	4.230	2.231	0.51	0.37	0.12
				Redd count	0.007	0.592	2.806			
				Wood count	0.035	0.080	2.164			
				Percent pool	<0.001	0.188	4.838			
	59	2.1	0.68	Intercept	0.030	4.804	2.228	0.47	0.44	0.09
				Redd count	0.010	0.610	2.679			
				Percent pool	<0.001	0.207	5.364			
	59	2.5	0.68	Intercept	0.129	-	-1.543	0.53	0.36	0.11
				Redd count	0.041	0.481	2.090			
				Temp	0.130	22.95	1.539			
				Temp <sup>2</sup>	0.141	-	-1.495			
				Percent pool	<0.001	0.202	5.109			
				Wood count	0.109	0.062	1.634			
	53	0.0	0.93	Intercept	<0.001	-	-5.202	0.69	0.29	0.02
				Temp	<0.001	1.167	9.886			
				Subbasin	<0.001	15.81	4.142			
				Density	0.001	-	-3.500			
				Temp*basin	<0.001	-	-5.498			
		1.6	0.92	Intercept	<0.001	-	-5.446	0.70	0.29	0.01
				Temp	<0.001	1.210	9.921			
				Subbasin	<0.001	15.77	3.915			
				Density	0.352	0.180	0.942			
				Temp*basin	<0.001	-	-5.236			
				Temp*density	0.176	-	-1.339			
	53	4.8	0.91	Intercept	<0.001	-	-4.931	0.63	0.34	0.03
				Temp	<0.001	1.115	8.988			
				Basin	0.001	12.94	3.460			
				Temp*basin	<0.001	-	-4.703			



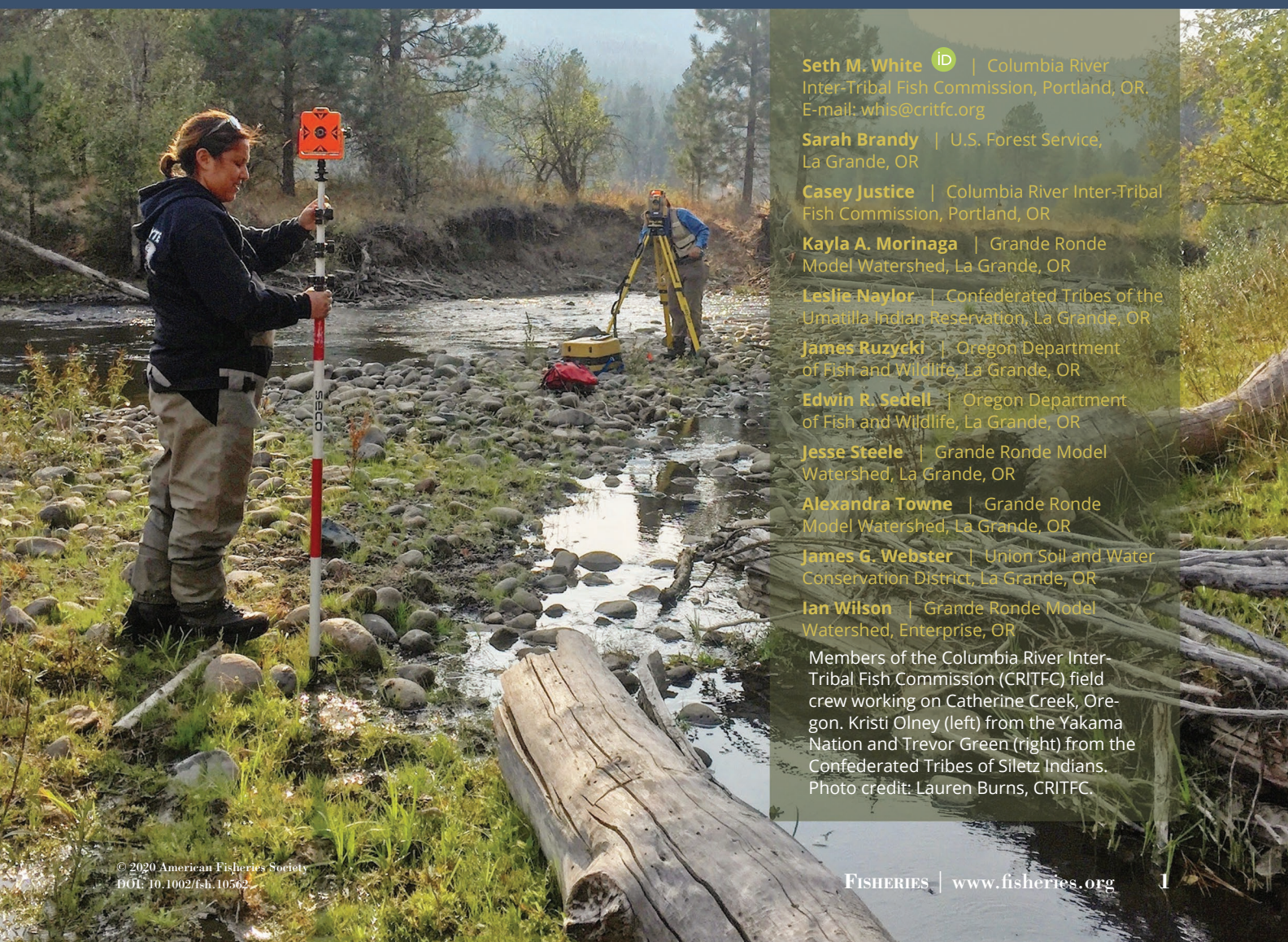
August size	53	0.0	0.89	Intercept	0.021	-	-2.390	0.58	0.41	0.01
				Aug. temp	<0.001	1.020	6.780			
				Basin	0.036	11.38	2.156			
				Density	<0.001	-	-4.695			
				Temp*basin	0.003	-	-3.097			
	53	1.5	0.89	Intercept	0.153	-	-2.517	0.60	0.39	0.01
				Temp	<0.001	1.074	7.005			
				Basin	0.048	11.08	2.034			
				Density	0.438	0.181	0.782			
				Basin*temp	0.005	-	-2.957			
	53	4.5	0.87	Intercept	0.180	-	-1.352	0.54	0.45	0.01
				Temp	<0.001	0.840	6.097			
				Basin	0.350	-	-0.946			
				Density	<0.001	-	-4.444			
				Basin*density	0.05	0.120	2.020			
Summer MSGR	53	0.0	0.58	Intercept	<0.001	6.371	3.580	0.14	0.71	0.16
				Temp	0.008	-	-2.760			
				Basin	0.110	-	-1.628			
				Temp*basin	0.104	0.338	1.656			
	53	0.85	0.58	Intercept	0.001	6.110	3.433	0.17	0.69	0.14
				Temp	0.013	-	-2.584			
				Basin	0.213	-	-2.584			
				Density	0.149	-	-1.475			
				Basin*temp	0.202	0.273	1.292			
	53	1.29	0.57	Intercept	0.001	4.980	3.494	0.14	0.71	0.15
				Temp	0.028	-	-2.266			
				Density	0.094	-	-1.713			
Summer <i>pCmax</i>	53	0.0	0.51	Intercept	<0.001	0.810	10.433	0.30	0.20	0.50
				Temp	<0.001	-	-4.567			
				Density	0.095	-	-1.783			
						0.004				
	53	0.53	0.49	Intercept	<0.001	0.762	10.250	0.26	0.22	0.52
				Temp	<0.001	-	-4.134			
	53	1.00	0.50	Intercept	<0.001	0.804	10.370	0.32	0.19	0.49
				Temp	<0.001	-	-4.622			
				Basin	0.350	0.016	0.994			
				Density	0.081	-	-1.770			

---

## **Appendix E – Published Fisheries paper on the Grande Ronde basin as a case study**

## PERSPECTIVE

# Progress Towards a Comprehensive Approach for Habitat Restoration in the Columbia Basin: Case Study in the Grande Ronde River



**Seth M. White**  | Columbia River Inter-Tribal Fish Commission, Portland, OR.  
E-mail: whis@critfc.org

**Sarah Brandy** | U.S. Forest Service, La Grande, OR

**Casey Justice** | Columbia River Inter-Tribal Fish Commission, Portland, OR

**Kayla A. Morinaga** | Grande Ronde Model Watershed, La Grande, OR

**Leslie Naylor** | Confederated Tribes of the Umatilla Indian Reservation, La Grande, OR

**James Ruzycski** | Oregon Department of Fish and Wildlife, La Grande, OR

**Edwin R. Sedell** | Oregon Department of Fish and Wildlife, La Grande, OR

**Jesse Steele** | Grande Ronde Model Watershed, La Grande, OR

**Alexandra Towne** | Grande Ronde Model Watershed, La Grande, OR

**James G. Webster** | Union Soil and Water Conservation District, La Grande, OR

**Ian Wilson** | Grande Ronde Model Watershed, Enterprise, OR

Members of the Columbia River Inter-Tribal Fish Commission (CRITFC) field crew working on Catherine Creek, Oregon. Kristi Olney (left) from the Yakama Nation and Trevor Green (right) from the Confederated Tribes of Siletz Indians. Photo credit: Lauren Burns, CRITFC.



Despite immense resources directed towards habitat restoration, recovering fish populations remains a daunting and perplexing issue. In 2015, recommendations for a comprehensive approach to habitat restoration in the Columbia River basin were published in *Fisheries*, which included elements of landscape ecology and resilience, broad public support, governance for collaboration and integration, and capacity for learning and adaptation. Using the Grande Ronde River basin as a case study, we convened a working group consisting of local restoration practitioners, managers, and researchers involved in habitat restoration research, monitoring, and evaluation to assess progress towards meeting these recommendations. We concluded that partnerships and collaborations in governance have been formed and research using a landscape perspective has been integrated into decision making, but efforts would benefit from gaining broader public support, formalizing an adaptive management strategy, and defining objectives and indicators for biological and ecological diversity. Continued progress will require consistent policy and funding support from the broader region. We envision this self-assessment at the 5-year milestone would be helpful to other groups facing similar challenges.

## INTRODUCTION

Historically, a diverse assemblage of fishes thrived in the Columbia River basin, owing to the region's dynamic landscapes (McPhail and Lindsey 1986). Anadromous Pacific salmon *Oncorhynchus* spp. and steelhead *Oncorhynchus mykiss* were particularly abundant, with the historical estimate of aggregate stocks averaging 10–16 million (NPCC 1986) as compared to a recent minimum estimate of 2.6 million (ODFW and WDFW, n.d.), with only 350 thousand of those being natural origin (CBPTF 2020). Although these declines are attributed to factors including ocean harvest, predation, and mortality from hydroelectric dams, degradation of tributary habitat conditions has also been implicated (McIntosh et al. 2000). Despite immense resources directed towards habitat improvement, recovering fish populations remains a daunting and perplexing issue. Columbia River habitat restoration exists in a sophisticated legal and regulatory landscape where states and tribes are recognized as equal co-managers (Blumm and Baermann 2020) and work together across multiple tribal, state, federal, and private jurisdictions. While advances in our understanding of technical aspects of restoration will continue to help, slow progress can be attributed to a deficiency of a comprehensive approach to restoration that recognizes conservation in the Columbia basin is embedded in a complex management landscape where ecological as well as socioeconomic and political factors need consideration (Hand et al. 2018).

Five years previously, recommendations for a comprehensive approach to habitat restoration in the Columbia River basin were articulated (Rieman et al. 2015). In spring and summer of 2019, restoration practitioners, managers, and researchers with longstanding experience in the basin formed a workgroup to implement a formal adaptive management strategy, starting with an in-depth study of calls to action made by Rieman et al. (2015) and a response detailing progress made in the Grande Ronde basin. In this paper, we present a case study from the Grande Ronde River, highlighting key accomplishments, lessons learned, and next steps towards achieving these goals. We envision these lessons—learned locally—will have broad applicability for habitat restoration throughout the Columbia River basin and beyond.

### Call for a Comprehensive Approach to Habitat Restoration

Rieman et al. (2015) outlined a comprehensive approach to habitat restoration in the Columbia River basin that could be achieved by rebalancing the goals of biological abundance and biological diversity, strengthening linkages between science and management, increasing public engagement, working across traditional ecological and social boundaries, and

developing a formal approach to learning from experience. The recommendations would be incorporated into every project at all levels including policy decisions, project planning, and management direction. The authors advocated for pursuing a comprehensive approach despite the complexity and cost, as new opportunities for efficiencies would arise and tradeoffs between the goals would become apparent. As one means to achieve these goals, Rieman et al. (2015) cited the need to recognize and champion local efforts that are innovative and effective. In this paper, we highlight aspects of one of those local efforts: the Grande Ronde River partnership.

## CASE STUDY METHODS

### Study Area

The Grande Ronde River is a large tributary of the Snake River, originating in the Blue Mountains of northeastern Oregon and flowing approximately 340 km to its mouth in southeastern Washington. The upper Grande River and its tributary Catherine Creek include the watershed upstream of the confluence of the Wallowa River (Figure 1). Land use activities since the mid-1800s including trapping American beaver *Castor canadensis*, logging, grazing, mining, water withdrawals, road construction, and urban development have degraded aquatic habitat conditions; for example, loss of coldwater refugia (Ebersole et al. 2003) and extensive channel simplification (White et al. 2017). Human-caused CO<sub>2</sub> emissions have contributed to a summer warming trend of Pacific Northwest streams of approximately 0.14–0.27°C per decade between 1976 and 2015 (Isaak et al. 2017, 2018). These warming trends are expected to contribute to range contraction and decreased capacity of salmonids in the basin (Justice et al. 2017). Climate change is also expected to negatively impact hydrology and availability of water resources (Clifton et al. 2018), as well as increase pathways for invasive species (Rahel and Olden 2008), which can have adverse effects on habitat (however, see Roche et al. 2020 for discussion of unexpected impacts of climate change on fish habitat and invasive species). In the Grande Ronde basin, habitat degradation has been implicated in the long-term decline and subsequent listing of local Chinook Salmon *O. tshawytscha* and steelhead (Figure 2), as well as populations of Bull Trout *Salvelinus confluentus* listed under the Endangered Species Act (ESA; NOAA 2008a).

Habitat restoration in the Grande Ronde River basin began in earnest in the mid-1980s, when the first Bonneville Power Administration (BPA)-funded project was implemented by the Oregon Department of Fish and Wildlife (ODFW) as documented by Beschta et al. (1991). Partly due to limited funding, early restoration efforts focused on small-scale



# UPPER GRANDE RONDE & CATHERINE CREEK PROJECTS 2017-2024

- 1.Lookingglass Conservation - 2023
- 2.Willow Creek Fish Passage - 2020
- 3.Indian Creek Fish Passage - 2021
- 4.Elmer Dam Fish Passage & Flow - 2021
- 5.CC37 LWD - 2022
- 6.CC38 - 2020
- 7.Red Mill Reach Phase I - 2019
- 8.Buffalo Land and Livestock Phase I - 2021
- 9.CC42 Adult Weir - 2024+
- 10.CC46-48.5 Opportunities - 2024+
- 11.State Parks Resotration - 2020
- 12.Hall Ranch - 2021
- 13.CC52 - 2023
- 14.LDS Camp - 2023
- 15.SF Catherine Creek Ditch - 2024+
- 16.Beaver Creek Dam Fish Passage - 2017
- 17.Mine Tailings Restoration Project - 2022
- 18.Woodlee Campground Restoration - 2019
- 19.Limber Jim (Schiller) Culvert - 2020
- 20.Limber Jim Creek Restoration - 2017
- 21.UGR Small Streams Restoration - 2019
- 22.UGR Small Streams Restoration - 2020
- 23.UGR Small Streams Restoration - 2021
- 24.UGR Culvert Replacements - 2017
- 25.Sheep Creek Restoration - 2019
- 26.Fly Creek Restorition Phases I-III - 2020
- 27.MUGR River Canyon Restoration - 2019
- 28.Bowman Habitat Restoration - 2020
- 29.Meadow Creek Starkey Forest LWD - 2023
- 30.Dark Canyon LWD - 2024
- 31.Dark Canyon Restoration Phase I&II - 2023
- 32.Longley Meadows Restoration - 2021
- 33.Whiskey Creek 244, Culvert - 2020

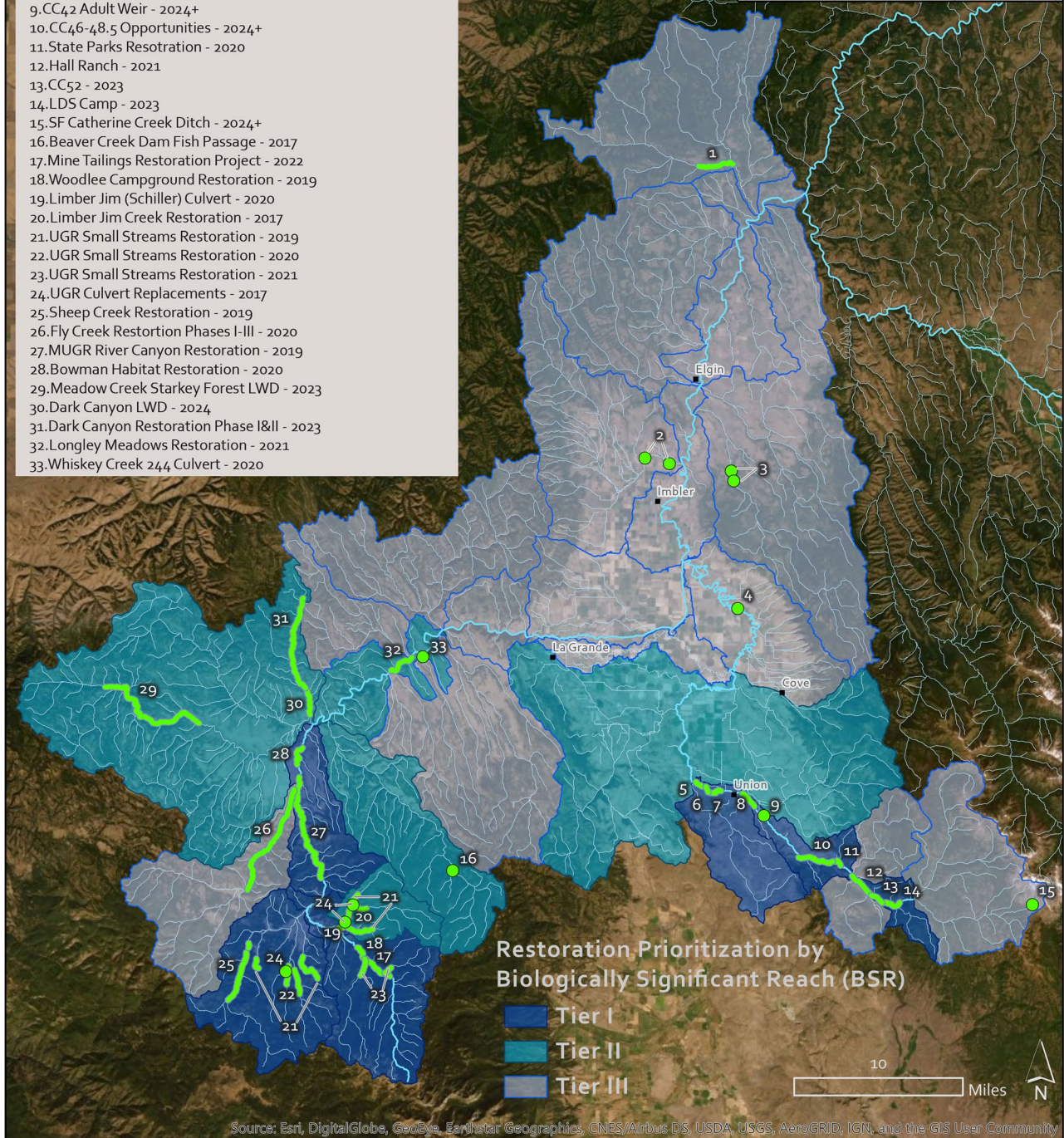
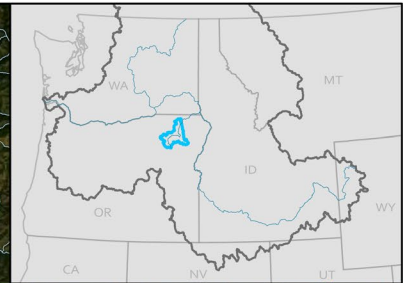


Figure 1. The upper Grande Ronde River and Catherine Creek watersheds in northeastern Oregon. Tier I-III conservation areas (high to low priority) from the Grande Ronde Atlas (Atlas) are shown along with restoration initiated or planned since 2017, when Atlas projects were first realized on the ground. Some restoration projects in Tier III (low priority) areas are passage improvements allowing fish to migrate into their historical range (i.e., projects 2-4).



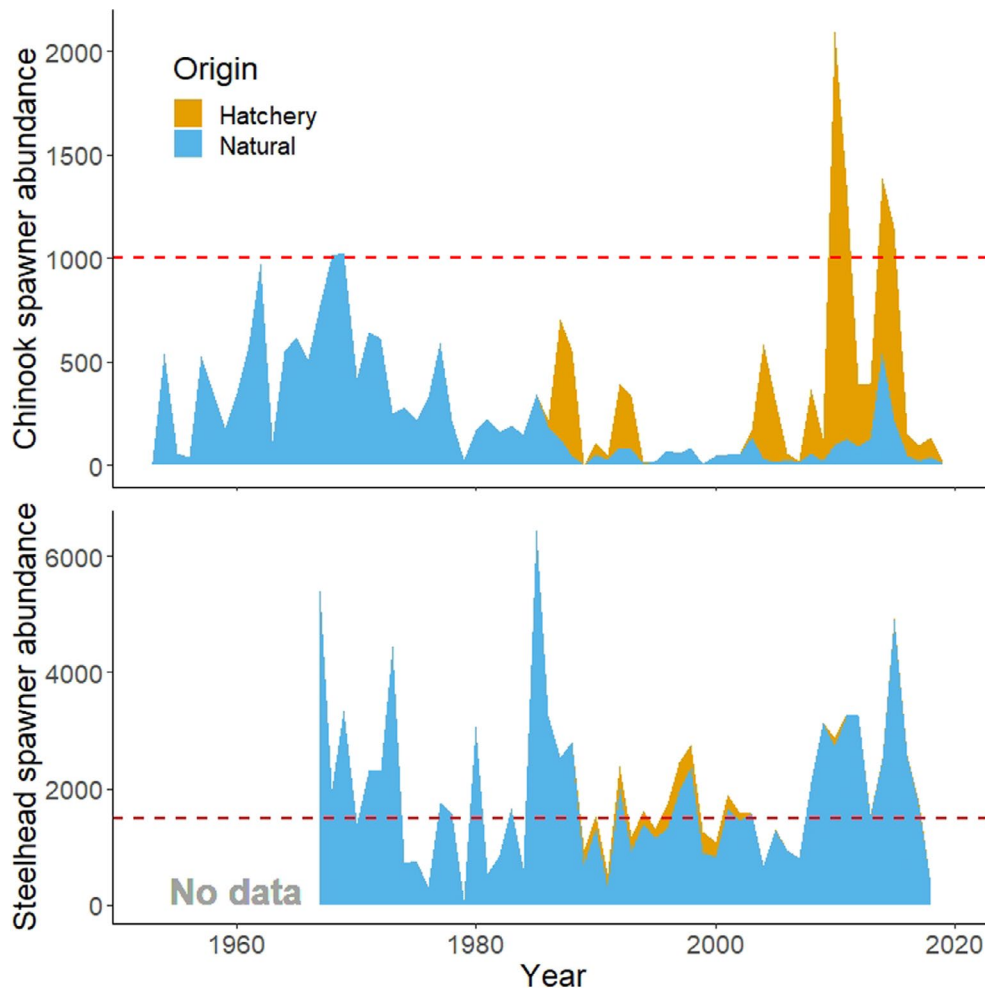


Figure 2. Abundance of hatchery and natural origin spring Chinook Salmon spawners (including jacks) returning to population areas for Grande Ronde upper mainstem during 1953–2019 (top panel) and summer steelhead during 1967–2018 (bottom panel). Red dashed lines represent minimum abundance thresholds considered viable and at low risk with a 95% probability of persistence over 100 years (NOAA 2017). Note different y-axis scale for each panel. (Data compiled by Oregon Department of Fish and Wildlife East Region Fish Research & Monitoring).

passage and fish screening, streambank stabilization, road improvements, and riparian conditions (Sedell 2018). To this day, there are concerns that restoration efforts may not overcome the rate of habitat degradation in the watershed, a worry that was underscored by results from an ecosystem diagnostic and treatment modelling exercise, which is a science-based planning tool incorporating local values and objectives (see Mobrand et al. 1995). The 2008 Federal Columbia River Power System Biological Opinion (NOAA 2008b) delivered mandates for BPA, the U.S. Bureau of Reclamation, and the U.S. Army Corps of Engineers to address habitat factors limiting salmon and steelhead populations in the upper Grande Ronde River and Catherine Creek, thus increasing funding for restoration. Starting in 2014, prioritizing stream reaches and restoration actions addressing critical limiting factors by life stage for ESA-listed populations became a central focus. This led to a collaborative effort to develop the Grande Ronde Atlas (henceforth referred to as Atlas), a dynamic tool that utilizes existing scientific data, current research evidence, and expert knowledge to prioritize restoration actions in biologically significant reaches. Once identified, restoration opportunities are scored and ranked using biological and other criteria; see Atlas Partners (2015) for a detailed description.

### Case Study Approach

We used the case study approach described by Yin (2018) to elucidate generalizable concepts through detailed assessment of the Grande Ronde partnership. Initial responses to the directives of Rieman et al. (2015) were developed in two, half-day workshops with Atlas partners. Essentially, each directive was discussed in meetings with the entire group (including but not limited to co-authors of this paper), with an emphasis on providing specific examples demonstrating (1) good progress, (2) adequate progress but with room for improvement, or (3) marginal progress. This qualitative scoring rubric reflected our ability to cite specific examples during the workshop and in subsequent discussions. For example, if ample evidence for strong community partnerships was evident in the form of positive feedback from the public, good attendance and participation at public meetings, and sustained public engagement with restoration, these would then become the basis for a “good” rating for the related directive. In contrast, if no specific examples of quantitative goals or indicators for biological diversity currently in practice could be gleaned from the participants, this would then become the basis for a “marginal” rating for the related directive, and so forth. After the in-person workshops, participants were

divided into smaller workgroups to develop written narratives on the topics most relevant to their interests and expertise. The sections were then combined into a single draft and shared with all participants to solicit final comments prior to drafting this article. While we recognize the Grande Ronde River does not represent every watershed perfectly, we maintain general insights can be extrapolated broadly, a key assumption of the case study method.

### PROGRESS ON RECOMMENDED ACTIONS

Here, we dive deeper into illustrative examples of the Grande Ronde partnership corresponding to the three categories of progress (good, adequate, and marginal). Corresponding topics are combinations of individual directives from Rieman et al. (2015) and include (1) building partnerships among scientists, managers, and the public (good progress); (2) integrating research findings with formal decision making (adequate progress); and (3) implementing measurable objectives and indicators for biological diversity as equal priority to abundance (marginal progress). While we focus on these specific aspects for our case study, an overview of all workshop findings can be found in Table 1.

#### Good Progress: Building Partnerships among Scientists, Managers, and the Public

Integration of science and management requires a local coordinating entity and ongoing commitment to invest in peer-learning opportunities. With the formation of the Grande Ronde Model Watershed (GRMW) Program in 1992—an organization that provides an interface between science and management and coordinates conservation on public and private land—restoration expanded to include additional partners. Atlas and GRMW have the explicit goal of bringing together and encouraging dialogue among managers, researchers, and stakeholders with a range of interests to allocate limited resources. The initial prioritization framework involved meetings between program managers, project sponsors, researchers, restoration implementers, and other experts from multiple local, state, tribal, regional, and national organizations as members of a science technical advisory committee (Tetra Tech 2017). Atlas participants rely on ongoing monitoring efforts (e.g., screw traps, adult weirs, snorkel and spawning surveys, and radio tracking data) and research findings (e.g., maps of modeled water temperature and habitat surveys) to prioritize restoration. As new information comes in from research, monitoring, and evaluation, Atlas updates priorities for restoration monthly. In addition, an annual State of the Science meeting hosted by GRMW provides an opportunity for scientists to showcase new research and monitoring techniques, as well as a forum for managers to communicate on-the-ground needs. Scoring of priority reaches for restoration is updated every 5 years. Improved collaboration with fisheries scientists because of Atlas has been critical to refining restoration strategies.

Community engagement is a key component of successful stream habitat projects (Hand et al. 2018), especially in rural communities where residents can be skeptical of restoration. Project information and accomplishments are often shared through individual agency websites and social media pages, local newspapers, professionally produced videos, and brochures (e.g., Figure 3). The GRMW produces *Ripples in the Grande Ronde* (<https://grmw.org/#rippleBox>), a quarterly online and print newsletter with an average circulation of

10,000 print copies. NOAA Fisheries, GRMW, and Columbia River Inter-Tribal Fish Commission (CRITFC) are currently collaborating on a short outreach film about river restoration in the Grande Ronde basin ([www.grmw.org/ourwatershed](http://www.grmw.org/ourwatershed)). The Union Soil and Water Conservation District (USWCD) provides the agricultural community with education and technical assistance for developing natural resource conservation projects, including stream restoration. Another example includes Union County's Place-based Water Planning (<https://bit.ly/3mpaEiG>), an effort that has brought together landowners, natural resource agencies, state, federal, local government, tribes, and others to tackle issues such as summer water deficit, declining aquifers, and flooding.

Economic stimulation from restoration efforts has helped rebuild communities in rural areas, including new approaches to rural development (Hibbard et al. 2015). Restoration contractors purchase numerous local goods and services, such as trees from private forestlands for stream restoration projects, providing benefits to the local economy. Restoration practitioners in the Grande Ronde basin use social and economic incentives for agricultural, ranching, and forestry operations. The Natural Resource Conservation Service (NRCS) has several incentive programs in exchange for implementation of conservation measures in partnership with the USWCD, such as irrigation efficiency upgrades, riparian fencing, upland water source development, grazing management plans, forest thinning, and conservation easements. The Freshwater Trust ([www.thefreshwatertrust.org](http://www.thefreshwatertrust.org)) also provides incentives for water quantity and quality conservation, such as lining or piping ditches to prevent water loss and leasing or purchasing water rights.

Community science (also referred to as citizen science) provides opportunities for the public to contribute to socio-ecological objectives of restoration, while increasing awareness and promoting stewardship (Edwards et al. 2018). In 2018, a new monitoring network coordinator position at GRMW was created to increase public outreach and involvement. In coordination with U.S. Forest Service (USFS) staff, plans include training volunteers to conduct surveys of Columbia spotted frogs *Rana luteiventris*, monitor freshwater mussels, and conduct aquatic macroinvertebrate surveys. Grande Ronde basin partners are actively seeking additional ways to increase public involvement, including a proposal recently funded through a USFS Youth and Community Engagement program that would provide learning opportunities about river restoration for high school classrooms and the public. However, funding for staff to continually recruit and train community scientists and volunteers will be necessary to maintain this momentum.

Although workshop participants considered this directive as one of their most successful, several barriers to sustaining partnerships between scientists, managers, and the public still exist. While education and outreach are critical for articulating the work conducted in the basin, funding staff for these tasks is challenging. Partners rely on existing staff to work outside their job duties, or on volunteers to fill the role of outreach specialists. The local Wallowa-Whitman National Forest employs public outreach specialists, but their focus has historically been on national forestland projects, recreation, and safety updates—however, this is changing to include press releases covering all forest activities including aquatic restoration. Outreach and education often follow project implementation, yet these efforts would benefit from earlier engagement of key players.

Table 1. Recommended actions towards a comprehensive approach for habitat restoration in the Columbia Basin (adapted from Rieman et al. 2015), with examples of progress in the upper Grande Ronde Basin since the formation of the Grande Ronde Atlas (Atlas) framework. Qualitative assessments of progress (marginal/red, adequate/yellow, or good/green) are indicated in the rightmost column.

Action	Directive	Examples of progress in the Grande Ronde basin	Progress
Rebalance the goals	Develop and communicate goals and measurable objectives for biological diversity that are held as equal priority to the goals and objectives for abundance	Atlas prioritizes restoration in areas with overlap in salmonid species use, life stages (Figure 1); multiple life history strategies of salmonids are considered; Confederated Tribes of the Umatilla Indian Reservation First Foods concept emphasizes ecological diversity and resilience	Marginal
	Directly engage all stakeholders and the public to broaden understanding of the critical value of biological diversity	Public outreach efforts emphasize the ecological value and ecosystem services provided by freshwater mussels, beaver, Pacific lamprey, and Columbia spotted frogs (Figure 7)	Good
	Develop indicators for monitoring that measure and communicate progress on abundance and biological diversity at multiple scales across the basin	Abundance criteria and indicators for VSPs exist at the population scale; Life-stage specific indicators for salmonids are expressed at the reach scale	Marginal
	Consider the implications of hatchery production for carrying capacity and diversity of wild fish as a basis for integrating hatchery production with habitat restoration	Hatchery genetic management plans list performance standards for limiting impact on carrying capacity; Life cycle models incorporating the contribution of supplemented to natural populations are in development	Adequate
Strengthen linkages between science and management	Use landscape sciences and technology in assessment and restoration planning and support and expand common application of relevant research, monitoring, modelling, and analytical tools	Remotely sensed information (Light detection and ranging and thermal infrared) used to develop a water temperature model and potential vegetation map, for the purpose of prioritizing areas where riparian restoration could mitigate future climate change in conjunction with life cycle model; carcass additions as a management tool evaluated using field experiments	Good
	Create and support communities of practice and peer-learning networks that demonstrate science–management integration; highlight new tools and analyses that are innovative and promote those with real potential for success	The Grande Ronde Model Watershed (GRMW) provides interface between science and management and coordination of restoration; development of Atlas involved intensive exchanges between researchers and managers including annual State of the Science meeting	Good
	Recommit to options for broadly based technical assistance to provide analytical support, constructive criticism, and feedback to proposed and ongoing projects	Projects are scrutinized internally by Atlas technical committee and reviewed by GRMW board of directors; broadly based technical assistance from outside the sub-basin's expertise was identified as a need	Adequate
Increase public engagement	Include education and outreach specialists as key players at the earliest stages of project development	Wallowa-Whitman National Forest uses public outreach specialist to communicate broad forest management plans; more resources are needed to support efforts at local scales	Good
	Engage people and organizations early through forums that encourage dialogue between managers, researchers, and stakeholders associated with a range of resource values	Atlas has the explicit goal of bringing together managers, researchers, and stakeholders; more engagement with the public as stakeholders is needed, requiring policy and funding support	Good
	Align ecological needs with social and economic incentives and consider benefits and costs to people and their communities	The Natural Resource Conservation Service and Freshwater Trust use incentives for landowners to engage in conservation measures; restoration contractors purchase trees from local landowners	Adequate
	Use a wide diversity of media and forums for public and community engagement	The GRMW publishes <i>Ripples in the Grande Ronde</i> with broad distribution to the community; NOAA, GRMW, and the Columbia River Inter-Tribal Fish Commission are producing a short public outreach film to gain broad support for salmon conservation efforts; Figure 3 provides an example of printed outreach materials for landowner incentives	Good
	Make public involvement and active learning through citizen science in monitoring and research a central element in project implementation	Opportunities to engage community science include K-12 classrooms monitoring nearby restoration projects (e.g., Sheep Creek; see Figure 6); efforts to enlist community scientists are just now gaining momentum	Adequate
	Recognize the social sciences as a critical element of scientific review and guidance and include social scientists as primary contributors to the advisory, review, and planning process	GRMW recently solicited guidance from a social scientist at Eastern Oregon University regarding community outreach efforts; diverse boards of directors at GRMW and the Union Soil and Water Conservation District provide social and economic review of restoration projects	Marginal

(Continues)

Another obstacle to partnership building results from different groups assigning different importance to ecological, social, cultural, and economic values, making the process of

aligning these values complex. For example, Columbia basin treaty tribes prioritize the ecological, subsistence, and cultural needs of fisheries resources above and beyond immediate



Table 1. (Continued)

Action	Directive	Examples of progress in the Grande Ronde basin	Progress
Work across traditional ecological and social boundaries	Highlight and support experiments in governance for collaborations that bridge agency and intellectual groups, local and regional organizations, governments, landowners, and science-management disciplines	Atlas is founded on partnerships between managers and researchers from multiple local, state, federal, and tribal organizations; Union County's Place-based Water Planning program has strong interdisciplinary and multiagency participation	Good
	Bring innovative and successful examples (including those from other resource and restoration disciplines) to others in the basin	Guidance for restoration prioritization draws from a wealth of literature from the PNW and from the Umatilla tribe's <i>River Vision</i> ; landscape-scale watershed assessment approaches applied in the basin were imported from approaches used internationally; lessons can be learned about applying adaptive management from the upper Columbia River basin groups	Adequate
Learn from experience	Identify clear, quantitative objectives, including diversity objectives that form the baseline for the adaptive management cycle	Quantitative objectives for fish abundance are more clearly defined (e.g., natural origin spawner abundance) but diversity objectives are gaining attention; examples of quantitative objectives for the Sheep Creek project are provided in Figure 6	Adequate
	Implement intentional, science-based management experiments that promote learning about landscapes, cost effective restoration actions, and understanding of their socio-ecological implications	Landscape-scale water temperature model used to evaluate which restoration strategies would be most effective under future climate change scenarios; Regional Action Effectiveness Monitoring program will provide general guidance on project-scale restoration effectiveness; experimental additions of fish carcasses conducted in upper Grande Ronde River helped evaluate carcass additions as a management tool	Good
	Incorporate options for citizen science in monitoring and experiential programs that help reduce monitoring costs and promote broader understanding of the results	New monitoring coordinator position at GRMW provides support for community science programs alongside U.S. Forest Service; plans include surveys for amphibian egg masses, freshwater mussels, and aquatic invertebrates using community scientists	Adequate
	Use formal models to guide more structured decision making and to communicate a broader vision of the system and its critical uncertainties to all involved	Quantitative life-stage and life-cycle models have assisted in decision making, but the overall adaptive management process could be improved by using formal models such as structured decision making (SDM). Atlas includes many—but not all—components of SDM. Continued funding and logistical support for monitoring programs will be required to meet this goal	Adequate

economic incentives, with the expectation that treaties between tribes and the United States would protect salmon so that tribes could always earn a moderate living through fishing (CRITFC 2014). Recognition of the lower Columbia River tribes as co-managers having an equal footing has gone a long way towards reforming and sustaining the relationships among tribes and other entities in the Columbia basin (Blumm and Baermann 2020). Meanwhile, values and preferences may differ among landowners, recreational and commercial fishers, the agricultural and forestry industries, and biodiversity conservation groups (CBPTF 2020).

#### Lessons learned and next steps:

- (1) Integration of science and management requires a local coordinating entity and ongoing commitment to invest in peer-learning opportunities. In the Grande Ronde, this was accomplished in part through the formation of the GRMW. Next steps include sustained commitment to provide effective forums encouraging science-management interface.
- (2) Improved collaboration between restoration practitioners and fisheries scientists has been critical to refining restoration and adaptive management strategies. In the Grande Ronde, this was accomplished through a series of face-to-face meetings between restoration scientists and practitioners. Next steps include continuing these regular implementation team meetings and providing scientists with information about future restoration projects to allow adequate planning for pre- and post-restoration assessments.

- (3) Community engagement is a key component of successful river restoration. In the Grande Ronde, this was accomplished with a series of written materials and in-person outreach and technical assistance to the local community, including landowners. Next steps include continuing these outreach efforts while attempting to engage the community at earlier stages, an activity that will require dedicated funding.

- (4) Community scientists and volunteers can increase capacity to achieve and document ecological responses to river restoration. In the Grande Ronde, this is being accomplished through finding opportunities for community members to collect field data for river health assessments. Next steps include securing funding dedicated to supporting staff to run community science programs.

#### Adequate Progress: Integrating Research Findings with Formal Decision Making

Landscape sciences and population-scale analytical tools represent a critical component of the restoration planning process. For example, remotely sensed thermal infrared and light detection and ranging (LiDAR) data were coupled with ground-based habitat measurements to develop a water temperature model for assessing restoration and climate change impacts on salmon populations (Justice et al. 2017). Since the publication of these findings and after the formation of Atlas, restoration actions have emphasized riparian vegetation



## SUCCESS STORIES

### The 6-Ranch

The 6-Ranch has been host to two separate restoration projects, co-owner James Nash says, "our experience with restoration and the partners has been very positive." The 6-Ranch has realized many benefits from their restoration projects, including a higher water table, the (decades absent) return of wild spawning anadromous fish, and the return of nesting eagles and other avian species. James Nash also now fulfills his lifelong dream of guiding fly fishermen on the 6-Ranch, a pursuit that supplements the ranch's net income.

### The Smith Family Trust

After a high water event on Catherine Creek, Glen Smith and his family wanted to stabilize their streambanks to minimize further erosion. Glen, an avid outdoorsman, was surprised to find that restoration could balance a sustainable cattle operation while benefitting fish and wildlife. The Smiths now enjoy an improved irrigation system, payments from enrolling 17 acres in a CREP easement and reap the benefits of a split-season water lease.

### The Oregon Ag. Foundation

Jean and Glen McKenzie, longtime philanthropists, left their farm to be managed by the Oregon Agricultural Foundation (OAF). The McKenzies wanted a balance of ecological sustainability and agricultural production, as well as educational opportunities for EOU faculty and students. OAF now has 150 acres enrolled in a CREP easement along Willow Creek and 650 acres of leased farm ground, both providing income for the Eastern Oregon University Foundation which funds scholarships and capital improvements.

## LANDOWNER PROGRAMS

### Instream Flow Restoration

The Freshwater Trust's instream flow restoration program offers landowners a financial incentive to manage water in ways that balance the instream needs of fish and their habitat with economic and social needs. This program involves a variety of options including irrigation efficiency upgrades, short or long-term leases, and late-season shut-offs. These flexible tools allow producers to maximize income, restore rivers, and keep water rights intact. Many factors are considered for flow restoration, including the landowner's long-term goals, type of agricultural production, irrigation methods, funding sources, water rights, and instream flow needs.

### Conservation Reserve Enhancement Program

The Conservation Reserve Enhancement Program (CREP) through the Farm Service Agency (FSA) targets farmland that is adjacent to rivers and streams, providing an opportunity for valuable habitat improvements on what is often marginal soil. For farmers and landowners facing crop damage from flooding, restoring habitat can also increase flood storage capacity, while significantly reducing farming risks. This voluntary program allows participants to receive an annual rental payment for their enrolled acres. FSA also provides cost-sharing for set up, conservation practice incentives, and bonuses based on individual size and type of easement.

### Natural Resource Conservation Service

The NRCS seeks to co-invest with local partners in innovative approaches to benefit farming, ranching, forest operations, local economies, and natural resources. Many programs exist for producers to make conservation a reality, including the Agricultural Conservation Easement Program (ACEP), Environmental Quality Incentives Program (EQIP), Conservation Stewardship Program (CSP) or the Healthy Forests Reserve Program (HFRP). These programs can assist in irrigation improvements, compensate producers for conservation practices, and offer easement rental payments.

grande ronde basin restoration partnership

# WHAT'S GOOD FOR FISH, IS GOOD FOR THE FARM

Find out if restoring fish habitat could add value to your property, while providing agricultural risk management and budgeting tools.

Figure 3. Example of public outreach materials that communicate alignment between ecological, social, and economic incentives in the Grande Ronde basin. (Flyer courtesy of the Grande Ronde Model Watershed.)

improvement in areas with summertime temperatures approaching critical thresholds for salmonids. Additionally, basin-wide bathymetric, thermal profile, and hydrologic data were combined with remotely sensed data to assess limiting habitat factors and prioritize restoration actions (USBOR 2012, 2014). Researchers have discovered mechanisms driving spatial patterns in ecosystem processes by evaluating stream metabolism and juvenile salmon abundance at the river network scale (Kaylor et al. 2019a) and assessing salmonid and overall food web responses to carcass additions (Kaylor et al. 2019b; Kaylor et al. 2020). In summer of 2020, CRITFC, GRMW, and BPA collaborated on obtaining remotely sensed, topobathymetric LiDAR data to assess river conditions across 76,188 acres of the Grande Ronde River and nearby Wallowa River watershed, including mainstem riparian and floodplains, but also larger fish-bearing tributaries. The forthcoming LiDAR data will allow researchers to evaluate a decade of vegetation change and map fish habitat quality and quantity across extensive portions of the watersheds.

Life cycle models have been developed to integrate population-scale biological and physical habitat data and assess long-term salmon population response to various restoration and hatchery supplementation scenarios (Pess and Jordan 2019). For example, Weber et al. (2018) demonstrated that hatchery supplementation of the upper Grande Ronde Chinook Salmon population coupled with aggressive habitat restoration are necessary to sustain populations above extinction thresholds, especially with future climate change. Next steps include the development of a Bayesian state-space model that will integrate life stage-specific biological and habitat data to estimate parameters of the Chinook Salmon life cycle (akin to Rivot et al. 2004) and evaluation of population responses

to a range of potential climate change, restoration, and other policy scenarios (similar to Crozier et al. 2008).

Not all restoration strategies suggested as optimal by model results are feasible within the current socioeconomic and political landscape as articulated by Hand et al. (2018). For example, in the Grande Ronde basin several large tracts of high intrinsic potential habitat for salmonids have been inaccessible to restoration and monitoring efforts because some landowners do not allow access to their property. Recent headway has been achieved through agency staff nurturing personal contacts with landowners, including field tours to nearby restoration projects and communication of common goals achieved through restoration and ranching (i.e., increased late-season water availability and pasture greenness). Other incentives have included irrigation efficiency improvements at no cost to landowners after removal of push-up dams that were impeding fish passage. By developing a more holistic "whole ranch" approach and tapping into programs to improve off-channel grazing efficiency—such as the NRCS Environmental Quality Improvement Program that provides spring developments and upland fencing, or the Farm Service Agency's Conservation Reserve Enhancement Program that provides financial incentives for creating riparian buffers—restoration practitioners can present a bundle of incentives to landowners that may otherwise be unwilling to participate in a project focused only on instream habitat and floodplains. The development of inter-agency coordination and cooperation within the Grande Ronde basin has been an important step in encouraging landowners to participate in restoration projects that cover several kilometers of stream, provide habitat complexity within the wetted channel and the floodplain, but are not detrimental to continuing their farm and ranching operations.

Most restoration efforts in the upper Grande Ronde basin are evaluated on an individual project basis rather than their cumulative effects; corresponding monitoring methods have not been standardized, nor consistently applied. One exception includes a watershed-scale assessment of riparian restoration required to cool water temperatures for salmonids facing climate change (Justice et al. 2017). Recognizing the need for a more standardized and comprehensive monitoring program, local researchers adopted the Columbia Habitat Monitoring Program (CHaMP 2016), with 471 visits to 162 sites within the Grande Ronde basin from 2011–2017 to assess status and trends in fish habitat conditions. However, CHaMP was abruptly terminated prior to its intended completion date due to concerns over high cost, lack of explicit comparison between impaired and reference conditions, and problems with survey repeatability. While there may be some validity to these concerns, termination of the program came at a price—most significantly the impaired ability to assess long term trends in habitat conditions throughout the Columbia Basin using a robust statistical survey design. Additionally, replacement of CHaMP with BPA's Action Effectiveness Monitoring program (Roni and O'Neal 2017) drastically reduced the spatial coverage of monitoring sites throughout the basin, thereby limiting the availability of habitat data for local decision making. Despite the termination of CHaMP, local efforts to assess cumulative restoration effectiveness have continued, including development of a new tributary habitat assessment protocol that couples rapid ground-based surveys with remotely-sensed imagery (White et al. 2020) and a compilation of information on the type and intensity of over 700 restoration efforts conducted since the mid-1980s to evaluate the long-term, cumulative impacts of restoration in the Grande Ronde basin (Benge 2016).

Quantitative models are used in the Grande Ronde basin to support decision making, including assessing limiting factors for salmon (Burke et al. 2010; NOAA 2017), estimating salmon population response to tributary habitat actions and climate change (Justice et al. 2017; Weber et al. 2018), and prioritizing restoration actions (Atlas Partners 2015; Justice et al. 2017). However, admittedly, these efforts have not been formally integrated into structured decision making (SDM) as recommended by several authors (Hilborn 1992; Conroy and Peterson 2013; Rieman et al. 2015), likely because of limited resources and expertise. Prioritization of restoration is currently guided by Atlas, which does include some elements of SDM. These include reviewing existing information to identify habitat impairments and limiting factors, identifying and coordinating with stakeholders, defining objectives, developing alternative restoration actions, estimating consequences of alternatives using a quantitative ranking system, and strategically selecting projects to maximize biological benefit. This process could be improved by including more specific, quantitative objectives, developing a broader set of management alternatives, and establishing a clear feedback loop in an adaptive management process to inform decision making (Figure 4).

Lessons learned and next steps:

- (1) Landscape sciences and quantitative, population-scale analytical tools are critical components of the restoration planning process; yet links between these analytical tools and management could be strengthened. In the Grande Ronde, this is accomplished by a combination of remote sensing, ground-based monitoring, and integration of

these data using statistical and mechanistic models. Next steps include development a formal structured decision-making process to help guide adaptive management.

- (2) Life cycle models can provide new insights and confirm existing assumptions about scenarios leading to population recovery or extirpation. In the Grande Ronde, a life cycle model indicated that aggressive riparian restoration was required to counteract climate change. Next steps include the development of a Bayesian state-space model to evaluate likely outcomes of a range of climate change, restoration, and other policy scenarios.
- (3) Restoration efforts should be evaluated as an overall population-scale strategy and include analyses of cumulative effects, in addition to assessment of individual restoration projects. In the Grande Ronde, this is accomplished by watershed-scale analyses of an extensive network of ground-based habitat monitoring and remote sensing. Next steps include applying a new tributary habitat assessment protocol and evaluation of long-term impacts of habitat improvement projects.
- (4) Optimal conservation solutions suggested by quantitative models need to be framed within the larger socioeconomic and political landscape. In the Grande Ronde, this is underscored by the inability to restore fish habitat in vast tracts of inaccessible private land. Next steps include adjusting scenarios addressed by quantitative models to account for the realities of the sociopolitical landscape, but also continuing to forge relationships with communities, including landowners, so that high-priority habitat on private land can be protected and restored.

#### **Marginal Progress: Implementing Measurable Objectives and Indicators for Biological Diversity as Equal Priority to Abundance**

Regional goals such as those stated in the ESA Recovery Plan (NOAA 2017) remain weighted toward abundance and in-river productivity thresholds for salmonids; although the plan includes provisions for diversity in population spatial structure, genetics, and life history strategies. These goals represent minimum values intended to maintain populations above extinction thresholds (CBPTF 2019), yet other plans in the region target higher abundances, with greater emphasis on ecosystem processes (e.g., NPT 2013). River restoration in the Grande Ronde basin historically focused on a narrow range of ecosystem components (e.g., instream habitat complexity and bank stability) across small spatial scales (hundreds of meters). Current restoration actions emphasize ecological or functional diversity by initiating larger projects (kilometers of river) and restoring natural fluvial processes and channel complexity by improving floodplain connectivity and off-channel habitats, increasing hyporheic exchange, and revegetating riparian zones (e.g., the Southern Cross project shown in Figure 5). In addition, Atlas prioritizes restoration actions in locations with overlap among multiple salmonid species, life stages, and life history strategies. Finally, incorporation of the Confederated Tribes of the Umatilla Indian Reservation (CTUIR) "First Foods" concepts into management practices embodies a shift towards managing rivers for ecological diversity and resilience. The First Foods approach, which is based on honoring reciprocity between humans and biota and their obligation to sustain each other, details a vision for resilient and functional river ecosystems, and has become the foundation of CTUIR's management approach (Quaempts et al.



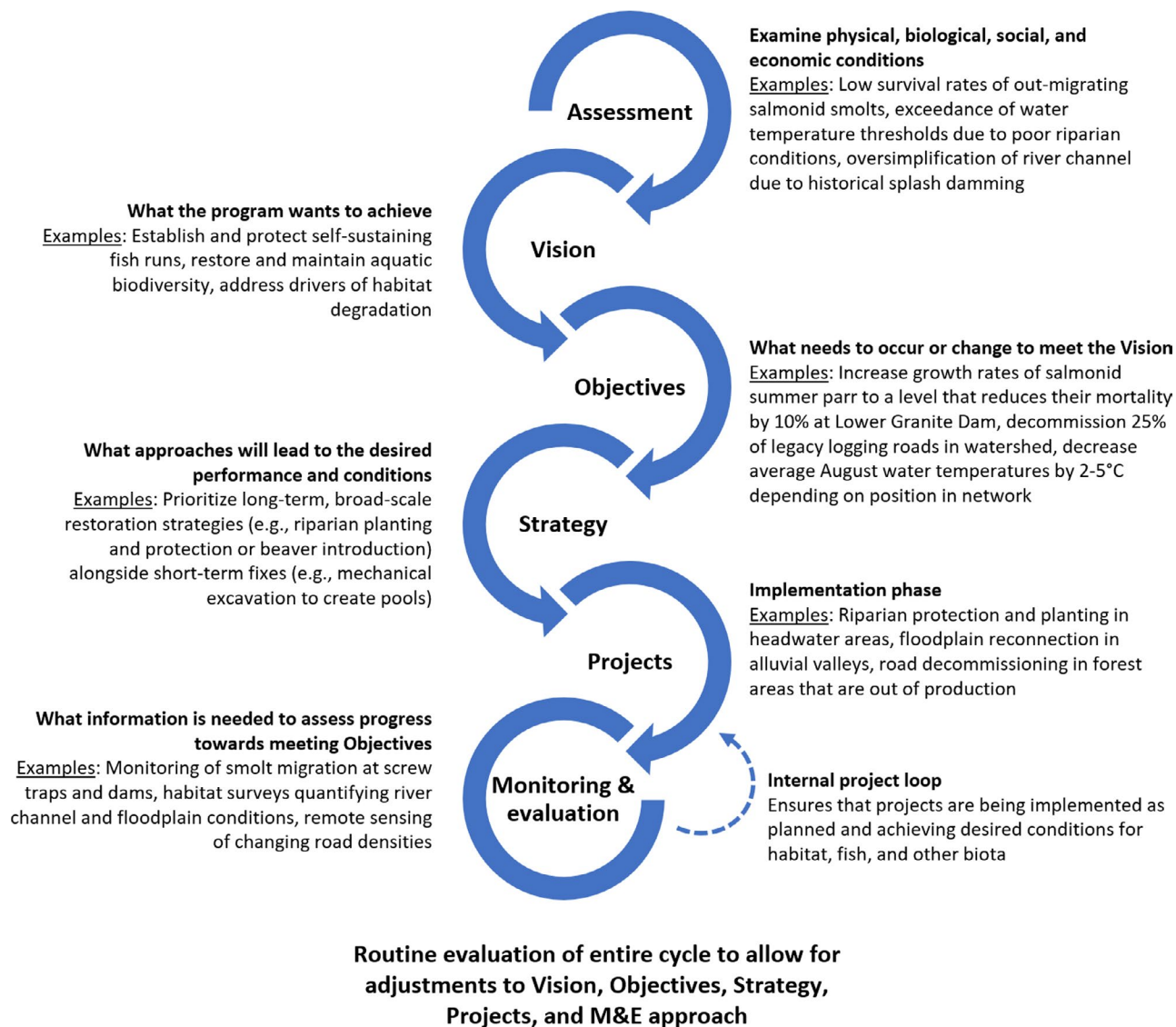


Figure 4. Adaptive management process with examples from the Grande Ronde basin. Monitoring, evaluation, and assessment form the backbone of learning and revising the vision, goals, objectives, strategies, and projects intended to improve tributary habitat conditions in support of salmon recovery and river ecosystem health. M&E = monitoring and evaluation. (Adapted from ISAB 2018.)

2018). Although restoration and management decisions have increasingly emphasized ecological diversity, a more focused effort is needed to develop and communicate quantifiable objectives for biological and functional diversity.

Indicators related to salmon and steelhead abundance and productivity are well developed, and data are robust owing to long-term collection of adult spawner and smolt data by ODFW and CTUIR. At the reach scale, life-stage specific indicators (e.g., juvenile salmon abundance, migration survival rates, pre-spawn mortality) are used to identify priority areas for restoration or adjust management actions (Sedell et al. 2018; White et al. 2018). Although some progress has been made in identifying diversity indicators and collecting the requisite data to quantify them, limited funding and uncertainty in measuring diversity has hindered progress. Recent research in the Grande Ronde basin has placed a greater emphasis on biological diversity by evaluating stream metabolism (Kaylor et al. 2019a), food webs of the entire fish assemblage and macroinvertebrate community (Kaylor et al. 2020), and novel prey availability indices (Sullivan and White 2017). A focused,

collaborative effort among basin partners and funding agencies will be needed to reach consensus on high priority indicators and standardized methods for computing them. We have begun this process by compiling several candidate biological and ecological indicators along with associated data sources and detailed definitions (Supplemental Table A).

For assessments of how individual or cumulative restoration projects affect indicators of abundance or diversity, a key problem articulated by Rieman et al. (2015) remains: Many localized restoration efforts lack measurable objectives, robust experimental designs, or a conceptual model for revising management plans using updated information. This problem is reiterated in a recent Independent Science Review Panel (ISRP) assessment of a synthesis of restoration effectiveness in the basin (ISRP 2018), and one that Atlas partners are actively seeking to address. For example, restoration practitioners took special care to clearly outline quantitative objectives for a recent project on Sheep Creek (Figure 6).

The implications of hatchery production on carrying capacity and diversity of wild fish needs to be considered in

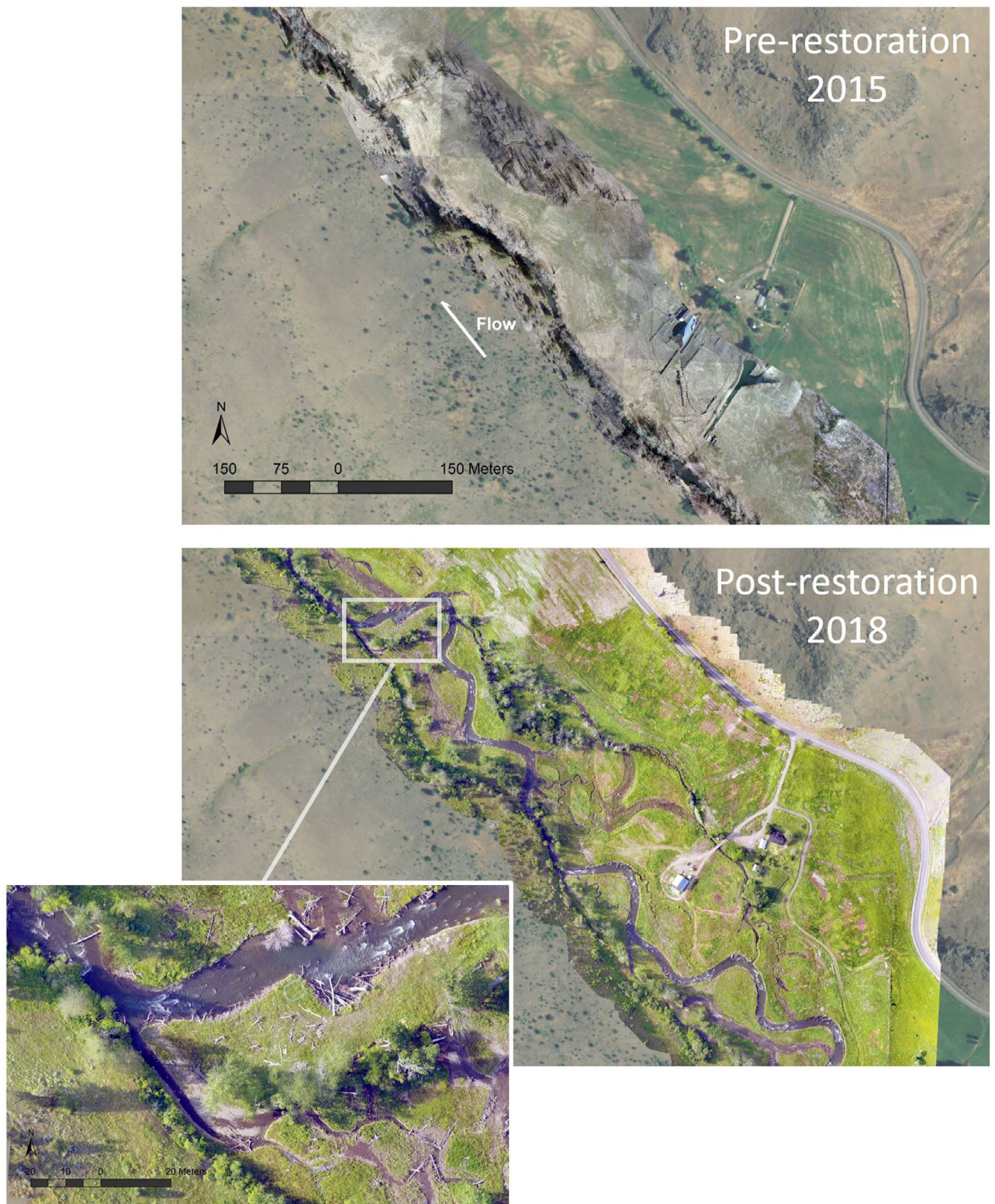


Figure 5. The Southern Cross site on Catherine Creek as an example of a large-scale project emphasizing ecological diversity through restoration of channel complexity and connectivity of floodplains and off-channel habitats.

context of habitat restoration. Salmon and steelhead hatcheries in the Grande Ronde Basin were authorized and developed to mitigate the effects of hydroelectric development via conservation, recovery, and harvest augmentation. All hatchery programs have a hatchery genetic management plan (HGMP)

detailing production goals for supplemented stocks (CTUIR 2011; ODFW 2011). These HGMPs have performance standards for spawning, rearing, and migration in freshwater, as well as estuarine habitat capacities. Monitoring of supplemented stocks includes measures of life-stage abundance and



## QUANTITATIVE OBJECTIVES OF SHEEP CREEK RESTORATION



The Sheep Creek Restoration Project encompasses 4.5 miles of the upper Grande Ronde River. Sheep Creek and its meadow habitats were not in proper functioning ecological condition (hydrologic, geomorphic, vegetative composition) due to historical practices such as beaver trapping, overgrazing, logging, road building, and an altered fire regime. The Sheep Creek Restoration project was implemented in 2019 by Trout Unlimited and the U.S. Forest Service.

### Quantitative objectives for habitat function included:

- Exclude cattle grazing from 145 acres of riparian habitat with 5.25 miles of fence to promote native riparian community
- Increase late-summer floodplain area by 30% after 2 years post-restoration
- Buffer seasonal high and low stream temperatures via increased groundwater inputs after 5 years of improved floodplain connection
- Add 1,500 pieces of large wood to the stream and floodplain
  - 72 channel spanning wood structures to backwater pools and activate side channels
  - 90 wood structures to provide velocity refuge and cover

### Quantitative objectives are monitored via:

- Riparian transects to track vegetation species composition and density
- Aerial photography and GIS analysis to monitor floodplain inundation at high and low streamflows
- Stream temperature data loggers to evaluate changes in temporal thermal regime
- Habitat surveys to evaluate retention of large wood and subsequent adjustments to cover and stream channel morphology

Figure 6. The Sheep Creek restoration project, a high priority project initiated in 2019 in the upper Grande Ronde River as an example of quantitative objectives and corresponding monitoring methods.

survival, distribution, and genetic composition. One impact of hatcheries is measured as productivity of hatchery origin fish relative to that of natural origin fish (“relative reproductive success”), providing necessary information for evaluating effects of hatchery stocks on overall carrying capacity of target fish populations. However, additional research is needed to elucidate the potential impacts of hatchery supplementation on natural origin populations, such as genetic diversity and variation in migration timing, age-at-return, and spatial distribution.

The well-documented plight of salmonids has dominated headlines, meeting agendas, and outreach efforts for decades. Meanwhile, other species such as Columbia spotted frog (Figure 7), western pearlshell freshwater mussels *Margaritifera falcata*, and beaver have largely been overlooked, although this is changing. For example, beaver impoundments have recently been identified as critical overwinter habitat for juvenile Chinook Salmon in the upper Grande Ronde River (Favrot and Jonasson 2020). Pacific Lamprey *Entosphenus tridentatus* are regarded as having high cultural and ecological



Figure 7. A Columbia spotted frog overlooking a restored section of the upper Grande Ronde River. Other important examples of biological biodiversity beyond salmon and steelhead include freshwater mussels, beaver, aquatic and terrestrial invertebrates, and Pacific lamprey. (Image courtesy of David Herasimtschuk, Freshwaters Illustrated.)

importance, yet are at high risk of extirpation in many rivers of the western United States, with stakeholder education seen as a critical step towards their recovery (Clemens et al. 2017). Efforts to communicate biodiversity values to the public in the Grande Ronde basin include a recent newsletter documenting the importance of freshwater mussels (Glidewell and Blevins 2018), though more work is needed to emphasize biodiversity.

Lessons learned and next steps:

- (1) Regionally as well as locally, objectives and indicators are still heavily biased towards fish abundance. In the Grande Ronde, goals are weighted towards abundance of ESA-listed salmonids. Next steps include increased attention to functional diversity of habitats and drawing from traditional knowledge emphasizing ecological diversity and resilience (e.g., CTUIR's First Foods concept).
- (2) A focused, collaborative effort among basin partners and funding agencies will be needed to reach consensus on high priority indicators. In the Grande Ronde, we propose that the development of these indicators become the focus of upcoming technical and policy exchanges such as the annual State of the Science meeting. As a start, we list several existing and proposed biological and ecological diversity indicators in Supplemental Table A.
- (3) Communication of ecological and biological diversity values has lagged in news headlines and other public outreach, as compared to the well-publicized plight of salmonids. In the Grande Ronde basin, *O. mykiss* and ESA-listed Chinook Salmon tend to be the central focus of outreach. Next steps include increased emphasis on biodiversity in public outreach materials. Communication of biodiversity values to the public through newsletters, presentations, field tours, and one-on-one meetings with landowners is a critical step in gaining support from local communities.

### CONCLUSIONS

We arrived at several conclusions about the progress, lessons learned, and next steps towards a comprehensive approach to habitat restoration. These conclusions were reached using a case study approach where specific issues in the Grande Ronde River illustrated broader conservation

themes in the Columbia basin and beyond (Table 1). Integration of science and management requires a local coordinating entity and ongoing commitment to invest in peer-learning opportunities, which includes improved collaboration between restoration practitioners, managers, and researchers. Community engagement is a key component of successful stream restoration and this can partially be achieved using community scientists and volunteers. Landscape sciences and quantitative, population-scale analytical tools are critical components of the restoration planning process; yet links between these analytical tools and management should be strengthened and formalized using a structured decision-making approach. Restoration efforts should be evaluated as an overall population-scale strategy and include analyses of cumulative effects on abundance and diversity indicators, in addition to assessment of individual restoration projects—a process drawing from both status and trends and action effectiveness monitoring. However, optimal conservation solutions suggested by quantitative models need to be framed within the larger socioeconomic and political landscape. Objectives and indicators are still heavily biased towards fish abundance; a next step includes developing a list of ecological diversity indicators and metrics (Supplementary Table A). This can be aided by traditional perspectives and local knowledge, such as CTUIR's First Foods concept that provides insights regarding the role of ecological diversity in salmon recovery. Communicating biodiversity values to the public through newsletters, presentations, and other outreach methods will be a critical step in gaining support from local communities.

We consider this self-assessment a stepping-stone towards realizing the directives from Rieman et al. (2015). Next steps include learning from others who have successfully adopted similar approaches (e.g., UCRTT 2014; UCSRB 2014; Hillman et al. 2016) as recommended by ISRP (2018) and continuing to share lessons learned. Current efforts from the Atlas partners involve developing a 5-year adaptive management plan coupled with a 20-year vision, recognizing that work is needed at multiple time scales for a long-term view of restoration. Finally, we encourage other groups to engage in a similar process of self-assessment and to share findings with the broader restoration community. These self-assessments should communicate not only the strengths of their programs, but also barriers to achieving goals and opportunities for improvement towards developing a comprehensive approach to habitat restoration in the Columbia basin.

### ACKNOWLEDGMENTS

This manuscript would not have been possible without the help of all the Atlas partners (too many to list) and countless others committed to restoration in the Grande Ronde basin. Timmie Mandish, formerly of BPA, provided much of the early conceptualization of Atlas. Dave Kaplow of BPA helped orchestrate subsequent Atlas meetings. Tom Cooney, retired from NOAA; Dale McCullough, retired from CRITFC; and Sean Welch of BPA provided guidance on the scientific principles behind Atlas. Stan Gregory and Chris Wood of the ISRP offered helpful advice and encouragement regarding this manuscript. Colleen Fagan, formerly of ODFW, and Coby Menton of GRMW were key participants of Atlas's Adaptive Management subgroup. Kasey Bliesner of ODFW compiled upper Grande Ronde spawner abundance data shown in Figure 2. The *Fisheries* Science Editor, two anonymous



reviewers, and Zach Penney and Rob Lothrop of CRITFC provided comments on manuscript drafts. We thank Tami Wilkerson at CRITFC for help with editing and formatting. Funding for the corresponding author and other CRITFC staff to prepare the manuscript was provided by BPA as part of the Columbia Basin Accords Agreement (Project # 2009-004-00).

#### ORCID

Seth M. White  <https://orcid.org/0000-0003-4918-6865>

#### REFERENCES

- Atlas Partners. 2015. Atlas implementation guidelines – Catherine Creek and upper Grande Ronde River. Available: <https://bit.ly/2jflbiq>. (December 2020).
- Benge, G. 2016. Mapping tributary habitat restoration projects in the upper Grande Ronde River to support landscape analysis. Master's thesis. Oregon State University, Corvallis.
- Beschta, R. L., W. S. Platts, and B. Kauffman. 1991. Field review of fish habitat improvement projects in the Grande Ronde and John Day River basins of eastern Oregon. Report to the Bonneville Power Administration. Portland, Oregon.
- Blumm, M. C., and C. L. Baermann. 2020. The Belloni decision and its legacy: United States v. Oregon and its far-reaching effects after a half-century. *Environmental Law* 49:347–386.
- Burke, J. L., K. K. Jones, and J. M. Dambacher. 2010. HabRate: a limiting factors model for assessing stream habitat quality for salmon and steelhead in the Deschutes River basin. Information Report 2010-03, Oregon Department of Fish and Wildlife, Corvallis.
- CBPTF (Columbia Basin Partnership Task Force). 2019. A vision for salmon and steelhead: goals to restore thriving salmon and steelhead to the Columbia River basin, phase 1 report of the CBPTF of the Marine Fisheries Advisory Committee. Available: <https://bit.ly/3o7Q8Un>. (December 2020).
- CBPTF (Columbia Basin Partnership Task Force). 2020. A vision for salmon and steelhead: goals to restore thriving salmon and steelhead to the Columbia River basin, phase 2 report of the CBPTF of the Marine Fisheries Advisory Committee. Available: <https://bit.ly/3lnDqPA>. (December 2020).
- CHaMP (Columbia Habitat Monitoring Program). 2016. Scientific protocol for salmonid habitat surveys within the Columbia Habitat Monitoring Program. Prepared for the Bonneville Power Administration, Project 2011–006-00. Available: <https://bit.ly/36mgUSK>. (December 2020).
- Clemens, B. J., R. J. Beamish, K. C. Coates, M. F. Docker, J. B. Dunham, A. E. Gray, J. E. Hess, J. C. Jolley, R. T. Lampman, B. J. McIlraith, M. L. Moser, J. G. Murauskas, D. L. G. Noakes, H. A. Schaller, C. B. Schreck, S. J. Starcevich, B. Streif, S. J. van de Wetering, J. Wade, L. A. Weitkamp, and L. A. Wyss. 2017. Conservation challenges and research needs for Pacific Lamprey in the Columbia River basin. *Fisheries* 42:268–280.
- Clifton, C. F., K. T. Day, C. H. Luce, G. E. Grant, M. Safeeq, J. E. Halofsky, and B. P. Staab. 2018. Effects of climate change on hydrology and water resources in the Blue Mountains, Oregon, USA. *Climate Services* 10:9–19.
- Conroy, M. J., and J. T. Peterson. 2013. Identifying and reducing uncertainty in decision making. Pages 192–231 in M. J. Conroy, and J. T. Peterson, editors. *Decision making in natural resource management: a structured, adaptive approach*. John Wiley & Sons, Chichester, UK.
- CRITFC (Columbia River Inter-Tribal Fish Commission). 2014. Spirit of the salmon: Wy-Kan-Ush-MiWa-Kish-Wit. Update. Columbia River Inter-Tribal Fish Commission, Portland, Oregon. Available: <http://plan.critfc.org>. (December 2020).
- Crozier, L. G., R. W. Zabel, and A. F. Hamlet. 2008. Predicting differential effects of climate change at the population level with life-cycle models of spring Chinook Salmon. *Global Change Biology* 14:236–249.
- CTUIR (Confederated Tribes of the Umatilla Indian Reservation). 2011. Grande Ronde endemic spring Chinook Salmon supplementation program: hatchery genetic management plan. Available: <https://bit.ly/37eEYpS>. (December 2020).
- Ebersole, J. L., W. J. Liss, and C. A. Frissell. 2003. Thermal heterogeneity, stream channel morphology, and salmonid abundance in Northeastern Oregon streams. *Canadian Journal of Fisheries and Aquatic Sciences* 60:1266–1280.
- Edwards, P. M., G. Shaloun, and D. Bedell. 2018. A unique role for citizen science in ecological restoration: a case study in streams. *Restoration Ecology* 26:29–35.
- Favrot, S. D., and B. C. Jonasson. 2020. Fall and winter movement dynamics of naturally produced spring Chinook Salmon parr in two neighboring interior Pacific Northwest natal rivers. *Transactions of the American Fisheries Society* 149:532–551.
- Glidewell, B., and E. Blevins. 2018. Helping freshwater mussels help river ecosystems. *Ripples in the Grande Ronde Spring Edition*: 4–5. Available: <https://bit.ly/3o8TgiL>. (December 2020).
- Hand, B. K., C. G. Flint, C. A. Frissell, C. C. Muhlfeld, S. P. Devlin, B. P. Kennedy, R. L. Crabtree, W. A. McKee, G. Luikart, and J. A. Stanford. 2018. A social-ecological perspective for riverscape management in the Columbia River basin. *Frontiers in Ecology and the Environment* 16:S23–S33.
- Hibbard, M., L. Senkyr, and M. Webb. 2015. Multifunctional rural regional development: evidence from the John Day watershed in Oregon. *Journal of Planning Education and Research* 35:51–62.
- Hilborn, R. 1992. Can fisheries agencies learn from experience? *Fisheries* 17(4):6–14.
- Hillman, T., P. Roni, and J. O'Neal. 2016. Effectiveness of tributary habitat enhancement projects. Report to Bonneville Power Administration, Portland, Oregon. Available: <https://bit.ly/3g2PtAZ>. (December 2020).
- Isaak, D. J., C. H. Luce, D. L. Horan, G. L. Chandler, S. P. Wollrab, and D. E. Nagel. 2018. Global warming of salmon and trout rivers in the northwestern U.S.: road to ruin or path through purgatory? *Transactions of the American Fisheries Society* 147:566–587.
- Isaak, D. J., S. J. Wenger, E. E. Peterson, J. M. Ver Hoef, D. E. Nagel, C. H. Luce, S. W. Hostetler, J. B. Dunham, B. B. Roper, S. P. Wollrab, G. L. Chandler, D. L. Horan, and S. Parkes-Payne. 2017. The NorWeST summer stream temperature model and scenarios for the Western U.S.: a crowd-sourced database and new geospatial tools foster a user community and predict broad climate warming of rivers and streams. *Water Resources Research* 53:9181–9205.
- ISAB (Independent Scientific Advisory Board). 2018. Review of the 2014 Columbia River Basin Fish and Wildlife Program. ISAB 2018–3, Portland, Oregon.
- ISRP (Independent Scientific Review Panel). 2018. Review of the Grande Ronde Model Watershed Synthesis, 1992–2016. ISRP 2018–11, Portland, Oregon. Available: <https://bit.ly/37lGHKf>. (December 2020).
- Justice, C., S. M. White, D. A. McCullough, D. S. Graves, and M. R. Blanchard. 2017. Can stream and riparian restoration offset climate change impacts to salmon populations? *Journal of Environmental Management* 188:212–227.
- Kaylor, M. J., S. M. White, W. C. Saunders, and D. R. Warren. 2019a. Relating spatial patterns of stream metabolism to distributions of juvenile salmonids at the river network scale. *Ecosphere* 10:e02781.
- Kaylor, M. J., S. M. White, E. R. Sedell, A. M. Sanders, and D. R. Warren. 2020. Carcass additions influence food webs through bottom-up and direct consumption pathways along a fish species assemblage gradient. *Ecosystems*. Available: <https://bit.ly/3qi9oAC>. (December 2020).
- Kaylor, M. J., S. M. White, E. R. Sedell, and D. R. Warren. 2019b. Carcass additions increase juvenile salmonid growth, condition, and size in an interior Columbia River basin tributary. *Canadian Journal of Fisheries and Aquatic Sciences* 77:703–715.
- McIntosh, B. A., J. R. Sedell, R. F. Thurow, S. E. Clarke, and G. L. Chandler. 2000. Historical changes in pool habitats in the Columbia River basin. *Ecological Applications* 10:1478–1496.
- McPhail, J. D., and C. C. Lindsey. 1986. Zoogeography of the freshwater fishes of Cascadia (the Columbia System and rivers north to the Stikine). in C. H. Hocutt, and E. O. Wiley, editors. *The Zoogeography of North American freshwater fishes*. John Wiley, New York.
- Mobrand, L., L. Lestelle, L. Gilbertson, R. Browning, D. Bryson, R. Carmichael, E. Claire, B. Hadden, C. Huntington, L. Kuchenbecker, and M. Shaw. 1995. Grande Ronde Model Watershed ecosystem diagnosis and treatment: template for planning status report for Grande Ronde Model Watershed project and progress report on the application of an ecosystem analysis method to the Grande Ronde watershed using spring Chinook Salmon as a diagnostic species. Final Report to the Bonneville Power Administration, Project 94-030, Portland, Oregon.
- NOAA (National Oceanic and Atmospheric Administration). 2008a. Supplemental comprehensive analysis of the Federal Columbia River



- Power System and mainstem effects of the Upper Snake and other tributary actions. NOAA Fisheries, Portland, Oregon.
- NOAA (National Oceanic and Atmospheric Administration). 2008b. Endangered Species Act Section 7(a)(2) consultation biological opinion and Magnuson-Stevens Fishery Conservation and Management Act essential fish habitat consultation: consultation on remand for operation of the Federal Columbia River Power System, 11 Bureau of Reclamation Projects in the Columbia Basin and ESA Section 10(a)(1)(A) Permit for Juvenile Fish Transportation Program (Revised and reissued pursuant to court order, NWF vs. SMFS, Civ. No. CV 01-640-RE [D. Oregon]).
- NOAA (National Oceanic and Atmospheric Administration). 2017. ESA recovery plan for Snake River spring/summer Chinook Salmon (*Oncorhynchus tshawytscha*) and Snake River basin steelhead (*Oncorhynchus mykiss*). NOAA Fisheries, Portland, Oregon.
- NPCC (Northwest Power and Conservation Council). 1986. Compilation of information on salmon and steelhead losses in the Columbia River Basin. Northwest Power Planning Council, Portland, Oregon.
- NPT (Nez Perce Tribe). 2013. Management plan 2013–2028. Nez Perce Tribe Department of Fisheries Resources Management, Lapwai, Idaho.
- ODFW (Oregon Department of Fish and Wildlife). 2011. Grande Ronde Basin Catherine Creek spring/summer chinook program: hatchery genetic management plan. Available: <https://bit.ly/2JlCcaB>. (December 2020).
- ODFW (Oregon Department of Fish and Wildlife), and WDFW (Washington Department of Fish and Wildlife). n.d. Status report: Columbia River fish runs and fisheries 1938–2002. Available: <https://bit.ly/3o9KyRw>. (December 2020).
- Pess, G., and C. E. Jordan. 2019. Characterizing watershed-scale effects of habitat restoration actions to inform life cycle models: case studies using data-rich vs. data-poor approaches. U.S. Department of Commerce, NOAA Technical Memorandum NMFS-NWFSC-151.
- Quaempts, E. J., K. L. Jones, S. J. O'Daniel, T. J. Beechie, and G. C. Poole. 2018. Aligning environmental management with ecosystem resilience: a First Foods example from the Confederated Tribes of the Umatilla Indian Reservation, Oregon, USA. *Ecology and Society* 23:29.
- Rahel, F. J., and J. D. Olden. 2008. Assessing the effects of climate change on aquatic invasive species. *Conservation Biology* 22:521–33.
- Rieman, B. E., C. L. Smith, R. J. Naiman, G. T. Ruggerone, C. C. Wood, N. Huntly, E. N. Merrill, J. R. Alldredge, P. A. Bisson, J. Congleton, K. D. Fausch, C. Levings, W. Pearcy, D. Scarnecchia, and P. Smouse. 2015. A comprehensive approach for habitat restoration in the Columbia Basin. *Fisheries* 40:124–135.
- Rivot, E., E. Prévost, E. Parent, and J. L. Baglinière. 2004. A Bayesian state-space modelling framework for fitting a salmon stage-structured population dynamic model to multiple time series of field data. *Ecological Modelling* 179:463–485.
- Roche, K., P. Jurajda, L. Šlapanský, and S. M. White. 2020. Turning back the tide? Local-scale impacts of climate change may have positive effects by restoring natural riverine habitat and reducing invasive fish density. *Freshwater Biology* 65:2010–2020.
- Roni, P., and J. O'Neal. 2017. Action effectiveness monitoring program 2016. Annual Report to the Bonneville Power Administration, Project 2016-001-00. Available: <https://bit.ly/3qgjX6Y>. (December 2020).
- Sedell, E., S. Tattam, A. Garner, C. Horn, K. Bliesner, J. Dowdy, S. Favrot, G. McMichael, E. Branigan, B. Power, O. Davis, and J. Ruzyski. 2018. Investigations into the life history of naturally produced spring Chinook Salmon and summer steelhead in the Grande Ronde River subbasin, 2017. Annual Report to the Bonneville Power Administration, Project 1992–026-04.
- Sedell, J. D. 2018. Grande Ronde Model Watershed synthesis: 1992–2016. Grande Ronde Model Watershed, La Grande, Oregon.
- Sullivan, S. P., and S. M. White. 2017. Methods supporting the development of food web metrics from benthic macroinvertebrate data. CRITFC Technical Report No. 17–05, Portland, Oregon.
- Tetra Tech. 2017. Catherine Creek and upper Grande Ronde River Atlas restoration prioritization framework: user's manual. Tetra Tech, Bothell, Washington.
- UCRTT (Upper Columbia Regional Technical Team). 2014. A biological strategy to protect and restore salmonid habitat in the Upper Columbia region. Draft report to the upper Columbia Salmon Recovery Board.
- UCSRB (Upper Columbia Salmon Recovery Board). 2014. Integrated recovery program habitat report. Upper Columbia Salmon Recovery Board, Wenatchee, Washington.
- USBOR (U.S. Department of the Interior, Bureau of Reclamation). 2012. The Catherine Creek tributary assessment, Grande Ronde River basin, Tributary Habitat Program, Oregon. USBOR, Boise, Idaho.
- USBOR (U.S. Department of the Interior, Bureau of Reclamation). 2014. Upper Grande Ronde River tributary assessment, Grande Ronde River basin, Tributary Habitat Program, Oregon. USBOR, Boise, Idaho.
- Weber, N., N. Bouwes, C. Justice, and S. White. 2018. Life-cycle model for upper Grande Ronde and Catherine Creek spring chinook: evaluation of habitat restoration and population recovery strategies, Report to the Bonneville Power Administration, Project 2009–004-00.
- White, S., C. Justice, L. Burns, D. Kelsey, D. Graves, and M. Kaylor. 2018. Assessing the status and trends of spring chinook habitat in the upper Grande Ronde River and Catherine Creek. Annual Report to Bonneville Power Administration, Project 2009–004-00.
- White, S., C. Justice, L. Burns, B. Staton, D. Graves, and M. Kaylor. 2020. Assessing the status and trends of spring chinook habitat in the upper Grande Ronde River and Catherine Creek. Annual Report to Bonneville Power Administration, Project 2009–004-00.
- White, S. M., C. Justice, D. A. Kelsey, D. A. McCullough, and T. Smith. 2017. Legacies of stream channel modification revealed using General Land Office surveys, with implications for water temperature and aquatic life. *Elementa Science of the Anthropocene* 5:3. Available <https://bit.ly/33v6lLm>. (December 2020).
- Yin, R. K. 2018. Case study research and applications: design and methods, sixth edition. SAGE, Los Angeles, California.

## SUPPORTING INFORMATION

Additional supplemental material may be found online in the Supporting Information section at the end of the article. [AFS](#)

**Supplementary Table A.** Indicators and metrics for biological and ecological diversity.

Indicator type	Indicator	Metric	Description	Data source
<b>Salmon/steelhead abundance<sup>1</sup></b>	Adult abundance	Abundance of natural origin spawners	Number of natural origin adults (age 3+) on the spawning grounds	Field
	Juvenile abundance	Abundance of natural origin summer parr	Number of natural origin juvenile parr during summer (July - September)	Field
		Abundance of natural origin juvenile fall migrants	Number of natural origin juveniles migrating out of their natal rearing areas during fall (October - December)	Field
		Abundance of natural origin juvenile spring migrants	Number of natural origin juveniles migrating out of their natal rearing areas during spring (March - June)	Field
		Abundance of natural origin smolts	Number of natural origin smolts surviving to Lower Granite Dam	Field
<b>Salmon/steelhead productivity<sup>1</sup></b>	Adult productivity	Pre-spawn survival of natural origin spawners	Survival of natural origin adults from return to tributary weirs to spawning	Field
		Total productivity of natural origin spawners (adults per spawner)	The number of surviving natural origin adult offspring (age 3+) per parent	Field
	Juvenile productivity	Tributary survival of summer parr	Survival of natural origin summer parr from natal rearing areas to Lower Granite Dam	Field
		Tributary survival of fall (early) migrants	Survival of natural origin fall migrants from tributary traps to Lower Granite Dam	Field
		Tributary survival of winter parr	Survival of natural origin winter parr from natal rearing areas to Lower Granite Dam	Field
		Tributary survival of spring (late) migrants	Survival of natural origin spring migrants from tributary traps to Lower Granite Dam	Field
		Freshwater productivity of natural origin spawners (smolts per spawner)	The number of natural origin smolt offspring surviving to Lower Granite Dam per parent	Field
	Juvenile to adult productivity	Smolt-to-adult return rate (SAR)	Survival of natural origin smolts from Lower Granite Dam to returning adults at Lower Granite Dam	Field
<b>Salmon/steelhead diversity<sup>1</sup></b>	Spawner distribution	Number and spatial arrangement of spawning areas	Number of major spawning areas (MaSAs), distribution of MaSAs, and quantity of habitat	Field/modeled

**Supplementary Table A** (continued)

Indicator type	Indicator	Metric	Description	Data source
			outside MaSA (ICTRT 2007, Table 8)	
		Spatial extent or range of population	Proportion of historical range occupied and presence/absence of spawners in MaSAs (ICTRT 2007, Table 9)	Field/modeled
		Change in gaps or continuities between spawning areas	Change in occupancy of MaSAs that affects connectivity within the population (ICTRT 2007, Table 10)	Field/modeled
	Phenotypic and genotypic variation	Major life history strategies	Distribution of major life history expression within a population (ICTRT 2007, Table 11)	Field
		Phenotypic variation	Reduction in variability of traits, shift in mean value of trait, loss of traits (ICTRT 2007, Table 12)	Field
		Genetic variation	Analysis addressing within and between population genetic variation (ICTRT 2007, Table 13)	Field/lab
	Gene flow	Spawner composition 1	Proportion of natural spawners that are out-of-ESU <sup>2</sup> spawners (ICTRT 2007, Figure 9)	Field
		Spawner composition 2	Proportion of natural spawners that are out-of-MPG <sup>3</sup> spawners	Field
		Spawner composition 3	Proportion of hatchery origin natural spawners derived from a within-MPG brood stock program, or within population (not best practices <sup>4</sup> ) program	Field
		Spawner composition 4	Proportion of hatchery origin natural spawners derived from a local (within population) brood stock program using best practices	Field
	Occupancy of diverse habitats	Distribution of population across habitat types	Change in occupancy across ecoregion types (ICTRT 2007, Figure 10)	Field
	Integrity of natural systems	Selective change in natural processes or impacts	Ongoing anthropogenic activities inducing selective mortality or habitat change within or out of population boundary (ICTRT 2007, Figure 14)	Modeled

**Supplementary Table A** (continued)

Indicator type	Indicator	Metric	Description	Data source
<b>Habitat quality/diversity</b>	Floodplain/side channels	River channel complexity index	River channel complexity index (RCI) = $S \cdot (1+J)$ where S = stream sinuosity, J = # of side channel junctions (Brown 2002)	Field/LiDAR/UAS <sup>5</sup>
		Side channel ratio	Length of side channels divided by length of main channel during base flow (Beechie et al. 2017)	Field/LiDAR/UAS
	Riparian condition	Riparian tree cover	Average percent tree canopy cover in the riparian zone (50 m stream buffer)	UAS/LiDAR
		Riparian tree height	Average tree height (m) in the riparian zone (50 m stream buffer)	UAS/LiDAR
		Riparian vegetation departure	Average percentage departure in current vegetation from simulated historical vegetation reference conditions in the riparian zone (100 m buffer; LANDFIRE 2016)	Satellite/Modeled
	River channel (cover)	Large wood <sup>6</sup> area percentage	Percentage of stream surface area covered by large wood during base flow	UAS
		Large wood frequency bankfull	Number of large wood pieces within the bankfull channel per 100 m stream length (Moore et al. 2017)	Field
		Large wood frequency wetted	Number of large wood pieces within the wetted channel during base flow per 100 m stream length (Moore et al. 2017)	Field
		Overhanging vegetation	Percentage of stream surface area covered by vegetation during base flow	UAS/LiDAR
		Undercut bank percentage	Percentage of the total bank length that is undercut	Field
	River channel (depth)	Bankfull width to depth ratio	Average bankfull width to depth ratio (Rosgen 1996)	Field/LiDAR
		Residual pool depth	Mean residual pool depth (max depth - thalweg <sup>7</sup> exit depth in meters; Mossop and Bradford 2006)	Field
	River channel (pools)	Large pool frequency	Number of large pools (> 20 m <sup>2</sup> area and > 0.80 m max depth) per km stream length (McIntosh et al. 2000)	Field

**Supplementary Table A** (continued)

Indicator type	Indicator	Metric	Description	Data source
		Medium pool frequency	Number of medium-sized pools (> 20 m <sup>2</sup> area and > 0.50 m max depth) per km stream length (McIntosh et al. 2000)	Field
	River channel (substrate)	Median sediment particle size	Median sediment particle size on the streambed surface in riffles (Wolman 1954)	Field
	Water quality	Coldwater refuge <sup>8</sup> density	Number of coldwater refuges per km stream length (Dugdale et al. 2015)	FLIR
		Maximum weekly maximum temperature	Maximum 7-day running average of daily maximum temperature (EPA 2003)	Field/Modeled
		Observed/Expected benthic macroinvertebrates	Ratio of observed to expected (O/E) benthic macroinvertebrate taxa as predicted by the River Invertebrate Prediction and Classification System (RIVPACS, Hawkins et al. 2000)	Field
<b>Habitat quantity</b>	Floodplain/side channels	Off-channel habitat bankfull	Surface area (m <sup>2</sup> ) of connected off-channel habitat during bankfull flow (NetMap 2020, Benda et al. 2016)	LiDAR
		Off-channel habitat base flow	Surface area (m <sup>2</sup> ) of connected off-channel habitat during base flow (NetMap 2020, Benda et al. 2016)	LiDAR
		Side channel length	Length (m) of side channels during low flow	Field/UAS
	Flow	Center of flow mass	Flow-weighted mean day of the water year (i.e., center of flow timing; USFS 2015)	Field/Modeled
		Mean annual flow	Mean of all daily flow measurements (m <sup>3</sup> ·s <sup>-1</sup> ) within a water year (Oct 1 - Sep 30; USFS 2015)	Field/Modeled
		Mean summer flow	Mean of all daily flow measurements (m <sup>3</sup> ·s <sup>-1</sup> ) during summer (Jun 1 - Sep 30; USFS 2015)	Field/Modeled
	River channel	Fast water area	Surface area (m <sup>2</sup> ) of fast water habitat (e.g., fast turbulent, fast non-turbulent, fast small side channels) during base flow	Field/UAS
		Length accessible anadromous fish habitat	Length (km) of accessible main channel habitat that is currently used by anadromous fish for spawning, rearing, or migration (StreamNet 2019)	Field/Modeled

**Supplementary Table A** (continued)

Indicator type	Indicator	Metric	Description	Data source
		Slow water area	Surface area (m <sup>2</sup> ) of slow water habitat (e.g., pools, off-channel units, slow small side channels) during base flow	Field/UAS

<sup>1</sup> Indicators required to calculate viable salmonid population (VSP) criteria (McElhany et al. 2000)

<sup>2</sup> ESU = Evolutionary Significant Unit

<sup>3</sup> MPG = Major Population Group

<sup>4</sup> Best practices refers to breeding, rearing, and release protocols that minimize effects of hatchery fish on natural population structure and fitness as in Flagg et al. (2004), Olson et al. (2004) and Mobrand et al. (2005).

<sup>5</sup> UAV=Unmanned aerial system (i.e., drone)

<sup>6</sup> Large wood = wood pieces  $\geq 0.15$  m diameter and  $\geq 3$  m length

<sup>7</sup> Thalweg = deepest portion of the stream channel

<sup>8</sup> Coldwater refuges = contiguous wetted area ( $> 1$  m<sup>2</sup>) with water temperature  $> 2$  °C colder than the ambient river temperature

## References

- Beechie, T.J., O. Stefankiv, B. Timpane-Padgham, J.E. Hall, G.R. Pess, M. Rowse, M. Liermann, K. Fresh, and M. Ford. 2017. Monitoring salmon habitat status and trends in Puget Sound: development of sample designs, monitoring metrics, and sampling protocols for large river, floodplain, delta, and nearshore environments. Page 185. National Oceanic and Atmospheric Administration, NOAA Technical Memorandum NMFS-NWFSC-137, Seattle, WA.
- Benda, L., D. Miller, J. Barquin, R. McCleary, T. Cai, and Y. Ji. 2016. Building Virtual Watersheds: A Global Opportunity to Strengthen Resource Management and Conservation. *Environmental Management* 57(3):722–739.
- Brown, A. G. 2002. Learning from the past: palaeohydrology and palaeoecology. *Freshwater Biology* 47(4):817–829.
- Dugdale, S. J., N. E. Bergeron, and A. St-Hilaire. 2015. Spatial distribution of thermal refuges analysed in relation to riverscape hydromorphology using airborne thermal infrared imagery. *Remote Sensing of Environment* 160:43–55.
- EPA (U.S. Environmental Protection Agency). 2003. EPA region 10 guidance for Pacific Northwest state and tribal temperature water quality standards. Page 49. U.S. Environmental Protection Agency, EPA 910-B-03-002, Region 10 Office of Water, Seattle, Washington.
- Flagg, T. A., C. V. W. Mahnken, and R. N. Iwamoto. 2004. Conservation hatchery protocols for Pacific salmon. *American Fisheries Society Symposium* 44:603–619.
- Hawkins, C. P., R. H. Norris, J. N. Hogue, and J. W. Feminella. 2000. Development and evaluation of predictive models for measuring the biological integrity of streams. *Ecological Applications* 10 (5): 1456–77.
- Heck, M. P., L. D. Schultz, D. Hockman-Wert, E. C. Dinger, and J. B. Dunham. 2018. Monitoring stream temperatures—a guide for non-specialists. Page 76. U.S. Geological Survey Techniques and Methods, book 3, chapter A25.
- ICTRT (Interior Columbia Technical Recovery Team). 2007. Viability criteria for application to interior Columbia Basin salmonid ESUs. Review draft March 2007. Available at: 48T [http://www.nwfsc.noaa.gov/trt/trt\\_viability.cfm48T](http://www.nwfsc.noaa.gov/trt/trt_viability.cfm48T).
- LANDFIRE. 2016. Vegetation departure (VDep) data from Landscape Fire and Resource Management Planning Tools Project, version 2.0.0. <https://www.landfire.gov/vdep.php> (accessed 10/15/2020).

**Supplementary Table A (continued)**

- McElhany, P., M. Ruckleshaus, M. J. Ford, T. Wainwright, and E. Bjorkstedt. 2000. Viable salmon populations and the recovery of evolutionarily significant units. U.S. Department of Commerce, National Marine Fisheries Service, Northwest Fisheries Science Center, NOAA Technical Memorandum NMFS-NWFSC-42. 156 p.
- McIntosh, B.A., J.R. Sedell, R.F. Thurow, S.E. Clarke, and G.L. Chandler. 2000. Historical changes in pool habitats in the Columbia River Basin. *Ecological Applications* 10 (5): 1478–96. [https://doi.org/10.1890/1051-0761\(2000\)010\[1478:HCIPHI\]2.0.CO;2](https://doi.org/10.1890/1051-0761(2000)010[1478:HCIPHI]2.0.CO;2).
- Mobrand, L. E., J. Barr, L. Blankenship, D. E. Campton, T. T. P. Evelyn, T. A. Flagg, C. V. W. Mahnken, L. W. Seeb, P. R. Seidel, and W. W. Smoker. 2005. Hatchery reform in Washington state: principles and emerging issues. *Fisheries* 30(6):11–23.
- Moore, K., K. Jones, J. Dambacher, and C. Stein. 2017. Aquatic inventories project: methods for stream habitat surveys. Page 89. Oregon Department of Fish and Wildlife, Version 27.1, Corvallis, OR.
- Mossop, B., and M. J. Bradford. 2006. Using thalweg profiling to assess and monitor juvenile salmon (*Oncorhynchus* spp.) habitat in small streams. *Canadian Journal of Fisheries and Aquatic Sciences* 63(7):1515–1525.
- NetMap. 2020. Floodplain mapping tools (Floodplain 2.0) from NetMap toolkit for ArcGIS 10.X, version 3.2.0, build date 02/28/2020. Developed by TerrainWorks. <https://terrainworks.com/>.
- Olson, D. E., B. Spateholts, M. Paiya, and D. E. Campton. 2004. Salmon hatcheries for the 21st century: a model at Warm Springs National Fish Hatchery. *American Fisheries Society Symposium* 44:581–598.
- Rosgen, D. 1996. Applied river morphology. Wildland Hydrology, Pagosa Springs, CO.
- StreamNet. 2019. Fish distribution – all species combined. Digital map. <https://www.streamnet.org/data/interactive-maps-and-gis-data/> (accessed 11/14/2019).
- USFS (United States Forest Service). 2015. Western US stream flow metric dataset: modeled flow metrics for stream segments in the western United States under historical conditions and projected climate change scenarios. Page 7.
- Wolman, M. G. 1954. A method of sampling coarse river-bed material. *Transaction of the American Geophysical Union* 35:951–956.